uOttawa

L'Université canadienne
Canada's university

FACULTÉ DES ÉTUDES SUPÉRIEURES ET POSTOCTORALES

uOttawa

L'Université canadienne
Canada's university

FACULTY OF GRADUATE AND POSDOCTORAL STUDIES

Lilian Navarro Ugueto

AUTEUR DE LA THÈSE / AUTHOR OF THESIS

M.Sc. (Earth Sciences)

GRADE / DEGREE

Department of Earth Sciences

FACULTÉ, ÉCOLE, DÉPARTEMENT / FACULTY, SCHOOL, DEPARTMENT

Depositional Architecture and Evolution of Deep-water Base-of-slope and Slope Channel Complexes in a Passive-margin Setting: Isaac Formation, Windermeer Supergroup (Neoproterozoic), Southern Canadian Cordillera

TITRE DE LA THÈSE / TITLE OF THESIS

Dr. W. Arnott

DIRECTEUR (DIRECTRICE) DE LA THÈSE / THESIS SUPERVISOR

CO-DIRECTEUR (CO-DIRECTRICE) DE LA THÈSE / THESIS CO-SUPERVISOR

EXAMINATEURS (EXAMINATRICES) DE LA THÈSE / THESIS EXAMINERS

Dr. A. Desrochers

Dr. A. Donaldson

Dr. C. Schroder-Adams

Gary W. Slater

Le Doyen de la Faculté des études supérieures et postdoctorales / Dean of the Faculty of Graduate and Postdoctoral Studies

DEPOSITIONAL ARCHITECTURE AND EVOLUTION OF DEEP-WATER BASE-OF-SLOPE AND SLOPE CHANNEL COMPLEXES IN A PASSIVE-MARGIN SETTING: ISAAC FORMATION, WINDERMERE SUPERGROUP (NEOPROTEROZOIC), SOUTHERN CANADIAN CORDILLERA

By

Lilian L. Navarro Ugueto

Thesis submitted to the
Faculty of Graduate and Postdoctoral Studies
In partial fulfillment of the requirements
For the *Master Scientiarum* degree in Earth Sciences

OTTAWA-CARLETON GEOSCIENCE CENTRE
FACULTY OF SCIENCE
UNIVERSITY OF OTTAWA

Library and Archives Canada

Published Heritage Branch

395 Wellington Street
Ottawa ON K1A 0N4
Canada

Bibliothèque et Archives Canada

Direction du Patrimoine de l'édition

395, rue Wellington
Ottawa ON K1A 0N4
Canada

Your file Votre référence
ISBN: 978-0-494-18451-6
Our file Notre référence
ISBN: 978-0-494-18451-6

NOTICE:
The author has granted a non-exclusive license allowing Library and Archives Canada to reproduce, publish, archive, preserve, conserve, communicate to the public by telecommunication or on the Internet, loan, distribute and sell theses worldwide, for commercial or non-commercial purposes, in microform, paper, electronic and/or any other formats.

The author retains copyright ownership and moral rights in this thesis. Neither the thesis nor substantial extracts from it may be printed or otherwise reproduced without the author's permission.

AVIS:
L'auteur a accordé une licence non exclusive permettant à la Bibliothèque et Archives Canada de reproduire, publier, archiver, sauvegarder, conserver, transmettre au public par télécommunication ou par l'Internet, prêter, distribuer et vendre des thèses partout dans le monde, à des fins commerciales ou autres, sur support microforme, papier, électronique et/ou autres formats.

L'auteur conserve la propriété du droit d'auteur et des droits moraux qui protège cette thèse. Ni la thèse ni des extraits substantiels de celle-ci ne doivent être imprimés ou autrement reproduits sans son autorisation.

In compliance with the Canadian Privacy Act some supporting forms may have been removed from this thesis.

While these forms may be included in the document page count, their removal does not represent any loss of content from the thesis.

Conformément à la loi canadienne sur la protection de la vie privée, quelques formulaires secondaires ont été enlevés de cette thèse.

Bien que ces formulaires aient inclus dans la pagination, il n'y aura aucun contenu manquant.

Canada

© Lilian Navarro Ugueto, Ottawa, Canada, 2006

DEPOSITIONAL ARCHITECTURE AND EVOLUTION OF DEEP-WATER BASE-OF-SLOPE AND SLOPE CHANNEL COMPLEXES IN A PASSIVE-MARGIN SETTING: ISAAC FORMATION, WINDERMERE SUPERGROUP (NEOPROTEROZOIC), SOUTHERN CANADIAN CORDILLERA

Lilian L. Navarro Ugueto

Approved as style and content by:

Dr. Keith Been
University of Ottawa
(Chairman of Committee)

Dr. André Desrochers
University of Ottawa

Dr. Claudia Schorder-Adams
Carleton University

Dr. Allan Donaldson
Carleton University

ABSTRACT

The Isaac Formation in the Neoproterozoic Windermere Supergroup crops out in the Castle Creek South area (southwestern Canadian Cordillera) and consists of a more than 1.2 km-thick, laterally continuous slope deposit formed along the ancestral passive margin of western North America. Within the study area, six channel complex sets have been recognized, of which two, named informally Channels 1 and 3, are the focus of this study. Channel 1 exposes an oblique section of base-of-slope channel deposits, whereas Channel 3 , at least in its lower part, is a flow-transverse section.

Channels 1 and 3 are 200-300 m thick and laterally extend over 1.1 km, and were initiated following two major falls of relative sea level. Detailed relationships between the intrachannel facies, architecture and geometry within both complex sets indicates that each comprises several vertically-stacked channel complexes that locally are separated by thin-bedded, mudstone-dominated turbidites interpreted to represent channel-abandonment deposits.

Each channel complex consists of several channel units, which, in turn, are composed of multiple channel fills. Channel fills are up to 30 m thick and show different infill geometries (amalgamated, semi-amalgamated or layered, non-amalgamated and accretionary), exhibiting systematic lateral changes in fill from channel axis to channel margin.

Multistory and multilateral fills in Channels 1 and 3 record a complex repetitive history of channel incision/bypass, aggradation, deactivation, migration and reincision. These erosional and depositional episodes are the result of changes in the equilibrium channel profile, flow parameters, and/or eustatic fluctuations.

RÉSUMÉ

La formation d' Isaac dans le groupe néoprotérozoïque de Windermere affleure dans la région au sud de Castle Creek (sud-ouest de la Cordillère canadienne) et se compose de plus de 1.2 km d'épaisseur de dépôts de pente latéralement continus s'étant formés le long de la marge passive ancestrale à l'ouest de l'Amérique du nord. Dans le secteur d'étude, six ensembles de complexes de chenaux ont été identifiés. Deux ont été appelés officieusement les chenaux 1 et 3 et seront examinés dans la présente étude. Le chenal 1 expose une section oblique de dépôts de bas de pente continentale. Quant au chenal 3, il expose une section transversale au paléocourant, du moins dans sa partie inférieure.

Les chenaux 1 et 3 ont de 200 à 300 m d'épaisseur, sont latéralement continus sur plus de 1.1 km et ont été formés durant deux importantes périodes de baisse du niveau relatif de la mer. L'étude détaillée des relations entre les facies intra-chenaux, l'architecture et la géométrie de chacun de complexes a permis de distinguer plusieurs complexes de chenaux empilés à la verticale. Ces derniers sont localement entrecoupés de minces dépôts de turbidites à haute teneur en boue (mudstone-dominated) qui sont interprétée comme étant des dépôts de chenal d'abandon.

Chacun des complexes de chenal est constitué de plusieurs unités de chenaux qui à leur tour se composent de plusieurs événements de remplissage de chenaux. Ces dépôts de remplissage ont jusqu'à 30 m d'épaisseur, se présentent sous différentes géométries de remplissage (amalgamées, semi-amalgamées ou posées, non amalgamée et d'accrétion), et montrent également des changements systématiques de mode remplissage lorsque l'on passe de l'axe du chenal à sa marge.

Le caractère multilatéral et multiétage du remplissage des chenaux 1 et 3 suggère une histoire complexe et réitérée des opérations d'incision/«bypass», d'aggradation verticale, de désactivation, de migration et de réincision lors de la formation de ces chenaux. Ces épisodes d'érosion et de déposition sont le résultat des changements de profil d'équilibre du chenal, des paramètres d'écoulement, et/ou des fluctuations du niveau marin.

RESUMEN

La Formación Isaac del Supergrupo Windermere de edad Neoproterozoica aflora en el área sur de Castle Creek (suroeste de la Cordillera Canadiense). Esta formación consiste de depósitos lateralmente continuos de talud continental con más de 1.2 km de espesor, que se formaron a lo largo del antiguo margen pasivo al Oeste de Norteamérica. En el área de estudio se reconocieron seis sets o conjuntos de complejo de canal, de los cuales dos, llamados informalmente Canal 1 y 3, representan los objetivos principales del presente estudio. El Canal 1 es expuesto en un corte oblicuo de depósitos de base de talud, mientras el Canal 3, al menos en su parte inferior, es expuesto en un corte perpendicular a la dirección de paleocorriente.

Los Canales 1 y 3 tienen aproximadamente 200-300 m de espesor, se extienden por más de 1.1 km y fueron depositados durante dos significativas caídas relativas del nivel del mar. Basado en el análisis detallado de las facies, elementos arquitectónicos y parámetros geométricos en ambos sets de complejo de canal, se distinguieron varios Complejos de canales, superpuestos verticalmente y que localmente están separados por estratos tabulares de capas delgadas de arenisca fina y lodolitas que se interpretan como depósitos de abandono del canal.

Cada Complejo de Canal consiste de numerosas Unidades de canal, que a su vez están compuestas de múltiples Rellenos de canales. Los Rellenos de canales alcanzan hasta 30 m de espesor y muestran diferentes geometrías de relleno (amalgamados, semi-amalgamados o estratificados, no amalgamados y acrecionales), exhibiendo a su vez cambios sistemáticos desde el eje del canal hasta sus márgenes.

El carácter múltiple y multilateral de los rellenos en los Canales 1 y 3 sugieren una historia compleja y repetitiva de incisión/"bypass", agradación, desactivación, migración y reincisión en los canales. Estos episodios de erosión y depositación son interpretados como el resultado de cambios en el equilibrio del perfil del canal, parámetros de flujos y/o fluctuaciones del nivel del mar.

EXTENDED ABSTRACT

The Isaac Formation in the Neoproterozoic Windermere Supergroup outcrops in the Castle Creek South area (southwestern Canadian Cordillera) contain more than 1.2 km thick of laterally continuous, turbidite slope deposits formed along the ancestral passive margin of western North America. Within the study area, six channel complex sets have been recognized, in which two of them, informally named Channel 1 and 3 are the focus of this study. Channel 1 exposes an oblique section of base-of slope channel deposits, whereas Channel 3 is flow-transverse, at least in its lower part, including slopes channel-levee and channel deposits.

The studied outcrops provide descriptions in detail emphasizing lithofacies, sedimentary structures, and other small-scaled features that cannot be observed in subsurface resolution. Furthermore, facies associations, architectural elements, significant surfaces, stacking patterns and lithofacies distribution were determined in order to provide important stratigraphic details on the lateral and vertical attributes of both channel-complex sets. Five facies association have been determined in intrachannel deposits of Channel 1 and 3 that consist of a spectrum of facies deposited from high- to low-concentration turbidity flows and include bypass-channel, lateral accretion packages, channel-fill, slump and channel-abandonment deposits.

Channel 1 and 3 are 200-300 m thick and at least 1.1 km wide, and were formed followed two major falls in relative sea level. Channels 1 and 3 consist of vertically-stacked channel complexes that are locally separated or capped by layered thin-bedded, mudstone-dominated sheets interpreted to represent channel-abandonment deposits. Each channel complex comprise several channel units, which in turn are made of multiple channel fills. Channel fills are individually up to 30 m thick and show different infill geometries (amalgamated, semi-amalgamated or layered, non-amalgamated and accretionary). Fills show systematic changes from the axis to margin, ranging from high net-to-gross, amalgamated, feldspathic-rich sandstone-conglomerate to low net-to-gross, non-amalgamated, interstratified sandstone-mudstone.

Multistory and multilateral fills suggest that numerous and repetitive episodes of channel incision/bypass, aggradation, deactivation, migration and reincision occur during the

formation of Channel 1 and 3, as a result of changes or adjustment in the equilibrium channel-profile, flow-parameters and base-level history.

Channel 1 and 3 are excellent outcrop analogues for understanding and predicting hydrocarbon reservoir architectures and compartmentalization geometries in tectonically-similar deep-marine strata.

AUTHOR'S DECLARATION

I declare that the work in this dissertation was carried out in accordance with the Regulations of the University of Ottawa. The work is original, except where indicated by special reference in the text, and no part of the dissertation has been submitted for any other academic award. Any views expressed in the dissertation are those of the author.

SIGNED: .....

DATE:.....

ACKNOWLEDGEMENTS

First and foremost, I give my thanks and appreciation to R. William (Bill) Arnott, without whom this work would not exist. For the countless hours of effort, patience and consideration I have received over the years, I sincerely thank you. Your incisive critical reading of this work is greatly appreciated. Gracias for always sharing your passionate and contagious enthusiasm for geology, and for encourage me "to see a world in a grain of sand". I thank also the Arnott family: Siobhan, Nelley, Hallie, Grady, and Bailey for tolerantly having me as a guest in their lovely house during my first month in Ottawa.

I express thanks to Gerald (Gerry) M. Ross for sharing his immeasurable experience with rocks of Windermere Supergroup in the southern Canadian Cordillera.

Academic financial support was provided by PDV, S.A. (CIED) and Departamento de Geología, Escuela de Geología, Minas y Geofísica, Universidad Central de Venezuela. Funding this thesis project was provided by the Windermere Consortium, which includes: Natural Sciences and Engineering Research Council of Canada, Geological Survey of Canada, Anadarko Canada, Canadian Natural Resources Ltd., Devon Canada, Encana, Nexen, and Shell.

I am grateful to the diligent crew of field assistants that were in Castle Creek during my two field seasons in the captivating cold wilds: Sonia Prefontaine, Krista Michol, Claude Farley, and Benoit_Michel Saumur. I would like to extend my sincere thanks to John Southard (M.I.T.) and Bruce Hart (McGill University) for eagerly lending a hand in the field.

My eternal gratitude to the McKirdy family: Liz, Brian, Karen, Ross, Bell, and Zeke, and to the Jones family: Cathy Greenhouse, Andy and Reed Jones. Trillions thanks for your help, support, and friendship in the mountains. Thanks Liz and Cathy for those mouth-watering dishes and for sometimes stopping by on the outcrop to have a word about the amazing scenery.

Special thanks to the Departments of Earth Science of UO and Carleton, and Ottawa-Carleton Geoscience Centre for letting me meet not only geologically-savvy people, but also some of the kindest persons I could encounter: Prof. Andre Lalonde, Prof. George Dix, Prof. Bahram Daneshfar, Prof. Joe Wallace, Helene De Gouffe, Edward W. Hearn, Sylvie Theriault, and Gita Kanags. Millions of thanks to Prof. Keith Benn (as Chairman of the Department at that time) for helping me without vacillation in one of my monetarily challenging times.

I thank members of committee Dr. André Desrochers, Dr. Allan Donaldson and Dr. Claudia Schorder-Adams and Dr. Keith Been (Chairman) for their helpful and insightful reviews.

My thanks to the Laboratories of UO: Ron Hartree aided with the XRD training, George Mrazek prepared thin sections, Monica Wilk-Alemany (ICP-AES Laboratory) taught me how to prepare some

samples for isotope analyses, Wendy Abdy, Paul Middlestead and Patricia Wickham (G.G. Hatch Isotope Laboratories) for kindly replying to my isotope inquires.

A big thank you to all undergrad, grad students and post docs of UO who have shared an office, a moment, a laugh and/or a big smile with me. My reverences to: Fedora González, Kelly Powis, Brad Simms, Hosein Mohammadzadeh, Agnès Dubois, Don Cummings, Simone Dumas (extra million of thanks for correcting my rudimentary French translation of the Abstract), and Susanne Leclair. Thanks to Juraj Farkas, Kenny Wallace, Lori Meyer, Erin Crear, Andre Koladich, Anne P. Peschler, Zishann Khan, Mark Smith, Ernesto Swarchz and Paul Gammon.

My thankfulness to the Executive Board of O.L.A. (Ottawa Latin-American Association) at UO of which I was part, especially Gabriela Larenas and Laura Avalos, as well as the numerous O.L.A. Members. Thanks for allowing me to be part of this group to promote and increase Latino/Hispanic awareness at UO through the planning of cultural, academic and social events, portraying positive aspects of Latin American cultures within the Canadian community.

I thank Herbert Wilhelm Fournier Bethke for being present. Desde aquel día que apretando fuertemente mi mano viraste mi mundo, ese día descubrí que esta vida no es una sola. Gracias por compartir tantas travesías conmigo, alentarme en los caminos espinosos y sonreír cada vez que parábamos a ver el horizonte.

I thank my family without reserve, mi encantadora mami Ilda Margarita Ugueto Marcano y mi hermano Freddy Alberto Navarro Ugueto. Their unconditional love and support means everything to me. I dedicate this work to my mother. Literalmente, sin ti yo no existiría. Cada palabra de aliento y reconvención que me has dado, sin duda alguna, han trascendido fronteras y llenado mis espacios. Gracias por tu extraordinaria humildad y ejemplo. Gracias por siempre recordarme que los valores humanos no se aprenden a través de los libros ni se transmiten en herméticas aulas.

DEDICATION

To my mother Ilda Margarita Ugueto Marcano,

"Although these works are not perfect as I could wish, yet any impartial observer will perceive the care and labour I have bestowed upon them so that if they do not merit praise they may at least earn blames".

Giorgio Vasari, on his own work, Lives of the Artists, 1568.

«Maigré l' imperfection regrettable de ces œuvres, tout observateur impartial appréciera l' attention et l' effort que ju leur ai consacrés, de telle sorte que, si elles ne méritent pas d' éloges, elles peuvent au moins gagner le blâmes»

Giorgio Vasari, sur son propre oeuvre, Les vies des meilleur, sculptures et architectes, 1568.

"Si bien estos trabajos no son perfectos como yo hubiese querido, cualquier observador imparcial percibirá el cuidado y esfuerzo que yo coloqué en ellos, por lo cual si ellos no merecen elogios, al menos ellos pueden ganar culpas".

Giorgio Vasari, sobre su propia obra, Vida de los más excelentes pintores, escultores y arquitectos, 1568.

Espejismos Invernales

De Lilian Navarro (Inédito, 2005)

Este desierto blanco no se parece a Ítaca ni es el fin del mundo
No existen sus vestigios ni quimeras

Una vez más
el viento lacera mis pulmones, deslizando lentamente su cuchilla
mientras la levedad nos cubre como una torva sublevada

A cada paso
el hielo crepita recitando nuestros nombres
y las escarchas se aprisionan a nuestras vértebras

La nieve es la terredad madura de las aguas
Polvo nacarado que nos devuelve el ilimitado vacío de la quintaesencia.

Wintry Mirages

By Lilian Navarro (Unedited, 2005)

This white desert is not Ithaca or the end of the world
there are not either their vestiges or chimeras

Anew
the wind slice up my lugs, slowly gliding its knife
whilst the levity covers us as an uprising whiteout

Every step
ice crackles reciting our names
and snowflakes seize our vertebras

The snow is the terrene maturity of the waters
Nacreous dust that bring back to us the vast emptiness of the quintessence.

TABLE OF CONTENTS

ABSTRACT ..... *ii*
RÉSUMÉ ..... **iii**
RESUMEN ..... **iv**
EXTENDED ABSTRACT ..... *v*
AUTHOR'S DECLARATION ..... *vii*
ACKNOWLEDGEMENTS ..... *viii*
DEDICATION ..... *x*
TABLE OF CONTENTS ..... *xii*
LIST OF FIGURES AND ILLUSTRATIONS ..... **xvii**
LIST OF TABLES ..... **xx**
CHAPTER 1: THESIS INTRODUCTION *1*
1.1. OUTLINE **1**
1.2. REGIONAL GEOLOGICAL SETTING **1**
1.2.1. Origin and Constitution of Canadian Cordillera 1
1.2.2. Cariboo Mountains, southern Canadian Cordillera 4
1.2.2.1. Regional Structural Context 5
1.2.2.2. Regional Stratigraphy: WINDERMERE SUPERGROUP 7
Age Constraints 8
Stratigraphic History 10
Windermere Turbidite System 14
1.3. CASTLE CREEK, CARIBOO MOUNTAINS (STUDY AREA) **15**
1.3.1. Location and Access 15
1.3.2.Previous Works 17
1.3.3. Structural Framework 18
1.3.4. Stratigraphy 18
1.3.4.1. Kaza Group 18
1.3.4.2. Cariboo Group 20
Isaac Formation 20
Cunningham and Yankee Belle formations 23
1.3.5. Slope Channels of the Isaac Formation: Channel Complexes 1 and 3 23
1.4. OBJECTIVES AND METHODOLOGY **24**
1.4.1. Objectives 24
1.4.2. Methodology 24
1.4.2.1. Fieldwork 24
1.4.2.2. Logging and Correlation techniques 25
1.4.2.3. Petrography 25
1.4.2.4. X-Ray Diffraction 25
1.4.2.5. Stable Isotopes 26

1.5. STATEMENT OF CONTRIBUTIONS 26

CHAPTER 2. FACIES, AND FACIES ASSOCIATION OF TWO DEEP-WATER SUBMARINE CHANNEL COMPLEX SETS (CHANNEL 1 AND 3) IN THE NEOPROTEROZOIC ISAAC FORMATION, WINDERMERE SUPERGROUP, CARIBOO MOUNTAINS, BRITISH COLUMBIA, CANADA 28

2.1. INTRODUCTION 28
2.1.1. Chapter Aims 28
2.1.2. Sediment Gravity Flows 28
2.1.2.1. Classifications of Sediment Gravity Flows 29
Low-density flows 31
High-density flows 31
Debris flows 32
2.1.2.2. Sediment Support Mechanism 32
Turbulence 32
Dispersive Pressure 32
Buoyancy 33
Hindered Settling 34
Matrix Strength 34
2.1.3. Submarine Channel 34
2.1.3.1. Types of Submarine Channel 35
Erosional Channels 35
Depositional Channel 35
Mixed Erosional-depositional Channel 35
2.1.3.2. Evolution of Submarine Channels 36
1) Channel inception 36
2) Channel bypass 36
3) Channel filling 38
4) Channel abandonment 38

2.2. FACIES DESCRIPTION AND INTERPRETATION 38
2.2.1. F1. Normally Graded to Massive Conglomerate and Sandstone 40
2.2.1.1. F1.1. Normally Graded Conglomerate to Sandstone and Normally Graded Sandstone 40
F1.1a. Normally Graded Conglomerate to Sandstone 40
F1.1b. Normally Graded Sandstone 43
2.2.1.2. F1.2. Massive Sandstone and Conglomerate 43
F1.2a. Massive Conglomerate 43
F1.2b. Massive Sandstone 44
2.2.1.3. Petrography and X-Ray diffraction 45
Petrographic analysis 45
Conglomerate 45
Sandstone 46
Carbonate clasts 46
XRD analyses: Carbonate clasts 47
2.2.1.4. Interpretation 48
Provenance 51
2.2.2. F2. Mudstone-clast Breccia 52
2.2.2.1. F2.1. Mudstone-clast breccia 52
2.2.2.2. F2.2. Mudstone-clast brecciated facies 54
2.2.2.3. Petrography, X-Ray Diffraction and Carbon Content analyses 60

Petrography 60
X-Ray Diffraction 60
Carbon Content 60
2.2.2.4. Interpretation 62
Mudstone clasts from local or updip erosion? 63
Mudstone clasts from brecciation of mudstone layers or clasts 65
Liquidization and Effective stress 65
Brecciation of mudstone clasts 66
2.2.3. F3. Cross-stratified and Parallel Stratified Sandstone 67
2.2.3.1. F3.1. Cross-stratified sandstone 67
2.2.3.2. F3.2. Parallel Stratified Sandstone 70
2.2.3.3. Petrography 71
2.2.3.4. Interpretation 71
Cross-stratified beds (Facies F3.1) 71
Provenance 73
Upper-Stage Plane Beds (Facies 3.2) 73
2.2.4. F4. Sandstone interbedded with mudstone and unlaminated mudstone 74
2.2.4.1. F4.1. Sandstone interbedded with mudstone 75
F4.1a. Structureless sandstone interbedded with mudstone 75
F4.1b. Laminated sandstone interbedded with mudstone 75
F4.1c. Cross-laminated sandstone interbedded with mudstone 75
2.2.4.2. F4.2. Mudstone 76
2.2.4.3.Petrography, X-ray Diffraction and Carbon Content analyses 77
Petrography 77
X-ray Diffraction and Carbon Content 77
2.2.4.4. Interpretation 77
Provenance 78

2.3. FACIES ASSOCIATIONS AND INTERPRETATIONS 78
2.3.1. FA1. Bypass-channel Association 79
2.3.1.1. FA1a. Thin-bedded siltstone-sandstone 79
2.3.1.2. FA1b. Thick to very thick conglomerate 79
2.3.1.3. FA1c. Thin-to-very thick bedded mudstone-clast breccia 81
2.3.1.4. Interpretation 83
2.3.2. FA2. Inclined-bed Association 83
2.3.2.1. FA2a. Inclined Sandstone-siltstone 83
2.3.2.2. FA2b. Inclined, Sandstone and mudstone-clast breccia beds 85
2.3.2.3. Interpretation 85
2.3.3. FA3. Channel-Fill Association 88
2.3.3.1. FA3a. Amalgamated thick bedded conglomerate and sandstone channel-fill 89
2.3.3.2. FA3b. Partly amalgamated, thick-to-thin bedded conglomerate and/or sandstone channel-fill 90
2.3.3.3. FA3c. Non-amalgamated thin bedded siltstone-sandstone channel-fill 91
2.3.3.4. Interpretation 92
2.3.4. FA4. Slumped siltstone-sandstone 93
2.3.4.1. Interpretation 93
2.3.5. FA5. Channel-abandonment association 95
2.3.5.1. Interpretation 98

2.4. CHAPTER SUMMARY 99

CHAPTER 3. ARCHITECTURE OF TWO DEEP-WATER SUBMARINE CHANNEL COMPLEX SETS (CHANNEL 1 and 3) IN THE NEOPROTEROZOIC ISAAC FORMATION, WINDERMERE SUPERGROUP, CARIBOO MOUNTAINS, BRITISH COLUMBIA, CANADA 101

3.1. INTRODUCTION 101
3.1.1. Chapter Aims 101
3.1.2. Channel Architecture and Hierarchy 102
3.1.2.1. Channel stacking pattern 102
3.1.3. Channel 1 and 3 Data 104

3.2. CHANNEL 1: Geometry and Architectural elements 104
3.2.1. Lower Channel Complex, Channel 1 104
3.2.1.1. Channel Unit Ch1.L-C1 106
3.2.1.2. Channel Unit Ch1.L-C2 106
3.2.1.3. Layered thin-bedded sheet (Ch1.L-S1) 108
3.2.1.4. Interpretation 109
3.2.2. Upper Channel Complex, Channel 1 109
3.2.2.1. Channel Unit Ch1.U-C1 110
3.2.2.2. Channel Unit Ch1.U-C2 115
3.2.2.3. Layered thin-bedded sheet (Ch1.U-S1) 119
3.2.2.4. Channel Unit Ch1.U-C3 121
3.2.2.5. Layered thin bedded sheet (Ch1.U-S2) 122
3.2.2.6. Interpretation 122

3.3. CHANNEL 3: Geometry and Architectural Elements 125
3.3.1. Lower Channel Complex (Ch3.L) 127
3.3.1.1. Channel Unit Ch3.L-C1 128
3.3.1.2. Channel Unit Ch3.L-C2 130
3.3.1.3. Channel Unit Ch3.L-C3 134
3.3.1.4. Channel Unit Ch3.L-C4 138
3.3.1.5. Interpretation 140
Ch3.L: Composite terraced basal surface and stacking pattern 143
Comparison of channel margins of Ch3.L with other systems 145
3.3.2. Middle Channel Complex, Channel 3 149
3.3.2.1. Channel Unit Ch3.M-C1 150
3.3.2.2. Channel Unit Ch3.M-C2 150
3.3.2.3. Interpretation 153
3.3.3. Upper Channel Complex, Channel 3 153
3.3.3.1. Channel Unit Ch3.U-C1 154
3.3.3.2. Channel Unit Ch3.U-C2 154
3.3.3.3. Layered thin-bedded sheet (Ch3.U-S1) 156
3.3.3.4. Interpretation 156

3.4. Comparison in channel configuration of both deep-water channels 157
3.4.1. Vertical variation 157
3.4.1.1. Lower Channel units 157
3.4.1.2. Middle Channel units 160
3.4.1.3. Upper Channel units 160
3.4.2. Channel-stacking patterns 161

3.5. Implications for deep-water hydrocarbon reservoirs **163**

3.6. CHAPTER SUMMARY **164**

CHAPTER 4. EVOLUTION OF TWO DEEP-WATER SUBMARINE CHANNEL COMPLEX SETS (CHANNEL 1 and 3) IN THE NEOPROTEROZOIC ISAAC FORMATION, WINDERMERE SUPERGROUP, CARIBOO MOUNTAINS, BRITISH COLUMBIA, CANADA ***165***

4.1. INTRODUCTION **165**

4.1.1. Chapter Aims 165

4.1.2. Deep-water sequence stratigraphy 165

4.2. EVOLUTION OF TWO SLOPE CHANNEL COMPLEX SETS OF ISAAC FORMATION, CASTLE CREEK AREA **168**

4.2.1. Significance of basal bounding surfaces 168

4.2.2. Evolution of Channel Complex Sets 1 and 3 173

4.2.2.1. Evolution of Channel 1 173

Incipient conditions 173

Stage 1 174

Stage 2 174

Stage 3 175

Transition Stage 1 to 3 175

4.2.2.2. Evolution of Channel 3 178

Incipient conditions 178

Lower Channel Complex: Evolution of a channel-levee complex 178

Stage 1 178

Stage 2 179

Stage 3 179

Transition Stage 1 to 3 182

Middle Channel Complex (Stages 1-3) 182

Upper Channel Complex (Stages 1-3) 183

4.3. CHAPTER SUMMARY **183**

CHAPTER 5. CONCLUSIONS ***184***

REFERENCES ***186***

APPENDIXES ***203***

APPENDIX I. Location of Sample, Log and Gamma Ray profiles **203**

APPENDIX II. Petrography Data **210**

APPENDIX III. X-Ray Powder Diffraction Data **234**

APPENDIX IV. Gamma Ray Profiles **240**

APPENDIX V. Facies distribution **246**

APPENDIX VI. Paper publication **253**

LIST OF FIGURES AND ILLUSTRATIONS

Figure 1.1. Hypothetical reconstructions of Rodinia at 1000 Ma....2
Figure 1.2. Morphogeologic belts of the western Canadian Cordillera....4
Figure 1.3. Physiographic map of southeastern Canadian Cordillera....5
Figure 1.4. Major dextral strike-slip faults in the Canadian Cordillera....6
Figure 1.5. General map of the Cariboo Mountains and the adjoining Quesnel Highlands and Rocky Mountains....7
Figure 1.6. Map of distribution of the Windermere Supergroup in the Canadian Cordillera....8
Figure 1.7. General stratigraphic correlation chart for the Windermere Supergroup....9
Figure 1.8. Composite stratigraphic column of Neoproterozoic strata in the Cariboo Mountains....10
Figure 1.9. Schematic configuration of Proterozoic to Lower Cambrian strata in the southern Canadian Cordillera. For references see text....12
Figure 1.10. Schematic representation for the Windermere Supergroup in western Laurentia....13
Figure 1.11. Hypothetical configuration of the Late Proterozoic rift basins (Adelaide, Sinian and Windermere basins) along southern Australia, south China and western North America,....13
Figure 1.12. Schematic paleogeographic reconstruction of the Windermere turbidite system in the southern Canadian Cordillera....14
Figure 1.13. Schematic restoration of the Windermere turbidite System....15
Figure 1.14. Location of the Castle Creek study area....16
Figure 1.15. Panoramic photos of Castle Creek outcrops....17
Figure 1.16. Composite stratigraphy in the Castle Creek south study area....19
Figure 1.17. Generalized map of the Kaza Group and Lower Isaac Formation in the Castle Creek area....21
Figure 1.18. Location of Channel 1 and 3 in the Castle Creek area (south) in the Cariboo Mountains, southern Canadian Cordillera....22
Figure 2.1. Downslope moving turbidity current....29
Figure 2.2. General classification of subaqueous sediment gravity or density flows....30
Figure 2.3. Sequences of low and high-density flow deposits....31
Figure 2.4. Schematic representations of particle support in sediment-gravity flow....33
Figure 2.5. Submarine channels....35
Figure 2.6. Submarine Channel types....36
Figure 2.7. Major stages of channel evolution....37
Figure 2.8. Subfacies F1.1a, normal graded conglomerate beds....41
Figure 2.9. Common scour-load structures in a normally graded sandstone bed....41
Figure 2.10. Typical load casts in a normally graded granule conglomerate....42
Figure 2.11. Load structure on the base of a normally graded granule conglomerate....42
Figure 2.12. Ball-and pillow, or pseudonodule structures....42
Figure 2.13. Massive conglomerate of subfacies F1.2a....44
Figure 2.14. Pebble conglomerate of subfacies F1.2a, massive conglomerate....44
Figure 2.15. Massive and normally graded sandstone beds....45
Figure 2.16. Schematic cross-section of a high-density or concentrated flow....49
Figure 2.17. Sketch of an experimental high-density, surge-type turbidity current....50
Figure 2.18. Formation of load and flame structures....51
Figure 2.19. Boulder mudstone clast embedded in an amalgamated Facies 2 bed in Channel 1....53
Figure 2.20. Grey elongated boulder mudstone clast in Facies 2, Channel 3....53
Figure 2.21. Elongated, boulder mudstone clast....54
Figure 2.22. Angular mudstone clast with conspicuously jagged edges....54
Figure 2.23. Mudstone clasts embedded in a sandstone matrix....56
Figure 2.24. Mudstone clasts in a coarse sandstone matrix....57
Figure 2.25. Mudstone clasts in a coarse sandstone matrix....58
Figure 2.26. Sandstone injections and mudstone clasts embedded in a coarse sandstone matrix....59
Figure 2.27. Comparison of TOC (total organic carbon) for Channel 1 and 3....62
Figure 2.28. Mud-clast rich, high-concentrated flow....64
Figure 2.29. Flow transformation of a hyperconcentrated flow....65
Figure 2.30. Schematic stages of deformation in the mud-clast brecciated facies....68

Figure 2.31. Cross-stratified sandstone bed (facies F3.1)....69
Figure 2.32. Deformed cross-bedding in cross-bedded sandstones, Channel 1. 70
Figure 2.33. Planar-tabular cross-stratified and parallel-stratified sandstone beds 71
Figure 2.34. Convolute bedding in Facies 4.1c....74
Figure 2.35. Heterolithic Facies 4.1c. 76
Figure 2.36. Heterolithic Facies 4.1c 76
Figure 2.37. Bypass Facies Association FA1a and FA1b....81
Figure 2.38. Bypass Facies Association FA1c....82
Figure 2.39. Inclined Sandstone-Siltstone Facies Association (FA2a)....84
Figure 2.40. Similarity between fluvial point bar and deep-water lateral accretion packages (LAP)....86
Figure 2.41. Hyperpycnal flows and other types of density flows....87
Figure 2.42. Schematic diagrams of different types of channel-fill associations (FA3)....88
Figure 2.43. Amalgamated conglomerate and sandstone channel-fill association....89
Figure 2.44. Loaded contact between thick bedded conglomerate and very coarse sandstone....90
Figure 2.45. Disrupted and strongly contorted strata of facies association FA4....94
Figure 2.46. Sandstone boudin-like structures....95
Figure 2.47. Strata in the lowermost part of the channel-abandonment facies association (FA5)....96
Figure 2.48. Lenticular beds in an abandoned channel (FA5) 96
Figure 2.49. Lenticular, coarse-grained sandstone beds in the basal Channel-abandonment facies (FA5) 97
Figure 2.50. Strata in the upper part of the channel-abandonment facies association (FA5)....98
Figure 3.1. Stratigraphic hierarchy of strata in Channel 1 and 3, Castle Creek South area....103
Figure 3.2. Schematic diagram of channel stacking pattern....103
Figure 3.3. Vertical and lateral stacked channel complexes of Channel 1....105
Figure 3.4. Photomosaic and line tracing of the Lower Channel Complex in Channel 1 107
Figure 3.5. Southeast panoramic view of the channel unit Ch1.L-C2 (lower channel complex), Channel 1..108
Figure 3.6. Photomosaic and line tracing of Lower Channel Unit in the Upper Channel Complex, Channel 1 111
Figure 3.6a. Measured sections in the SE of Lower Channel Unit in the Upper Channel Complex, Channel 1 (Ch1.U-C2). 112
Figure 3.6b. Correlation diagram for the NW part of channel unit Ch1.U-C1 in the Upper Channel Complex, Channel 1....113
Figure 3.7. Some mudstone-clast breccia zones in the lowermost channel unit of upper channel complex C1U, Channel 1....114
Figure 3.8. Laterally discontinuous, mudstone-clast breccia bed in Ch1.U-C1. 115
Figure 3.9. Coarse, normal graded, cross-bedded sandstone interstratified with thin-bedded facies in the uppermost part of Ch1.U-C1....116
Figure 3.10a. Measured sections in the SE of Middle and Upper Channel Unit in the Upper Channel Complex, Channel 1 (Ch1.U-C2)....117
Figure 3.10b. Representative measured sections through the NW part of channel units Ch1.U-C2 and Ch1.U-C3 in the Upper Channel Complex, Channel 1 118
Figure 3.11. Erosion surfaces at the base of channel fills in Ch1.U-C2....119
Figure 3.12. Layered thin-bedded interval, Ch1.U-S1, overlying the channel unit Ch1.U-C2 in Channel 1..120
Figure 3.13. Representative log of fine-grained sheet deposits at the top of Upper Channel Complex, Channel 1 123
Figure 3.14. A simplified model for the development of erosional zones of Channel 1....124
Figure 3.15. Vertical and lateral stacked channel complexes of Channel 3, Castle Creek South....126
Figure 3.16 Correlation diagram of levee deposits adjacent to the northwest (outer-bend) channel margin. .129
Figure 3.17a. Outcrop distribution of the lowermost channel unit Ch3.L-C1 in Channel 3....131
Figure 3.17b. Outcrop distribution of the lowermost channel unit Ch3.L-C1 in Channel 3....132
Figure 3.17c. Outcrop distribution of the lowermost channel unit Ch3.L-C4 in Channel 3....133
Figure 3.18. Close-up of pebble conglomerate with orange-brownish weathering (ankeritic), carbonate clasts, w....134
Figure 3.19. Erosion surfaces in Ch3.L-C2. 135
Figure 3.20. Photomosaic and line drawing of southeast margin of lower channel complex of Channel 3 (Ch3.L) 136
Figure 3.21. Characteristics of channel fills in Ch3.L-C3. 137

Figure 3.22. Photomosaic and line tracing of northwest margin of uppermost channel unit in Lower channel complex of Channel 3 (Ch3.L- C4) 138
Figure 3.23. Close ups of the erosional basal surface in the northwest margin of channel unit Ch3.L-C4..... 139
Figure 3.24. Channel-fill strata along the northwest margin of channel unit Ch3.L-C4..... 139
Figure 3.25. Graphic comparison of terraced composite surfaces identified in Lower Channel 3, Castle Creek south study area and other channel-levee systems..... 146
Figure 3.26. Diagrams showing the cross-section of a) aggrading submarine channel and b) aggrading and laterally migrating submarine channel complex at various times. 149
Figure 3.27. Photomosaic of channel unit Ch3.M-1, Middle Channel Complex of Channel 3..... 151
Figure 3.28. Photomosaic of channel unit Ch3.M-C2, Middle Channel Complex of Channel 3 152
Figure 3.29 Photomosaic of Upper Channel Complex of Channel 3 155
interval. B) Measured stratigraphic section collected in channel unit Ch3.U-C2, Channel 3. For legend see Fig. 3.4. C) Inset photo is a..... 155
panoramic-view showing truncation surfaces at the base of Ch3.U-C2. Person for scale..... 155
Figure 3.30. Schematic representation of the equilibrium channel profile 159
Figure 3.31. Schematic representation of three different channel responses to the old and new equilibrium profiles: graded, erosional and aggradation 159
Figure 3.24. Schematic diagram of different channel-stacking patterns observed in channel fills of Channel 1 and 3 162
Figure 4.1. Simplified relative sea-level curve highlighting the depositional system during base-level fall and lowstand..... 167
Figure 4.2. Schematic model for the stratigraphic sequences of slope channel complex sets of the Isaac Formation (Castle Creek south study area). Based on sequence-stratigraphic model of Plint and Nummedal (2000), see Fig. 4.1. 169
Figure 4.3. Schematic diagram illustrating the five main evolutionary episodes of Channel 1..... 176
Figure 4.4. Schematic diagram illustrating the fourth main evolutionary stages of Channel 3. 180
Figure I.1. Photo Index of Channel 1 and 3 in the Castle Creek South study area. 204
Figure I.2. Photomosaic with location of samples, logs and gamma-ray logs in (southeast) Channel 1 205
Figure I.3. Photomosaic with location of samples, logs and gamma-ray logs in (northwest) Channel 1 206
Figure I.4. Photomosaic with location of samples. logs and gamma-ray logs in (southeast) Channel 3 207
Figure I.5. Photomosaic with location of samples, logs and gamma-ray logs in (northwest) Channel 3 208
Figure I.6. Photomosaic with location of samples, logs and gamma-ray logs in (northwestern) Channel 3 ... 209
Figure II.1. Feldspathic arenite of facies F1 218
Figure II.2. Subfeldspathic arenite of facies F1 218
Figure II.3. Extremely poorly sorted, petromict conglomerate (Facies F1)..... 219
Figure II.4. Perthitic feldspar in feldspathic arenite (facies F1)..... 219
Figure II.5. Feldspar grain with perthite intergrowth in a subfeldspathic arenite (facies F1) 220
Figure II.6. Fragmented and altered..... 220
Figure II.7. Fragmented plagioclase in feldspathic arenite (facies F1). 221
Figure II.8. A feldspar grain in the matrix of a petromict conglomerate (facies F1)..... 221
Figure II.9. Pseudomatrix in feldspathic arenite of facies F1. 222
Figure II.10. Quartz overgrowth in petromict conglomerate (Facies F1)..... 222
Figure II.11. Deformed chloritized grain (possibly shale) in a subfeldspathic arenite (facies F1)..... 222
Figure II.12. Pore-filling carbonate cement in feldspathic arenite (facies F1) 223
Figure II.13. Calcite cementation in a petromict conglomerate (facies F1)..... 223
Figure II.14. Dolomitization of interstitial matrix and/or cement in a subfeldspathic arenite (facies F1)..... 223
Figure II.15. Dedolomitisation in a subfeldspathic arenite (facies F1). 224
Figure II.16. Dolomitization in carbonate-clast conglomerate (facies F1). 224
Figure II.17. Ooid grain in a carbonate-clast conglomerate (facies F1). 225
Figure II.18. Ooid from carbonate-clast conglomerate (facies F1). 225
Figure II.19. Ooid in carbonate-clast conglomerate (facies F1). 226
Figure II.20. Composite ooids in carbonate-clast conglomerate (facies F1). 226
Figure II.21. Composite ooids in carbonate-clast conglomerate (facies F1) 227
Figure II.22. Composite ooids in carbonate-clast conglomerate (facies F1) 227
Figure II.23. Alteration of grain and matrix of carbonate-clast conglomerate..... 228
Figure II.24. Pelsparite-clast in conglomerate (facies F1)..... 228

Figure II.25. Early calcite cement in carbonate-clast conglomerate. 229
Figure II.26. Microfractures in carbonate-clast conglomerate facies F1. 229
Figure II.27. Partial silicification of calcite in carbonate-clast conglomerate (facies F1). 229
Figure II.28. Authigenic quartz in carbonate-clast conglomerate (facies F1). 230
Figure II.29. Microbial structure in a carbonate-clast conglomerate (facies F1). 230
Figure II.30 Microbial fabric in fragment of carbonate embedded in debris-flow deposit. 231
Figure II.31. Dolomitized microbial boundstone from carbonate-clast debrite 231
Figure II.32. Replacement dolomite in carbonate-clast debrite. 231
Figure II.33. A mudstone clast from the brecciated facies (facies F2.2) 232
Figure II.34. Matrix from the breccia facies (facies F2.1) 233
Figure II.35. Sub feldspathic sandstone of cross-stratified facies (facies F3) 233
Figure II.36. Structureless sandstone (facies F4) 233
Figure II.36. Structureless sandstone (facies F4) 233
Figure III.1. X-ray diffractograms for samples from Channel 1 and 3 analyzed as random bulk powders. 236
Figure IV.1. Gamma-ray curve for measured section in the axis of Channel 1 241
Figure IV.2. Geophysical gamma-ray logs for the marginal succession of Channel 1. 242
Figure IV.3. Gamma-ray logs for the intrachannel deposits of Channel 3. 243
Figure IV.4. Gamma-ray logs for proximal levee deposits immediately beneath and adjacent to the strata in the Lower part of Channel 3. 244
Figure IV.5. Gamma-ray logs for the distal levee deposits adjacent to the lower part of Channel 3. 245
Figure V.1. Representative Facies types, distribution and N:G percentage in the Lower Channel Unit of Channel 1 247
Figure V.2. Facies types, distribution and N:G percentage in the representative sections of Upper Channel Unit of Channel 1 249
Figure V.3. Facies types, distribution and N:G percentage in the representative sections of Lower Channel Complex of Channel 3 251
Figure V.4. Facies types, distribution and N:G percentage in the Middle and Upper Channel Units of Channel 3 252

LIST OF TABLES

Table 2.1. Summary of facies and subfacies described in this study. 39
Table 2.2. Total organic carbon content determined from Channel 1 and 3 61
Table 2.3. Facies association description and interpretation 80
Table II.1. Petrographic analysis of 8 siliciclastic rock samples from Channel 1in the Castle Creek South study area. 211
Table II.2. Petrographic analysis of 30 samples of siliciclastic rocks from Channel 3 in the Castle Creek study area. 212
Table II.3. Petrographic analysis of 8 carbonate-clasts samples from Channel 1 and 3 in the Castle Creek South study area. 216
Table II.4. Petrographic analysis of 10 carbonate-clast samples from debrite unit that underlies Channel 3 in the Castle Creek South study area. 217
Table III.1. Mineralogical analysis of samples from Channel 1 and 3 using XRD 235
Table V.1. Chart of lithofacies distribution and percentage of sandstone in Lower Channel Complex of Channel 1 (Ch1.L). 247
Table V.2. Chart of lithofacies distribution and percentage of sandstone in Upper Channel Complex of Channel 1 (Ch1.U). 248
Table V.3. Chart of lithofacies distribution and percentage of sandstone in Lower Channel Complex of Channel 3 (Ch3.L). 250
Table V.4. Chart of lithofacies distribution and percentage of sandstone in Middle and Upper Channel Complexes of Channel 3 (Ch3.M, Ch3.U). 252

CHAPTER 1: THESIS INTRODUCTION

1.1. OUTLINE

This thesis is set up as follows: **Chapter 1** presents a literature review on the regional geological setting of Neoproterozoic rocks of the southern Canadian Cordillera, and specifically the local geology of the Castle Creek study area. Subsequently, the objectives and contribution of this thesis are presented. **Chapter 2** discusses the sedimentologic, compositional and isotopic characteristics of two channel complex sets in the Lower Isaac Formation, and **Chapter 3** tabulates the geometrical framework of these channel complex sets, with emphasis on the major controls that affected their development and compared with worldwide examples is presented.. In **Chapter 4**, the stratal evolution of two slope channel complexe sets is discussed **Chapter 5** summarizes the principal findings and conclusions of this study, and discusses them in context with the objectives of the thesis.

The CD-ROM that accompanies this volume provides a colour version of each chapter of this thesis as a portable document format (PDF) file.

1.2. REGIONAL GEOLOGICAL SETTING

1.2.1. Origin and Constitution of Canadian Cordillera

The Canadian Cordillera, located in western Canada, was formed during the Late Jurassic and Cretaceous as a part of the inversion of the older rifted margin of the western North America Craton (NAC). It was generated by the collision and accretion of allochthonous terranes that produced crustal thickening, folding, thrust faulting, and metamorphism (Monger and Price 1979; Monger et al. 1982; Gabrielse et al. 1991; Reid et al., 2002).

The history of the Cordillera began with the first stages of a diachronous break-up and dispersal of the supercontinent *Rodinia* during the Neoproterozoic at ~600-800 Ma (Karlstrom et al., 2001). This event led to the opening of a new ocean basin between Gondwana (Australia, East Antarctica and India) and Laurentia (ancestral North America), which later became the Pacific Ocean, called then *Panthalassa*. Reconstructing the initial configuration of Rodinia and the relative position of its constituent fragments has been

highly controversial (Fig. 1.1), with several studies variously suggesting that the counterpart of North America Craton may be (1) the Siberian platform (Sears and Price 1978, 2000; Monger and Price, 1979), (2) southwestern U.S. and East Antarctica (SWEAT model; Moores, 1991; Daziel, 1991; Borg and DePaolo, 1994), (3) South China (Li et al., 1995, 2002), (4) North China (Piper and Rui, 1997), (5) Argentina (Daziel, 1997), (6) Australia and Western U.S (AUSWUS model; Karlstrom et al.,1999, 2001; Burret and Berry, 2000), and (7) Australia and Mexico (AUSMEX model; Wingate et al., 2002).

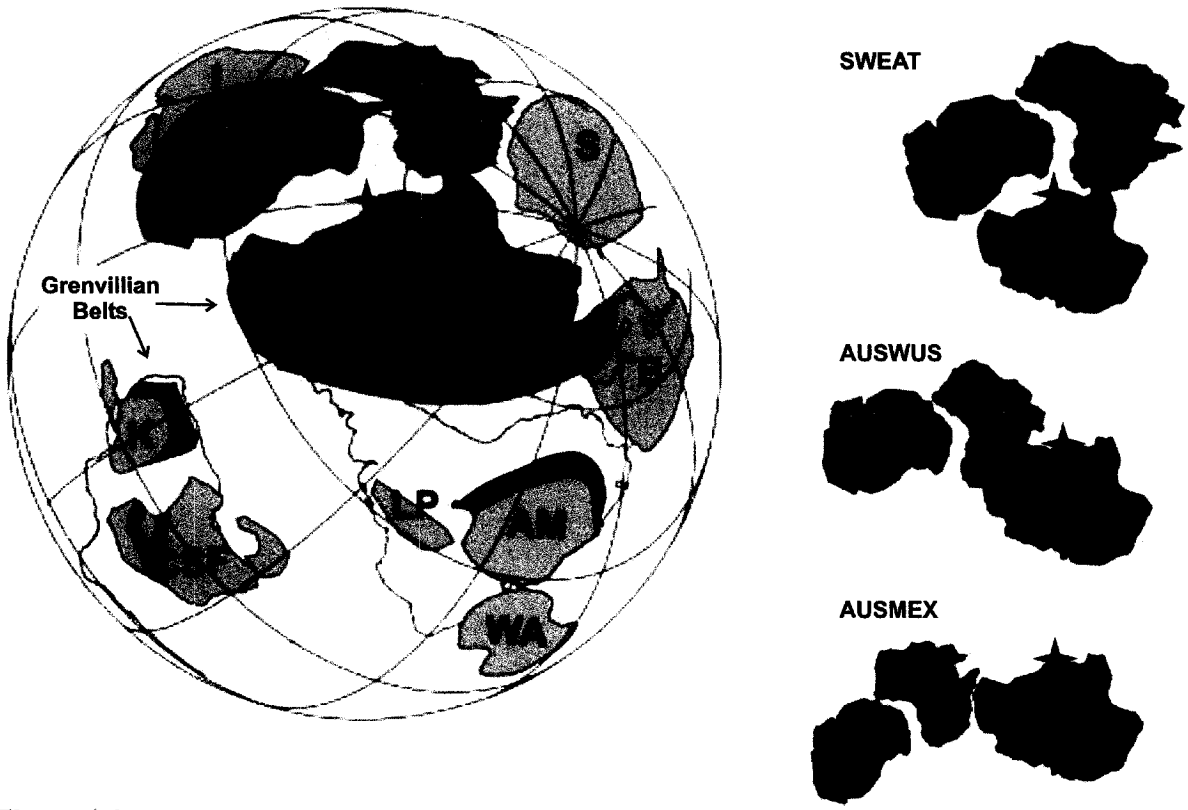

Figure 1.1. Hypothetical reconstructions of Rodinia at 1000 Ma (Modified from Cordani et al., 2003). Dalziel et al.'s (2000) Rodinia and the SWEAT (Moores, 1991), AUSWUS (Karlstrom et al., 1999) and AUSMEX (Wingate et al., 2002) configurations. I, India; M, Madagascar; AN, Antarctica; A, Australia; S, Siberia; L, Laurentia; B, Baltica; CGM, Coats Land/Grunehogna/Maudheim; K, Kalahari; CSF, Congo – São Francisco; LP, Río de la Plata; AM, Amazonia; WA, West Africa. Dark strips represent the Grenvillian-age orogenic belts. Red star represent the location of the Windermere Basin.

The continental rifting-drifting that created the initial Cordilleran continental margin of the NAC and its adjacent ocean was followed by a Late Neoproterozoic to Late Jurassic miogeocline-platform stage (Price, 1994). During this stage, sediments were deposited on the Interior Platform of the NAC and in the flanking continental terrace wedge, or Cordilleran Miogeocline (Monger and Price, 1979). Paleozoic sedimentation was largely constrained to

the miogeocline, where to the west a thick, relatively continuous, cyclic sequence of carbonates and minor fine-grained clastics was mostly deposited. To the east coarse-grained clastics, derived from the Precambrian crystalline shield, were deposited along shorelines of the advancing sea (Slind et al., 1994).

Subsequently, the growth and mountain-building of the Cordillera (i.e. thickening of the crust) occurred in the Late Jurassic to Early Eocene (Monger and Price, 1979). The evolution of the Cordillera imposed a load upon the lithosphere, which responded by downward flexing. As a consequence a foreland basin was formed ahead of the emerging mountain belt. The active construction of the foreland fold-thrust belt and foreland basin was terminated by Early and Middle Eocene crustal extension in the central part of the Cordillera (Price, 1994).

The formation of the Cordillera resulted in the development of five morphogeological belts (or linear geological provinces). These belts, or superterranes, are oriented sub-parallel to the north-northwest trend of the Cordillera, and are differentiated based on a combination of lithological, structural, tectonic, metamorphic, and physiographic attributes (Gabrielse et al., 1991). The belts are the result of terranes accreted onto the western margin of the NAC. The exact timing and the amount of accretion is still a source of much debate. From west to east the belts are: Insular, Coast, Intermontane, Omineca, and Foreland (Fig. 1.2).

The *Insular Belt* comprises the Insular Mountains and Saint Elias Range and was formed after the collision of the allochthonous Insular superterrane with the NAC and further deformation of the Intermontane terranes during the mid-Cretaceous (Gabrielse et al., 1991). The *Coast Plutonic Belt* includes the Coast and Cascade Mountains and is considered to be a major plutonic-metamorphic suture zone resulting from the Middle Cretaceous collision between the exotic Insular superterrane and Intermontane superterrane. The *Intermontane Belt* includes Interior, Stikine and Yukon plateaus and Skeena Mountains and was formed approximately in the Early Jurassic.

The *Omineca Crystalline Belt* comprises the Purcell, Selkirk, Monashee, Cariboo, Omineca, Cassiar and Selwyn mountains and is another important suture zone or welt in which intense metamorphism and plutonism took place during Paleozoic and locally Early Mesozoic time (Monger et al., 1982). The *Foreland Belt*, including the Rocky, Mackenzie and Franklin mountains, was created as a result of an oblique collision between exotic terranes and the NAC that detached, compressed, thickened and folded; and then thrust,

metamorphosed and transported eastward sedimentary rocks originally deposited on the passive continental margin over the craton (Price, 1994, Monger and Price, 1979). Sediments formed from the erosion of the emerging Cordillera accumulated in the foreland basin that lay to the east.

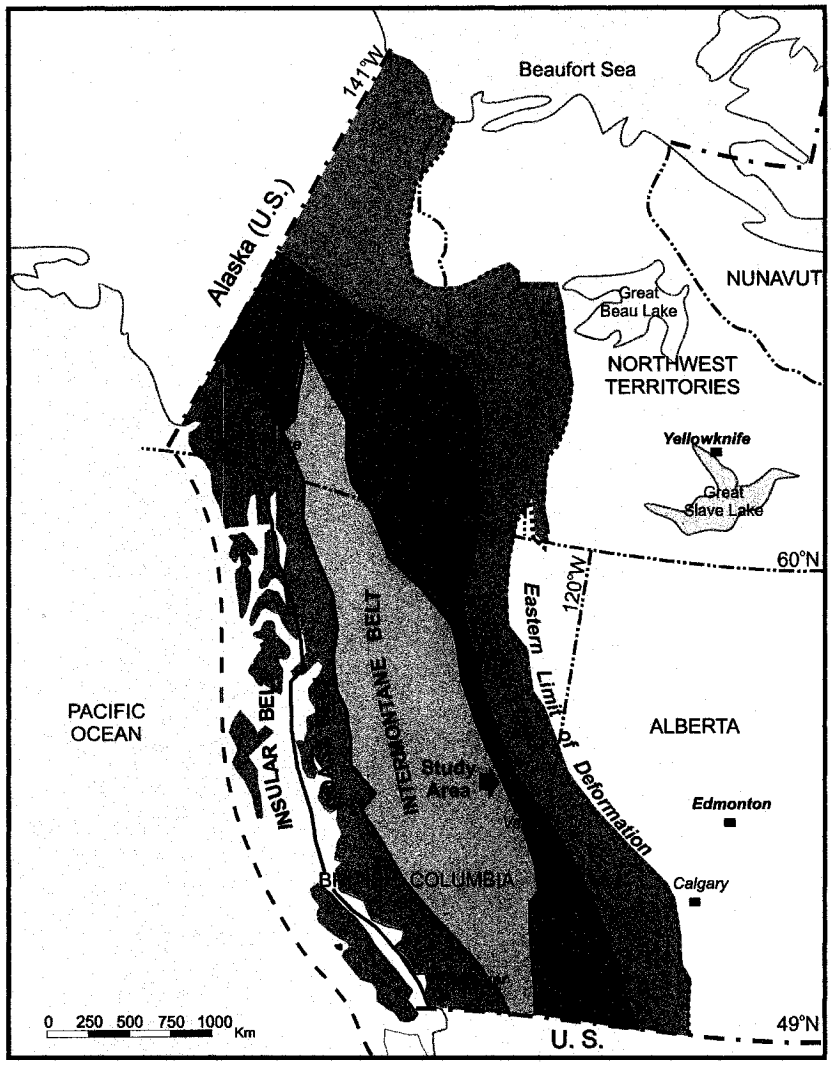

Figure 1.2. Morphogeologic belts of the western Canadian Cordillera. The study area is located in the central part of the Omineca Crystalline Belt (Modified from Wheeler and McFeely, 1991 and Gabrielse et al., 1991).

1.2.2. Cariboo Mountains, southern Canadian Cordillera

The Cariboo Mountains are located within the Omineca Belt (Fig. 1.2) in the northernmost range of the Columbia Mountains (Fig. 1.3), east-central British Columbia. They are bounded to the east by the Fraser River system that flows along the Southern Rocky

Mountain Trench and Rocky Mountains and on the west by the Quesnel Highlands. Maximum relief is approximately 4000 m but generally is about 2000 m.

1.2.2.1. Regional Structural Context

The Cariboo Mountains are situated near the southern termination of the Northern Rocky Mountain Trench Fault and are bounded by the Southern Rocky Mountain Trench to the east and the Fraser River strike-slip fault system to the west (Fig. 1.4). The major regional structures of the Cariboo Mountains are kilometer-scale, northwest-trending folds that, from east to west, are the Premier Anticlinorium, the Isaac Lake Synclinorium, Lanezi Arch or Anticlinorium, the Black Stuart Synclinorium and Lightning Creek Anticlinorium (Campbell et al., 1973; Fig. 1.5).

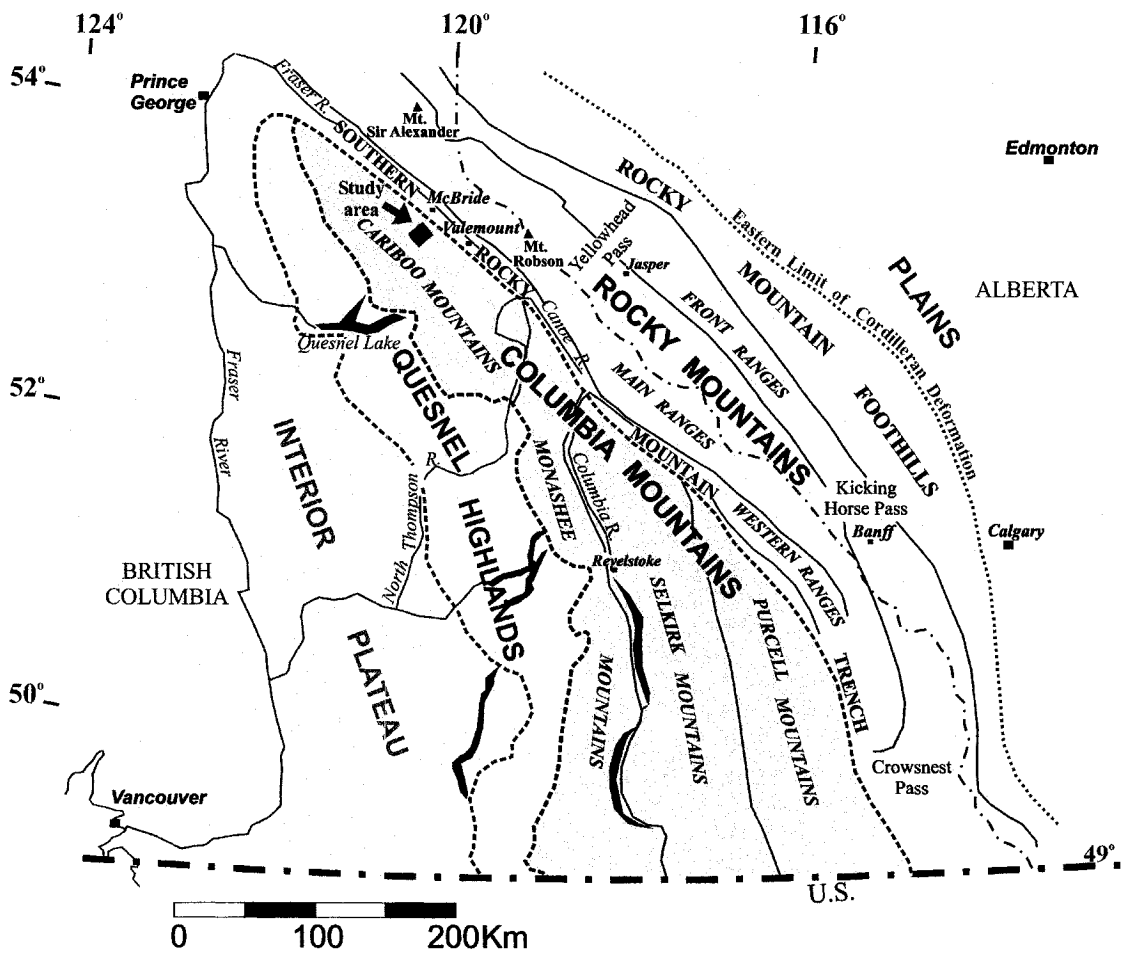

Figure 1.3. Physiographic map of southeastern Canadian Cordillera (Modified from Murphy and Rees, 1983), showing the location of Cariboo Mountains in the Canadian Cordillera and the position of the study area (arrow).

There is a distinctive contrast and variation in the structural style and metamorphic grade between northern and southern Cariboo Mountains (Campbell et al., 1973; Murphy, 1987b; Reid et al., 2002). In the northern Cariboo Mountains, upright to overturned folds that were formed during Jurassic deformation are common (Murphy, 1987b), and rocks metamorphosed to subgreenschist facies are widespread. In contrast, tight to nearly isoclinal and overturned folds are typically found in the southern Cariboo Mountains, where rocks were affected by higher grades of metamorphism (Reid et al., 2002).

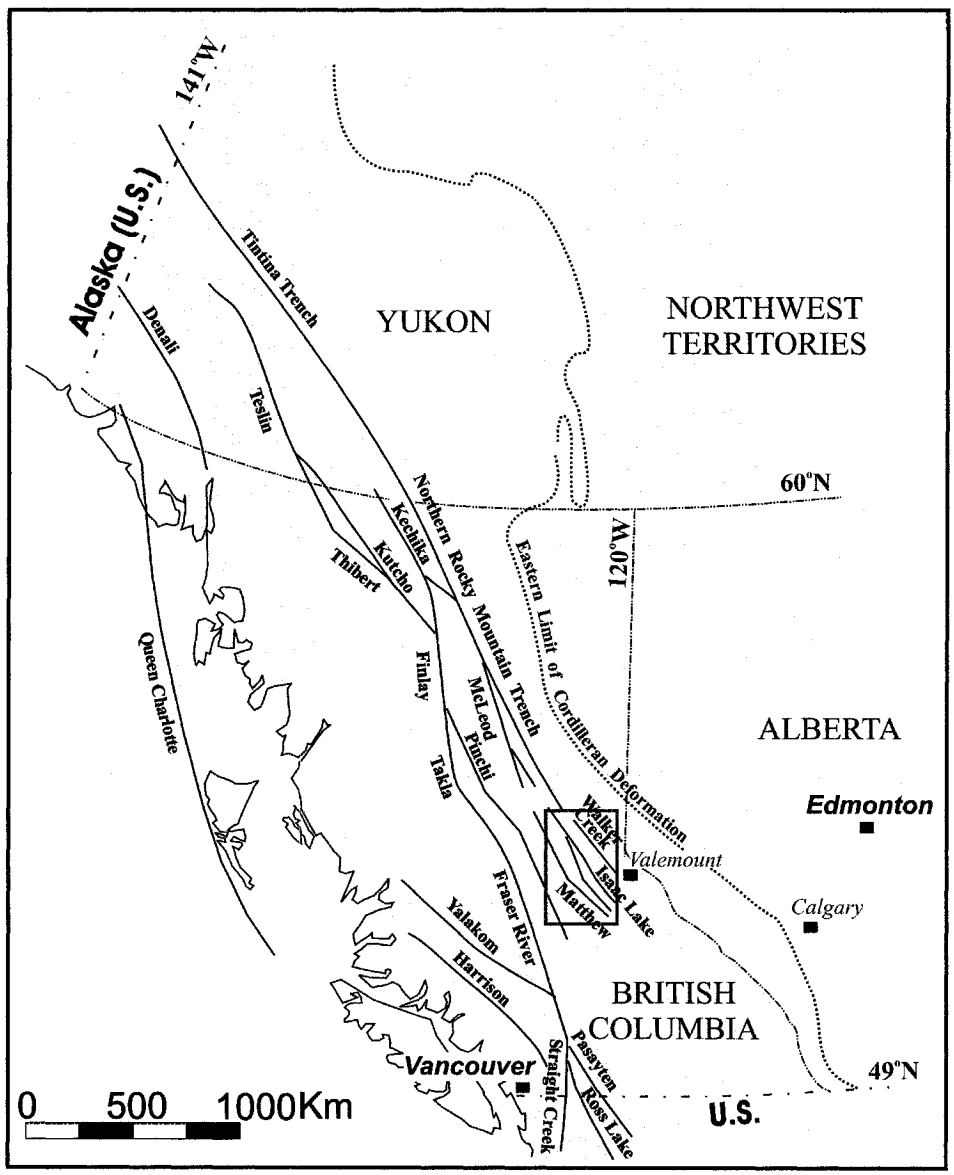

Figure 1.4. Major dextral strike-slip faults in the Canadian Cordillera (Modified from Reid et al., 2002) that form the eastern and western limits of Cariboo Mountains (gray square).

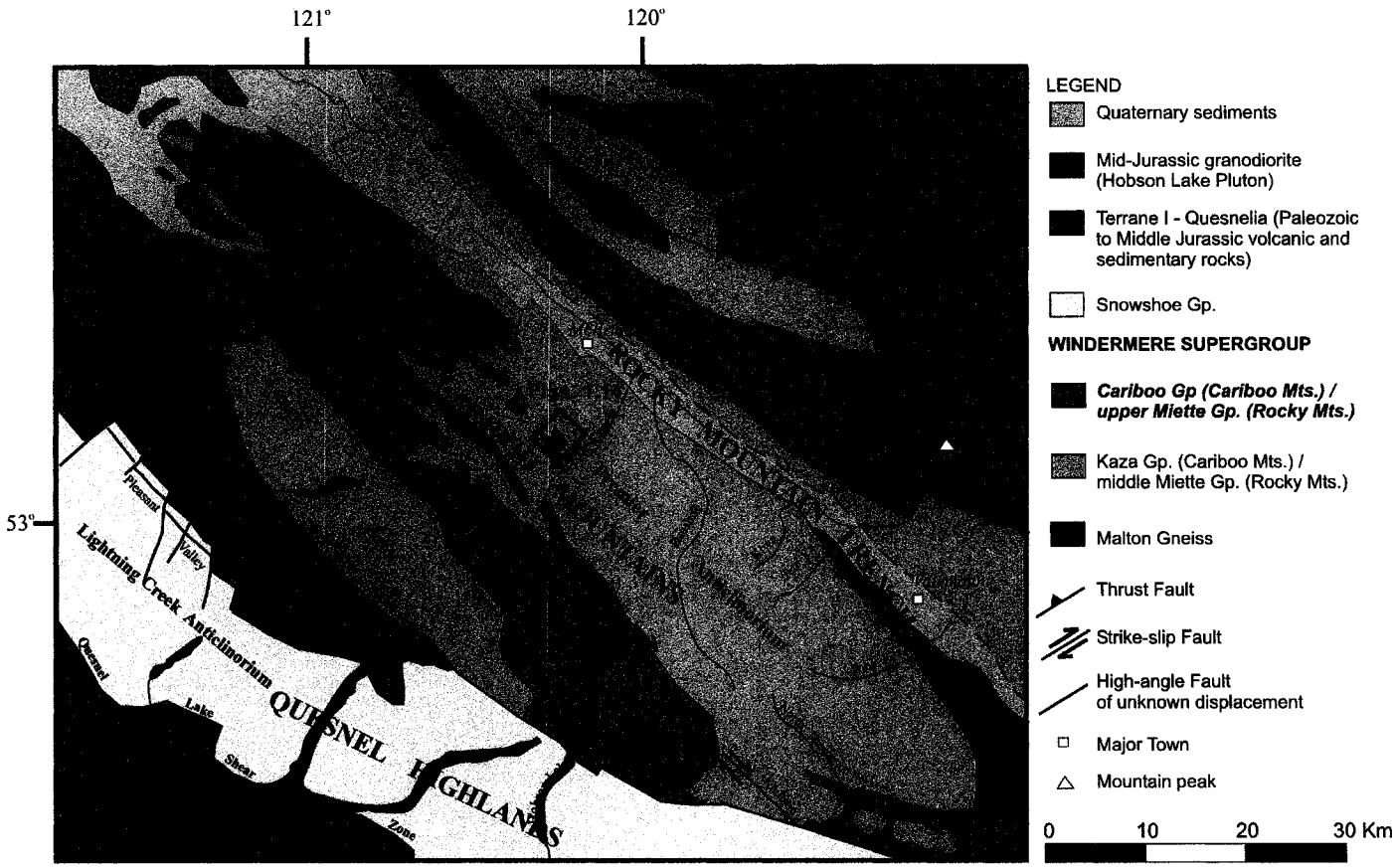

Figure 1.5. General map of the Cariboo Mountains and the adjoining Quesnel Highlands and Rocky Mountains (Modified from Murphy 1987, Reid et al., 2002). The location of the study area (red square) is shown with respect to regional areas and geological features.

1.2.2.2. Regional Stratigraphy: WINDERMERE SUPERGROUP

The term Windermere System was used to describe Precambrian rocks in the Purcell Mountains in the Windermere area of southeast British Columbia by Walker (1926). Later, the term Windermere Supergroup was proposed by Gabrielse (1972) and Reesor (1973). The Windermere Supergroup forms a widespread Neoproterozoic sedimentary assemblage that extends from northern Canada to the Sonora Desert in northern Mexico (Fig. 1.6), a distance of over 4000 km/ 2500 mi (Steward, 1972).

The stratigraphy of the Windermere Supergroup in southern Canadian Cordillera is extremely complex, and nomenclature varies from region to region. As a result, a vast stratigraphic nomenclature has been applied and different regional correlations have been reported from the Purcell, Selkirk, and Rocky Mountains to Cariboo Mountains (Fig. 1.7).

In the Cariboo Mountains, the sedimentary succession comprises Upper Neoproterozoic rocks (Fig. 1.8), that stratigraphically-upward consist of the Kaza Group, Isaac Cunningham and Yankee Belle formations (Cariboo Group). Some of these units are described in detail in section 1.3.3.

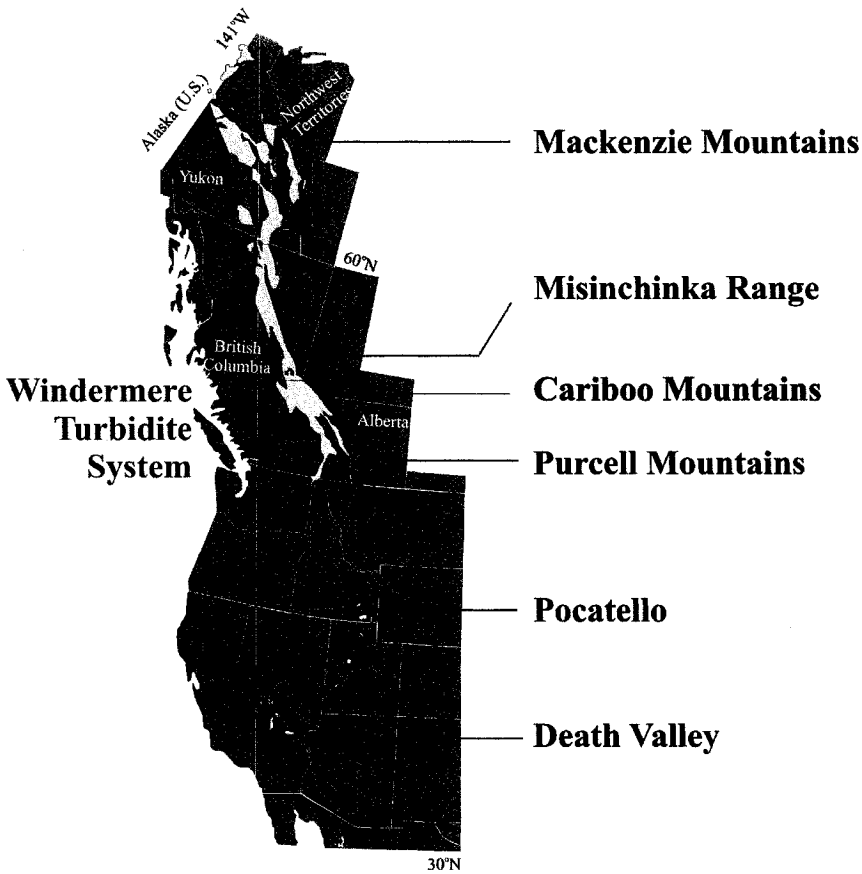

Figure 1.6. Map of distribution of the Windermere Supergroup in the Canadian Cordillera and Western U.S. (Modified from Ross et al., 1995). The turbidite system of this unit is enclosed in a rectangle. Additionally, Cariboo Mountains are highlighted.

Age Constraints

The Windermere Supergroup succession in the southern Canadian Cordillera is poorly dated with radiometric ages. The geochronologic constraints bracket this stratigraphic unit between 762-728 Ma at the base (Devlin et al., 1988, Ross et al., 1995) and 569.6 ± 5.3 Ma at the top (Colpron et al., 2002), see figs. 1.7 and 1.8. The most recent Re–Os radiogenic data obtained from chlorite-grade black shales of the upper Old Fort Point Formation (regional marker of Kaza Group), indicate that the best estimate of the depositional age for this marker horizon is 607.8 ± 4.7 Ma (Kendall et al., 2004).

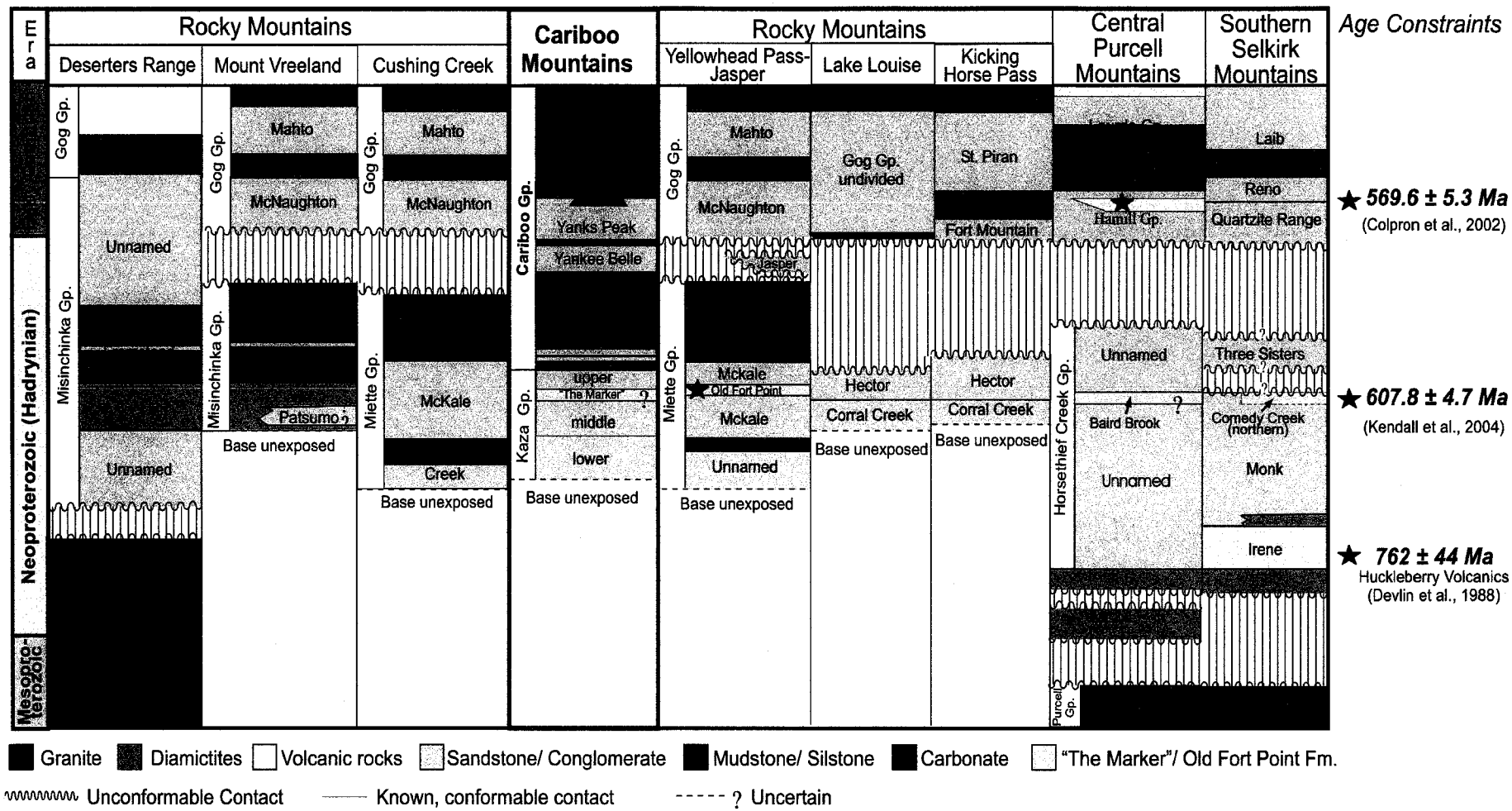

Figure 1.7. General stratigraphic correlation chart for the Windermere Supergroup (modified from Hein and McMechan, 1994). Lithological information based on Aitken and McMechan (1991), Fritz, et al. (1991), Gabrielse and Campbell (1991), Parrish (1991), and Hein and McMechan 1994. The section in the Cariboo Mountains is enclosed in a red rectangle. See Figs. 1.3 and 1.5 for regional location. Known age constraints for the Windermere Supergroup are shown on the right, and the stars indicate the stratigraphic position of rocks dated.

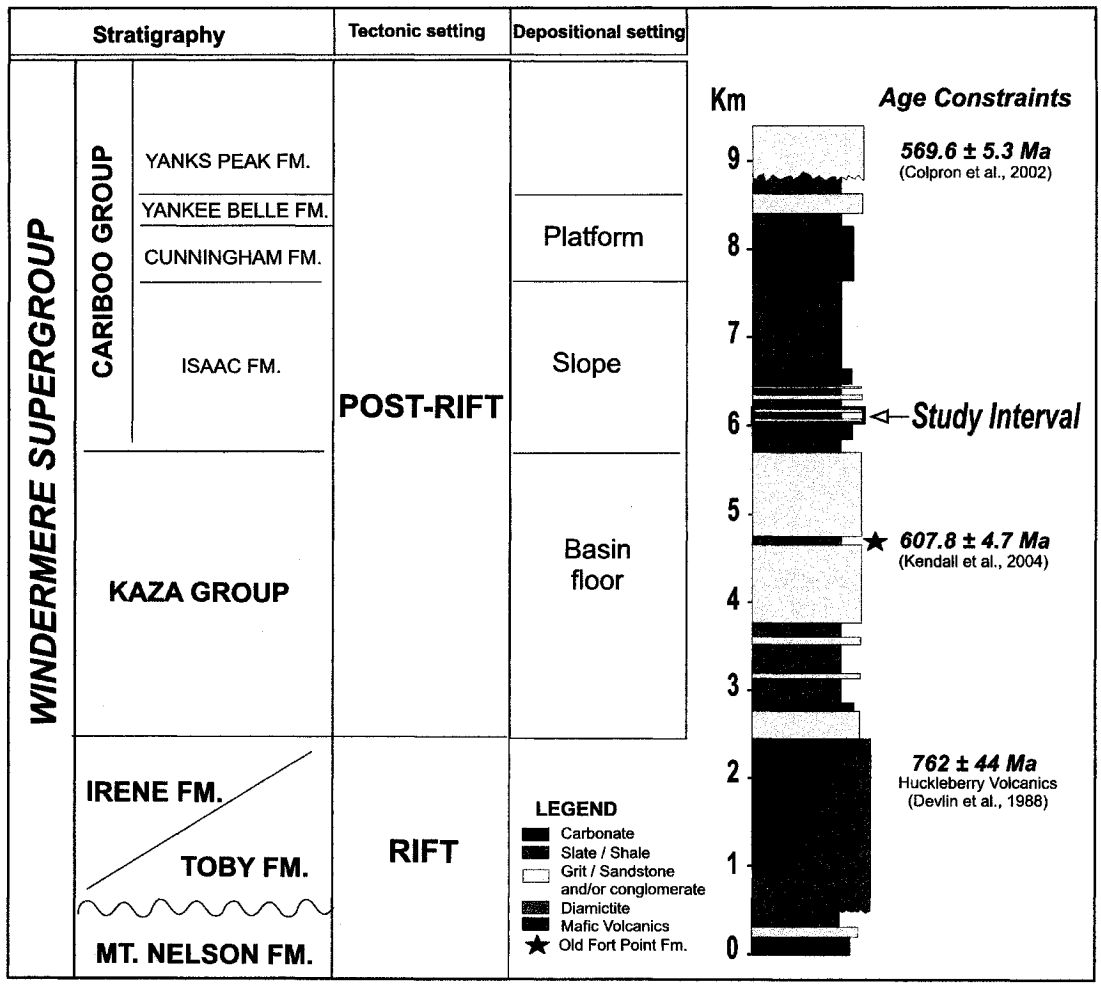

Figure 1.8. Composite stratigraphic column of Neoproterozoic strata in the Cariboo Mountains (Modified from Ross, et al. 1995). The interval studied in this work (red rectangle) comprises the Lower Isaac Formation. Reported age constraints for the Windermere Supergroup are shown on the right.

Stratigraphic History

The Late Proterozoic (Hadrynian, 700-800 Ma,) Windermere Supergroup was deposited along the western margin of North America. The 9 km-thick sedimentary sequence of the Windermere Supergroup unconformably overlies two very thick, sedimentary assemblages, the Purcell Supergroup and Muskwa assemblage (Fig. 1.9).

The Purcell (Belt) Supergroup, which is dated at 1500-1350 Ma (McMechan and Price, 1982) comprises a more than 11 km-thick accumulation of clastic and carbonate rocks that occurs mostly in southeastern British Columbia and southwestern Alberta (Ressor, 1957). The Muskwa assemblage, which consists of a 6 km-thick succession of dolomite, limestone and coarse- to fine-grained siliciclastics is limited to northern British Columbia and has been

tentatively correlated with rock successions of the Purcell Mountains (Bell, 1968) and Mackenzie Mountains (800-1200 Ma, Hein and McMechan, 1994).

Windermere strata are interpreted to have been deposited during the growth of a passive margin that succeeded an earlier history of continental breakup and separation during the formation of the Panthalassa, or proto-Pacific Ocean (Gabrielse, 1972; Ross, 1991). However, some authors (Stewart, 1972; Bond and Komiz, 1984) have suggested that Windermere deposition occurred in a single or complex of continental margin rift basins, whereas others (Simony and Aitken, 1990), inferred its deposition to be linked to a different tectonic setting (e.g. foreland basin).

Strata of the Windermere Supergroup suggest lateral facies changes from shallow continental shelf rocks in the western U.S.A. and northern Canada grading west and northwestward (basinward) into slope and basin floor (Fig. 1.10; Eisbacher 1985, 1992; Ross 1991). In addition, the persistence of sulfide minerals, particularly pyrite, implies extensive bacterial reduction of seawater sulfate in a basin characterized by anoxic/ euxinic conditions (Ross et al., 1995).

During Windermere sedimentation, two worldwide Neoproterozoic glaciations occurred (Fig. 1.9), and are recorded by the Toby Formation, which is a glaciogenic unit interbedded with the Irene Formation in southern B.C., and possibly corresponds with the global-scale Sturtian glaciation at ~750 M.a. (Ross et al., 1995), and the Vreeland Formation that consists of younger glaciogenic sediments deposited in the northern Cordillera (Hein and McMechan, 1994; McMechan, 2000).

The Windermere Supergroup succession, according to Eisbacher (1985, 1992), correlates with the Adelaide succession of eastern Australia and the Sinian succession of China (Fig. 1.11). These three successions have very similar sedimentary sequences and tectonic histories, and therefore may have been joined in Laurentia before 750 M.a. (Powell et al., 1994; Li et al., 1995, 2002; Karlstrom et al., 2001).

The Neoproterozoic rift and then drift episode was followed by a younger episode of continental rifting and subsequent sedimentation during the Early Paleozoic (Gabrielse and Yorath, 1991). Paleozoic sediments were deposited on a rapidly subsiding stable passive margin at a time marked by a worldwide rise of relative sea level and transgression (Hein and McMechan, 1994).

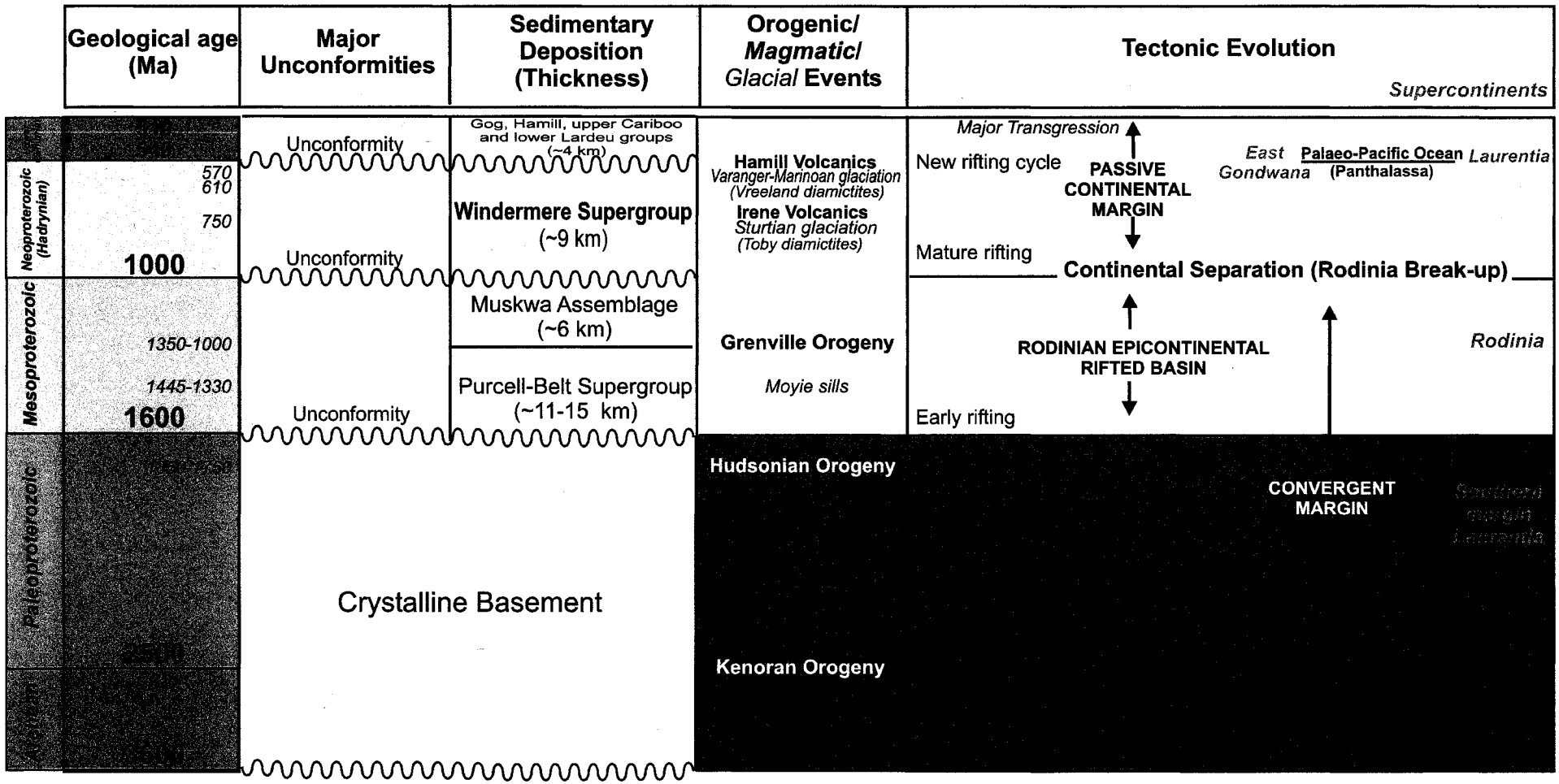

Figure 1.9. Schematic configuration of Proterozoic to Lower Cambrian strata in the southern Canadian Cordillera. For references see text.

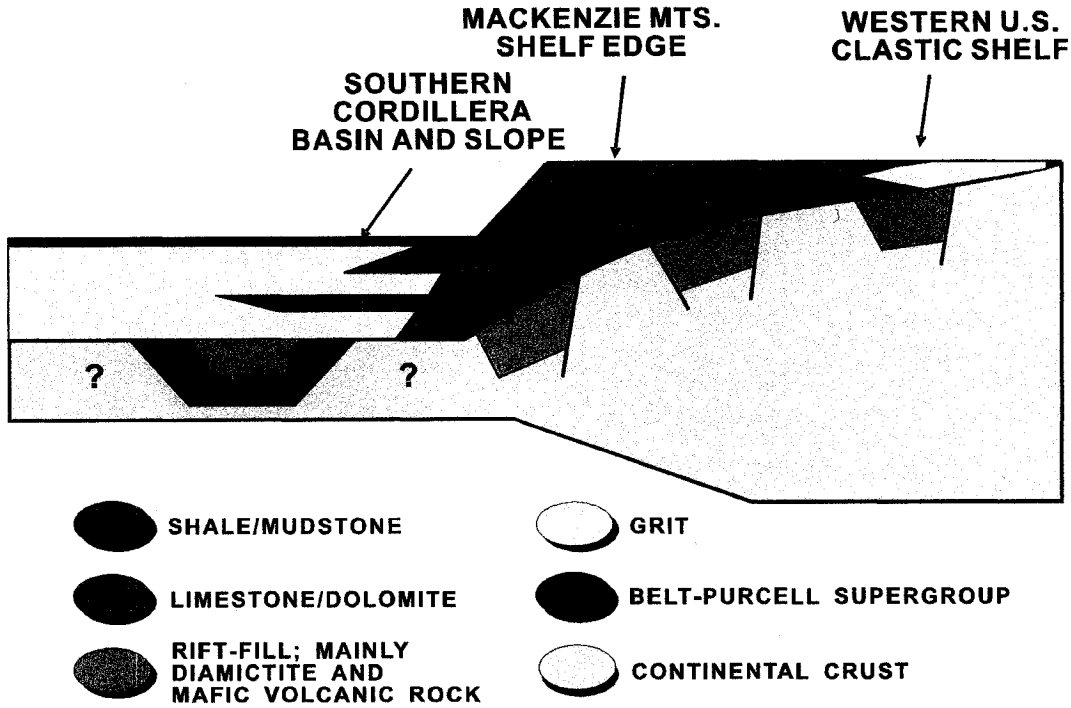

Figure 1.10. Schematic representation for the Windermere Supergroup in western Laurentia (Modified from Ross et al., 1991). Note that most deep-water deposits of the Windermere Supergroup are situated in the southern Canadian Cordillera.

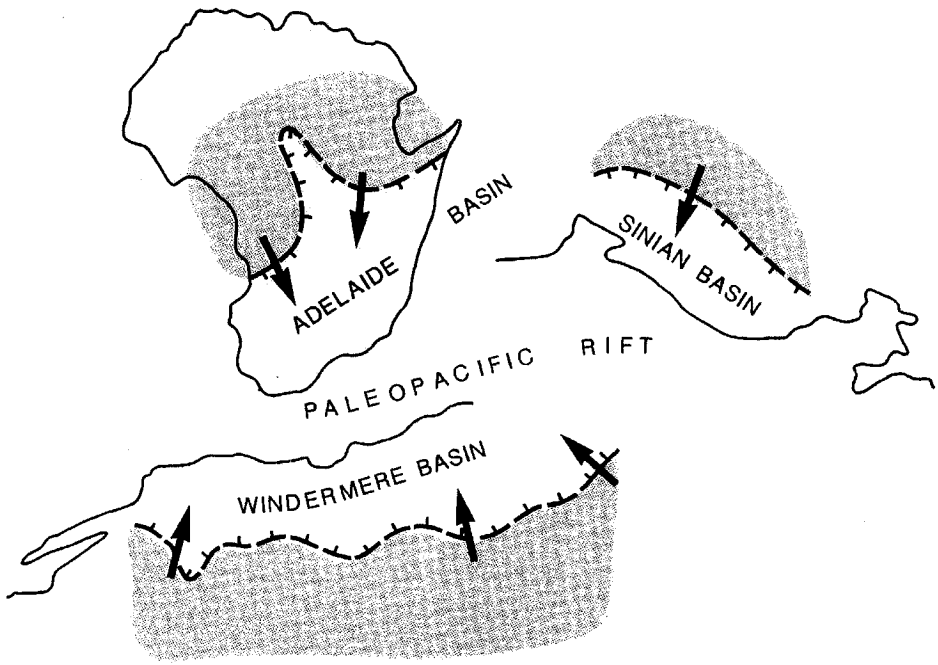

Figure 1.11. Hypothetical configuration of the Late Proterozoic rift basins (Adelaide, Sinian and Windermere basins) along southern Australia, south China and western North America, respectively (Eisbacher, 1985). The colored areas indicate cratonic blocks and pericratonic basins; the arrows indicate relative directions of sediment transport.

Windermere Turbidite System

Deep-marine strata of the Windermere turbidite system are exposed in Lake Louise and Cariboo Mountain areas of the southern Canadian Cordillera (Fig. 1.6 and 1.12; Ross, 1991). This turbidite basin would be classified as a "Type A" basin (Mutti and Normark, 1987), where the basin formed on oceanic crust and was supplied by a large, long-lived sediment source with little or no related tectonic activity.

The palinspastically unrestored size of the Windermere turbidite system is ~35,000 km^2, 11,700 mi^2 (Ross and Murphy 1988; Ross 1991). However, the latest attempt at a minimum palinspastic reconstruction of this system estimated that it is no less than 160,000 km^2 (Ross, 2003a) and as a result is comparable in scale to modern passive margin turbidite systems, such as the Amazon and Mississippi fans (Fig. 1.13).

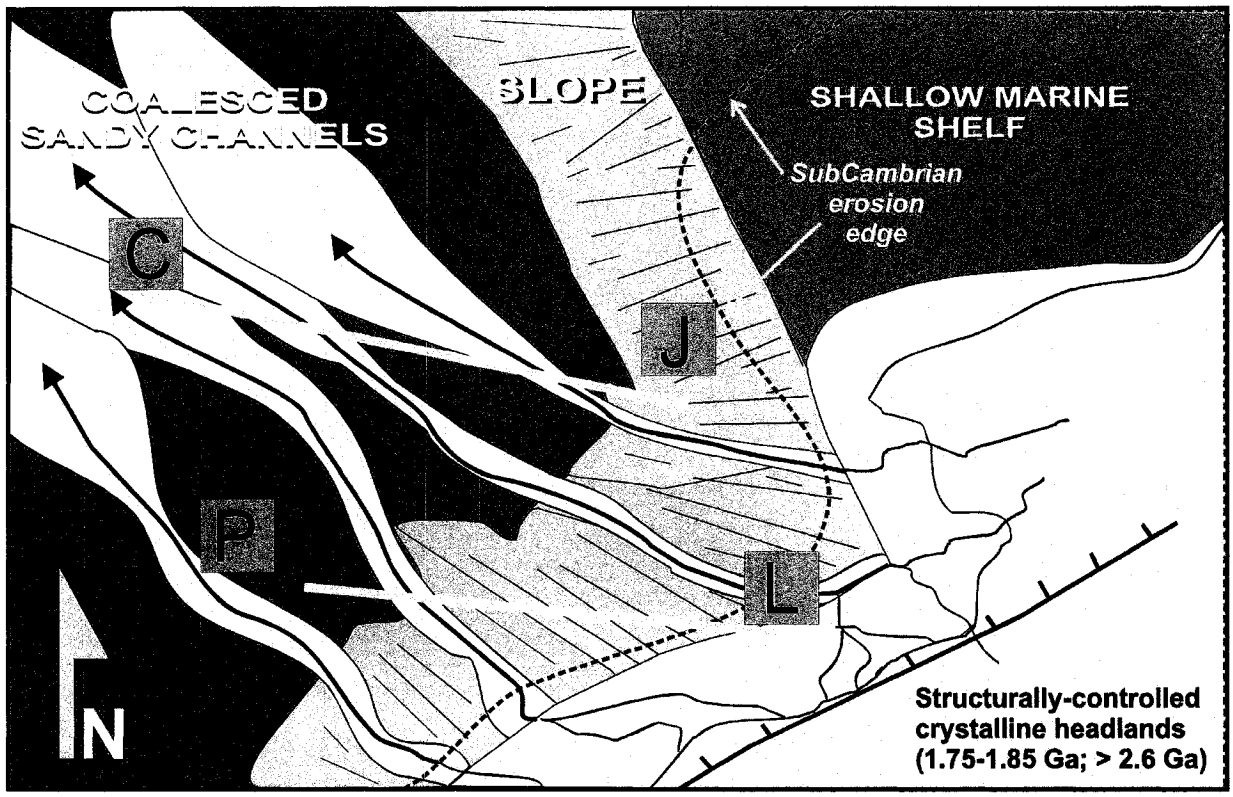

Figure 1.12. Schematic paleogeographic reconstruction of the Windermere turbidite system in the southern Canadian Cordillera (Ross 2000). Note the northwestward change from submarine canyon deposits located in the Lake Louise area (L) passing downslope into lower slope/ base-of-slope deposits in the Jasper (J) and Purcell (P) areas and finally into basin floor strata in the Castle Creek area.

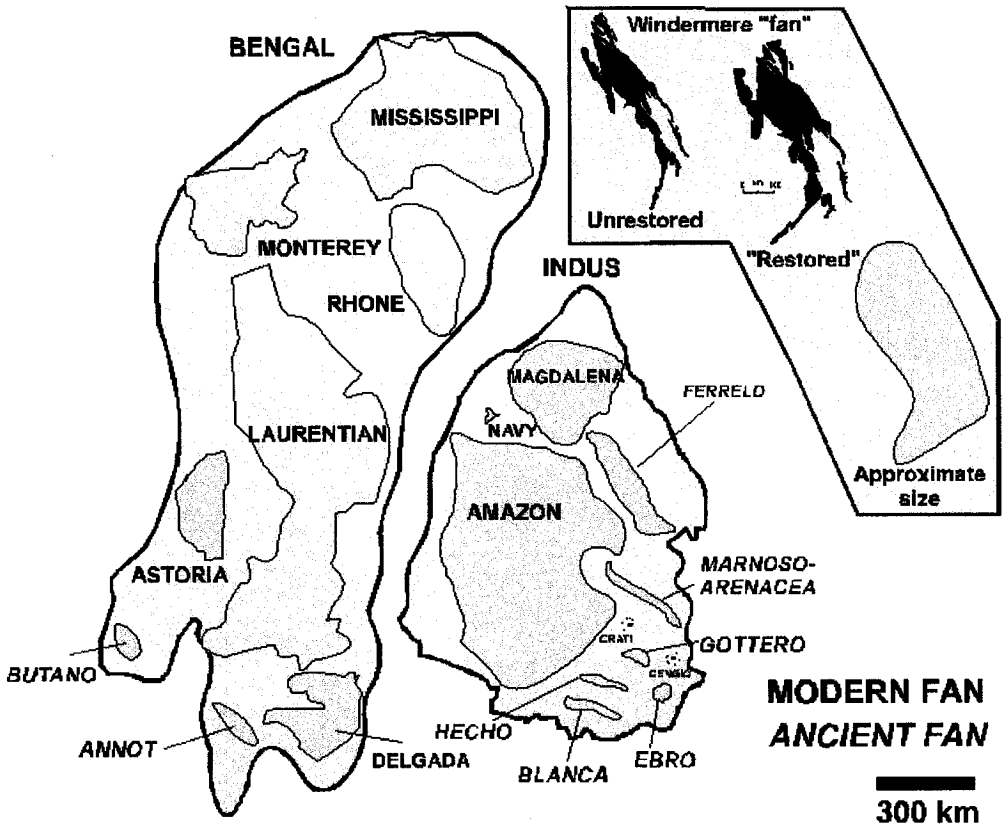

Figure 1.13. Schematic restoration of the Windermere turbidite System (Ross, 2000) and comparison with other well-known ancient and modern fan systems (Barnes and Normark, 1985). Ancient and modern examples are written in red and black letters, respectively.

1.3. CASTLE CREEK, CARIBOO MOUNTAINS (STUDY AREA)

1.3.1. Location and Access

The study area is located in east-central British Columbia between 53° and 53°25' N and 120°02' and 120°03' W, on the southwest side of Castle Creek (Fig. 1.14), which is a major tributary of the Fraser River in the Cariboo Mountains (Fig. 1.3 and 1.5). At Castle Creek the study area has been informally divided into two major areas, Castle Creek North and South; this study was in the southern area.

Due to rapid retreat of glaciers (<100 years) in the Castle Creek area, pristine periglacial outcrops are exposed, especially near the margins of these large ice masses (Fig. 1.15). In addition, low grade of metamorphism has preserved primary sedimentary textures and structures, and simple, large, open styles of folding makes the Castle Creek area an exceptional place to study the Neoproterozoic rocks of the Windermere Supergroup.

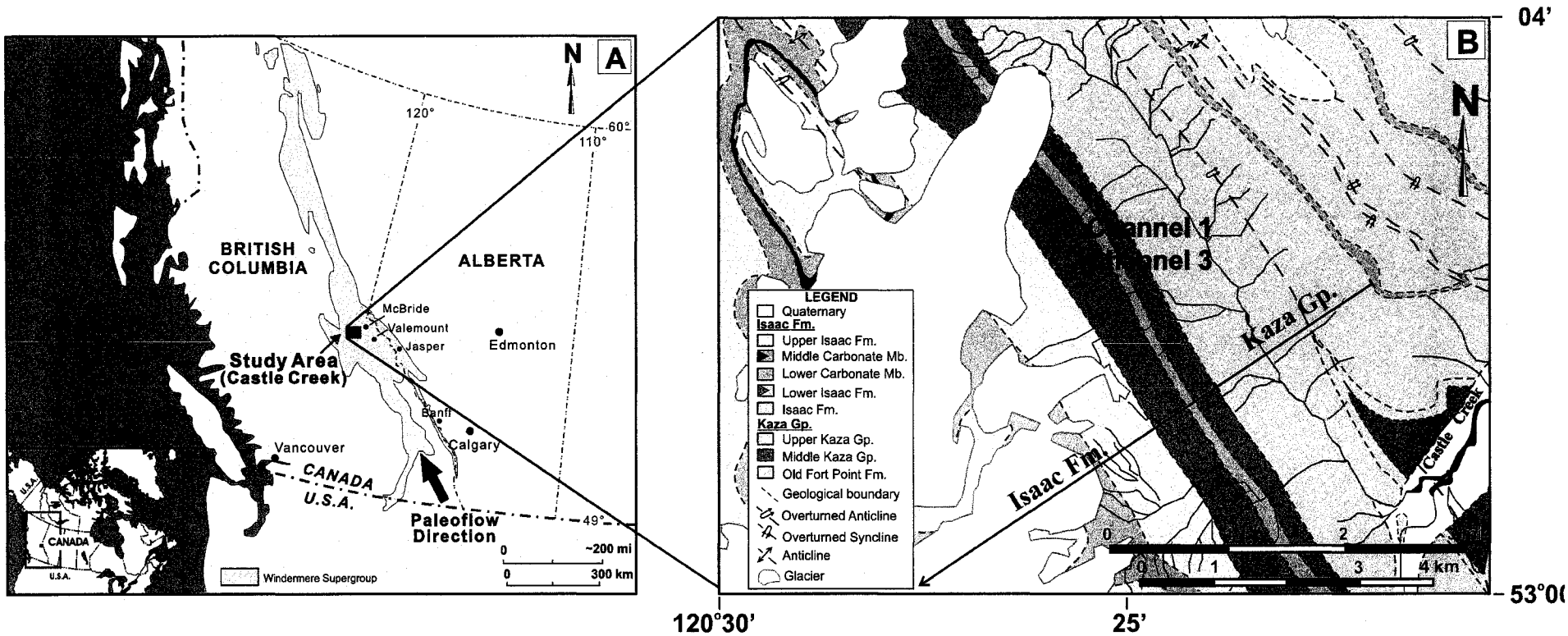

Figure 1.14. Location of the Castle Creek study area shown in relation to: (A) map of western Canada illustrating the distribution of Windermere strata (Modified from Ross and Murphy, 1989). Note the location of the study area (red square), Cariboo Mountains, British Columbia. Outcrop distribution and inferred palaeocurrent trend are from Ross and Murphy (1989) and Ross (1991). (B) Geological map of Castle Creek, study area, highlighting the location of both Channel Complexes 1 and 3 (Modified from Ross and Ferguson, 2003, part of 93H/1 Eddy map-sheet). Note that in the study area (red square) siliciclastic rocks of the Lower Isaac Formation are located on the west limb of an overturned anticline.

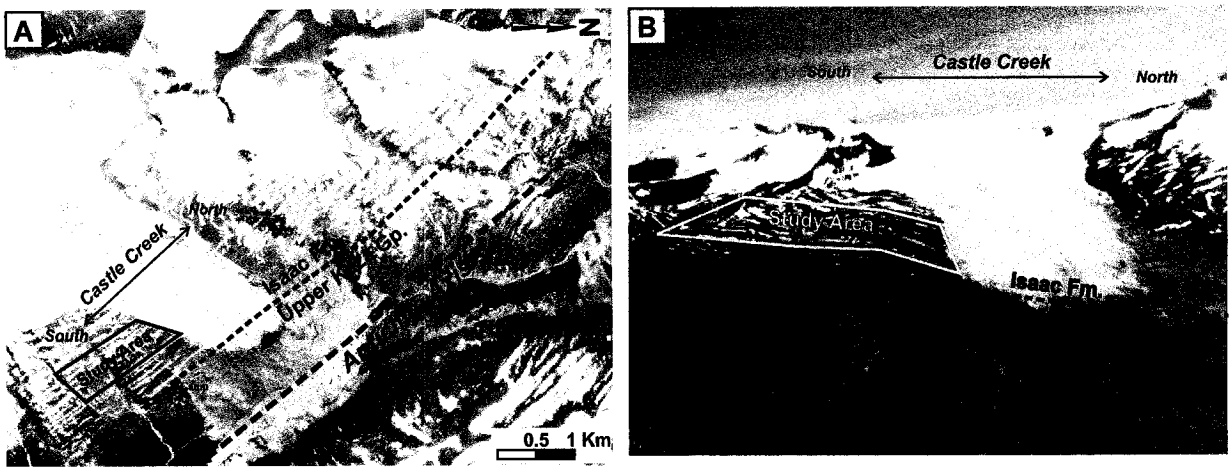

Figure 1.15. Panoramic photos of Castle Creek outcrops in (a) the 1970's and (b) recently (2004), showing the periglacial exposure of the Kaza Group and Isaac Formation (e.g. yellow zones in left photo). The whiter zones indicate glacial cover. (Left photo taken by Ross, G. and right photo taken by Arnott, R.W.C.).

Because road-access is limited in the mountainous central and eastern part of Cariboo Mountain, the access to the study area is principally by helicopter.

1.3.2.Previous Works

The first major geological work of the Castle Creek area was by Campbell et al. (1973). This work included a geological map of the McBride area (1:250,000) and a comprehensive report that included details of regional stratigraphy and correlation of the Proterozoic and Lower Paleozoic rocks with those in the Rocky Mountains, Rocky Mountain Trench, and other areas in the southern Cariboo Mountains and Interior Plateau. Additionally, Campbell et al. (1973) provided important data about major regional geological structures and cross sections, metamorphic episodes, and economic and commercial interests in the area.

Subsequently, there has been a number of structural and regional works carried out in the Castle Creek and surrounding areas (e.g. Murphy and Rees 1983; Murphy 1987a,b; Ross and Murphy 1988; Thompson and Ross 1990; Ross 1991; Ross et al., 1995; Ross, 2000; Reid et al., 2002; among others). Many of these studies were compiled and summarized by Aitken and McDonough (1990), Gabrielse and Campbell (1991) and Hein and McMechan (1994). Recently, Ross and Ferguson (2003) published a detailed map (1:50,000), integrating regional data. Notwithstanding these works, no detailed sedimentological, stratigraphic or architectural analyses have been published concerning the deep-water channels of the Isaac Formation in the Castle Creek area or vicinities.

1.3.3. Structural Framework

The Castle Creek area occurs in the western part of the Premier Anticlinorium (Fig. 1.5), a kilometer-scale upright fold structure that plunges northwest and comprises large Jurassic southwest-verging to overturned folds that dip steeply to moderately to the northwest (Murphy and Journey, 1982; Murphy, 1987a,b). Structural elements in this area are complex and indicate a polyphase history of deformation that includes at least four major episodes of folding, multiple generations of faults, planar foliations, lineations, joints, cleavages, and high angle crenulations (Murphy and Rees, 1983; Murphy 1987a,b). Specifically, strata of the Windermere Supergroup in the study area are well-exposed on the steeply dipping limb of a west-verging overturned anticline (Fig. 1.14).

1.3.4. Stratigraphy

In the Castle Creek study area, the Windermere Supergroup consists mostly of strata of the Kaza Group and Isaac Formation (Lower Cariboo Group, Fig. 1.16). The Upper Cariboo Group comprises the Cunningham and Yankee Belle formations and is not exposed in the area.

1.3.4.1. Kaza Group

Diverse terminology has been used to describe the Kaza Group in the Cariboo Mountains (Campbell et al., 1973; Pell and Simony, 1982, 1987; Murphy and Rees, 1983; Murphy, 1987; Ross and Murphy, 1988; Ross et al., 1995). The unit is about 2-4 km thick and is composed of metasandstone interbedded with metaconglomerate, metasiltstone, metashales, and local carbonate-rich intervals. In the Castle Creek area, almost 800 m thick of upper Kaza Group strata are well exposed (Fig. 1.16).

Included in the Kaza Group is a distinctive and regionally extensive unit termed the Old Fort Point Formation (Ross and Murphy, 1988). The regional equivalence of this marker with other units in the southern Canadian Cordillera is not *sensu stricto*, because of local sedimentary differences. However, it has been suggested that a general relationship exists among them (Fig. 1.7), and that the Old Fort Point Formation in the middle Miette Group of the Jasper area (Ross and Murphy, 1988) and the Cushing Creek area (Carey and Simony, 1985; Hein and McMechan, 1994), lower Hector Formation of the Lake Louise area (Charlesworth et al., 1967; Arnott and Hein, 1986), upper Horsethief Creek Group, including

Comedy Creek unit of northern Selkirk Mountains area (Reesor, 1957; Poulton and Simony, 1980; Pell and Simony, 1981, 1982, 1987; Ross and Murphy, 1988; Gasbry and Brown, 1993) and carbonate division called Baird Brook Division of the central Purcell Mountains (Poulton and Simony, 1980; Kubli and Simony, 1992) form a single basinwide correlative stratal unit. This unit comprises a distinctive upward-thinning sequence of chloritic siltstones, rhythmic marble-siltstone, and carbonaceous-sulfidic pelite (Ross and Murphy 1988).

The Kaza Group has been interpreted to consist of deep-marine basin-floor strata deposited on the passive margin of the western North American Craton (Ross et al., 1995), and that the Old Fort Point marker unit represents a regional highstand systems tract succession formed as a result of a major sea level rise (Ross and Murphy, 1988).

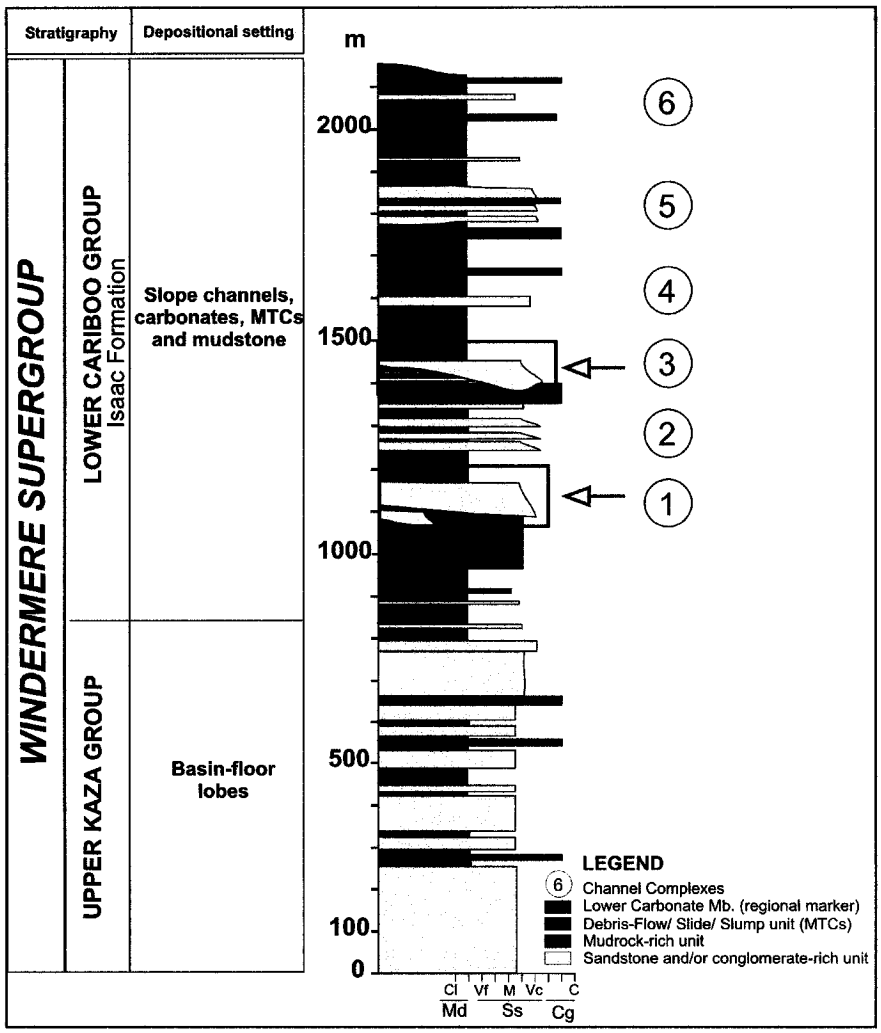

Figure 1.16. Composite stratigraphy in the Castle Creek south study area. The numbers indicate major channelized units; Channel 1 and 3 are two of the lowermost channel complexes.

1.3.4.2. Cariboo Group

The Cariboo Group lies conformably above the Kaza Group and reaches a maximum thickness of approximately 5 km in the western Cariboo Mountains and thins eastward along the western limit of the Rocky Mountain Trench (Fig. 1.5). It has been divided along the Canadian Cordillera into seven stratigraphic units (Fig. 1.8), which from oldest to youngest are: Isaac, Cunningham, Yankee Belle, Yanks Peak, Midas, Mural and Dome Creek formations (Campbell et al., 1973). In the greater Castle Creek area, Isaac, Cunningham and Yankee Belle formations are exposed (Fig. 1.8).

Isaac Formation

The Isaac Formation in the Cariboo Mountains is the lowermost unit of the Cariboo Group, overlying strata of the Kaza Group (Figs. 1.6, 1.7 and 1.8). It consists of metamudstone, metasiltstone and metashale interbedded with six metaconglomerate and metasandstone intervals, and two carbonate intervals. Strata are typically pyritic, particularly in the lower part of the formation.

The metaconglomerate and metasandstone intervals have been commonly termed "**grits**" (Gabrielse ,1972; Young et al. 1973; Brown et al., 1978; Poulton and Simony, 1980; Murphy, 1990). This term is restrictive because it is used to describe only clastic sediment containing abundant angular, siliceous grains ranging from 2 to 8 mm in diameter in a finer-grained matrix. Another term associated with the Isaac metasandstone is "**psammite**", which is an obsolete term that describes clastic sediment or sedimentary rock composed of sand-size particles. Psammite is sometimes used to indicate the metamorphic equivalent of arenite or sandstone.

At the Castle Creek study area, the 1300 m thick, lower unit of the Isaac Formation is composed of persistent and distinctive pale-grey-weathering, bluish grey siltstone and mudstone that is interstratified with pinkish brown-weathering, yellowish brown sandstone-conglomerate that locally form intervals up to 100 m thick (Fig. 1.16). The Isaac Formation is correlated with the East Twing Formation of the upper Miette Group in the central and east Rocky Mountains and upper Framstead, Chowika and Cut Thumb formations of the Misinchinka Group in the Deserter Range and Mount Vreeland in the Northwest Rocky Mountains (Fig. 1.7, Campbell et al., 1973).

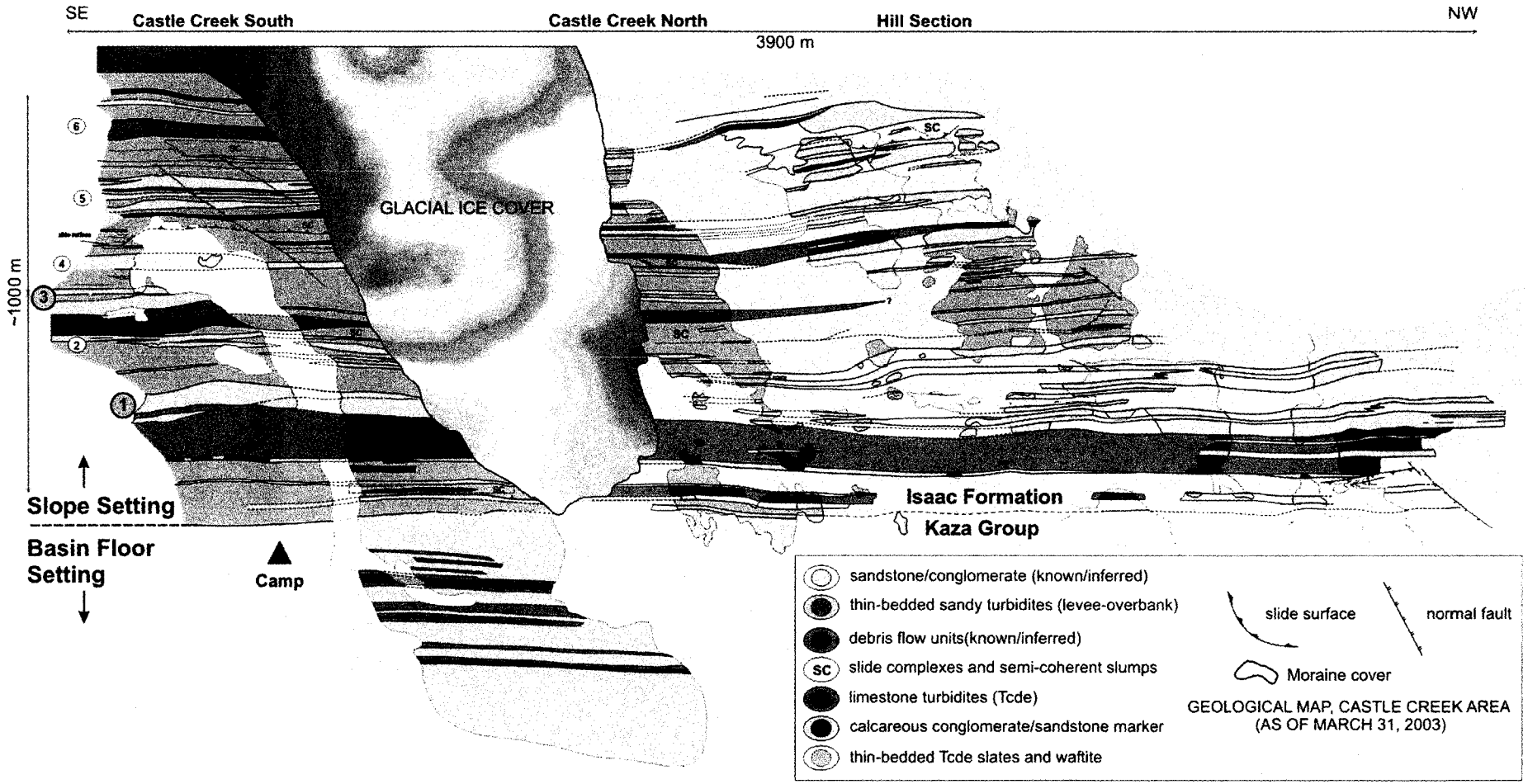

Figure 1.17. Generalized map of the Kaza Group and Lower Isaac Formation in the Castle Creek area (From Windermere Consortium, in progress), illustrating the slope to basin floor variations in lithofacies and internal stratigraphy. Shown are the locations of Channel Complexes 1-6, highlighting Channel 1 and 3 studied in this work.

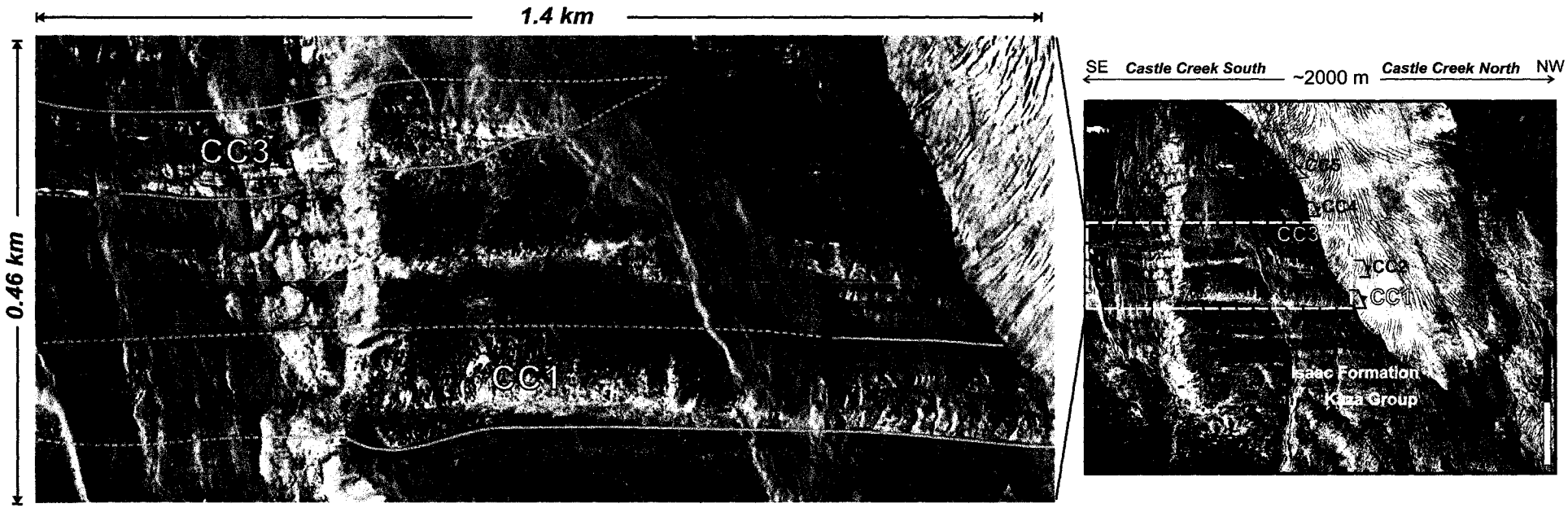

Figure 1.18. Location of Channel 1 and 3 in the Castle Creek area (south) in the Cariboo Mountains, southern Canadian Cordillera.

Moreover, an approximately 150 m thick carbonate member, informally termed the first Isaac Carbonate marker, is exposed in the study area. The first Isaac Carbonate marker is one of two tabular carbonate intervals in the Isaac Formation that form regionally-correlatable markers (Ross, 1991, 1995). These horizons may be related to other platformal units in the southern Cordillera, including Yellowhead Platform and Upper Limestone Unit of Northern Dogtooh Mountains (Poulton, 1973; Ross et al., 1995).

The Isaac Formation has been interpreted to have been deposited on the passive-margin slope of Neoproterozoic western North America (Ross et al., 1995). The two major carbonate intervals represent resedimented deep-water carbonates derived from a shallow-water carbonate platform (Ross, 1991). The Isaac deep-water sedimentary system is a typically mud-rich depositional system, locally interrupted by sand deposition. Similar modern systems include the Mississippi, Indus, Amazon, Bengal, Nile, Magdalena, Laurentian, Monterey, Mozambique, Astoria, and Valencia submarine fans (Reading and Richards,1994; and Stow and Mayall, 2000).

Cunningham and Yankee Belle formations

The Isaac Formation is overlain conformably by the Cunningham and Yankee Belle formations. In the northern Cariboo Mountains the Cunningham Formation reaches a maximum thickness of about 550 m, whereas the Yankee Belle Formation is up to about 900 m thick (Gabrielse and Campbell, 1991). The Cunningham Formation consists mostly of oncolitic and intraclastic carbonates. The Yankee Belle Formation is recognized by a rhythmic sequence of alternating limestone, siltstone and shale that changes upward to shale and sandstone. Both units are interpreted to have been deposited on a shallow-marine, high-energy shelf (Ross et al., 1995).

1.3.5. Slope Channels of the Isaac Formation: Channel Complexes 1 and 3

Stratigraphically upward, the 2.5 km thick succession of Windermere Supergroup stratigraphy in the Castle Creek study area indicates a transition from basin-floor to continental slope sedimentation (Figs. 1.14 and 1.15). As mentioned in the previous section 1.3.4., basin-floor deposits are recorded by the Upper Kaza Group and slope to toe-of-slope deposits comprise the Lower Isaac Formation (Fig. 1.17). These slope deposits are dominated by siltstones and silty/sandy mudstones interpreted to be turbidites, debrites,

slump or slide deposits. Moreover, these mudrocks are interbedded with sandstone-conglomerate and carbonate intervals. The sandstone-conglomerate interval are interpreted to be very-thick sand-filled channels encased in mudrocks (Fig. 1.16). This project focused on two of these channel-fill deposits informally termed Channel 1 and 3 (Fig. 1.18).

1.4. OBJECTIVES AND METHODOLOGY

1.4.1. Objectives

The principal objective of this project is to describe intrachannel deposits of channel complex sets 1 and 3 of the Isaac Formation in the Castle Creek South study area. Specifically, it includes the identification, interpretation and spatial distribution of lithofacies, lithofacies assemblages and architecture elements that fill these channels. Emphasis will be placed on the overall vertical and lateral stratigraphic relationships and the reconstruction of depositional environment and processes. A second objective is to evaluate the major mineralogical, petrographic and geochemical attributes of Isaac channel-fill mudstone, sandstone and conglomerate in order to assess sediment provenance and sedimentary conditions that operated during transport and slope deposition.

1.4.2. Methodology

1.4.2.1. Fieldwork

Fieldwork was conducted over two summer seasons (July to August 2002 and 2003). During the first summer emphasis was placed on measuring vertical sections, correlating and sampling (samples locations are shown in Appendix 1) in both channel complexes, and making gamma-ray profiles for each measured section. During the second summer, helicopter-shot photomosaics were used with ground-based work to map-out major bounding surfaces.

Fieldwork was carried out on two superbly exposed channel fills that are exposed on the overturned limb of an anticline that was recently deglaciated. Outcrop quality, however, is variable and in places, particularly on the southeast side of the most areally-extensive moraine in the area, bedrock obscured by glacial debris or vegetation, especially lichen.

1.4.2.2. Logging and Correlation techniques

In total, 65 detailed bed-by-bed stratigraphic sections were measured in both channel complexes. Sections record lithology, grain size, thickness, internal primary and secondary sedimentary structures and where possible, palaeocurrent direction.

Bed correlation between logs and detailed mapping of significant surfaces was done by "walking out" beds and surfaces along the outcrop surface. This allowed the identification of important architectural elements within the channel fills and establishment of the lateral and vertical facies relationships. In general, the accessibility of the outcrop was very good, but local steep cliffs required visual observations to trace laterally major surfaces.

In addition, gamma-ray spectrometry (GRS) data were collected at the surface, measuring total radioactivity. Data obtained from logs, correlation panels and gamma-ray profiles have all been captured digitally.

1.4.2.3. Petrography

A total of 60 samples were collected for thin-section analysis, prepared at the University of Ottawa and evaluated with Olympus SZ61 and BX41 microscopes (full featured stereo microscope and reflected light upright microscope respectively). These data assisted in describing grain size, mineralogy, alteration and microstructure. Carbonate thin sections were stained following the standard procedure using Alizarin Red S and potassium ferrocyanide (Dickson, 1966).

1.4.2.4. X-Ray Diffraction

X-ray diffraction is a phenomenon in which the atomic planes of a crystal cause an incident beam of X-rays (if wavelength is approximately the same magnitude as the interatomic distance) to interfere with one another as they leave the crystal. Each crystalline solid has a unique X-ray diffraction pattern which may be used as a "fingerprint" for its identification. In this work, therefore, this technique was used to determine the approximate mineralogical composition of rocks based on the standards of the International Centre for Diffraction Data (ICDD).

A total of 39 mudstone, mudstone-clast and carbonate-clast samples were selected for bulk rock analysis with X-ray powder diffraction in the XRD Lab of University of Ottawa. During the preparation of these samples the method outlined by Buhrke et al. (1998) was

used to 1) take a representative specimen from the bulk and "homogeneous" sample, 2) grind each sample down to particles that have a standard particle size of 45μm or less and promote random orientation and distribution of the crystallites (i.e. crystals with at least one microscopic or submicroscopic dimension) and 3) use a method of powder preparation that would not cause distortion or destruction of the crystal lattice (i.e. geometric description of the periodicity of a crystalline arrangement).

1.4.2.5. Stable Isotopes

A total of 24 samples for isotopic analysis were collected from mudstone and mudstone fragments of the Isaac intra- and extra-channel deposits in order to examine organic carbon content (TOC or %C). Bulk rock samples were first oven dried, crushed and then reacted and digested with (pre-made) 10% hydrochloric acid for 1 hour to eliminate inorganic carbon occurring principally as carbonate cement and then spun in a centrifuge (Hermle model Z510) at a maximum speed of 2500 revolutions per minute. Subsequently, samples were decanted and rinsed three times with distilled water to eliminate any excess chlorine ions, and then heated at 60°C for two days to dry them. Later, samples were analyzed in a NC 2500 elemental analyzer (mass spectrometer) to determine overall amount of C (%C, %H, %N, %S).

1.5. STATEMENT OF CONTRIBUTIONS

Although some work has been done in the Castle Creek area, mostly structural geology (Campbell et al., 1973; Murphy and Journeay, 1982; Murphy and Rees, 1983; Murphy, 1987a,b; Reid et al., 2002; Ross and Ferguson, 2003; among others), few have reported on the sedimentological and stratigraphic characteristics of these strata (Murphy and Rees, 1983; Ross and Murphy, 1988; Thompson and Ross, 1990; Ross, 1991; Ross et al., 1995). The Isaac Formation consists typically of fine-grained rocks, mostly slates and silty mudstones and its study has been overlooked. Nevertheless, very thick sandstone and conglomerate intervals occur in these mudrocks and form impressive channel-fill deposits. This study, therefore, is the first to report on the characteristics and stratal geometries of two thick intrachannel deposits in the Isaac Formation.

These data, in turn, provide significant insight into reservoir quality distribution in subsurface deep-marine channel hydrocarbon reservoirs. In particular, deep-marine channel

and channel-levee deposits, which represent important hydrocarbon reservoirs, require a better understanding of stratal architecture and reservoir distribution (Slatt, 2002). Accordingly, the superb exposures of channel fills in the Isaac Formation provide an meaningful analogue for better understanding depositional processes, stratal geometry and channel evolution in deep-marine settings.

CHAPTER 2. FACIES, AND FACIES ASSOCIATION OF TWO DEEP-WATER SUBMARINE CHANNEL COMPLEX SETS (CHANNEL 1 AND 3) IN THE NEOPROTEROZOIC ISAAC FORMATION, WINDERMERE SUPERGROUP, CARIBOO MOUNTAINS, BRITISH COLUMBIA, CANADA

2.1. INTRODUCTION

A summary describing the processes and classification of gravity flows, and channel types and evolution is first presented in order to develop some of the concepts used herein. Subsequently, description of facies and facies association and respective interpretations are presented.

2.1.1. Chapter Aims

This chapter presents a detailed analysis of the facies and facies association in two channel complex sets 1 and 3 formed on the Neoproterozoic passive-margin slope of western Canada using the methodology described in Chapter 1. This analysis concentrates on the Castle Creek South study area. The specific characteristics of sedimentary facies that make up intrachannel deposits in the Isaac Formation are poorly documented and some processes that form these deposits are poorly understood. Thus, the primary aims of this chapter are to better understand the facies and facies associations that constitute intrachannel deposits of both channel complexes.

2.1.2. Sediment Gravity Flows

Sediment gravity flows (also know as sedimentary density flows of Mulder and Alexander, 2001, or gravite of Gani, 2003) are flows of sediment or a mixture of sediment and water that move downslope due to gravity; e.g. turbidity currents (Fig. 2.1.). These flows are the primary mechanism that transports and deposits sediments in deep-water environments, located at bathyal water depths (i.e. more than 200 m deep).

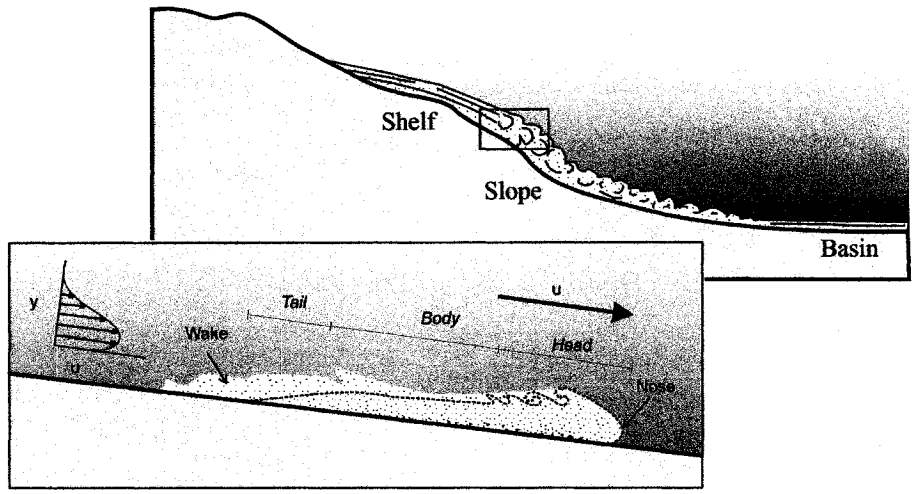

Figure 2.1. Downslope moving turbidity current. In an ideal sequence of events a turbidity current is initiated upslope by underflow or failure (e.g. slump triggered by earthquake). The flow head tends to accelerate downslope, and erodes the substrate. Those sediments become incorporated into the flow (mainly in the body and tail), and in turn increase the density contrast with the ambient fluid.

2.1.2.1. Classifications of Sediment Gravity Flows

Based on the interpreted importance of various mechanisms or conditions, numerous classifications schemes for sediment-gravity flows have been proposed. These include (1) sediment concentration (Bagnold, 1962), (2) rheology (Dott, 1963; Postma, 1986; Shanmugan, 2000), (3) sediment-support mechanism (Middleton and Hampton, 1973; Middleton 1993), (4) combination of rheology and sediment-support mechanism (Lowe 1982, Gani, 2004), (5) field description (Bouma, 1962; Guibaudo, 1992), (6) combination of rheology and field description (Mutti, 1992; Pickering et al., 1989), and (7) combination of flow properties and sediment-support mechanism (Mulder and Alexander, 2001). Herein, subaqueous gravity or density flows are classified using the most commonly used classification schemes (Fig. 2.2) that subdivides sediment-gravity flows into three major categories: low-density flows, high-density flows and debris flows.

Low- and high- density flows are differentiated, respectively, in terms of low and high sediment concentration (*C*). *C* represents the proportion, expressed either as weight percentage (Lowe, 1982; and others) or volume percentage (Mulder and Alexander, 2001), of sedimentary particles that are suspended in the flow. Debris flows are density flows that contain sufficient mud that flow rheology, and consequently flow behaviour, is affected.

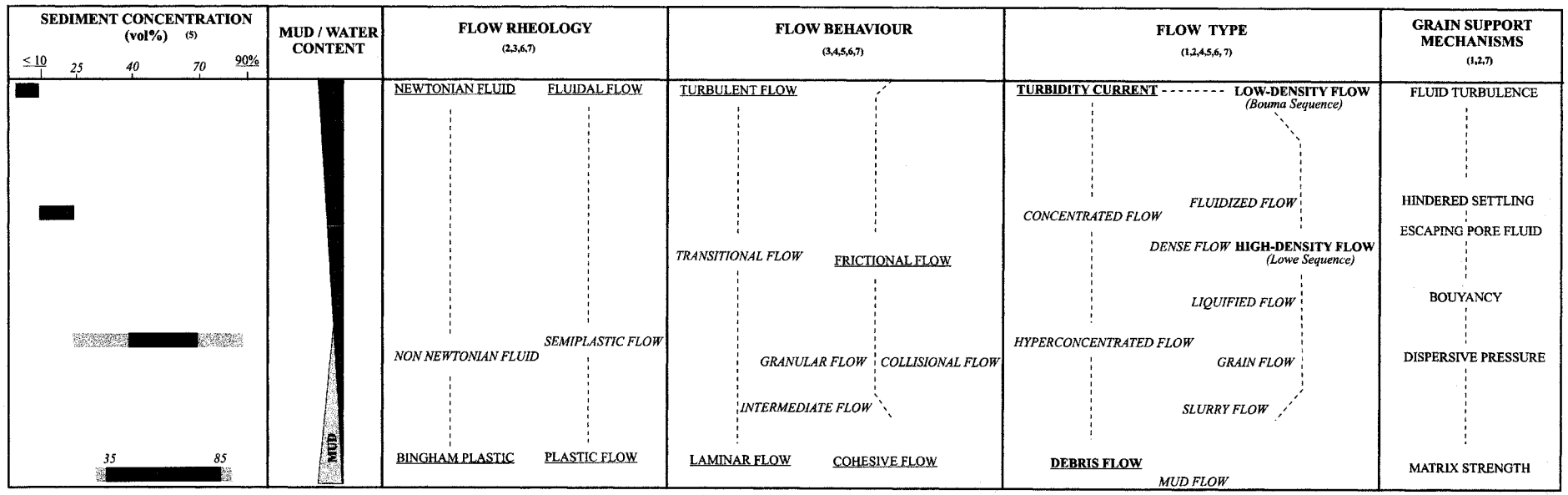

Figure 2.2. General classification of subaqueous sediment gravity or density flows showing different classifications of gravity flows according to the predominant flow rheology, flow behaviour and grain-support mechanisms. The spectrum of flow conditions is represented by dashed lines. Based on (1) Middleton and Hampton (1973), (2) Lowe (1982), (3) Shanmugan (2000), (4) Lowe and Guy (2000), (5) Mulder and Alexander (2001), (6) Dagnustpa (2003), and (7) Gani (2004).

Low-density flows

Low-density flows are sediment-gravity flows with sediment concentration less than 9 vol% (Bagnold, 1962), in which the sediment is supported by fluid turbulence. This flow is mostly turbulent (high Reynolds number –i.e. ratio between inertia and viscous forces, greater than ~2000), and behave with a fluidal or Newtonian rheology, where the fluid (i.e. flow) lacks strength. Suspension deposition from turbidity currents creates turbidites, with succeeding sedimentary structures that correspond with the typical T_{a-d} divisions of the Bouma Sequence (Fig. 2.3; Bouma, 1962).

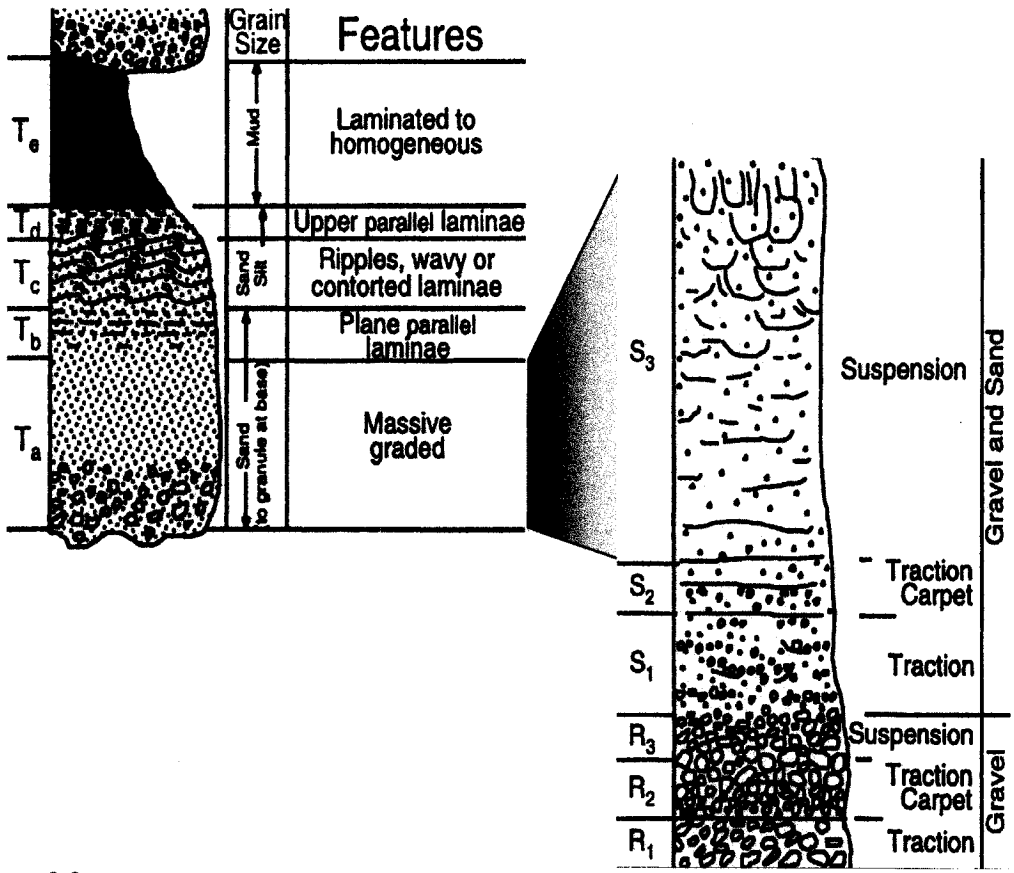

Figure 2.3. Sequences of low and high-density flow deposits. At the left, Bouma Sequence turbidites (Bouma, 1962); at right, classical Lowe Sequence of high-density turbidity currents (Lowe, 1982).

High-density flows

During the past decades there has been growing evidence suggesting subaqueous gravity flows are genetically more complex than simply low-density turbidity currents. Those flows with sediment concentrations from 10 to 25 vol% (concentrated) and greater

(hyperconcentrated) have been termed high-density turbidity currents by Lowe (1982). These flows are transitional (Reynolds numbers between 500 and 2000), and can behave variably as turbulent and/or laminar flows. These dense and frictional flows are sufficiently competent to transport coarse particles (from coarse sand to gravel).

During the movement of high-density flows, a number of different sediment-supporting mechanisms coincide in time and/or space, including turbulence, dispersive pressure, hindered settling, upward escaping fluid, buoyancy, and matrix strength. Deposition from high-density flows is interpreted to form vertical succession of sedimentary structures described in the Lowe Sequence (Fig. 2.3; Lowe, 1982).

Debris flows

Characteristically, debris flows exhibit a Bingham (plastic) rheology where the fluid (i.e. flow) possesses strength owing to the presence of cohesive material (mud). Sediment particles, therefore, are supported by matrix strength and commonly are up to boulder in size. These flows are typically laminar (low Reynolds numbers, less than ≈500) and deposit "en masse", forming debrites.

2.1.2.2. Sediment Support Mechanism

As pointed out earlier, particles in sediment gravity flows may be supported by one or more sediment support mechanisms. Each of these mechanisms is briefly described below and illustrated in Fig. 2.4.

Turbulence

Turbulence is linked to the irregular movement of fluid elements termed (turbulent) eddies (e.g. motions of a fluid in directions differing from, and locally opposite to the direction of the larger-scale current, especially in a circular motion). Sediment remains suspended when the speed of upward turbulence equals or exceeds the settling speed of the particle (Fig. 2.4a).

Dispersive Pressure

Dispersive pressure is a support mechanism that becomes increasingly more efficient and important with increasing sediment concentration (Fig. 2.4b). Dispersive pressure arises

because of grain collisions, involving exchangeable kinetic energy and transferable momentum. This exchange of momentum helps to maintain the colliding particles in suspension (Bagnold, 1954). Dispersive pressure causes the dilatation of the granular material undergoing shear, and therefore results in a consequential normal stress (Middleton and Hampton 1973). Dilation, however, serves to reduce the effectiveness of dispersive pressure (Le Roux, 2003).

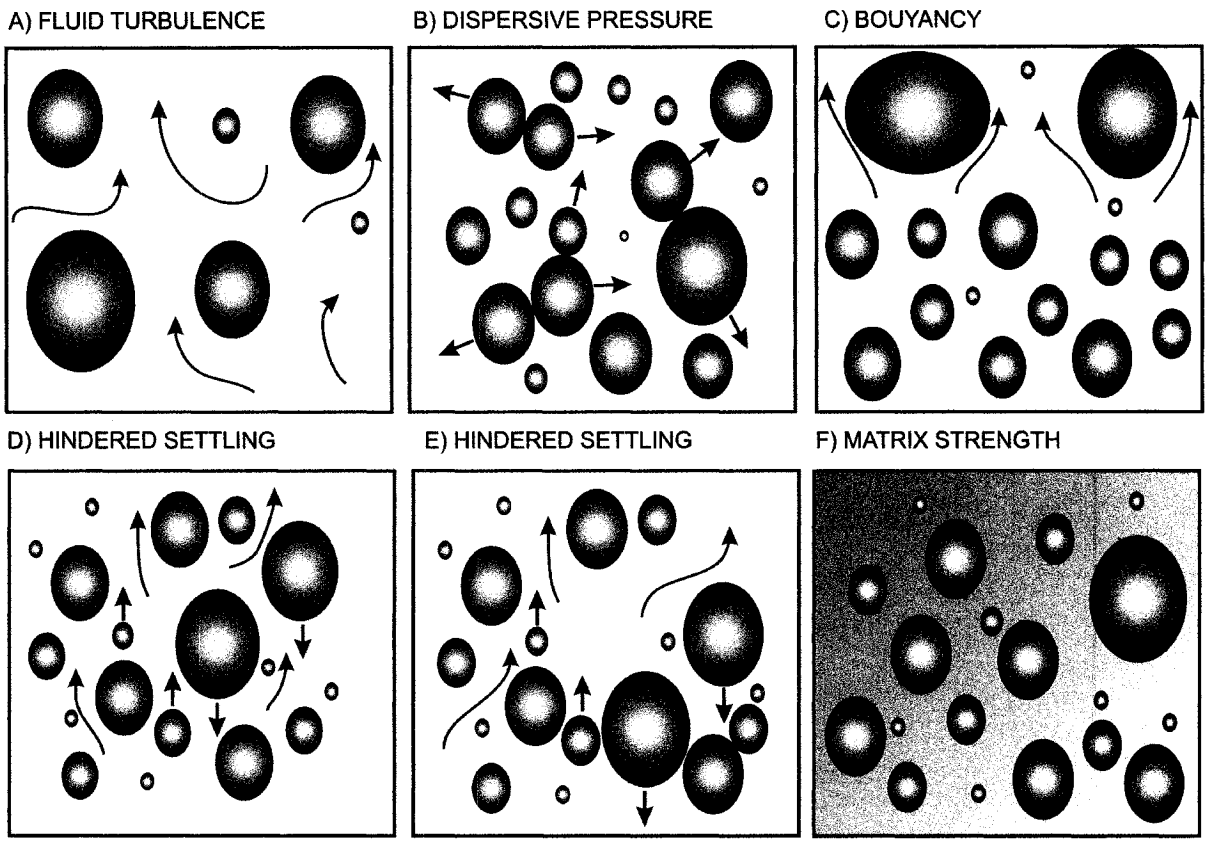

Figure 2.4. Schematic representations of particle support in sediment-gravity flow: (a) fluid turbulence, in which particles are held in suspension by upward-directed turbulent eddies; (b) dispersive pressure created by particles-particles collision; (c) buoyancy, where largest and densest particles could be floating and maintained in suspension for longer period; (d) hindered settling, in which the upward flow of a fluid-fine sediment mixture creates drag on settling, larger particles, reducing their settling velocities because of (e) the collision and clutter of particles; and (f) matrix strength, in which cohesion of interstitial fine particles (grey background) create strength within flow and thereby allow it to suspend large particles.

Buoyancy

Buoyancy is a sediment support mechanism that plays an important role in the segregation of some large-diameter and heavy particles in intermediate to highly concentrated granular dispersions (Fig. 2.4c). Buoyancy decreases the effective settling velocity of these particles

and delays its sedimentation (Druit, 1995). The concept of buoyancy was first discussed by the Greek Philosopher Archimedes, in what is known as Archimedes Principle: *Any object, wholly or partly immersed in a fluid, is buoyed up by a force equal to the weight of the fluid displaced by the object.* Therefore, buoyancy refers to a force which creates motion and displaces a fluid due to the differences in density and pressure it has with its environment until equilibrium is reached.

Hindered Settling

Hindered settling is another support mechanism that becomes increasingly important as sediment concentration increases (Fig. 2.4d,e). Hindered settling occurs when neighboring particles interfere with the vertical settling of individual particles because of particle crowding. Hindered settling promotes a strong upflow of fluid and fine sediment that hampers the free settling velocities (i.e. rate at which sediment particles tend to sink in a clear fluid under gravitational forces) of larger particles by collisions and shear with finer and/or lighter particles that get swept upwards by the displaced fluid (Davies, 1968). Based on experimental observations, Druitt (1995) suggested that the effect of hindered settling is clearly visible at intermediate sediment concentrations (20-44 vol%), and also is greater when the difference between particle size and/ or density is large.

Matrix Strength

Matrix strength represents an important mechanism of grain support in which the interstitial matrix composed of a mixture of clays and mud particles with water promotes an increase of particle cohesion within the flow, and subsequently generates sufficient strength to prevent the settling of large particles (Fig. 2.4f).

2.1.3. Submarine Channel

A submarine channel is a negative topographical element produced by confined turbidity currents that follow a major, long-term pathway or conduit for local basinward sediment transport (Fig. 2.5; Mutti and Normak, 1987). Submarine channels traverse the continental slope (inclined on average about 2-4 degrees, but up to 25 degrees).

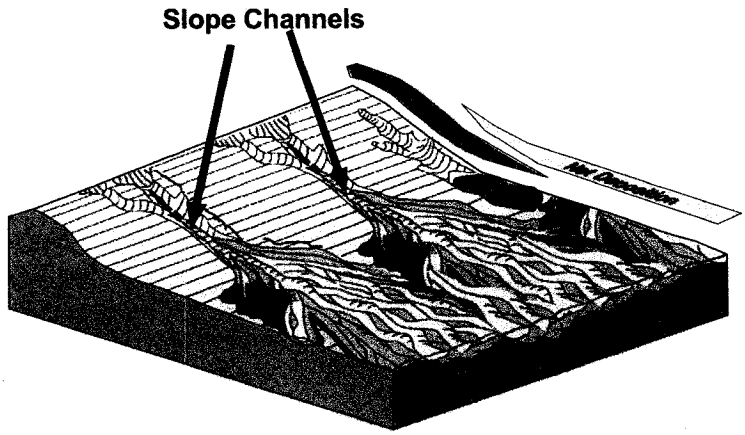

Figure 2.5. Submarine channels. They are major geomorphologic elements that provide the principal conduits for transport of sediment from the continental or shallow-marine/shelf to deep-marine environments.

2.1.3.1. Types of Submarine Channel

Three channel types are recognized in modern and ancient systems: erosional, depositional, and mixed erosional-depositional (Fig. 2.6; Mutti and Normak 1987). The origin and formation of each channel type is linked to characteristic processes, as discussed below.

Erosional Channels

An erosional channel is created by the erosion and local removal of the substrate (Fig. 2.6a). These channels are identified by (1) the lower elevation of the channel floor compared to the surrounding sea floor surface, (2) truncation of sidewall strata and (3) the lack of levees (Field et al., 1996).

Depositional Channel

Depositional channels are formed by deposition of sediment along the channel, forming channel-margin levees (Fig. 2.6b). This channel system consists of channel floor and levee system that with time (i.e. deposition) becomes increasingly more elevated above the surrounding sea floor.

Mixed Erosional-depositional Channel

A mixed channel is produce by a combination of channel-margin deposition (levees) and erosion of the substrate in the axis of the channel (Fig. 2.6c). Levees are usually present on

both sides of the channel and the channel floor may occur above or below the level of the surrounding sea floor.

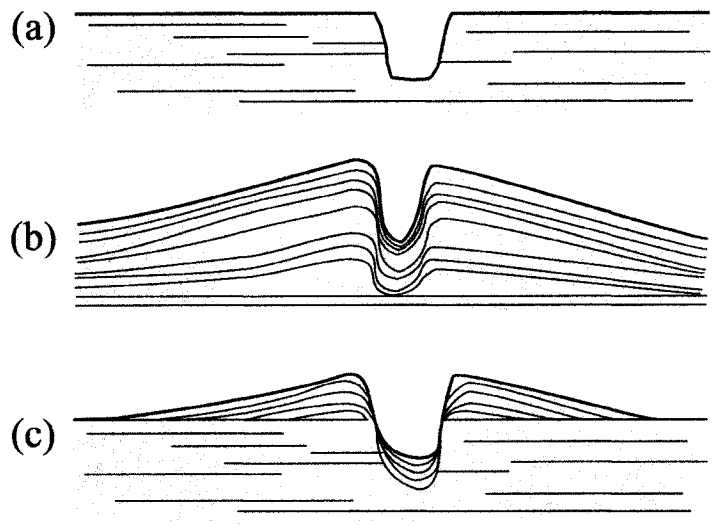

Figure 2.6. Submarine Channel types: a) erosional, b) depositional, and c) erosional-depositional or mixed (Modified from Pickering et al., 1995; after Lee, 2004).

2.1.3.2. Evolution of Submarine Channels

Based on the channel-fill model proposed by Pickering et al. (1995) and Clark and Pickering (1996), channel evolution (Fig. 2.7) is divided in four main stages or phases that can be repeated and involve inception, bypass, filling and abandonment.

1) Channel inception

This stage corresponds with channel initiation and is dominated by net erosion, where multiple erosive flows travel basinward and progressively incise and form a complex, stepped erosional surface (e.g. major deep scour). These channels thereafter become a conduit for basinward transport of sediment by gravity flows, but with nondeposition (Fig. 2.7a).

2) Channel bypass

Following the initial erosion stage and formation of the major down-cutting surface of the channel, large-volume flows mostly bypass, or traverse this natural conduit to reach more basinward areas (e.g Mutti, 1977).

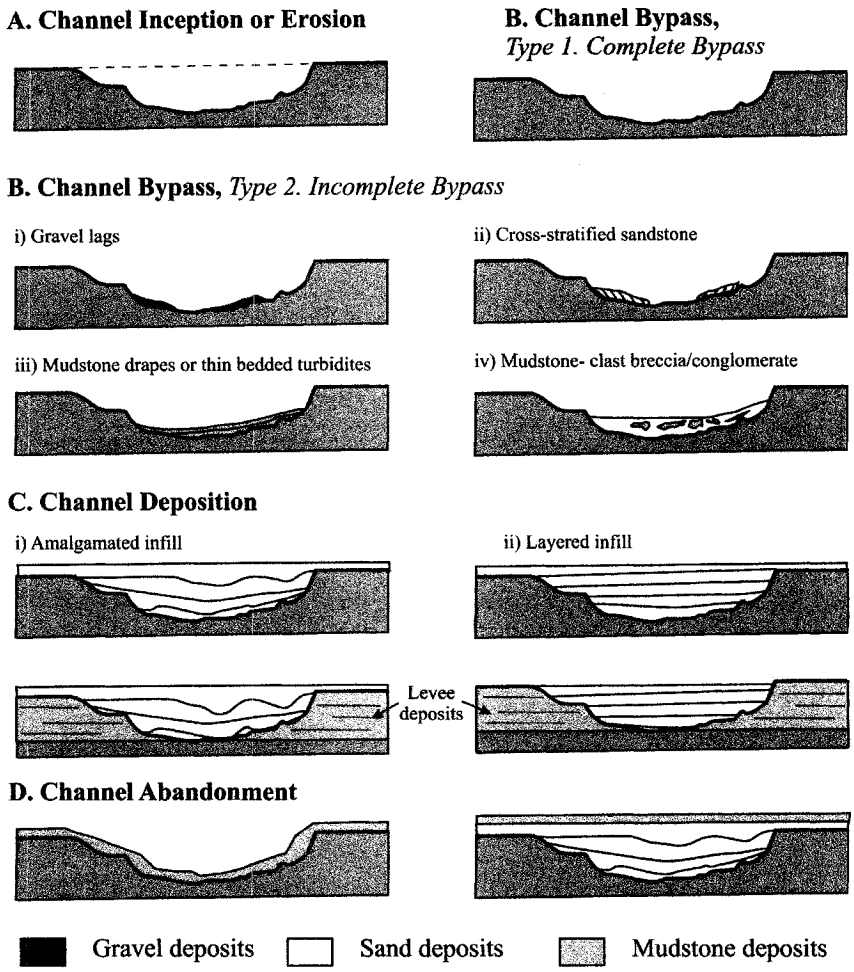

Figure 2.7. Major stages of channel evolution (Modified from Beaubouef et al., 1999): (1) erosion or inception, (2) bypass, (3) deposition and (4) abandonment. See the text for more detailed discussion.

There are different kinds of sediment by-pass (erosional and depositional) end-members, illustrated in Fig. 2.7b, termed complete and incomplete bypass, respectively. Complete bypass occurs where efficient flows transfer completely sediment to the basin with no additional erosion along the base of the channel but also no deposition. Incomplete bypass, on the other hand, occur where flows only partly transport the sediment. These flows therefore leave behind fractions of their load within the channel because of the progressive loss of momentum and competence. Bypass deposits are termed lag or residual deposits, and generally consist of thin and lenticular beds (Beaubouef et al., 1999).

Four types of incomplete-bypass deposits are recognized: (i) deposits that generally consist of the largest particles, commonly gravel, in the flow (cf. bypass type 1 of Beaubouef et al., 1999), (ii) deposits formed by intensive reworking of older sedimentary deposits by

traction currents along the channel bottom, developing cross stratification (cf. bypass type 1 of Beaubouef et al., 1999), (iii) deposits that consist of fine-grained turbidites left behind by tails of turbidity currents (cf. bypass type 2 of Beaubouef et al., 1999); and iv) deposits that were formed from irregular scouring of the channel floor, generating common mud intraclasts. At the same time sediments are bypassing the channel, levees are gradually being constructed to their maximum height along the channel margins by overspill and flow stripping. These processes attest to the magnitude of the flows moving through the channel. Levee construction confine progressively the intrachannel flows.

3) Channel filling

With time the efficiency of flows decreases because of diminution of volume and loss of momentum, so that sediment bypass consequently becomes reduced and levee growth is dramatically slowed. Gravel- and sand-rich flows become arrested within the channel. During the major depositional period of the channel infill (Fig. 2.7c), thick, laterally extensive (i) amalgamated or (ii) layered intrachannel deposits onlap or interfinger directly onto the margins of the channel, or onto the levee deposits that were constructed at their margins.

4) Channel abandonment

As flows continue to weaken and lose more momentum and competence, they eventually become unable to transport sediment through the channel, and the channel becomes abandoned. This stage could be caused by channel avulsion or relative sea-level rise (Beaubouef et al., 1999), and is characterized by an upward-thinning and -fining sequence, composed of fine-grained sediments that partially or completely fill residual topography (Fig. 2.7d).

2.2. FACIES DESCRIPTION AND INTERPRETATION

In this study, based on lithology, grain size, sorting, sedimentary structures, bed thickness, bed contacts and other relevant descriptive information, four major lithofacies and ten subfacies have been recognized in Channel 1 and 3 of the Lower Isaac Formation in the Castle Creek study area (Table 2.1). Each lithofacies is described in detail and interpreted below.

Facies	Subfacies		ıinant Grain Size/ Matrix	Sorting	Physical Sedimentary structures	Bed Thickness (range in meters)	Others	Comparative Facies	Interpretation
F1.Normally Graded to Massive Sandstone and Conglomerate	F1.1. Normally Graded Sandstone and Conglomerate	F1.1a. Normally Graded Conglomerate to Sandstone	ıle and pebble/ e to very coarse sand	Well Sorted	Normal Grading	Medium to very thick (0.2-7 m)	* Load structures * Horizontal sand injections * Pseudonodules	Ta[1], R3[2]	Differential settling during the gradual or rapid aggradation of single or multiple gravelly high-density turbidity or concentrated flows or a decrease of sediment supply associated with rapid waning flow
		F1.1b. Normally Graded Sandstone	coarse to coarse medium sand	Well Sorted	Normal Grading	Medium to very thick (0.1-2.6 m)	* Load structures * Flame structures	Ta[1], S3[2]	Differential settling during the gradual or rapid aggradation of single or multiple sandy high-density turbidity or concentrated flows or a decrease of sediment supply associated with rapid waning flow
	F1.2. Massive Sandstone and Conglomerate	F1.2a. Massive Conglomerate	ıle and pebble der)/ e sand	Poorly Sorted	None	Medium to very thick (0.1-4 m)	* Load bases	Ta[1], R3[2]	Rapid suspension deposition from single or multiple gravelly high-density turbidity or concentrated flows caused by progressive aggradation, with high aggradation rates caused by high sediment fallout
		F1.2b. Massive Sandstone	ıe sand	Poorly Sorted	None	Medium to very thick (up to 1 m)	* Minor load bases	Ta[1], S3[2]	Rapid suspension deposition from single or multiple sandy high-density turbidity or concentrated flows caused by progressive aggradation, with high aggradation rates caused by high sediment fallout
F2. Mudstone-clast Breccia									
	F2.1. Mudstone-clast Breccia		e to boulder/ ım sand up to pebble	Poorly Sorted	None	Thick to very thick (0.2-10.6 m)	* Injections	F3[3]	Suspension or "en masse" deposition from sandy-gravelly high-density turbidity currents or hyperconcentrated flows with abundant partially consolidated mud clasts, derived from erosion of underlying or lateral adjacent beds and/or upstream erosion and transport within flow.
	F2.2. Mudstone-clast Brecciated facies		e to boulder/ ım sand up to pebble	Poorly Sorted	None	Thick to very thick (0.36-1.5 m)	* Injections * Fragmentations of mudstone layers and clasts	F3[3]	Some clasts show post-depositional brecciation and soft-sediment deformation as a result of liquidization processes (liquefaction and/ or fluidization).
F3. Cross-stratified and Parallel stratified Sandstone	F3.1. Cross-stratified Sandstone		ıe and very coarse	Well Sorted	Cross-stratification	Thin to thick (0.05- 0.5m)	* Contorted cross-stratification	S1[2],F6[3]	Deposition under high-velocity unidirectional flow conditions from tractional reworking by sandy high-density turbidity currents or concentrated flows
	F3.2. Parallel-stratified Sandstone		ıe sand	Moderate to Well Sorted	Parallel lamination	Thin to medium (0.04- 0.16 m)		S1[2],F7[3]	Deposition under upper-flow regime conditions in sandy high-density turbidity currents or concentrated flows
F4. Sandstone interbedded with Mudstone and Unlaminated Mudstone		F4.1a. Structureless Sandstone and Mudstone	ıand and silty mud	Well sorted	None	Thin to medium (0.15- 0.3 m)	Flame structures	Ta? and Td-e[1]	Rapid suspension deposition with high sediment fallout with limited traction, followed by suspension deposition of mud
	F4.1 Sandstone interbedded with Mudstone	F4.1b. Laminated Sandstone and Mudstone	ım to very fine sand lty mud	Well sorted	Parallel Lamination	Very thin to thick (0.03- 0.4 m)	Flame structures	Tb and Td-e[1]	Deposition under high energy upper- flow- regime plane bed conditions, followed by mud deposition
		F4.1c. Rippled Sandstone and Mudstone	Fine to very fine sand and silty mud (to silt)	Well sorted	Cross-lamination	Very thin to medium (0.02- 0.15 m)	* Flame structures * Convolute structures	Tc and Td-e[1]	Traction plus sediment fallout deposition under lower flow regime ripple conditions, followed by mud deposition
	F4.2. Mudstone		Silty mud or clay	Well Sorted	None	Very thin to thick (0.2- 5 m)	Flame structures	Td or Te[1]	Low energy suspension deposition from a waning turbidity current, or hemipelagic suspension deposition

[1] Bouma (1962), [2] Lowe (1982), [3] Mutti (1992)

Table 2.1. Summary of facies and subfacies described in this study.

2.2.1. F1. Normally Graded to Massive Conglomerate and Sandstone

One of the most common facies in the intrachannel deposits of Channel 1 and 3 is normally graded and massive sandstone and conglomerate, representing subfacies F1.1 and F1.2 respectively. These strata make up a considerable proportion of the Facies Association FA3.

2.2.1.1. F1.1. Normally Graded Conglomerate to Sandstone and Normally Graded Sandstone

Many conglomerate and sandstone beds (subfacies F1.1.a and F1.1b respectively), principally in Channel 1 are coarse-tail graded. Some beds, however, are only graded in the upper part of the bed.

F1.1a. Normally Graded Conglomerate to Sandstone

Normally graded conglomerate to sandstone beds consist of clast-supported granule to pebbly conglomerate that grade upward to coarse or very coarse sandstone. Beds range from 0.22 to 6.5 m thick, with a modal thickness around 1.5 m. Generally very thick beds, up to 7 m thick in Channel 1 and 2.36 in Channel 3, consist of amalgamated or partly amalgamated beds. In the conglomeratic part of the bed, the dominant clast size is granule and fine pebble (0.3 to 0.5 cm) with a coarse to very coarse sandstone matrix. Local coarse pebble-size quartz clasts (up to 3 cm long) are also present. Larger clasts ranging from 0.3 to greater than 45 cm, with a mode of approximately 1-2 cm are more common in Channel 3 (Fig. 2.8). Sub-angular to sub-rounded grains of quartz (grey, white, and blue) are abundant, and feldspar clasts (white) are rare to common. Large carbonate clasts (brown-orange weathered) occur only in Channel 3, and with variable abundance (up to 20%). Additionally, elongated mudstone clasts are rare to common with dimensions that range from 0.10 to 1.5 m.

Bed bases are generally erosive and dominated by gentle or shallow scours. Loaded and undulatory basal contacts are also common. Local scour-load surfaces are observed as well (Fig. 2.9). Soft-sediment deformation structures are locally developed, including: (1) extensive basal load casts (Fig. 2.10) with irregular protuberances or lobes up to 30 to 50 cm deep, (2) horizontal sand injections that are up to 25 cm long and are observed locally at the base of conglomerate and sandstone beds, (3) flames structures in the underlying fine

sandstone and mudstone beds (Fig. 2.11), and (4) localized pseudonodules or "ball-and-pillow" structures are formed by multiple beds or layers and have dimensions that range from 0.62 to 2.5 m in length and from 0.23 to 0.9 m in height (Fig. 2.12). Individual conglomerate beds are laterally discontinuous and typically traceable for only a few tens of meters.

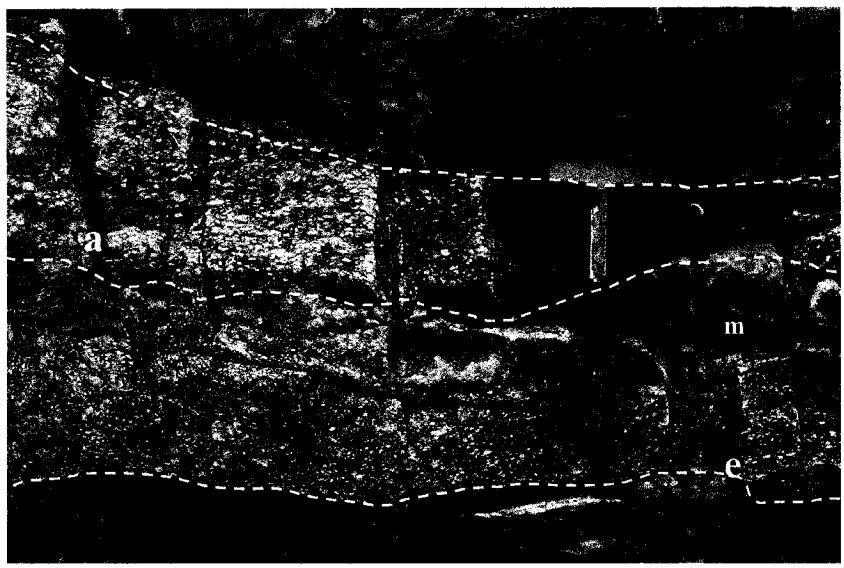

Figure 2.8. Subfacies F1.1a, normal graded conglomerate beds in Channel 3, showing typical erosive bases (e) and amalgamation surfaces (a). Light gray quartz and white feldspar clasts are abundant, and large mudstone clasts (m) are observed locally. The top and bottom of the beds are marked by dashed lines.

Figure 2.9. Common scour-load structures in a normally graded sandstone bed (subfacies F1.1a) in Channel 3. Note the "U"-shape scour (arrow) that later was loaded.

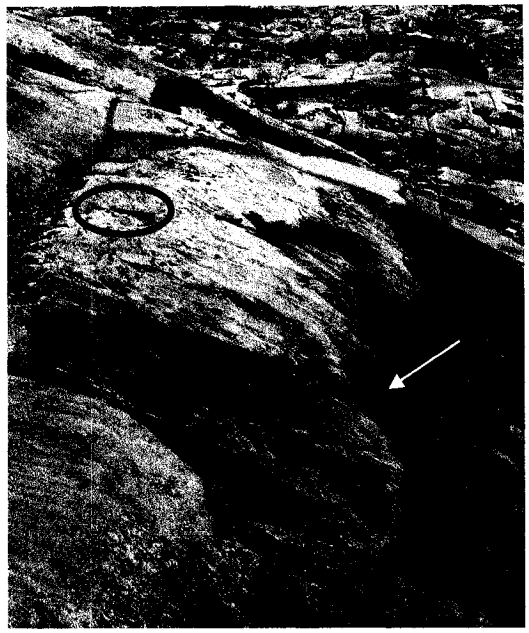

Figure 2.10. Typical load casts in a normally graded granule conglomerate (subfacies F1.1a) in Channel 1. Note the extensive, decimeter-scale protuberances (arrow) at the base of a thick amalgamated bed. Hammer for scale.

Figure 2.11. Load structure on the base of a normally graded granule conglomerate bed (Facies 1.1a) in Channel 1 that has a flame of fine sandstone and mudstone squeezed upward between them.

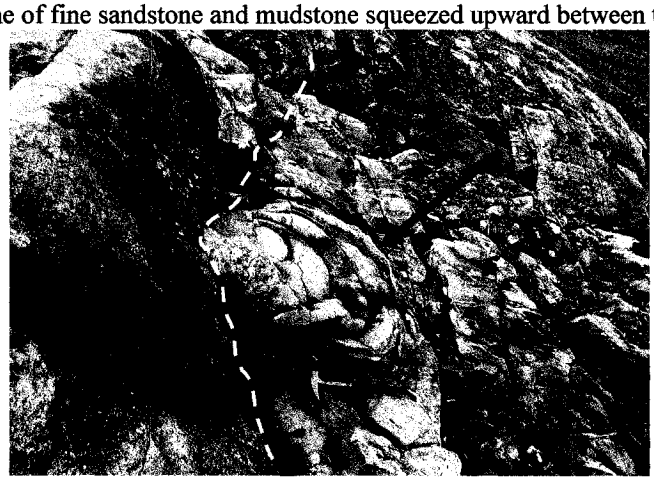

Figure 2.12. Ball-and pillow, or pseudonodule structures in normally graded conglomerate and sandstone beds (subfacies F1.1a) in Channel 3. Note the meter-scale pseudonodule (arrow). The top of the structure is truncated by an erosion surface (dashed line).

F1.1b. Normally Graded Sandstone

In general, this subfacies consists of very coarse sandstone that grades vertically upward to coarse or medium sandstone. Locally, dispersed up to 1 m-long (boulder size) mudstone clasts are present, especially at the base or at the top of beds. Quartz or feldspar clasts, smaller than 5 cm (granule to cobble), are locally observed above the bed bases. Normally graded sandstone beds range from 0.1 to 2.6 m thick in Channel 1, and to 1.92 m thick in Channel 3. Like strata of subfacies F1.1a, strata of subfacies F1.1b are commonly amalgamated and laterally discontinuous, and locally are pinched out or eroded. Beds are typical erosionally based, showing characteristic concave upward and mud-draped scours. Combined (erosive and loaded), loaded and undulatory bases are also present. Very irregular load and flame structures are common at the base of beds. Load structures are up to 60 cm deep.

2.2.1.2. F1.2. Massive Sandstone and Conglomerate

Subfacies F1.2 consists of massive conglomerate (subfacies F1.2a) and sandstone (subfacies 1.2b). They are more common in Channel 3.

F1.2a. Massive Conglomerate

Subfacies F1.2a consist of 0.1 to 4 m thick beds (up to 2.15 m thick in the Channel 3) of poorly sorted, clast-supported conglomerate (Fig. 2.13). Clasts average between 0.4 and 0.6 cm (granule to pebble), but some are up to 4 cm (pebble). The matrix is coarse sandstone, although medium and very coarse sandstone are also observed. Sub-rounded quartz and feldspar clasts are common to abundant. Locally in Channel 3, pebble- to boulder- size carbonate (Fig. 2.14) and mudstone clasts are common to rare with the long-axes are more than 10 cm long. Mudstone clasts range from irregular elongate to angular flat shapes. Carbonate clasts are typically rounded and contain mostly grains of ooids, composite ooids, peloids and stromatolite intraclasts.

Basal bedding contacts are diffuse, and beds with more than 2 m thick tend to be amalgamated. Wavy or undulatory and erosional bases are also observed (Fig. 2.13). Beds can generally be followed for few hundreds meters laterally.

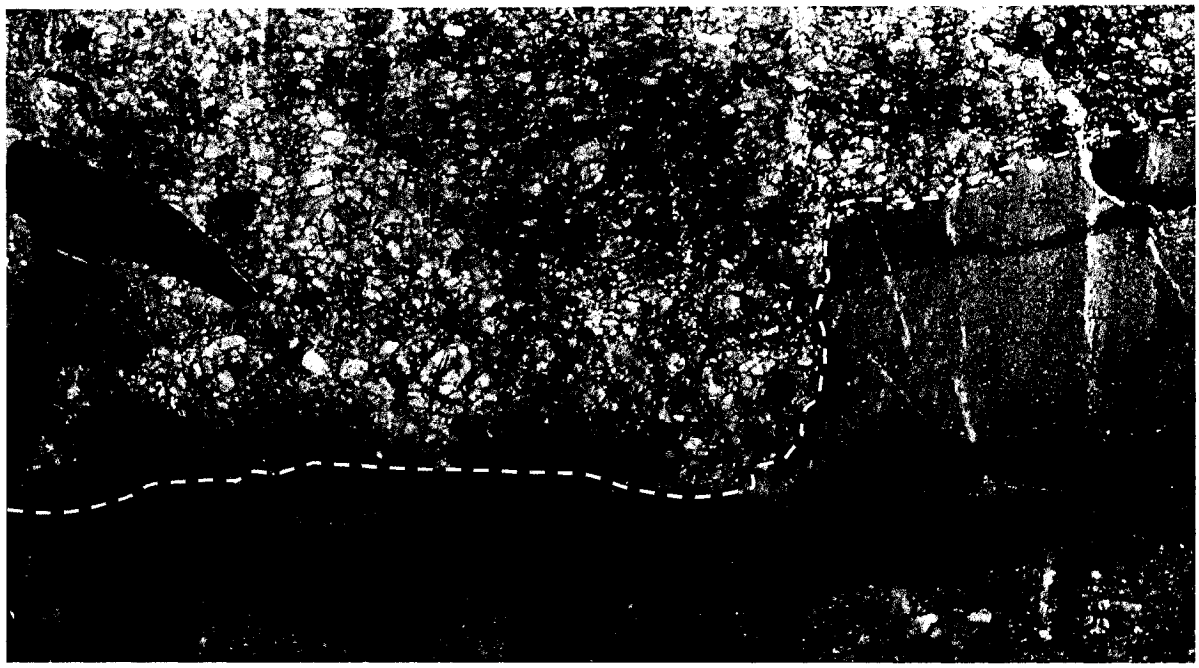

Figure 2.13. Massive conglomerate of subfacies F1.2a in Channel 3. Note the irregular scour (dashed line) at the base of a thick bed. The abundance of quartz and/or feldspar (white) pebble clasts

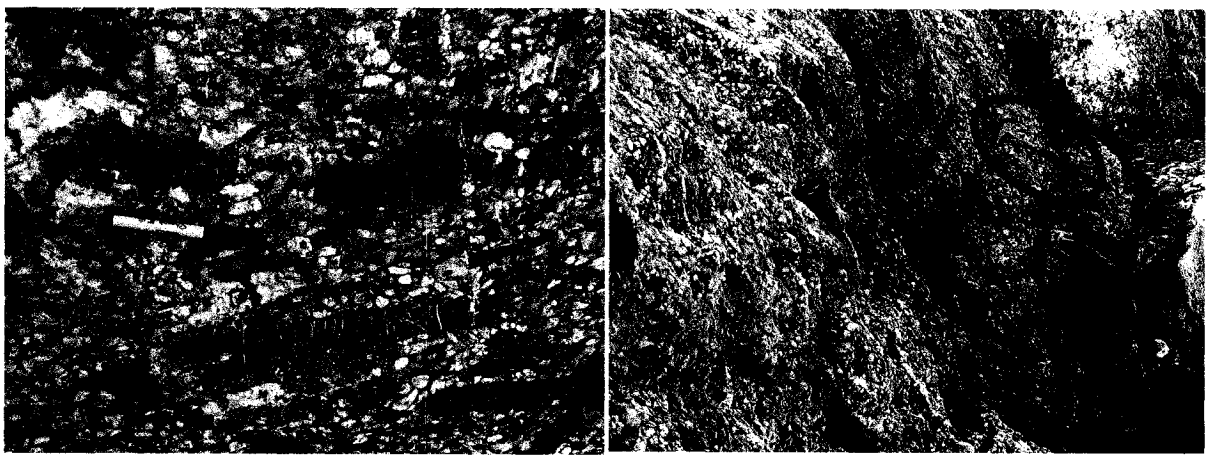

Figure 2.14. Pebble conglomerate of subfacies F1.2a, massive conglomerate in Channel 3. Note the dispersed large carbonate clasts (brown-orange weathered) that are embedded in a coarse-grained matrix. This matrix contain abundant quartz and feldspar pebbles. Carbonate clasts are up to boulder size (right photo).

F1.2b. Massive Sandstone

Massive sandstone consists of medium- to thick-bedded (up to about 1 m) sandstone (Fig. 2.15) that is typically coarse grained, although some beds are very coarse, medium or fine. Locally, beds contain dispersed large mudstone clasts several centimeters up to 25 cm long (boulder) at the base. The bases of massive sandstone beds are typically erosional and

loaded. Common load structures occurs along their undulatory bases are also observed. Water-escape structures were not observed.

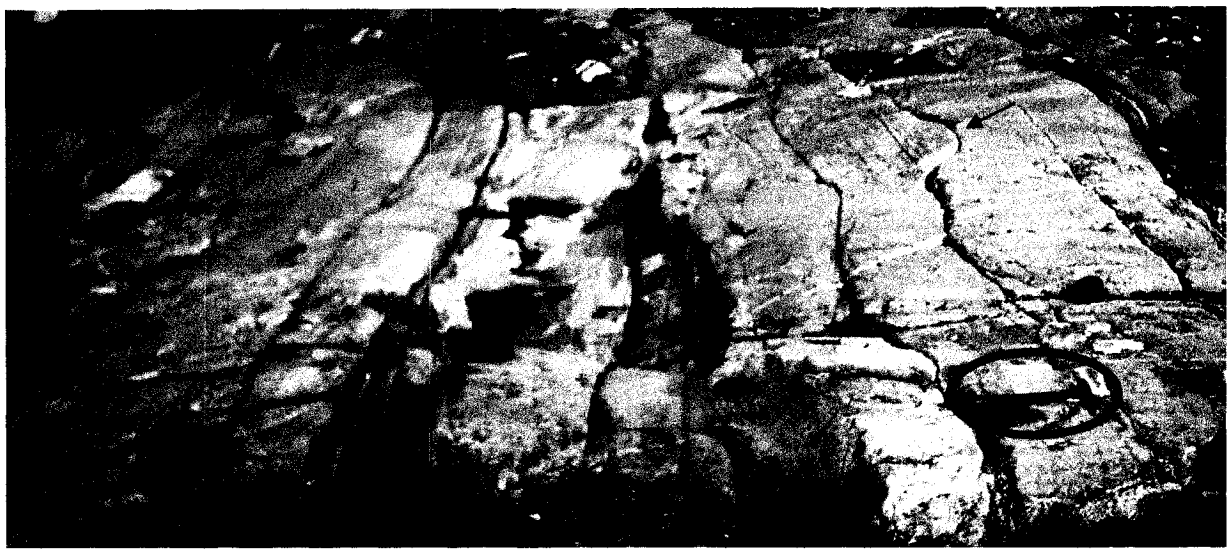

Figure 2.15. Massive and normally graded sandstone beds of subfacies F1 in Channel 3. Note the U-shaped scour (arrow).

2.2.1.3. Petrography and X-Ray diffraction

Petrographic analysis

For location of samples see Appendix I and for tabulated data of petrographic results and photomicrographs of siliciclastic facies F1, see Table II.1 and II.2 and Figs. II.1-II.15 in Appendix II.

Conglomerate

Granule conglomerate of facies F1 are classified as petromict, and consist primarily of polycrystalline quartz clasts (>70%). The next most abundant grain types are monocrystalline quartz with strong undulatory extinction, and feldspar. The conglomerate beds are extremely poorly sorted, and contain high percentages of matrix, including silt to very coarse-sand detrital grains and recrystallized matrix. Detrital grains are mostly monocrystalline quartz and feldspar (plagioclase and alkali feldspar). Feldspar grains are generally fractured or altered, and some also show perthitic intergrowths. The recrystallized matrix consists of fine-grained quartz, muscovite and chlorite, plus small amounts of

tourmaline, chlorite, zircon and pyrite. Some conglomerate beds have a micritic matrix or sparry calcite cement.

Sandstone

Most coarse to very coarse- sandstones of facies F1 classify as sub-feldspathic and feldspathic arenites, generally with 4-9 % feldspar, but some contain as much as 15% feldspar. Feldspar grains are mostly plagioclase and K-feldspar. Some alkali feldspar grains show perthitic texture (e.g. lamellar intergrowth of Na-rich feldspar in a K-rich feldspar). Some plagioclase show partitioned and bent twining. Monocrystalline quartz with very undulose extinction is the most abundant grain (> 40%). Polycrystalline quartz with a polygonal fabric of interlocking crystals and with elongated, lenticular, interlocking, sutured crystals are also common, especially in conglomerate, which typically make up 2-15% and exceptionally as much as 30% of the grains. Lithic rock fragments are present only in trace amounts, including siltstone and sandstone clasts. Detrital mica, principally muscovite, is a common component of these sandstones, comprising up to 2% of the grains. Diagenetic and post-diagenetic pyrite grains are common (up to 3%), and show framboid and cubic shapes respectively. Pyrite grains typically show partial or complete replacement by Fe-oxyhydroxides (mostly goethite). Zircon, epidote, biotite, chlorite and tourmaline are other minerals observed. Some deformed chloritized grains were observed.

Most sandstones have considerable percentages (up to 35%) of recrystallized matrix (related to the Mesozoic metamorphism) composed of finely crystalline quartz, muscovite and/or chlorite. The sandstones normally contain altered feldspars, forming secondary matrix or pseudomatrix that later was recrystallized. Interstitial sparry calcite cement is common, up to 20%. Rhombic ferroan dolomite crystals occurs in conjunction with calcite cement, as a dolomitized or dedolomitized replacement. Quartz overgrowths are also observed.

Carbonate clasts

Five groups of carbonate clasts were recognized in the Channel 3 (see petrographic results and photomicrographs in Table II.3 and Figs. II.16-II.28 in Appendix II). One group is composed mostly of microspar (4-30 μ m) as a result of neomorphism of a primary micritic matrix. These clasts of microsparite or mudstone (classification of Folk, 1962 and Dunham, 1962, respectively) contain a small percentage (less than 5%) of detrital quartz. A second

group consists of completely dolomitized mudstone. These clasts originally consisted of micrite or microcrystalline calcite (<5 μm) that were first have been neomorphosed to microspar and then almost completely dolomitized to a mosaic of fine crystalline dolomite. Some dolomite crystals are zoned. Additionally, up to 2% detrital quartz (with the exception of one sample that has 30%), and traces of muscovite and pyrite were identified. Interstitial spar cement and microfractures filled with calcite and quartz are commonly observed.

A third group consists predominantly of spar (>50 μm) as a result of neomorphism of a micritic matrix or of pore-filling cement. Clasts of sparite or crystalline carbonate (classification of Folk, 1962 and Dunham, 1962) include an important percentage (more than 15%) of detrital quartz. A fourth group of carbonate clasts is found exclusively in channel-fill conglomerate, containing abundant allochems such as ooids and composite ooids, or recrystallized peloids. Even though matrix and allochems in these clasts have been selectively recrystallized to microspar, pseudospar and/or spar, and later dolomitized, signs of original fabric are relatively well-preserved. At least two or three generations of carbonate cement are observed: fine-, medium- and coarse- crystalline cements, in which the first two are closely related.

In addition to the previously described clasts, another group of carbonate clasts is typical of the debrite unit (see petrographic results and photomicrographs in Table II.4 and Figs. II.29-II.32 in Appendix II) that underlies Channel 3. It is composed of carbonate fragments with crypto-algal features (resembling stromatolite, and classified as biolithite or boundstone according to Folk, 1962 and Dunham, 1962, respectively) with small percentage (less than 5%) of detrital quartz. These fragments exhibit a distinctive layered structure, where layers of micrite that have been neomorphosed to microspar are interbedded with layers of irregular, elongated fenestral pore-spaces filled with dark micrite, possibly representing the original microbial mat layer. Some clasts have been partially dolomitized.

XRD analyses: Carbonate clasts

Minerals identified from carbonate clasts sampled from intrachannel deposits of Channel 3, and underlying debrite, include dolomite, ankerite and occasionally calcite (Table III.1, Appendix III). Quartz, muscovite and plagioclase are other minerals recognized.

2.2.1.4. Interpretation

Facies 1 corresponds to the basal T_a division of a classical Bouma sequence (Fig. 2.2, Bouma, 1962). The Bouma A-division is a matter of much debate, and has been attributed to deposition from (1) turbulent suspension (Bouma, 1962; Middleton and Hampton, 1973), (2) antidune phase of the upper-flow-regime (Harms and Fahnestock, 1965; Walker 1967), (3) high-density turbidity currents (Lowe, 1982), (4) sandy debris flows (Shanmugam, 1996, 1997), (5) sustained, high-density turbidity currents (Kneller and Branney, 1995; Branney and Kokelaar, 1999), (6) concentrated flows (Mulder and Alexander, 2001), and others. In this study, Facies 1 is interpreted to have been deposited from single or multiple sandy or gravelly, high-density turbidity flows (Fig. 2.2; Lowe, 1982) or similarly concentrated flows (Mulder and Alexander, 2001). This facies is equivalent with the S3 and R3 division of Lowe (1982).

High-density or high-concentration flows are generally interpreted to be highly stratified. Stratified or bipartite flows (Fig. 2.16) are composed of two parts: lower and upper. The lower part contains a sediment volume concentration that is sufficiently high to damp turbulence (above 10 vol% based on Bagnold, 1954), but not so high as to cause frictional freezing. In this part of the flows, hindered settling (see introductory section 2.1.2.2, p. 34) becomes an important sediment-support mechanism and adds to the suppression of turbulence (Li and Davies, 2001). The upper part of the flow, on the other hand, has lower sediment concentration and is mostly supported by fluid turbulence.

Coarse-grained flows with a thick turbulent upper part tend to deposit coarse-tail graded beds (Russell and Arnott, 2003). These beds suggest differential grain settling during deposition from concentrated flows (Mulder and Alexander, 2001), or a decrease in coarse sediment supply associated with a depletive or rapidly waning flow (Kneller and Branney, 1995; Kneller, 1995). Normal graded bedding in high-concentration flows has been commonly reported from the geological literature, and dates back to the early works of Kuenen and Migliorini (1950) and Kuenen (1953). More recently, however, Kneller (1995) and Shamungan (2002) point out that in many cases normal graded beds are depositionally complex.

Coarse-grained flows with a thick frictional basal part form massive deposits. These deposits suggest higher instantaneous rates of sediment deposition beneath a rapidly

collapsing turbulent suspension (Middleton and Hampton, 1973; Arnott and Hand, 1989; Allen, 1991; Vrolijk and Southard, 1997; Russell and Arnott, 2003).

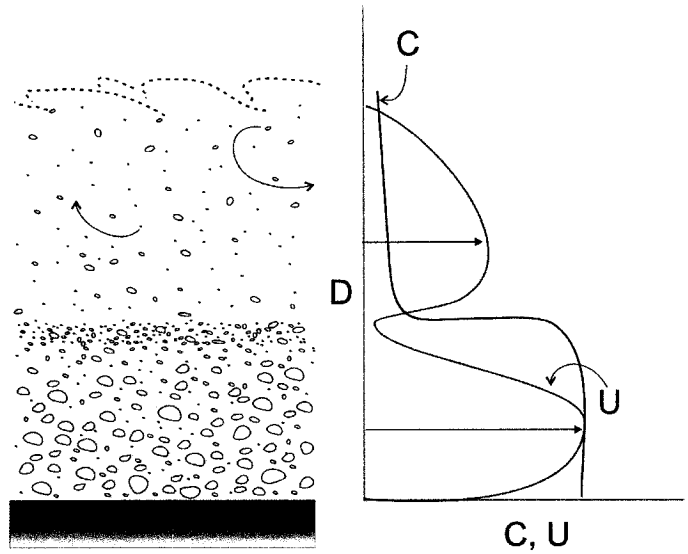

Figure 2.16. Schematic cross-section of a high-density or concentrated flow (Modified from Branney and Kokelaar, 1998). The sediment concentration (C) and velocity (U) profiles measured from the bed thickness (T) are shown in the right. Note the high sediment concentration in the basal part of the flow and the low concentration and high turbulence in the upper part. Some authors (Vrolijk and Southard, 1997; Branney and Kokelaar, 1998) have experimentally observed that a low-velocity layer occurs between the two portions of the flow.

Alternative theories of how high-concentration flows deposit, such as progressive aggradation, cannot be verified in this study area. This theory is based on the assumption that deposition occurs from sustained high-density turbidity currents with a non-turbulent, low-velocity layer (depositional boundary layer of Branney and Kokelaar, 1992; or the laminar sheared layer by Vrolijk and Southard, 1997). The intermediate layer between the non-turbulent lowermost part of the flow and the turbulent upper part of the flow occurs initially near the substrate and progressively moves upward during bed aggradation (Branney and Kokelaar, 1992). Features which are commonly associated with these deposits, such as dewatering structures, were not observed in this study.

Large or "outsized" mudstone clasts commonly occur in the middle or top of Facies 1 beds. These clasts may be the result of erosion by high-density or concentrate flows and then preferentially transported along a density interface in the density-stratified flow (Fig. 2.17; Postma et al., 1988). Clasts glide and are supported by buoyancy, and accumulate along the density interface as a result of selective particle filtering according to clast density (Branney and Kokelaar, 2002). Buoyancy (see introductory section 2.1.2.2., p. 33-34) decreases the

effective settling velocity of these particles and delays its deposition (Druit, 1995). Consequently, these clasts are buoyed above the flow boundary layer and are unable to sink through it (Branney and Kokelaar, 2002). When the lower laminar part of the flow freezes or aggrades upward, the clasts stop gliding ("floating") and deposit along the position of the interface.

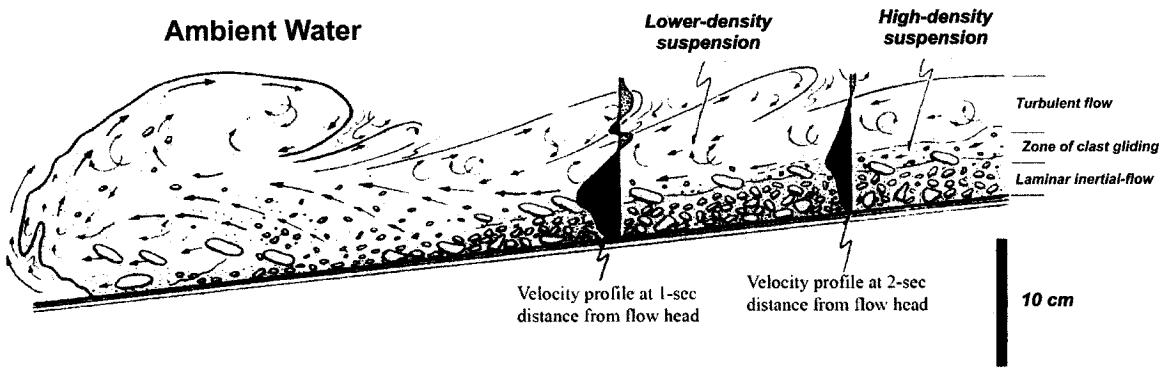

Figure 2.17. Sketch of an experimental high-density, surge-type turbidity current moving along a 25° slope, and head velocity of 108 cm/sec. Larger clasts preferentially glide in the body of the flow and also along the rheological interface (highlighted pinkish zone) between the non-turbulent (laminar inertia) lower part of the flow and turbulent upper part (modified from Postma et al., 1988; p. 51).

Postdepositional structures, such as load and flame structures, ball-and-pillow and horizontal injections are common in strata of Channel 1 and 3, and are interpreted as indicators of soft-sediment deformation by liquidization or liquification processes (i.e. fluidization and/or liquefaction). For a more detailed discussion of these terms see p. 65. Loaded and undulatory bases and flame structures are common along the contact between conglomerate or sandstone (facies F1) and mudstone (facies F4). The latter facies will be discussed below in section 2.2.4., p 74. These structures are associated with liquefaction of a poorly consolidated (water saturated) underlying mud layer because of rapid deposition of the coarse sediment, which forms a density inversion between the overlying coarser, denser sediment and the underlying fine-grained sediment layer. Gravitational instability along the interface between these layers caused the overlying dense sediment (mostly sand) to partially sink into the underlying, muddy sediment, forming load casts and flame structures (Fig. 2.18). More intensive liquefaction resulted in the formation of laterally extensive ball-and-pillow or pseudonodule structures, in which coarse sand becomes isolated and enveloped in the finer sediment. Pseudonodules observed in the study area (Channel 3) are erosionally

truncated on their upper part, indicating that deformation occurs during deposition. Sand injections that intrude into underlying or laterally adjacent thick, fine-grained strata suggest that locally the sand become liquefied, and driven by high pore pressures, was squeezed into the less permeable, cohesive sediment.

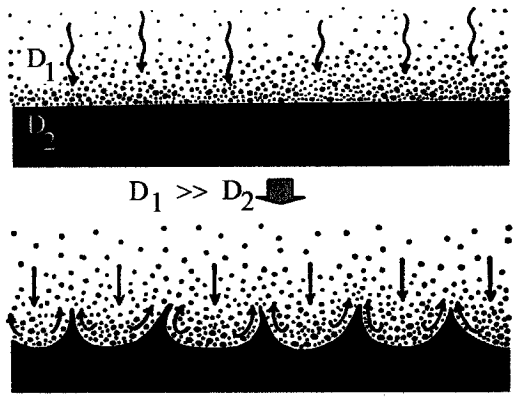

Figure 2.18. Formation of load and flame structures (modified from Ricci Lucci, 1995). Due to the difference of densities between D_1 (sand) and D_2 (mud), the sand layer (D_1) sinks as bulbous or rounded lobes (loads) into D_2. In the case of flame structures, the sinking sand causes the lower density mud to be squeezed upward as upward-taping protrusions (resembling flames).

Provenance

Pervasive alteration of feldspars to clay minerals and subsequent formation of pseudomatrix is observed in samples of facies F1. This secondary matrix or pseudomatrix of Dickinson (1970) was formed by mechanical compaction and squeezing of these ductile or labile grains into intergranular pore space during burial, which became recrystallized to fine white mica (i.e. muscovite) and chlorite. Since the proportion of pseudomatrix in these sandstones exceeds 10% in some cases, the original percentage of feldspars was greater than what is now observed. Therefore, the principal source of detritus for the passive-margin slope deposits of Channel 1 and 3 was immature (feldspathic-rich). Moreover, the abundance of mechanically and chemically unstable minerals, like feldspar, indicates that erosion was rapid and that transport was rather short before deposition. In other words, they probably have a relatively local origin. The preservation of perthitic textures in some feldspars suggests that they were derived from a plutonic (possibly granitic) source from the adjacent cratonic Canadian Shield.

The carbonate clasts in deposits of Channel 3 indicate a distinctive change in provenance during the deposition of this stratigraphic unit. Some of these clasts are ooids and composite ooids, which suggest derivation from a coeval tropical or subtropical carbonate platform, where water was, at least locally, relatively shallow (5 to 15 m deep) and high-energy (Tucker, 2001). Different textural generations of cements indicate that early phases of cementation occurred in these rocks (early diagenesis) and was affected considerably by later episodes of dissolution, cementation, and dolomitization.

2.2.2. F2. Mudstone-clast Breccia

This facies is common in Channel 1 and 3, especially in facies associations FA1 and FA2.

2.2.2.1. F2.1. Mudstone-clast breccia

Facies 2 consists of ungraded, structureless, mudstone-clast conglomerate and/or breccia that are clast- or matrix-supported, with percentage of mudstone clast greater than 15%. Silty mudstone clasts range from pebble (5 cm) to boulder (average 75-100 cm), however larger clasts are observed locally in Channel 1, ranging up to boulder size (e.g. 2 m, Fig. 2.19). Clasts exhibit a typical greyish color, but some are black. Clasts also are generally elongated (Fig. 2.20), and show a random or more common sub-parallel-to-bedding fabric. The matrix comprises a poorly sorted mix of grains that range from medium sand to pebbles (up to 3.5 cm). Beds are a few decimeters (0.2 m) up to 10.6 m thick in Channel 1 and up to 8.5 m thick in Channel 3. On average, beds are 0.8 m thick in Channel 1 and 1.2 m thick in Channel 3.

Where mudstone gravel clasts are very angular to angular, the rock is classified as a breccia; where clasts are sub-rounded to rounded, they are classified as conglomerates. However most mudstone clasts are angular. These clasts are silty and locally laminated or interstratified with fine sandstone. Primary sedimentary structures, including parallel lamination and cross-lamination commonly occur in the sandstone layers (Fig. 2.21). Minor clay-rich mudstone clasts are also observed. The base of Facies F2.1 is erosive, indicated by extensive deep and shallow scours. Thick beds (greater than 2 m) locally correspond to highly amalgamated beds in both Channels 1 and 3, including local lenses of conglomerate and sandstone. Injection features are observed locally and water escape structures are absent.

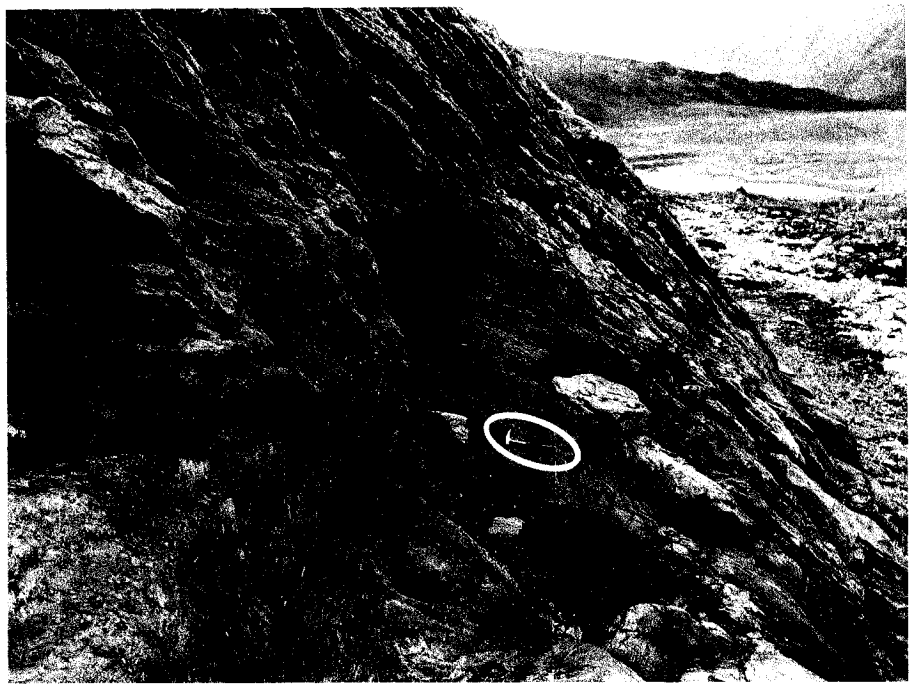

Figure 2.19. Boulder mudstone clast embedded in an amalgamated Facies 2 bed in Channel 1.

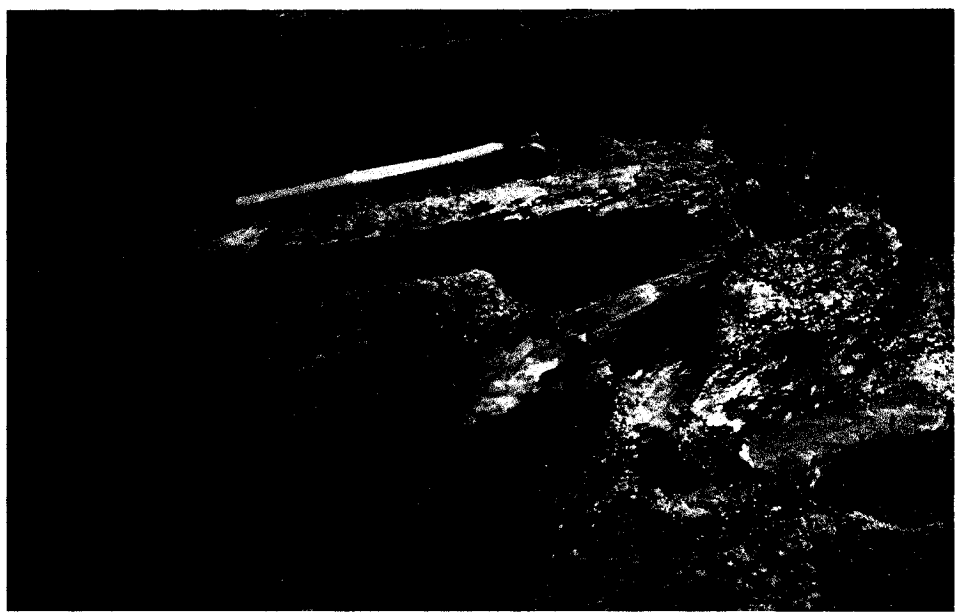

Figure 2.20. Grey elongated boulder mudstone clast in Facies 2, Channel 3. The matrix is composed of granule to coarse sandstone.

Figure 2.21. Elongated, boulder mudstone clast (grey) in Facies 2, Channel 1; showing internally parallel laminated fine sandstone.

2.2.2.2. F2.2. Mudstone-clast brecciated facies

Subfacies F2.2 consists of ungraded, structureless clast-supported breccia. In comparison with the clasts in facies F2.1, mudstone clasts of subfacies F2.2 show uncommon shapes (Fig. 2.22) and are closely packed, with the matrix filling small fissures and spaces between them.

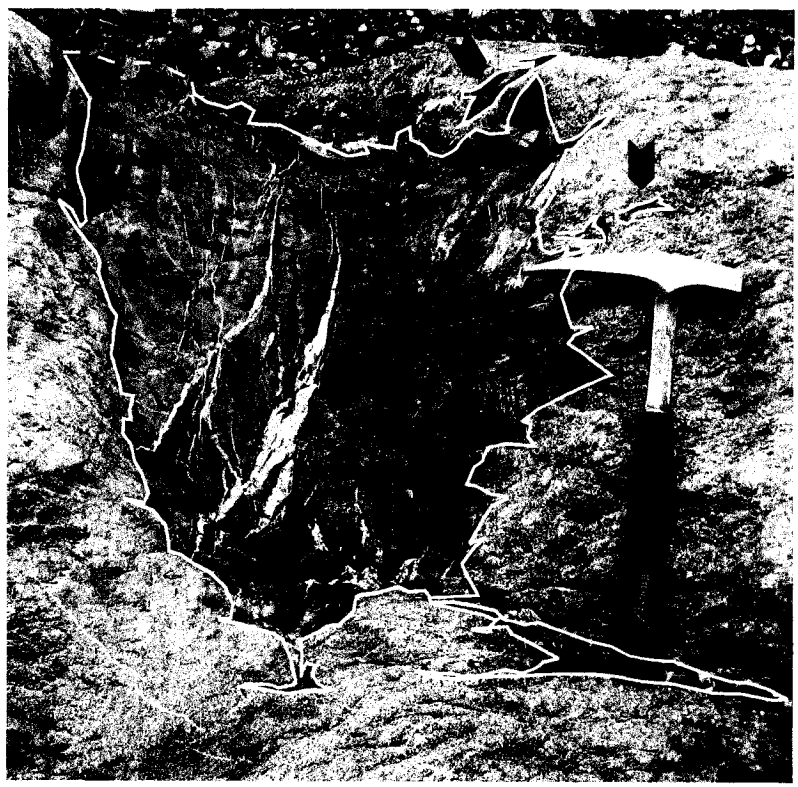

Figure 2.22. Angular mudstone clast with conspicuously jagged edges (Channel 1). Note the irregular and ragged margins of the clast, in which the sand matrix appears to be wedged and injected, producing a serrate mudstone clast that in places has been partially fragmented (arrows).

Silty mudstone clasts range from pebbles (3 cm) to boulders (150 cm), and exhibit a distinctive grey color and sub-parallel-to-bedding fabric. Some mudstone clasts exhibit local internal lamination, including interstratified fine sandstone, showing well-preserved parallel or cross-lamination. The matrix is poorly sorted, comprising a mix of grains that range from coarse sand to pebbles (up to 2.5 cm); isolated patches of coarser grains are observed locally (Fig. 2.23).

Clasts consist of diffusely laminated mudstone or interstratified mudstone and fine sandstone. Based on their unusual shapes, there are three main types of mudstone clasts in subfacies F2.2. One is distinguished by large clasts with slab or blocky shapes, that are 2-20 cm thick and 15-210 cm long. Thus, they show a high ratio between the long and the short axes that ranges from 7 to 10. Moreover, the surface of the long sides of these clasts is smooth and flat, whereas the margin of their short sides are rounded, pointed or irregularly serrated (Fig. 2.24, 2.25). Another type of mudstone clasts is represented by small to large clasts with platy forms (0.5-5 cm thick and 7-43 cm long); in which their ratio of long:short axes is high, from 8 to 15. Characteristically, these clasts are sharply pointed and have irregular edges (Fig. 2.23). The third type of mudstone clast is characterized by very angular clasts with variable sizes that range from 0.8-39 cm thick and 2-67 cm long. These clasts show atypical shapes, in some cases contorted and deformed, with extremely jagged borders (Fig. 2.22, 2.25, 2.26). These clasts appear partly or totally detached from other mudstone clasts or beds.

Breccia beds are generally a few decimeters (0.3 up to 0.76 m) to 1.5 meter thick, and are interbedded between thick beds of coarse sandstone or conglomerate (facies F1) that exhibit diffuse or erosive upper and/or lower contacts. Clastic injections are common, and typically oriented parallel to laminations within the mudstone (Fig. 2.24, 2.25). Injected sand was sourced from laterally adjacent, underlying and/or overlying coarse-grained beds (Fig. 2.25). Laterally, breccia strata grade into layers of mudstone or mudstone interbedded with fine sandstone that locally show erosive upper contacts and horizontal clastic injections (Fig. 2.24).

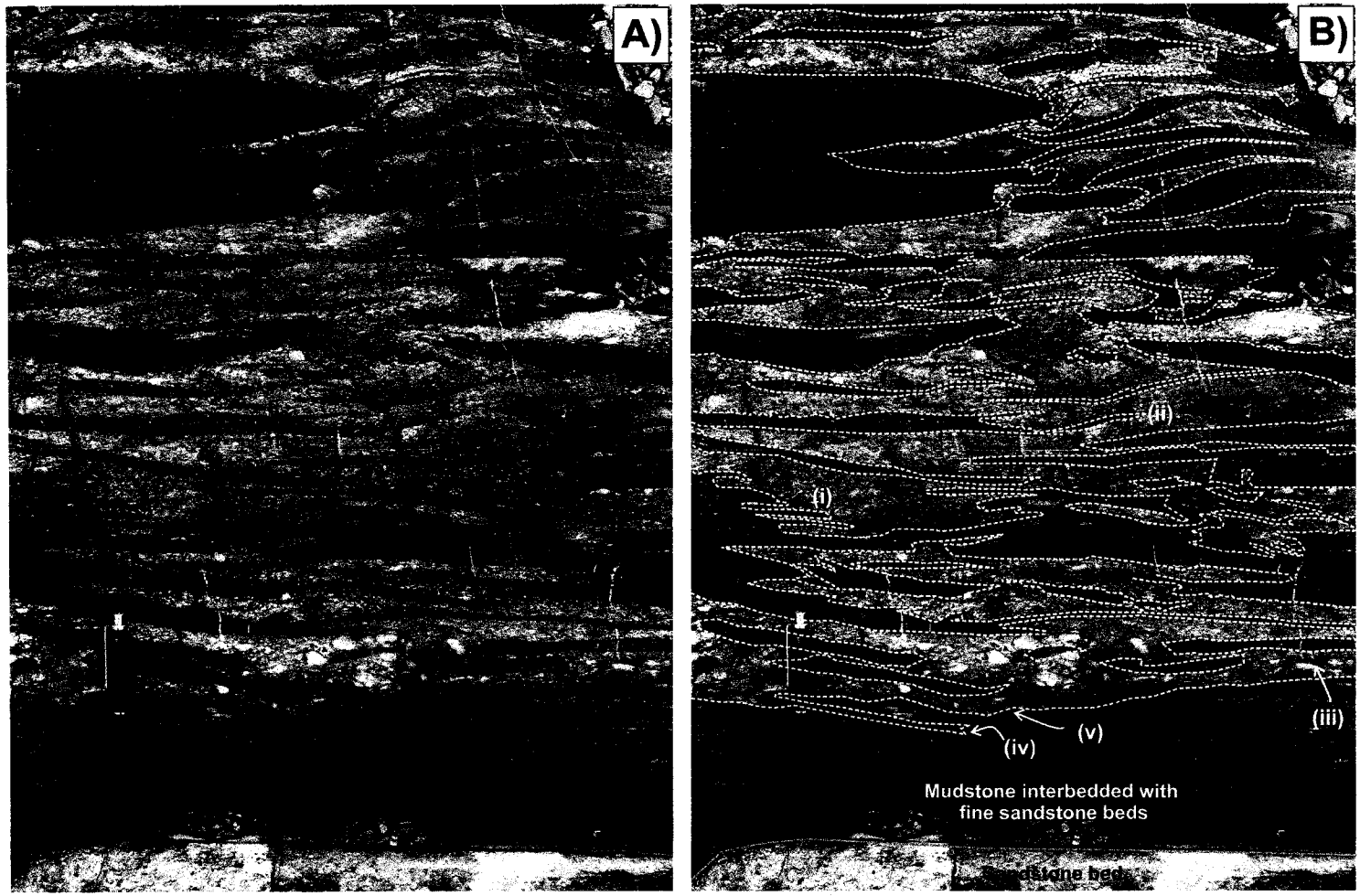

Figure 2.23. Mudstone clasts embedded in a sandstone matrix, Channel 3. A) non-interpreted and B) interpreted. Mudstone clasts (grey) are closely packed and show a sub-parallel fabric of the apparent a-axis. Note the short-side margins of some mudstone clasts are ragged or serrated (i) and strangely pointed (ii). Matrix infilling consists of coarse sand with dispersed pebble clasts (iii) and is sourced from the overlying conglomerate bed. Coarse sediment has been injected into underlying mudstone bed (iv), which has been truncated partially (v). Thick, yellow lines indicate a sharp contact between fine-grained beds and underlying coarse sandstone beds; and dotted, yellow lines represent margins of mudstone clasts and matrix.

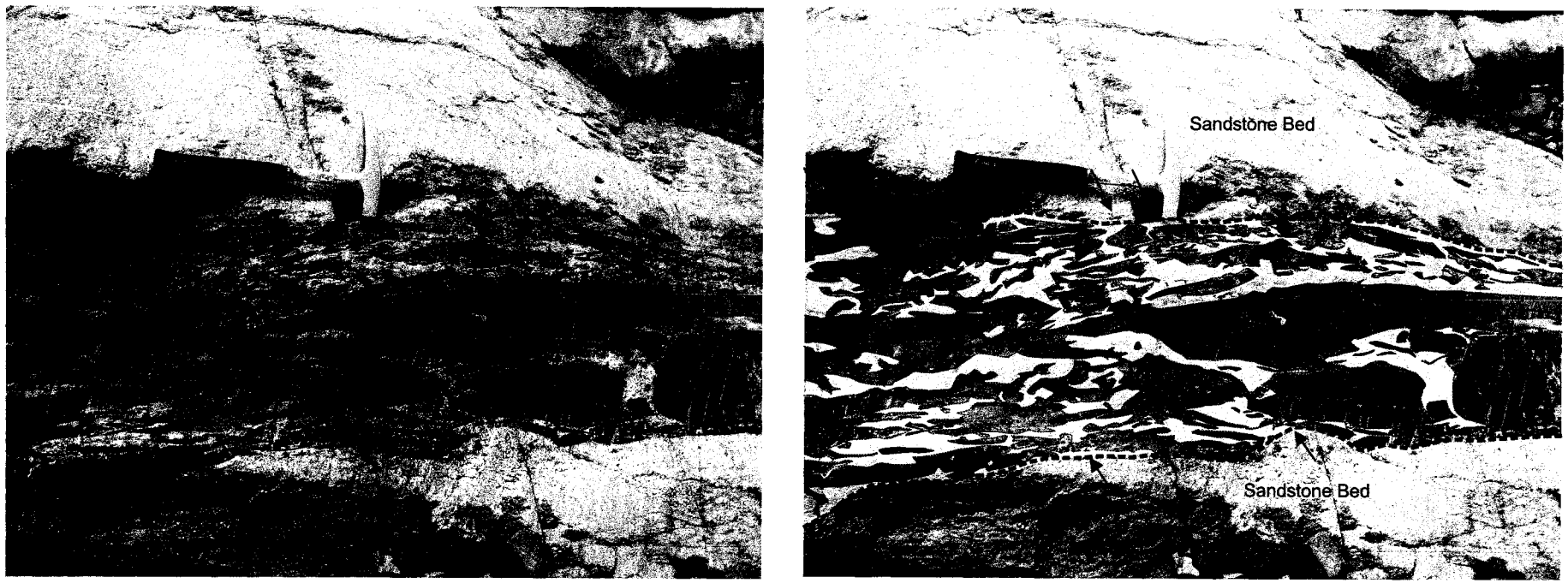

Figure 2.24. Mudstone clasts in a coarse sandstone matrix, Channel 1. Left, non-interpreted and Right, interpreted. Note the uncommon shapes and brecciation or disintegration of large mud clasts by the matrix infilling, which preferentially invades parallel to lamination. The clasts are closely packed and stacked. and the intruded sand matrix is partly sourced from the upper and lower beds (arrows). The thick dotted lines demarcates the lower and upper boundaries of the mud clast-rich layer. Light areas show the distribution of sand matrix.

Figure 2.25. Mudstone clasts in a coarse sandstone matrix, Channel 1. Note the brecciation of a mudstone interval forming large blocky and small irregular mudstone clasts (yellow arrow) that are closely packed and also locally attached. Brecciation occurs as a result of matrix injection within the mudstone layer (black arrow). Rip-down clasts are also distinguished (red arrow).

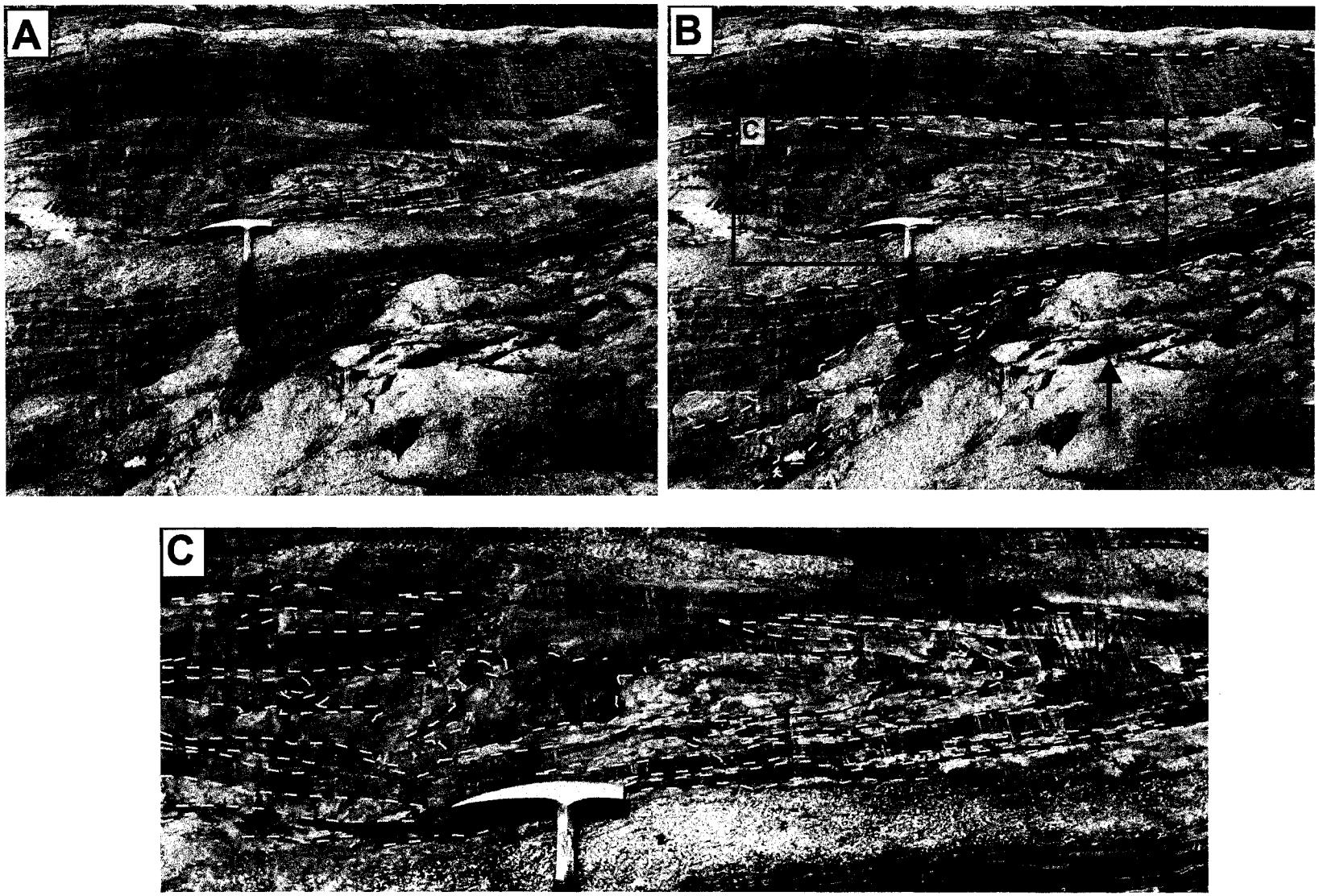

Figure 2.26. Sandstone injections and mudstone clasts embedded in a coarse sandstone matrix, Channel 1. A) non-interpreted and B,C) interpreted. In (B), some mudstone clasts (arrow) originated from the ripping down of a overlying mudstone bed now appears partly disaggregated. In (C), some mudstone clasts could have been formed due to matrix injection throughout mudstone bed.

2.2.2.3. Petrography, X-Ray Diffraction and Carbon Content analyses

Petrography

Mudstone clasts are mostly composed of abundant clay minerals and silt size grains of quartz (see petrographic results and photomicrographs in Table II.2 and Figs. II.33-II.34 in Appendix II; for sample location see Appendix I). The matrix surrounding mudstone clasts in these breccias is a poorly sorted mixture of silt to very coarse sand. Coarser matrix grains are composed (in order of abundance) of quartz, plagioclase and K-feldspar. Pyrite, zircon and muscovite are also observed. The fine-grained recrystallized matrix consists of microcrystalline quartz, chlorite and muscovite. In a number of cases, some clasts show microfractures and also injective interpenetration of matrix grains around their borders, especially along the lamination.

X-Ray Diffraction

Minerals identified from mudstone clasts (facies F2.1) include (see Table III.1 in Appendix III): quartz, chlorite, muscovite, plagioclase, K-feldspar, calcite, dolomite, ankerite and goethite. Many small peaks were unidentified, which suggest that several other minerals may exist but are in very small quantities.

Carbon Content

Even though rocks in the study area have experienced low-grade metamorphism, they have preserved many primary isotopic signatures (Ross, 2003a). In view of this, random samples of mudstone-clasts breccias (facies F2.1) and nearby mud-rich facies deposited in the intra- and extra-channel areas of Channel 1 and 3 were analyzed for comparison of total organic carbon content (TOC). A compilation of the carbon-content data for each channel is shown in the Table 2.2 and Fig. 2.27. Total organic carbon (TOC in weight percent) is used here as test tool to constrain the contributions from specific sources.

Overall, TOC values from slope deposits for the Isaac Formation in Castle Creek are up to 4 wt% (Ross, 2003a), and in contrast values from basinal deposits of the Upper Kaza Group are significantly below detection limits, less than 0.02 wt% (Meyer, 2004). Variations of TOC in Channel 1 and 3 of the Isaac Formation are generally low and correlate well with

lithology. However, the TOC data is not very insightful to elucidate clear relationship between mudstone clasts and their possible source. TOC values range from 0.11 to 1.8 wt%, with mudstone turbidites, mud matrix of carbonate-clast debrites having the highest values (average 0.26 and 0.98 wt% respectively) and mudstone clasts from breccia facies and mud matrix of quartz-debrites (average 0.18 and 0.16 wt% correspondingly) typically have slightly lower values.

	#	SAMPLE ID	FACIES	LITHOLOGY	TOC (wt%)
CHANNEL 1	1	112	F2.1	Mudstone clast	**0.14**
	2	113	F4	Thin bedded turbidite	**0.20**
	3	115	F2.1	Mudstone clast	**0.13**
	4	150	F4	Thin bedded turbidite	**0.11**
	5	151	F2.1	Mudstone clast	**0.13**
	6	152	F2.1	Mudstone clast	**0.13**
	7	153	F2.1	Mudstone clast	**0.13**
	8	169	F4	Thin bedded turbidite	**0.45**
	9	170	F2.1	Mudstone clast	**0.13**
	10	171	F2.1	Mudstone clast	**0.09**
	11	172	F2.1	Mudstone clast	**0.20**
	12	173	F4	Thin bedded turbidite	**0.26**
CHANNEL 3	13	9	F2.1	Mudstone clast	**0.34**
	14	18		Carbonate-clast debrite (mud matrix)	**0.15**
	15	24	F4	Thin bedded turbidite	**0.16**
	16	43	F4	Thin bedded turbidite	**0.22**
	17	68	F2.1	Mudstone clast	**0.23**
	18	69	F2.1	Mudstone clast	**0.22**
	19	70	F2.1	Mudstone clast	**0.25**
	20	84		Carbonate-clast debrite (mud matrix)	**1.80**
	21	88		Quartz-clast debrite (mud matrix)	**0.16**
	22	155	F4	Thin bedded turbidite	**0.18**
	23	156	F2.1	Mudstone clast	**0.25**
	24	163	F4	Thin bedded turbidite	**0.36**

Table 2.2. Total organic carbon content determined from Channel 1 and 3 (Isaac Formation). See Appendix I for samples location.

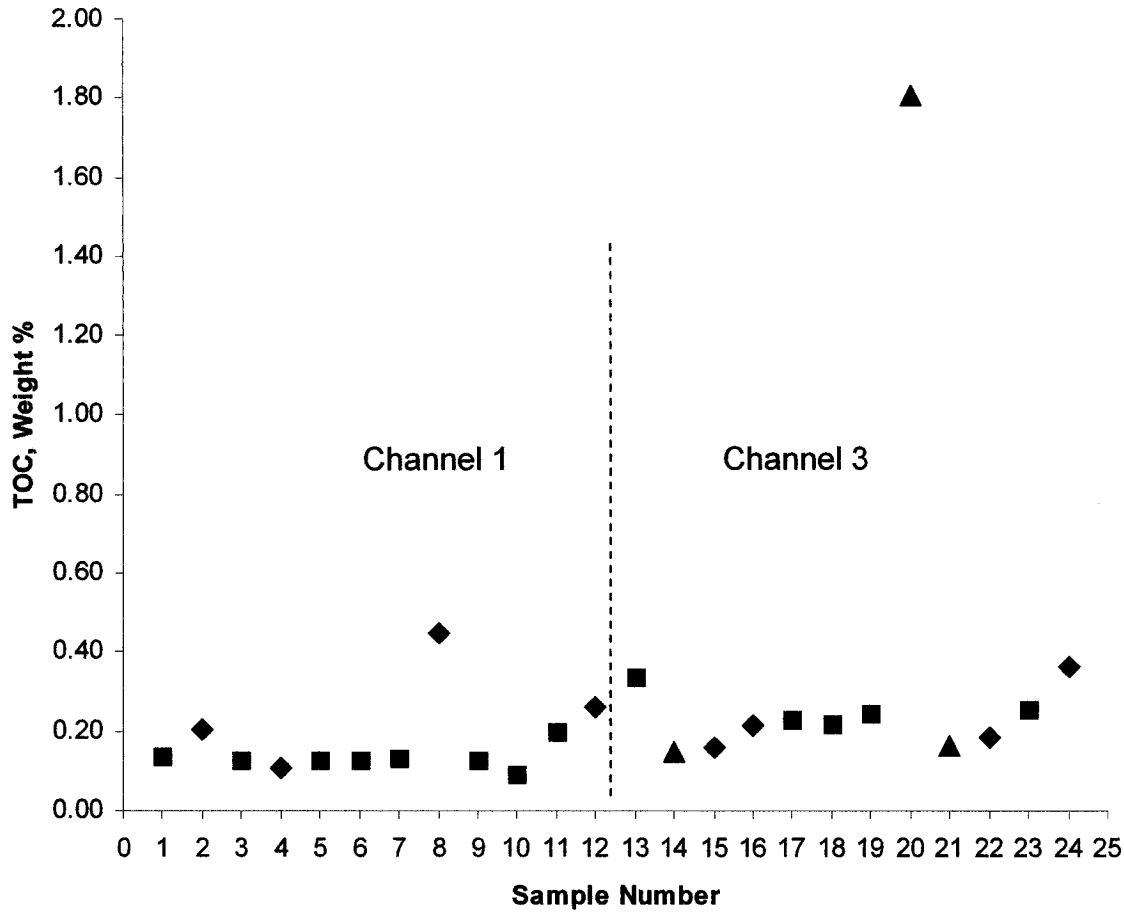

Figure 2.27. Comparison of TOC (total organic carbon) for Channel 1 and 3 (Isaac Formation): mudstone clasts of breccia facies F2.1 (square), and adjacent thin bedded turbidite (diamond) and debrites (triangle). Note that on average TOC values are between 0.1 to 0.4 wt%. One mudstone sample from the matrix of a carbonate-clast debrite has a much higher organic carbon content compared to the other samples.

2.2.2.4. Interpretation

Understanding the origin of mudstone clasts in the breccia lithofacies is crucial to interpreting the dynamics of the flows from which they were deposited. Facies F2 of Channels 1 and 3 shows features that suggest three different origins, which are interpreted to be closely analogous to the three major groups A, B and C of Johansson and Stow (1995). These origins are (a) rip-up clasts derived from erosion of the underlying or laterally adjacent strata; (b) clasts derived from upstream erosion and downflow transportation within the flow; and (c) clasts mainly derived from post-depositional processes, such as liquefaction, rip-

down, instrastratal flow, and injection. Facies F2 is likely comparable with the facies F3 of Mutti (1992).

Mudstone clasts from local or updip erosion?

Mudstone clasts of subfacies F2.1 in Channel 1 and 3 have an intraformational origin, resulting from local or updip erosion (rip-up clasts) by strong sandy-gravelly high-density (Lowe, 1982) or hyperconcentrated flows (Mulder and Alexander, 2001). Locally, breccias beds are adjacent to an underlying fine-grained beds, which could be considered as a local source for the clasts. However, comparison of the TOC values of mudstone clasts and underlying mudstone turbidites are not conclusive. The slightly low or high TOC content in some of the clasts that is appreciably different from the TOC concentration of local fine-grained deposits suggest some mudstone clasts most probably come from other areas (e.g. shales eroded in up-dip).

The occurrence of erosive contacts at the base of facies F2.1 beds implies that these flows were strongly erosional before deposition. The processes that caused the deposition of clast-rich strata may have occurred this way:

(1) initially, flows tended to be frictional and sufficiently strong to erode compacted muddy sediments in upstream and local areas;

(2) during the downstream movement of these flows, the coarsest and densest particles were progressively concentrated into the head of flow whereas finer and less dense particles collected into the sediment cloud that follows behind the head (Middleton, 1966; Middleton and Hampton, 1973, 1976; Hand, 1997). Thus, eroded mud clasts were progressively incorporated into the body of the flow, forming a stratified high-concentration flow (Fig. 2.17).

Stratification in the body of the flow arose rapidly (Fig. 2.28) during sorting of clasts by turbulence and hindered settling occurred. Finer grains were preferentially elutriated and swept up into the lower sediment-concentration, upper part (Davies, 1971) and into the tail of the flow. In contrast, coarser grains, including mud clasts, were concentrated in the lower portion of the flow. For that reason, the matrix in facies F2.1 is predominantly coarse. Moreover, outsized clasts, like those described in subfacies F2.1, could have been supported

by buoyancy and clast-to-clast interaction (Hampton, 1979; Postma et al., 1986; Druitt, 1995).

The abundance of mud clasts within the flow (some subfacies F2.1 beds contain more than 50% mudstone clasts) affected its behaviour by (a) greatly reducing the settling velocity because of particle-particle interaction, which is increased because of the large surface of the mud clasts (Baldock et al., 2004); (b) reducing particle segregation by promoting grain interlocking due to the corners and edges of their angular and non-spherical shapes (Davies and Kaye 1971), (c) overloading the flow, or (d) disintegrating mud clasts and adding clay particles to the flow and consequently suppressing turbulence (Lowe and Guy, 2001; Baas and Best, 2002);

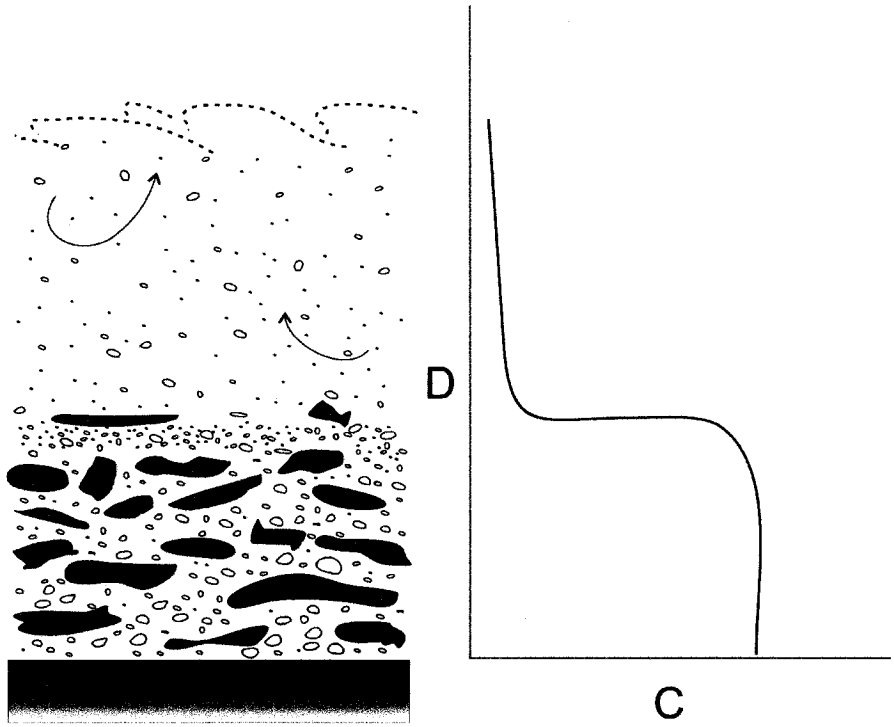

Figure 2.28. Mud-clast rich, high-concentrated flow with schematic concentration profile. Note the framework or cage of mud and coarser clasts in the highly concentrated, lower part of the flow that thereafter behaves as a debris flow, while the upper low concentrated section of flow is supported by turbulence.

(3) during downslope transport, the mud-clast rich portion of the flow was likely gradually transformed into a hyperconcentrated flow (Mulder and Alexander 2001) that could behave as intermediate to debris flow (c.f. cohesionless debris flow of Postma, 1986; slurry flow of Lowe and Guy 2000; linked debris flow of Haughton et

al., 2003), depending largely on sediment concentration. The upper part of the flow, in contrast, tended to be an overcharged turbulent flow (Fig. 2.29).

(4) The mud-clast rich portions of the flow waned or decelerated until interlocking between particles caused *en masse* freezing and sedimentation took place.

Figure 2.29. Flow transformation of a hyperconcentrated flow (Modified from Aird, 2001). A stratified flow with a lower mud-clast rich, highly-concentrated flow (A) that is overridden by an upper turbulent part of the flow that was progressively enriched with elutriated fines, especially in the rear of flow (B).

Mudstone clasts from brecciation of mudstone layers or clasts

Mudstone clasts of facies F2.2 are interpreted to be formed under burial conditions that promoted the formation of abundant and local disturbances within and around mudstone clasts and mudstone beds. These disturbances are associated with soft-sediment deformation as a result of liquidization processes (liquefaction and/ or fluidization).

Liquidization and Effective stress

Liquidization or liquification is the process related to the transformation of sediment into a liquid state and which then behaves as a viscous fluid (Allen 1977, 1982). Liquidization of sand occurs when the grains lose intergranular contact and become suspended within the fluid (Owen, 1987). Upon liquidizing, the weight of the grains is transferred to the fluid producing or adding to an excess of pore-fluid pressure or overpressure (i.e. pressure of

fluids that occupy pore spaces in the sediment). Specifically, high pore-fluid pressure affects the Effective Stress.

Effective stress does not represent the contact stress between particles but instead the distribution of load sustained by the sediment over its entire surface area. This stress is "effective" in that it causes important changes in the threshold shear stress needed to initiate failure of the sediment. An excess of pore-fluid pressure reduces the effective stress on the particles, and accordingly reduces the threshold shear stress.

The two major processes of liquidization are fluidization and liquefaction (Nichols, 1995). *Fluidization* occurs when a continuous upward flow of fluid (external pore fluid) passes through the sediment, whereas *liquefaction* occurs when a transitory fluid (internal pore fluid) supports the sediment grains.

Brecciation of mudstone clasts

Mudstone-clast breccia or conglomerate associated with turbidites commonly show disturbance of their clasts (Mutti and Nilsen, 1981; Chough and Chun, 1988; Mutti, 1992; Lowe and Guy, 2000; Mulder and Alexander, 2001; Kawakami and Kawamura, 2002). Examples of these disturbances are described in facies F2.2, and include unusual shapes of mudstone clasts and sand injection within clasts. These clasts are interpreted to be strongly affected by deformational processes, forming "brecciated layers".

Fragmented clasts have a distinctive close packing and appear to be the disaggregated remnants (i.e. adjacent clasts can be fitted back together) of an original mud clast or mud layer that now are supported in a poorly sorted matrix composed of particles similar to the underlying and/or overlying sandstone beds.

Large, blocky or platy mudstone clasts with ragged or pointed edges in facies F2.2 are interpreted to be formed by the injection of liquefied sand derived from overlying and/or underlying beds into a (partially eroded) mudstone interval. Sand injections observed along internal layering in some mudstone clasts suggest that significant deformation took place along cohesionless silty or sandy laminae in these clasts. These laminae may have acted as permeability pathways (plane of weakness) along which sand was injected and effectively fractured. Furthermore, mudstone clasts with irregular margins may have been formed by intense brecciation or fragmentation resulting from overpressure in the sandstone beds causing injection and ripping-down of the overlying mudstone interval. Rip-down process

occurs when the underlying sandstone liquefies and disaggregates (rip-down) parts of the overlying mudstone interval (Chough and Chun, 1988).

In general, these abnormal mud-clasts preserved different deformational stages according to their level of fragmentation or brecciation (Fig. 2.30). The initial stage occurs at the surface (i.e. during deposition of overlying sand bed) and is characterized by an incipient fragmentation, in which minimal fracturing and injection by early liquefied sand is preferentially created along irregular erosion surfaces at the top of a muddy layer.

Intermediate and advanced fragmentation stages occur in the subsurface during burial. Increased loading or overloading induces an increase in pore pressure in the sand and compaction of mud. This eventually became a trigger that causes the overpressure to suspend the sand. The liquefied sand intruded, especially along lamination, into the more compacted mud. Most intrusions are clastic sills, suggesting that they formed at very shallow burial depths (Jolly and Lonergan, 2002). Intense liquefaction and mobilization progressively formed mudstone clasts that are fragmented, bent, closely packed or dispersed, or partially detached from the parent muddy layer. These features were preserved as pore fluid pressure dissipated, sand injection ceased and the granular framework restored.

2.2.3. F3. Cross-stratified and Parallel Stratified Sandstone

Facies F3 consists of cross-stratified and parallel-stratified sandstone (subfacies 3.1 and 3.2, respectively). This facies is included in Facies Association FA2.

2.2.3.1. F3.1. Cross-stratified sandstone

Subfacies F3.1 is found only in Channel 1. It is composed of well-sorted, coarse and very coarse sandstone with common sub-rounded granule quartz clasts and cobble mudstone clasts that range from 5 to 15 cm long and are generally oriented sub-parallel to the cross-stratification (Fig. 2.31). The base of medium- to large-scale cross-stratified sandstone is commonly erosive. Individual cross-stratified sets range from 0.05 to 0.5 m thick, and foresets are commonly normally graded and dip between 12 to 25°, contorted foreset are observed locally (Fig. 2.32). Cosets consisting of 2 or 3 sets are observed, but single sets are more common.

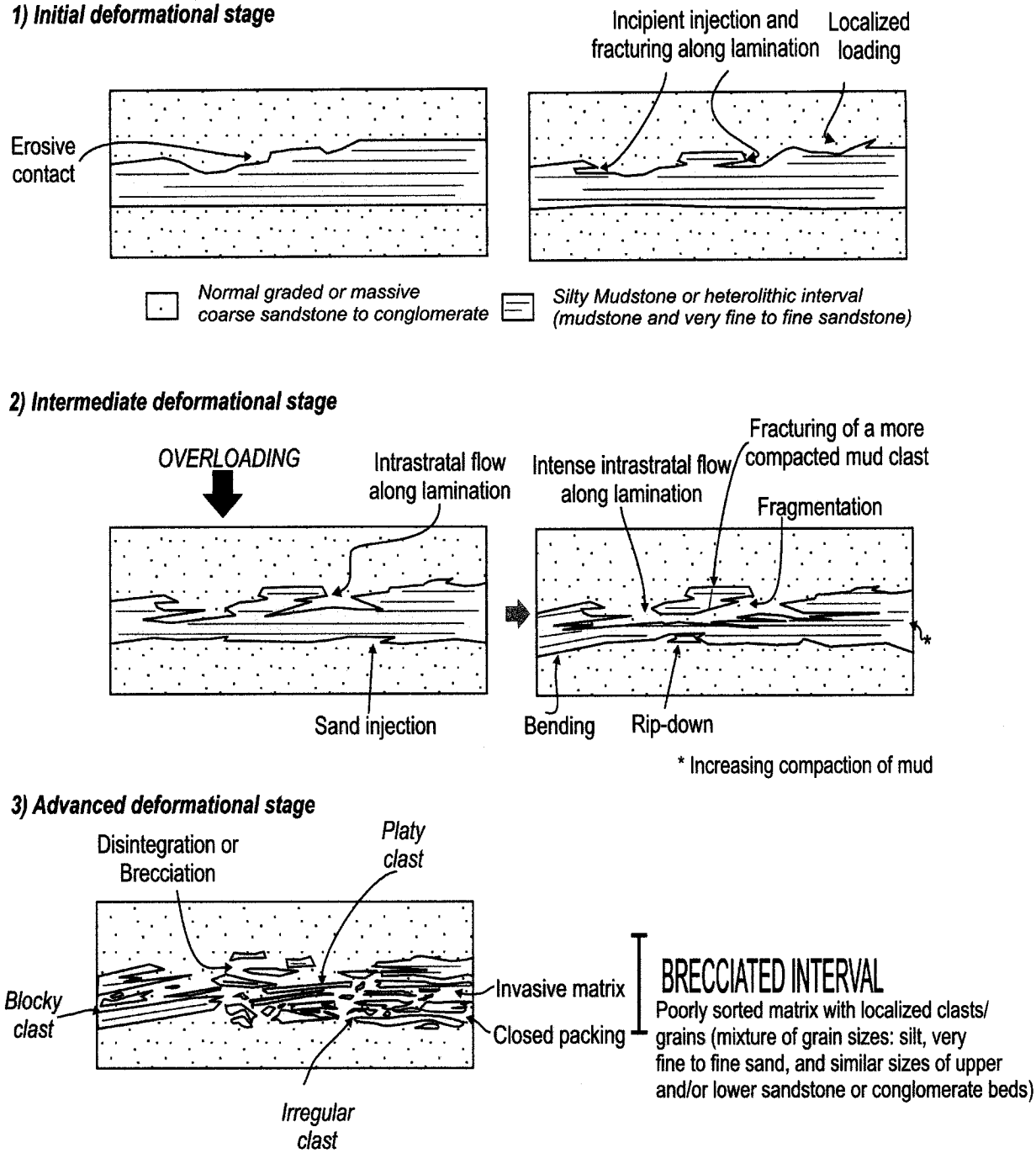

Figure 2.30. Schematic stages of deformation in the mud-clast brecciated facies. 1) During incipient deformation induced by differential loading of overlying turbidite deposits, the mudstone layer is slightly deformed around its irregular top and minor fractures and fissures along the lamination or internal layering are filled by liquefied sand matrix; 2) With overloading and transformation to a liquidization stage (intermediate deformation), the growth of instrastratal flow of liquefied sand and rip down sand injections take place due to high pore pressures, generating common fracturing and consequent fragmentation of mud clasts. 3) Advanced deformation is determined by the progressive brecciation or disintegration of mud clasts as a result of the lateral expansion of instrastratal flow, which caused an extensive incursion of liquefied matrix between the disintegrated fragments. This deformation is enhanced by liquefaction and posterior fluidization of the overlying and underlying beds between the now brecciated layer.

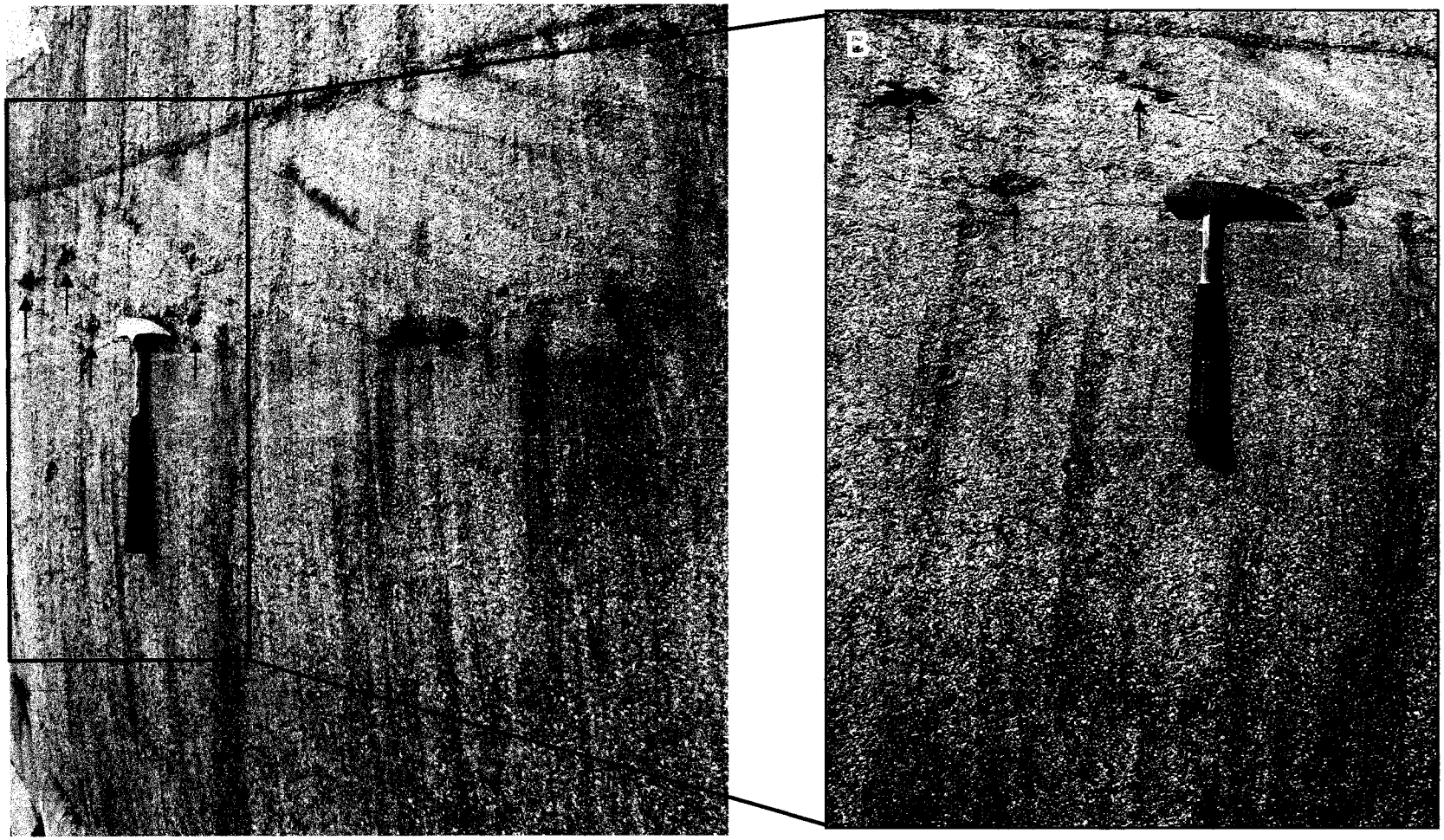

Figure 2.31. Cross-stratified sandstone bed (facies F3.1), Channel 1. A) Large-scale view of cross-stratified and normally graded sandstone beds (Facies (facies F3.1 and F1.1a respectively). B) Close up of normally graded granule conglomerate overlain abruptly by a 27 cm thick dune stratified coarse sandstone. Note dispersed mudstone clasts (dark grey) that occur near the bases of bed sets and foresets (arrows). Linears parallel to the hammer correspond to glacial striae.

Because the outcrop is typically two-dimensional, making accurate paleocurrent measurements was extremely difficult. However, a small number of three-dimensional exposures of trough axes generally indicate paleoflow toward the northeast (20-40°).

2.2.3.2. F3.2. Parallel Stratified Sandstone

Subfacies F3.2 consists of planar laminated, coarse sandstone. Beds typically range from millimeters to over a decimeter thick (0.04 to 0.16 m), but in rare cases can be as much as a few meters thick (Fig. 2.33 Some beds are normally graded. Laminae typically are sub-parallel to the basal contact, stratification is diffuse to sharp and laterally continuous. Tops and bases of beds are diffuse or sharp with little evidence of erosion or loading.

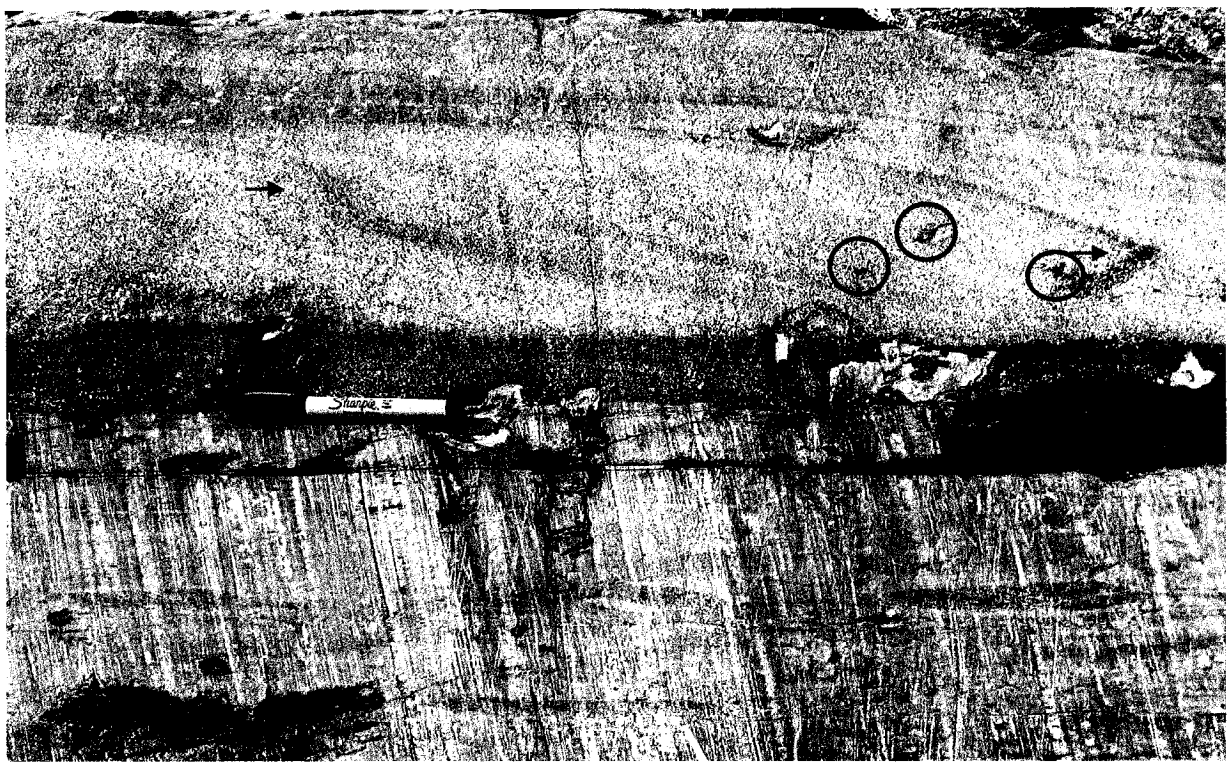

Figure 2.32. Deformed cross-bedding in cross-bedded sandstones, Channel 1. Noted simple recumbent fold or overturned cross-bedding (black arrows). Minor granule-size mudstone clasts (circles) are found dispersed along the foresets.

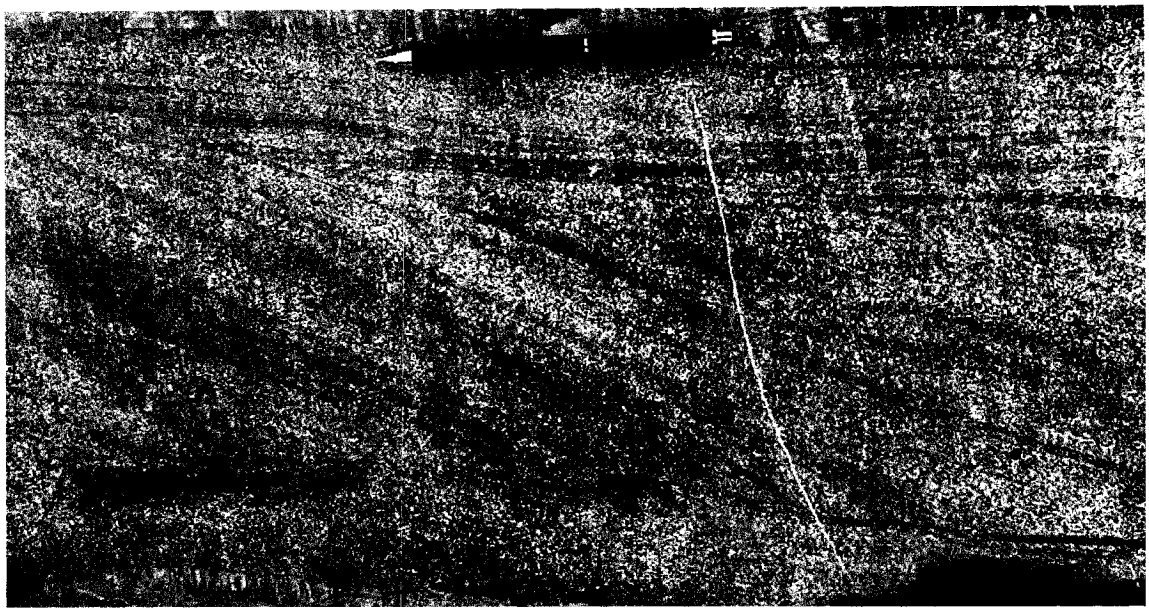

Figure 2.33. Planar-tabular cross-stratified and parallel-stratified sandstone beds (Channel 1).

2.2.3.3. Petrography

Framework grains of cross-bedded sandstone are dominated by monocrystalline quartz grains (as much as 75%), and up to 6% of various feldspar types (including K-feldspar and plagioclase), and pyrite (see petrographic results and photomicrographs in Table II.1 and Fig. II.35 in Appendix II). Feldspars also tend to be altered. Rocks are classified as subfeldspathic sandstone. Strata are well sorted and generally consist of coarse to very coarse sand size grains.

Sandstone is estimated to contain a considerable amount (up to 15%) of blocky calcite cement that show common rims of iron oxide (possibly hematite), which produce the characteristic reddish colours in these rocks. Additionally, low percentage (3%) of recrystallized matrix of quartz are distinguished. Quartz and feldspar grains commonly show evidence of corrosion or leaching by the calcite cement. Microfractures filled with quartz are common.

2.2.3.4. Interpretation

Cross-stratified beds (Facies F3.1)

Medium- and large-scale cross-stratification has been observed and documented in ancient and modern deep-water deposits (Allen, 1970; Flemming, 1978; Hiscott and

Middleton, 1979; Lowe, 1982; Valentine et al., 1984; Bouma and Coleman, 1985; Lykousis, 2001; Shanmugam, 2002). Still, the formation of these structures by turbidity currents remains controversial in the geological literature because of the depositional dissimilarity between suspension settling from turbidity currents and tractive conditions from cross-beds (Walker, 1965; Pickering et al., 1989; Shanmugan, 2002). Briefly, cross-bedding in turbidites has been variously interpreted to be the product of traction caused by (1) moderate-to-high density currents (Piper, 1970; Winn and Dott, 1979), (2) high density turbidity currents (Lowe, 1982), (3) low-density turbidity currents (Martinsen, 1994), (4) concentrated density-flow (Alexander and Mulder, 2001), (5) deep-water tidal bottom currents (Shanmugam et al., 1995; Shanmugam, 2002), and (6) aggradational tractional reworking under steady concentrated density flows (Grecula et al., 2003). In this study, subfacies F3.1 is interpreted to indicate traction transport and deposition under turbulent, unidirectional flow conditions that generated subaqueous dunes (Fig. 2.30). This subfacies corresponds to the S1 division of Lowe sequence (Lowe, 1982) and F6 facies of the classification of Mutti (1992). It is not associated with the Tc division of the classical Bouma sequence, since Bouma (1962) stated cross bedding was absent in this division.

Medium- to large-scale cross-sets within large subaqueous dunes are formed in sufficiently strong and energetic flows (Collinson and Thompson, 1982), in which sediment concentration is low enough that flow separation occurrs.

The thickest cross-beds in subfacies F3.1 are composed of very coarse sandstone (coarsest size). This coincides with the earlier observations of Flemming (2000a, 2000b) who suggested that the dimensions (height and length) of deep-water dunes are controlled by grain size, unlike subaqueous dunes formed in experiments at flumes and in rivers, where dunes scale to turbulence related to water depth (Southard and Boguchwal, 1990; Carling, 1999). Other parameters that could act in the formation of these dunes are flow velocity and sediment concentration (less than 30 volume % according Davies 1968).

Cross beds in the study area are typically composed of well-sorted sandstone, which suggests tractional sorting of the bedload because of selective entrainment (Li and Komar, 1992) or because of particle segregation depending on physical and mechanical properties, such as particle density, size, and shape (Williams, 1976; Dolgunin and Ukolov, 1995; Dolgunin et al., 1998; Branney and Kokelaar, 2002).

Normally graded cross-stratification observed in facies F3.1 suggests gravity sorting during slipface avalanching (Kleinhans, 2004). Additionally, the presence of mudstone clasts in cross beds reflects local erosion from the muddy bottom during tractional reworking. Cross-stratified sandstone with a grain size similar to the underlying sandstone (facies F1) bed implies the dune was formed largely by tractional reworking of the underlying bed (Kneller and McCaffrey, 2003). Cross-stratified sandstone with dissimilar grain size suggests up-dip sediment source and that cross-stratification was formed by a subsequent and unrelated flow.

Deformed cross-bedding indicates that some dunes were affected by soft-sediment deformation. Grain avalanching (grainflow) on the lee side of subaqueous dune bedforms results in characteristically loosely or openly packed sand grains, which are susceptible to later liquefaction (Allen, 1972; Owen, 1996). Many deformed cross-bedded sandstones are found in the study area are associated with flame structures. This observation may indicate that they are the product of compression and buckling of foresets during the partial collapse of a liquefied bedform (Allen, 1985). However, in other beds cross-bedding has been recumbently-folded, especially at the top of the set. This deformation is most probably related to current shear (tangential shear) acting over a liquefied bed (Collinson and Thompson, 1982; Owen, 1996).

Provenance

Cross-bedded sandstones (facies F3.1) are texturally mature but mineralogically immature. Common quartz and feldspar grains were derived from the erosion of the same crystalline igneous plutonic source that provided the detritus discussed earlier in Facies F1. Pervasive Neoproterozoic carbonate precipitation observed in the study area (e.g. in cross beds of the Upper Kaza Group) are suggested to be derived from anaerobic oxidation of methane (Meyer, 2004). The growth and methane oxidation rates of anaerobic methanotrophic Archaea in combination with sulphate-reducing bacteria could have allow the evolution of ancient microbial pathways (Teske et al., 2003).

Upper-Stage Plane Beds (Facies 3.2)

Parallel-bedded strata were deposited from upper-flow-regime, sandy turbidity flows.

This lithofacies is interpreted to be comparable to the S1 division of Lowe (1982) and F7 division of Mutti (1992).

Since high rates of sediment fallout tend to obscure lamination (Arnott and Hand, 1989), these deposits most probably occur under high velocities, but moderate to low aggradation rates. The slow rate of deposition enhances grain size differentiation of particles, which is manifested in the normally graded laminae of Subfacies 3.2.

Upper-stage parallel-laminated, coarse sandstone beds commonly lack basal scours surfaces and consist of the same or slightly finer sediment than the underlying normally graded/massive and cross-bedded sandstone (facies 1 and 3.1) beds, which indicate that the parallel-laminated interval was formed due to a change (decreasing or increasing) of flow strength or sediment concentration with time, but at relatively high-velocity flow conditions.

2.2.4. F4. Sandstone interbedded with mudstone and unlaminated mudstone

Facies 4 consists of medium- to thinly-bedded sandstone interstratified with mudstone (subfacies 4.1.), or unlaminated mudstone (subfacies 4.2.). This facies forms part of Facies Association FA1, FA2 and FA3. Soft sediment deformation structures are common, including convolute lamination, which is more common in Channel 1 (Fig. 2.34), and flame structures at the base of beds where they overlie coarser sandstone. Flame structures have sharp, pointed crests preferentially inclined toward the northwest.

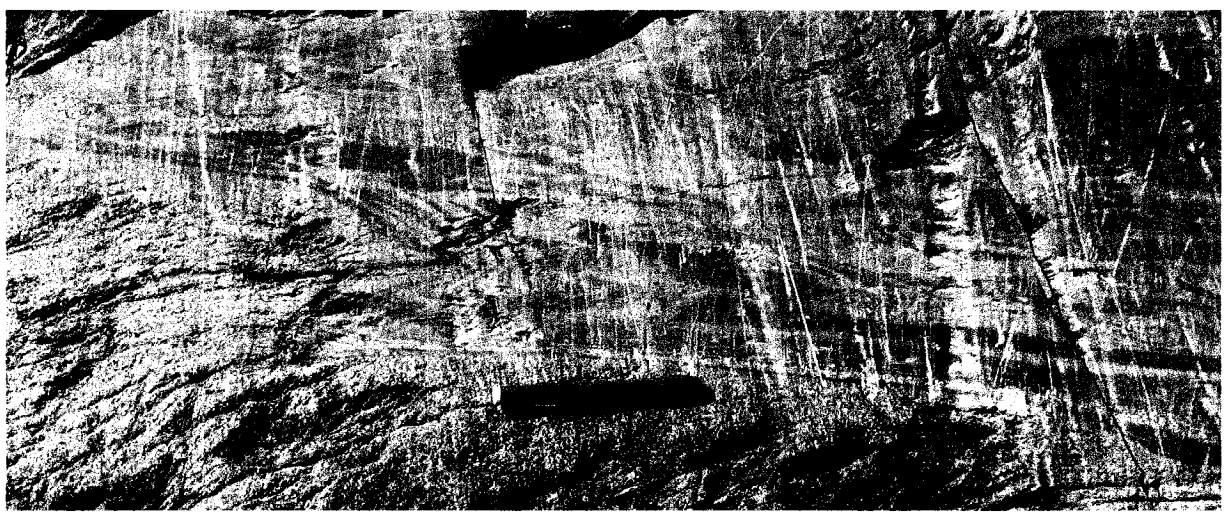

Figure 2.34. Convolute bedding in Facies 4.1c, consisting of interbedded rippled cross-laminated/laminated sandstone (brownish) and mudstone (grey), Channel 1. Note the irregular folding and contortion of beds.

2.2.4.1. F4.1. Sandstone interbedded with mudstone

Subfacies 4.1 consists of interstratified sandstone and mudstone stacked to form meter-scale intervals that commonly fine and thin upward. The proportion of sandstone and mudstone varies, forming heterolithic intervals that range from 1 to 60 m thick. Layers of medium to dark grey, 0.3 to 20 cm-thick mudstone typically occur at the top of individual couplets and are composed mostly of coarse silt and mud. Clay-rich mudstone is Uncommon and occurs particularly in beds <2 cm thick. Most mudstone beds are structureless, but discontinuous parallel lamination can be discerned locally. Mudstones are commonly pyritized and sharply overlie sandstone beds.

Pinkish to brownish-grey sandstone interbeds range from 0.5 to >25 cm thick, with most in the range of 2 to 10 cm thick. Beds consist of well sorted, structureless, cross-laminated or parallel laminated, fine to very fine sandstone.

F4.1a. Structureless sandstone interbedded with mudstone

Structureless sandstone interstratified with mudstone is common and occurs 20 to 30 cm thick beds. Sandstones are sharp-based, fine grained, well sorted, and of the order of 15 cm thick. Locally, they are massive or normally graded.

F4.1b. Laminated sandstone interbedded with mudstone

Laminated sandstones interbedded with mudstone form couplets from 0.5 to 45 cm thick. Sandstone intervals are medium- to very fine-grained, range from 0.3 to 40 cm, and show parallel to wavy lamination.

F4.1c. Cross-laminated sandstone interbedded with mudstone

Small-scale cross-laminated, fine and very-fine sandstone (Subfacies 4.1b) are interbedded with mudstone and form couplets from 0.2 to 15 cm thick (Fig. 2.35, 2.36). Sandstones consist typically of a single cross-stratified set that is 0.5-5 cm thick, although multiple (up to three) sets were also observed. Sandstones have sharp and erosional bases. Lenticular or isolated beds, were also observed (Fig. 2.35). Beds of up to 10 cm thick, medium cross-stratified sandstone, locally, as well are rare.

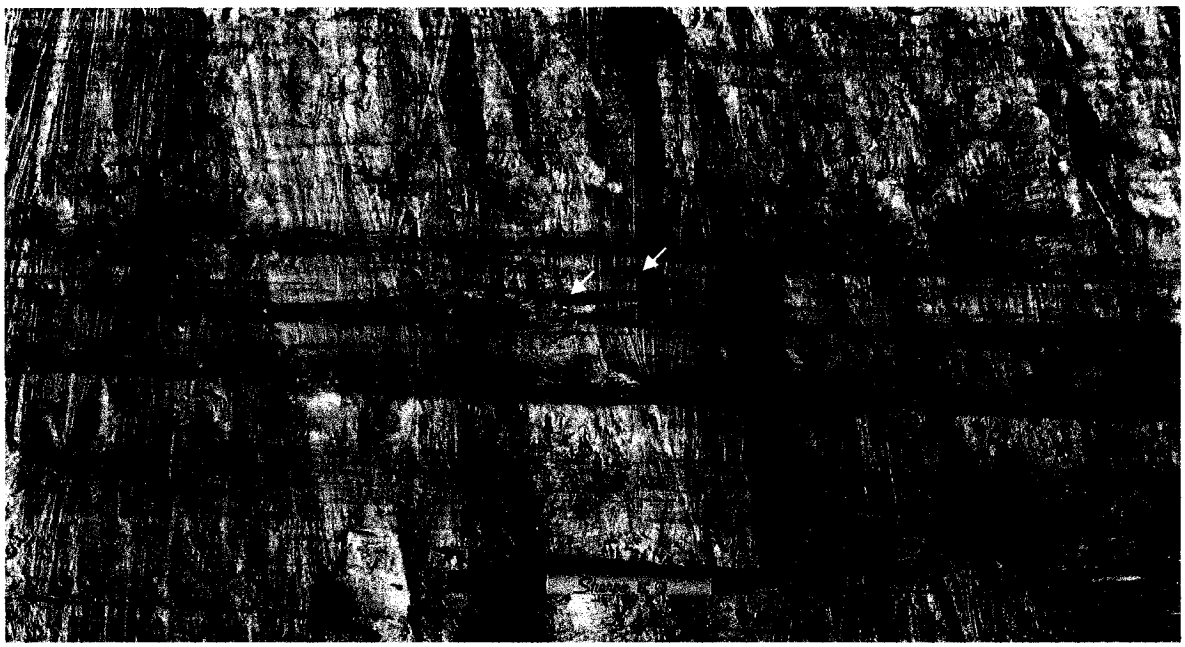

Figure 2.35. Heterolithic Facies 4.1c. Note the stacked, single-set-thick, ripple cross-laminated fine sandstone (Tc) interbedded with grey mudstone (Tde,Te), Channel 1. Thin-bedded sandstone lenses interpreted as starved ripples are also distinguished (e.g. white arrows).

Figure 2.36. Heterolithic Facies 4.1c, showing detail of interbedded small-scale, ripple cross-laminated fine sandstone (T_c) and grey mudstone (T_d,T_e), Channel 1.

2.2.4.2. F4.2. Mudstone

Unlaminated to diffusely laminated beds of mudstone overlies normal graded, massive or cross-stratified facies in Channel 1 and 3. They are up to 20 cm thick and sharp-based. Rare, up to 10 cm thick, small-scale cross-laminated very-fine sandstone beds are locally

interstratified. Clay-rich mudstone succession occurs peculiarly at the topmost of Channel 1, and is 5 m thick. Flame structures are common.

2.2.4.3.Petrography, X-ray Diffraction and Carbon Content analyses

Petrography

Fine-grained sandstone samples of facies F4 consists predominantly of quartz (>54%), and lower amounts of K-feldspar (less than 5%) and up to 3% plagioclase (see petrographic results and photomicrographs in Table II.2 and Fig. II.36 in Appendix II). Detrital muscovite is the most common accessory mineral, and commonly displays bent and deformed shapes. Minor cubic or framboid pyrite grains show partial or complete oxidation (probably to goethite). The matrix is highly recrystallized and contains high amounts (>10%) of finely crystalline quartz and chlorite, and rarely muscovite. Significant alteration of plagioclase feldspar has produced a pervasive pseudomatrix. Additionally, a considerable percentage (30%) of micritic matrix has been locally identified.

X-ray Diffraction and Carbon Content

XRD analyses of mudstone in facies F4 qualitatively identifies the major mineral content in these strata (see Appendix III). Quartz, chlorite and muscovite are the most common minerals. Plagioclase and minor K-feldspar are also recognized. Additionally, calcite is present in most samples, and ankerite is rarely identified. Carbon content results are presented in Table 2.2. and Fig. 2.27, and were discussed previously (see facies F2, p. 58-60).

2.2.4.4. Interpretation

Facies 4.1 was deposited by waning fine-grained, low density turbidity currents, wherein sediment was suspended by fluid turbulence. Structureless fine sandstone of subfacies F4.1a (T_a division of Bouma, 1962) suggests high rates of suspension sediment deposition, with little traction (Arnott and Hand 1989, Allen 1991). Planar laminated medium sandstone of subfacies F4.1b (T_b division of Bouma, 1962) indicates deposition from high energy upper-flow-regime plane bed flows. Subfacies F4.1c, which consists typically of single-set-thick cross-laminated or rarely cross-stratified sandstone (T_c division of Bouma, 1962), indicates

bed load transport with minimal deposition from suspension under lower-flow-regime ripple or dune conditions. Lenticular or isolated ripple cross-stratified sandstone beds are indicative of local sediment starvation.

Following deposition of the sandstone part of each couplet, silty mudstone layers (T_d, T_{de} divisions of Bouma, 1962) were deposited by suspension settling of silt and mud particles. Laminated mudstone most probably indicates traction plus fall-out with sorting of silt grains from disaggregated clay flocs in the viscous sublayer of the flow (Guibaudo, 1992).

Silty mudstone (facies F4.2) that commonly overlie massive/normal graded or cross-bedded sandstone (facies 1 and 3.1 in that order) beds is interpreted to have been deposited under low energy traction and suspension conditions. Such conditions were probably related to a waning of the flow that allowed mostly fine grain suspension deposition. Clay-rich mudstones, on the other hand, were deposited by hemipelagic settling.

The most common postdepositional structures observed in facies 4 are flame and convolute lamination. *Flame structures* were formed as a result of liquefaction of underlying mudstone layer (for a more detail discussion see facies F1, p. 50-51). ***Convolute lamination*** implies hydroplastic deformation of partially liquefied sediment soon after deposition. Most axial planes of folds are inclined to the west, coincident with the dominant paleoflow direction, possibly due to convolution associated with current drag. However, some examples appear to be a result of a density inversion within the heterolithic interval during deposition, and deformation is merely related to restoration of a stable density gradient.

Provenance

The significant amount of matrix and pseudomatrix from altered plagioclase indicates that the sandstones of facies F4 are mainly subfeldspathic or feldspathic, depending on the original feldspar content. Like other strata, sandstones of facies F4 were most probably sourced from local, dominantly felsic plutonic rocks that were likely part of the Canadian Shield igneous complex.

2.3. FACIES ASSOCIATIONS AND INTERPRETATIONS

Intrachannel deposits of Channel 1 and 3 have been subdivided into five facies associations that are comparable to the earlier classifications of Pickering et al. (1995), Clark

and Pickering (1996), Beaubouef et al., 1999 (see Fig. 2.7). These facies associations are summarized in Table 2.3; for a more detailed discussion of each sedimentary facies see the previous section 2.2.

2.3.1. FA1. Bypass-channel Association

FA1 drapes the basal erosion surfaces of channel units and consists of thin bedded siltstone-sandstone (FA1a), thick to very thick conglomerate (FA1b) and mudstone-clast breccia (FA1c). Examples of FA1 are common in Channel 3, but consist only of FA1c in Channel 1.

2.3.1.1. FA1a. Thin-bedded siltstone-sandstone

Above a basal erosion surface, up to 2 m thick, thin-bedded packages consist mainly of thin- to medium- bedded, fine to medium sandstone and siltstone (facies F4, Fig. 2.37a-c), locally interbedded with medium bedded, mudstone-clast breccia and/or coarse-to-very coarse sandstone (facies F1 and F3).

Sandstone is typically parallel and ripple cross-laminated (single or common multiple sets), but structureless beds are also observed (facies F4b, F4c, and F4a). Beds range from 0.1-30 cm thick. Thin beds are laterally persistent for several hundred meters. In places, gradual thickening away from an interpreted channel axis is observed (increase of 1.5-2 m over 200 m of lateral distance).

Even though this assemblage drapes the erosional surface at the base of channel fill, the evidence of scour is observed between beds. Thin beds are conformably overlain by thick beds, but some become eroded in the axial part of the channel. FA1a represents up to 2% of a channel fill.

2.3.1.2. FA1b. Thick to very thick conglomerate

Facies association FA1b comprises thick to very thick (>1 m), normal graded and massive conglomerate (facies F1.1a and F1.2a respectively) that overlie the deeply to shallowly scoured base of an individual channel story. Clast-supported conglomerate are composed mostly of coarse granule and pebble clasts, and locally contain boulder carbonate clasts (Fig. 2.37d). Beds have limited lateral continuity, although some can be traced laterally up to 500 m. FA1b occurs in the axis of channel fills in the lower part of Channel 3.

Facies Association		Thickness (m)	Description	Interpretation
FA1. Bypass-channel association	FA1a. Thin-bedded siltstone-sandstone	Up to 2	Fine to medium, parallel, ripple cross-laminated or structureless sandstone interbedded with siltstone (heterolithic strata). Locally, mudstone-clast breccia and/or coarse-to-very coarse sandstone are also interstratified. Erosive base.	Deposition from the tail of bypassing flows that were traveling downslope.
	FA1b. Thick to very thick conglomerate	1-2	Normal graded and massive, clast-supported conglomerate. Deeply to shallowly scoured channel base.	Deposition from the gravelly fractions of sediment load that were "left-behind" during the passage of bypass flows through the channel
	FA1c. Thin to very thick bedded mudstone-clast conglomerate	Up to 10	Irregular lenses to laterally extensive, continuous zones of mudstone-clast breccia. Deep to shallow erosion channel base. Conglomerate and sandstone beds are locally interbedded.	Mudstone clasts from erosion of fine-grained sediments on the channel floor or underlying channel fills and possibly also parts of the lateral adjacent levee beds.
FA2. Inclined bed association	FA2a. Inclined Sandstone-siltstone	0.2 to 3	Medium- to thick-bedded, cross-bedded, coarse sandstone interstratified with thin-bedded heterolithic strata. Beds typically dip from 2-5° against the erosion channel base. Located at the top of Channel 1.	Lateral accretion packages formed during periods of bypass in a migrating sinuous channel. Cross-stratified sandstone interbedded with thin-bedded heterolithic strata from alternating periods of deposition of coarse-grained, traction high-concentration turbidity flows and deposition of fine-grained, low-concentration turbidity flows.
	FA2b. Inclined Sandstone and mudstone-clast breccia beds	<4	Very coarse to coarse sandstone intercalated with discontinuously lenticular intervals of thick-bedded mudstone-clast breccia. Strata are subparallel but dipping inclined up to 10° to the erosional channel base. Located at the top of lower Channel 3.	Lateral accretion packages formed during periods of bypass in a migrating sinuous channel. Mudstone-clast breccia interbedded with coarse sandstone from deposition of traction-suspension dominated conglomerate and high concentration sandy turbidites.
FA3. Channel-fill association	FA3a. Amalgamated thick bedded conglomerate and sandstone channel-fill	3-20	Thick-bedded, normal graded to massive conglomerate and sandstone, and local thick-bedded mudstone-clast breccia. Significant bed amalgamation. Laterally and vertically fining upward.	Channel filled with deposition from gravelly and sandy, high-concentration turbidity flows.
	FA3b. Partly amalgamated, thin- to thick-bedded conglomerate and/or sandstone channel-fill	2-30	Thick-bedded, normal graded to massive, conglomerate or coarse-to very coarse-grained, sandstone in the channel axis that become laterally interstratified, into thin-bedded siltstone-sandstone. Walking away from the channel axis, clear variation from intermediate to less bed amalgamation. Fining upward trend.	Channel fills with deposition of high-concentration turbidity flows, in the channel axis that progressively became smaller, less erosive, and muddier toward the margins in order to allow the preservation of fine-grained interbeds.
	FA3c. Non-amalgamated thin bedded siltstone-sandstone channel-fill	2-10	Heterolithic strata, consisting of cross-laminated or laminated, medium to fine sandstone and siltstone. Thinning upward tendency, punctuated by local thickening and thinning intervals. Medium- to thick-bedded normal graded, medium to very coarse sandstone locally interstratified. Located in the upper part of Channel 1 and middle of Channel 3.	Channel fills by thinly bedded fine-grained strata deposited from low-concentration turbidity flows.
FA4. Slumped siltstone-sandstone association		3	Deformed strata of thin- to medium-bedded, very fine to fine sandstone interbedded with siltstone, cross-stratified, medium to very coarse sandstone, and mudstone clast breccia. Isolated sandstone boudin-like structures. Erosion base. Located in Channel 1 and 3.	Slump deposits derived from upslope and were redeposited within the channel.
FA5. Channel-abandonment association		5 to 65	At the base, lenticular interbeds of massive or cross-stratified, very-coarse to medium sandstone, typically display compensational stacking pattern. Classic fining and thinning upward trend. Overlain channel fills. Located typically in the uppermost part of Channel 1 and 3.	Thin bedded, fine-grained strata deposited from low-concentration flows, marking channel abandonment. Deposition of lenticular coarse sandstone filling restricted topography at top of the channel conduit.

Table 2.3. Facies association description and interpretation

2.3.1.3. FA1c. Thin-to-very thick bedded mudstone-clast breccia

Breccia zones (facies F2) are highly amalgamated, laterally extensive, and commonly overlie a deep erosion surface, especially in the channel axis. Beds range from 0.5 m up to 8 m thick and contain of clasts of mudstone (Fig. 2.38a,b). Locally, remnants of conglomerate and sandstone beds are observed. Thicker zones (more than 10 m) are observed in Channel 1. Strata of FA1c represent up to 15-20% of the intrachannel deposits, and show variable lateral continuity, ranging from discontinuous lenses to hundred-meter wide continuous zones.

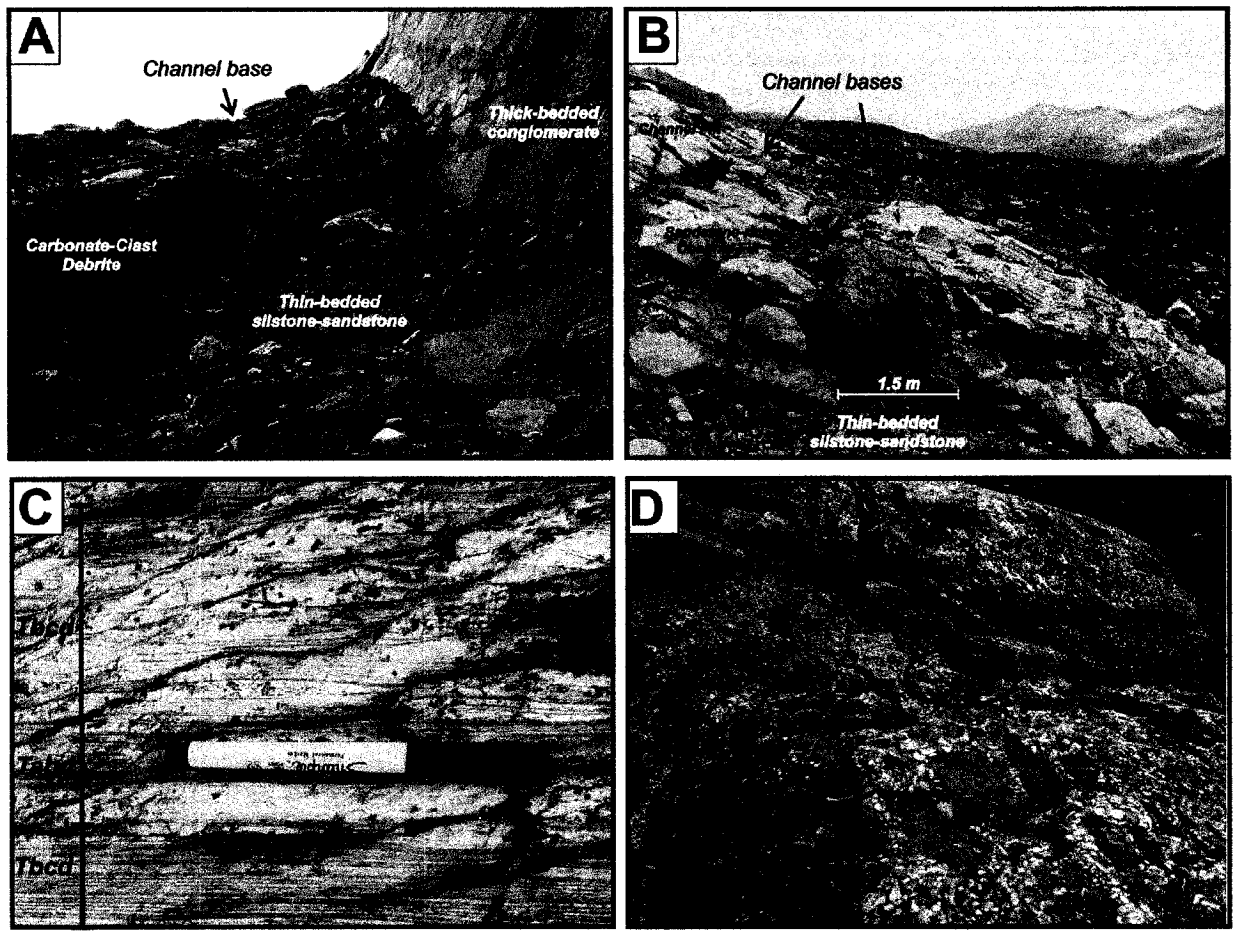

Figure 2.37. Bypass Facies Association FA1a and FA1b. (A) Thin bedded turbidites deposited at the base of Channel 3 are bounded below by the debrite marker and above by channel-filling conglomerate. The photo is taken looking toward the southeast. Stratigraphic top is to the right (Photo taken by S. Khann, 2004). (B) Thin bedded turbidites deposited above an erosion surface in the upper part of Channel 3 near its margin. The photo is taken looking toward the northwest. Stratigraphic top is to the left of the photo. (C) Close up of thin bedded turbidites shown in photo B, that are composed of fine to coarse sandstone interbedded with siltstone. Note the millimeter- and centimeter-scale thickness of the beds and repetitive successions (D) Massive clast-supported conglomerate consisting of up to cobble-size, carbonate clasts (brown- orange weathered) in a quartz- pebble-rich matrix (white) overlie the base of a channel story.

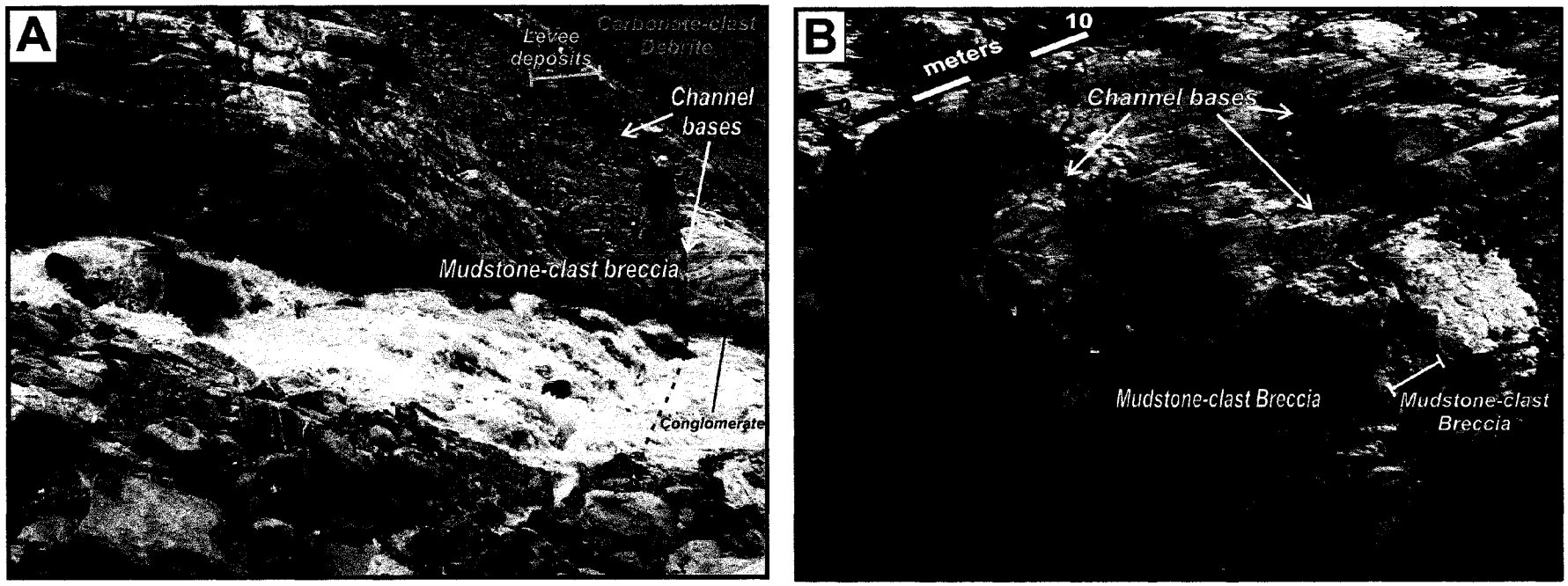

Figure 2.38. Bypass Facies Association FA1c. Intraclast breccia overlying deep erosion surface (red dashed lines) that truncates underlying conglomerate and sandstone beds, and levee deposits.

2.3.1.4. Interpretation

FA1 is related to the passage of bypass flows through the channel (see Fig. 2.7). Flows of this kind are interpreted to be low to moderately concentrated, energetic and highly efficient and are associated with the original formation of the erosional conduit (Kneller 2003). The denser and coarser parts of the head and body of these flows transited the channel conduit, bypassed the area and moved farther downdip. During their passage, they occasionally 'left behind' lag or residual deposits (Beaubouef *et al.*, 1999; Gardner & Borer, 2000; Gardner et al., 2003) that characterize incomplete bypass.

The three bypass facies associations of FA1 are the result of episodes of incomplete bypass. Thin-bedded packages of FA1a (cf. *incomplete bypass type 2* of Beaubouef *et al.*, 1999) represented incomplete Bouma sequences (T_{be}, T_{bce}, T_{bcd} and T_{cde}) that were deposited by low- to medium-concentration tails of bypassing flows. Gravel beds of FA1b are similar to *incomplete bypass type 1* described by Beaubouef *et al.* (1999) and are considered to be the result of progressive loss of competence in the bypassing flows wherein the coarsest fractions (pebble or gravel) of sediment load are left stranded in the channel. Mudstone-clasts breccias of FA1c, on the other hand, are related to erosion of fine-grained sediments exposed on the channel floor or underlying channel fills and possibly also parts of the laterally adjacent levees.

2.3.2. FA2. Inclined-bed Association

The inclined-bed association consists of two distinctive lithologies: sandstone-siltstone (FA2a) and sandstone-breccia (FA2b). The first is observed in Channel 1, whereas the second occurs in Channel 3. These strata occur characteristically adjacent to the base of channels, in particular those located at the top of Channel 1 and 3.

2.3.2.1. FA2a. Inclined Sandstone-siltstone

At its base, the inclined-bed association is composed of medium- to thick-bedded coarse-grained dune cross-bedded sandstone (facies F3a) intercalated with thin-bedded sandstone-siltstone (facies F4). Cross-beds commonly exhibit post-depositional deformation. In contrast, thinly-bedded sandstone-siltstone (facies F4) predominates toward the top of the association. FA2a ranges from 0.2 to 3 m thick and depends on depth of channel incision.

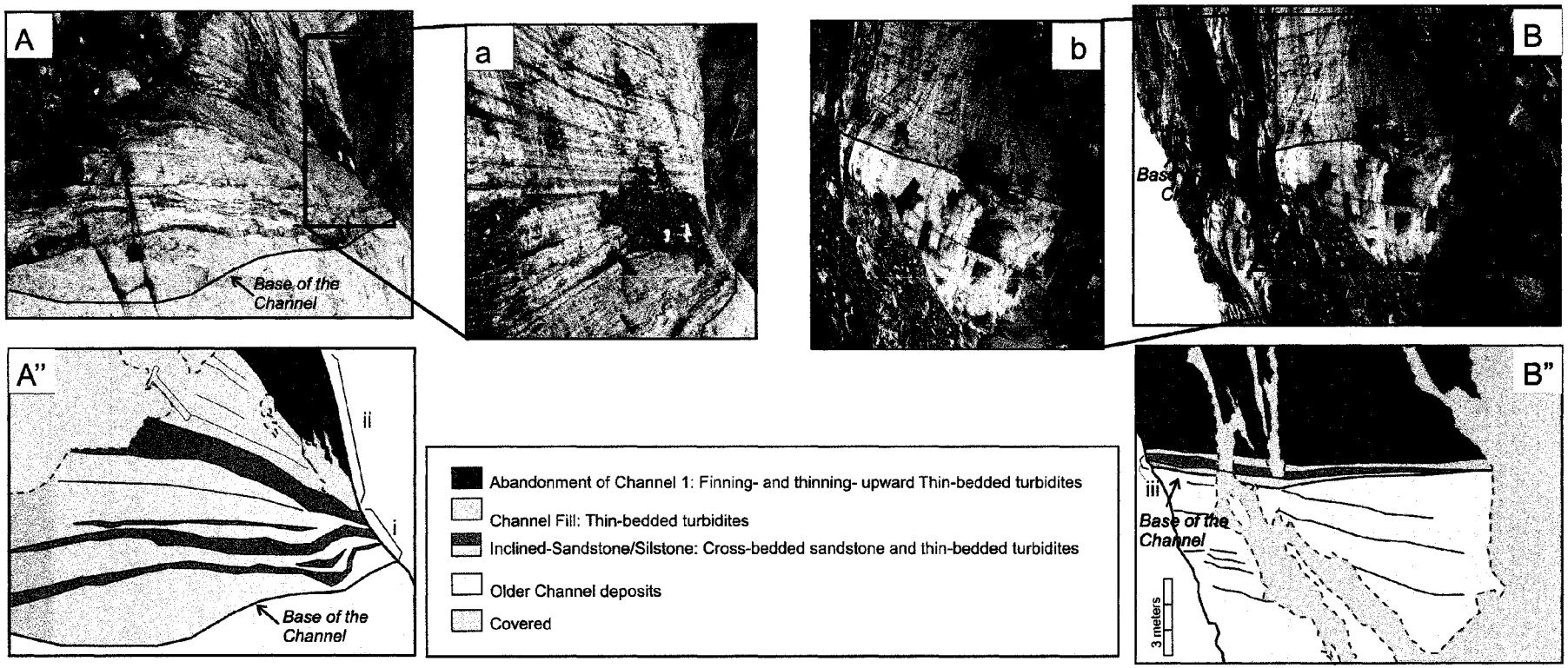

Figure 2.39. Inclined Sandstone-Siltstone Facies Association (FA2a). A-a-A") Oblique view, the photo is taken looking to the NW (Photo taken by R.W.C. Arnott, 2004). Note details of the lithofacies that dominate this package: i) semi-amalgamated packages of cross-bedded sandstone and sandstone-siltstone, ii) abruptly overlain by thin-bedded turbidites that show lithological variations: the lower succession (light green) is characterized by thinly-bedded turbidites (Tde) and the upper succession (dark green) shows a clear fining- and thinning-upward trend of thin-bedded turbidites (Tcde). B-b-B") Continuation of the channel scour to the left of photo A, oblique view, photo looking to the SE. iii) cross-bedded sandstone and sandstone-siltstone thin and fine laterally at the margin of a mud-filled (light green) channel.

Beds typically thin and fine toward the northwest and downlap onto the surface at the base of the channel (Fig. 2.39). In general, strata dip from 2-5°. Inclined-beds are conformably overlain by mudstone-filled channels (facies association FA3c). FA2a makes up about 3% of intrachannel deposits.

2.3.2.2. FA2b. Inclined, Sandstone and mudstone-clast breccia beds

Facies association FA2b is at least 4 m thick and consists of very coarse to coarse sandstone (facies F1) stratified with discontinuous lenses of thick-bedded mudstone-clast breccia (facies F2) at the northwestern margin of Channel 3. These strata correlate laterally to thick and amalgamated conglomerate and sandstone (facies F1) in the channel axis. Beds are of the order of 1 meter-thick (up to 1.25 m) and can be traced laterally about 100 m. In general, beds are subparallel but inclined (up to 10°) to the channel base, dipping toward the northwest. Bed amalgamation is variable. Discontinuous lenticular patches of mudstone-clast breccia are common in the lower part of channel fills. Strata of FA2b erosively overlie fine-grained, thinly bedded levee deposits. FA2b represents up to 2% of intrachannel deposits.

2.3.2.3. Interpretation

FA2 is interpreted as lateral accretion packages (LAP, *sensu* Abreu et al. 2003), deposited during periods of sediment bypass in a laterally migrating sinuous channel. According to the classification scheme of Abreu et al (2003), FA2a is a non-amalgamated LAP and FA2b is a semi-amalgamated LAP. FA2a is composed of coarse-grained, traction-dominated high-concentration turbidites (cross-stratified sandstone) at the base and fine-grained, low-concentration turbidites (thin-bedded sandstone-siltstone) toward the top. FA2b, on the other hand, comprises a heterogeneous assemblage of traction-suspension dominated conglomerate (mudstone-clast breccia) and high concentration sandy turbidites (coarse sandstone). The internal geometry (e.g. stacking pattern and degree of bed amalgamation) and lithology of LAPs varies and depends on channel geometry, flow conditions (including changes in flow magnitude and energy, and sediment discharge) and caliber of sediment load (Abreu et al., 2003, Miall, 1996).

Deposition of deepwater LAPs is considered to be analogous to point bars in sinuous fluvial channels (Figure 2.40, Abreu et al., 2003), where active cutbank erosion occurs on the

outer bend and deposition, or accretion, on the inner bend, or point bar, of the meander (Fig. 2.40).

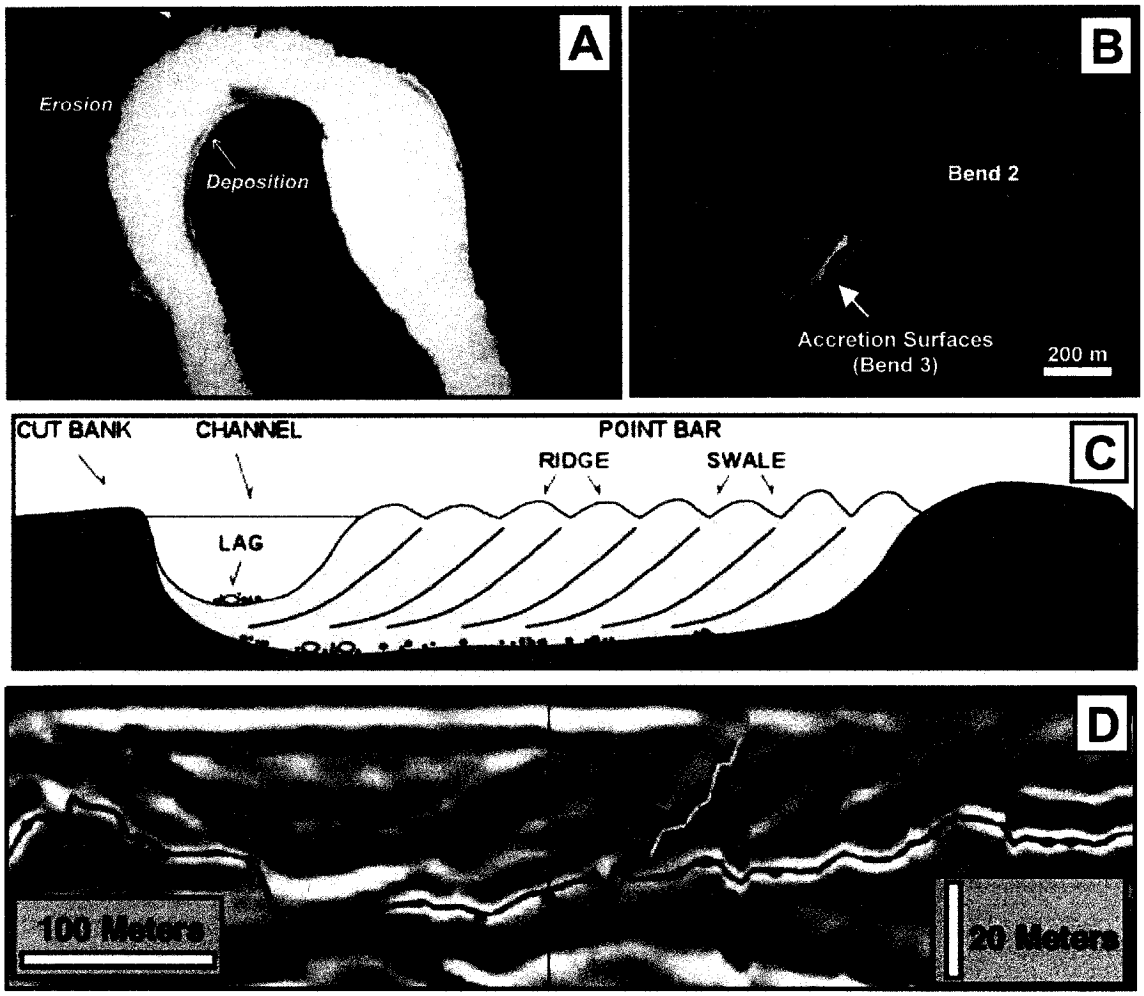

Figure 2.40. Similarity between fluvial point bar and deep-water lateral accretion packages (LAP). Point bars (A and C) and LAPs (B and D from Abreu et al., 2003) are deposited on the inside meander bend, during and following erosion on the outer bank. (A) Aerial photo of a meander in the Fraser River, British Columbia, Canada. (B) Accretion surfaces within a LAP in Channel bend 3 (Green Channel Complex), offshore Angola, which are parallel to the channel margin and dip toward the channel. (C) Development of fluvial point-bar (modified from Galloway and Hobday 1983). (D) Shingled reflections in seismic profile of Channel bend 5 (Green Channel Complex), offshore Angola (From Abreu et al, 2003).

Abreu et al. (2003), based on work of Elliot (2000) in the Ross Formation in Ireland, suggested that deepwater LAPs might be related to hyperpycnal (underflowing) flows emanating from on up-slope delta front. These flows formed when high-density, sediment-laden river water exceeded the density of the marine water in the receiving basin, plunged to the bottom and flowed downslope (Fig. 2.41). Underflows can travel considerable distances and transport large volumes of sediments (Mulder and Alexander 2001). Additionally, these

flows can be sustained for hours to weeks and even months. The deposits of such flows are suggested to be common in the world's marine basins and the rock record, for instance Mulder and Syvitski (1995) estimated that 66% of the 230 worldwide rivers that they studied are capable of producing underflows into marine basins because of high suspended sediment concentrations during floods with return periods of 1000 years or less. Plink- Björklund et al. (2002) pointed out that hyperpycnal flows possibly reach deep-water slope or basin floor mostly during sea-level lowstands, when the rivers debouche along the shelf edge and directly onto the continental slope. However, despite their theoretical commonality, hyperpycnal-flow deposits have been rarely reported from the geological record, and thus, important issues about their evolution are still unknown.

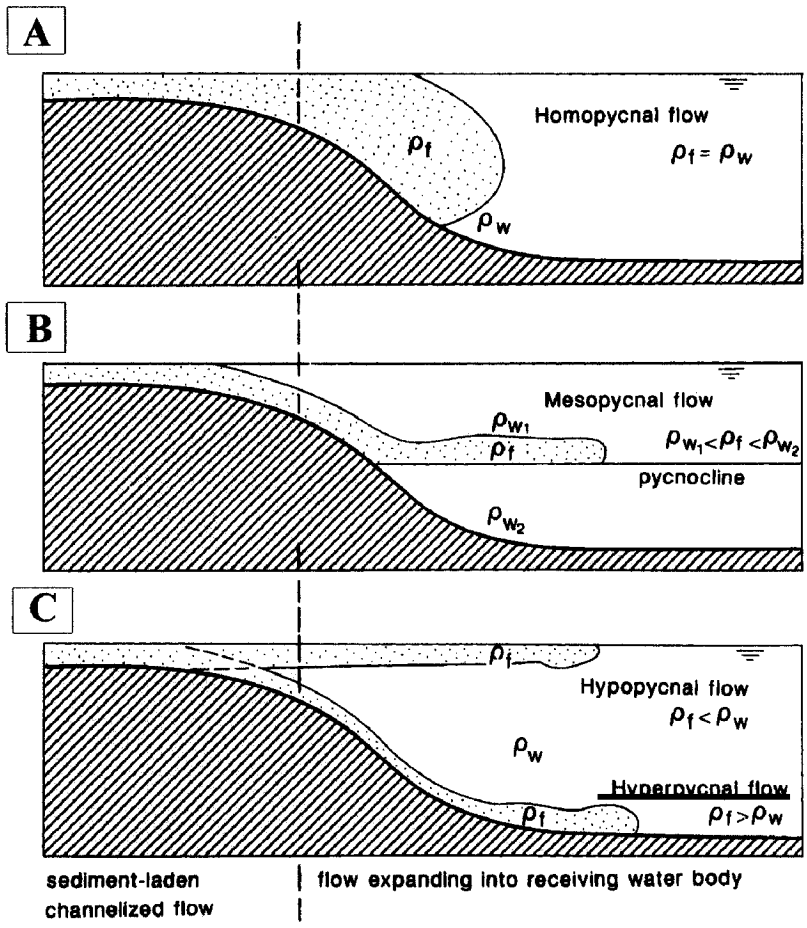

Figure 2.41. Hyperpycnal flows and other types of density flows (From Mulder and Alexander, 2001); in which ρ_f = density of flow; ρ_w = density of ambient fluid or water (ρ_{w1} and ρ_{w2} = densities of water in stratified body). A) homopycnal flow: $\rho_f = \rho_w$, B) mesopycnal flow: $\rho_{w1} < \rho_f < \rho_{w2}$, C) hypopycnal flow: $\rho_f < \rho_w$, and hyperpycnal flow: $\rho_f > \rho_w$.

2.3.3. FA3. Channel-Fill Association

The FA3 facies association forms approximately 75-85% of the fill of Channel 1 and 3. Channel fills are of the order of 3-30 m thick. There are three kinds of channel fill described in this study, ranging from highly amalgamated, thick-bedded conglomerate/sandstone to non-amalgamated, thin-bedded siltstone-sandstone (Fig. 2.42). Commonly, FA3 erosionally overlies previously discussed facies associations (FA1, FA2). Channels are shallow (less than <5 m), but up to 10 m deep local scours are observed which also coincided with the channel axis.

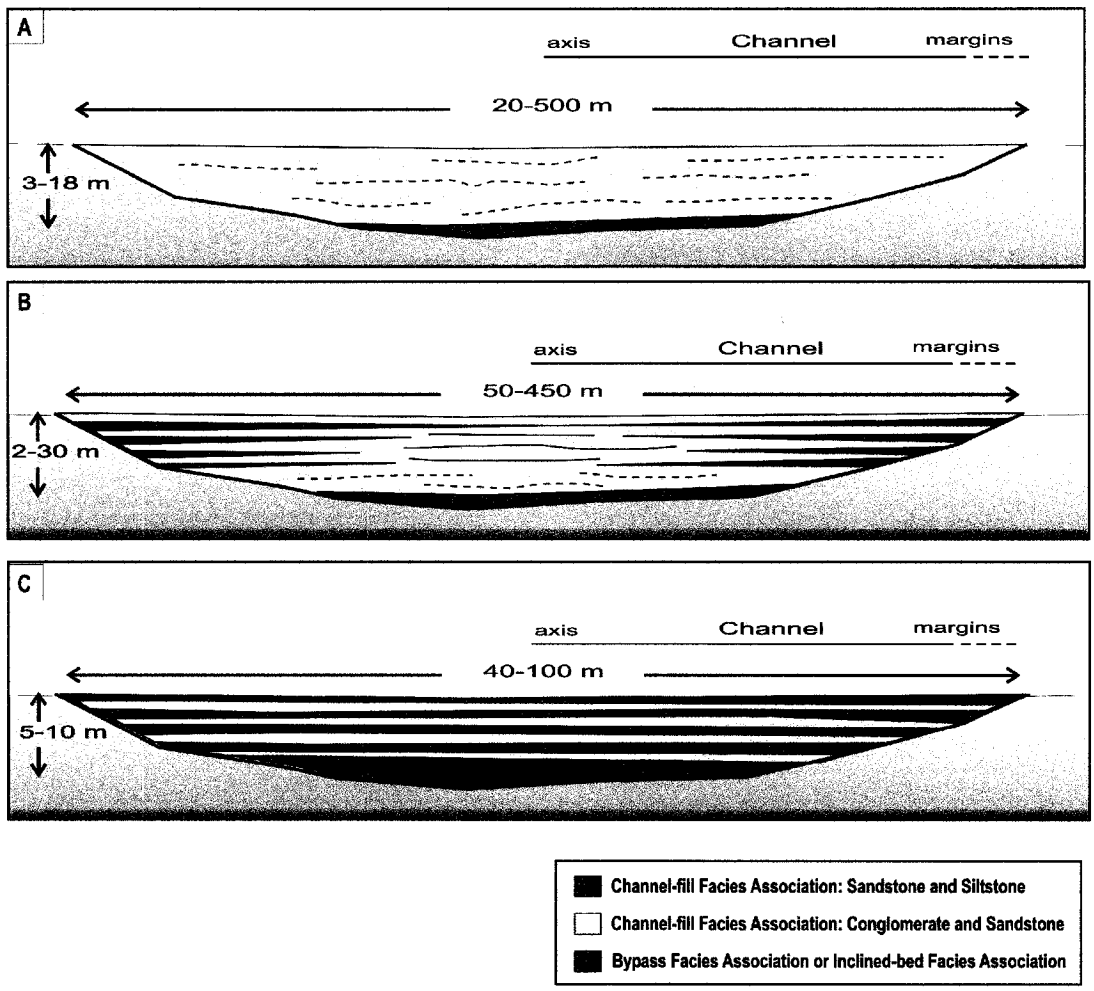

Figure 2.42. Schematic diagrams of different types of channel-fill associations (FA3), consisting of: A) amalgamated, thick-bedded conglomerate and sandstone, B) partially amalgamated, thick- to thin-bedded conglomerate and/or sandstone in the channel axis that laterally grades to more interstratified, heterolithic facies toward the margins, and C) non-amalgamated, thin-bedded siltstone-sandstone, with local beds that are lenticular, pinching out toward the channel margins. Bypass facies assemblages that underlie FA3 are occasionally absent

2.3.3.1. FA3a. Amalgamated thick bedded conglomerate and sandstone channel-fill

Some channels of Channel 1 and 3 are filled predominantly with thick-bedded, normal graded to massive conglomerate and sandstone (facies F1 and F2); and minor thick-bedded mudstone-clast breccia (facies F3a). Beds are highly amalgamated (Fig. 2.43), ranging from 30 cm to 2.5 m in thickness. Rare examples are up to 7 m thick, and occur mostly in Channel 1. Normally graded conglomerate and sandstone are coarse-tail graded, with clasts that vary, respectively, from granule to pebble, and coarse to very coarse sand (rarely medium sand). Clasts up to boulder size, are common in Channel 3.

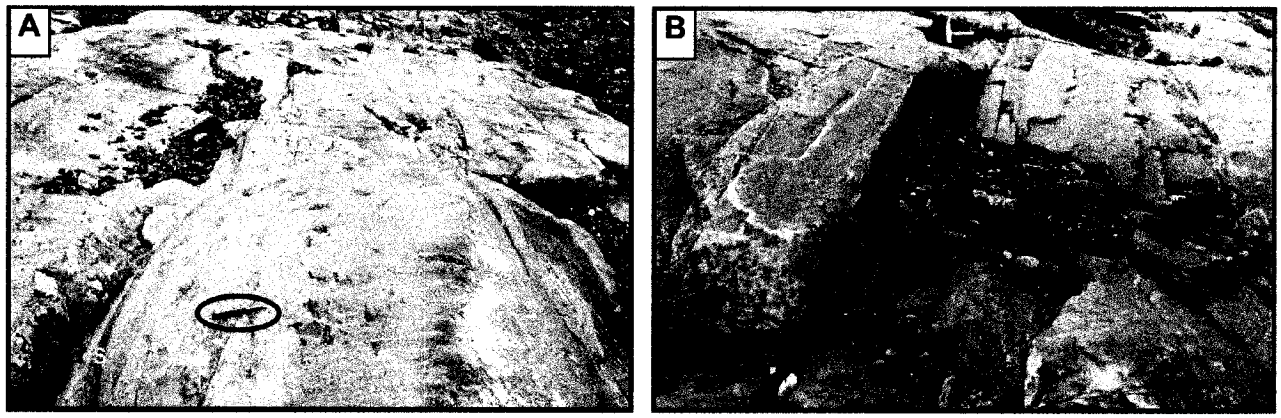

Figure 2.43. Amalgamated conglomerate and sandstone channel-fill association; showing high degree of amalgamation between thick-bedded, fine pebble to granule conglomerate and very coarse to coarse sandstone, which A) rarely are interbedded with thinly-bedded siltstone (s), and B) show characteristic scour bases (arrow). Oblique views, both photos are taken looking to the northwest. Stratigraphic top is on the left of the photos. Photo A is from Channel 1 and photo B is from Channel 3.

Beds bases are sharp, locally scoured, and commonly loaded (Fig. 2.44). Toward the top of a channel fill, important lithological changes are observed. For example, coarse-grained beds in Channel 1 became more interstratified with 5-20 cm thick, cross-stratified coarse sandstone (subfacies F3a) and up to 3 cm thick, unlaminated siltstone (subfacies F4d). Locally, there is also a clear lateral change toward the channel margin from massive coarse sandstone with rare cross-bedded sandstone to interbedded cross-bedded sandstone, interstratified with siltstone-fine sandstone and uncommon massive coarse sandstone, to thin bedded siltstone and fine sandstone and rare massive or cross-bedded sandstone.

In addition to laterally fining, channel fills also fine upward marked by more abundant and thickly preserved fine-grained interbeds. For instance, the upper part of some of these fills in Channel 3 grade abruptly upward into an about 1 m thick succession of thin-bedded siltstone interbedded with structureless, parallel laminated and/or rippled, very fine to medium sandstone (subfacies F4a-c).

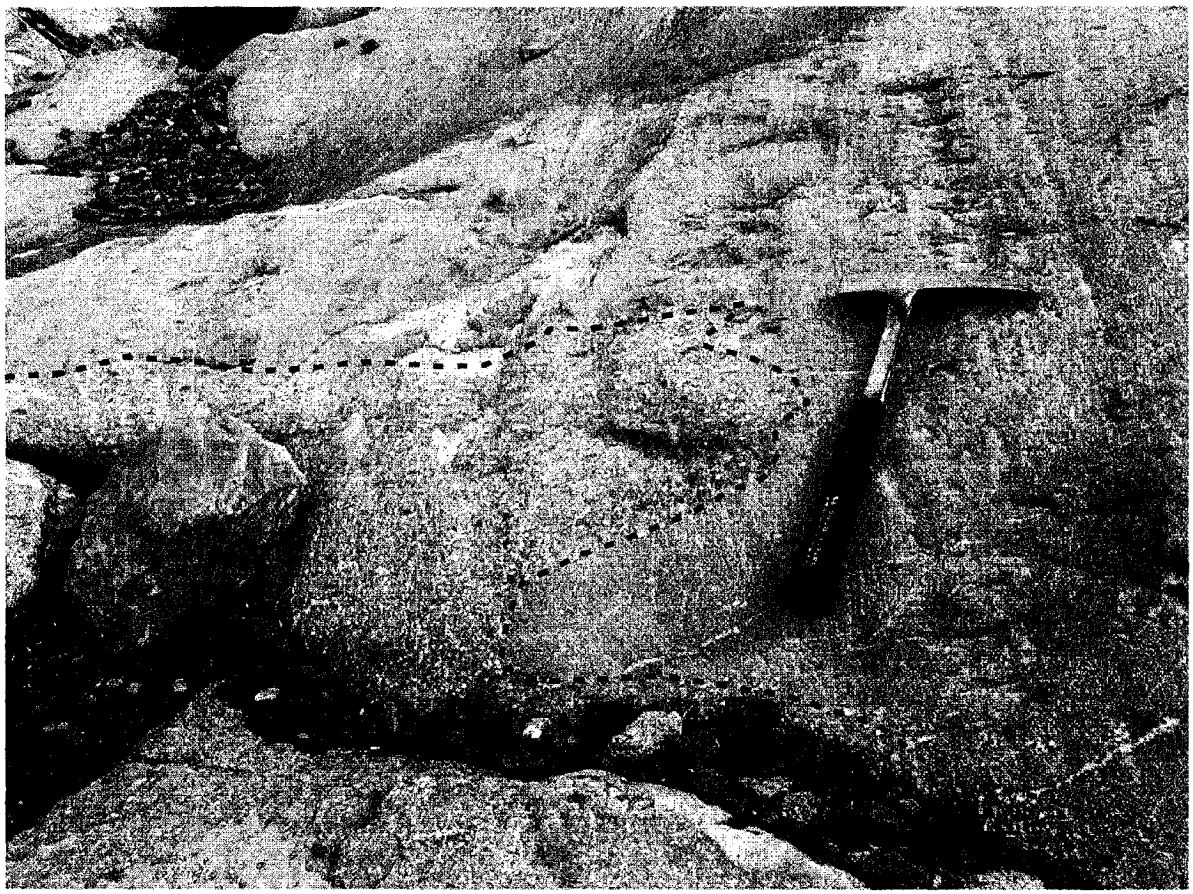

Figure 2.44. Loaded contact between thick bedded conglomerate and very coarse sandstone, which are common in facies association FA3a. Photo is from Channel 1.

2.3.3.2. FA3b. Partly amalgamated, thick-to-thin bedded conglomerate and/or sandstone channel-fill

Some channel fills (Fig. 42, b) are characterized by a more layered or stratified sandstone-dominated infill that is composed of partially amalgamated normal graded to massive sandstone (subfacies F1b and F2b). Strata are coarse to very coarse grained, with common abundant granule and pebble clasts at the base. Other channel fills show also partly

amalgamated infill, but they are composed of massive and normal graded conglomerate (subfacies F1a and F2a) with smaller grain sizes (granule and fine-pebble clasts) than facies association FA3a. The mean thickness of sandstone and conglomerate range between 1.2 and 2 m; however, thicker beds (more than 3 m thick) occur in Channel 1. Some amalgamation surfaces are locally expressed as rip-up mudstone clast horizons/zones apparently "floating" within a bed, but can often be traced laterally into a siltstone parting between two separate sandstone and conglomerate beds. Generally, beds have loaded or mixed (scoured and loaded) bases.

In contrast to facies association FA3a, laterally continuous, thin-bedded siltstone-sandstone interbeds (facies F4) are more common, even in the channel axis. Interbeds consist mostly of either thin- to medium-bedded (less than 15 cm), cross-laminated and/or parallel-laminated fine sandstone intercalated with siltstone (facies F4b-c) or thin to medium bedded (1-20 cm thick), unlaminated silty mudstone or siltstone (facies F4d). Moreover, medium bedded (up to 30 cm thick), cross-stratified coarse sandstone (facies F3a), observed exclusively in Channel 1, are common. Decimeters thick, parallel-stratified, coarse sandstone (facies F3b) are also common, but are observed mostly in Channel 3.

In the upper part of channel fills, beds become less amalgamated as intercalated coarse- and fine-grained strata become common. Also toward the channel margins, coarse-grained-rich strata in FA3b become laterally less amalgamated (e.g. southeast margin of Channel 3) and beds tend to onlap, fine and thin rapidly over around 100 m to the margins (Fig. 2.42).

2.3.3.3. FA3c. Non-amalgamated thin bedded siltstone-sandstone channel-fill

Some channels in the upper part of Channel 1 (Fig. 2.37) and middle of Channel 3, are filled mostly with fine-grained facies (Fig. 2.42c). Facies association FA3c is an up to 10 m thick sequence, composed of alternating beds of medium to fine sandstone and siltstone. Sandstone beds are typically small-scale, non-climbing (ripple) cross-laminated (facies F4), in which single sets are 2-3 cm thick, and thick multiple (2-3) sets are more common (up to 20 cm thick). Beds are laterally continuous and traceable for several hundred meters. A general thinning-upward trend is recognized, but local thickening and thinning successions are also observed. Some fine sandstone are structureless and laminated.

Locally, the fine-grained strata is interstratified with medium- to thick- bedded (10-40 cm thick), normal graded, medium to very coarse sandstone (facies F2), with rare dispersed mudstone clasts at their bases. Some of these beds in Channel 3 pinch out toward the northwest.

2.3.3.4. Interpretation

The three different depositional styles observed in channel fills of Channel 1 and 3 are related to the character of the turbidity current that traveled through these channels. These flows were less efficient compared to the earlier mostly erosive bypass flows, and as a consequence deposited much of the sediment within the channel.

Channel-fills of FA3a are composed mostly of normal graded and massive conglomerate and sandstone (T_a Bouma or R_3/S_3 Lowe divisions) that were deposited from gravel- and sand-rich, high-concentration turbidity flows. These flows transported the largest clasts observed in Channel 1 and 3 and were highly erosive causing significant bed amalgamation. Moreover, these flows were highly stratified; for instance in the lower channel complex of Channel 3, the upper turbulent portions of these flows were able to overspill and construct adjacent levee deposits.

Channel fills of FA3b consist mostly of sandstone and minor fine conglomerate and were deposited also by high-concentration turbidity flows. However, these deposits are less amalgamated and more interstratified with thin-bedded turbidites, not only in the upper part of the fills but also toward the channel margins, suggesting important upward and lateral changes in the flow character. Flows that deposited FA3b may have been smaller, less concentrated, and richer in fine-grained sediment. Localized scours at the base of sandstone beds are considered to represent occasional turbulent bursts that locally scoured the bed and subsequently were filled.

Channel fill FA3a and FA3b show a typical upward-fining trend that is interpreted to indicate reduction in sediment caliber and/or flux or waning flow conditions. The occurrence of cross-bedding at the top of FA3a and throughout FA3b fills and in Channel 1 is interpreted to indicate a decrease in sediment concentration and as a consequence flow separation and traction transport. In contrast, channel fill FA3c was filled by thinly bedded T_{cd}, T_{cde} Bouma turbidites that are related to deposition from lower-energy, low-concentration turbidity currents.

2.3.4. FA4. Slumped siltstone-sandstone

Facies association FA4 consists of slump units that were recognized in Channel 1 and 3, and lies directly on erosion surfaces. One lies at the base of a semi-amalgamated channel-fill in the upper part of Channel 1; another lies at the base of a non-amalgamated heterolithic channel-fill in the middle of Channel 3, and the other at the top of an isolated sandstone-filled channel in the upper part of Channel 3. FA4 ranges from 1 to 2.25 m thick and consists of deformed thin- to medium-bedded (1 to 10 cm thick), very fine to fine sandstone interbedded with siltstone (facies F4). Fine sandstone beds have sharp bases and are ripple and parallel laminated, but locally are also massive. Siltstone commonly exhibits millimeter-scale lamination. Locally, up to 20 cm thick, cross-stratified, medium to very coarse sandstone (facies F3a) are commonly observed. Small (<1 cm) rip-up clasts (facies F2a) occur at the base of some sandstone or siltstone beds. Deformed strata commonly exhibit chaotically disrupted bedding and small-scale, open, rounded, overturned folds (Fig. 2.45). In the upper part of Channel 3, deformed intervals occurs, and bedding has been detached and sandstone boudin-like features (less than 1 m long) (Fig. 2.46).

2.3.4.1. Interpretation

Contorted and folded strata of FA4 that typically overlie a laterally extensive scour surface are interpreted to be related to downslope slumping of semi-consolidated background slope sediments that then were redeposited within the channels.

During movement the sediment mass deformed intensely and produced a wide variety of deformation structures, including folds and boudins. The occurrence of these structures suggests extensive plastic deformation during movement. Folds are characteristic in the basal and middle parts of slump units because of comparatively higher shear (Martinsen, 1994). Likewise, boudins resulted from deformation within the basal shear zone, in which early extensional faulting occurred, and was subsequently followed by the intrusion of fine-grained "ductile" layers (i.e. shale) that were squeezed into the gaps, partially destroying the extensional fractures (faults).

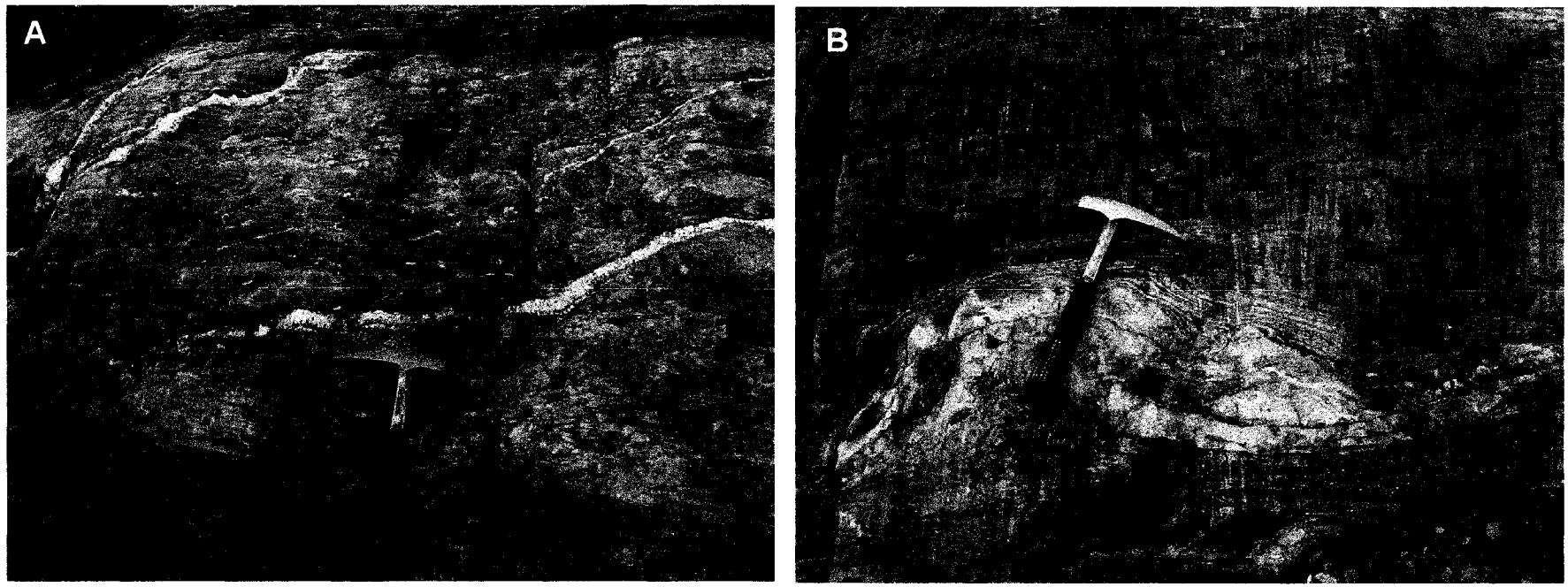

Figure 2.45. Disrupted and strongly contorted strata of facies association FA4. Some slump intervals have a characteristic chaotic appearance. Primary bedding has been evidently distorted (A) and also folded (B). Photo is from middle of Channel 3.

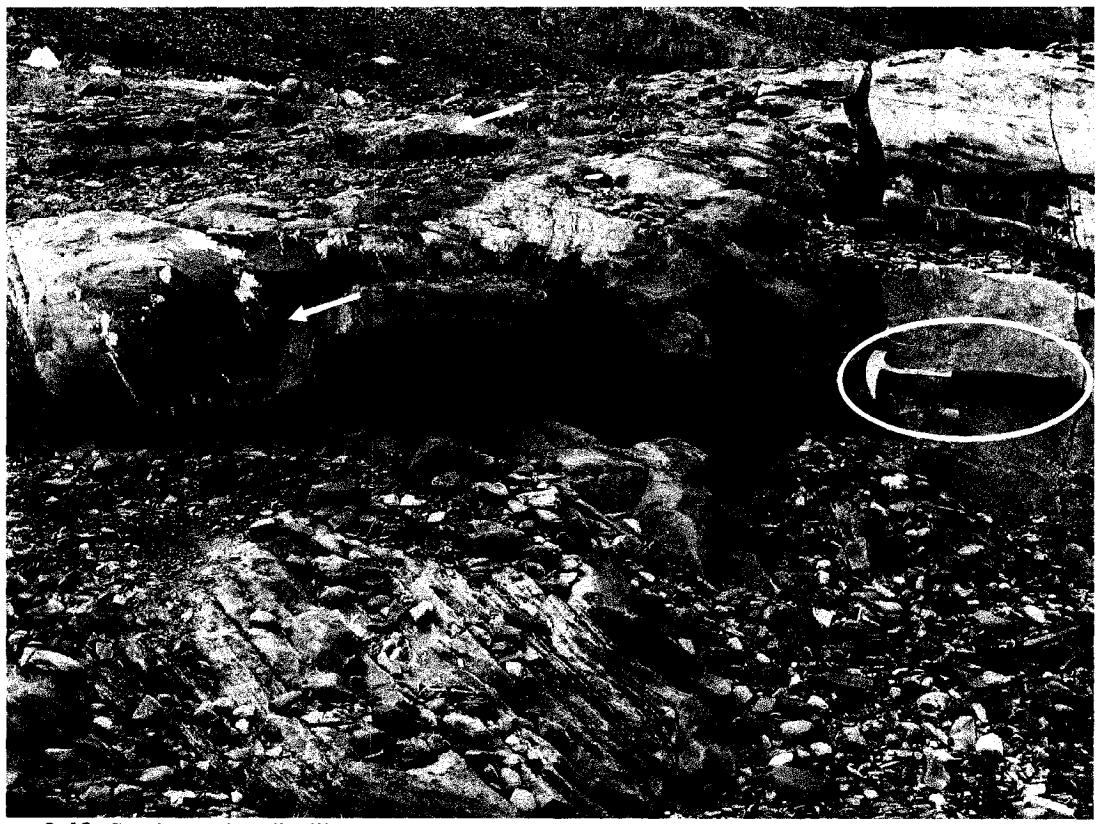

Figure 2.46. Sandstone boudin-like structures (arrows) embedded within a contorted sequence, FA4. Photo is from upper part of Channel 3.

2.3.5. FA5. Channel-abandonment association

A prominent fine-grained tabular unit (Facies association FA5) commonly occurs in the uppermost part of Channels 1 and 3. Additionally, it occurs at the top of the lower and middle part of Channel 1 and the middle part in Channel 3. FA5 abruptly overlies channel-fill association (FA3). It can be traced laterally for more than 1-1.5 km. Strata are 5 to 65 m thick, consist mostly of facies F4 and locally facies F1, and show a distinctive fining- and thinning- upward trend.

The basal part of FA5 is typically composed of repetitive heterolithic units of intercalated fine-to-very fine cross-laminated and parallel-laminated sandstone and silty mudstone or siltstone. Stratal units range from 2 to 20 cm thick (Fig. 2.47). Small-scale cross-laminated beds are 1-3 cm thick and stack to form multiple (2 or 3) cosets up to 10 cm thick. Siltstone beds are just a few centimeters thick and massive. The sandstone/siltstone ratio is approximately 2:3.

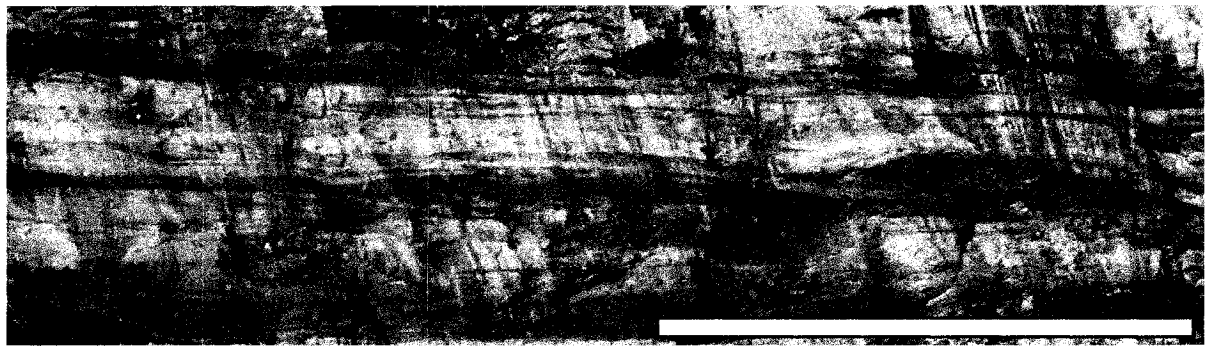

Figure 2.47. Strata in the lowermost part of the channel-abandonment facies association (FA5), consisting of multiple sequence of cross-laminated, fine-grained (brown) sandstone interbedded with grey siltstone. Photo is from uppermost part of Channel 1.

At the base of FA5, coarser beds are commonly interbedded with the heterolithic facies. Beds are 10-32 cm thick and consist of massive, very-coarse to medium sandstone. Beds have scoured or loaded bases. Beds are wedge shaped (pinch out one side only) or lens shaped (pinch out both side), and generally stack in a compensational pattern (Figs. 2.48 and 2.49).

Figure 2.48. Lenticular beds in an abandoned channel (FA5), showing pinch out terminations (arrows) with a compensational-stacking arrangement. Photo is from middle part of Channel 3.

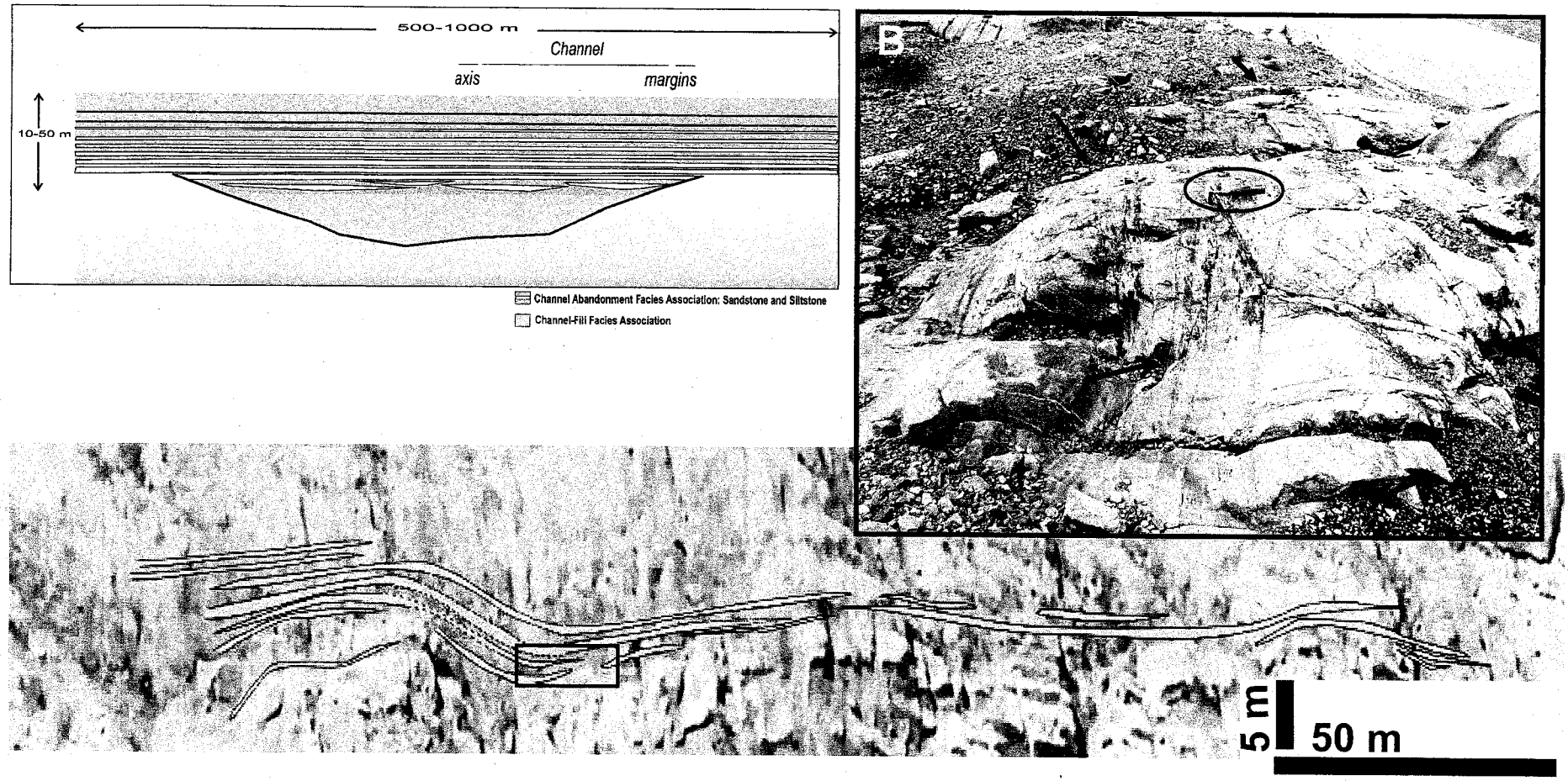

Figure 2.49. Lenticular, coarse-grained sandstone beds in the basal Channel-abandonment facies (FA5). A) Schematic mapping of some of these beds in an (unrestored) photomosaic reconstruction. B) Detail photo, indicating pinch-out terminations (arrow). These pinch out can be clearly seen in the field, but it is difficult to illustrate them in a close view. Photos are from uppermost part of Channel 1.

Upward the heterolithic strata changes from sandstone-dominated to more siltstone-dominated (Fig. 2.50). The siltstone-dominated upper part is composed of well sorted, cross-laminated and parallel-laminated very fine sandstone typically less than 1 cm thick (0.2 to 0.5 cm). Single ripple cross-laminated set are the most common. Massive and parallel-laminated siltstone beds with dark mudstone bands at their tops are increasingly abundant toward the top of FA5. Bed thickness of siltstone gradually increases from 2-4 cm thick in the middle part of FA5 to 12-15 cm to the upper part of FA5. Thus, sandstone/siltstone ratio decreases significantly (below 1:3).

The topmost part of FA5 is a clay-rich mudstone interval, which in the uppermost part of Channel 1 is a several meter thick claystone interval

Figure 2.50. Strata in the upper part of the channel-abandonment facies association (FA5). Note alternation of single-set, thinly-bedded, cross-laminated, very fine-grained sandstone (brown) and grey siltstone. Photo is from uppermost part of Channel 1.

2.3.5.1. Interpretation

The thin bedded, fine-grained successions at the top of Channel 1 and 3 are interpreted to record the change to low density, low competence sediment-gravity flows during the deactivation of the channel system. Thin-bedded, strata consist of upper division turbidites that were deposited as intrachannel flows became progressively less capable of transporting coarse-grained sediment.

Lenticular coarse sandstone beds (T_a or T_c intervals) at the base of FA5 represent the terminal competent flows in the study area. These flows most probably occurred in an exploited pre-existing negative topographic areas where some flows, however, were still focused (Grecula et al., 2003).

The progressive upward thinning of fine-grained sandstone in conjunction with thickening of siltstone beds confirms the decreasing of flow competence during the last stage of channel evolution. The claystone interval at the top of FA5 in Channel 1 is interpreted to record a change to exclusively hemipelagic deposition.

2.4. CHAPTER SUMMARY

There are four main lithofacies identified in intrachannel deposits of Channel 1 and 3. The most common Facies F1 consists of (coarse-tail) normally graded and massive sandstone and conglomerate (T_a Bouma or R_3/S_3 Lowe divisions), that are interpreted to have been deposited by high-concentration turbidity flows. Depending on the sediment concentration and principal support mechanism, deposition of these coarse-grained flows may occur by differential grain settling during the gradual or rapid aggradation of the flow, or collapse fallout from suspension associated with rapid deceleration of the flow.

Facies F2 is distinguished by mudstone-clast breccias (F_3 Mutti division) deposited from suspension or freezing deposition from sandy-gravelly high-concentration flows enriched with partially consolidated mud clasts that were derived from erosion of the underlying or laterally adjacent beds and/or upstream erosion and transport within the flow. In addition, brecciated facies may have been formed from post-depositional remobilization and soft-sediment deformation as a result of liquidization processes.

Facies F3 is composed of cross-stratified and parallel-laminated sandstone (T_c and T_b Bouma intervals) that, respectively, were deposited under tractional reworking and upper-flow regime conditions by sandy high-concentration turbidity flows. In contrast, facies F4 consists of heterolithic intervals (T_{a-d} interbedded with $T_{de,e}$ Bouma divisions) that were deposited from relatively high- or intermediate-concentration flows followed by low-concentration (muddier) turbidity flows.

Five facies association (at the level of organization of architectural elements) have been defined, and consist of one or more lithofacies. FA1 corresponds to bypass-channel facies associations of thin-bedded siltstone-sandstone, thick- to very thick-bedded conglomerate, and thin- to very thick-bedded mudstone clast breccia, bounded by basal erosion surfaces. They occur as a result of the initial transit of low to moderately concentrated, energetic and very efficient bypassing flows through the channel, depositing in basinward areas. Likewise,

inclined bed association (FA2) represents lateral accretion packages formed during significant periods of bypass in a laterally migrating sinuous channel.

Channel-fill association FA3 is the primary facies group that has been recognized and is characterized by thick-bedded conglomerate-sandstone to thin-bedded siltstone-sandstone deposited from high- to low-concentration turbidity flows. The degree of amalgamation of these deposits varies according to the flow character that was filling the channel. Locally, contorted and chaotic units (facies association FA4) were found in Channel 3 and is considered to be a slump deposit derived from upslope sources and locally deposited within the channel. Finally, the fine-grained succession (FA5), cropping out in the uppermost part of channel complexes is interpreted to be deposited from low-concentration turbidity flows during phases of complete channel abandonment.

Petrographically, conglomerate and sandstone from the passive-margin slope deposits of Channel 1 and 3 exhibit considerable feldspar content (up to 15%, or more). Feldspars have been strongly altered, forming a pervasive pseudomatrix that became recrystallized to fine-grained white mica (i.e. muscovite) and chlorite. The high content of plagioclase and potassium feldspars suggest that sediment was derived from a plutonic (possibly granitic) source area, probably from the Canadian Shield. Nevertheless, some conglomerate in Channel 3 contain boulder clasts of carbonate mudstone and crystalline carbonate with abundant ooids, peloids or fragments of stromatolites. Some clasts have been early cemented or partially neomorphosed and dolomitized. The occurrence of these clasts suggests an additional carbonate source area during the filling of Channel 3, most likely from a coeval tropical or subtropical carbonate platform.

CHAPTER 3. ARCHITECTURE OF TWO DEEP-WATER SUBMARINE CHANNEL COMPLEX SETS (CHANNEL 1 and 3) IN THE NEOPROTEROZOIC ISAAC FORMATION, WINDERMERE SUPERGROUP, CARIBOO MOUNTAINS, BRITISH COLUMBIA, CANADA

3.1. INTRODUCTION

A synopsis describing the hierarchy and architectural classification of channels is first introduced in order to establish some of the concepts and terminology used hereafter. The following chapter addresses the internal geometry, architectural elements, and facies distribution of Channel 1 and 3 in the Castle Creek South study area, and then concludes with a discussion of their similarities and sedimentary controls, and reservoir implications.

3.1.1. Chapter Aims

This chapter presents a detailed analysis of the architectural elements of two channel complex sets formed on the Neoproterozoic passive-margin slope of western Canada. The purpose of this analysis was to characterize the vertical and lateral changes in the fill of individual deep-water channels that comprise the Isaac Formation at Castle Creek, B.C. This was accomplished by measuring detailed, closely spaced (typically <20 meters) stratigraphic sections, and then correlating individual beds, bed sets and stratal units. The data can help to better constrain geological models that describe the configuration and evolution of complex channelized deep-marine systems. The objectives of this chapter, therefore, are to identify the hierarchy of architectural elements within Channel 1 and 3, and establish their geometry, dimensions, facies distribution, lateral and vertical continuity. Since this work provides the degree of detail needed in intra-reservoir characterization and modelling, few remarks about how some facies architecture recognized in Channel 1 and 3 could affect reservoir analogues are presented at the end of this chapter.

3.1.2. Channel Architecture and Hierarchy

Architectural elements, *sensu lato*, are the large-scale facies association that form the (two- or) three-dimensional "building blocks" of a particular depositional system (Walker and James, 1992). Architectural elements in deep-water clastic settings refer to mappable three-dimensional geomorphologic features observed in modern and ancient turbidite systems, including channels, overbank or levee deposits, lobes, etc (see Mutti, 1992; Clark and Pickering 1996; Posamentier and Kolla, 2003).

Several classification schemes for architectural elements of submarine channels have been proposed (Mutti and Normak, 1987; Pickering et al., 1995; Garner and Borer, 2000; Sprague et al., 2002; Abreu et al., 2003; Moraes et al., 2004). However, is used here a hybrid classification for deep-water channels that combines and summarizes these classifications (Fig. 3.1). In this classification, a discrete *channel fill*, also termed as a channel storey, is defined as a negative relief geomorphic feature through which a large number of turbidity currents are confined and directed downslope (Mutti et al., 2000). Individual channel fills are typically less than 10 m deep and 200 m long. A *channel unit* comprises two or more channel fills, which are interpreted to be genetically related. A *channel complex* consists of two or more distinct stacked channel units. A *channel complex set*, in turn, is composed of two or more channel complexes, each delimited by a shift of facies or abandonment surface at its base and top (Abreu et al., 2003). Finally, a *channel system* is the highest order hierarchical element and consists of more than two genetically related channel complex sets.

3.1.2.1. Channel stacking pattern

The connectivity and stacking of individual channel fills is observed in outcrop or seismic sections is related to the interactive relationships between lateral channel migration and aggradation during the evolution of a channel system (Clark and Pickering, 1992; Mchargue, 1991). Other factors (as shown in Fig. 3.2) that may impact channel stacking patterns include: channel sinuosity, rate of sediment accumulation, sand/mud ratio of sediment supplied (net-to-gross ratio), and the degree of channel confinement.

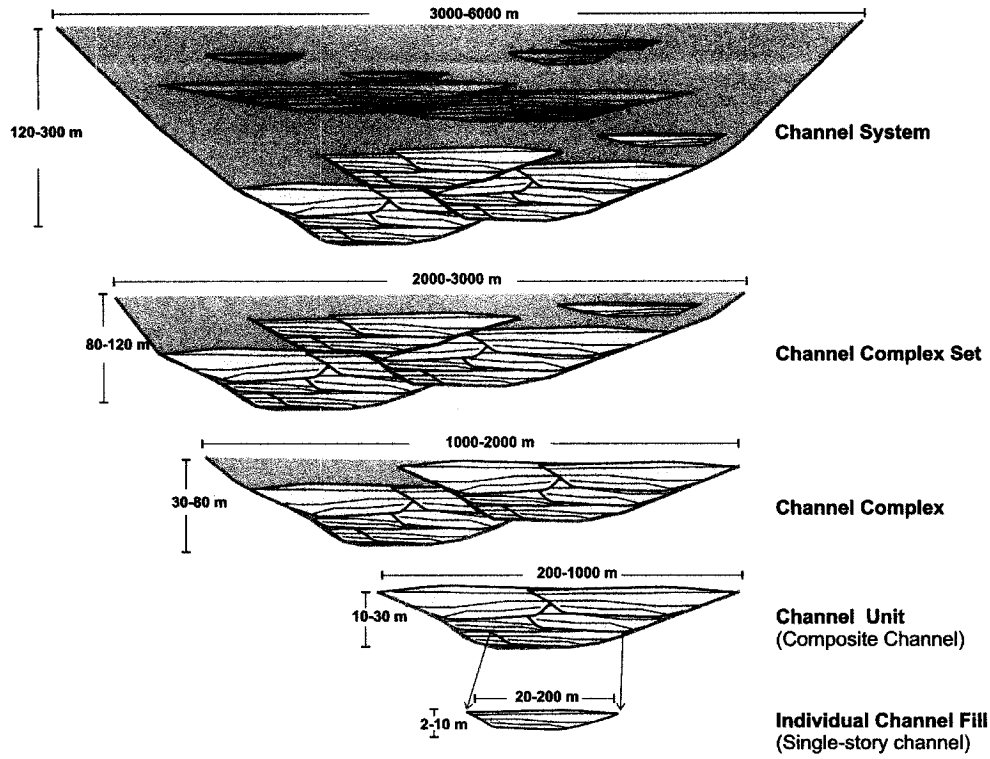

Figure 3.1. Stratigraphic hierarchy of strata in Channel 1 and 3, Castle Creek South area.

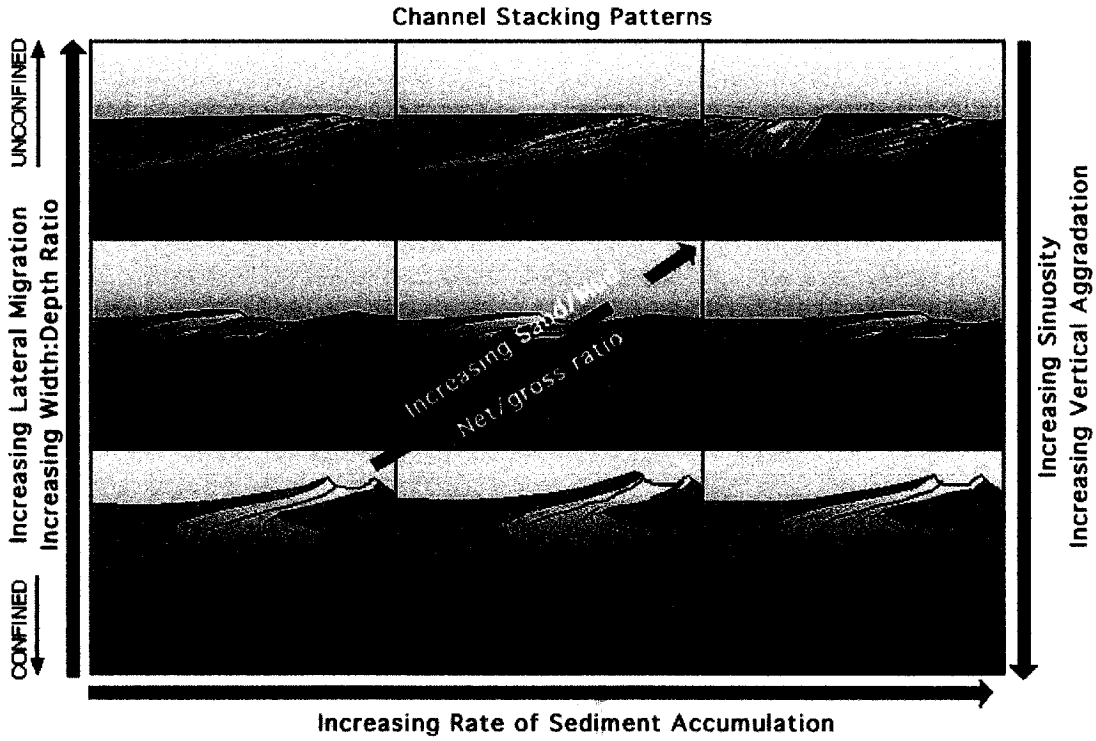

Figure 3.2. Schematic diagram of channel stacking pattern, showing how width: depth ratio of stacked channel complexes relates to lateral migration and vertical aggradation of individual channel storeys (after Clark and Pickering, 1996).

3.1.3. Channel 1 and 3 Data

A total of 67 measured vertical sections and 28 scintillometer profiles were collected and mapped onto air-photomontages in the field, and their locations are included in Appendix I. Thirteen cross-sections or correlation panels constructed to illustrate facies distribution and geometry of intrachannel strata in Channel 1 and 3 are shown in this chapter. Gamma-ray logs are presented in Appendix IV. Channel 1 is oriented oblique to the general northwest paleoflow direction determined from a small number of cross-stratified structures. In contrast, Channel 3, or at very least the lower channel complex, is oriented almost perpendicular to the general paleoflow. Moreover, a quantitative analysis based on data obtained from measured sections is presented in Appendix V.

3.2. CHANNEL 1: Geometry and Architectural elements

In the study area, Channel 1 is generally less than 200 m thick, and although the lateral margins are incompletely exposed, its width is estimated to be of the order of 2 to 3 km. The orientation of the outcrop face is southeast-northwest (330°), oblique to the general axis (~40°) of the channel network in Channel 1 (Fig. 3.3). Based on the hierarchical classification proposed in section 3.1.2, Channel 1 is a channel complex set divided into lower and upper channel complexes (denoted as Ch1.L and Ch1.U in Fig. 3.3) that range from 30 to 90 m thick, and individually comprise several channel units composed of more than two channel fills. Major erosion surfaces at the base of individual channel units and fills are generally shallow (less than 1 m deep), but locally are up to 11 m deep. Bedding surfaces are typically parallel to the basal surface of the channel. Locally, irregular scour-and-fill and load structures have also been observed.

3.2.1. Lower Channel Complex, Channel 1

The lower channel complex (Ch1.L) is poorly exposed in the study area, being mostly covered by vegetation and/or moraine. It overlies a brown/grey-weathering, carbonate marker unit, up to 250 m thick, that is composed mostly of allodapic limestone and dolostone accumulated at the base-of-slope. This unit consists of thin-bedded carbonate turbidites (T_{cde}), blocks of slumped limestone, and laminated calcareous siltstone and shale interbeds. Upward this unit becomes increasingly mixed with siliciclastic sediment and eventually becomes interstratified with siliciclastic sandstone turbidites.

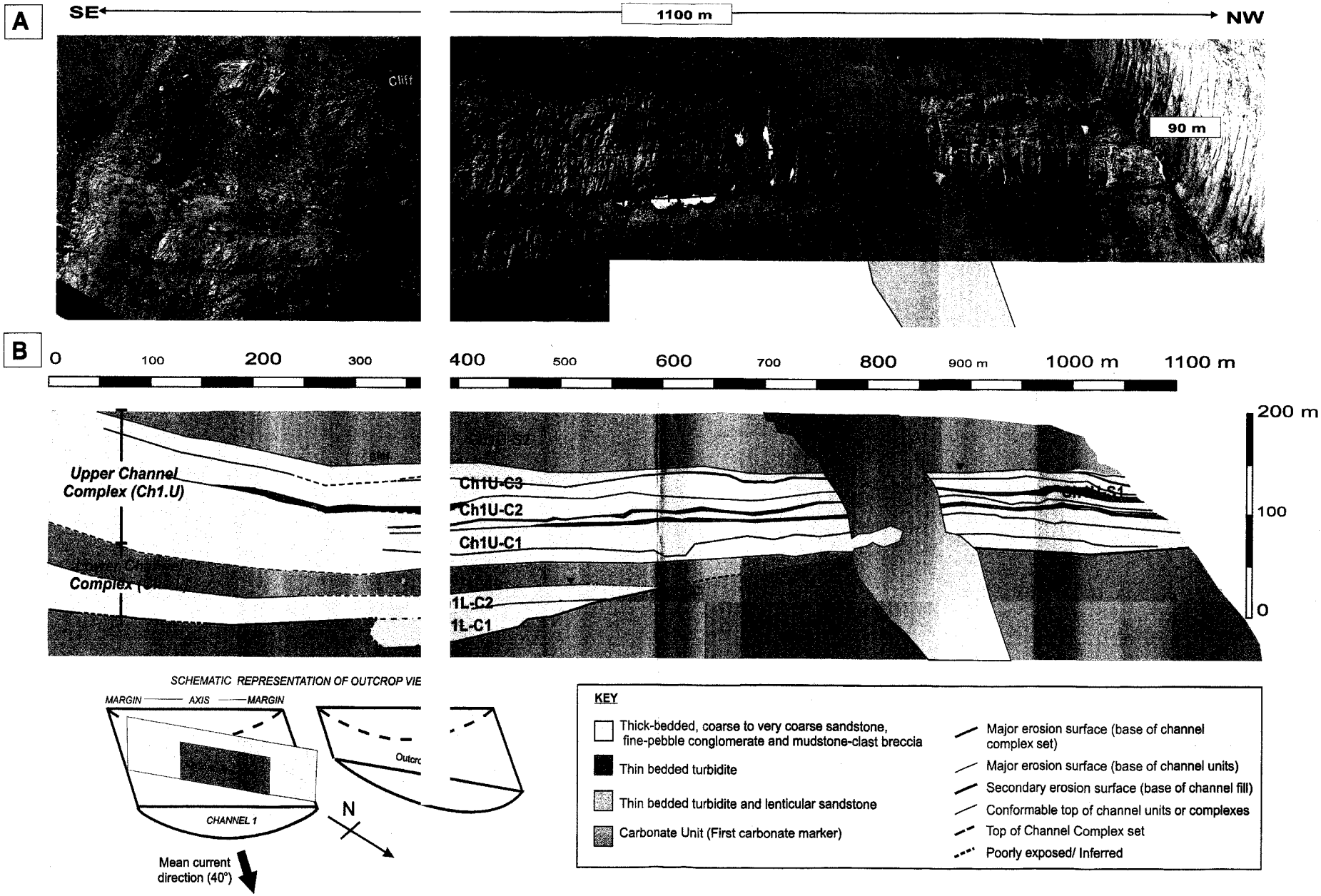

Figure 3.3. Vertical and lateral stacked channel complexes of Channel 1, Castle Creek South. (A) Oblique-view, photomosaic showing the 1.1 km-wide outcrop belt. (B) Simplified schematic architectural panel showing channel complexes of Channel 1, highlighting the major channel units and fills. Note the oblique orientation of the outcrop face in relation to mean paleoflow direction. For map location of logs and samples see Figs. I.1-I.3 in Appendix I.

Two channel units are recognized in Ch1.L. Each is up to a few decameters thick and in one case is over 600 m wide. These channel units illustrate the character of Ch1.L along its northwestern margin (Fig. 3.4).

3.2.1.1. Channel Unit Ch1.L-C1

The lower channel unit (Ch1.L-C1) is an apparently single channel with a convex-up geometry and an asymmetrical erosional basal surface. It is less than 250 m wide and ranges from 11-20 m thick in the axial part of the channel. The most common facies association (architectural element) observed in this channel unit is the partly amalgamated channel-fill facies association (FA3b; see chapter 2, section 2.3 for discussion).

The channel-form element observed in Ch1.L-C1 shows a partly amalgamated to layered infill. The channel fill consists predominantly of thick-bedded, very coarse to coarse, massive sandstone and normally graded conglomerate in the axial part. Laterally, bed thickness decreases from an average of 1.3-1.6 m to 0.6-1.1 m in the partly exposed northwest margin (Fig. 3.4; and table V.1 and Fig. V.1 in Appendix V). Away from the channel axis, the more amalgamated coarse-grained beds are interbedded with thin-bedded, fine-grained sandstone and mudstone. Therefore, the average sandstone percentage (net-to-gross) changes gradually from 99% in the channel axis to 86% near the channel margin. Additionally, several beds lap onto the basal erosion surface exposed along the northwestern margin.

3.2.1.2. Channel Unit Ch1.L-C2

The upper channel unit Ch1.L-C2 is a multistory channel incised into not only the underlying channel unit Ch1.L-C1 but also the regional carbonate marker (see Fig. 3.4). Ch1.L-C2 is more than 18 m thick and is of at least across a width exposed over 600 m. It can be traced for more than 1 km at the southeast end of the study area, where inferred deposits of this channel unit show significant facies changes and increase in thickness. In the southeastern area, Ch1.L-C2 consists of two sandstone-dominated channel fills separated by a >5 m thick fine-grained interchannel interval (Fig. 3.5).

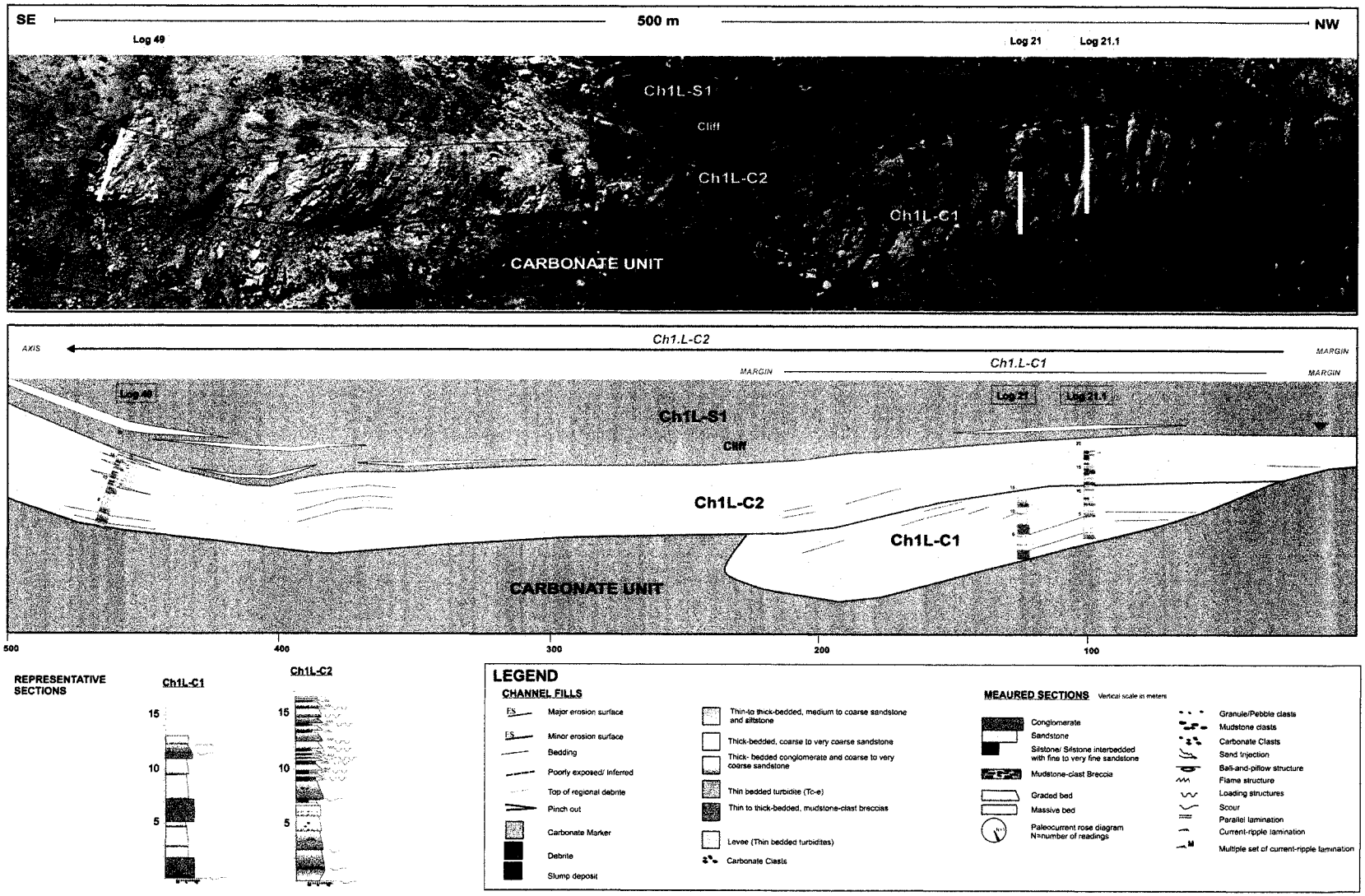

Figure 3.4. Photomosaic and line tracing of the Lower Channel Complex in Channel 1 illustrating bedding geometry, facies and architectural elements. This schematic has attempted to removed the most evident topographical effect.

The channel unit consists mostly of decametre-thick, partly amalgamated channel fills (FA3b, for general details of facies association see chapter 2, section 2.3), composed of 0.4 to 1.6 m thick, normally graded conglomerate and sandstone that upward become more interstratified with fine-grained beds (Fig. 3.4). Similar to Ch1.L-C1, beds thin laterally and onlap the northwest channel margin. Moreover, some beds pinch-out laterally, especially in the upper part of the channel unit. Sandstone net-to-gross varies laterally from 91% in the channel axis to 70% near the margin (table V.1 and Fig. V.1 in Appendix V).

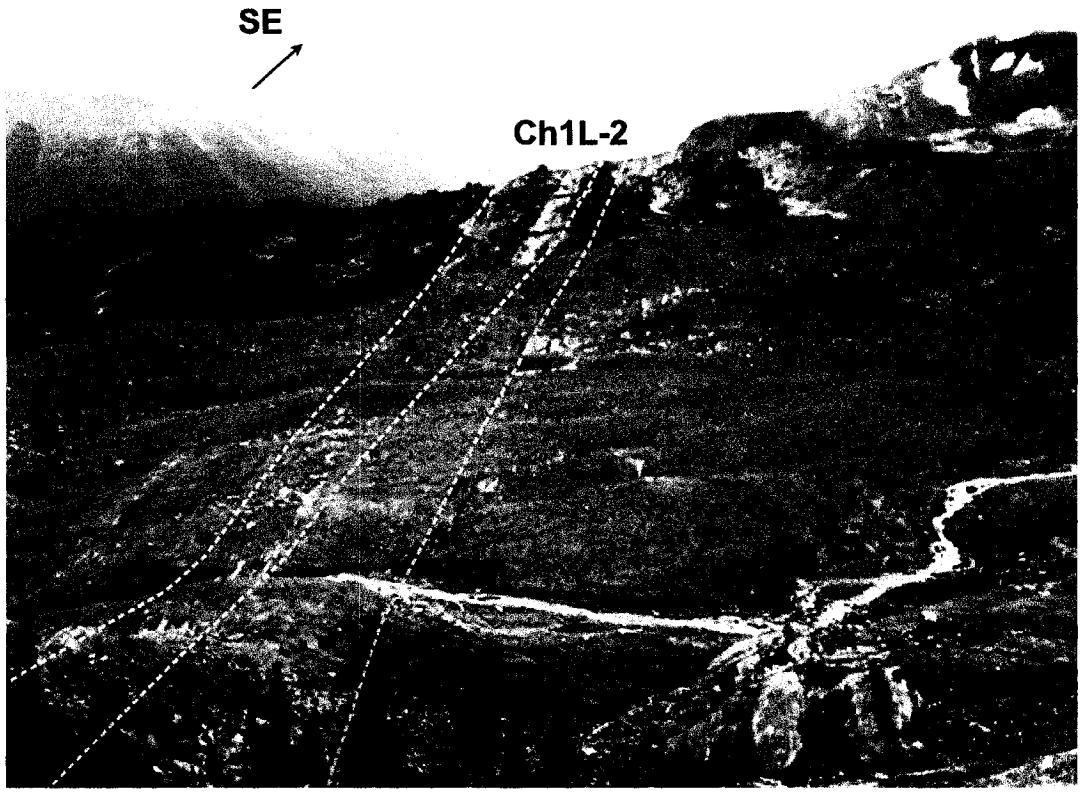

Figure 3.5. Southeast panoramic view of the channel unit Ch1.L-C2 (lower channel complex). Channel 1. Sandstone-dominated channel fills are denoted with yellow dotted lines and the fine-grained dominated intervals are indicated with green dotted lines.

3.2.1.3. Layered thin-bedded sheet (Ch1.L-S1)

The top of Ch1.L-C2 marks the top of the lower channel complex of Channel 1 (Ch1.L). This surface is overlain by an approximately 10 m thick, tabular or sheet-like interval (Ch1.L-S1) consisting of mostly thin-bedded (up to 5 cm thick), heterolithic facies with common ripple cross- and parallel-lamination sandstone (FA5 facies association). Medium bedded (20 cm) lenticular beds of coarse sandstone occur at the base of the interval.

3.2.1.4. Interpretation

The architecture of the Lower Channel Complex of Channel 1 (Ch1.L) illustrates multiple episodes of incision and infill. The almost 10 m deep, basal surface of Ch1.L-C1 represents the initial episode of erosion along the top of a regional deep-water carbonate interval (sequence stratigraphic significance of this interval will be discussed in the chapter 4), and is similar to channels described by Eschard et al. (2003) from outcrops in Pakistan. Initial incision was the result of highly efficient flows that most probably were preferentially routed through topographically low areas during a long-term episode of bypass. The lower, thick-bedded, coarse-grained high-concentration sandy turbidites in Ch1.L-C1 record the earliest stages of channel infill related to a change to more sand-rich, less efficient flows.

The upper channel unit (Ch1.L-C2) is wider than Ch1.L-C1 and consists of semi-amalgamated channel fills (FA3b) made up mostly of sand-rich, high-concentration turbidites that upward and laterally become gradationally interstratified with fine-grained, low-concentration turbidites. The upward change to less amalgamated sandstone observed in the upper part of these fills and toward the (northwestern) channel margin is inferred to indicate deposition from smaller, lower concentration, more mixed (sand/mud) flows. The thin bedded, fine-grained interval that separates two channel fills beyond the southeastern part of the study area might correspond to temporary deactivation of Ch1.L-C2.

The layered thin bedded sheet (Ch1.L-S1) that caps the uppermost channel fill of Ch1.L-C2 was deposited from muddy, low-concentration turbidity currents (FA5) that represent a complete abandonment of the lower channel complex (Ch1.L), possibly associated with a decreasing sediment supply and flow energy (Eschard et al., 2003), or upstream channel avulsion.

3.2.2. Upper Channel Complex, Channel 1

The upper channel complex of Channel 1 (Ch1.U) is about 90 m thick and more than 1.6-2 km wide, but only 1.1 km was mapped in this study. It overlies channel complex Ch1.L in the southeast and the carbonate marker unit in the northwest. At least three distinct channel units have been recognized in Ch1.U (Fig. 3.3), and they are typically 20-30 meters thick.

3.2.2.1. Channel Unit Ch1.U-C1

The lowermost part of Ch1.U-C1 is 22-45 m thick and is characterized by a broad (intermediate to high aspect ratio (i.e. width/depth)) channel unit, e.g. width:depth is 1600:45. It comprises numerous amalgamated, vertically-stacked, turbidite-filled channels. Basal surfaces are commonly laterally extensive, shallow (<1 m) and parallel to the erosion surface at the base of Ch1.U-C1 (Fig. 3.6). In the axial areas, however, basal surfaces are locally steeply scoured. The relatively low relief of the channels and their typically high bed amalgamation makes them difficult to distinguish individually in areas with poor lateral continuity or exposure.

Channel fills in the lower part of Ch1.U-C1, consist mostly of highly amalgamated, thick-bedded (in average 0.8-1.5 m) conglomerate and coarse to very coarse sandstone (FA3a facies association; see Fig. 3.6a, 3.6b). In the middle and upper part of Ch1.U-C1, channel fills display distinct vertical and lateral facies variations.

Channel-axis deposits consist typically of thick bedded, amalgamated mudstone-clast breccia (FA1c facies association) overlying a basal erosion surface. Breccias include outsized mudstone clasts (1-1.5 m diameter) and make up to 23% of the stratal succession in the axial areas. Lenses of fine conglomerate and sandstone are generally interbedded within the thickest breccia beds. The lateral continuity of breccia beds is variable. The occurrence and stacking of breccia layers in the channel axis form asymmetrical, erosional zones, that are almost 100 m wide and 3-10 m deep (Fig. 3.7). Laterally away from the axis, the channel becomes shallower and strata become finer and interbedded with siltstone near the channel margin.

Channel-margins deposits are dominated by FA3b facies association composed of moderately amalgamated, thick bedded (up to 1.3 m), normally graded and massive conglomerate and sandstone and lesser amounts of basal mudstone-clast breccia (Fig. 3.6b, 3.8). Gradationally upward and laterally, these strata become progressively more interstratified with coarse-grained, cross-bedded sandstone (facies F3.1) and fine sandstone interbedded with mudstone (facies F4; Fig. 3.6b).

Lateral continuity of the fine-grained beds is poor, from 1-2 m to a maximum of a few hundred of meters. Medium-scale, cross-bedded sandstone suggest paleoflow toward the northeast (20-40°).

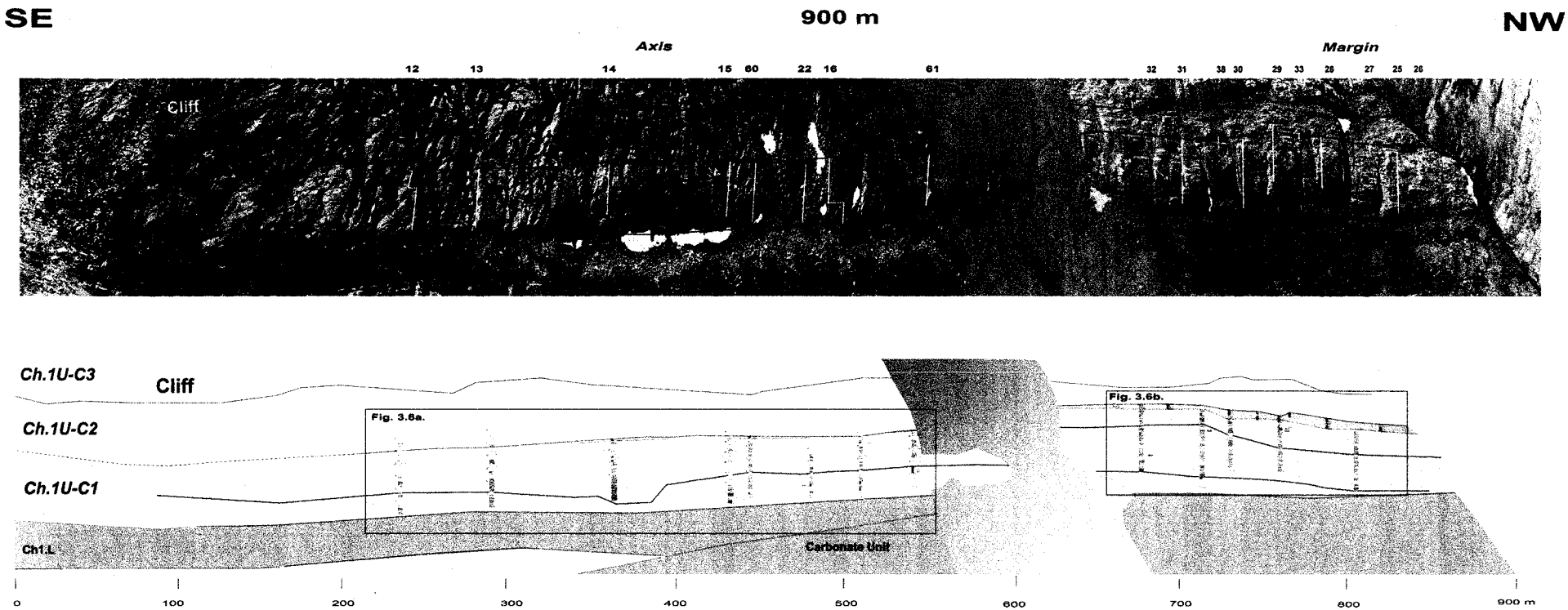

Figure 3.6. Photomosaic and line tracing of Lower Channel Unit in the Upper Channel Complex, Channel 1 illustrating bedding geometry, facies and architectural elements.

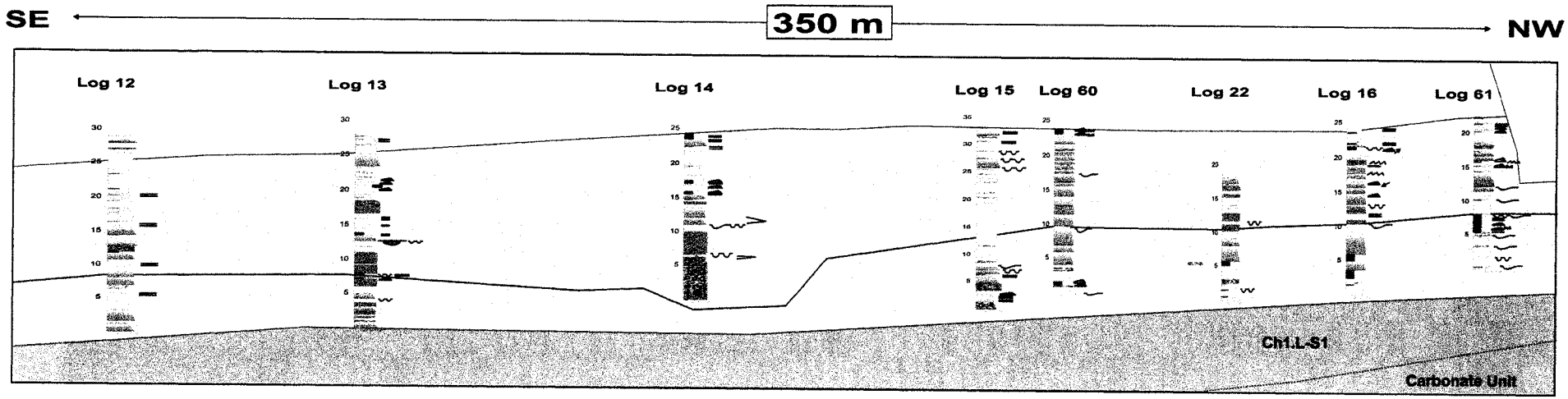

Figure 3.6a. Measured sections in the SE of Lower Channel Unit in the Upper Channel Complex, Channel 1 (Ch1.U-C2). For legend see Fig. 3.4

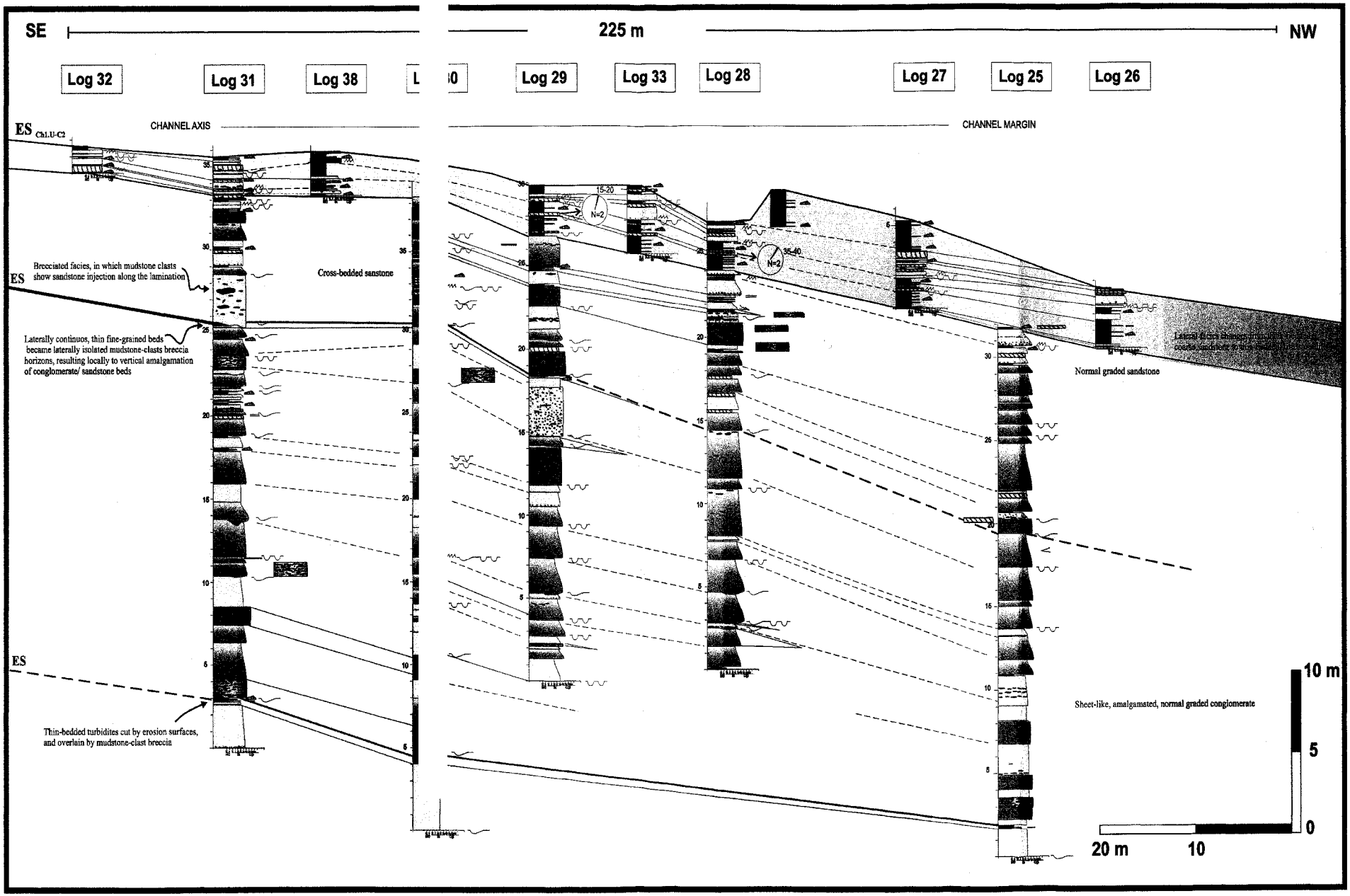

Figure 3.6b. Correlation diagram for the NW part of channel unit Ch1.U-C1 in the Upper Channel Complex, Channel 1 illustrating bedding geometry and facies. For legend see Fig. 3.4

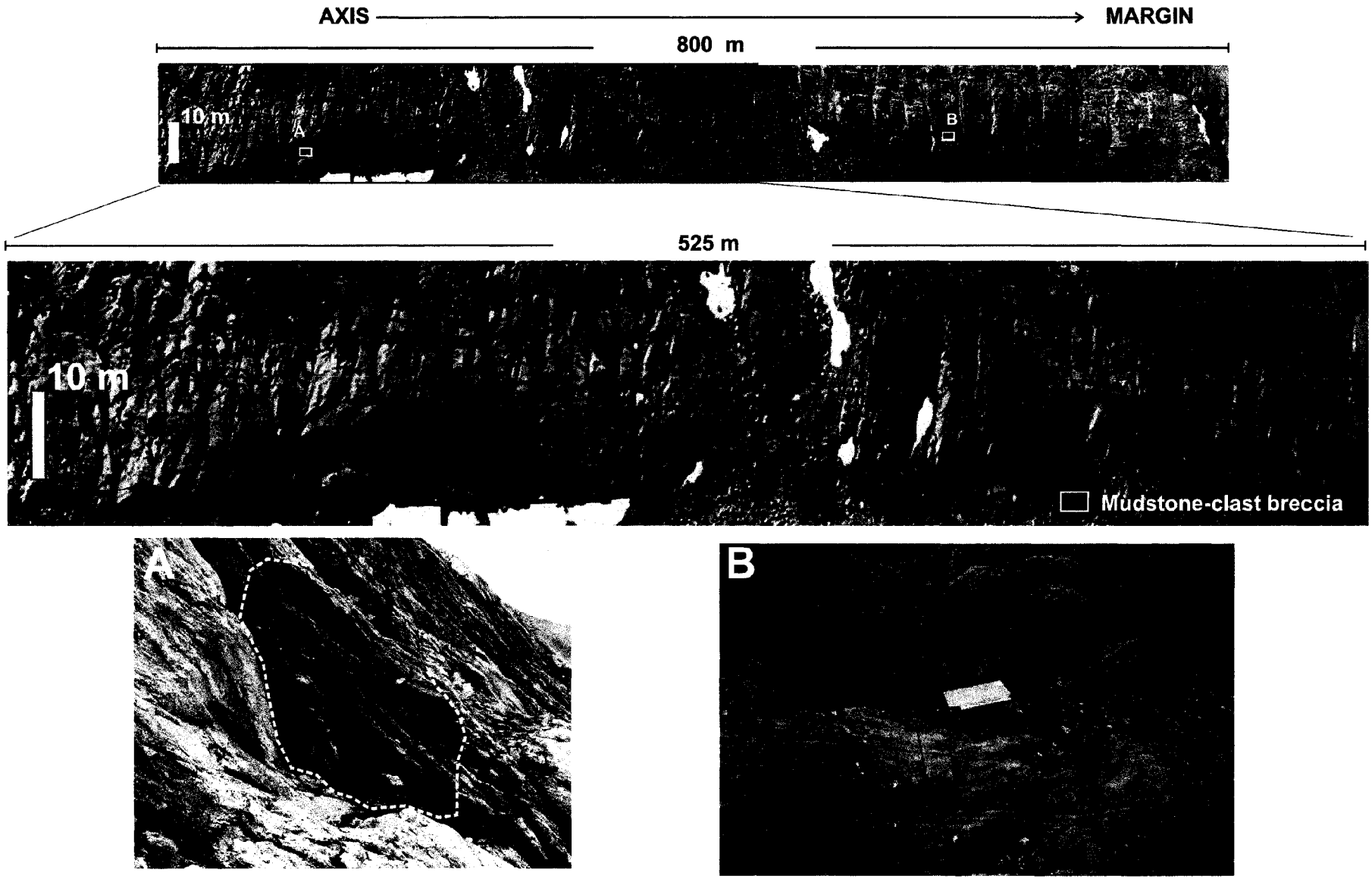

Figure 3.7. Some mudstone-clast breccia zones in the lowermost channel unit of upper channel complex C1U, Channel 1. Note the depth and lateral extent of these zones. A) Detail of boulder mudstone clast (roughly enclosed by white dotted line) in a breccia zone within the channel axis. Hammer for scale. Oblique view, looking northwest. B) Close-up of mudstone-clast breccia lying on top of thinly-bedded, fine-grained unit. Fieldbook for scale.

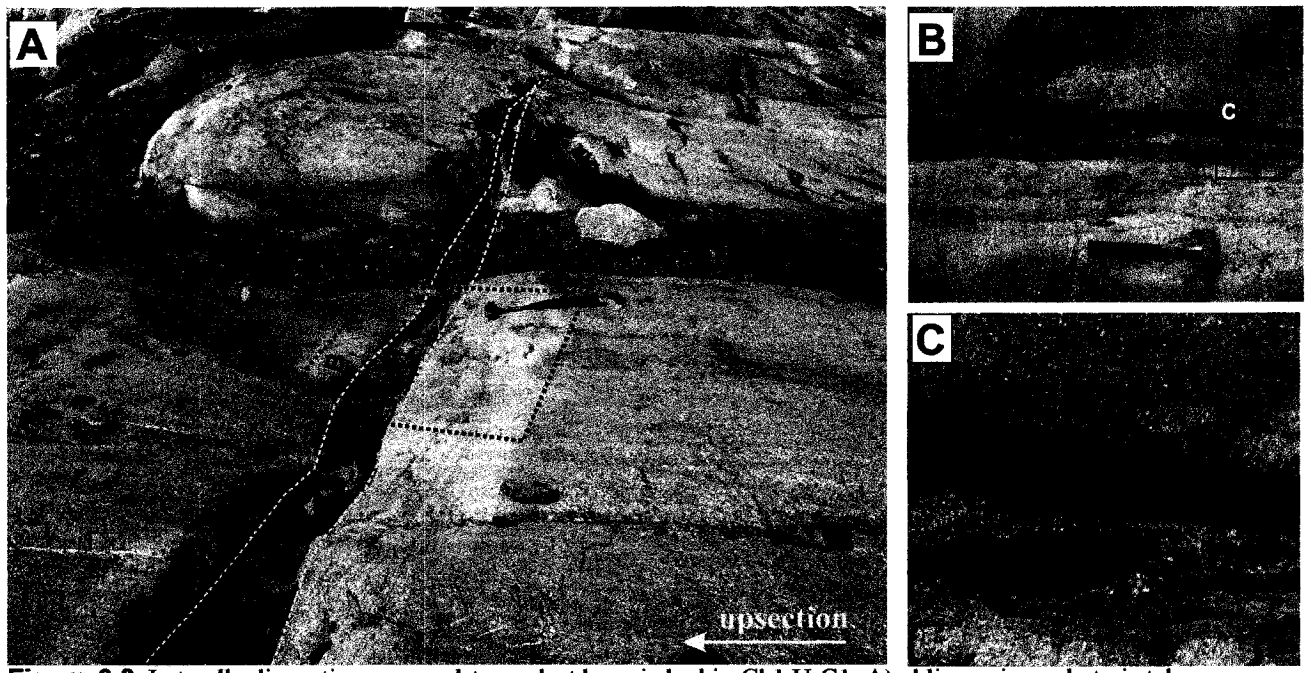

Figure 3.8. Laterally discontinuous, mudstone-clast breccia bed in Ch1.U-C1. A) oblique view, photo is taken looking northwest. B) detail of photo A and C) inset, in which the breccia matrix is slightly coarser than the underlying and overlying sandstone beds.

Bed thickness decreases slightly upward and beds become less amalgamated. Moreover, the percentage of sandstone/conglomerate (net-to-gross) decreases rapidly toward the channel margins (from 98 to 84%; see Fig. V. 2 and table V.2 in Appendix V).

In the uppermost part of Ch1.U-C1, coarse-grained beds laterally fine, thin and quickly become (in less than a few hundred meters) more interbedded with heterolithic facies toward the northwestern channel margin (Fig. 3.6b, 3.9; see Fig. V.2 and table V.2 in Appendix V). Loading and deformational structures are common in channel unit Ch1.U-C1, but are most common in the uppermost part.

3.2.2.2. Channel Unit Ch1.U-C2

The middle channel unit (Ch1.U-C2) is at least 1.1 m wide (estimated to be >1.6 km wide) and up to 25 m thick (Fig. 3.3), with intermediate to high aspect ratio (e.g. 64). Ch1.U-C2 scours into the uppermost part of Ch1.U-C1, especially in the channel-axis areas (Fig. 3.10, 3.10a). Ch1.U-C2 consists of at least three stacked channel fills that each have a basal erosion surface draped by thin-bedded mudstone or sandstone-siltstone (FA1a facies association; Fig. 3.11) or mudstone-clast breccia (FA1b facies association). The percentage of FA1 strata is less (up to 5%) than that in the lower channel unit (Ch1.U-C1). Even though

channels show relative low erosional relief (<1 m), localized steeply dipping (up to 3-4 m deep) scours are observed, mostly in the axis of the channel.

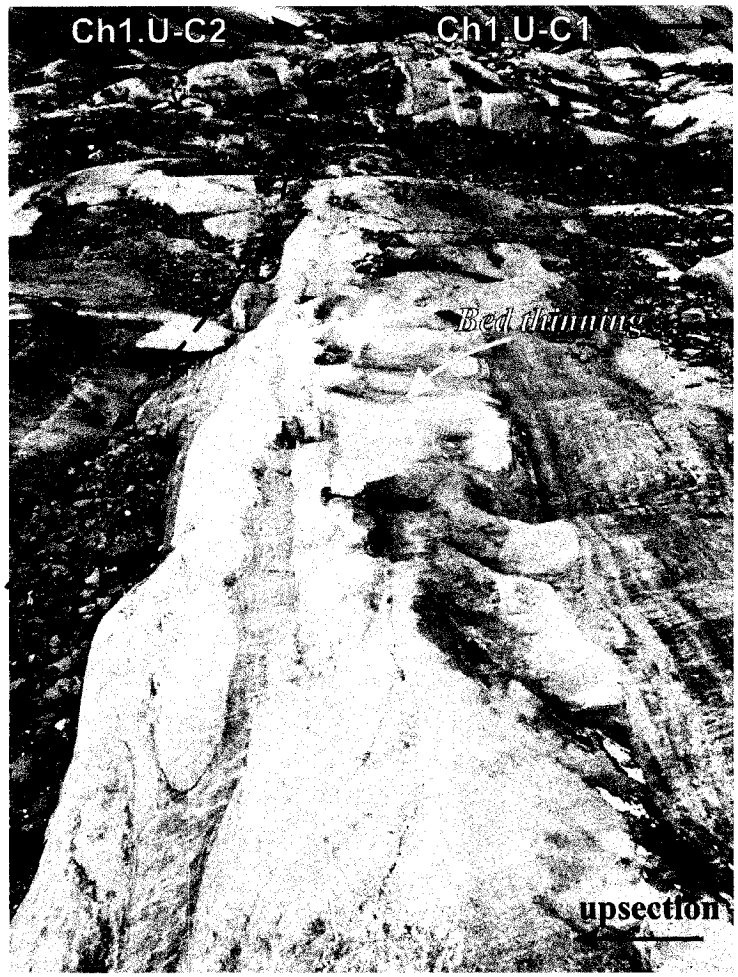

Figure 3.9. Coarse, normal graded, cross-bedded sandstone interstratified with thin-bedded facies in the uppermost part of Ch1.U-C1. Note the dramatic thinning of the beds toward the channel margin (top of photo). Oblique view, looking northwest.

The channel fills are sand-rich and composed of thick-bedded (>0.4 m), normal graded sandstone commonly interbedded with cross-bedded sandstone and thin-bedded sandstone and siltstone (Fig. 3.10, 3.10a, 3.10b). In comparison with Ch1.U-C1 (lower channel unit), cross-bedded sandstone and fine-grained beds are considerably more common (up to 15%) in Ch1.L-C2. Minor granule conglomerate beds are also observed. Away from the channel axis, beds become distinctly less amalgamated and more laterally continuous, forming more interstratified strata near the channel margins (Fig. 3.10b). Like Ch1.U-C1, Ch1.U-C2 shows a lateral decrease of sandstone/conglomerate ratio from 89-95% in the channel axis to 70% near the margins (see table V.2 and Fig. V.2 in Appendix V).

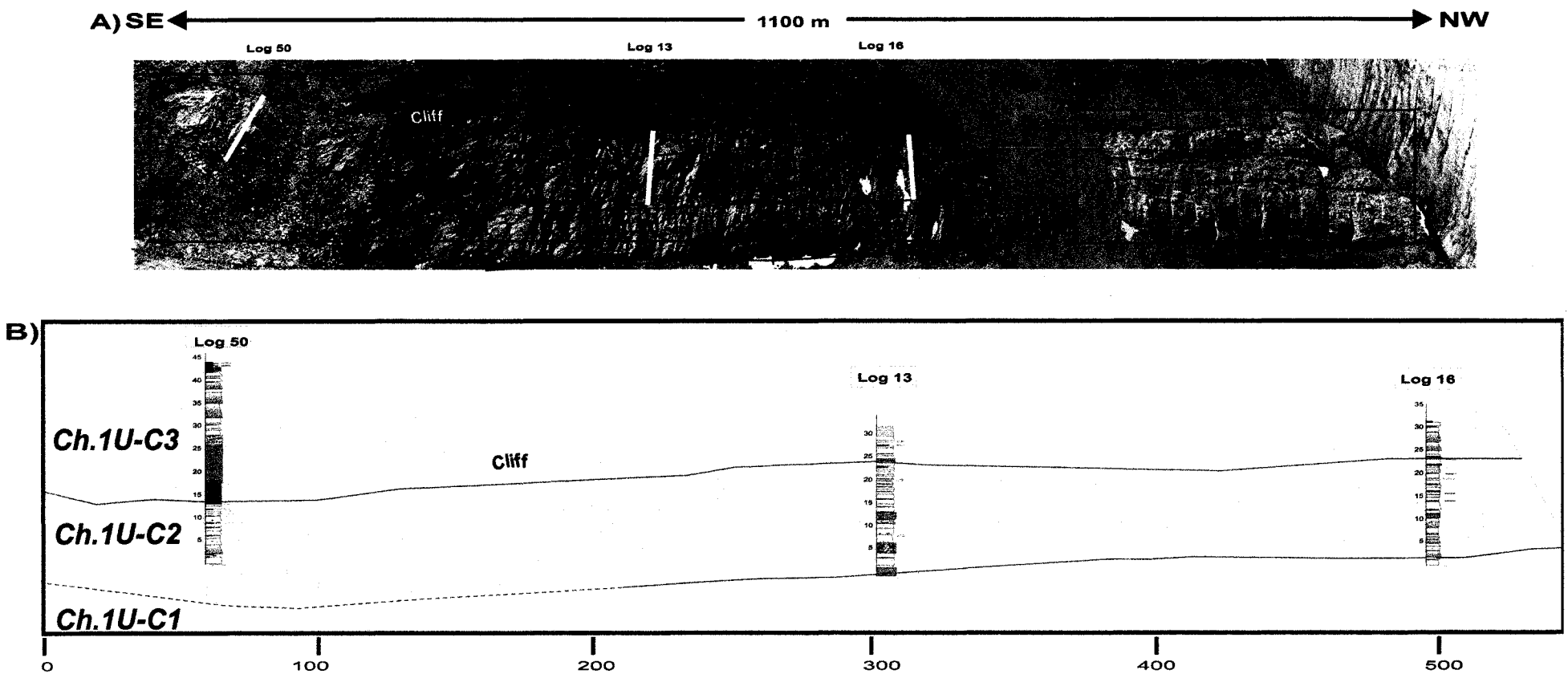

Figure 3.10a. Measured sections in the SE of Middle and Upper Channel Unit in the Upper Channel Complex, Channel 1 (Ch1.U-C2). The location of the logs is shown in a (A) photomosaic and line tracing of both channel units in the Upper Channel Complex, Channel 1. For legend see Fig. 3.4.

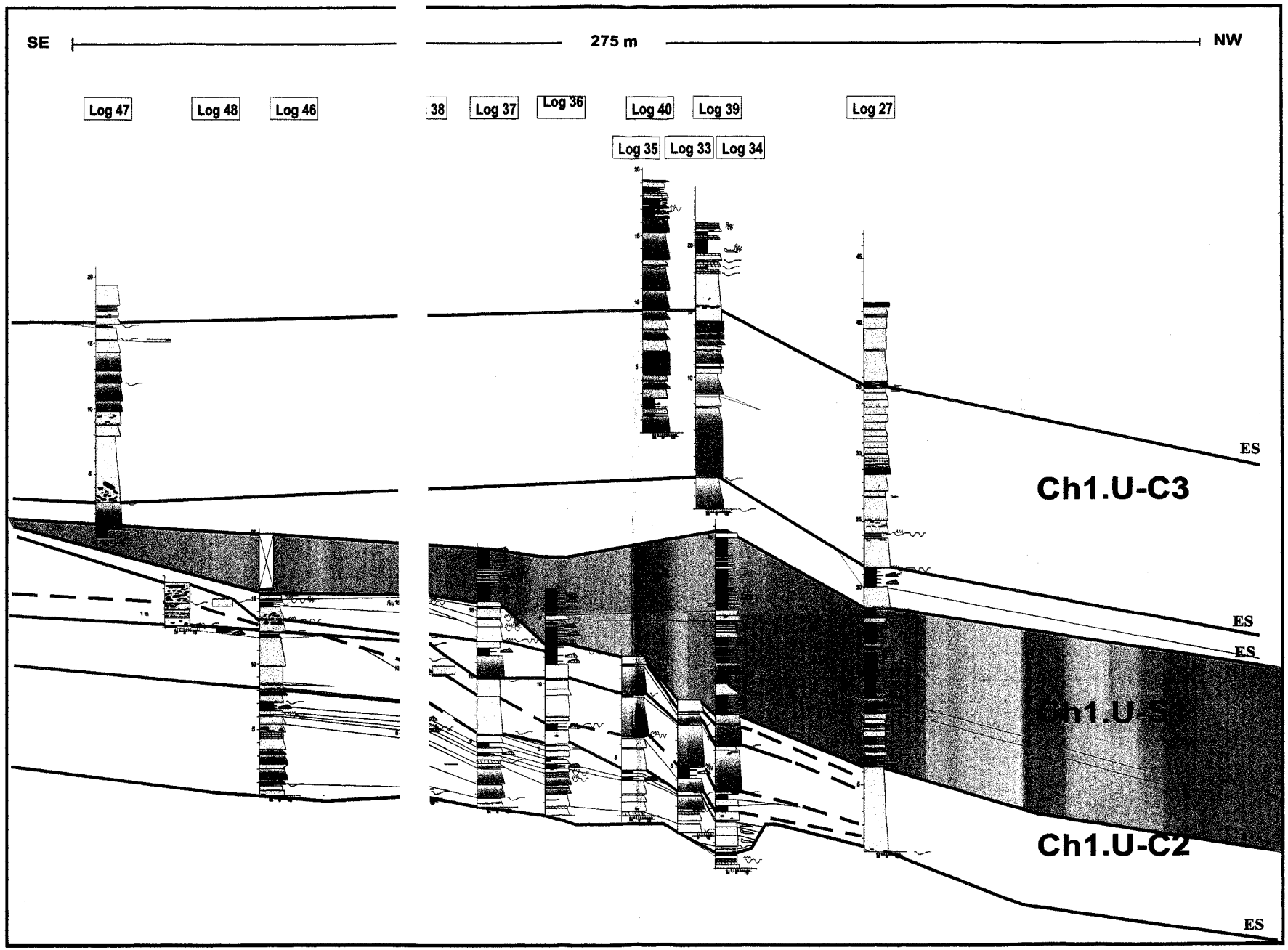

Figure 3.10b. Representative measured sections through the NW part of channel units Ch1.U-C2 and Ch1.U-C3 in the Upper Channel Complex, Channel 1 illustrating bedding geometry and facies. For legend see Fig. 3.4

Channel fills also change upward from partly amalgamated sandstone to less or non-amalgamated sandstone. Post-depositional features (e.g. flames, brecciated facies, deformed cross-beds and load structures) are common in the channel unit.

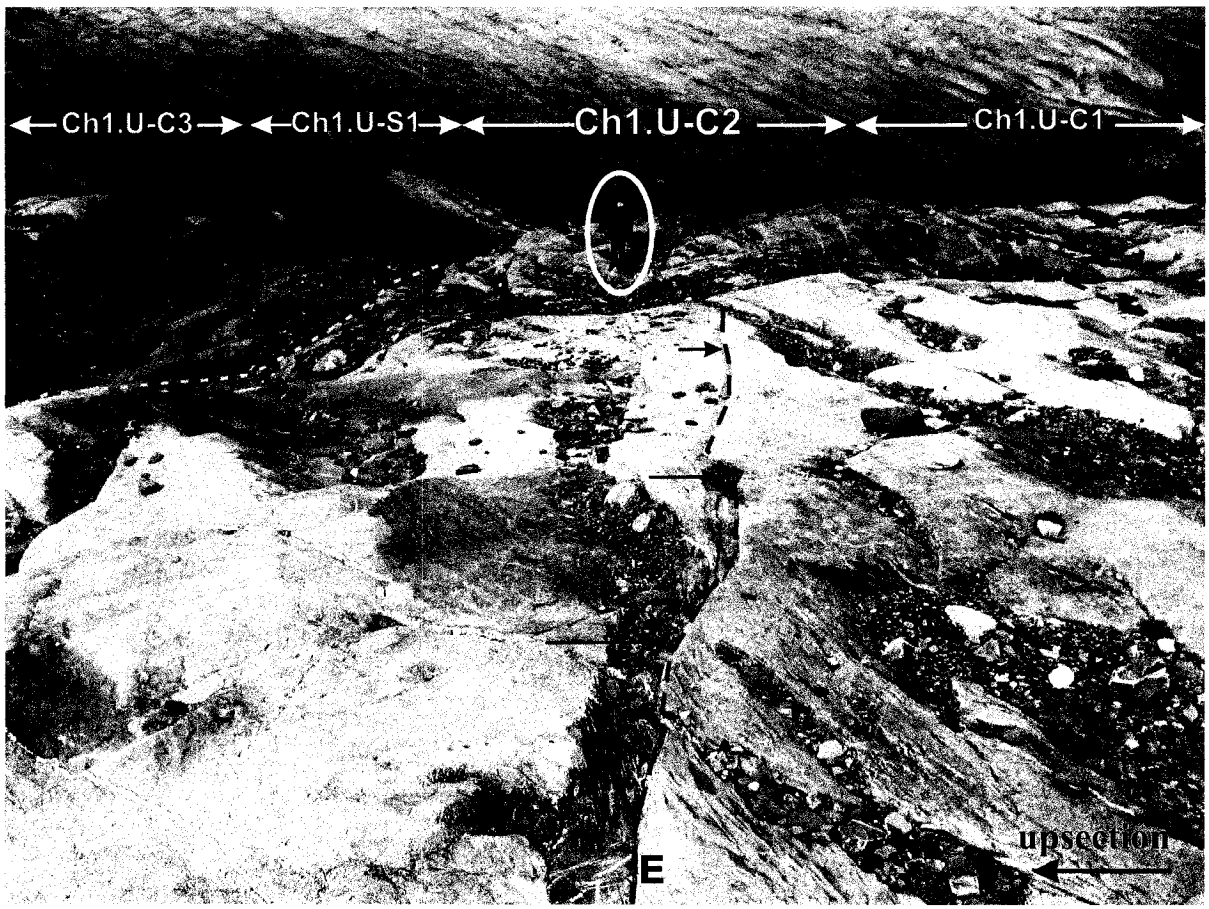

Figure 3.11. Erosion surfaces at the base of channel fills in Ch1.U-C2 (red dashed lines). Note the erosion surface, denoted with letter E, is draped by thin-bedded (5-20 cm thick) silty mudstone or siltstone bed. Channel fills in Ch1.U-C2 are dominated by amalgamated to semi-amalgamated, normal graded, very coarse sandstone, locally interbedded with mudstone beds. Ch1.U-C2 is capped by a interval of fine-grained turbidites (Ch1.U-S1). Person for scale. Oblique view, photo is taken looking to the northwest.

3.2.2.3. Layered thin-bedded sheet (Ch1.U-S1)

A distinctive, 12-15 m-thick layered succession (Ch1.U-S1) with low average sandstone content overlies the uppermost fill of Ch1.U-C2, and appears to drape the residual topography (Fig. 3.10b). This succession thickens laterally toward the northwest and is gradually truncated to the southeast by the overlying channel unit, Ch1.U-C3 (Fig. 3.12). It consist of thinly-bedded (average 3 cm), interbedded/interlaminated ripple- and parallel-laminated fine sandstone and siltstone (FA5 facies association).

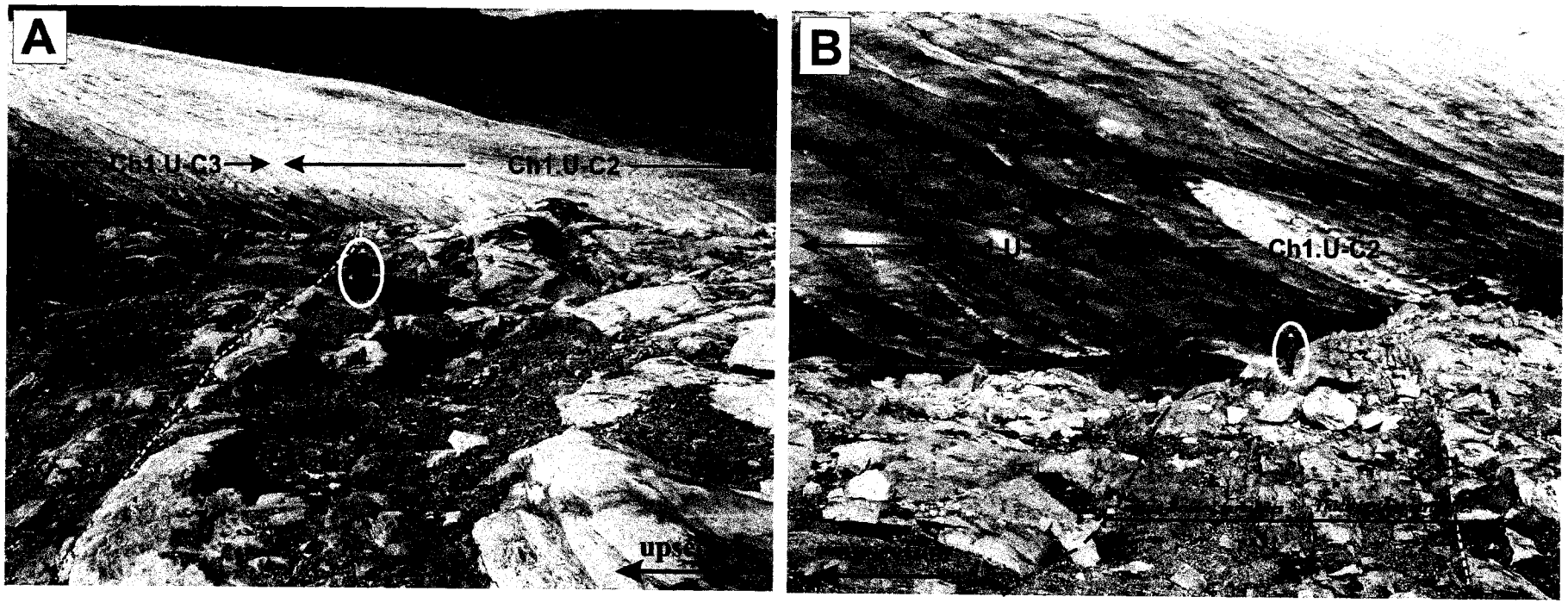

Figure 3.12. Layered thin-bedded interval, Ch1.U-S1, overlying the channel unit Ch1.U-C2 in Channel 1. A) This interval consists mostly of thin-bedded, fine-grained turbidites beds. B) Note thick-bedded, coarse-grained sandstones occur at the base of the interval. Person for scale. Oblique views, looking to the northwest. Photo A was taken on the left (southeast) side of photo B.

In lower part of Ch1.U-S1, some thick (up to 0.5 m), normal graded or cross-bedded coarse sandstone beds are interstratified with the fine-grained facies (Fig. 3.12b). Most beds occurring in the succession are laterally continuous, with the exception of these coarse-grained beds that typically to pinch out in less than 100 m or onlap the basal surface.

3.2.2.4. Channel Unit Ch1.U-C3

The uppermost channel unit (Ch1.U-C3), which is 20-30 thick and more than 1.1 m wide, consists of three or four vertically stacked, channel fills (Fig. 3.3; and Fig. 3.10b). Erosion surfaces at the base of the channel fills are characteristically shallow, although some are locally steep. The erosion surfaces incise underlying channel fills, forming a well-connected composite channel geometry. Laterally discontinuous, mudstone-clast breccia and thin-bedded sandstone and siltstone (facies associations FA1a and FA1c respectively) generally overlie channel bases. Locally, an up to 3 m thick slump interval (facies association FA4) located in the southeast of the study area overlies the channel base, but can only be traced a few meters laterally.

Channel fills are characterized by semi-amalgamated, thick-bedded (average thickness of 1.3 m), normal graded and massive, coarse sandstone beds in channel axis that become non-amalgamated at the channel margins (facies association FA3b) due to common thin, fine-grained interbeds (up to 10-15%, see table V.2 and Fig. V.2 in Appendix V). Well-sorted, very coarse to coarse, cross-bedded sandstone is common in the upper part of Ch1.U-C3. Similar to the underlying channel units, post-depositional structures (e.g. flames, loaded bases, deformed cross-beds, brecciated facies, etc) are common.

The uppermost channel fill of Ch1.U-C3, in the northwestern part of the study area, consists of lateral-accretion deposits. These deposits comprise heterolithic strata, inclined at about 5^{o} to the channel base, which mainly consist of fine sandstone and silty mudstone interbedded with cross-bedded coarse sandstone (FA2a, see section 2.3.2 in chapter 2). Inclined strata are overlain by channel-fill deposits that consist of non-amalgamated, thinly bedded, siltstone-sandstone (facies association FA3c).

3.2.2.5. Layered thin bedded sheet (Ch1.U-S2)

Ch1.U-3 is capped by a more than 50 m thick, fine-grained, upward-fining and -thinning, layered succession (Ch1.U-S2, Fig. 3.13). In the lower part of this succession (overlying the top of Ch1.U-C3) fine-grained strata interfinger with lenticular beds of massive or cross-bedded coarse sandstone (see section 2.3.5 in previous chapter 2). Stratigraphically-upward, layered sheets are more common, showing an overall tabular geometry. Strata are composed of thin-bedded, cross-laminated, fine sandstone and silty mudstone (facies F4.1) that show an upward decrease in sandstone/mudstone ratio from 2/3 to less than 1/3, and ultimately grade into a few meters-thick, clay-rich interval (facies F4.2).

3.2.2.6. Interpretation

Outcrop exposures of the upper channel complex of Channel 1 (Ch1.U) allow detailed examination of its architecture, and clearly demonstrate that the complex channel geometries are related to numerous episodes of incision and channel fill. The basal surface of Ch1.U indicates a prolonged period of incision by strong, bypassing turbidity flows that widened the channel (Fig. 3.14a). In the lower channel unit (Ch1.U-C1), the mudstone-clast breccia that overlies the laterally extensive, erosion surface represents the erosional remnants or zones associated with (bypass) incision alternating with periods of channel deposition. Channel axes tend to mark deeper zones where turbidity flows were preferentially directed, whereas channel margins experienced less intense erosion and minor deposition (Fig. 3.14b).

Amalgamated breccia beds observed in the axial areas were more affected by differential erosion. Elliot (2000a,b) observed similar laterally extensive surfaces, termed megaflute erosion surfaces, in the Ross Formation in western of Ireland, and suggested that they were related to widespread erosion by a single turbidity current. The distribution of erosion surfaces and breccias in Channel 1 suggests that they too were formed during incision and sediment bypass through incipient channels (Fig. 3.14c-d), but most probably by several turbulent flows that deposited the thick, amalgamated beds of mudstone-clast breccia. These channels were characteristically shallow with minor aggradation and migrated freely laterally (Fig. 3.14d). The superposition of several channels with a similar thalweg position could have created the deep erosional zones (Fig. 3.14d).

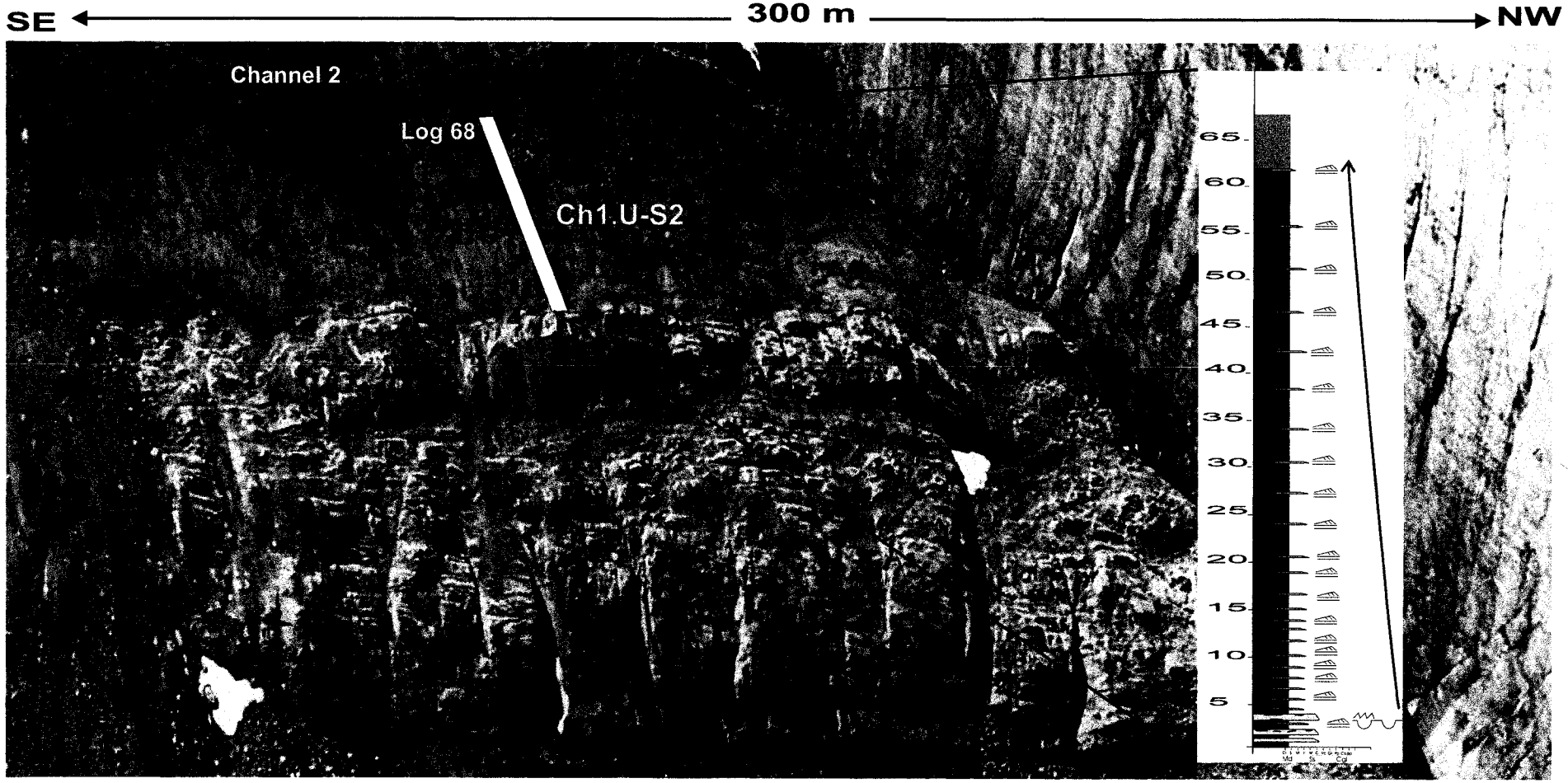

Figure 3.13. Representative log of fine-grained sheet deposits at the top of Upper Channel Complex, Channel 1 showing fining- and thinning- upward trend. For legend see Fig. 3.4

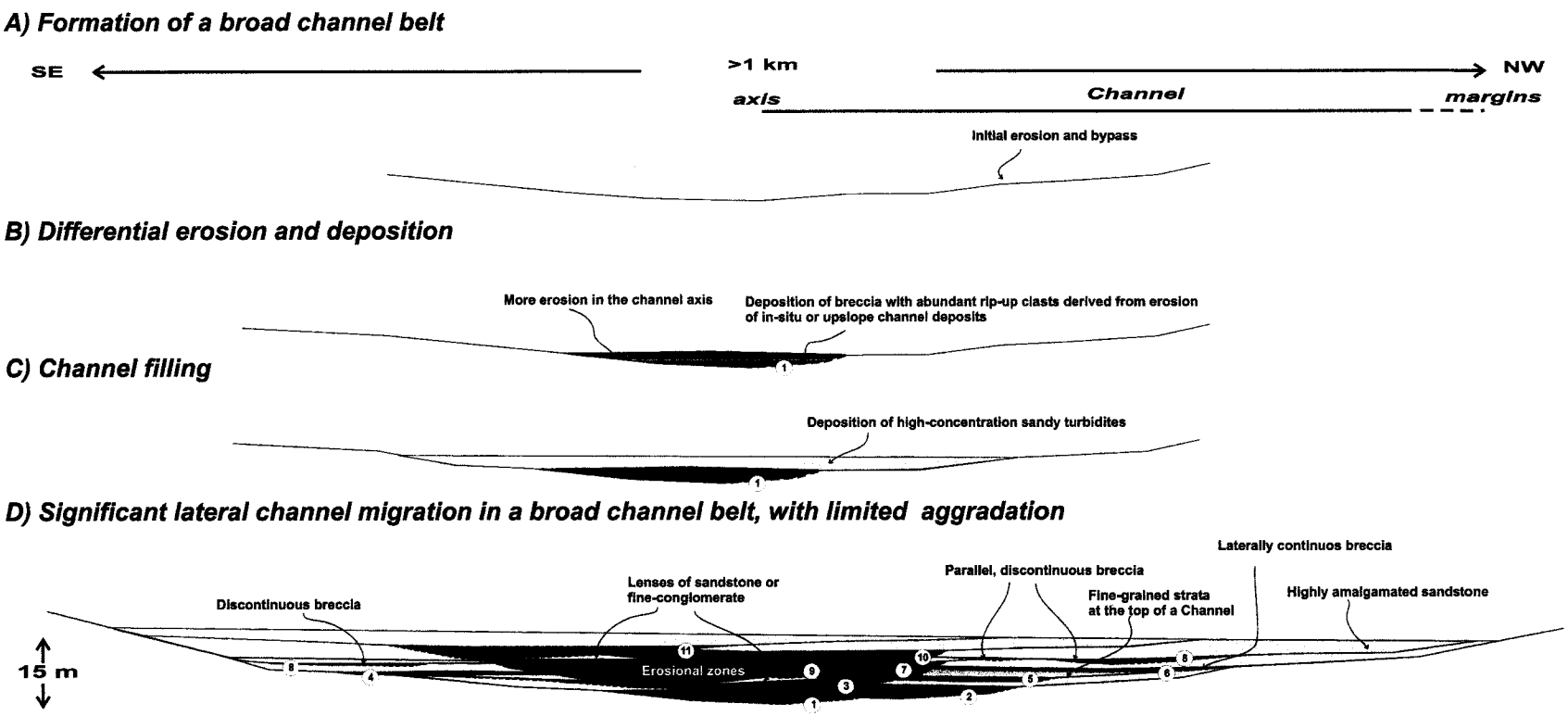

Figure 3.14. A simplified model for the development of erosional zones of Channel 1. (A) Initial channel erosion and bypass from highly-efficient flows, (B) Flows became more focused in the channel axis, that locally accentuated erosion, (C) Channel filling was limited to thick, amalgamated coarse sandstone strata, D) As a channel fills and reduces accommodation space, it rapidly migrates laterally, eroding older deposits and widening the channel belt. These channels are shallow and once filled they deactivate promptly. Fine-grained strata deposited at the top of the channel correspond to deactivation and have low preservation potential because the strata are eroded by younger channels. Laterally extensive, continuous or discontinuous, erosional remnants at the base of channels (numbered) in Channel 1 indicates the occurrence of these bypass/erosion events. The vertical superposition of several channel axes, that takes place generally in the axis of the channel complex, formed erosional zones that contain thick, variably amalgamated breccia with lenticular beds of coarse-grained deposits.

Depositional episodes in Ch1.U-C1 are recorded by stacked multistorey, amalgamated channel-fill successions that consist mostly of pebble and sand-rich, high-concentration turbidites. In these successions, erosion of thin-bedded, fine-grained deposits or mudstone-clast breccia beds, most probably during the early stages of the event that deposited the overlying turbidite, caused extensive amalgamation of sandstone/conglomerate beds.

The middle and upper channel units (Ch1.U-C2 and Ch1.U-C3) are characterized by multiple semi-amalgamated channels that are interpreted to be aggradational channels. Some channel deposits contain either fine-grained or breccia beds at their bases that are interpreted as bypass deposits, and indicating short-term reincision stages (c.f. Samuel et al., 2002). The magnitude of the bypassing flows is less significant than those that formed Ch1.U-C1. Individually, channel fills consist of FA3b strata deposited from mostly sand-rich, high-concentration turbidity currents, that alternated with fine-grained, low-concentration currents. The interval of thin-bedded turbidites (Ch1.U-S1) that occurs between the middle and upper channel units is considered to indicate a temporary deactivation of the channel system or abandonment of the channel conduit, which later was re-established during the inception and filling of Ch1.U-C3.

The uppermost channel element in Ch1.U is composed of inclined strata and mud-rich channel fill interpreted to be associated with a more sinuous channel. This dramatic change in channel configuration occurred just prior to deposition of mud-dominated turbidites Ch1.U-S2 that correspond to the terminal deactivation of this channel complex set (Channel 1).

3.3. CHANNEL 3: Geometry and Architectural Elements

Channel 3 is almost 150 m thick, and although its southeast margin is rather poorly exposed, its width is of the order of 1.5-1.6 km. Channel 3 is a channel complex set (see chapter 3.1.2 for terminology discussion) composed of three (lower, middle and upper) channel complexes informally termed Ch3.L, Ch3.M, Ch3.U, respectively (Fig. 3.15). Channel complexes range from 30-80 m thick, and individually comprise at least two channel units, which in turn consist of two or more channel fills. The top of Channel 3 is abrupt and is marked by the superposition of Channel 4.

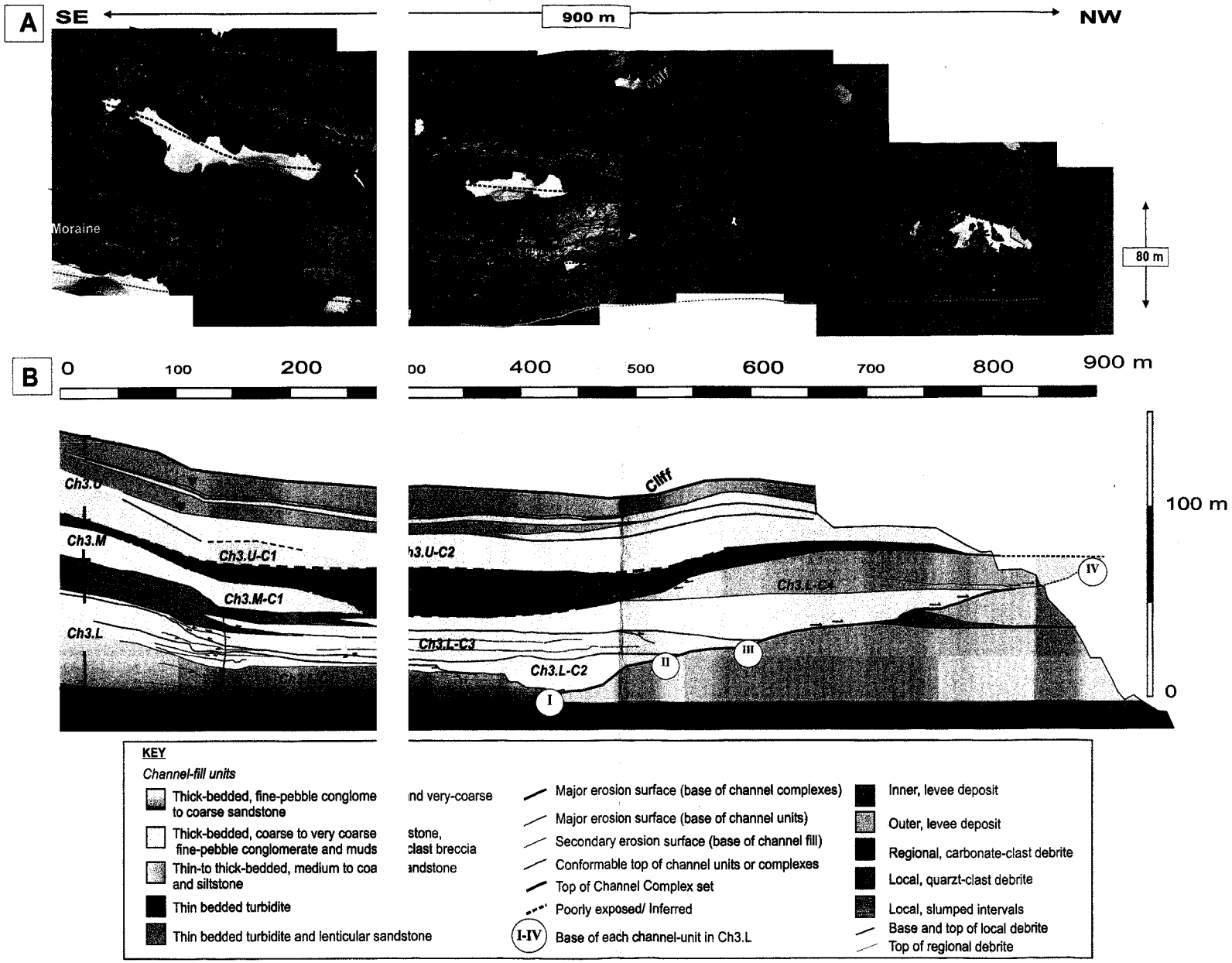

Figure 3.15. Vertical and lateral stacked channel complexes of Channel 3, Castle Creek South. (B) Oblique view, aerial photomosaic showing channel complexes Ch3.L, Ch3.M and Ch3.U, highlighting the major channel fills and extra-channel deposits. (C) Detailed schematic representation illustrating lithofacies distribution and architectural elements in Fig. 3.15B.This schematic has attempted to removed the most evident topographical effect.

3.3.1. Lower Channel Complex (Ch3.L)

Ch3.L is an approximately 80 m-thick channel-levee complex. It comprises four distinct channel units (C1 to C4) that stack vertically in an aggrading lateral offset pattern along the northwest margin of the Channel Complex (Fig. 3.15). Channel units are separated by major erosion surfaces that can be traced across the study area (~1 km). Each channel unit comprises two or more channel fills, which are interpreted to be genetically related.

The basal surface of Ch3.L-C1 is a smooth, shallow-dipping surface (<1°) that becomes steeper and more irregular along the channel margins, especially the northwest margin. This surface is a composite surface with a terraced or 'step and flat' geometry, similar to that described by McHargue (1991) on the Indus Fan and Eschard et al. (2003) from Cretaceous outcrops in Pakistan. The lower part of the surface incises the top of a regionally-extensive debris-flow deposit with abundant large, subangular to rounded, dispersed carbonate clasts (Fig. 3.15), including fragments of stromatolites and carbonate mudstone. Erosion surfaces at the base of successive channel units (Ch3.L-C2 to Ch3.L-C4) are similarly shallow, parallel to the surface at the base of the Channel Complex, and erode underlying channel units. Locally, however, some surfaces scour deeply into underlying channel units (up to 10 m deep), e.g. Ch3.L-C2 and Ch3.L-C3. Surfaces are steeper along the northwest margin (slopes up to 25°), where they also incise adjacent levee deposits and a quartz-clast debrite.

Channel units of Ch3.L are bounded on both side by levee deposits. These strata were initially described and studied in a reconnaissance level of detail by the author. Later, a more detailed study was carried out by graduate student Zishan Khan. The following relates to the author's field notes, and in part from Khan's work (Khan et al., 2005), which also appears in Navarro et al. (in press), see Appendix VI. Levee deposits on the northwest side are subdivided into two kinds based on their lithofacies and distance from the channel margin: proximal and distal. At the base of the levee deposits, a laterally extensive, up to 3 m thick, amalgamated succession consisting mostly of massive and cross-stratified sandstone and mudstone-clast breccia is observed.

Proximal levee strata reach a maximum thickness of over 55 m at the crest, and are composed of repeating intervals or packages made up of two vertically-stacked facies assemblages (Fig. 3.16, and Fig. IV.4 in Appendix IV). Khan et al. (2005) pointed out that these intervals show a lateral offset to the northwest. The basal facies assemblage is less than

10 m thick and comprises medium- to thick-bedded (0.3-0.7 m), parallel-laminated medium sandstone and multiple set, ripple- cross-laminated, fine to medium sandstone. The upper facies assemblage ranges from 7 to 15 m thick and is thinner and finer, consisting of thin-bedded (1-4 cm), very fine to fine sandstone interbedded with up to 20 cm thick, siltstone. Fine-grained facies gradually increase away from the channel margin over distances of 500 m.

An up to 7 m-thick interval of silty mudstone with dispersed pebble clasts of quartz (Fig. 3.15) is abruptly interbedded within the uppermost proximal levee. This interval is sharply overlain by a 1.5 m-thick, coarse sandstone that fines laterally to medium sandstone and thins to less than 40 cm over 200 m.

In comparison with the proximal levee, the sandstone/mudstone ratio is dramatically lower in the distal levee. These strata consists mostly of up to 30 m-thick fine-grained intervals of thin bedded (0.5-6 cm) parallel- and cross-laminated, fine to very fine sandstone interbedded with siltstone (Fig. 3.16, and Fig. IV.5 in Appendix IV). Locally, these intervals fine and thin upward. Moreover, the fine-grained intervals are interstratified with up to 4-5 m thick successions of thick-bedded (0.5-1.5 m), amalgamated, medium-grained sandstone and mudstone-clast breccia.

Levee deposits on the southeast side generally interfinger with channel-fill strata along the channel margin and consist mostly of thin bedded (0.5-2 cm) very fine sandstone and siltstone, that in the proximal areas are locally interbedded with thicker sandstone beds (Fig. 3.15). These latter strata include medium- to thick-bedded (>0.2 m) massive sandstone and medium- to thick-bedded (0.15-0.5 m), fine to medium sandstone with multiple (3 or 4) sets of non-climbing ripple cross-stratification. Southeast levee strata fine and thin rapidly laterally over a distance of less than a few decameters (10's meters) toward the southeast.

3.3.1.1. Channel Unit Ch3.L-C1

The lowermost channel unit Ch3.L-C1 consists of at least three channel fills that are broad (at least 1.1 km wide and up to 15 m thick) and have high width/depth ratios (over 50). The lateral continuity of these channel fills is, thus, high (Clark and Pickering, 1996).

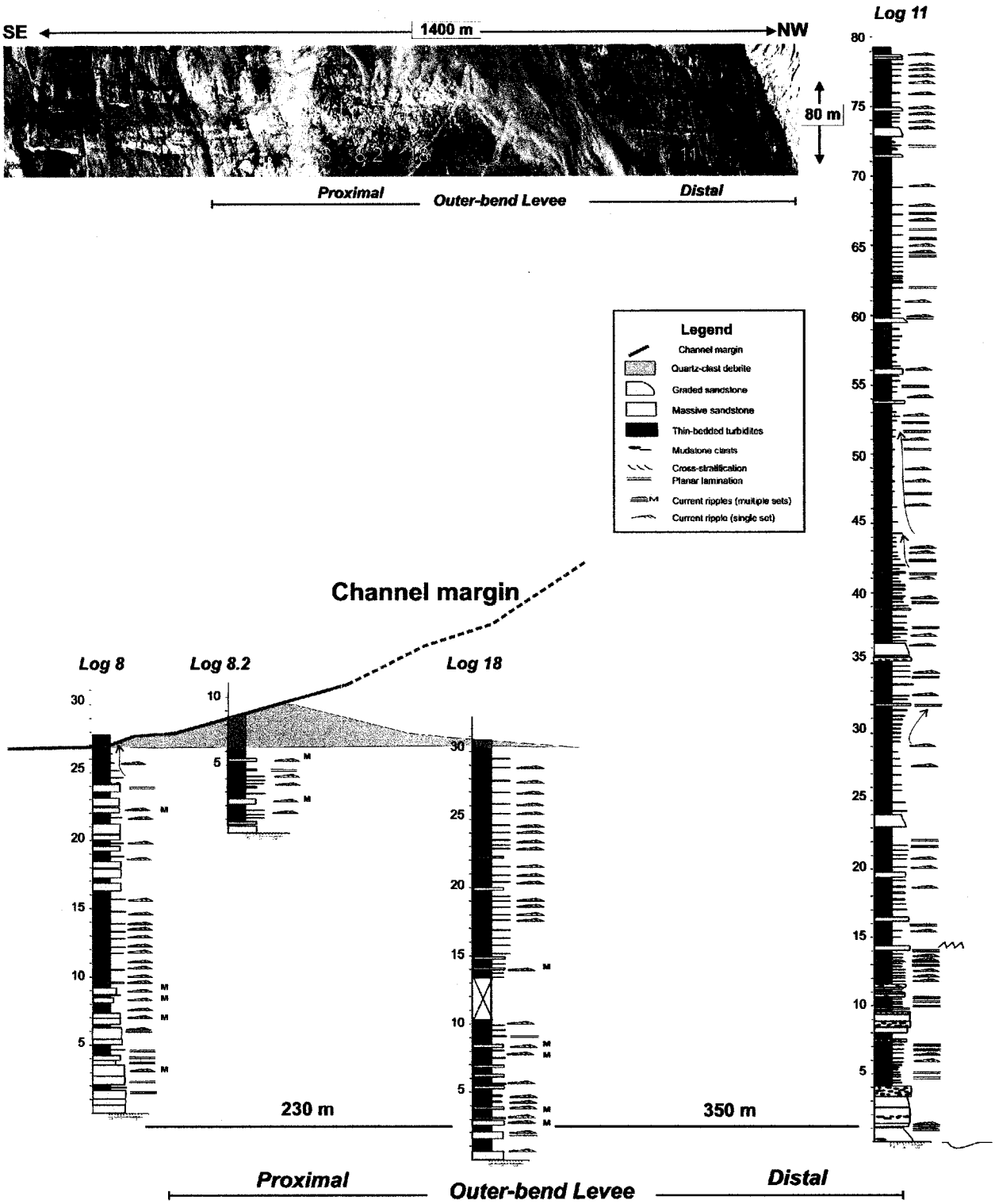

Figure 3.16 Correlation diagram of levee deposits adjacent to the northwest (outer-bend) channel margin.

At the base of channel fills, two subfacies FA1a,b are observed. FA1a occurs at the base of Ch3.L-C1 (Fig. 2.37a), and is up to 2.5 m thick and consists mostly of thin- to medium-

bedded siltstone and normal graded, massive and parallel-laminated, fine- to medium-grained sandstone. Additionally, clast-supported conglomerate (FA1b, Fig. 2.37d) with occasional carbonate clasts occur at the base of channel fills and is less than 2 m thick.

Channel-fill strata overlying FA1 are mostly amalgamated, thick-bedded, normally-graded and massive, pebbly and granule conglomerate and very coarse to coarse sandstone with minor mudstone-clast breccia (FA3a, Fig. 3.17a). Conglomerate is poorly sorted with abundant pebble or granule clasts of quartz and feldspar, and some contain angular to subrounded, boulder carbonate clasts (Fig. 3.18). Beds are up to 3 m thick with common scoured bases. Net-to-gross typically are more than 80% (see Table V.3 and Fig. V.3). Overall, channel fills change upward from typically amalgamated conglomerate to less amalgamated sandstone and fine sandstone interbeds with siltstone become increasingly common.

3.3.1.2. Channel Unit Ch3.L-C2

Channel unit Ch3.L-C2 comprises two channel fills that have slightly different vertical facies assemblages in comparison to those in the underlying channel unit. Even though the south margin of the channel unit is not exposed in the study area, Ch3.L-C2 is estimated to be >1 km wide and up to 15 m thick (Fig. 3.15). The base of Ch3.L-C2 overlies abruptly the channel unit Ch3.L-C1 and its adjacent levee unit.

A prominent up to 8 m-thick, laterally-extensive, mudstone-clast (rip-up) breccia (FA1c facies association; Fig. 3.17b, 3.19) overlies a major erosion surface at the base of Ch3.L-C2. Clasts consist of abundant, angular mudstone clasts dispersed in a poorly-sorted matrix of medium sandstone to pebble conglomerate (up to 3.5 cm). Mudstone clasts (in some cases greater than 0.3-0.5 m) are characteristically oriented parallel to the basal bedding contact, however disorganized fabrics and sand injections, comparable to those previously illustrated by Mutti and Nilsen (1981) occur locally. Breccia zones are highly amalgamated, including local lenticular beds or remnants of conglomerate and sandstone embedded within breccia.

Channels are 1-8 m deep and are filled with normally graded and massive very coarse sandstone and lesser amounts of poorly sorted, clast-supported, pebble and granule conglomerate (Fig. 3.17b). Average bed thickness is 1.2-1.5 m. Locally, thin-bedded (1-20 cm), fine sandstone and siltstone are interbedded with the thicker beds. The average net-to-gross is > 90%.

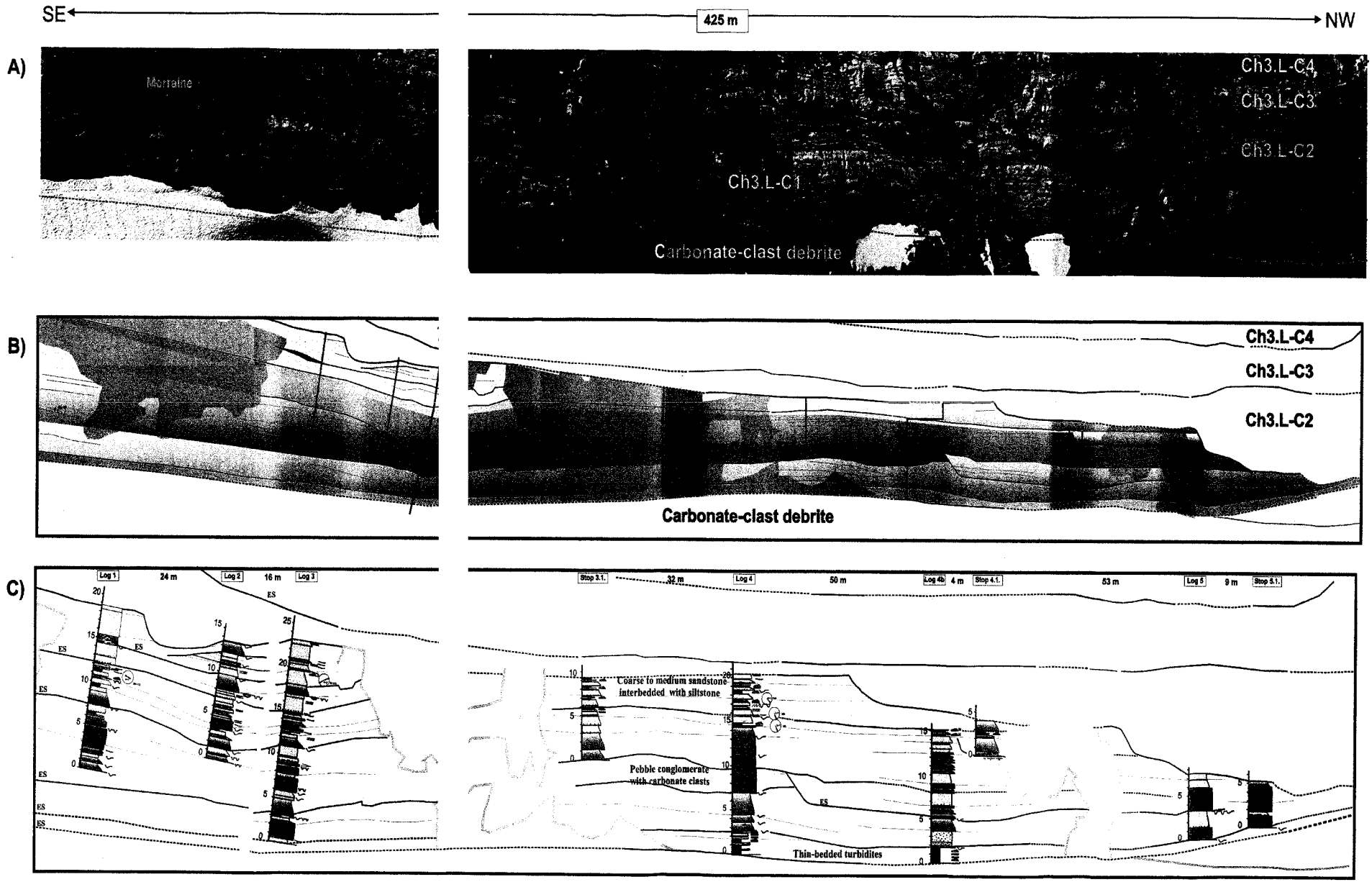

Figure 3.17a. Outcrop distribution of the lowermost channel unit Ch3.L-C1 in Channel 3 with measured sections and correlation panel showing the basal succession of thin-bedded turbidites and the dominance of amalgamated conglomerate/sandstone in the channel fills. For legend see Fig. 3.4.

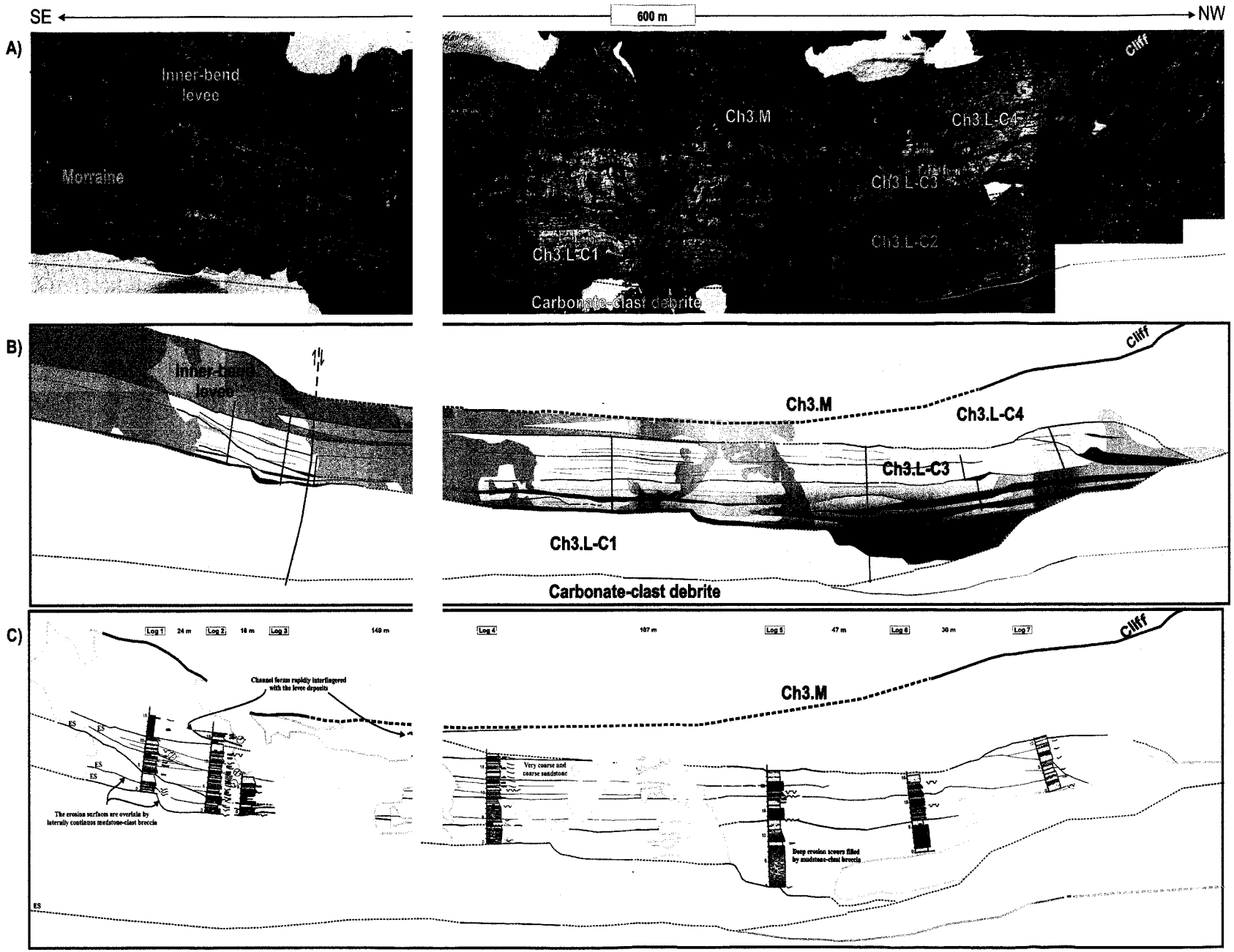

Figure 3.17b. Outcrop distribution of the lowermost channel unit Ch3.L-C1 in Channel 3 with measured sections and correlation panel showing a variable channel infilling composed of amalgamated sandstone, conglomerate and mudstone breccia. For legend see Fig. 3.4

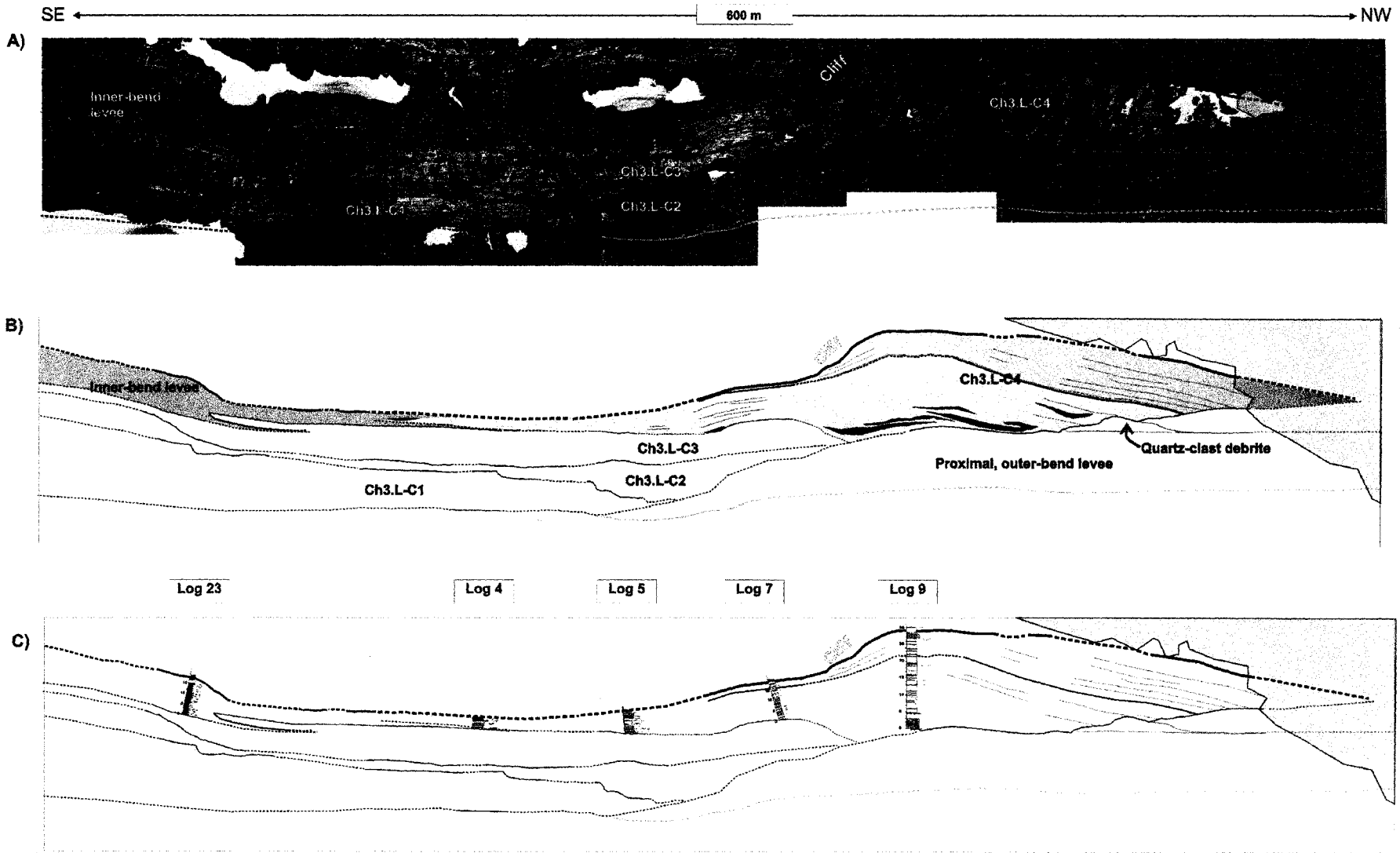

Figure 3.17c. Outcrop distribution of the lowermost channel unit Ch3 L-C4 in Channel 3 with measured sections and correlation panel. For legend see Fig. 3.4

Figure 3.18. Close-up of pebble conglomerate with orange-brownish weathering (ankeritic), carbonate clasts, white to light grey, quartz and/or feldspar pebbles, and dark grey, angular mudstone clasts. Ch1.L-C1 (Photo taken by G. Ross).

3.3.1.3. Channel Unit Ch3.L-C3

Ch3.L-C3 is approximately 600 m wide, 7-15 m thick, and consists of three vertically-stacked channel fills with well-exposed (both) margins (Fig. 3.15). Channel fills in Ch3.L-C3 are significantly narrower than those in the underlying channel units (Ch3.L-C1 and Ch3.L-C2), and are offset laterally and interfinger with flanking southeast levee strata. The aspect ratio in Ch3.L-C3 is intermediate to high (39-86).

The basal surface of Ch3.L-C3 scours up to 10 m deep into underlying strata (Ch3.L-C2), and in most places is overlain by mudstone-clast breccia (FA1c facies association). Bases of individual channel storeys are sharp and shallow, but locally some are steep and deeply incised (up to 5 m; Fig. 2.38b). Mudstone-clast breccia overlies the scoured bases. Clasts are abundant and embedded in a distinctive coarse-grained matrix (coarse sandstone to fine pebble conglomerate). Breccia units or zones are typically laterally continuous and can be traced more than 400 m, but some are locally discontinuous and lenticular (Fig. 3.17c).

In contrast to underlying channel units, channel fills in Ch3.L-C3 become increasingly sandy upward and more interbedded with parallel and/or cross-laminated fine sandstone and mudstone (Fig. 3.17c). Thickness of mudstone beds ranges from 1 to 8 cm. Few paleocurrents measured from three-dimensional current ripples and dunes indicate that paleoflow was slightly toward the northeast (20°).

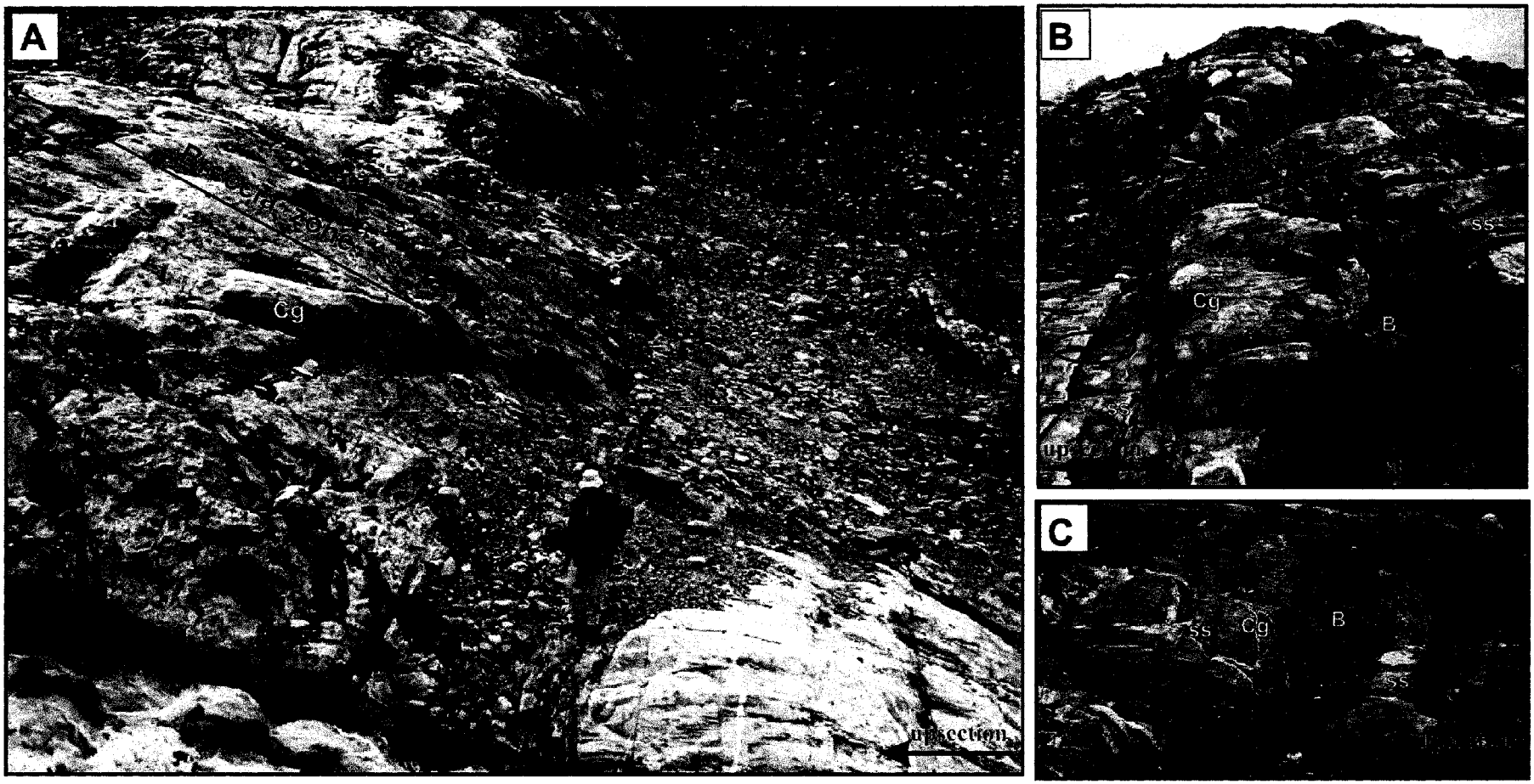

Figure 3.19. Erosion surfaces in Ch3.L-C2. A) The major erosion surface at the base of Ch3.L-C2 (red dashed line) truncates the underlying conglomerate-dominated, channel unit Ch3.L-C1 (see Fig. 2.38 a). Mudstone-clast breccia zones (B) that overlie this surface are highly amalgamated with local lenses or remnants of conglomerate (Cg) and sandstone (ss). B) Some conglomerate beds have erosional bases that truncate the underlying sandstone strata. C) Some breccia overlies irregular, erosional bases.

Channel fills are characteristically semi-amalgamated (FA3b, Fig. 3.17c). Channel-axis strata are dominated by thick-bedded (up to 2.3 m), normally graded and massive, coarse to very coarse sandstone and minor clast-supported, granule conglomerate that commonly are interbedded with thin-bedded and fine-grained strata (Fig. 2.15, 2.43b, 3.19c). These axial strata grade laterally into less-amalgamated sandstone toward the southeast margin, where marginal strata consist mostly of interbedded thick- to medium-bedded massive and normal graded sandstone, thin-bedded sandstone and mudstone. Toward the southeast margin coarse-grained strata tend to thin and fine rapidly, over a few 100 meters laterally, onlapping the channel margin (Fig. 3.15, 3.20, 3.21).

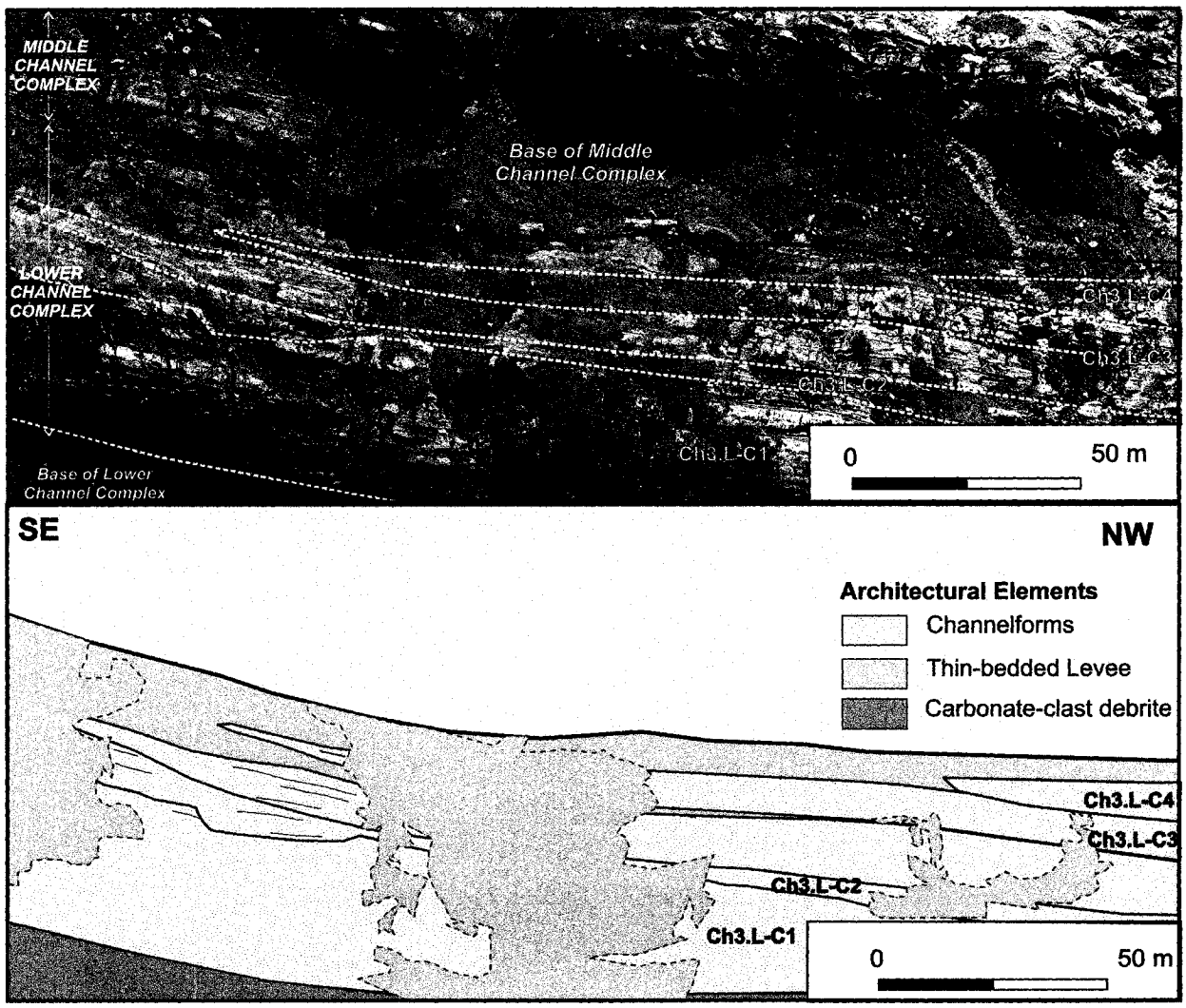

Figure 3.20. Photomosaic and line drawing of southeast margin of lower channel complex of Channel 3 (Ch3.L) illustrating architectural elements of channel and extra-channel (levee) deposits. Note how channel units Ch3.L-C3 and Ch3.L-C4 interfinger laterally with thin-bedded levee strata (see Fig. 3.14b).

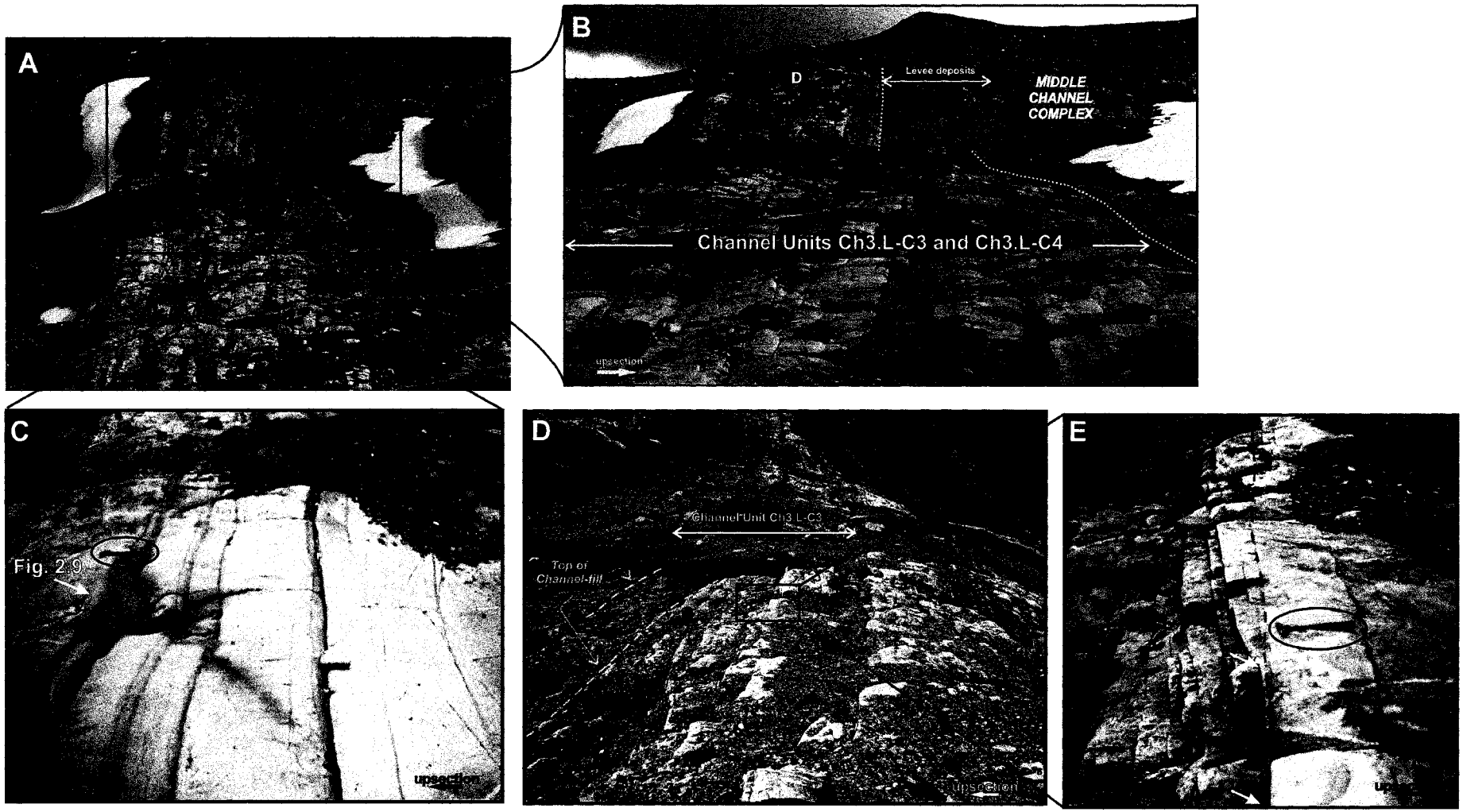

Figure 3.21. Characteristics of channel fills in Ch3.L-C3. A-B) Semi-amalgamated channel elements are composed mostly of massive and normally graded, brownish yellow sandstone with thin-bedded, grey mudstone interbeds. C) Sandstone beds have typical erosional and undulatory bases, and local U-shaped scours (arrow). D-E) Some beds onlap against the basal erosion surface of channel fills. Oblique views, A-C) looking to the northwest and D-E) looking to the southeast.

3.3.1.4. Channel Unit Ch3.L-C4

Ch3.L-C4 is the uppermost channel unit of Ch3.L and is approximately 600 m wide and up to 30 m thick (aspect ratio is low to intermediate: 14-60). It comprises three main channel fills, which are offset 100 m to the northwest. Like channel fills in Ch3.L-C3, fills of this unit not only interfinger with flanking levee strata along the southeast margin, but also lap onto the adjacent debrite and levee strata along the opposite (northwest) margin (Fig. 3.15, 3.22, 3.23).

Toward the channel axis of Ch3.L-C4, a major erosional surface scours the underlying channel unit (Ch3.L-C3). Overlying this erosion surface, an up to 3 m thick, inclined succession (FA2b facies association) is recognized. It is composed of partially amalgamated, massive sandstone interstratified with mudstone-intraclast breccia (Fig. 3.17c).

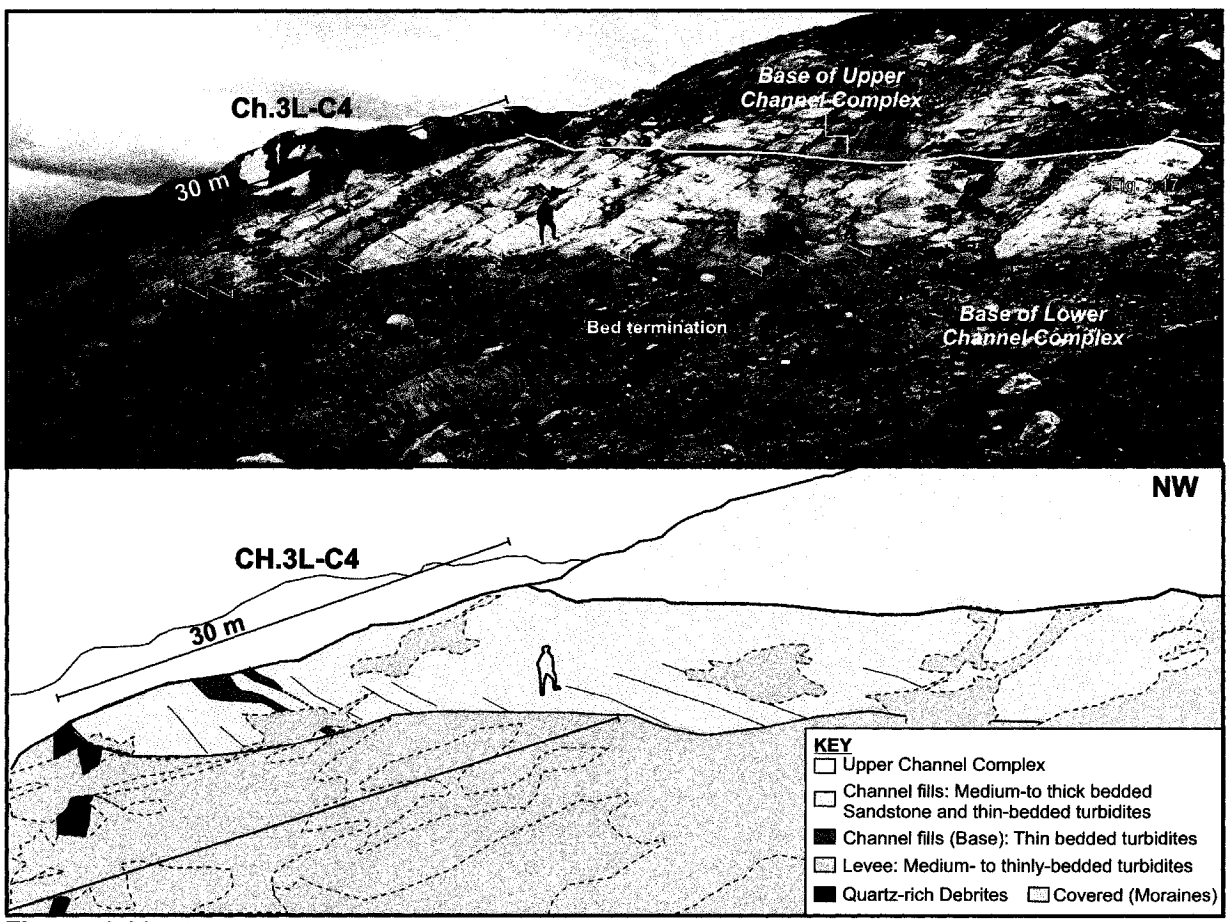

Figure. 3.22. Photomosaic and line tracing of northwest margin of uppermost channel unit in Lower channel complex of Channel 3 (Ch3.L- C4), illustrating architectural elements of channel and extra-channel deposits. Note the channel fill of channel unit Ch3.L-C4 onlap quartz-clast debrite and fine-grained levee deposits.

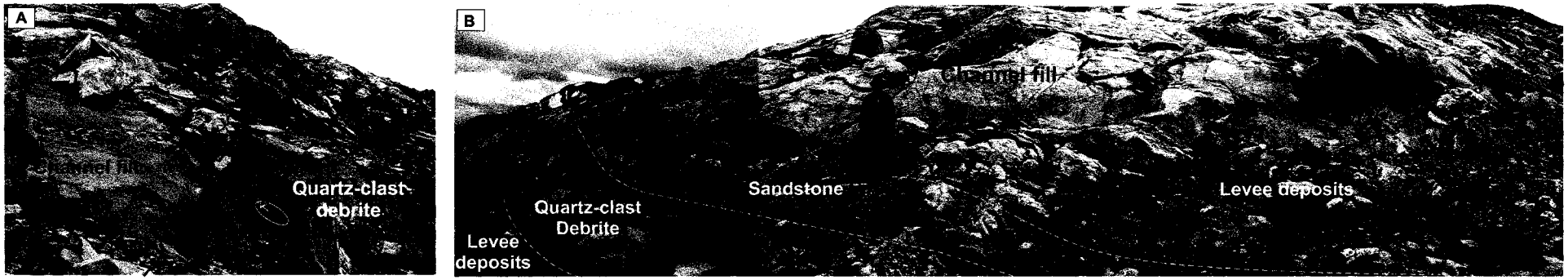

Figure. 3.23. Close ups of the erosional basal surface in the northwest margin of channel unit Ch3.L-C4. (A) The surface is extremely irregular and (B) it sharply truncates adjacent debrite and levee deposits.

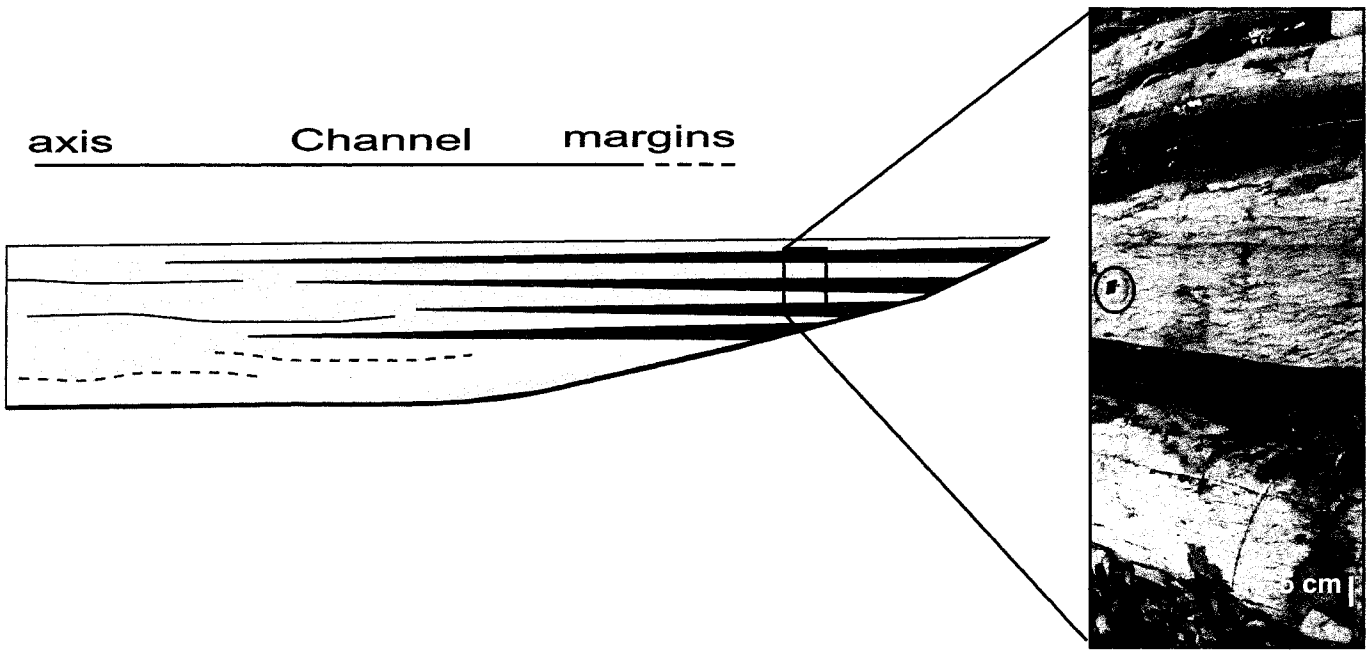

Figure. 3.24. Channel-fill strata along the northwest margin of channel unit Ch3.L-C4 consists of non-amalgamated sandstone separated by siltstone. Compass (circled) for scale. (photograph taken by Z. Khan, 2004).

Toward channel margins, lensoid-shaped breccia beds show limited lateral continuity (less than 100-150 m), and are subparallel but gently inclined to the channel base (Fig. 3.17c). This inclined succession is somewhat comparable to the semi-amalgamated lateral accretion package in the Big Rock Quarry (Jackfork Group) described by Abreu et al. (2003).

Additionally, scour surfaces at the base of some individual channel fills in Ch3.L-C4 are draped by fine-grained strata (FA1a facies association (Fig. 2.37b,c; see section 2.3, chapter 2)). These successions are up to 1 m thick and include thin-bedded (0.1 to 30 cm thick), fine to medium sandstone interbedded with mudstone. Medium-grained sandstone beds are mostly structureless and plane-parallel laminated, whereas fine sandstone are multiple set, ripple cross-laminated and parallel-laminated. Rare unlaminated mudstone beds are also observed.

Basal successions are in general overlain by semi-amalgamated channel fills (FA3b), consisting of medium- to thick-bedded (up to 2-2.6m), normally-graded and massive, coarse to very-coarse sandstone and granule conglomerate in the channel axis. Coarse-grained strata typically thin over less than a few hundred meters (100-200 m) toward the margins and become better stratified. These channel-off-axis or channel-margin strata are made up of thin- to thick-bedded (less than 1.5 m), well sorted, coarse sandstone, but are more interbedded with thin- to medium-bedded silty mudstone and very-fine sandstone (Fig. 3.24, Fig. IV.3) compared to the channel-axis strata. Mudstone beds thicken slightly toward the margin and reach thicknesses up to 32 cm. Accordingly, the net-to-gross ratio decreases toward the channel margin, ranging from 93% in the channel axis to 70% at the margins (Table V.3 and Fig. V.3 in Appendix V).

3.3.1.5. Interpretation

The architecture of the Lower Channel Complex of Channel 3 resulted from multiple episodes of incision, levee construction, channel infill and abandonment. The basal surface of the lower channel unit, Ch3.L-C1 coincided with erosion along the top of a regionally extensive, carbonate-clast debrite (the stratigraphic significance of this interval will be discussed in Chapter 4).

Debris-flow deposits overlain by channel-levee systems have been previously reported in the literature (Weimer, 1991; Piper et al., 1997; Pirmez et al., 1997; Manley and Flood, 1998;

Maslin et al., 1998; Beaubouef and Friedman, 2000; Brami et al., 2000; Winker and Booth, 2000; Posamentier and Kolla, 2003; Samuels et al., 2003). The carbonate-clast-rich debrite probably had a moderately uneven surface topography that preferentially diverted the initial, relatively unconfined, highly efficient flows through topographical lows. The fine-grained succession (T_{b-e} turbidites) overlying the basal erosion surface of Ch3.L-C1 is related to phase of incision and bypass and represents deposition from the low-concentration tails of highly energetic turbulent suspensions. During this phase, most sediment was transported and eventually deposited farther basinward.

As sediments bypassed the channel, levees were being progressively developed along the margins of the channel by overspill and flow stripping. More flow stripping occurred along the outer channel-bend levee (e.g. Peakall et al., 2000) and resulted in the deposition of the sand-rich, lowermost part of the proximal levee along the northwest channel margin. With distance from the channel, these flows decelerated and deposited finer-grained sediment on the distal levee. Simultaneously, but on the other side of the channel, the lowermost part of the inner levee was deposited.

As the levees built upward, intrachannel flows become progressively more confined. The onset of channel filling was most probably related to an increase in sediment flux and caliber, and accordingly, a decrease in flow efficiency. Moreover, Piper and Normark (1983) contended that a consequence of flow stripping is a considerable loss of momentum of the intrachannel flows, which then leads to sediment deposition downstream.

Channels in the lower part of Ch3.L-C1 began to fill with the coarsest deposits in the channel complex, recorded by thick-bedded, normally graded and massive pebble conglomerate and conglomeratic sandstone. These deposits are interpreted to have been deposited by gravel- and sand-rich, high-concentration turbulent flows. Channels in Ch3.L-C1 were most probably wide and comparatively shallow and formed a complex amalgamation of overlapping channel fills. Some of these channels show deep, basal erosion surfaces that are overlain by pebble conglomerate lags suggesting secondary episodes of cut-and-fill as the channel complex filled and migrated laterally.

Stratigraphically-upward, conglomerate content and bed amalgamation decreases and sandstone-dominated strata become more common in the upper channel fills of Ch3.L-C1.

This suggests a waning of flow conditions or a decrease in sediment caliber and/or supply to the system.

The bases of channel units Ch3.L-C2 and Ch3.L-C3 show prominent (locally 8-10 m deep) erosion surfaces that are interpreted to indicate major periods of channel reincision. Erosion most probably removed a considerable amount of the underlying channel succession and adjacent levee. Thick, laterally extensive horizons or zones of matrix-supported, mudstone-intraclast breccia were deposited above the erosion surface. Patches and lenses of sandstone and conglomerate within the breccia zones are inferred to be erosional remnants of deposits related to reincision.

In comparison to channels in Ch3.L-C1, channels in Ch3.L-C2 and Ch3.L-C3 show changes in channel morphology, which in turn are most probably related to changes in flow discharge. These channel fills are narrower and stack vertically. In addition, they show an abrupt lateral offset (migration) with local incision between them. Erosion surfaces are commonly overlain by thick, mudstone-clast breccia beds with great lateral continuity, and correspond to the bypass facies association.

Along the northwest channel margin, channel fills onlap an erosive surface that separates them from their adjacent, genetically-related levee strata. This surface is related to the greater amount of erosion along the outer-bend side of the channel, continuously migrated in that direction (northwest). In contrast, along the southeast margin, channel fills (especially those in the upper part of Ch3.L-2 and in Ch3.L-C3) interfinger with fine-grained levee deposits. This suggests lower-energy deposition on the inner-bend levee.

Stratigraphically upward, channel fills of Ch3.L-C3 and Ch3.L-C4 became narrower and more sandstone-rich, perhaps in response to changes in flow or slope conditions of the system, and therefore comparable to some examples of channels on the modern Indus Fan and Niger Delta slope (McHargue, 1991; Deptuck et al., 2003). Moreover, channel-fill strata show clear convergence via onlap toward both margins, and a lateral decrease in bed amalgamation away from the axis as intercalated thinly bedded, fine-grained turbidites become increasingly common. The lateral-fining and -thinning trends of channel-margin strata imply that flows were smaller, muddier and less dense along their lateral margins (McCaffrey and Kneller, 2001; Kneller, 2003).

The uppermost channel unit, Ch3.L-C4, illustrates a major change in channel configuration, defined by a basal semi- to fully-amalgamated lateral accretion package that overlies a major erosion surface. The unit consists of the inclined facies association (FA2b) and is composed of partially to completely amalgamated massive sandstone interbedded with thick, discontinuous patches of mudstone-rich breccia. These deposits represent periods of sediment bypass, eroding older channel and levee deposits at the outer bend of the channel, and also suggest lateral migration of a possible sinuous channel system.

The characteristics of adjacent outer- and inner-bend levee deposition has been already described in the preceding channel units. However, the outer levee associated with Ch3.L-C4 is overlain sharply by a pebbly quartz-clast debrite, which in turn is capped by a thick, coarse sandstone turbidite. Due to the occurrence of floating quartz clasts, the debrite is not related to in-situ levee wall failure, but instead is likely related to failure of up-slope levee deposits that slumped into the channel and were carried downslope. Overspill and deposition of the debris flow along the outer bend would have almost instantaneously added a significant amount of topography to the levee. As a consequence, subsequent levee growth was marked by the deposition of thin bedded, fine-grained turbidites.

Channel fills of Ch3.L-C4 are composed of highly amalgamated, thick, high- and low-concentration turbidites in the channel axis and less- to non-amalgamated heterolithic strata toward the margins. Similar to Ch3.L-C1, some fills are characterized by a unit of thin bedded turbidites overlying the basal erosion surface and indicate deposition from the tails of by-pass flows. At the margins of Ch3.L-C4, the typical thinning of beds toward the levee is similar to beds along the margins of Ch3.L-C3.

Ch3.L: Composite terraced basal surface and stacking pattern

At first glance, the base of the lower channel complex in Channel 3 (Ch3.L) could be considered a master surface that defines the boundary between channel and channel-margin levee deposits, and was formed during a single period of incision that preceded numerous infill events. However, this surface is a composite surface with a terraced geometry formed by the merging of four major erosional surfaces along the northwest margin. Along the southeast margin, the base shows an interfingered or serrated geometry. The dissimilar geometries of these margins, in conjunction with the complex vertical and offset stacking pattern of the four channel units in Ch3.L, are intrinsically associated with the progressive

northwestward migration of the entire channel system. Likewise, the lateral migration is reflected in the levee deposits along the northwest margin, which show a commensurate offset in the adjacent coarse-grained proximal levee deposits (Khan et al., 2005).

Channel-unit deposits record multiple episodes of channel inception and fill, separated by sharp significant surfaces or boundaries. These surfaces are indicative of major reincision episodes that interrupted otherwise continuous channel migration, demonstrating that some channel complexes underwent periodic readjustment or rejuvenation during their evolution. Events of abrupt channel migration can be triggered by periodic channel plugging due to (1) levee slumping (Kolla et al., 2001) or (2) debris-flow failures (Deptuck et al., 2003) typically along the outer bend of the channel.

After each reincision or episode of rapid, abrupt channel migration (*sensu stricto* Deptuck et al., 2003), levee and channel growth resumed and gradually migrated laterally. Channel and genetically-related levee deposits show striking differences and stratal relationships depending on which side of the channel they were formed. The northwest side represents the outer-bend channel margin, whereas the southeast side corresponds to the inner-bend channel margin. Sharper and steeper reincision surfaces along the northwest margin imply that channel-axes migrated and preferentially, eroded into the outer (cut-bank) levee deposits. In contrast, most channel-fill deposits interfinger with the levee deposits on the southeastern margin, except for those in the lowermost part of the channel complex (Ch3.L-C1) that terminate against both channel margins, suggesting that earlier channel units eroded inner levee deposits too, but with time erosion became restricted only to the opposite (outer bend) side of the channel complex.

Abrupt onlap of channel strata against genetically-related levee deposits suggests that levee construction preceded channel infilling. Moreover, channel infill was associated with diminution of flow conditions (e.g. flow velocity, capacity, and competence). It is inferred that channel aggradation occurred incrementally and at the same time that the channel was migrating laterally, allowing the preservation of proximal levee deposits along the cut-bend (outer bank) margin of the channel.

Finally, the upward change from wider, more erosive channels to narrower, probably more sinuous channels, is recognized in Ch3.L, and is interpreted to be as a result of long-term changes in flow or slope conditions of the system. Similar architectural styles and

episodic evolution of channel-levee systems have been previously reported from the sedimentary record, including Cerro Toro Formation, Chile (Beaubouf, 2004; Hubbard et al., 2004), Pab Formation, Pakistan (Eschard et al., 2003), and in offshore hydrocarbon reservoirs (1-10 km wide) in the Indus Fan (McHargue, 1991; Von Rad and Tahir, 1997), Bengal fan (Huschber et al., 1997), Angola fan (Kolla et al., 2001) and Niger River Delta (Deptuck et al., 2003).

Comparison of channel margins of Ch3.L with other systems

The terraced and serrated channel margins of Ch3.L have been recognized in a number of seismically resolved confined-channel complexes that occur on a variety of horizontal and vertical scales (e.g. Indus Fan, Indonesia fan and Niger Delta) and also in outcrop (e.g. Cerro Toro Formation, Chile and Pab Formation in Pakistan) (See Fig. 3.25). These channel complexes, whether they have outer levees (sensu Husberch, 1997; Deptuck, et al., 2003) or not, have three common characteristics, which together have a direct effect on the generation of this distinctive channel-margin configuration:

a) Outer-bend vs. inner-bend levee deposition

All modern examples of submarine channel systems (e.g. Niger Delta, Indus fan, etc) that exhibit composite surfaces contain channels with moderate to high sinuosities. As channel sinuosity increases, turbidity currents have a higher potential for overbank and overspill at the channel bends, and as a consequence, levee development. One notable feature of these submarine levees is their lack of bilateral symmetry, because levee deposition or aggradation is considerably greater on the outer compared to the inner bank (Fig. 3.26a). For example, in high sinuosity deep-water channels, the outer-bend levee is three to four times higher compared to the opposite (inner) levee (Straub et al., 2004), as the consequence of superelevation of the dense current over the outer bank (Peakall et al., 2000; Kolla et al., 2001; Straub et al., 2004).

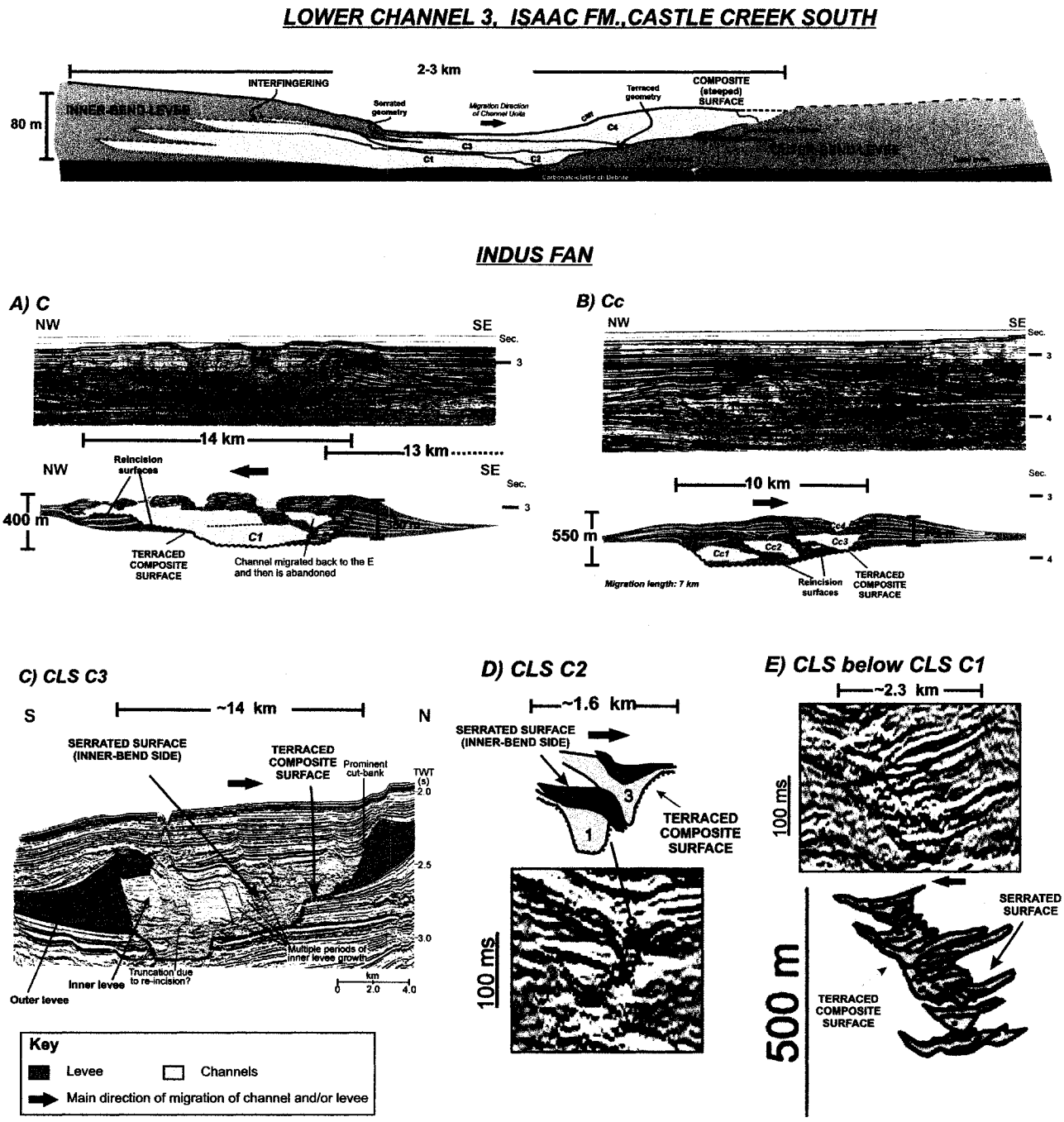

Continued...

Figure 3.25. Graphic comparison of terraced composite surfaces identified in Lower Channel 3, Castle Creek south study area and other channel-levee systems, such as (a,b) the channel complexes C and Cc of McHargue (1991) and (c-e) the channel complex system CLS C3, C2, and below C1 of Deptuck, et al. (2003) in the Indus Fan; (f-g) channel complex Benin Major of Deptuck, et al. (2003) in the Niger Delta; (h) leveed channel complex in the Indonesia Fan (Posamentier and Kolla, 2003); (i) channel complex set 3 of the Cerro Toro Formation, Chile (Beaubouef, 2004); and (j-k) channel complexes in the Pab Formation, Pakistan (Eschard, et al., 2003). Note all these examples have similar channel margin geometry even though they occur at significantly different scale.

Continuation Fig. 3.25…

LOWER CHANNEL 3, ISAAC FM.,CASTLE CREEK SOUTH

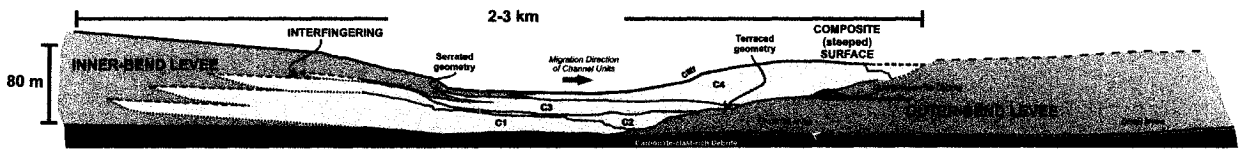

BENIN MAJOR, NIGER DELTA

F) Erosional fairway

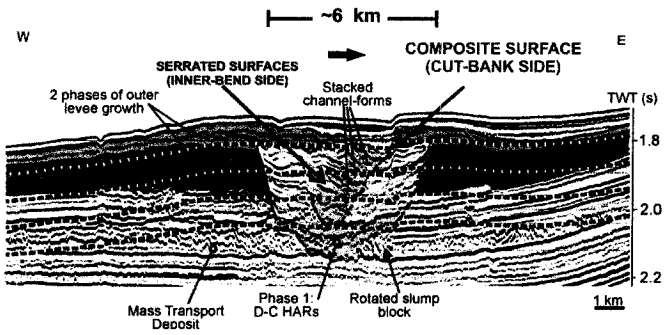

G) Meander loop 1

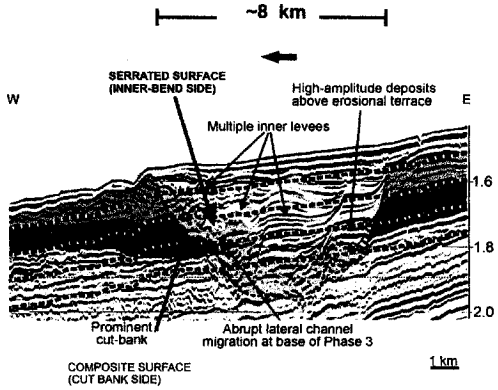

OFFSHORE EASTERN BORNEO, KALIMANTAN, INDONESIA FAN

H) Channel Complex

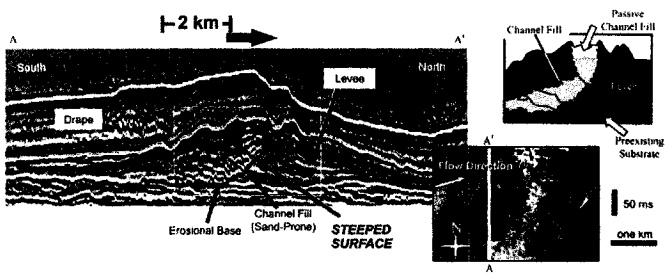

CERRO TORO FM., CHILE

I) Channel Complex Set 3

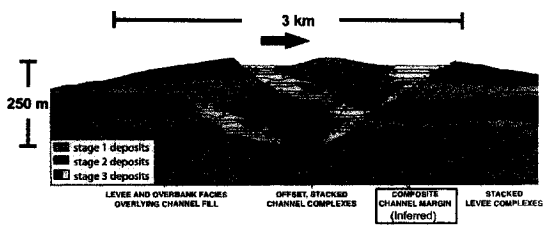

PAB FM., PAKISTAN

J) Channel Complex in the Canyon mouth

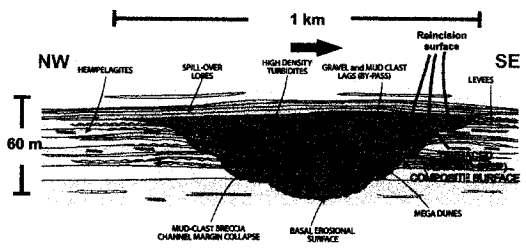

K) Channel Complex in the Mid-Fan

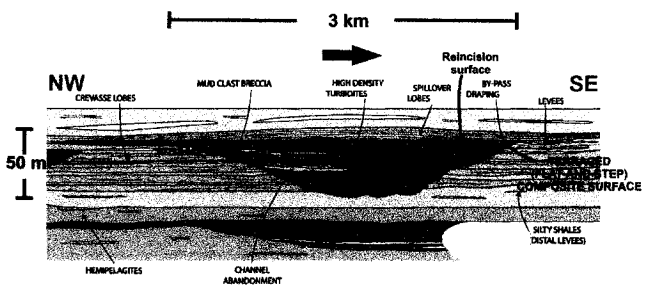

The high sinuosity of these channel systems can induce strong secondary flow circulation. Keevil et al. (2005) found that the secondary flow in submarine channel bends has a reverse sense of rotation (from the inside to the outside of the bend) compared to sinuous fluvial channels. Secondary flow plays a major role in determining the distribution of erosion and deposition around the channel perimeter, and also in establishing the spatial distribution of sediment grain size and sorting across the channel bend. High rates of sediment deposition on the outer levee leads to a sharp and steeper channel margin, compared with the more gentle slope on the inner-bank side. Sediment distribution in submarine levees varies depending on which side of the channel they were constructed. The coarsest sediment preferentially accumulates near the outer bank where thick flows predominate, whereas relatively thinner, fine-grained deposits prevail on the inner bank (Straub et al., 2004; Mohrig et al., 2004).

b) Channel aggradation accompanied with lateral migration

All the channel complexes presented in the fig. 4.5 show consistent evidence for considerable channel aggradation following levee deposition. Aggradation within the channel significantly decreased the levee relief (Fig. 3.26a). Channels tended to aggrade vertically as well as migrate laterally toward the outer-bank. Since channel aggradation was insufficient to balance the high outer-bank topography, the bank occasionally collapsed and temporarily plugged the channel. This forced the channel to abruptly shift laterally, while at the same time maintaining the principal direction of migration. This peculiar migratory evolution is characteristic of modern sinuous submarine channels, and is probably related to the reversed direction of secondary flow circulation (Keevil et al., 2005) and hydrodynamic conditions.

c) Multiple episodes of channel and levee growths

Most modern and ancient deep-water channel-levee complexes with composite bases consist of vertically-stacked, lateral-offset, channel-forms and levees that are interpreted to be the result of numerous (at least three) periods of channel-levee growth (Fig. 3.26b). Each episode of channel-levee growth is marked by an abrupt channel shift. The superposition of a new channel-levee system above an older one, but with significant lateral offset, is delineated by a serrated inner-bank margin and a terraced or benched outer-bank margin.

A) Submarine channel-levee

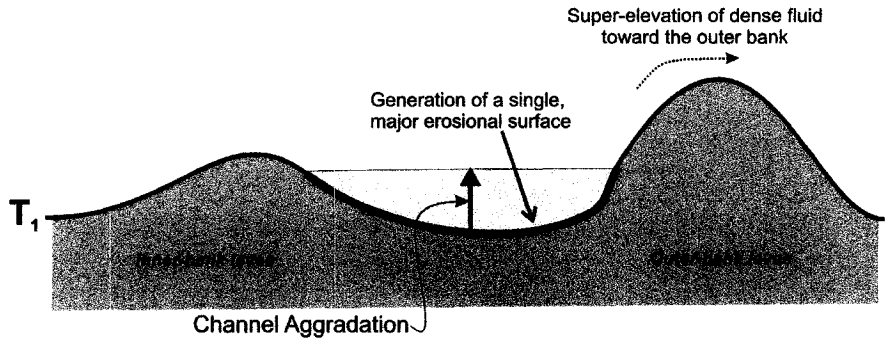

B) Submarine channel-levee complex

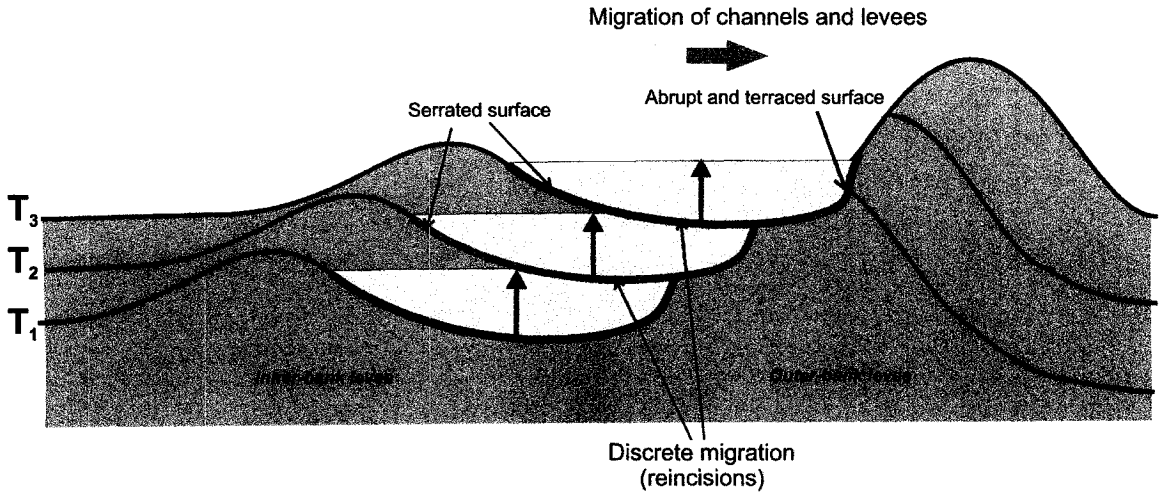

Figure 3.26. Diagrams showing the cross-section of a) aggrading submarine channel and b) aggrading and laterally migrating submarine channel complex at various times. The diagram shows that the base surface of the channel-levee complex is different on each side of the channel.

3.3.2. Middle Channel Complex, Channel 3

Middle channel complex of Channel 3 (Ch3.M) is poorly exposed in the study area, and consists of two distinct channel units that stack vertically, with a maximum thickness of 17 m (Fig. 3.15). The width of the complex is more than 1.1 km. These units are laterally offset toward the northwest. Channel units are separated by major erosion surfaces that locally can be traced across the study area. Even though a channel unit is defined by two or more channel fills (see section 3.1.2 in this chapter), the individual fills in Ch3.M could not be differentiated due to limited outcrop exposure. Thus, channel units have been distinguished on the basis of facies changes and erosional truncation of beds.

The base of Ch3.M-C1 overlies abruptly Ch3.L, incising mostly its uppermost channel unit Ch3.L-C4 and southeast levee intervals. The surface is flat and shallow-dipping (<1°), but becomes steeper along the southeast channel margin. The base of the overlying channel unit Ch3.M-C2 is also shallow, but along both margins, it is deeply incised Ch3.M-C1 and becomes steep on both margins with slopes up to 30-40°.

3.3.2.1. Channel Unit Ch3.M-C1

Ch3.M-C1 is poorly exposed in the study area where it is <300 m wide and is 13-16 m thick (Fig. 3.27). Channel margins are mostly covered. It comprises amalgamated channels filled with medium- to thick-bedded (up to 2.3 m), very coarse and coarse massive sandstone with subordinate clast-supported conglomerate (mostly FA3a). Massive sandstone beds contain abundant granule clasts and rare mudstone clasts at their bases. Normally graded, parallel-bedded sandstone beds, containing sand injections and flame structures, are common through the section. Stratigraphically-upward, coarse-grained strata commonly alternate with intervals of thin-bedded, fine sandstone with planar and/or ripple cross-lamination interbedded with siltstone (Fig. 3.27). Fine-grained intervals range from 1-46 cm thick.

3.3.2.2. Channel Unit Ch3.M-C2

Channel unit Ch3.M-C2 is up to 10 m thick, and is only well exposed in the NW side of the study area. Ch3.M-C2 is composed of non-amalgamated channel fills (FA3c, see section 2.3.3, chapter 2; Fig. 3.28). An up to 1 m-thick interval of deformed strata (FA4, see section 2.3.4, chapter 2) occurs in the lower part of Ch3.M-C2 and directly overlies the basal erosion surface. This interval is composed of contorted medium-bedded, very fine to coarse sandstone interbedded with siltstone (FA4, see section 2.3.4, chapter 2). Finer-grained sandstones are ripple- and parallel-laminated, whereas coarser sandstone are massive and dune-cross-stratified. Scattered mudstone clasts occur at the base of coarse-grained sandstone beds (Fig. 2.45).

Channel fills consist mostly of single and multiple sets of cross-laminated fine sandstone interbedded with siltstone (Fig. 3.28b). Minor medium- to thick-bedded (up to 40 cm thick), normal graded, medium to very coarse sandstones are also observed. These beds pinch out toward the northwest (Fig. 3.28c). In most places (excluding vertical cliff faces), beds are moderately traceable.

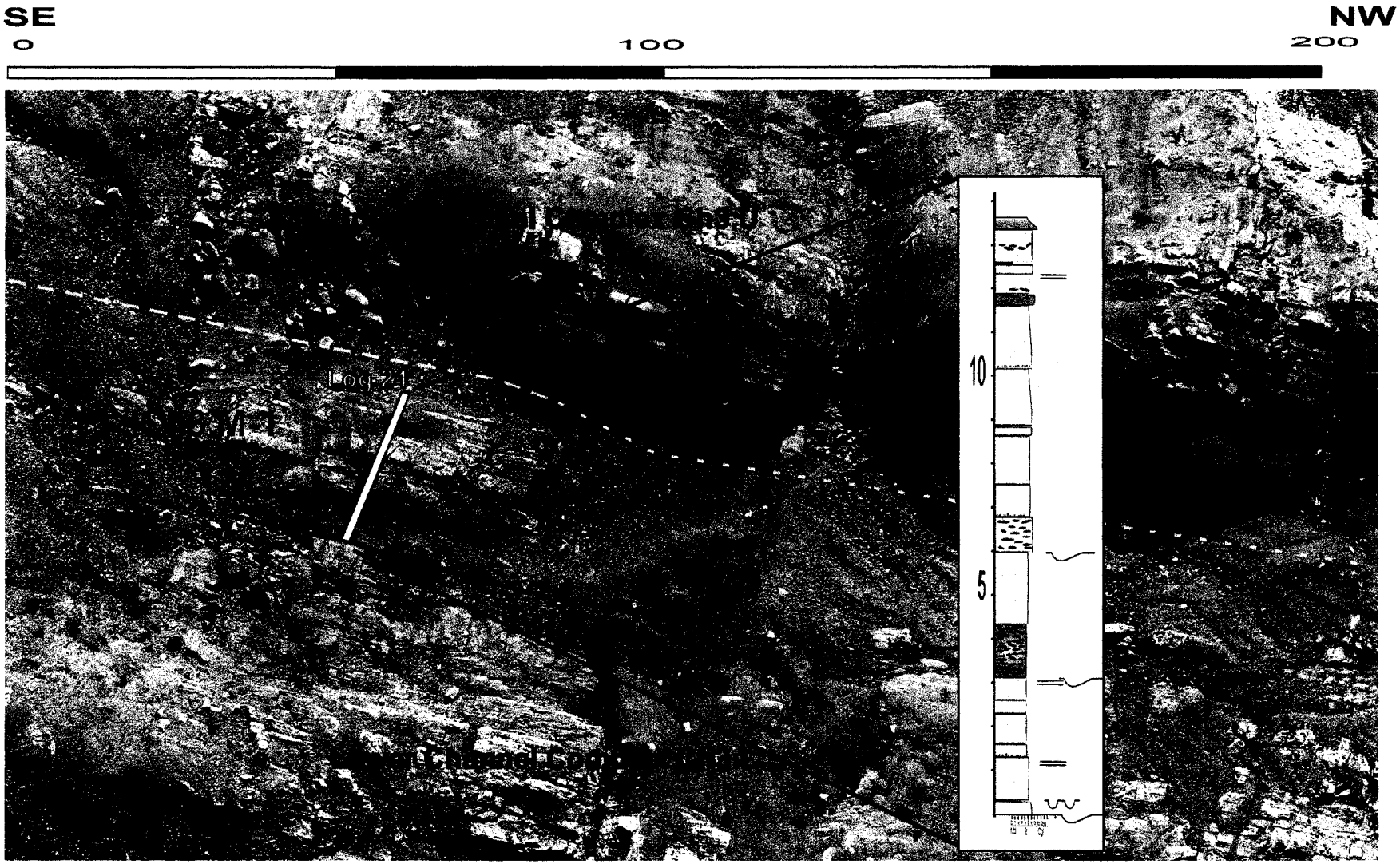

Figure 3.27. Photomosaic of channel unit Ch3.M-1, Middle Channel Complex of Channel 3, highlighting several bedding surfaces and measured section. For legend see Fig. 3.4.

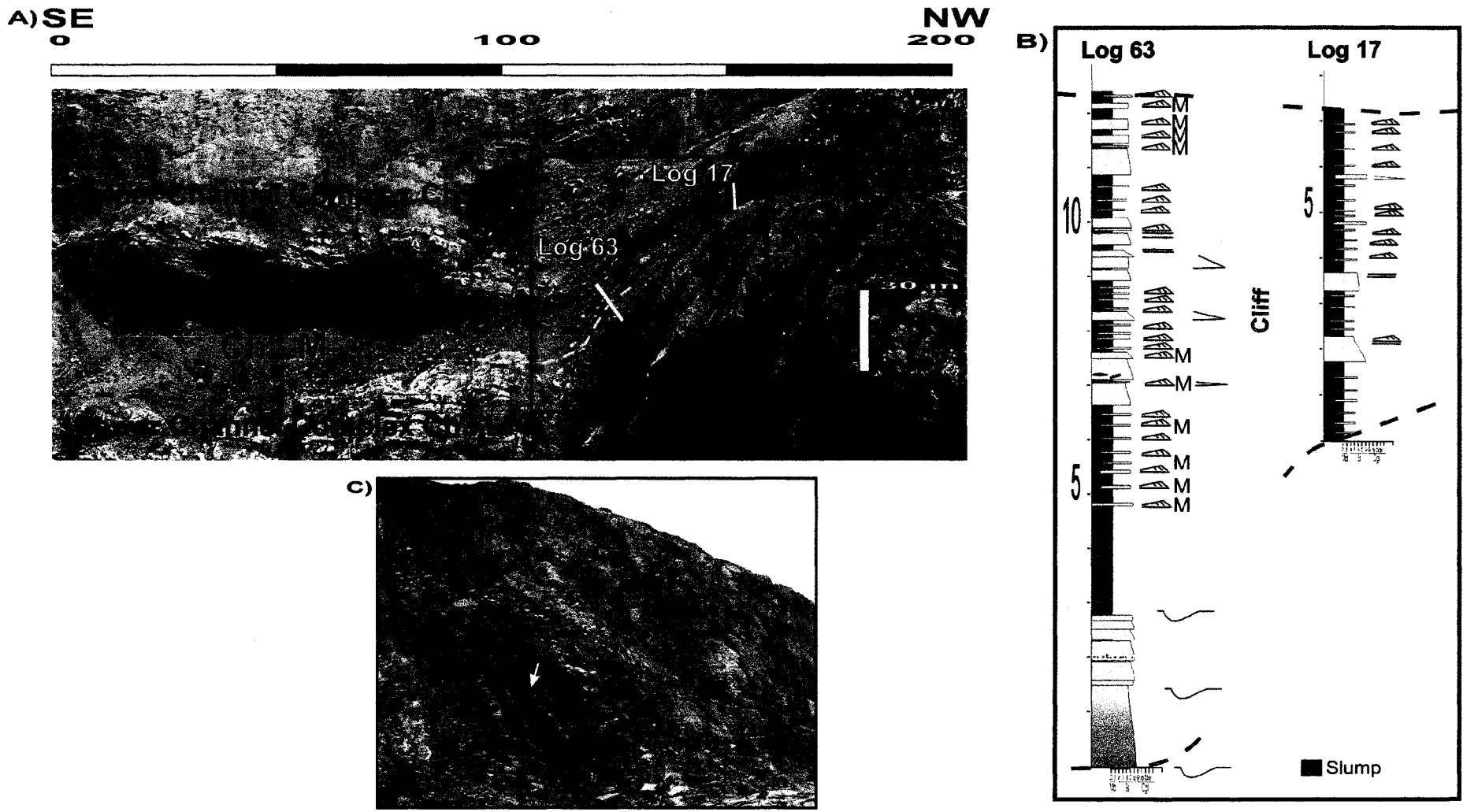

Figure 3.28. Photomosaic of channel unit Ch3.M-C2, Middle Channel Complex of Channel 3, highlighting the basal erosional surface of a slump interval. A) This channel is filled by thin bedded turbidites. B) Representative log of channel unit Ch3.M2, Channel 3. For legend see Fig. 3.4. C) Inset photo is a cliff-view showing truncation surfaces at the base and top of Ch3.M-C2. Some thicker medium to coarse sandstone beds thin and pinch out (arrow) obliquely upward. Person for scale.

3.3.2.3. Interpretation

The middle channel complex Ch3.M is interpreted to represent a new phase of channel deposition. The base of Ch3.M-C1 marks a dramatic change in the channel history, perhaps associated with a shift in channel position. This change is initiated by an episode of incision by large bypass turbidity flows that eroded deeply into the southeast levee and the upper channel fills of Lower Channel 3.

The channel fill phases were dominated by sand-rich turbidity flows. These flows were smaller and less efficient than the earlier bypassing flows, and formed thick amalgamated deposits. Vertical changes from thick, sandstone-rich strata to thinner, more heterolithic facies suggest a reduction of sediment discharge or flow velocity (Grecula et al., 2003; Eschard, et al., 2003), possibly related to a backstep of the sediment staging area.

The base of Ch3.M-C2 marks another change in the channel complex and is associated with channel incision and rejuvenation. Erosion by by-passing high-energy currents eroded almost all the northwest margin of Ch3.M-C1. Deformed strata near the base of Ch3.M-C2 represent slump deposits most likely sourced from a failure of the northwest channel wall. The slump failure occurred during channel incision or during the early stage of channel fill, when sediments along its margins were most unstable and more susceptible to collapse. This was succeeded by infilling of Ch3.M-2 with mostly mud-rich, low-concentration turbidites (T_{cde}). Thick, coarse-grained sandstone (T_a turbidites) rapidly pinch out toward the northwest. These strata suggest a gradual infilling of a largely abandoned channel.

3.3.3. Upper Channel Complex, Channel 3

The upper channel complex in Channel 3 (Ch3.U) strikes across the study area and is more than 1.1 km wide (Fig. 3.15). It is about 50 m thick and comprises at least two amalgamated channel units in the lower half of the complex and a laterally extensive, sheet-like, fine-grained interval in the upper half of the complex that locally is interbedded with an isolated channel fill. Channel units are vertically stacked and show a lateral offset toward the northwest.

The lower channel unit (Ch3.U-C1) lies sharply on the middle channel complex Ch3.M, whereas the upper channel unit (Ch3.U-C2) truncates part of Ch3.U-C1 and both channel

complexes Ch3.M and Ch3.L on the northwest. The bases of these channel units are demarcated by sharp and shallow (locally stepped) erosion surfaces.

3.3.3.1. Channel Unit Ch3.U-C1

Ch3.U-C1 is about 300 m wide and is up to 20-25 m thick. It consists of amalgamated channel fills (FA3a) made up of thick-bedded, normal graded, dispersed granule to very coarse to medium sandstone (Fig. 3.29). Sandstone thickness varies, but generally is up to 1.2 m. Locally, interbedded mudstone and/or fine cross-laminated sandstone are common, and range from a few to tens of centimetres thick.

3.3.3.2. Channel Unit Ch3.U-C2

Ch3.U-C2 consists of amalgamated channel fills that are more than 1 km wide and collectively up to 25 m thick. Individual channel fills range from 2 to 10 m thick. Only a few channel fills have been recognized with confidence. They are characterized by high width:depth ratios, and have vertical stacking with lateral offset toward the northwest.

The bases of the channel fills are marked by shallow erosion surfaces that locally become steep (Fig. 3.29). The lateral continuity of the channel fills is high to intermediate (based on criteria of Clark and Pickering, 1996).

Thick-bedded, mudstone-clast breccia beds commonly overlie the erosion surface at the base of channel fills. Fills are highly amalgamated (FA3a) and consist mostly of thick-bedded, normal graded, very coarse to medium sandstone, with subordinate thick-bedded, normal graded conglomerate to sandstone (Fig. 3.29).

Commonly, sandstone beds have abundant, up to 6 mm, granule and pebble clasts at their bases, and range from several centimetres to 2.29 m thick. Conglomerate beds are up to 2.53 m thick. Sandstone and conglomerate beds are locally capped by 1-2 cm-thick mudstone. In the upper channel fills, coarse-grained beds are interbedded with thin- to medium-bedded (10-23 cm thick) intervals of mudstone and very fine cross-laminated sandstone.

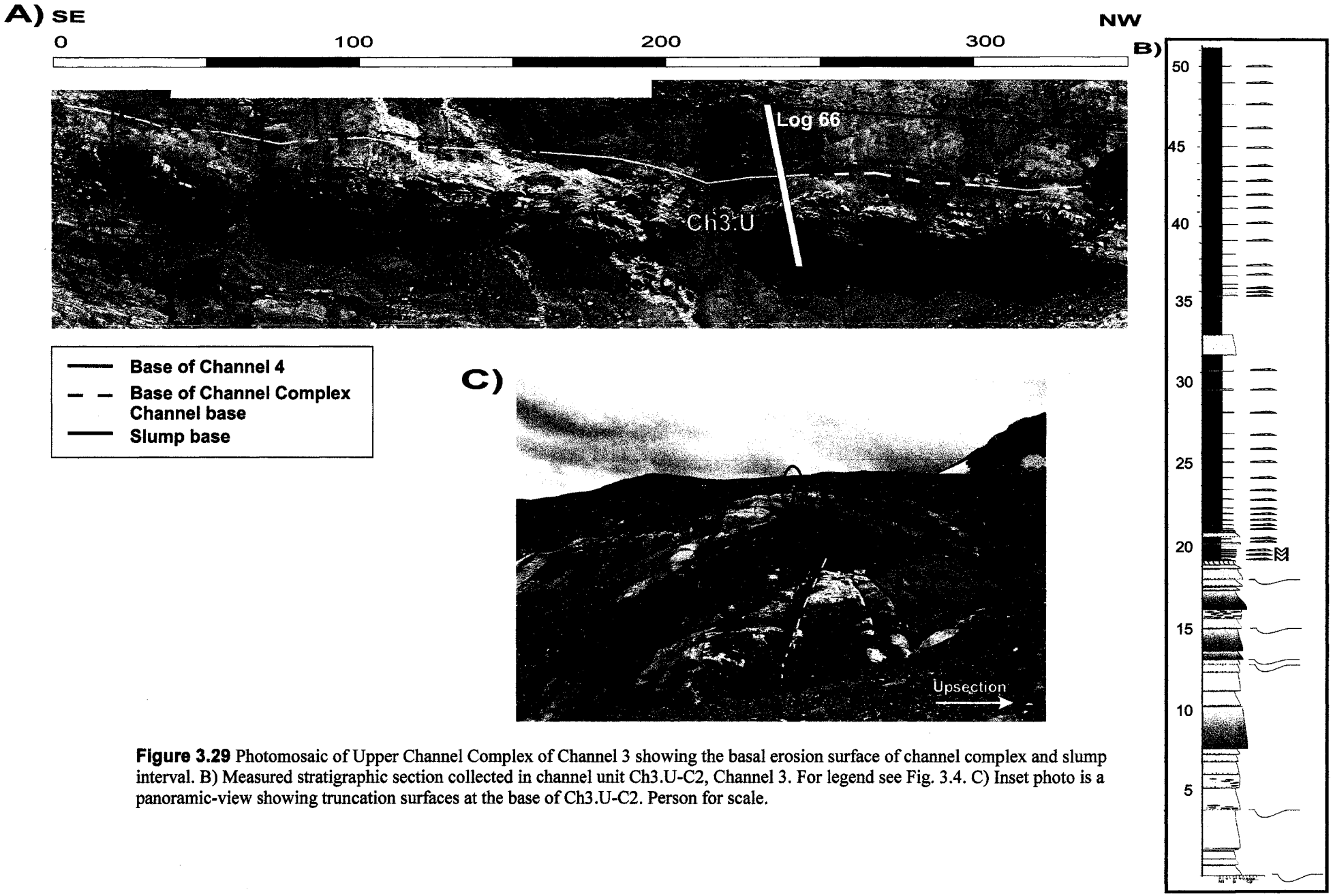

Figure 3.29 Photomosaic of Upper Channel Complex of Channel 3 showing the basal erosion surface of channel complex and slump interval. B) Measured stratigraphic section collected in channel unit Ch3.U-C2, Channel 3. For legend see Fig. 3.4. C) Inset photo is a panoramic-view showing truncation surfaces at the base of Ch3.U-C2. Person for scale.

3.3.3.3. Layered thin-bedded sheet (Ch3.U-S1)

Ch3.U-C2 is conformably overlain by an up to 20 m thick, fine-grained succession (Ch3.U-S1). At its base, strata are interbedded with beds of massive or cross-bedded, coarse sandstone. These beds are generally discontinuous over relatively short distances (pinching-out in one or both directions).

Fine-grained strata are composed of thin-bedded, cross-laminated fine sandstone and silty mudstone (Fig. 3.29). Multiple sets (2-3) of ripple cross-laminated sandstone are common in the lower part, but single sets predominate toward the top. Moreover, cross-laminated sandstone layers typically fine and thin upward from 5 cm to 0.2 mm. In contrast, mudstone beds increase in abundance and thickness and range from 1 to 20 cm. Locally, thin-bedded (5 to 10 cm thick), cross-bedded and massive, coarse and medium sandstone are observed.

An isolated, 1.5-2 m thick channel fill is encased within the upward-fining mudstone-rich strata, and consists of amalgamated beds of medium to coarse sandstone (FA3a). This discrete channel fill is overlain by a succession of contorted beds and isolated boudin-like structures (Fig. 2.46), with thickness on the order of 2-2.3 m (FA4).

3.3.3.4. Interpretation

The upper channel complex clearly demonstrates several periods of channel reactivation, in which both channel units represent successive phases of erosion, infill and abandonment. The base of Ch3.U-C1 corresponds to incision and bypass of turbidity flows that eroded underlying deposits of Middle Channel 3. Subsequent depositional phases were recorded by multistorey channel fills deposited from high-concentrated, sandy turbulent flows.

The base of Ch3.U-C2 indicates a short-term channel reincision event that might have been triggered by slump failure along the northwest channel margin that caused the channel system to abruptly migrate laterally. Similar events occurred during growth of the Lower Channel Complex (Ch3L). Channel fills show laterally extensive basal erosion surfaces overlain by mudstone-clast breccia, which together are interpreted to be indicative of high-energy bypass processes. Channel-fill deposits that consist of normal graded sandstone (T_a turbidites, S3 Lowe division) were deposited by high-concentration turbulent flows.

The top of the Upper Channel Complex (Ch3.U-S1), which consists of thin-bedded fine-grained strata (T_{cde}) deposited from low-concentration turbidity currents, marks the terminal deactivation of Channel 3. The deactivation phase was interrupted by late-stage incision of a single channel. This channel was progressively but intermittently filled by small-scale, high-concentration sandy flows that deposited amalgamated sandstone (T_a). This channel is overlain by a contorted interval, interpreted to be a slump deposit that abruptly plugged the channel. This slump indicates slope instability, which locally may have been exacerbated because of channel abandonment.

3.4. Comparison in channel configuration of both deep-water channels

The architectural elements defined in this study show considerable spatial and temporal variability in both Channel 1 and 3. Individual channels stack vertically and form a channel complex set (Channel 1 and 3) that overlies an areally extensive deep-water deposit (sequence stratigraphic implications of these intervals will be discussed in Chapter 4). Notwithstanding differences in the general geometry of both channel complex sets, some channel complexes and their constituent composite fills (e.g. Upper channel complex in Channel 1 (Ch1.U) and Lower Channel-levee complex in Channel 3 (Ch3.L)) show morphological similarities in terms of comparable vertical and lateral trends in lithofacies, and types of infills and character of significant surfaces. These similarities most probably reflect comparable relationships in the principal factors that control sediment transport and deposition in slope settings, including: accommodation, flow conditions, sediment flux and caliber, equilibrium profile and level fluctuations (Husberch et al., 1997; Pirmez et al., 2000; Kneller 2003; Posamentier and Kolla, 2003).

3.4.1. Vertical variation

3.4.1.1. Lower Channel units

Channel fills in the lower part (or lower channel units) of channel complexes in Channel 1 and 3 are wide (commonly >1 km) and highly amalgamated, forming a stacked, nested geometry. Fills are more amalgamated in their axes where basal erosion surfaces tend to be

locally deep, including local erosional zones. Erosion surfaces are typically overlain by amalgamated, laterally discontinuous mudstone-clast breccia deposits, gravelly strata or thin-bedded turbidites, suggesting intense sediment reworking and bypass. These strata are overlain by channel deposits. Channels were free to migrate laterally and cannibalize previously deposited sediment, eventually developing a broad sheet-like belt near the base of the channel complex.

The dominance of erosive processes is associated with low rates of vertical aggradation due to limited accommodation space. Slope accommodation is determined by the equilibrium profile (Fig. 3.30) of the channel. Equilibrium profile is a graded, concave-upward profile that adjusts to base level in a manner similar to fluvial systems (Pirmez et al., 2000). Samuels et al. (2003), based on Takahashi (2001), postulated that the equilibrium gradient of slope depends on flow characteristics (e.g. density and thickness) and maximum grain size of sediment load.

Submarine channels that show little aggradation (e.g. Mayall and Steward, 2000; Kolla et al., 2001, Samuels et al. 2003) tend to migrate laterally in a horizontal plane. These channels are described as graded or neutral channels (Kneller, 2003; Fig. 3.31), in their attempt to maintain the same equilibrium profile. In the study area, channels in the lower part of Channel 1 and Channel 3 mostly probably were initially graded and could have changed with time to became locally more erosional when the slope profile was lowered.

In large part, changes in slope profile reflect changes in flow conditions. Initially flows were regular, highly-efficient, and likely to bypass the slope and be deposited farther down slope. These flows are only recorded as remnants (bypass deposits) of originally more extensive deposits, and occur as thin bedded turbidites, mudstone-clast breccia and/or interstratified gravel lag layers. Any sudden change to more energetic flows could cause an abrupt migration in channel position (Kolla et al. 2001). These flows had higher momentum and were more focused toward the channel axis (Husberch et al., 1997), forming erosion surfaces like the erosional zones in Ch1.U-C1 or Ch3.L-C2.

A change to coarser and/or larger flows initiated deposition of the coarsest conglomerate and/or sandstone within the channel. These channel fills have the highest net-to-gross ratio and ranging from 75 to 95%.

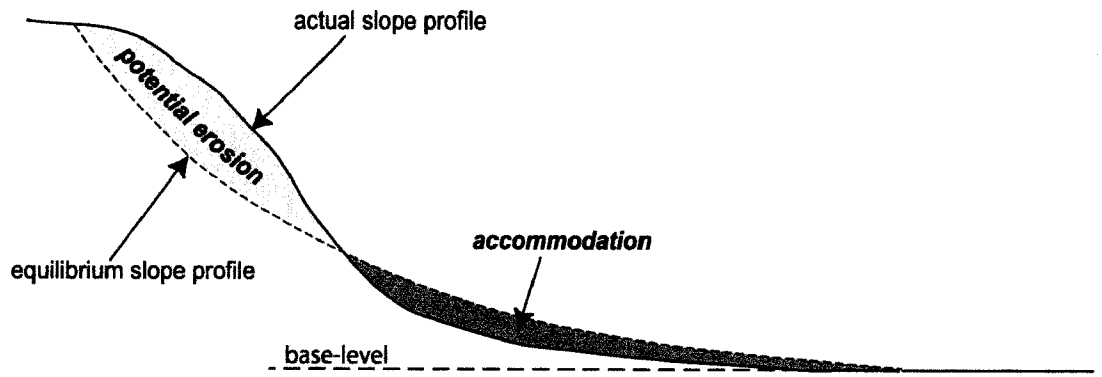

Figure 3.30. Schematic representation of the equilibrium channel profile (From Samuels et al., 2003). If the actual slope profile is below the equilibrium profile, there is positive accommodation, which in turn is compensated by deposition. In contrast, if the actual slope profile is above, there is potential erosion (negative accommodation of Kneller, 2003). Baselevel in deep-water systems is the deepest point that flows reach in the basin.

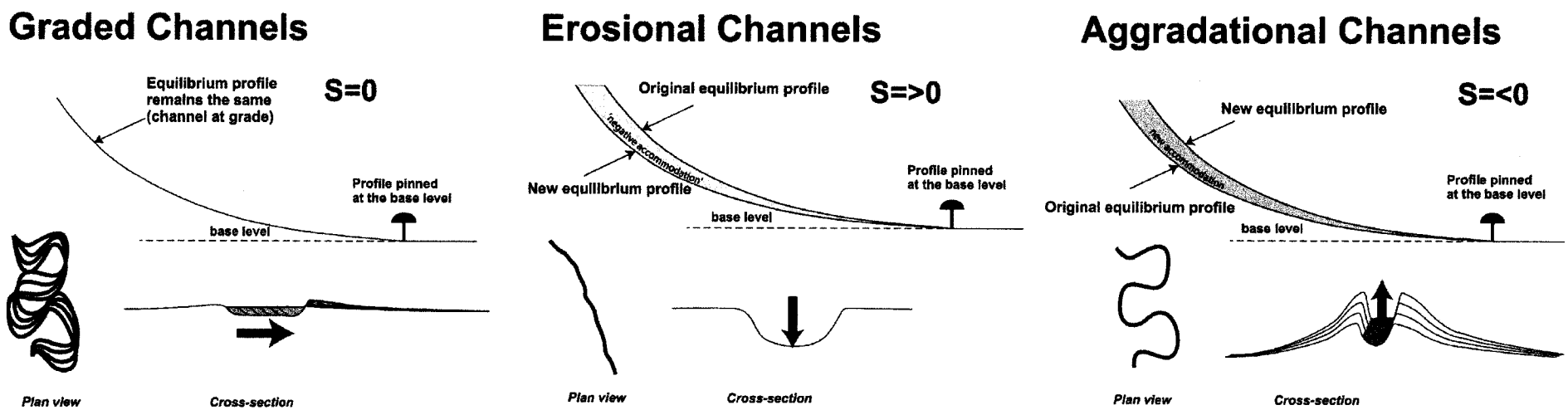

Figure 3.31. Schematic representation of three different channel responses to the old and new equilibrium profiles: graded, erosional and aggradation, shown in their respective general plan and cross-sectional views (From Kneller, 2003).

In the middle, and in particular in the upper part of the lower channel units, the degree of amalgamation decreases upward, as interbedded mudstone and fine-grained sandstone become more common. Moreover, fine-grained strata at the top of the channel units are better developed and more thickly preserved. This vertical change indicates that considerable aggradation occurred toward the tops of channels, and is intrinsically connected to a decrease in flow velocity, efficiency, thickness and/or density.

3.4.1.2. Middle Channel units

Channel fills in the middle part (or middle channel units) of channel complexes of Channel 1 and 3 have typically shallow basal erosion surfaces, although some are deeply scoured. Mudstone-clast breccia and mudstone drapes commonly overlie these surfaces and were deposited by bypass flows signifying channel inception. Channel fills are typically semi-amalgamated or layered with lower net-to-gross ratios that the underlying channel fills, ranging from 70 to 89%. Channel fills consist mostly of sandstone and conglomerate, commonly interbedded with thin-bedded, fine-grained turbidites. Conglomerate beds are slightly less coarse than in the lower channel units. This vertical trend is related to a tendency toward less energetic, less dense, smaller, sandier and less efficient flows (Samuels et al., 2003; Kneller, 2003) with sufficient accommodation space for channel aggradation. Aggradational channels are associated with lower slope gradient, and commonly are associated with the backstepping of sediment supply system (Samuels et al., 2003).

Two important features are common at the top of the middle channel units in Channel 1 and 3. The first is the occurrence of thin-bedded, fine-grained turbidites interpreted to represent temporary abandonment of the channel system. The second is laterally extensive and locally deeply scoured erosion surfaces truncating underlying channel units, which characterizes episodes of channel migration induced by dramatic changes in flow parameters.

3.4.1.3. Upper Channel units

Channel fills in the upper part (or upper units) of channel complexes in Channel 1 and 3 are similar to those in the middle channel units, but have a comparatively lower sandstone-mudstone ratio. Individual channels in the upper units have generally flat, basal erosion surfaces, overlain by bypass deposits that make up a smaller proportion of the channel fill. Channel fills are less amalgamated because of better preserved interbedded fine-grained

strata. The degree of amalgamation of channel fills diminishes upward and laterally. This vertical facies change is linked with higher rates of aggradation in the system caused by upward changes in the equilibrium channel profile related to changes in sediment load and flow character (Kneller, 2003).

Although it is impossible to derive channel sinuosity from a two-dimensional cross-section, the inclined facies association (lateral accretion packages) in the upper part of some channel complexes suggests an upward increase in channel sinuosity. These channels, in comparison with those in the lower in section, are also significantly narrower. These observations are consistent with remarks of other works, for example Elliot (2000) and Eschard et al. (2003), who documented meandering turbiditic channels at the top of channel complexes in the Ross Formation (Ireland) and Pab Formation (Pakistan), respectively.

The overall decrease in sediment supply is followed by a complete deactivation of the channel system, which is identified by the mudstone-rich turbidite succession that drapes the entire channel system.

3.4.2. Channel-stacking patterns

As mentioned in section 3.1.2, channel-stacking patterns are related to the interaction of lateral channel migration and vertical aggradation. These processes are also closely related to the flow conditions, including flow volume, velocity, competence, and frequency (McHargue, 1991).

Channel fills within some channel complexes (e.g. Ch1.U, lower part of Ch3.L) in Channels 1 and 3 show three common stacking patterns, which vary stratigraphically upward. Channel fills in the lower part of the channel complexes exhibit high lateral migration, which is associated with a less "confined" system (see Fig. 3.2), particularly in Channel 1, in which high rates of sediment deposition significantly exceeded the low rates of accommodation space. As a consequence, width: depth ratio and sandstone:mudstone ratios tend to be high and bed amalgamation is common.

Channel fills in the middle and upper part of the studied channel complexes, on the other hand, show two different stacking relationships: combined aggradation and migration, and aggradation with little migration. The combined stacking pattern is recognized in the middle part of Ch.3.L, and is related to a complex oblique channel migration, in which channels were aggrading as the channel continuously migrated preferentially toward the cut-bank side,

forming the terraced composite basal surface (see the end of section 3.3.1 for a detailed discussion). Continuous lateral migration was interrupted by episodes of abrupt channel migration. This type of stacking pattern occurs when the rate of sediment deposition is greater than the accommodation space. The width:depth and sandstone:mudstone ratios of channels gradually decrease upward, as a result of the progressive reduction in sediment supply.

The second aggradational stacking geometry is identified in middle and upper parts of Ch.1.U and upper part of Ch.3.L, in which rate of sediment deposition was accommodated within the channel space. This vertical channel aggradation was accompanied by some lateral migration. Typically, the width:depth ratio of channels is high to intermediate, and sandstone:mudstone ratio diminishes slightly upward.

In the uppermost part of the studied channel complexes, LAP's deposits suggest an increase in the channel sinuosity, which occurs when rates of sediment deposition are sufficiently high, even though the width of the thalweg belt decrease.

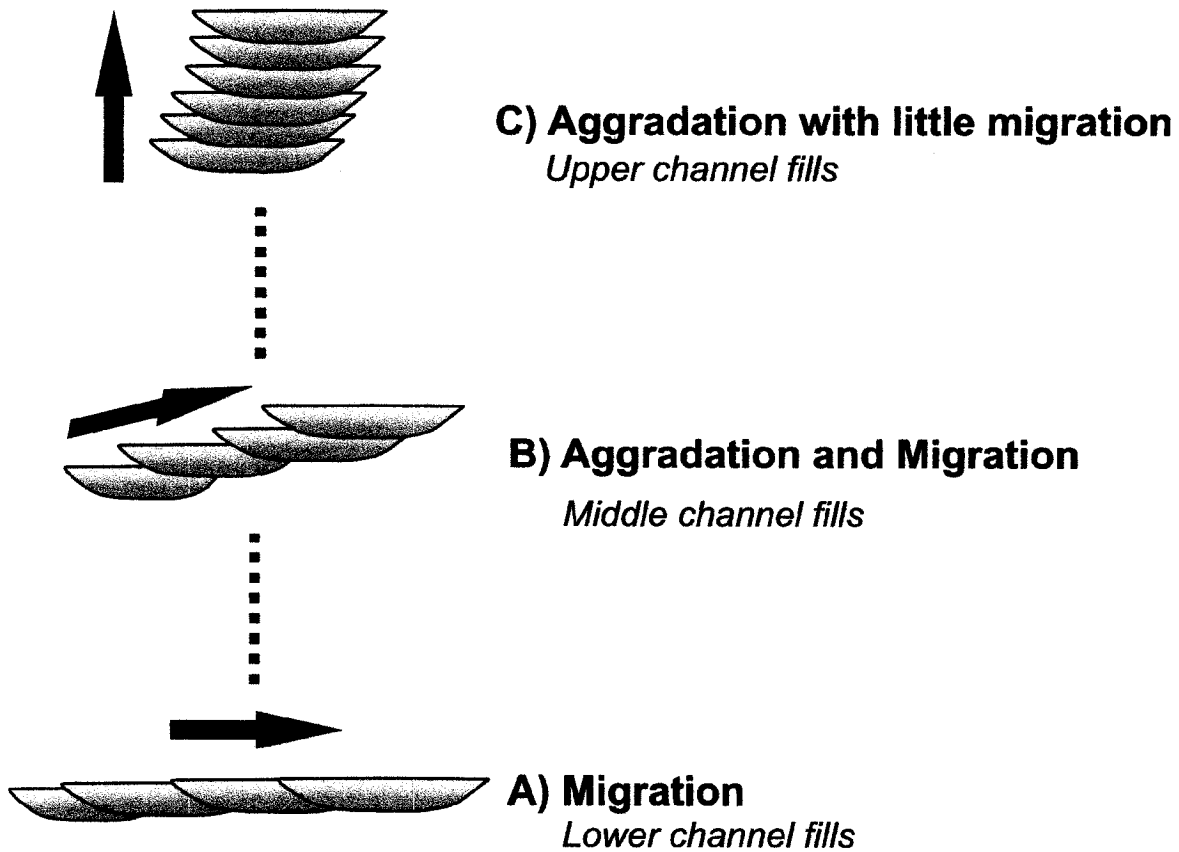

Figure 3.24. Schematic diagram of different channel-stacking patterns observed in channel fills of Channel 1 and 3, based on the degree of lateral migration and vertical aggradation.

3.5. Implications for deep-water hydrocarbon reservoirs

A brief discussion of important reservoir implications related to channel development in the slope setting is presented below. Channel 1 and 3 are comparable to modern offshore deep-water systems in the Arabian Sea (McHargue, 1991) and West Africa (Kolla et al., 2001; Fonnesu, 2003; Abreu et al., 2003; Deptuck et al., 2003; Adeogba et al., 2005), and thus can be useful analogs for predicting and estimating the stratal architecture of slope channel hydrocarbon reservoirs.

High-resolution outcrop studies are key to building reservoir architectural models (Slatt, 2000). In this study, Channel 1 and 3 provide important sedimentological and architectural data at a scale that is seismically unresolvable, but which can be used to provide geostatistical data for constructing geologically reliable reservoir models.

In the axial parts of both Channel Complex sets, channel fills have high reservoir quality with excellent horizontal and vertical connectivity, and their N:G ratios range from 80 to 100%. These fills consist almost exclusively of stacked, amalgamated clast-supported conglomerate and coarse-grained sandstone (see stratigraphy columns of Channel 1 and 3 in this chapter, gamma-ray profiles in Appendix V, and facies distribution percentage in Appendix VI). Fine-grained layers that occur within channel fills are typically laterally discontinuous somewhere along their length. In contrast, the fine-grained, laterally-continuous turbidites that occur rarely at the top of channel fills (especially in Channel 1) probably would form local barriers to fluid flow.

Mudstone rip-up clast breccias commonly occur at the base of some channel fills. These breccia zones reduce significantly reservoir volume locally (Elliot, 2000), but most probably cause little change in the permeability because of good communication through the sandstone matrix surrounding the loosely packed mud-clasts.

Reservoir quality decays as grain-size and bed thickness decrease vertically and laterally toward the channel margins. In the upper channel fills of Channel 1 and 3, N:G ratios decrease (from 90% to 70%) as strata become progressively less amalgamated. Typical rapid and direct thinning of beds toward the channel margins (similar in broad terms to the type A, pinch-out geometry of McCaffrey and Kneller, 2001), which is well illustrated in upper channel unit of Lower Channel 3, will result in excellent reservoir quality all the way to the

bed termination. However, the common occurrence of siltstone interbeds will most probably negatively affect the vertical connectivity between individual sandstone beds.

Locally, differences in the contact between channel sandstone and levee deposits along the southeast and northwest margin of lower Channel 3, being either sand-on-mud or sand-on-sand, would have a negative or positive impact on cross-flow between these elements.

3.6. CHAPTER SUMMARY

Two major intrachannel architectural elements, channels and thin-bedded sheets, are recognized in Channel 1 and 3 of the Isaac Formation at the Castle Creek South study area. Mapping the spatial and temporal distribution of these elements, based on the observed vertical and lateral facies changes, sandstone geometries and major erosion surfaces provides a detailed understanding of their internal architecture and evolution.

Channel 1 and 3, which are both estimated to be more than 1.1 km wide, represent channel complex sets that consist of two and three stacked channel complexes, respectively. Channel complexes are of the order of 30-50 m thick and individually comprise several channel units, which in turn are made up of more than two channel fills. Major erosion surfaces at the base of individual channel units are typically shallow, with local deep scours, and are overlain by thin-bedded turbidites, conglomerate layers and mudstone-clast breccia, interpreted to be bypass deposits associated with varying degrees of erosion during channel inception.

Channel fills show an upward change from high net-to-gross, amalgamated sandstone-conglomerate to lower net-to-gross interstratified sandstone-mudstone, which is interpreted to indicate upward changes in the equilibrium channel profile, and accordingly, changes in accommodation space. In the lower part of some channel complexes, channel fills are amalgamated because of low rates of aggradation and consequent sediment reworking and bypass. In their middle and upper parts, however, higher rates of aggradation resulted in better preservation of interbedded fine-grained strata. Non-amalgamated, heterolithic channel fills are rare and occur at the top of some channel complexes, indicating passive deactivation of the channel system. Channel complexes are draped by a laterally extensive, thin-bedded sheet units that represents temporary or final channel abandonment.

CHAPTER 4. EVOLUTION OF TWO DEEP-WATER SUBMARINE CHANNEL COMPLEX SETS (CHANNEL 1 and 3) IN THE NEOPROTEROZOIC ISAAC FORMATION, WINDERMERE SUPERGROUP, CARIBOO MOUNTAINS, BRITISH COLUMBIA, CANADA

4.1. INTRODUCTION

A summary of deep-water strata and their sequence stratigraphic significance is first introduced to set the conceptual framework for the discussion presented later, which focuses solely on the evolution of Channel 1 and 3. Special attention is paid to the relationships between the architecture of the channels, whether they show similar characteristics or not, in relation to their slope position. Additionally, a brief discussion about important reservoir implications of channel development in the slope setting is presented.

4.1.1. Chapter Aims

This chapter discusses temporal and spatial evolution of two channel complex sets formed on the Neoproterozoic passive-margin slope of western Canada. The models condense the observations and interpretations of this study into a number of schematic diagrams that provide a conceptual framework to better understand and predict the stratigraphic occurrence, distribution, and facies variability of deep-water slope channel reservoirs.

4.1.2. Deep-water sequence stratigraphy

Recent progress in deep-water siliciclastic research and development of applicable stratigraphic models has been motivated by the demand to explore and exploit high-cost hydrocarbon reservoirs. This economic interest in deep-water depositional systems has contributed significantly to the identification of the architectural elements that make up these deposits, including channels, levee, overbank, crevasse splays, debris flow, lobes, etc. However, a precise understanding of the sedimentological variables that control the construction of these features is still poorly known.

The intrinsic relationship between deep-water sequences and changes of sea level are widely recognized (Posamentier and Kolla, 2003), and provide a general understanding of

the geologic framework of slope and fan deposits. However, it is important to note that some turbidite systems are controlled instead by tectonic and/or climatic factors that are unrelated to sea level position (e.g. Scott et al., 2000, Gonzalez et. al., 2003; Jeannette et al., 2003; Mutti et al., 2003).

Deep-water sedimentation rate increases considerably during relative sea-level fall (Satur et al., 2000; Coleman, 2000; Gardner et al., 2003; Samuels et al., 2003; Posamentier and Kolla, 2003). As shown in Fig. 4.1, several models have been presented in the literature that associate depositional successions (or system tracts) to times of falling and/or lowstand of sea level (e.g. Posamentier and Vail, 1988; Hunt and Tucker, 1992, 1995; Kolla et al., 1995; Plint and Nummedal, 2000; among others). These models differ with respect to nomenclature, but more importantly, the position of bounding surfaces and/or stratal stacking patterns. Notwithstanding terminological differences, the top of the highstand system tract (sequence deposited during slowing rates of relative sea-level rise and stillstand) is marked by an erosional unconformity that is initiated as sea level begins to fall.

A depositional sequence is defined as a relatively conformable succession of genetically related strata bounded by unconformities or their correlative conformities. It consists of major stratal surfaces and system tracts that were formed during specific intervals in a cycle of relative sea level change. The base of a sequence (Fig. 4.1) is termed a sequence boundary (SB, type 1) by some authors (Van Wagoner et al., 1988; Posamentier et al., 1988, Van Wagoner et al., 1990, Kolla et al., 1995). However, Hunt and Tucker (1992, 1995) and Plint and Nummedal (2000) argued that this surface is not areally widespread, and is formed before the lowest point of sea level fall. This surface therefore should not be considered the SB, but instead as the basal surface of the forced regression (Hunt and Tucker, 1992, 1995) or regressive surface of marine erosion (Plint and Nummedal, 2000). This surface is formed as relative sea level falls (equivalent to the forced regression of Posamentier et al., 1990, 1992), the continental shelf becomes progressively more exposed as the shoreline shifts basinward. As a result of subaerial exposure, rivers commonly begin to incise the shelf and shelf margin, especially if the shoreline falls below the shelf-slope break. This, in turn, results in a considerable volume of sediment being supplied to the upper slope, and subsequently transported downslope onto the lower slope and basin floor, forming toe-of-slope deposits and basin-floor fans (e.g. Cummings and Arnott, 2005). Fans may consist of a

series of feeder channels and at their termini distinct fan lobes. Additionally, sediment overburden and elevated pore pressures creates instability on the upper part of the slope that elevates gravitationally-driven failure, and related slump and slide deposits. Deposits formed during this period of sea-level fall are included as part of the early lowstand system tract (Posamentier et al., 1991,1992), forced regressive wedge system tract (Hunt and Tucker, 1992), forced regressive system tract (Helland-Hansen and Gjelberg, 1994; Hunt and Tucker, 1995), or falling-stage system tract (Plint and Nummedal, 2000). In general, falling relative sea-level is periodically interrupted by small-scale stillstand or rises of relative sea level (Kolla et al., 1995).

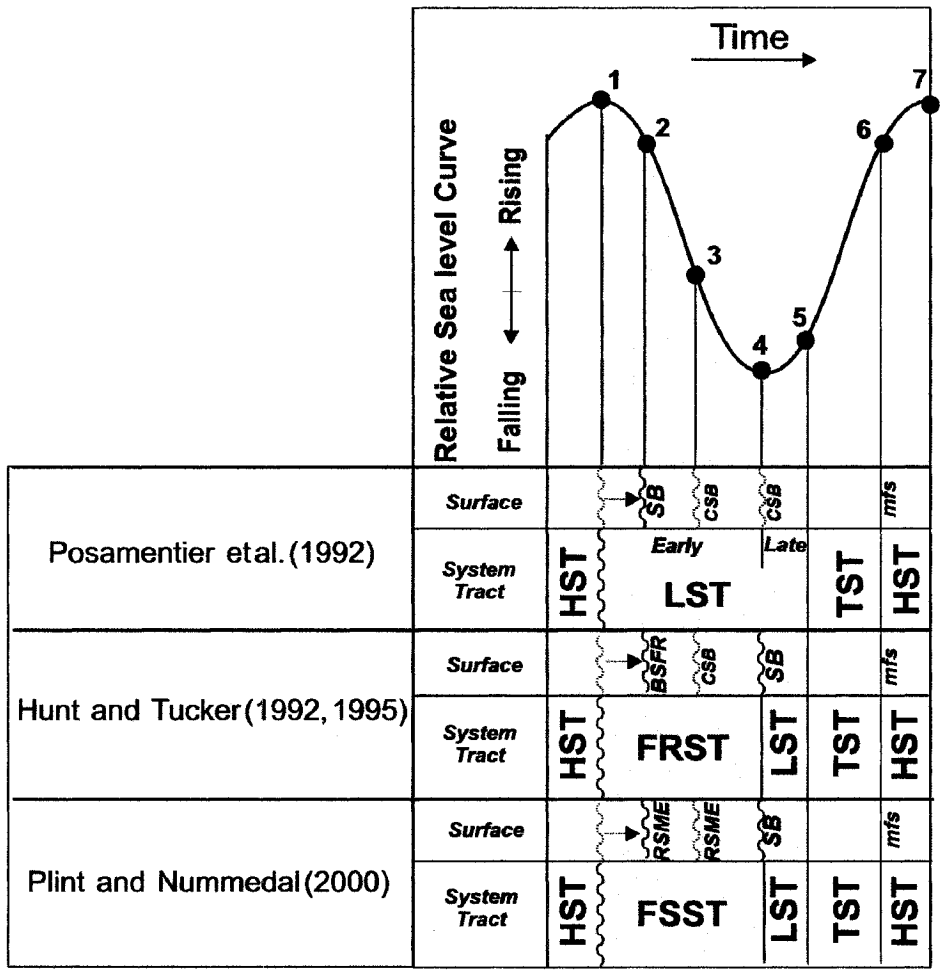

Figure 4.1. Simplified relative sea-level curve highlighting the depositional system during base-level fall and lowstand (Modified from Hunt and Tucker, 1995). The timing of the major stratal surfaces and systems tracts follows the sequence stratigraphic models of Posamentier et al. (1992), Hunt and Tucker (1992,1995) and Plint and Nummedal (2000). HST=Highstand system tract; LST=Lowstand system tract; TST=Transgressive system tract; FRST=Forced regressive system tract; FSST=Falling stage system tract; SB=Sequence boundary; CSB=Composite sequence boundary; mfs=Maximum flooding surface; BSFR=Basal surface forced regression; RSME=Regressive surface of marine erosion.

At lowstand (i.e. normal regression of Posamentier et al., 1992), the lowest point of sea level fall is reached and subsequently relative sea level begins to rise slowly. Sediments are transported down incised valleys that flood and form estuaries or are carried beyond the shelf margin into deep water and form extensive slope and basin-floor coarse clastic deposits. Strata deposited during lowstand (Fig. 4.1) are considered to form the late lowstand system tract (Posamentier et al.,1992), lowstand prograding wedge (Hunt and Tucker, 1992) or lowstand system tract (Hunt and Tucker, 1995; Plint and Nummedal, 2000). The base of the lowstand depositional system represents the sequence boundary according to Hunt and Tucker (1992, 1995) and Plint and Nummedal, (2000). This surface is developed as a single composite surface due to the slow rate of sedimentation at this time (Posamentier, et al., 1992; Kolla et al., 1995).

During transgression, as relative sea level rises, sediments are mostly trapped in estuaries and effectively prevented from reaching the shelf. Accordingly sediment supply to the slope and basin floor is decreased significantly. In addition, a second episode of shelf margin instability occurs forming widespread mass movement deposits. Peak relative sea level rise generates the maximum flooding surface that coincides with a condensed section across the shelf and areas more basinward, marking transition to the highstand system tract.

4.2. EVOLUTION OF TWO SLOPE CHANNEL COMPLEX SETS OF ISAAC FORMATION, CASTLE CREEK AREA

4.2.1. Significance of basal bounding surfaces

Identifying major bounding surfaces in deep-water channel systems in the Castle Creek study area is crucial to understanding the stratal architecture and depositional history in relation to changes of relative sea level. The bases of channel complex sets 1 and 3 are erosional, and each are interpreted to have formed during a major fall of relative sea level (Fig. 4.2). These bases also mark the initiation of two different channel systems (1 and 3, respectively).

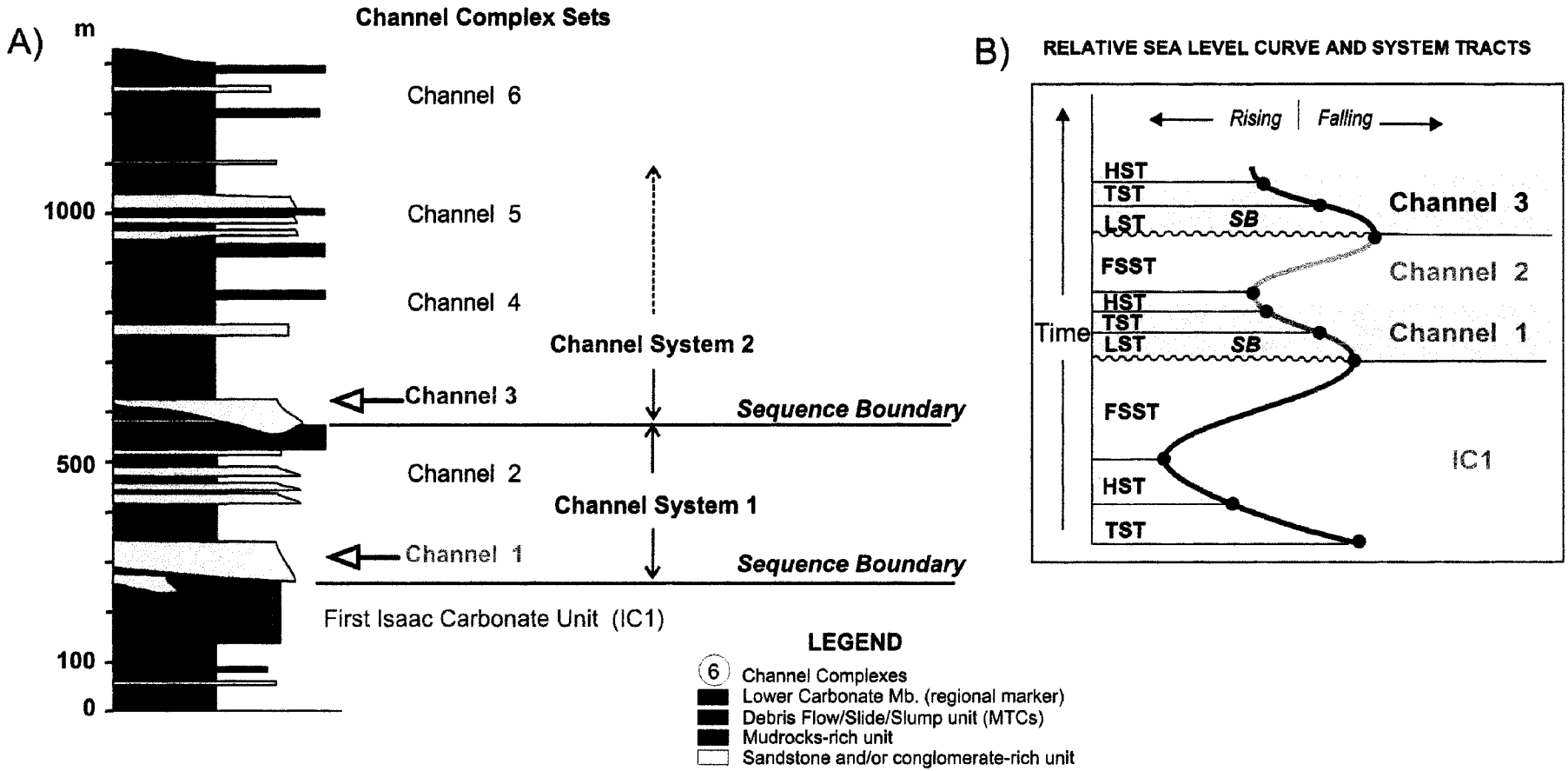

Figure 4.2. Schematic model for the stratigraphic sequences of slope channel complex sets of the Isaac Formation (Castle Creek south study area). Based on sequence-stratigraphic model of Plint and Nummedal (2000), see Fig. 4.1.

Channel 1 overlies a regionally-extensive, approximately 250 m thick, deep-water carbonate unit that consists of fine-grained limestone, limestone turbidites, and slump deposits. Stratigraphically-upward, carbonates became gradually more interbedded with siliciclastic turbidites. The carbonate unit is informally named the *first Isaac carbonate*, or IC1 of Ross et al. (1995), and represents a regionally extensive stratigraphic marker in the Isaac Formation related to prograding carbonate platform (Ross et al., 1995), which during the Neoproterozoic were typically ramps (Grotzinger, 1989; Grotzinger and James, 2000).

The IC1 is interpreted to have been deposited during a major (possibly third-order) sea level rise (Ross et al., 1995; Ross, 2003b) that may be related to waxing and waning of extensive Neoproterozoic ice sheets (Arnott, R.W.C., 2005, personal communication). During the long-term sea level rise (Fig. 4.2), the shelf was flooded and as a consequence a broad platform developed during the transgressive and highstand system tracts (TST and HST, respectively), which is recorded in the lower and middle part of IC1. During HST, carbonate production on the adjacent shallow-water shelf was so high that more sediment was produced than could be accumulated on the platform top, and the excess sediment was exported into the adjacent basin. Basinward transport promotes margin progradation, thereby expanding the width of the platform and the size of the carbonate factory (Coniglio and Dix, 1992). Higher sedimentation rates may have periodically overloaded the upper slope/outer shelf causing gravitational instability, which is a major contributing factor in generating turbidity currents (Middleton and Hampton, 1976). Thus, it is reasonable to expect a higher frequency of carbonate-transporting turbidity currents during times of high slope-to-basin sedimentation, which for platforms appears to correlate with highstands of relative sea level. Highstand shedding of turbidites, for example, has been well documented in the Quaternary sections surrounding the Bahamas (Droxler and Schlager, 1985; Reijmer et al., 1991; Anselmetti et al., 2000).

The carbonate factory was effectively shut-down during the end of the highstand with the onset of falling relative sea level (or FSST of Plint and Nummedal, 2000). Classical sequence stratigraphic models (Van Wagoner et al., 1988; Posamentier et al., 1988, Van Wagoner et al., 1990, etc) suggest that during falling sea level, fluvial systems incise the subaerially exposed continental shelf, causing sediment to bypass the shelf and be fed directly to the slope and basinal regions. Here, it is suggested that the carbonate platform in

IC1 was exposed only for a short time during FSST, and so rivers aggraded progressively on the extensive outer shelf. As a consequence, a voluminous reservoir of siliciclastic material was ponded near and at the shelf edge, with only a limited amount discharged to the slope. This resulted in deposition of the mixed siliciclastic-carbonate turbidites that crop out in the upper part of IC1. Similar morphological and depositional characteristics of the platform have been documented in the Quaternary Great Barrier Reef (Woolfe et al, 1998; Rankey et al., 1999; Page et al., 2003).

The broad carbonate platform could remain unaffected by small sea level fluctuations, but when sea level on the shelf surpassed a critical depth, large-quantities of feldspathic-rich clastic sediment staged in the middle and outer shelf were released to the slope and deposited in the base-of-slope (Channel 1). The lack of carbonate clasts in strata of Channel 1 supports the interpretation that subaerial exposure and erosion of the former carbonate platform was restricted.

The base of Channel 1 coincides with the top of IC1 and marks a new phase of siliciclastic deposition in the Isaac Formation (Fig. 4.2). This basal surface corresponds to a sequence boundary formed by submarine channel incision and is interpreted to represent a maximum (third-order) lowstand of sea level (LST). Deposition and backfilling of Channel 1 took place mostly during the late lowstand and early transgressive system tracts (LST and TST respectively). Superimposed on the long-term relative sea level oscillation were higher-frequency (fourth or fifth) oscillations. Samuels et al. (2003) suggested that short-term oscillations in sea level could cause changes in flow parameters that initiate episodes of erosion or aggradation in the channel system; for instance, a relative sea-level rise is commonly linked with a reduction in size, density and competence of flows, but the opposite occurs during relative sea-level fall. The top of Channel 1 is marked by the presence of thinly-bedded turbidites and claystone-rich strata that imply transgressive conditions (TST) during the time of major sea level rise.

With rising sea level, accommodation space gradually increased on the platform or ramp, resulting in deposition of a succession of shallow-water carbonates. At the same time but on the slope, laterally-accreting sinuous channels that crop out in the lower part of Channel 2 were formed (Arnott, 2005). During the initial stages of falling sea level (FSST), the platform became exposed and favoured deep-water deposition. A more than 90 m-thick

carbonate-clast-rich debrite and slump unit, which forms part of a regionally extensive, major mass transport complex, was deposited above Channel 2. These mass-transport and -flow deposits are interpreted to coincide with a time of slope instability when sediment flux and shelf bypass were at a maximum. Clasts eroded from shallow water carbonate (e.g. stromatolite, ooid, and grainstones) were incorporated in the debris flows and exported into deep water. Posamentier and Kolla (2003) pointed out that large-scale debris-flow or mass-transport deposits typify the base of depositional sequences in offshore Indonesia.

Channel 3 erosively overlies the thick debris-flow deposit and marks an important inflection point in the sea level curve, generating a high-order sequence boundary in the Isaac Formation (Fig. 4.2). Absence of a high resolution chronostratigraphic framework does not allow the precise determination of the hierarchical order of the bounding surface (sequence boundary), but it is presumed that it is a third- or fourth-order surface. This sequence boundary was formed by deep submarine incision on the slope during the late sea-level fall to lowstand (LST). In the LST, fluvial systems that had already incised the narrow carbonate platform tended to feed directly into the lower-slope and basin-floor areas. The lobe-like deposit above the base of Channel 3 was formed during this lowstand of sea level. The lobe-like strata suggest that the initial flows were relatively unconfined and sand-rich.

These strata are overlain by leveed channel deposits (Lower Channel 3 or Ch3.L), indicating that flows were progressively more mud-rich, and built up channel-margin levees by channel overspill and flow stripping. The channelforms in the lower Ch3.L were filled with the last vestiges of carbonate sediment shed at the lowest point of sea-level, when maximum subaerial exposure and incision of shelf occurred. Posamentier and Kolla (2003) emphasized that leveed channel deposits dominate during the late stage of a sea-level cycle. Channel elements form the middle and upper part of Channel 3 and were deposited during the early rise of sea level (TST). The occurrence of multiple periods of channel erosion and aggradation could be associated with short-term sea level oscillation (fourth order of Samuel, et al, 2003 or fifth order of Badalini et al., 2000), that generated multiple vertically-stacked, channel units. The top of Channel 3 is characterized by fine-grained turbidites and rare slump deposits, implying the deactivation of the channel system during highstand.

4.2.2. Evolution of Channel Complex Sets 1 and 3

Careful mapping and section measuring has been used to identify and map a number of erosion surfaces and channel elements in both Channels 1 and 3. These stratal surfaces have helped elucidate the geometry and stacking patterns of individual channels, and, in turn, have aided the interpretation of the overall channel evolution from channel inception to fill and abandonment.

The genetic evolution of deep-water channels is considered to be controlled by the interplay of allocyclic (external) forcing mechanisms, such as changes in relative sea level (Posamentier and Vail, 1988; Posamentier and Kolla, 2003), and autocyclic (internal) mechanisms, like equilibrium profile, avulsion, and thalweg migration (Pirmez et al., 2000). Additionally, changes in flow parameters, including flow concentration and flow thickness, are additional factors affecting the channel evolution (McHargue, 1991; Kneller, 2003; Kolla et al., 2003; McCaffrey and Kneller, 2004). McCaffrey and Kneller (2004) suggested that autocyclic factors may dominate during periods of high rates of sediment input, whereas allocyclic controls are more influential when input rates are lower.

The reconstructed evolution of Channel 1 and 3 show repetitive developmental trends that can be explained by different combinations of external and internal mechanisms or factors. Therefore, two particular evolution models are proposed below.

4.2.2.1. Evolution of Channel 1

The impact of external and internal factors on channel-stacking architecture and lithofacies distribution during the formation of channel units in Channel 1 is summarized in Fig. 4.3, and discussed next.

Incipient conditions

Before the inception of Channel 1, a regionally-extensive deep-water carbonate unit, informally termed the first Isaac carbonate, was deposited (Fig. 4.3A). This carbonate unit (see section 3.2.1 in chapter 3) contains a variety of coarse- and fine-grained carbonate facies, including slumps and to a lesser extent siliciclastic strata, and is inferred to represent mostly highstand deposition (see section 4.2.1, this chapter).

With a major fall of relative sea level, Channel 1 was formed above a sequence boundary (see section 4.2.1, this chapter). The delivery of a large volume of terrigenous sediments to the slope and basin predominated at this time. Channel 1 reveals a multistage depositional history that includes episodes of (1) incision and bypass (2) filling as well as (3) abandonment. These phases are mostly recorded in five channel units that comprise Channel 1.

Stage 1

Channel 1 was initiated by erosion at the base of Ch1.L (Fig. 4.3B). Formerly, the channel was poorly confined and large, efficient, highly erosive flows were diverted through topographic lows along the top of the carbonate unit (Fig. 4.3B). Later flows, confined to individual channel units eroded the top of underlying channel fills and locally the carbonate unit.

As a result of intense channel bypass and incision, channel bases were lowered causing flows to becoming progressively more confined. Except for Ch1.L-1 (<300 m), channel units in Channel 1 are generally wide and basal erosion surfaces can be traced laterally for more than 600 m. Sediments deposited during bypass have a low degree of preservation, because of erosion by subsequent flows. In particular, mudstone-clast breccia and thin-bedded turbidites that overlie some of these surfaces were the product of incomplete bypass flows that left behind parts of their load within the channel (e.g. Beaubouef et al., 1999). These bypass facies can be laterally discontinuous, and in some cases can represent a significant percentage of the channel-axis strata.

Stage 2

Channels began to fill when flow efficiency, momentum and velocity decrease due to changes in sediment volume and caliber. Flows also become more focused toward the channel axis (Fig. 4.3B'). A consistent upward change in the infilling nature of most channel units has been observed in Channel 1. Initially, channels began to fill with thick-bedded, normally graded and massive sandstone as a result of deposition from coarse-grained, high-concentration, sandy, turbulent flows.

These infill strata onlap the basal erosion surfaces. Later (stratigraphically upward), thick, sandstone-dominated strata became progressively more interbedded with cross-bedded

sandstone and thin-bedded, fine-grained turbidites indicating waning flow conditions or a decrease in sediment caliber and/or supply to the system. This occurs as a common depositional response to a general backstep of the channel system (Gardner et al., 2003, Eschard et al., 2003).

Stage 3

In the final stage, channels continue to fill but, sediment supply diminished considerably, especially if relative sea level rises (Kneller, 2003). Flows weaken gradually losing competence and momentum, and ultimately become unable to carry sediment through the channel. Semi- to non-amalgamated sandstone interbedded with thin-bedded turbidites and minor cross-bedded sandstone are typically deposited during this stage (Fig. 4.3B''). Commonly, channels became deactivated and fine-grained sediment uniformly draped the area.

Transition Stage 1 to 3

The transition from Stage 3 to 1 in the channel fills is marked by partial or complete erosion of older strata (e.g. fine-grained channel abandonment succession at the top of the underlying unit. Deposition in Channel 1 was interrupted by periodic reincision events. Each major reincision event coincided with the formation of a new channel unit (Fig. 4.3C-F) that possibly was related to a high-order sea-level fall (fourth order of Samuels et al., 2003), which in turn caused a reduction in the slope profile (loss of slope accommodation) by erosion and channelization (Imran et al., 1999; Pirmez et al., 2000). However, some of the major reincision or reactivation surfaces could also have been formed during stillstand or rising sea level, but in these cases they are related to important changes in flow conditions (i.e. sediment caliber and supply, and flow volume or density). Examples of deepwater channels and lobeforms formed during rising or high stand of sea level have been recognized by Kolla et al. (2003), Keller (2003) and McCaffrey and Kneller (2004).

The final depositional phase in Channel 1 occurred as the entire system was blanketed with thin-bedded, fine-grained turbidites, which probably was associated with a major rise in sea-level. The uppermost claystone layer corresponds to hemipelagic deposition related to local deactivation of the system, possibly upflow avulsion, or deactivation related to highstand and sediment starvation in deep parts of the basin.

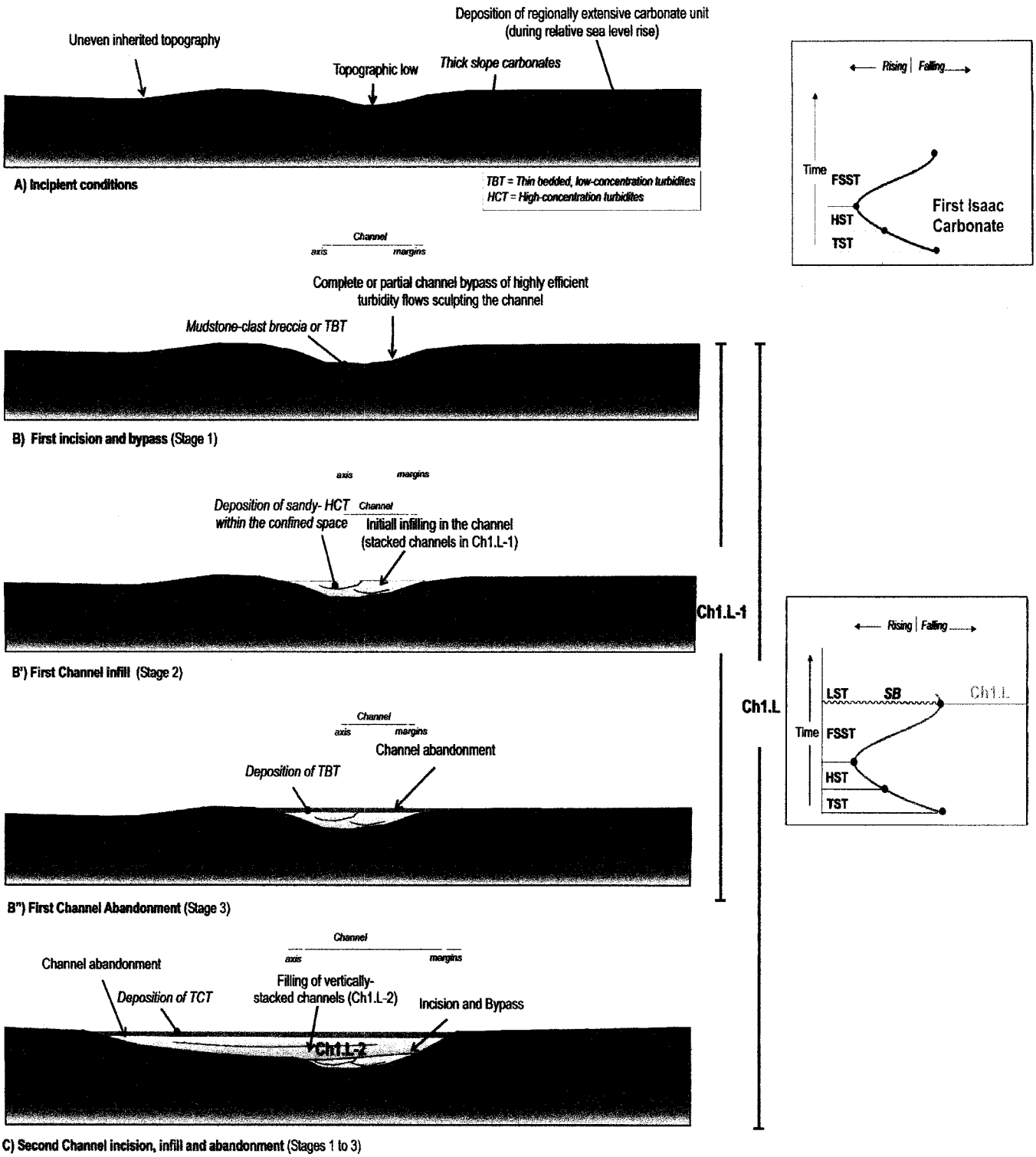

Continued...

Figure 4.3. Schematic diagram illustrating the five main evolutionary episodes of Channel 1. For explanation refer to the text. Schematic model, o the right, for the generation of Channel 1 through a major relative sea-level cycle.

...Continuation Fig. 4.4

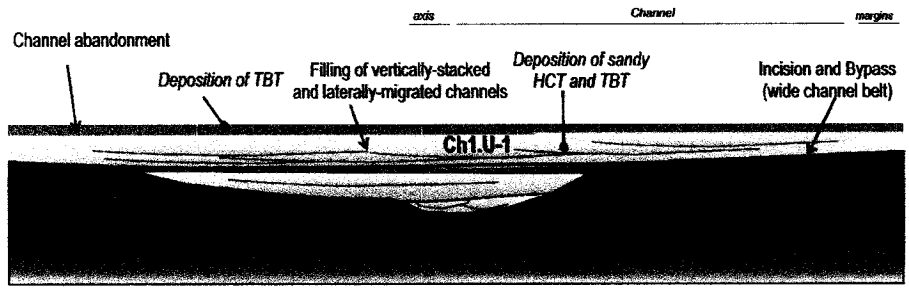

D) Third Channel incision, infill and abandonment (Stages 1-3)

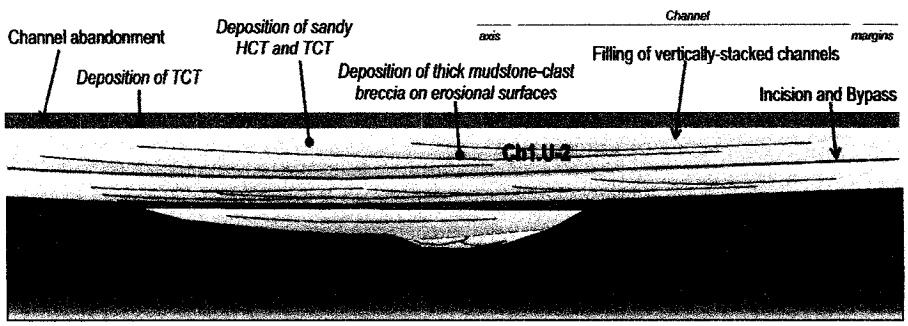

E) Fourth Channel incision, infill and abandonment (Stage 1-3)

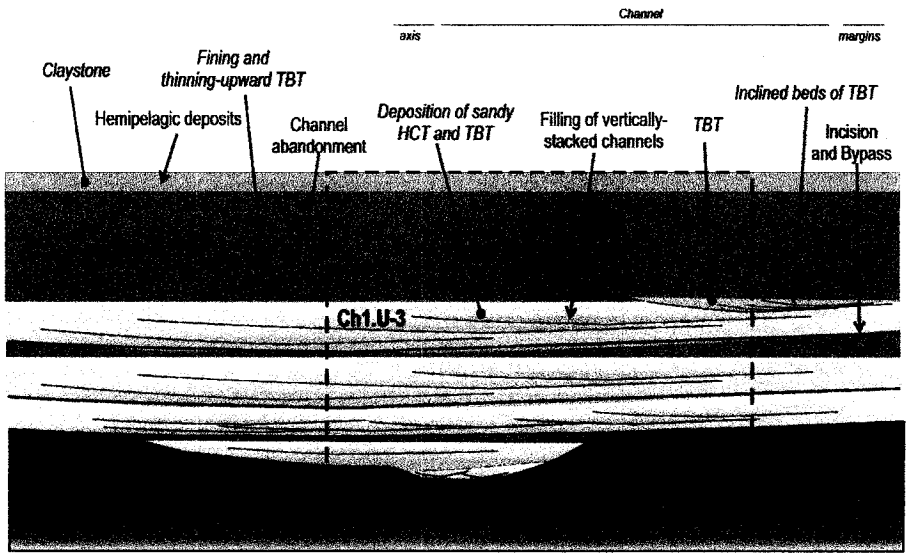

F) Fifth Channel incision, infill and complete abandonment (Stage 1-3)

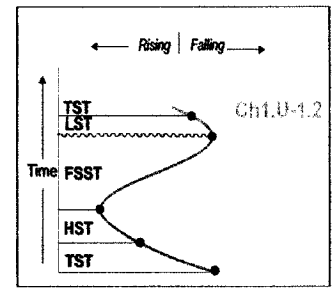

Ch1.U

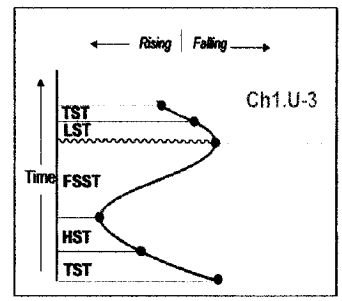

4.2.2.2. Evolution of Channel 3

The evolution of Channel 3 can be subdivided into an early stage of slope instability followed by three major episodes of erosion and then deposition (lower, middle and upper channel complexes).

Incipient conditions

Before the inception of Channel 3 an up to 90 m (295 ft) thick, carbonate clast, mud-rich, matrix-supported, areally-extensive debris-flow deposit that forms part of a major mass-transport complex or MTC, blanketed the study area. This debris-flow deposit probably coincided with a major fall of relative sea level (see section 4.2.1, this chapter). The upper surface of the debris-flow deposit was most likely irregular, which as a consequence helped focus later relatively unconfined, turbidity currents downslope. At Castle Creek, these early flows probably emplaced thick, coarse-grained, potentially lobe-shaped deposits (Fig. 4.4A). These strata, in turn, initiated the confinement of subsequent flows and promoted the localization and development of Ch3.L.

Lower Channel Complex: Evolution of a channel-levee complex

The first depositional phase of Channel 3 was marked by recurring stages of levee growth followed by channel fill, forming Ch3.L (Figure 4.4A-D). Each stage is defined by a particular channel geometry, channel and levee stacking pattern and the nature of adjacent levee deposits.

Stage 1

The first stage was characterized by levee aggradation and channel by-pass (Fig. 4.4B). In this stage, the channel was weakly confined, and as a consequence of superelevation of turbidity currents as they rounded the bend, facilitated the overspill of high-density flows along the outer channel-bend, resulting in the deposition of the sandier, lowermost part of proximal levee packages on the northwest channel margin. Lateral waning and thinning of these flows due to decrease in sediment competence and concentration lead to the deposition of fine-grained turbidites on the distal levee.

During levee aggradation, highly efficient, largely bypassing flows were sculpting and widening the channel (Mutti, 1992; Clark and Pickering, 1996; Mutti et al., 2003) due to disequilibrium between flow and slope conditions (Samuels et al., 2003; Kneller, 2003), creating laterally extensive erosion surfaces. Bypass flows transported much of their sand and coarser sediment farther downslope, leaving behind a residuum of thinly-bedded turbidites, mudstone-clast breccia and inclined package of sandstone and breccias, typically in channel axes.

Stage 2

The second stage was distinguished by the continuation of levee building and the initiation of channel filling (Fig. 4.4C). Rapid levee aggradation during the early part of stage 2 was caused by overbank deposition from bypass flows that resulted in blanket deposition of finer-grained, more mud-rich levee facies on both sides of the channel. Deposition on the northwest distal levee was interrupted by overbank-splay deposits. Levee growth at this time was sufficient to confine almost all flows to the more axial parts of the channel.

The beginning of channel fill was caused by an increase in sediment caliber and/or sediment flux of the intrachannel flows. Channels were initially filled with thick-bedded, normally graded and massive conglomerate and granule/pebble dispersed sandstone. In contrast, later channels were increasingly filled with thick-bedded, normally graded and massive sandstone. This vertical change in sandstone content is indicative of waning flow conditions, which could be associated also with a decrease in sediment caliber and/or supply.

Stage 3

In comparison to stages 1 and 2, channel aggradation increased significantly during stage 3 (Fig. 4.4D) due to a reduction in flow competence, capacity and velocity. Channel fills consisting mostly of partially amalgamated sandstone turbidites were deposited in the channel axes, whereas less amalgamated, more interbedded thick-bedded coarse sandstone and thin-bedded turbidites were deposited toward the channel margins. This indicates that in the axial part of the channel, flows were still high-energy, sand-rich, and erosive. Along the channel margins, by contrast, flows are muddier, less dense and hence deposited finer, more interstratified deposits. Stage 3 was terminated by channel abandonment and deposition of thin, fine sandstone turbidites.

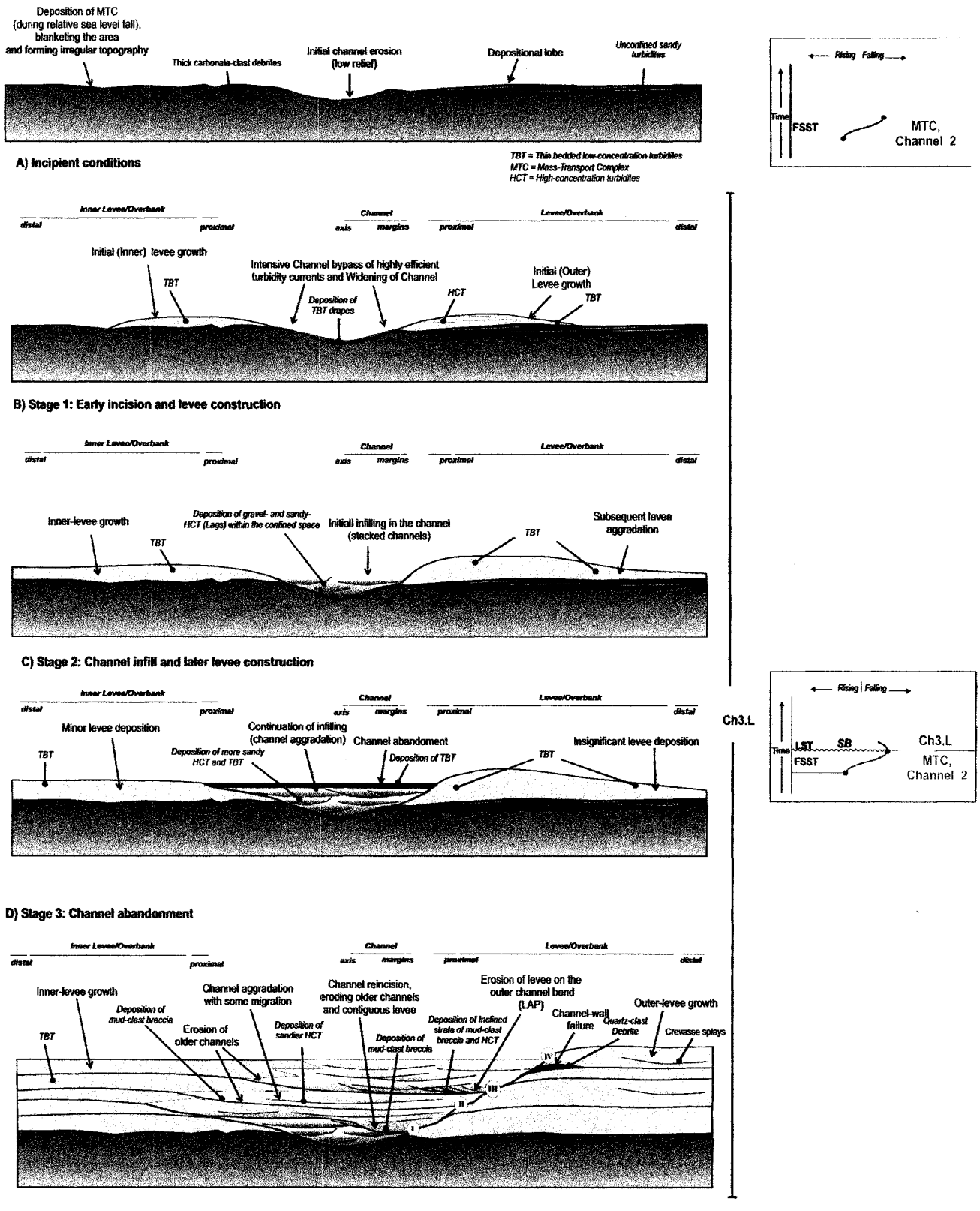

Figure 4.4. Schematic diagram illustrating the fourth main evolutionary stages of Channel 3. For details see text. Schematic model, o the right, for the generation of Channel 3 through a major relative sea-level cycle.

...Continuation Fig. 4.4

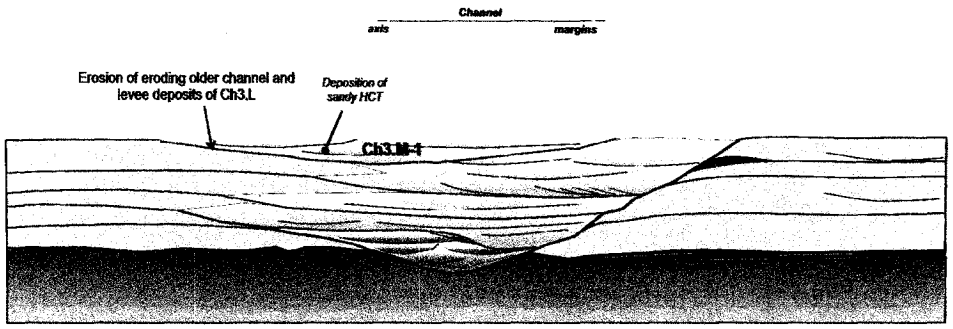

F.1) Middle Channel Complex in Channel 3

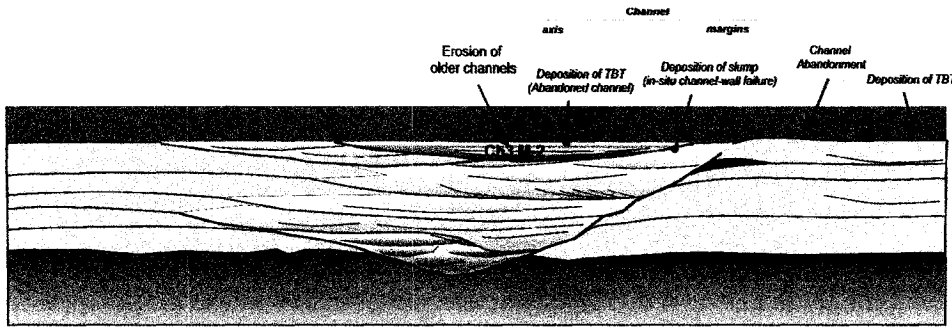

F.2) Middle Channel Complex in Channel 3

Ch3.M

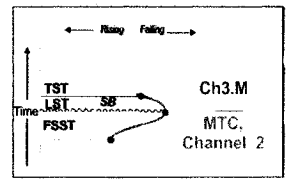

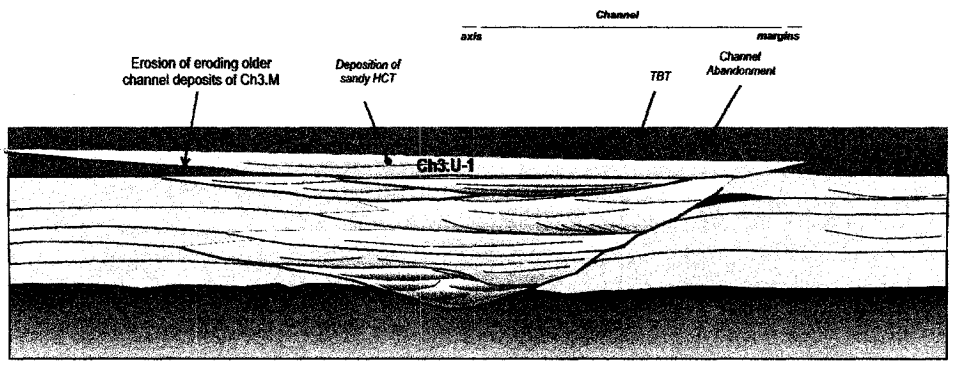

G.1) Upper Channel Complex in Channel 3

Ch3.U

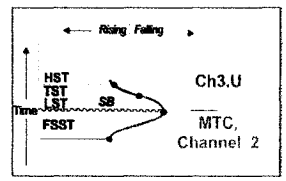

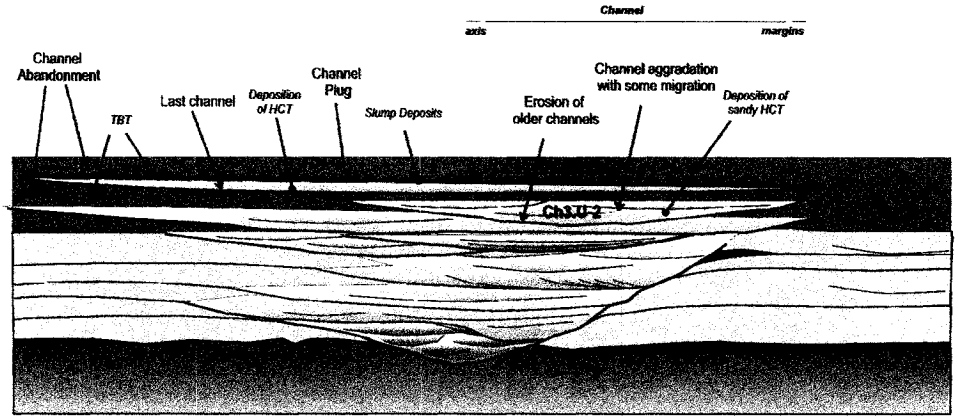

G.2) Upper Channel Complex in Channel 3

Transition Stage 1 to 3

The transition from Stage 3 to Stage 1 of the succeeding channel-levee unit is abrupt and marked by partial or complete erosion of the fine-grained channel abandonment succession at the top of the underlying unit. The major erosion surfaces or channel re-incisions may be associated with fourth-order sea-level fall (Samuels et al., 2003).

Multiple re-incision events at the base of channel units Ch3.L-2 and Ch3.L-3 represent abrupt or punctuated migration of the channel system (in the sense of Deptuck et al., 2003; Kolla et al., 2001; see chapter 3). Erosion at the base of channel unit Ch3.L-4, in contrast, was probably linked to a more gradual migration of the system (Deptuck et al., 2003). Recurring episodes of erosion occurred during the overall northwest migration of the entire system. Erosion preferentially occurred along the outer channel bend, and formed the composite terraced erosion surface observed at the base of Channel 3.

Middle Channel Complex (Stages 1-3)

The middle channel complex Ch3.M (for details see section 3.3.2 in chapter 3) records a complex (multistage) history of channel inception-fill-abandonment during the evolution in Channel 3.

The bases of Ch3.M-1 and Ch3.M-2 are characterized by major erosion surfaces that are laterally continuous across the study area. These erosional features represent important changes in channel development, and are interpreted to coincide with episodes of incision when bypassing turbidity flows eroded deeply into older intra- and extra-channel deposits (Fig. 4.4.G1). The deformed deposits observed at the base of Ch3.M-2 (e.g. Fig. 4.4.G2) are associated with local slump failures that took place along the (northwest) channel margin during sediment bypass.

Subsequently, as bypassing flows became less efficient and smaller, filling of channel relief occurred. The filling of Ch3.M-1 was dominated by sand-rich turbidity flows (Fig. 4.4.G2). In contrast, the heterolithic channel-fill in Ch3.M-2 (Fig. 4.4.G1) represents a passive channel fill and suggests a major change in depositional conditions due to a decrease in sediment discharge or flow velocity, possibly related to momentary abandonment of the entire channel system. Alternatively, it may be related to a major shifting of the channel position caused by an upcurrent avulsion.

Upper Channel Complex (Stages 1-3)

The Upper Channel Complex (Ch3.U) marks a late-stage rejuvenation of the channel system due to an increase in sediment flux, and corresponds to the final phase of channel activity (erosion, infill and then deactivation). During the early stages of Ch3.U (for details see section 3.3.3 in chapter 3), erosion was extensive, and hence parts of underlying channel complexes Ch3.L and Ch3.M were locally removed. The erosive base of Ch3.U-1 and Ch3.U2 indicate separate episodes of erosion by efficient, high-energy turbidity flows that transported sediment farther basinward (Fig. 4.4.G2).

Changes in flow parameters (decrease in flow size and flow efficiency, or increase in sand/mud ratio) initiated sedimentation within the channels in Ch3.U. Depositional events in Ch3.U are manifest as multistory channel fills deposited mostly from sandy, high-concentration turbulent suspensions. Like channels in Ch3.L and Channel 1, the stacking of Ch3.U-1 and Ch3.U2 show a relatively moderate degree of lateral offset toward the northwest.

Channel filling in Ch3.U was terminated by deposition of low-concentration turbidity currents (Fig. 4.4G2). However, this terminal deposition was interrupted at least once by incision and limited fill of a solitary channel. This channel is overlain by slump deposits, which most likely plugged the remaining channel space.

4.3. CHAPTER SUMMARY

Channel 1 and 3 overlie major sequence boundaries that are most likely related to two (third-order) lowstands of sea level. The evolution of Channel 1 is inferred to characterize a base-of-slope channel complex set, whereas evolution of Channel 3 is inferred to define a lower-slope channel complex set. Multiple phases of channel development are recognized in both channel complex sets, and are closely linked with a recurring history of channel incision, aggradation and lateral migration.

CHAPTER 5. CONCLUSIONS

1. Four main lithofacies were described in detail from channel deposits of Channel 1 and 3 of the Isaac Formation at Castle Creek. Lithofacies were further subdivided into subfacies according to grain size and sedimentary structures. Normally graded and massive sandstone and conglomerate is the most common facies (Facies F1). Subordinate mudstone-clast breccia (Facies F2) show evidence of depositional and post-depositional origin. Cross-stratified sandstone (subfacies F3.1) is observed exclusively in Channel 1. Facies F4 includes heterolithic strata consisting of fine-grained, thinly-bedded, upper division turbidites.

2. Five facies associations have been identified in Channel 1 and 3. FA1 and FA2 correspond to different kinds of by-pass deposits that overlie basal erosion surfaces. FA3 comprises three styles of channel fill: amalgamated, semi-amalgamated and non-amalgamated. FA4 consists of local, contorted and chaotic units that commonly are observed in Channel 3. FA5 includes thin-bedded, fine-grained turbidites associated with channel abandonment.

3. Petrographic and XRD analyses indicate that there is little mineralogical variation between facies. High feldspar content in strata (conglomerate and sandstone) of Channel 1 and 3 suggest that the sediment source area was dominantly plutonic, from the cratonic Canadian Shield. Additionally, some conglomerate with boulder carbonate clasts in the lower part of Channel 3 indicate that these clasts were supplied from an adjacent carbonate platform.

4. The most common architectural elements identified in Channel 1 and 3 are: channel forms and sheets. The good exposure and lateral continuity of these elements allow to establish their hierarchical arrangements and areal distribution. Channel 1 and 3 are two channel-complex sets, estimated to be more than 1.1 km wide, consisting of two and three stacked channel complexes respectively. Channel complexes are further subdivided into channel units, which consist of two or more channel fills. Channel units are individually separated by major complex erosion surfaces that coincide with reincision or rejuvenation events in the channel system. Channel units and fills show vertical and lateral stacking patterns that provide insight into understanding the temporal differences in vertical aggradation and lateral migration of each channel set. Important variations in lithofacies, geometry and internal bed

amalgamation according to position (axial or marginal) within each channel fill was also identified.

5. In general, both channel complex sets have similar stratal architecture, which is interpreted to be the product of interaction between autocyclical processes (e.g. equilibrium channel profile, avulsion) that drive short-term morphological evolution of the channel systems, and allocyclical processes (e.g. changes in relative sea level) that most probably have longer-term effects. Individual channel complexes commonly exhibit upward changes from high net-to-gross, amalgamated sandstone-conglomerate to lower net-to-gross interstratified sandstone-mudstone. In addition, erosion, bypass and sediment reworking in the lower part of the channel complex contrast with higher rates of channel deposition and aggradation in the middle and upper parts of the complex.

6. Both Channel 1 and 3 represent major lowstand deposits that overlie regionally extensive, sedimentary markers that record the initiation of two main channel systems in the Isaac Formation. Channel 1 overlies a highstand deep-water carbonate interval and Channel 3 overlies a large-scale mass transport complex (intraslope slump and debrite) associated with a major episode of upper slope/outer shelf destabilization and mass wasting.

7. A well-exposed channel-levee complex in the lower part of Channel 3 shows a distinctive basal surface with an erosive, terraced geometry along the northwest margin (cut-bank or outer-bend levee) and a serrated geometry along the opposite margin (inner-bend levee). This surface formed as a result of striking differences in levee sedimentation on opposite sides of a sinuous channel bend, combined with large-scale patterns of channel aggradation and migration.

REFERENCES

Abreu, V., M. Sullivan, C. Pirmez, and D. Mohrig, 2003, Lateral accretion packages (LAPs): an important reservoir element in deep water sinuous channels: *Mar. Petrol. Geol.*, **20**, p. 631-648.

Aird, P., 2001, *Introduction to deepwater sedimentary environments. Open-File Report*, Kingdom Drilling, 16 p.

Aitken, J.D. and D.M.R. McDonough, 1990, *Late Proterozoic glaciation, rifting and eustacy, as illustrated by the Windermere Supergroup.* Geological Association of Canada, Nuna Research Conference, Invermere and Valemount, British Columbia, 10.27 p.

Aitken, J.D. and M.E. McMechan, 1991, Middle Proterozoic Assemblages, *in* Gabrielse, H. and Yorath, C. J., eds., *Geology of the Cordilleran Orogen in Canada, Chapter 2.* Geol. Survey Can., Geology of Canada, No 4 (also GSA, The Geology of North America, vol. **G-2**), p. 97-124.

Allen, J.R.L., 1977, The possible mechanics of convolute lamination in graded sand beds. *J. Geol. Soc, London.* **134**, p. 19-31.

Allen, J.R.L., 1982, *Sedimentary structures: their character and physical basis.* v.**2**, Elsevier, Amsterdam, 663 p.

Allen, J.R.L., 1985, *Principles of Physical Sedimentology.* George Allen and Unwin. 272 p.

Allen, J.R.L., 1991, The Bouma division A and the possible duration of turbidity currents. *J. Sed. Petrol.*, **61 (2)**, p. 291-295.

Anselmetti, F. S.,; G. P. Eberli, and Z.-D. Ding, 2000, From the Great Bahama Bank into the Straits of Florida: A margin architecture controlled by sea-level fluctuations and ocean currents, *GSA Bulletin*, **112 (6)**, p. 829–844.

Arnott, R.W.C., 2005, Architecture of Lateral Accretion Deposits in Deep-Marine Sinuous Channel Fills, *abs.*, AAPG Annual Convention, Program with Abstracts, Calgary, Canada, p. A6.

Arnott, R. W.C. and B.M. Hand, 1989, Bedforms, primary structures and grain fabric in the presence of suspended sediment rain. *J. Sed. Petrol.*, **59 (6)**, p. 1062-1069

Arnott, R.W.C. and F.J. Hein, 1986, Submarine canyon fills of the Hector Formation, Lake Louise, Alberta: Late Precambrian syn-rift deposits of the proto-Pacific miogeocline. *Bull. Can. Petrol. Geology*, **34**, 395-407.

Ashley G. M., 1999, Classification of large-scale subaqueous bedforms: A new look at and old Problem. *J. Sed. Petr.*, **60 (1)**, 160-172.

Baas, J.H. and J.L. Best, 2002, Turbulence modulation in clay-rich sediment-laden flows and some implications for sediment deposition. *J. Sed. Res.*, **72 (3)**, 336-340.

Badalini, G., B. Kneller and D. Winker, 2000, Architecture and Processes in the Late Pleistocene Brazos-Trinity Turbidite System, Gulf of Mexico Continental Slope, *in* P. Weimer, R. M. Slatt, J. Coleman, N.C. Rosen, H. Nelson, A. H. Bouma, M. J. Styzen, and D. T. Lawrence, eds., *Deep-water reservoirs of the world*: GCSSEPM Foundation 20th Annual Research Conference, p. 16-33.

Bagnold, R.A., 1954, Experiments on a gravity–free dispersion of large solid spheres in a Newtonian fluid under shear. *Proc. Roy. Soc. London*, Ser. A., **225 (1160)**, 49-63.

Bagnold, R.A., 1956, The flow of cohesionless grains in fluids. *Philosophical Transaction of the Royal Society of London, Series A: Mathematical and Physical Sciences*, **249 (964)**, 235-297.

Bagnold, R.A., 1962, Auto-suspension of transported sediment: turbidity currents. *Proc. Roy. Soc. London*, Ser. **A, 265 (1322)**, 315-319.

Baldock, T.E., M.R. Tomkins, P. Nielsen and M.G. Hughes, 2004, Settling velocity of sediments at high concentrations. *Coastal Eng.*, **51**, 91-100.

Barnes, N.E., and Normark, W.R., 1985, Diagnostic parameters for comparing modern submarine fans and ancient turbidite systems. *in* Bouma, A.H., W.R. Normark and N.E. Barnes, eds., *Submarine Fans and Related Turbidite Systems:* New York, Springer-Verlag, p. 13-14.

Beaubouef, R.T., and S. J. Friedman, 2000, High resolution seismic/sequence stratigraphic framework for the evolution of Pleistocene intra slope basins, western Gulf of Mexico: depositional models and reservoir analogs, *in* P. Weimer, R. M. Slatt, J. Coleman, N.C. Rosen, H. Nelson, A. H. Bouma, M. J. Styzen, and D. T. Lawrence, eds., *Deep-water reservoirs of the world*: GCSSEPM Foundation 20th Annual Research Conference, p. 40-60.

Beaubouef, R.T., C. Rossen, F.B. Zelt, M.D. Sullivan, D.C. Mohrig, and D.C. Jennette, 1999, *Deep-water Sandstones, Brushy Canyon Formation, West Texas.* Field Guide for AAPG Hedberg Field Research Conference. AAPG Continuing Education Course Note Series # **40**, 2nd ed., 48 p.

Bell, R.T., 1968, Proterozoic stratigraphy of northeastern British Columbia. *Geol. Surv. Can.*, Paper **67-68**, 75 p.

Best, J., 1996, The fluid dynamics of small-scale alluvial bedforms. In Carling, P.A. and M.R. Dawson, eds., *Advances in Fluvial Dynamics and Stratigraphy*. Wiley, Chischester, p. 67-125.

Boardman, M.R., and A.C. Neumann, 1984, Sources of periplatform carbonates: Northwest Providence Channel, Bahamas. *J. Sediment. Petrol.*, **54**, p. 1110-1112.

Boggs, S. Jr., 1992, *Petrology of sedimentary rocks*. Macmillan Pub. Co., New York, 707 p.

Bond, G.C. and M.A. Kominz, 1984, Construction of tectonic subsidence curves for the early Paleozoic miogeocline, southern Canadian Rocky Mountains- implications for subsidence mechanisms, age of breakup, and crustal thinning. *GSA Bull.*, **95**, p. 155-173.

Borg, S. G. and D.J. DePaolo, 1994, Laurentia, Australia, and Antarctica as a Late Proterozoic supercontinent: Constraints from isotopic mapping. *Geology*, **22**, p. 307-310.

Bouma, A. H., 1962, *Sedimentology of some Flysch Deposits. A graphic approach to facies interpretation.* Elsevier, Amsterdam, 168 p.

Bouma, A.H. and J.M. Coleman, 1985, Peira Cava turbidite systems, France. *In* Bouma, A.H., Normark, W.R., and Barnes, N.E., eds., *Submarine Fans and related turbidite systems*. Springer-Verlag, New York, p. 217-222.

Brami, T.R., C. Pirmez, C.A. Heeralal, and K.L. Holman, 2000, Late Pleistocene deep-water stratigraphy and depositional processes, offshore Trinidad and Tobago, *in* P. Weimer, R. M. Slatt, J. Coleman, N.C. Rosen, H. Nelson, A. H. Bouma, M. J. Styzen, and D. T. Lawrence, eds., *Deep-water reservoirs of the world*: GCSSEPM Foundation 20th Annual Research Conference, p. 104-115.

Branney, M.J. and P. Kokelaar, 1992, A reappraisal of ignimbrite emplacement: progressive aggradation and changes from particulate to non-particulate flow during emplacement of high-grade ignimbrite. *Bull. Volcanol.*, **54**, p. 504-520.

Branney, M.J. and P. Kokelaar, 2002, *Pyroclastic density currents and the sedimentation of ignimbrites.* Geol. Soc. London, Mem., **27**, 143 p.

Brown, R.L., C.R. Tippet and L.S. Lane, 1978, Stratigraphy, facies changes and correlations in the northern Selkirk Mountains, southern Canadian Cordillera. *Can. J. Earth-Sci.*, **15**, p. 1129-1140.

Buhrke, V.E., R. Jenkins and D.K. Smith, 1998, A practical guide for the preparation of specimens for X-Ray fluorescence and X-Ray diffraction analysis. *Wiley - VCH*, New York, 333 p.

Burret, C. and R. Berry, 2000, Proterozoic Australia- Western United States (AUSWUS) fit between Laurentia and Australia. *Geology*, **28 (2)**, p. 103-106.

Burwash, R.A.; C.R. McGregor and J. Wilson, 1994, Chaper 5: Precambrian Basement beneath the Western Canada Sedimentary Basin, *in* Mossop, P.G. and Shetse, I., comps., *Geological Atlas of the Western Canada Sedimentary Basin.* Calgary, Can. Soc. Petrol. Geol. and Alberta Res. Council, 510 p.

Campbell, R. B., E. W. Mountjov, and F.G. Young , 1973, *Geology of McBride Map-Area, British Columbia (93-H). Geol. Surv. Can.*, Paper **72 (35)**, 104 p.

Carey, J.A. and P.S. Simony, 1985, Stratigraphy, sedimentology, and structure of Late Proterozoic Miette Group., Cushing Creek area, B.C. *Bull. Can. Petrol. Geology*, **33 (2)**, p. 184-203.

Carling, P.A., 1999, Subaqueous gravel dunes. *J. Sed. Res.*, **69 (3)**, p. 534-545.

Charlesworth, H.A.K., J.L. Weiner, A.J. Akerhurst, H.V. Bielenstein, C.R. Evans, R.E. Griffiths, D.B. Remington, M.R. Stauffer, and J. Steiner, 1967, Precambrian Geology of the Jasper Region, Alberta. *Res. Council Bull.*, **23**, 74 p.

Cheel, R.J. and G.V. Middleton, 1986, Horizontal lamination formed under upper flow regime plane bed conditions. *J. Geol.*, **94**, p. 489-504.

Chough, S.K. and Chun, S.S., 1988, Intrastratal rip-down clasts, Late Cretaceous Uhangri Formation, southwest Korea. *J. Sed. Petrol.*, **58**, p. 530-533.

Clark, J.D. and Pickering, K.T., 1996, Architectural elements and growth pattern of Submarine Channel: Application to Hydrocarbon Exploration. *AAPG Bull.* **80 (2)**, p. 194-221.

Clark, J.D., N.H. Kenyon and K.T. Pickering, 1992, Quantitative analysis of the geometry of submarine channels: Implications for the classification of submarine fans. *Geology*, **20 (5)**, p. 633-636.

Coleman, J.J. Jr., 2000, Carboniferous submarine basin development of the Ouachita Mountains of Arkansas and Oklahoma, *in* A.H. Bouma and C.G. Stone, eds., *Fine-grained turbidite systems*, AAPG Mem. **72**, SEPM Spec. Pub. N° **68**, p.21-32.

Collinson J.D. and D.B. Thompson, 1982, *Sedimentary Structures.* George Allen & Unwin. London, 194 p.

Colpron, M. J. M. Logan, and J. K. Mortensen, 2002, U–Pb zircon age constraint for late Neoproterozoic rifting and initiation of the lower Paleozoic passive margin of western Laurentia. *Can. J. Earth Sci.*, **39**, p. 133-143

Coniglio, M. and G. R. Dix, 1992, Carbonates slopes, R.G. Walker and N.P. James, eds., *Facies models-response to sea level change*. Geol. Assoc. Can., St. John's, p. 349-373.

Cordani, U.G., M.S. D'Agrella-Filho, B.B. Brito-Neves and R.I.F. Trindade, 2003, Tearing up Rodinia: the Neoproterozoic palaeogeography of South American cratonic fragments: *Terra Nova*, **15**, p. 350–359.

Crevello, P.D., and W. Schlager, 1980, Carbonate debris sheets and turbidites, Exuma Sound, Bahamas. *J. Sediment. Petrol.*, **50**, p. 1121-1148.

Dagustpa, P., 2003, Sediment gravity flow -the conceptual problems. *Earth Sci. Rev.*, **62**, p. 265-281.

Davies, R., 1968, The experimental study of the differential settling of particles in dispersion at high concentrations. *Powder Technol.*, **2**, p. 43-51.

Davies, R. and B.H. Kaye, 1971, Experimental investigation into the settling behaviour of dispersions. *Powder Technol.*, **5**, p. 61-68.

Daziel, I.W.D., 1991, Pacific margins of Laurentia and East Antarctica-Australia as a Conjugate pair Evidence and implications for an Eocambrian supercontinent. *Geology*, **19**, p. 598-601

Daziel, I.W.D., 1997, Neoproterozoic- Paleozoic geography and tectonics: Review, hypothesis, environmental speculation. *GSA Bull.*, **109 (1)**, p. 16-42.

Deptuck, M. E., G. S. Steffens, M. Burton, and C. Pirmez, 2003, Architecture and evolution of upper fan channel-belts on the Niger Delta slope and in the Arabian Sea: *Mar. Petrol. Geol.*, **20**, p. 649-676.

Devlin, W.J., H.K. Brueckner and C.G. Bond, 1988, New isotopic data and a preliminary age for volcanics near the base of the Windermere Supergroup, northeastern Washington, USA. *Can. J. Earth- Sci.*, **25**, p. 1906-1911.

Dickinson, W.R., 1970, Interpreting detrital modes of sandstone and arkose. *J. Sed. Petrol.*, **40**, p. 695–707.

Dickinson, W.R., 2004, Evolution of the North American Cordillera. *Annu. Rev. Earth and Planetary Sciences*, **32**, p. 13-45

Dickson, J.A.D., 1966, Carbonate identification and genesis as revealed by staining. *Journ. Sediment. Petrol.*, **36**, p. 491-505.

Dolgunin, V.N. and A.A. Ukolov, 1995, Segregation modeling pf particle rapid gravity flow. *Powder Technol.*, **83**, p. 95-103.

Dolgunin, V.N., A.N. Kudy and A.A. Ukolov, 1998, Development of the model of segregation of particles undergoing granular flow down an inclined chute. *Powder Technol.*, **96**, p. 213-218.

Dott, R.H. Jr., 1963, Dynamics of subaqueous gravity depositional processes. *AAPG Bull.*, **47**, p. 104-128.

Dott, R.H. Jr., 1964, Wacke, graywacke, and matrix - What approach to immature sandstone classification? *J. Sed. Petrol.*, **34**, p. 625-632.

Droxler, A.W., and Schlager, W., 1985, Glacial versus interglacial sedimentation rates and turbidite frequency in the Bahamas. *Geology*, **13**, p. 799-802.

Droxler, A.W., W. Schlager, and C.C. Whallon, 1983, Quaternary aragonite cycles and oxygen-isotope record in Bahamian carbonate ooze. *Geology*, **11**, p. 235-239.

Druitt, T.H., 1995, Settling behaviour of concentrated dispersions and some volcanological applications. *J. Volcanol. Geotherm. Res.*, **65**, p. 27-39.

Eisbacher, G.H., 1985, Late Proterozoic Rifting, Glacial Sedimentation, and sedimentary cycles in the light of Windermere deposition, Western Canada. *Paleogeograpy, Palaeoclimatology, Palaeoecology*, **51**, p. 231- 254.

Eisbacher, G.H., 1992, The Windermere Supergroup – Healthy tectonic and eustatic signals from a geriatric supercontinent. *Geologische Vereinigung. 82nd Annual meeting, Abstracts*, p. 11-12.

Elliot, T., 2000a, Megaflute erosion surfaces and the initiation of turbidite channels: *Geology*, **28 (2)**, p. 119-122.

Elliot, T., 2000b, Depositional Architecture of a Sand-rich, channelized turbidite system: The Upper Carboniferous Ross Sandstone Formation, Western Ireland: *Gulf Coast Section, SEPM 20th Annual Research Conference*, p. 342-373.

Eschard, R., E. Albouy, R. Deschamps, T. Euzen, and A. Ayub, 2003, Downstream evolution of turbiditic channel complexes in the Pab Range outcrops (Maastrichtian, Pakistan). *Mar. Petrol. Geol.*, **20**, p.691–710.

Field, M.E., J.V. Gardner and D.B. Prior, 1999, Geometry and Significance of Stacked Gullies on the Northern California Slope. *Marine Geology*, **154(1-4)**, p. 271-286.

Fisher, R.V., 1983, Flow transformation in sediment gravity flows. *Geology*, **11**, p. 274-274.

Flemming, B.W., 2000a, The role of grain size, water depth and flow velocity as scaling factors controlling the size of subaqueous dunes, *in* Trentesaux, A. and T. Garlan, eds., *Marine Sandwave Dynamics. Proceedings.* Int. Workshop, March 23-24 2000, Univ. of Lille 1, SHOM, France, p. 53-60.

Flemming B.W., 2000b, On the dimensional adjustment of subaqueous dunes in response to changing flow conditions: a conceptual process model, *in* Trentesaux, A. and T. Garlan, eds., *Marine Sandwave Dynamics. Proceedings.* Int. Workshop, March 23-24 2000, Univ. of Lille 1, SHOM, France, p. 61-68.

Fritz, W.H., M.P. Cecile, B.S. Norford, D. Morrow, and H.H.J. Geldsetzer, 1991, Cambrian to Middle Devonian Assemblages, *in* Gabrielse, H. and C. J. Yorath , eds., *Geology of the Cordilleran Orogen in Canada, Chapter 2*. Geol. Survey Can., Geology of Canada, No 4 (also GSA, The Geology of North America, vol. **G-2**), p. 151-218.

Gabrielse, H., 1972, Younger Precambrian of the Canadian Cordillera. *American J. Science*, **272**, 521-536.

Gabrielse, H. and C.J. Yorath, 1991, Tectonic synthesis, *in* Gabrielse, H. and C.J. Yorath, eds., *Geology of the Cordilleran Orogen in Canada, Chapter 18*: Geol. Survey Can., Geology of Canada, no. 4 (*also* Geological Society of America, The Geology of North America, v. G-2), p. 677-705.

Gabrielse, H. and R.B. Campbell, 1991, Part A. Upper Proterozoic Assemblages, *in* Gabrielse, H. and C. J. Yorath, eds., *Geology of the Cordilleran Orogen in Canada, Chapter 6*. Geol. Survey Can., Geology of Canada, No 4 (also GSA, The Geology of North America, vol. **G-2**), p. 125-150.

Gabrielse, H., J.W.H. Monger, J. O. Wheeler and C.J. Yorath, 1991, Part A. Morphogeological belts, tectonic assemblages, and terranes, *in* Gabrielse, H. and C. J. Yorath, eds., *Geology of the Cordilleran Orogen in Canada, Chapter 2*. Geol. Survey Can., Geology of Canada, No 4 (also GSA, The Geology of North America, **G-2**), p. 15-28.

Gani, M.R., 2003, Crisis for a general term referring to all types of sediment gravity flow deposits: Gravite. *2003 GSA Annual meeting*, Seattle, Washington, Official Program with Abstracts, **34 (7)**, p. 171.

Gani, M.R., 2004, From Turbid to Lucid: A Straightforward Approach to Sediment Gravity Flows and Their Deposits. *The Sedimentary Record*, SEPM, **2 (3)**, p. 4-8.

Gardner, M. H., and M. D. Borer, 2000, Submarine channel architecture along a slope and basin profile, Brushy Canyon Formation, West Texas, *in* Bouma, A.H. and C.C. Stone, eds., *Fine-grained turbidite systems*, AAPG Mem. **72**/SEPM Spec. Pub. **68**, p. 195-214.

Glaser, K.S., and A.W. Droxler, 1991, High production and highstand shedding from deeply submerged carbonate banks, northern Nicaragua Rise. *J. Sediment. Petrol.*, **61**, p. 128-142.

Gonzalez, A. P., D.S. Anderson and N.F. Hurley, 2003, Tectonic Controls on Delta-Front and Deepwater Sandstone Stratigraphy: Lewis Shale and Fox Hills Sandstone of the Northern Great Divide Basin, Wyoming, (*abs.*). AAPG Annual Convention, volume abstract, Dallas, USA.

Grasby, S.E. and R.L. Brown, 1993, New correlations of the Hadrynian Windermere Supergroup in the northern Selkirk Mountains, British Columbia. *Current Research, Part A*, Geol. Surv. Can., Paper **93-1A**, p. 199-206.

Grecula, M., S.S. Flint, H de V. Wickens, and S.D. Johnson, 2003, Upward-thickening patterns and lateral continuity of Permian sand-rich channel fills, Laingsburg Karoo, South Africa: *Sedimentology*, **50**, p. 831-853.

Grotzinger, J.P., 1989, Facies and evolution of Precambrian carbonates depositional systems: emergence of the modern platform archetype, *in* P.D. Crevello, J.L. Wilson, J.L. Sarg, and J.F., Read, eds., *Controls on Carbonate Platform and Basin Development*, SEPM Spec. Pub. **44**, p. 79-106.

Grotzinger, J.P. and James, N.P., 2000, Precambrian Carbonates: Evolution of Understanding, *in* J.P. Grotzinger and N.P. James, eds., *Carbonate Sedimentation and diagenesis in the evolving Precambrian world*, SEPM Spec. Pub. **67**, p. 3-20.

Guibaudo, G., 1992, Subaqueous sediment gravity flow deposits: practical criteria for their field description and classification. *Sedimentology*, **39**, p. 423-454.

Hampton, M.A., 1975, Competence of fined-grained debris flow. *J. Sed. Petrol.*, **45 (4)**, p. 834-844.

Hampton, M.A., 1979, Buoyancy in debris flows. *J. Sed. Petrol.*, **49**, p. 753-758.

Hana, J.C., and C.H. Moore, 1979, Quaternary temporal framework of reef to basin sedimentation, Grand Cayman, B.W.I. (abs.), *GSA* Abstr. Progr., **11**, p. 438.

Hand, B. M., 1997, Inverse grading resulting from coarse-sediment transport lag. *J. Sed. Res.* **67 (1)**, p. 124-129

Harms, J.C. and R.K. Fahnestock, 1965, Stratification, bedforms and flow phenomena (with an example from Rio Grande). In Middleton G.V., *ed.*, *Primary Sedimentation Structures and their hydrodynamic interpretation. SEPM Spec. Publ.*, **12**, p. 84-115.

Harris, M.T., 1994, The foreslope and toe-of-slope facies of the middle Triassic Latemar buildup (Dolomites, Northern Italy). *J. Sediment. Res.*, **B64**, p. 132-145.

Haughton, P.D.W., S.P. Barker and W.D. Mcaffrey, 2003, "Linked" debrites in sand-rich turbidite systems – origin and significance. *Sedimentology*, **50**, p. 459-482.

Hein, F.J. and M.E. McMechan, 1994, Chapter 6: Proterozoic and Lower Cambrian Strata of the Western Canada Sedimentary Basin, *in* Mossop, P.G. and I. Shetse, comps., *Geological Atlas of the Western Canada Sedimentary Basin*. Calgary, Can. Soc. Petrol. Geol. and Alberta Res. Council, p. 57-68.

Helland-Hansen, W., and J.G. Gjelberg, 1994, Conceptual basis and variability in sequence stratigraphy: a different perspective. *Sedimentary Geology*, **92**, p. 31-52.

Hine, A.C., R.J. Wilber, J.M. Bane, A.C. Neumann, and K.R. Lorenson, 1981, Offbank transport of carbonate sands along open, leeward bank margins: northern Bahamas, *Mar. Geol.*, **42**, p. 327-348.

Höy, T., 1989, The age, chemistry, and tectonic setting of the Middle Proterozoic Moyie sills, Purcell Supergroup, southeastern British Columbia. *Can. J. Earth Sci.*, **26**, p. 2305-2317.

Hubbard, S. M., B. W. Romans, S.A. Graham and D.R. Lowe, 2004, Downstream variability in deep-water channel deposit character and associated sedimentary processes, Cretaceous Cerro Toro Formation outcrop belt, Magallanes Basin, Chile (abs.), GSA Abstracts with Programs, v. **36 (5)** p. 373.

Hubscher, C., V. Spieb, M. Breitzke, and M.E. Weber , 1997, The youngest channel-levee system of the Bengal Fan: results from digital sediment echosounder data. *Marine Geology*, p. 125-145.

Hunt, D., and M.E. Tucker, 1992, Stranded parasequences and the forced regressive wedge systems tract: deposition during base-level fall. *Sedimentary Geology*, 81, p. 1-9.

Hunt, D., and M.E. Tucker, 1995, Stranded parasequences and the forced regressive wedge systems tract: deposition during base-level fall- reply. *Sedimentary Geology*, **95**, p. 147-160.

Imran, J. G. Parker and C. Pirmez, 1999, A nonlinear model of flow in meandering submarine and subaerial channels. *J. Fluid Mech.*, **400**, p. 295-331.

Jeannette, D.C. K. Fouada, T. Wawrzynieca, D. Dunlapa, R. Muñoz, J. Meneses-Rocha, 2003, Slope and basin-floor reservoirs from the Miocene and Pliocene of the Veracruz Basin, southeastern Mexico, *Mar. Petrol. Geol.*, **20**, 587-600.

Johansson, M. and D.A.V. Stow, 1995, A classification scheme for shale clast in deep-water sandstone, *in* Hartley, A.J. and D.J. Prosser, eds., *Characterization of Deep Marine Clastic Systems. Geol. Soc , Spec. Publ.*, **94**, p. 221-241.

Jolly, R.J.H. and L. Lonergan, 2002, Mechanism and controls on the formation of sand intrusions. *J. Geol. Soc.*, **159**, p. 605-617.

Karlstrom, K.E., K.-I. Åhäll, S.S. Harlan, M.L. Williams, J. McLelland and J.W. Geissman, 2001, Long-lived (1.8-1.0 Ga) convergent orogen in the southern Laurentia, its extension to Australia and Baltica, and implications for refining Rodinia. *Precambrian Research*, **110**, p. 5-30.

Karlstrom, K.E., S.S. Harlan, M.L. Williams, J. McLelland, J.W. Geissman, and K.-I. Åhäll, 1999, Refining Rodinia: Geologic evidence for the Australia- western U.S. connection in the Proterozoic. *GSA Today*, **9 (10)**, p. 1-7.

Kawakami, G. and M. Kawamura, 2002, Sediment flow and deformation (SFD) layers: Evidence for instrastratal flow in laminated muddy sediments of the Triassic Osawa Formation, Northeast Japan. *J. Sed. Res.*, **72**, p. 171-181.

Keevil, G., J. Peakall, K. Amos and J. Best, 2005, Flow structures in experimental sinous submarine channels, *abs.*, Sinuous Channels, Wynn, R. B., and Cronin, B., *eds.*, *Sinous channels: Genesis, geometry and architecture*, Joint meeting of UK TAPS group and the Geological Society of London's Marine Studies Group, p. 10.

Kendall, C. St. C. and Schlager, W., 1981, Carbonates and relative sea level changes. *Mar. Geology*, **44**, 181-212.

Kendall, B.S., R.A. Creaser, G.M. Ross, and D. Selby, 2004, Constraints on the timing of Marinoan "Snowball Earth" glaciation 187Re–187Os dating of a Neoproterozoic, post-glacial black shale in Western Canada. *Earth and Planetary Science Letters*, **222**, p. 729-740.

Khan, Z., L. Navarro, and R.W.C. Arnott, 2005, Architectural analysis and evolution of a Neoproterozoic deep-marine levee complex, Isaac Formation, Windermere Supergroup, Southwestern Canadian Cordillera, *abs.*, Sinuous Channels, Wynn, R. B., and Cronin, B., *eds.*, *Sinous channels: Genesis, geometry and architecture*, Joint meeting of UK TAPS group and the Geological Society of London's Marine Studies Group, p. 34.

Kier, J.S. and O.H. Pilkey, 1971, The influence of sea level changes on sediment carbonate mineralogy, Tongue of the Ocean, Bahamas. *Mar. Geol.*, **11**, p. 189-200.

Kleinhans, M.G., 2004, Sorting in grain flows at the lee side of dunes. *Earth-Sci. Rev.*, **65 (1-2)**, p. 75-102.

Kneller, B.C., 1995, Beyond the turbidite paradigm: physical models for deposition of turbidites and their implications for reservoir prediction, *in* Hartley, A.J. and Prosser, D.J., eds., *Characterization of deep marine clastic systems. Geol. Soc. London, Spec. Publ.*, **94**, p. 31-49.

Kneller, B., 2003, The influence of flow parameters on turbidite slope channel architecture: *Mar. Petrol. Geol.*, **20**, p. 901-910.

Kneller B.C. and C. Buckee, 2000, The structure and fluid mechanics of turbidity currents: a review of some recent studies and their geological implications. *Sedimentology*, **45**, suppl. **1**, p. 62-94.

Kneller, B.C. and M.J. Branney, 1995, Sustained high-density turbidity currents and the deposition of thick massive sands. *Sedimentology*, **42**, p. 607-616.

Kolla, V., H.W. Posamentier and H. Eichenseer, 1995, Stranded parasequences and the forced regressive wedge systems tract: deposition during base-level fall- discussion. *Sedimentary Geology*, **95**, p. 139-145.

Kolla, V., H.W. Posamentier and P. Bourges, 2003, Lobe- and Sheet-form Depositional Elements and Channel Avulsions and Occurrence in Deepwater Settings, *abs.*, AAPG Annual Convention, Program with Abstracts. Salt Lake City, USA.

Kolla, V., H.W. Posamentier, M. Fachmi, and L.J. Wood, 2004, Modes of evolution of deep-water and fluvial channels, *abs.*, AAPG Annual Convention, Program with Abstracts, Dallas, USA, **13**, p. A77.

Kolla, V., P. Bourges, J.M. Urruty, and P. Safa, 2001, Evolution of deep-water Tertiary sinuous channels offshore Angola (west Africa) and implications for reservoir architecture: *AAPG Bull.*, **85**, p. 1371-1405.

Komar, P.D., 1971, Hydraulic jumps in turbidity currents. *GSA Bull.*, **82**, p. 1477-1488.

Kubli, T.E. and P.S. Simony, 1992, The Dogtooth High, northern Purcell Mountains, British Columbia. *Bull. Can. Petrol. Geology*, **40 (1)**, p. 36-51.

Kuenen, P.H., 1953, Significant features of graded bedding. *Bull. AAPG*, **37(5)**, p. 1044-1066.

Kuenen, P.H. and C. I. Migliorini, 1950, Turbidity currents as a cause of graded bedding: *J. Geol.*, **58**, p. 91-127.

Le Roux, J.P., 2003, Can dispersive pressure cause inverse grading in grain flows? - Discussion. *J. Sed. Res.*, **73 (2)**, p.333-334.

Leclair, S.F., 2002, Preservation of cross-strata due to the migration of subaqueous dunes: an experimental investigation. *Sedimentology*, **49**, p. 1157-1180.

Leclair, S.F. and J.S. Bridge, 2001, Quantitative interpretation of sedimentary structures formed by river dunes. *J. Sed. Res.*, **71(5)**, p. 713- 716.

Lee, S., 2004, *Sedimentary processes recorded by continental slope morphology, Ph.D.'s thesis*, University of Bristol, Bristol, U.K., 204 p.

Li, M.Z. and .D. Komar, P., 1992, Selective entrainment and transport of mixed size and density sands: Flume experiments simulating the formation of black-sand placers. *J. Sed. Petrol.*, **62 (4)**, p. 584-590.

Li, Z. and A.G. Davies, 2001, Turbulence closure modeling of sediment transport beneath large waves. *Cont. Shelf Res.*, **21**, p. 243-262.

Li, Z., L. Zhang and C. McA. Powell, 1995, South China in Rodinia: Part of the missing link between Australia- East Antarctica and Laurentia? *Geology*, **23 (5)**, p. 407-410.

Li, Z., X. Li, H. Zhou, and P.D. Kinny, 2002, Grenvillian continental collision in South China: New SHRIMP U-Pb zircon results and implications for the configuration of Rodinian. *Geology*, **30 (2)**, p. 163-166.

Lowe, D. R., 1975, Water escape structure in coarse-grained sediments. *Sedimentology*, **22**, p. 157-204.

Lowe, D. R., 1982, Sediment gravity flows: II. Depositional models with special reference to the deposits of high-density turbidity currents. *J. Sed. Petrol.*, **52 (1)**, p. 279-297.

Lowe, D.R. and M. Guy, 2000, Slurry flow deposits in the Britannia Formation (Lower Cretaceous), North Sea: a new perspective on the turbidity current and debris flow problem. *Sedimentology*, **47**, p. 31-70.

Lykousis, V., 2001, Subaqueous bedforms on the Cyclades Plateau (NE Mediterranean) - evidence of Cretan Deep Water Formation? *Cont. Shelf Res.*, **21**, p. 495-507.

Lynts, G.W., J.B. Judd and C.F. Stehman, 1973. Late Pleistocene history of Tongue of the Ocean, Bahama. *GSA Bull.*, **84**, p. 2605-2684.

Manley, P.L. and R.D. Flood, 1988. Cyclic sediment deposition within the Amazon Deep-sea Fan: *AAPG Bull.*, **72**, p. 912-925.

Martisen, O., 1994, Chapter 5. Mass movements, *in* A.Maltman, ed., *The geological deformation of sediments*. Chapman & Hall, London, p. 127-165.

Maslin, M., N. Mikkelsen, C. Vilela, and B. U. Haq, 1998, Sea-level and gas-hydrate-controlled catastrophic sediment failures of the Amazon fan: *Geology*, **26**, p. 1107-1110.

McCaffrey, W. and B. Kneller, 2001, Process controls on the development of stratigraphic trap potential on the margins of the confined turbidite system and aids to reservoir evaluation. *AAPG Bull.*, **85 (6)**, p. 1-18.

McCaffrey, W.D. and B. Kneller, 2004, Autocyclic vs. Allocyclic Controls on Aggradational Channel Progradation, Back Fill and Avulsion (abs.), *AAPG Bull.*, **88 (13**, Supplement).

McHargue, T. R., 1991, Seismic Facies, processes and evolution of Miocene Inner fan Channel, Indus Submarine Fan, in Weimer, P. and M.H. Link, eds., *Seismic facies and sedimentary processes of submarine fan turbidite systems*, New York, Springer-Verlag, p. 403-416.

McMechan, M.E., 2000, Vreeland Diamictites- Neoproterozoic glaciogenic slope deposits, Rocky Mountains, northeast British Columbia. *Bull. Can. Petrol. Geol.* **48 (3)**, p. 246-261.

McMechan, M.E. and R.A. Price, 1982, Superimposed low-grade metamorphism in the Mount Fisher area, southeastern British Columbia - implications for the East Kootenay orogeny. *Can. J. Earth Sci.*, **19 (3)**, p. 476-489.

Meyer, L., 2004, Internal architecture of an ancient deep-water, passive margin, basin-floor fan system, Upper Kaza Group, Windermere Supergroup, Castle Creek, British Columbia, Master's Thesis, University of Calgary, Calgary, Alberta, 175 p.

Miall, A. D., 1996, *The Geology of fluvial deposits. Sedimentary facies, Basin analysis, and Petroleum geology*. Berlin, Springer, 582 p.

Middleton, G.V., 1966, Experiments on density and turbidity currents I. Motion of the head. *Can. J. Earth Sci.* **3 (4)**, p. 523-546.

Middleton, G.V., 1993, Sediment deposition from turbidity currents. *Annu. Rev. Earth Planet. Sci.*, 21, p. 89-114.

Middleton, G.V. and Hampton, M.A., 1973, Sediment gravity flows: mechanics of flow and deposition, *in* Middleton, G. V. and A. H. Bouma, eds., *Turbidites and Deep Water Sedimentation. Short Course Notes*, No **1**, SEPM (Pacific Section), Los Angeles, p. 1-38.

Middleton, G.V. and Hampton, M.A., 1976, Subaqueous sediment transport and deposition by sediment gravity flows. In Stanley, D.J. and Swift, D.J.P., eds., *Marine Sediment transport and Environmental Management*. John Wiley and Sons, New York, p. 197-218.

Mohrig, D., K.M. Straub, J. Buttles, and C. Pirmez, 2005, Channel levees built by turbidity currents in the laboratory, *abs.*, Fall Meeting AGU, San Francisco, USA

Mohrig, D., K.X. Whipple, M. Hondzo, C. Ellis, and G. Parker, 1998, Hydroplaning of subaqueous debris flows. *GSA Bull.*, **110 (3)**, p. 387-394.

Monger, J.W.H. and Price, R.A., 1979, Geodynamic evolution of the Canadian Cordillera-Progress and problems. *Can. J. Earth Sci.*, **16**, p. 770-791.

Monger, J.W.H., J.G. Souther and H. Gabrielse, 1972, Evolution of the Canadian Cordillera: A Plate Tectonic Model. *Amer. J. Sci.*, **272**, p. 577 - 602.

Monger, J.W.H., R.A. Price, and D.J. Tempelman-Kluit , 1982, Tectonic accretion and the origin of the two major metamorphic welts in the Canadian Cordillera. *Geology*, **10**, p. 70-75.

Moores, E.W., 1991, Southwest U.S.-East Antarctic (SWEAT) Connection: A hypothesis. *Geology*, **19**, p. 425-428.

Moraes, M.A.S., P.R. Blaskovski and P. Joseph, 2004, The Grès d'Annot as an analogue for Brazilian Cretaceous sandstone reservoir: comparing convergent to passive-margin confined turbidites, *in* Joseph, P. and S.A. Lomas, eds., *Deep-water Sedimentation in the Alpine Basin of SE France: New perspective on the Grès d'Annot and related systems*. Geological Society, London, Spec. Pub., 221, p. 419-435.

Moretti, M., J.M. Soria, P. Alfaro and N. Walsh, 2001, Asymmetrical soft-sediment deformation structures triggered by rapid sedimentation in turbiditic deposits (Late Miocene, Guadix Basin, Southern Spain), *Facies*, **44**, p. 283-294.

Mulder, T. and Alexander, J., 2001, The physical character of subaqueous sedimentary density flows and their deposits. *Sedimentology*, **48**, p. 269-299.

Mulder, T. and J.P.M. Syvitski, 1995, Turbidity Currents Generated at River Mouths during Exceptional Discharges to the World Oceans, *J. Geology*, **103**, p. 285- 299.

Mullins, H.T., 1983, Modern carbonate slopes and basins of the Bahamas, *in* Cook, H.E. (ed.) *Platform Margin and Deep-Water Carbonates*. SEPM., Short Course Notes, **12**, p. 4.1-4.138.

Murphy, D.C., 1987a, Kaza Group, eastern Wells Gray Park, British Columbia. *Current Res., Part A., Geol. Surv. Cana.*, Paper **87-1A**, p. 735-742.

Murphy, D.C., 1987b, Superstructure/infrastructure transition, east-central Cariboo Mountains, British Columbia: geometry, kinematics and tectonic implications. *J. Struct. Geol.*, **9 (1)**, p. 13-29.

Murphy, D.C., 1990, Stratigraphy and structure, southern Rocky Mountains Trench to the headwaters of the North Thompson River, Cariboo Mountains, British Columbia. *Current Research, part E*, Geol. Surv. Can., Paper **90-1E**, p. 71-80.

Murphy, D.C. and C.J. Rees (1983) Structural transition and stratigraphy in the Cariboo Mountains, British Columbia. *Current Research*, part A, Geol. Surv. Can., Paper **83-1A**, p. 245-252.

Murphy, D.C. and J.M. Journeay, 1982, Structural style in the Range, Cariboo Mountains, southern British Columbia: Preliminary Results. *Geol. Surv. Can.*, Paper **82-1A**, p. 289-292.

Mutti, E., 1992, *Turbidite Sandstone*. AGIP, Milan, Italy, 275 p.

Mutti, E., 1977, Distinctive thin-bedded turbidite facies and related depositional environments in the Eocene Hecho Group (south-central Pyrenees, Spain). *Sedimentology*, **24**, p. 107-131.

Mutti, E. and Normark, W. R., 1987, Comparing examples of modern and ancient turbidite system: Problems and Concepts, *in* Leggett, J.K. and Zuffa, G.G. (1987) *Marine Clastic Sedimentology. Concepts and Case Studies*, Graham & Trotman, p. 1-38.

Mutti, E. and T.H. Nilsen, 1981, Significance of intraformational rip-up clasts in deep-sea fan deposits. Abs. *IAS*, 2nd Eur. Reg. Meeting, Bologna, Italy, p. 117-119.

Mutti, E., R. Tinterri, G. Benevelli, D. di Biase, G. Cavanna, 2003, Deltaic, mixed and turbidite sedimentation of ancient foreland basins, *Mar. Petrol. Geol.*, **20**, 733–755.

Navarro, L. and R.W.C. Arnott, 2004, Architecture of two deep-marine submarine Channel Complexes in the Neoproterozoic Isaac Formation, Windermere Supergroup, Cariboo Mountains, British Columbia, Canada (abs.). *Geological Association of Canada-Mineralogical Association of Canada, Joint Annual Meeting: Lake to Lake*, St. Catharines, v. **29**, p. 495.

Nichols, R.J., 1995, The liquificaction and remobilization of sandy sediments. In Hartley, A.J. and Prosser, D.J., eds.,. *Characterization of Deep Marine Clastic Systems. Geol. Soc. London, Spec. Publ.*, **94**, p. 63-76.

Owen, G., 1987, Deformation processes in unconsolidated sands, *in* Jones M.E. and R.M.F. Preston, eds., *Deformation of Sediments and Sedimentary Rocks. Geol. Soc. London, Spec. Pub.*, **29**, p. 11–24.

Owen, G., 1996, Experimental soft-deformation: structures formed by the liquefaction of unconsolidated sands and some ancient examples. *Sedimentology*, **43**, p. 279-293.

Page, M.C., G.R. Dickens, and G.B Dunbar, 2003, Tropical view of Quaternary sequence stratigraphy; siliciclastic accumulation on slopes east of the Great Barrier Reef since the last glacial maximum. *Geology*, **31 (11)**, p.1013-1016.

Paola, C., S. M. Wiele and M.A. Reinhart, 1989, Upper-regime parallel lamination as the result of turbulent sediment transport and low-amplitude bed forms. *Sedimentology*, **36**, p. 47-59.

Parrish, R.R., 1991, Precambrian Basement Rocks of the Canadian Cordillera, *in* Gabrielse, H. and C.J. Yorath, eds., *Geology of the Cordilleran Orogen in Canada, Chapter 2.* Geol. Survey Can., Geology of Canada, No 4 (also GSA, The Geology of North America, vol. G-2), p. 89-96.

Peakall, J., McCaffrey, B., and Kneller, B., 2000, A process model for the evolution, morphology, and architecture of sinuous submarine channels. *J. Sed. Res.*, **70**, p. 434-448.

Pell, J. and P.S. Simony, 1982, Hadrynian Horsethief Creek Group/ Kaza Group Correlations in the southern Cariboo Mountains, British Columbia. *Current Research, Part A.* Geol. Surv. Can., Paper **82-1A**, p. 305-308.

Pell, J. and P.S. Simony, 1987, New Correlations of Hadrynian strata, south-central British Columbia. *Can. J. Earth Sci.*, **24**, p. 301-312.

Pell, J. and P.S. Simony,1981, Stratigraphy, Structure and Metamorphism in the southern Cariboo Mountains, British Columbia. *Current Research, Part A.* Geol. Surv. Can., Paper **81-1A**, p. 227-230.

Pickering, K.T., Clark, J.D., Ricci Lucci, F., Smith, R.N., Hiscott, R.N. and Kenyon, N.H., 1995, Architectural element analysis of turbidite systems, and selected topical problems for sand-prone deep-water system, *in* Pickering, K.T., Hiscott, R.N., Kenyon, N.H., Ricci Lucci, F., and Smith, R.D., eds., *Atlas of deep water environments: Architectural style in turbidite systems.* London, Chapman and Hall, p. 1-10.

Pickering, K.T., R.N. Hiscott and F.J. Hein, 1989, *Deep marine environments.* London, Harper-Collins (now Chapman & Hall), 416 p.

Piper, D.J.W.,1970, A Silurian deep sea fan deposit in western Ireland and its bearing on the nature of turbidity current. *J. Geol.*, **78**, p. 509-522.

Piper D. J. W., C. Pirmez, P. L. Manley, D. Long, R. D. Flood, W. R. Normark, and W. Showers, 1997, Mass-transported deposits of the Amazon Fan, *in* R. D. Flood, D. J. W. Piper, A. Klaus, and L. C. Peterson, eds., *Proceedings of the ocean drilling program scientific results*, **155**, p. 109-146.

Piper, D.J.W. and W.R. Normark, 1983, Turbidite depositional patterns and flow characteristics, Navy Submarine fan, California Borderland, *Sedimentology*, **30**, 681-694.

Piper, J.D.A. and Z.Q. Rui, 1997, Paleomagnetism of Neoproterozoic glacial rocks of the Hubei Shield: the North China block in Gondwana. *Tectonophysics*, **283**, p. 145-171.

Pirmez, C., R. H. Hiscott, and J. D. Kronen, 1997, Sandy turbidite succession at the base of channel-levee systems of the Amazon Fan revealed by FMS logs and cores: unraveling the facies architecture of large submarine fans, *in* R. D. Flood, D. J. W. Piper, A. Klaus, and L. C. Peterson, eds., *Proceedings of the ocean drilling program scientific results*, **155**, p. 7-33.

Pirmez, C., R. T. Beaubouef, S. J. Friedman, and D. C. Mohrig, 2000, Equilibrium profile and baselevel in submarine channel: Examples from Late Pleistocene systems and implications for architecture of deepwater reservoirs, *in* P. Weimer, R. M. Slatt, J. Coleman, N.C. Rosen, H. Nelson, A. H. Bouma, M. J. Styzen, and D. T. Lawrence, eds., *Deep-water reservoirs of the world*: GCSSEPM Foundation 20th Annual Research Conference, p. 782-805.

Plink- Björklund, P., and R. Steel, 2004, Initiation of turbidity currents: outcrop evidence for Eocene hyperpycnal flow turbidites. Sedimentary Geology, **165 (1-2)**, p. 29-52.

Plint, A.G. and D. Nummedal, 2000, The falling stage system tract: recognition and importance in sequence stratigraphy analysis, *in* Hunt, D. and R.L. Gawthorpe, eds., *Sedimentary responses to forced regressions*. Geological Society, London, Spec. Publ., **172**, 1-17.

Posamentier H.W and P.R. Vail, 1988, Eustatic controls on clastic deposition II – Sequence and system tract models, *in* C.K. Wilgus, B.S. Hastings, C.G. St. C. Kendall, H.W. Posamentier, C.A. Ross, and J.C. Van Wagoner, eds., *Sea Level Changes- An integrated approach.* SEPM, Spec. Pub., **42**, 125-154.

Posamentier H. W and V. Kolla, 2003, Seismic geomorphology and stratigraphy of depositional elements in deep-water settings: *J. Sed. Res.*, **73**, p. 367-388.

Posamentier, H.W., G.P. Allen, and D.P. James, 1990, Aspects of sequence stratigraphy: recent and ancient examples of forced regressions (abs.), *AAPG Bull.*, **74**, p. 742.

Posamentier, H.W., G.P. Allen, D.P. James, and M. Tesson, 1992, Forced regressions in a sequence stratigraphic framework: Concepts, examples, and exploration significance. *AAPG Bull.*, **76**, p. 1687-1709.

Posamentier, H.W., R.D. Erskine, and R.H. Jr. Mitchum, 1991, Models for submarine-fan deposition within a sequence-stratigraphy framework, in P. Weimer and M.H. Link, eds., *Seismic facies and sedimentary processes of submarine fans and turbidite systems*. Springer-Verlag, New York, p. 127-136.

Postma, G. ,1986, Classification for sediment gravity-flow deposits based on flow conditions during sedimentation. *Geology*, **14**, p. 291-294.

Postma, G., W. Nemec and K.L. Kleinspehn, 1988, Large floating clast in turbidites: a mechanism for their emplacemplacement. *Sed. Geol.*, **58**, p. 47-61.

Poulton, T.P. and P.S. Simony, 1980, Stratigraphy, sedimentology, and regional correlation of the Horsethief Creek Group (Hadrynian, Late Precambrian) in the northern Purcell and Selkirk Mountains, British Columbia. *Can. J. Earth Sci.*, **17**, p. 1708-1724.

Poulton, T.P., 1973, Upper Proterozoic 'Limestone Unit', northern Dogtooth Mountains, British Columbia. *Can. J. Earth Sci.*, **10**, p. 292-305.

Powell, C. McA., W.V. Priss, C.C. Gatehouse, B. Krapez and Z.X. Li, 1994, South Australian record of a Rodinian epicontinental basin and its mid-Neoproterozoic breakup (~700 Ma) to form the Palaeo-Pacific Ocean. *Tectonophysics*, **237**, p. 113-140.

Price, R.A. (1994) Chapter 2.Cordilleran Tectonics and the Evolution of Western Canada Sedimentary Basin. *In* Mossop, P.G. and Shetse, I. (comps.) *Geological Atlas of the Western Canada Sedimentary Basin.* Calgary, Can. Soc. Petrol. Geol. and Alberta Res. Council, p. 13-24.

Rankey, E.C., S.L. Bachter, and J. Kaufman, 1999, Controls on stratigraphic architecture of mixed carbonate/siliciclastic systems: A case study from the Holder Formation (Pennsylvanian, Virgilian), Sacramento Mountains, New Mexico, *in* P.M. Harris, A.H. Saller and J.A. Simo, eds., *Advances in carbonate sequence stratigraphy; application to reservoirs, outcrops and models*, SEPM, Spec. Publ., **63**, p. 127-150.

Read, J.F., 1985, *Carbonate platform models*: *AAPG Bull.*, **69**, p. 1-21.

Reading H.G. and M. Richards, 1994, Turbidite Systems in Deep-Water Basin Margins Classified by Grain Size and Feeder System. *AAPG Bull.*, **78 (5)**, p. 792–822.

Reesor, J. E., 1957, Geology of the Lardeau (east-half) map area, British Columbia. *Geol. Surv. Can., Mem.* 369, 129 p.

Reesor, J.E., 1957, The Proterozoic of the Cordillera in southeastern British Columbia and southwestern Alberta, *in* Gill, J.E., ed., *The Proterozoic of Canada. Royal Soc. Can., Spec. Publ.*, **2**, p. 150-177.

Reid, L.F., P.S. Simony, and G.M. Ross, 2002, Dextral strike-slip faulting in the Cariboo Mountains, British Columbia: a natural example of wrench tectonics in relation to Cordillera tectonics. *Can. J. Earth Sci.*, **39**, p. 953-970.

Reijmer, J.J.G., Ten Kate, W.G.H., Sprenger, A., and Schlager, W., 1991. Calciturbidite composition related to exposure and flooding of a carbonate platform (Triassic, Eastern Alps). *Sedimentology*, **38**, p. 1059-1074.

Reijmer, J.J.G., W.G.H. Ten Kate, A. Sprenger, and W. Schlager, 1991, Calciturbidite composition related to exposure and flooding of a carbonate platform (Triassic, Eastern Alps). *Sedimentology*, **38**, p. 1059-1074.

Ricci Lucci, F., 1995, *Sedimentographica. Photographic Atlas of sedimentary Structures.* 2nd ed., Columbia University Press, New York, 255 p.

Ross, G.M., 1991, Tectonic setting of the Windermere Supergroup revisited. *Geology*, **19**, p. 1125-1128.

Ross, G. M. ,2000, The Proterozoic Windermere Supergroup: an on-land continental margin turbidites system, Open File 3932, Calgary, Geological Survey Canada.

Ross, G. M., 2003a, The Windermere Turbidite System: A Window into the Neoproterozoic Deep-Water World. *GSA, Abstracts with Programs*, **35 (6)**, p. 472.

Ross, G. M., 2003b, Slope Carbonate deposition in the Neoproterozoic Windermere turbidite system (Western Canada) significance in basin analysis (*abs.*). *Slope Conference, Submarine Slope Systems: processes, products and predictions*, Liverpool, p. 71.

Ross, G. M., 2003c, The Neoproterozoic Windermere turbidite system (Western Canada): An analogue for petroleum exploration in modern passive margin turbidite systems (*abs.*): *Slope Conference, Submarine Slope Systems: processes, products and predictions*, Liverpool, p. 72.

Ross, G.M., J.D. Bloch and H.R. Krouse, 1995, Neoproterozoic strata of the southern Canada Cordillera and the isotopic evolution of seawater sulfate. *Precambrian Research*, **73**, p. 71-99.

Ross, G.M. and C.A. Ferguson, 2003, *Geology and structure cross-sections, Eddy, British Columbia. Geol. Surv. Can.*, Map **1967A**, scale 1:50,000.

Ross, G. M. and D.C. Murphy, 1988, Transgressive stratigraphy, anoxia, and regional correlations within the late Precambrian Windermere grit of the southern Canadian Cordillera. *Geology*, **16**, p. 139-143.

Ross, G.M. and R.R. Parrish, 1991, Detrital zircon geochronology of metasedimentary rocks in the southern Omineca Belt, Canadian Cordillera. *Can. J. Earth- Sci.*, **28**, p. 1254-1270.

Russel, H.A.J. and R.W.C. Arnott, 2003, Hydraulic-jump and hyperconcentrated-flow deposits of a glaciogenic subaqueous fan: Oak ridges moraine, southern Ontario, Canada: J. Sedimentary Research, **73**, p. 887-905.

Samuels, A., B. Kneller, S. Raslan, A. Sharp, and C. Parsons, 2003, Prolific deep marine slope channels of the Nile Delta, Egypt. *AAPG Bull.*, **87**, p. 541-560.

Satur, N., Hurst, A., Cronin, B.T., Kelling, G. And Gurbuz, K., 2000, Sand body geometry in a sand-rich, deep-water clastic system, Miocene Cingoz Formation of southern Turkey. *Mar. Petrol. Geol.*, **17**, p. 239-252.

Schlager, W., J. Reijmer, and A.W. Droxler, 1994, Highstand shedding of carbonate platforms, *J. Sediment. Res.*, **B64**, p. 270-281.

Scholle, P.A. and D.S. Ulmer-Scholle, 2003, A color guide to the petrography of carbonate rocks: grains, texture, porosity, diagenesis, AAPG Mem. 77, 474 p.

Scott, E.D., A.H. Bouma and H.DeVille Wickens, 2000, Influence of tectonics on submarine fan deposition, Taqua and Laingsburg subbasins, South Africa, *in* A.H. Bouma and C.G. Stone, eds., *Fine-grained turbidite systems*, AAPG Mem. **72**, SEPM Spec. Pub. N° **68**, p.47-56.

Sears, J. W. and R.A. Price, 1978, The Siberian Connection: A case for Precambrian separation of the North America and Siberian cratons. *Geology*, **6**, 267-270.

Sears, J.W. and R.A. Price, 2000, New look at the Siberian connection: No SWEAT. *Geology*, **28**, p. 423-426.

Shanmugam, G., 1996, High-Density Turbidity Currents: Are they sandy debris flows?. *J. Sed. Res.*, **66**, p. 2-10.

Shanmugam, G., 1997, The Bouma sequence and the turbidite mind set. *Earth- Sci. Rev.*, **42**., p. 201-229.

Shanmugam, G., 2000, 50 years of the turbidite paradigm (1950s-1990s): deep-water processes and facies models- a critical perspective. *Mar Petrol. Geol.*, **17**, p. 285-342.

Shanmugam, G., T.D. Spalding and D.H. Rofheart, 1995, Deep-marine bottom-current reworked sand (Pliocene and Pleistocene), Ewing Bank 826 Field, Gulf of Mexico, *in* Winn, R.D. Jr. and J.M. Armentrout, eds., *Turbidites and associated deep-water facies*. SEPM Core Workshop N° **20**, p. 25-54.

Simony, P.S. and J.D Aitken, 1990, The Windermere Supergroup and its tectonic context: outline and problems. In Aitken, J.D. and McDonough, D.M.R. (comps): *Late Proterozoic Glaciation, Rifting and Eustacy, as Illustrated by the Windermere Supergroup*. Geol. Assoc. Can., Nuna Research Conference, Invermere and Valemount, British Columbia, *Field Trip Guidebook*, p. 1-11.

Slind O.L., G.D. Andrews, D.L. Murray, B.S. Norford, D.F. Paterson, C.J. Salas, and E.E. Tawadros, 1994, Chapter 8. Middle Cambrian to Lower Ordovician Strata of the Western Canada Sedimentary Basin, *in* Mossop, P.G. and Shetse, I., comps., *Geological Atlas of the Western Canada Sedimentary Basin*. Calgary, Can. Soc. Petrol. Geol. and Alberta Res. Council, p. 87-108.

Southard, J.B. and L.A. Boguchwal, 1990, Bed configurations in steady unidirectional water flows. Part 2. Synthesis of Flume data. *J. Sed. Petrol.*, **60 (5)**, p. 658-679

Sprague, A.R., M.D. Sullivan, K.M. Campion, G.N. Jensen, F.J. Goulding, T.R. Garfield, D.K. Sickafoose, C. Rossen, and D.C. Jennette, 2002, The physical stratigraphy of deep-water strata: A hierarchical approach to the analysis of genetically-related stratigraphic elements for improved reservoir prediction. *National AAPG/SEPM meeting abstracts*, Houston, Texas, March 10-13, p.10–13.

Stewart, J.H., 1972, Initial deposits in the Cordilleran Geosyncline: Evidence of late Precambrian (<850 m.y.) Continental separation. *GSA Bull.*, **83**, p. 1345-1360.

Stow, D.A.V. and M. Mayall, 2000, Deep-water sedimentary systems: new models for the 21st century. *Mar. Petrol. Geol.*, **17**, p. 125-135.

Straub, K.M., D. Mohrig, and J. Buttles, 2004, Experimental Study of Sinuous Channel Evolution Associated with Depositional Turbidity Currents, *abs.*, Fall Meeting AGU, San Francisco, USA.

Takahashi, T., 2001, Mechanics and simulation of snow avalanches, pyroclastic flows and debris flows; *in*: W.D. McCaffrey, B.C. Kneller and J. Peakall (eds.) *Particulate Gravity Currents*, Int. Assoc. Sedimentol., Spec. Publ., **31**, 11–43.

Tarasov, A.T., 1974, Classification of injection structures. *Geotectonics*, **6**, p. 342-345.

Teske, Andreas, A. Dhillon and M. L. Sogin, 2003, Genomic Markers of Ancient Anaerobic Microbial Pathways: Sulfate Reduction, Methanogenesis, and Methane Oxidation. *Biol. Bull.*, **204**, p. 186–191.

Thompson, J.A. and G.M. Ross, 1990, Field Trip 3: Late Proterozoic stratigraphy in the Mcbride area (British Columbia): Windermere turbidites, condensed intervals and the vanished carbonate platform, *in* Aitken, J.D. and McDonough, D.M.R. (comps.) *Late Proterozoic glaciation, rifting and eustacy, as illustrated by the Windermere Supergroup*. Geological Association of Canada, Nuna Research Conference, Invermere and Valemount, British Columbia, p. 7.1-7.13.

Valentine, P.C., R.A. Cooper and J.R. Uzmann, 1984, Submarine sand dunes and sedimentary environments in Oceanographer Canyon. *J. Sed. Petr.*, **54 (3)**, p. 704-715.

Van Den Berg, J. H., Van Gelder, A. and Mastbergen, D. R., 2002, The importance of breaching as a mechanism of subaqueous slope failure in fine sand. *Sedimentology*, **49**, p. 81- 95

Van Wagoner, J.C., H.W. Posamentier, R.M. Mitchum, P.R. Vail, J.F. Sarg, T.S. Loutit, and J. Hardenbol, 1988, An overview of the fundamentals of sequence stratigraphy and key definitions, *in* C.K. Wilgus, B.S. Hastings, C.G.St.C. Kendall, H.W. Posamentier, C.A. Ross, J.C. Van Wagoner, eds., *Sea-level changes: an integrated approach*. SEPM Spec. Publ., **42**, p. 39-45.

Vecsei, A., and D.G.K. Sanders, 1997, Sea-level highstand and lowstand shedding related to shelf margin aggradation and emersion, Upper Eocene-Oligocene of Maiella carbonate platform, Italy. *Sediment. Geol.*, **112**, p. 219-234.

Von Rad, U., M. Tahir, 1997, Late Quaternary sedimentation on the outer Indus shelf and slope (Pakistan): evidence from single-resolution seismic data and coring. *Marine Geology*, 138, p. 193-236.

Vrolijk, P.J. and Southard, J.B., 1997, Experiments on rapid deposition of sand from high velocity flows: *Geoscience Canada*, **24**, p. 45–54.

Walker, J.F., 1926, Geology and mineral deposits of Windermere map-area, British Columbia, Geol. Surv. Can., Mem **148**, 69 p.

Walker J.F., 1965, The origin and significance of the internal sedimentary structures of turbidites: *Proc. Yorkshire Geol. Soc.*, **35**, p. 1-32.

Walker, R.G., 1967, Turbidite sedimentary structures and their relationships to proximal and distal environments. *J. Sed. Petrol.*, **37**, p. 25-43.

Walker, R. G. and James, N.P., 1992, *Facies models-response to sea level change*. Geol. Assoc. Can., St. John's, 409 p.

Weimer, P., 1991, Seismic facies, characteristics and variations in channel evolution, Mississippi Fan (Plio-Pleistocene), Gulf of Mexico, *in* P. Weimer, and M.H. Link, eds., *Seismic facies and sedimentary processes of modern and ancient submarine fans*: New York (Springer-Verlag), p. 323-347.

Wentworth, C.K., 1922, A scale of grade and class terms for clastic sediments. *J. Geology*, **30**, p. 377-392.

Wheeler, J.O. and McFeely, P., 1991, Tectonic assemblage map of the Canadian Cordillera and adjacent parts of the United States of America. Geol. Surv. Can., Map 1712A, scale 1: 2,000,000.

Williams, J.C., 1976, The segregation of particulate materials: A review. *Powder Technol.*, **15**, p. 245-251.

Wingate, M.T.D., S.A. Pisarevsky and D.A.D. Evans, 2002, Rodinia connections between Australia and Laurentia: no SWEAT, no AUSWUS? *Terra Nova*, **14 (2)**, p. 121-128.

Winker, C.D., and J. R. Booth, 2000, Sedimentary dynamics of the salt-dominated continental slope, Gulf of Mexico; integration of observations from the seafloor, near-surface, and deep subsurface, *in* P. Weimer, R. M. Slatt, J. Coleman, N.C. Rosen, H. Nelson, A. H. Bouma, M. J. Styzen, and D. T. Lawrence, eds., *Deep-water reservoirs of the world*: GCSSEPM Foundation 20th Annual Research Conference, p. 1059-1086.

Winn, R.D. Jr. and R.H. Jr. Dott, 1979, Deep-water fan-channel conglomerates of late Cretaceous age, southern Chile. *Sedimentology*, **26**, p. 203-228.

Woolfe, K.J., P. Larcombe, T. Naish and R.G. Purdon, 1998, Lowstand rivers need not incised the shelf: An example from the Great Barrier Reef, Australia, with implications for sequence stratigraphic models. *Geology*, **26 (1)**, p. 75-78.

APPENDIXES

APPENDIX I. Location of Sample, Log and Gamma Ray profiles

This appendix includes a photo index with an aerial photo compilation showing location of sample sites (yellow), measured stratigraphic logs (designated by the letter S) and gamma-ray profiles (designated by the initials "Gr") in Channel 1 and 3.

PHOTO INDEX

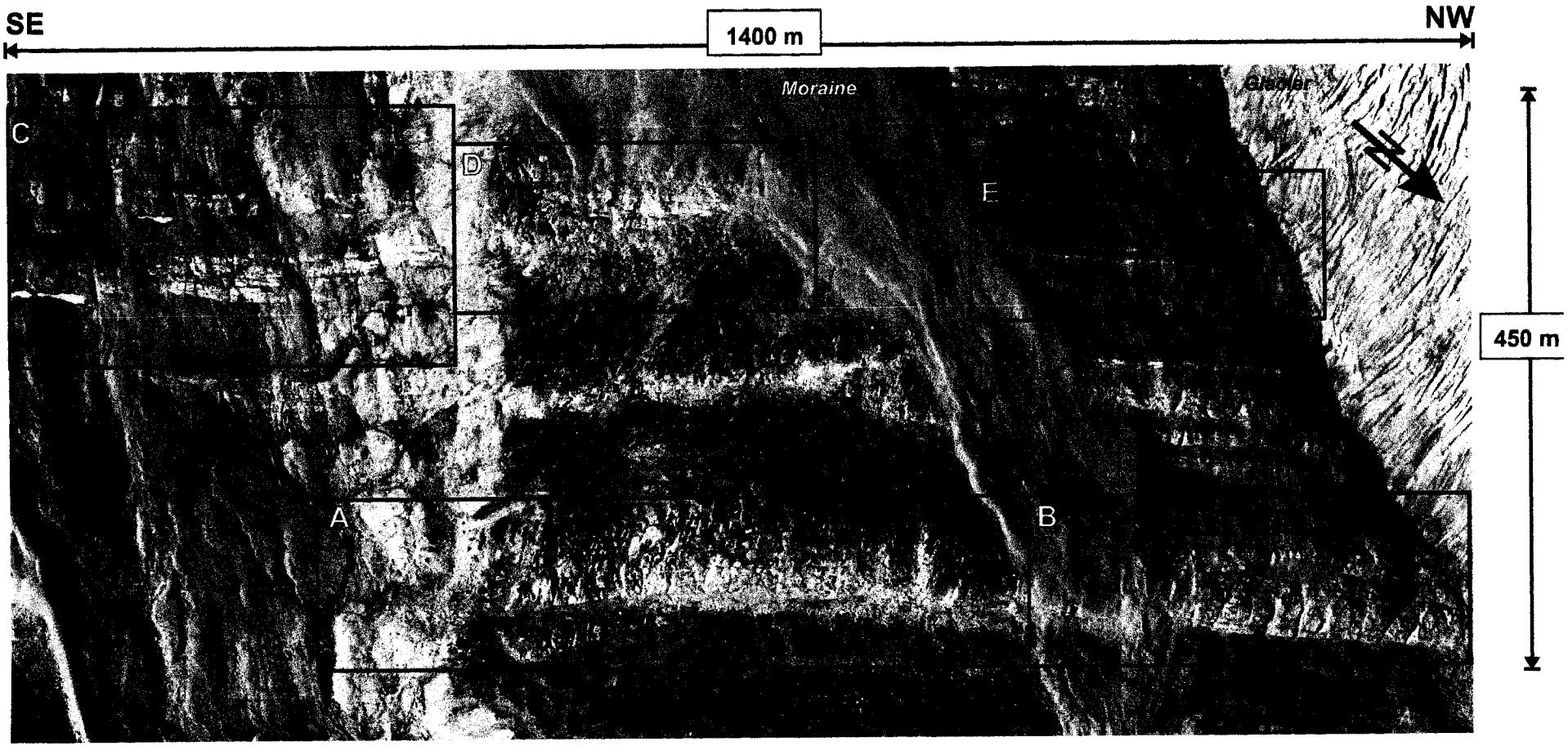

Figure I.1. Photo Index of Channel 1 and 3 in the Castle Creek South study area.

Figure I.2. Photomosaic with location of samples, logs and gamma-ray logs in (southeast) Channel 1, Castle Creek South study area. For general location see Fig. I.1.

PHOTO B

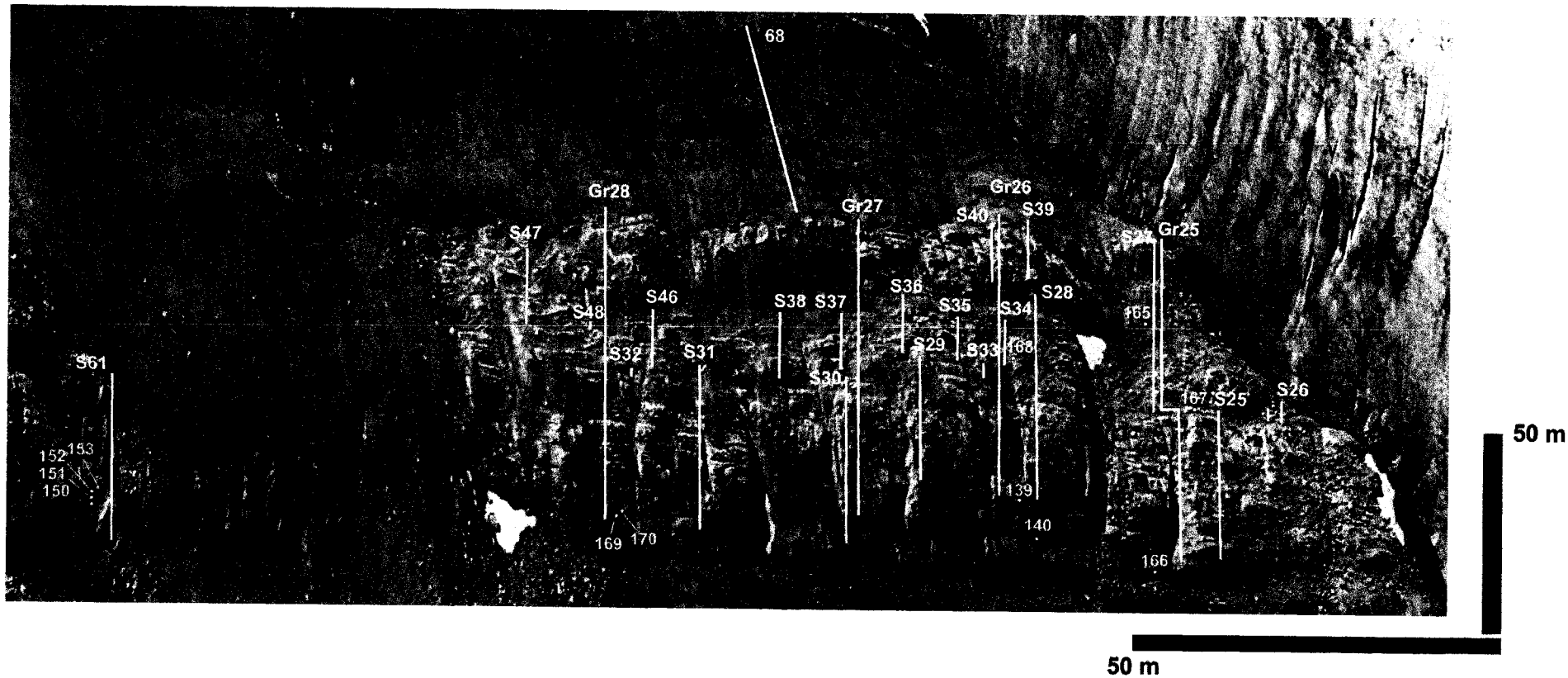

Figure I.3. Photomosaic with location of samples, logs and gamma-ray logs in (northwest) Channel 1, Castle Creek South study area. For general location see Fig. I.1.

PHOTO C

Figure I.4. Photomosaic with location of samples. logs and gamma-ray logs in (southeast) Channel 3, Castle Creek South study area. For general location see Fig. I.1.

PHOTO D

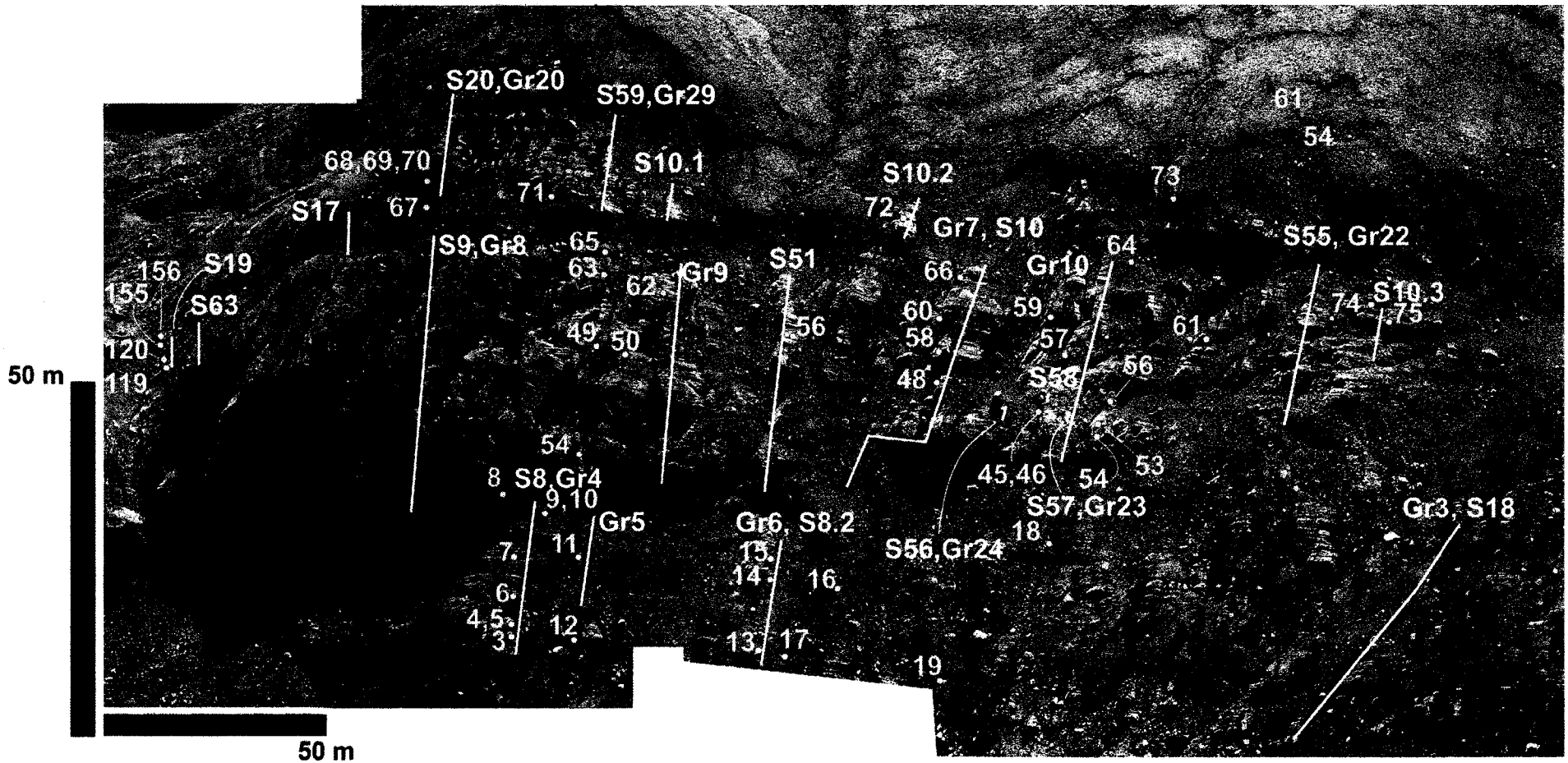

Figure I.5. Photomosaic with location of samples, logs and gamma-ray logs in (northwest) Channel 3, Castle Creek South study area. For general location see Fig. I.1.

PHOTO E

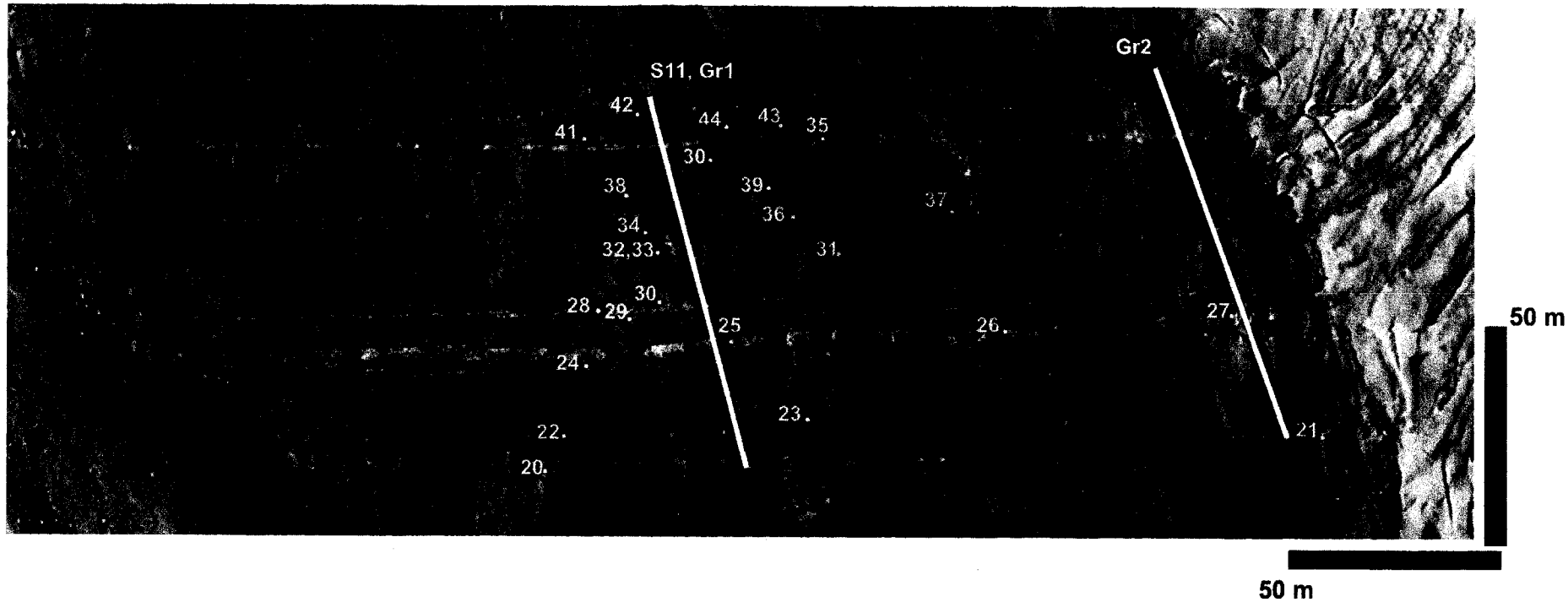

Figure I.6. Photomosaic with location of samples, logs and gamma-ray logs in (northwestern) Channel 3, Castle Creek South study area. For general location see Fig. I.1.

APPENDIX II. Petrography Data

This appendix includes textural, compositional and microstructural analysis of 38 thin-section samples of mudstone, sandstone and conglomerate and 8 samples of carbonate from Channel 1 and 3. Additionally, 13 carbonate samples from carbonate and debrite units underlying Channel 1 and 3 were studied for comparative purposes. For sample location see Appendix 1.

Grain size was classified according to the Wentworth scale (Wentworth, 1922). Visual estimates of mineral abundances and constituents were made using the chart of Scholle (2003, p. xii). Classification of sandstone and conglomerate follows the classification of Dott (1964) and Boggs (1992, p. 151), respectively.

Carbonates were classified according to Dunham (1962) and Folk (1962). Carbonate-dominated rocks (50%-75% carbonate) were described as pure carbonates with the grain size of the siliciclastic fraction added as a major modifier after the principal name (e.g., skeletal wackestone with quartz). Siliciclastic-dominated lithologies (>50%-75% siliciclastic) were described as pure siliciclastic rocks with the addition of the main carbonate constituent after the principal name (e.g., quartz siltstone with ooids).

SAMPLE ID	FACIES	LITHOLOGY	TEXTURE					GRAIN FRAMEWORK										MATRIX		CEMENT				CLASSIFICATION OF SEDIMENTARY PROTOLITH (Dott, 1964; Boggs,1992)	COMMENTS
			Grain Size (mm)			Wentworth Grain Size Classification (max., min, avg)	Sorting (*)	Quartz	K-feldspar	Plagioclase	Rock Fragments	Muscovite	Pyrite	Zircon	Tourmaline	Hematite	Chlorite	Recrystallized matrix (**)	Micrite	Quartz overgrowth	Calcite	Siderite or Fe-dolomite	Goethite		
			Maximum	Minimum	Average																				
114	F1	Sandstone	2.9	0.73	1.1	Granule, coarse sand, *very coarse sand*	m-p	65		4			1		Tz		Tz	30		Tz				Subfeldspathic arenite	Abundant monocrystalline quartz; Pervasive alteration of feldspar, forming pseudomatrix; Quartz overgrowth are rare; Matrix contain abundant fine muscovite and chlorite, and fine quartz; Abundant monocrystalline quartz
165	F1	Sandstone	4.4	0.44	1.76	Pebble, medium sand, *very coarse sand*	m-p	26		24	Tz			Tz			Tz	22			3			Feldspathic Arenite	Micrite is locally recrystallized by sparite; Deformation of plagioclase; Alteration of Plagioclase, locally to calcite; Chlorite with anomalous blue interference colors; Abundant mono- and polycrystalline quartz
167	F1	Sandstone	3.3	0.68	1.36	Granule, fine sand, *very coarse sand*	p	45		5	Tz						Tz	15	10		25			Subfeldspathic Arenite	Alteration of plagioclase, in some cases to calcite cement; Abundant monocrystalline quartz; Chloritization of shale
137	F1	Conglomerate	5	0.8	3	Pebble, very coarse sand, *granule*	m-w	60		5	Tz				Tz		Tz	35						Petromict Conglomerate	Abundant polycrystalline quartz; Cubic and framboid pyrite with goethite or hematite rims are common; Siltstone fragment is observed; Alteration of feldspar, locally forming pseudomatrix; Deformation twinning of plagioclase; Chlorite show anomalous blue interference colors; Matrix consist of fine muscovite and minor fine- to coarse-grained quartz; Pressure fringes of quartz around some grains
138	F1	Conglomerate	4.7	1.47	2.51	Pebble, very coarse sand, *granule*	m-p	48		7							Tz	20	15		2			Petromict Conglomerate	Microvein filled by quartz; Deformation of plagioclase; Alteration of Plagioclase; Chlorite with anomalous blue interference color; Micrite is locally recrystallized by sparite or blocky calcite cement
139	F1	Conglomerate	4.4	2.2	2.5	Pebble, very coarse sand, *granule*	vp	35		5	Tz		2					50			8			Petromict Conglomerate	Alteration of feldspar to fine muscovite, locally forming pseudomatrix; Calcite crystals show brownish rims of Fe-oxide (e.g. hematite), formed prior the metamorphism; Abundant polycrystalline quartz; Extensive recrystallization in the matrix; Fragment of fine sandstone is observed; Matrix consist of fine muscovite and minor fine- to coarse-grained quartz
140	F1	Normal graded conglomerate (top)	6.6	1.6	1.47	Pebble, very coarse sand, *coarse sand*	vp	42		6		Tz		Tz			2	35			15			Subfeldspathic arenite	Perthite texture of Plagioclase; Chlorite with anomalous blue interference colors; Alteration of Plagioclase; Local dolomitization; Matrix is composed of grains of quartz, feldspar, etc and recrystallized matrix (i.e. mixture of fine-to medium-grained quartz and minor muscovite and chlorite); Common metamorphic muscovite
168	F3	Cross-stratified sandstone	3.3	0.55	1.89	Granule; coarse sand; *very coarse sand*	m-w	75	2	4			1					3			15			Subfeldspathic arenite	Microvein filled by quartz; Pervasive alteration of plagioclase to calcite cement; Corrosion of quartz grains by calcite; Abundant monocrystalline, very undulatory quartz; Minute non-cubic pyrite; Sutured contacts and recrystallization around grain margins

(*) vp= very poorly sorted; p= poorly sorted, m=moderately poorly sorted, w= well sorted. (**) Recrystallized matrix= Recrystallized fine to medium quartz, and fine-grained muscovite and chlorite Tz=Traces (<1%)

Table II.1. Petrographic analysis of 8 siliciclastic rock samples from Channel 1in the Castle Creek South study area.

SAMPLE ID	FACIES	LITHOLOGY	TEXTURE					GRAIN FRAMEWORK										MATRIX		CEMENT				CLASSIFICATION OF SEDIMENTARY PROTOLITH (Dott, 1964; Boggs,1992)	COMMENTS
			Grain Size (mm)			Wentworth Grain Size Classification (max., min, avg)	Sorting (*)	Quartz	K-feldspar	Plagioclase	Rock Fragments	Muscovite	Pyrite	Zircon	Tourmaline	Hematite	Chlorite	Recrystallized matrix (**)	Micrite	Quartz overgrowth	Calcite	Siderite or Fe-dolomite	Goethite		
			Maximum	Minimum	Average																				
1	F1	Sandstone	0.88	0.36	0.68	Coarse sand, medium sand, *coarse sand*	w	68	11	6			Tz	1	Tz			10		Tz	2	2		Subfeldspathic arenite	Alteration of Feldspar; Abundant monocrystalline quartz; Perthite texture of feldspars; Longitudinal to sutured contacts; Recrystallized matrix of fine to medium quartz and minor fine muscovite and chlorite; Abundant quartz subgrain boundaries; The K-feldspar is mostly orthoclase
59	F1	Sandstone	2.9	0.15	1.5	Granule, fine sand, *very coarse sand*	m-p	53	10	10	Tz	1		1		Tz		22		3				Feldspathic arenite	Abundant monocrystalline quartz; Recrystallized matrix of fine quartz and minor fine muscovite; The K-feldspar is mostly orthoclase; Fragment of fine sandstone is observed; Matrix with abundant fine muscovite and chlorite; Pervasive alteration of Feldspar, forming pseudomatrix; Perthite texture of feldspars
71	F1	Sandstone	1.76	0.22	0.97	Very coarse sand, fine sand, *coarse sand*	w	70		15			3	Tz			Tz	20		2				Subfeldspathic Arenite	Alteration of plagioclase to fine white mica; Abundant monocrystalline quartz; Recrystallized matrix is composed muscovite and chlorite (that is locally altered to hematite) and minor and localized fine-grained quartz
73	F1	Sandstone	0.73	0.14	0.63	Coarse sand, fine sand, *coarse sand*	m	69	4	5			1	Tz			1	20						Subfeldspathic arenite	Chlorite show anomalous blue interference colors; Abundant monocrystalline quartz; Cubic and framboid pyrite are common; Matrix with abundant fine muscovite; Pervasive alteration of Feldspar, forming pseudomatrix
74	F1	Sandstone	2.2	0.36	0.38	Granule, medium sand, *medium sand*	m	50	12	10	Tz		Tz	1			1	15		2	6			Feldspathic Arenite	Perthite texture of Plagioclase; Alteration of plagioclase to fine muscovite; Micrite is recrystallized by sparite or blocky calcite cement; First-generation of quartz overgrowth are observed; Deformed feldspars; Chloritization of shale; Cubic pyrite show rims of Fe-oxides; Abundant monocrystalline quartz; Alteration of plagioclase to calcite cement; Matrix is composed of fine to coarse-grained quartz and minor muscovite
92	F1	Sandstone	2.2	0.4	0.73	Granule, medium sand, *coarse sand*	p	66	13	1		Tz						23	5	Tz	2			Subfeldspathic Arenite	Deformation of muscovite; Perthite texture of Plagioclase; Alteration of plagioclase; Abundant monocrystalline quartz
93	F1	Sandstone	4.4	0.22	0.88	Pebble, fine sand, *coarse sand*	vp	61	18	2	Tz		1		Tz			15	2	1				Feldspathic Arenite	Fragment of fine-grained sandstone; Perthite texture of Plagioclase; Cubic pyrite; Alteration of plagioclase to fine muscovite, forming pseudomatrix; Deformation twinning of plagioclase; Chlorite show anomalous blue interference colors
98	F1	Sandstone	1.1	0.28	0.55	Very coarse sand, medium sand, *coarse sand*	m	70	9	2			Tz					10	2		7			Subfeldspathic Arenite	Recrystallized matrix is composed of abundant fine quartz and minor fine white mica (e.g. muscovite); Perthite texture of Plagioclase; Alteration of Plagioclase to fine muscovite; Abundant monocrystalline quartz; Recrystallization of primary micrite to sparite or blocky calcite cement

(*) vp= very poorly sorted; p= poorly sorted, m=moderately poorly sorted, w= well sorted. Tz=Traces (<1%) (**) Recrystallized matrix= Recrystallized fine to medium quartz, and fine-grained muscovite and chlorite

Table II.2. Petrographic analysis of 30 samples of siliciclastic rocks from Channel 3 in the Castle Creek study area.

...Continuation

SAMPLE ID	FACIES	LITHOLOGY	TEXTURE					GRAIN FRAMEWORK										MATRIX		CEMENT				CLASSIFICATION OF SEDIMENTARY PROTOLITH (Dott, 1964; Boggs, 1992)	COMMENTS
			Grain Size (mm)			Wentworth Grain Size Classification (max., min, avg)	Sorting (*)	Quartz	K-feldspar	Plagioclase	Rock Fragments	Muscovite	Pyrite	Zircon	Tourmaline	Hematite	Chlorite	Recrystallized matrix (**)	Micrite	Quartz overgrowth	Calcite	Siderite or Fe-dolomite	Goethite		
			Maximum	Minimum	Average																				
100	F1	Sandstone	2.7	0.9	1.95	Granule, coarse sand, *very coarse sandstone*	m	48	1	10			1					35	5		1	Tz		Subfeldspathic Arenite	Alteration of plagioclase to microcrystalline calcite, and minute crystals of brownish Fe-dolomite or siderite
106	F1	Sandstone	1.1	0.18	0.63	Very coarse sand, fine sand, *coarse sand*	m-p	48	12	10			Tz	Tz				30			3	2		Feldspathic Arenite	Pervasive sutured grain boundaries enclosing neoblasts; Microcline with typical tartan twin; Some feldspars show deformation and folded twins; Cubic pyrite; Alteration of plagioclase to fine muscovite, forming pseudomatrix; Perthite texture of Plagioclase; Abundant monocrystalline quartz
110	F1	Sandstone	1.1	0.55	1.3	Very coarse sand, coarse sand, *very coarse sand*	m-p	70	7	2			Tz	Tz			Tz	20		Tz				Subfeldspathic Arenite	Abundant mono- and polycrystalline quartz; Chlorite with anomalous blue interference colors; Alteration of plagioclase to fine muscovite; Perthite texture of Plagioclase; Recrystallized matrix is composed fine-grained quartz and minor muscovite
117	F1	Sandstone	2.1	0.4	0.73	Granule, medium sand, *coarse sand*	vp	47	25	2					Tz			20	3			3		Feldspathic Arenite	Presence of minute crystals of brownish Fe-dolomite or siderite; Cubic pyrite are observed; Alteration of plagioclase to fine muscovite; Microvein filled by quartz; Abundant monocrystalline quartz
128	F1	Sandstone	1.1	2.2	1.46	Very coarse sand, medium sand, *very coarse sand*	w-m	56	10	4				Tz				16	10	1	3			Feldspathic Arenite	Recrystallized matrix is composed fine-grained quartz and minor muscovite and chlorite; Chlorite with anomalous blue interference colors; Alteration of plagioclase to fine muscovite, forming pseudomatrix; Perthite texture of Plagioclase; Abundant monocrystalline quartz Microvein filled by quartz; Cubic pyrite are observed; Alteration of plagioclase; Deformation twinning of plagioclase; Pervasive sutured quartz grain boundaries
129	F1	Sandstone	0.55	0.15	0.44	Coarse sand, fine sand, *medium sand*	m	68	10	5		2	1					15						Subfeldspathic Arenite	
132	F1	Sandstone	1.26	0.31	0.88	Very coarse sand, medium sand, *coarse sand*	m	44	10	4			Tz	1			1	40						Feldspathic Arenite	Perthite texture of Plagioclase; Alteration of plagioclase to fine muscovite; Cubic pyrite is observed; Chlorite with anomalous blue interference colors; Abundant monocrystalline quartz
133	F1	Sandstone	1.1	0.18	0.55	Very coarse sand, fine sand, *coarse sand*	m-p	41	20	3				Tz			1	35						Feldspathic Arenite	Abundant monocrystalline quartz; Chlorite show anomalous blue interference colors; Alteration of plagioclase to fine muscovite, forming pseudomatrix; Perthite texture of Plagioclase
154	F1	Sandstone	2.2	0.37	1.76	Granule, medium sand, *very coarse sand*	m-p	55		10			Tz	Tz				22	23		13			Subfeldspathic Arenite	Alteration of Plagioclase, in some cases to calcite; Calcite is partially replaced Fe-dolomite; Abundant monocrystalline quartz; Cubic pyrite are common

...Continuation

SAMPLE ID	FACIES	LITHOLOGY	TEXTURE: Grain Size (mm) Maximum	Minimum	Average	Wentworth Grain Size Classification (max., min, *avg*)	Sorting (*)	GRAIN FRAMEWORK: Quartz	K-feldspar	Plagioclase	Rock Fragments	Muscovite	Pyrite	Zircon	Tourmaline	Hematite	Chlorite	MATRIX: Recrystallized matrix (**)	Micrite	CEMENT: Quartz overgrowth	Calcite	Siderite or Fe-dolomite	Goethite	CLASSIFICATION OF SEDIMENTARY PROTOLITH (Dott, 1964; Boggs,1992)	COMMENTS
157	F1	Sandstone	2.5	0.36	0.44	Granule, fine sand, medium sand	vp	47	15	3				Tz			Tz	30				5		Feldspathic Arenite	Alteration of Plagioclase to minute crystals of brownish Fe-dolomite or siderite; Perthite texture of Plagioclase; Cubic pyrite are observed; Abundant monocrystalline quartz and common polycrystalline quartz
159	F1	Sandstone	2.2	0.18	0.25	Granule, fine sand, *medium sand*	w	45	1	12	Tz	1	1		Tz			40						Subfeldspathic Arenite	Obvious preferred mineral orientation; Abundant monocrystalline quartz; Cubic and framboid pyrite with goethite or hematite rims are common; Fragment of siltstone; Alteration of Feldspar, forming pseudomatrix; Matrix contain fine muscovite, and minor quartz and chlorite
160	F1	Sandstone	2.2	0.11	0.55	Very coarse sand, fine sand, *coarse sand*	vp	52	7	1					Tz			40						Subfeldspathic Arenite	Chlorite show anomalous blue interference colors; Abundant monocrystalline quartz; Cubic pyrite are observed; Alteration of plagioclase to fine muscovite, forming pseudomatrix; Perthite texture of Plagioclase
161	F1	Sandstone	2.93	0.49	1.47	Very coarse sand, medium sand, *very coarse sand*	o-m	50		20			Tz	Tz				26	4					Feldspathic Arenite	Alteration of Plagioclase to fine white mica; Micrite is locally replaced by minute; Crystals of brownish Fe-dolomite; Abundant monocrystalline quartz; Cubic pyrite are common; Microvein filled by quartz; Orientation of minerals; Matrix contain mostly of recrystallized fine quartz
162	F1	Sandstone	0.55	0.18	0.36	Coarse sand, fine sand, *medium sand*	w	61	6	2			1					10			20			Subfeldspathic Arenite	Corrosion of quartz and feldspar grains by calcite; Alteration of plagioclase to fine white mica, forming pseudomatrix; Some feldspars show deformation and folded twins; Pervasive sutured contacts and subgrains and neoblasts in the grain contacts; Abundant monocrystalline quartz; Recrystallized matrix is composed medium-grained quartz and minor muscovite; Cubic pyrite
90	F1	Conglomerate	8	0.44	6	Pebble, medium sand, *pebble*	Vp	66	3	5	Tz		2				2	10	10		2			Petromict Conglomerate	Chloritization of shale; Abundant polycrystallin quartz; Cubic pyrite are common, and they hav been altered to goethite or hematite; Perthite textur of feldspar; Chlorite shows anomalous blu interference colors; Micrite is recrystallized b calcite cement; Pervasive alteration of feldspa forming pseudomatrix; Some feldspar are altered t minute rhombic crystals of dolomite or ankerite
91	F1	Conglomerate (top)	7	1.1	1.2	Pebble, very coarse sand, *very coarse sand*	p	43	7	3				1				40	4	Tz	2			Subfeldspathic Arenite	Deformed feldspars; Abundant polycrystalline quartz; Pervasive alteration of plagioclase; Perthite texture of Plagioclase; Micrite is recrystallized by sparite or blocky calcite cement; Matrix is composed of up to coarse-sand grains of quartz, feldspar, etc; Recrystallized matrix (i.e. mixture of fine-to medium-grained quartz and minor muscovite and chlorite)

...Continuation

SAMPLE ID	FACIES	LITHOLOGY	TEXTURE: Grain Size (mm) Maximum	Minimum	Average	Wentworth Grain Size Classification (max., min, avg)	Sorting (*)	GRAIN FRAMEWORK: Quartz	K-feldspar	Plagioclase	Rock Fragments	Muscovite	Pyrite	Zircon	Tourmaline	Hematite	Chlorite	MATRIX: Recrystallized matrix (**)	Micrite	CEMENT: Quartz overgrowth	Calcite	Siderite or Fe-dolomite	Goethite	CLASSIFICATION OF SEDIMENTARY PROTOLITH (Dott, 1964; Boggs,1992)	COMMENTS
101	F2.1	Mudstone-clast breccia (matrix)	5	0.35	3.3	Pebble, medium sand, *granule*	vp	59	2	9			2					30						Subfeldspathic Arenite	Pressure fringes around some grains; Common polycrystalline quartz; Alteration of Plagioclase; Orientation of minerals; Perthite texture of Plagioclase; Cubic pyrite are common; Matrix is an assemblage of predominant muscovite, and recrystallized fine quartz
70	F2.2	Mudstone-clast breccia (matrix)	4.5	0.07	0.73	Pebble; very fine sand; *coarse sand*	vp	64	1		<1	1	1	<1				21					12	Subfeldspathic arenite	Alteration of plagioclase to a) clay minerals, creating pseudomatrix, and b) minute crystals of brownish Fe-dolomite or siderite; Goethite as a alteration product by oxidation of pyrite; Rock fragment of siltstone; Common polycrystalline quartz.; Large mudstone clast composed mostly of very fine- to fine- grained quartz grains, and clay minerals; Interpenetration of coarse quartz grains along the short-side margin of a large mudstone clast; Cubic pyrite are common; Large mudstone clast is composed of clay minerals and silt quartz; Mudstone clast show sub-vertical fracture, in which authigenic clay minerals and iron oxides (relatively non-luminescent, or darker brown) precipitated after fracturing plus accumulations of relatively insoluble silicate minerals, including feldspars and remnants of quartz grains; Abundant monocrystalline quartz; Some feldspar grains show strong deformation twins
45	F4	Structureless sandstone	0.22	0.05	0.09	Fine sand; coarse silt; *very fine sand*	w	66	1	1		1	1					30						Subfeldspathic arenite	Cubic pyrite with rims of goethite; Deformed detrital muscovite; Localized concentration of matrix; Alteration of plagioclase, creating pseudomatrix
49	F4	Cross-laminated sandstone	0.6	0.05	0.07	Coarse sand; coarse silt; *very fine sand*	m-p	54	3	1			2					40						Subfeldspathic arenite	Non-cubic pyrite that has been altered to goethite; Alteration of plagioclase to clay mineral (fine muscovite), creating pseudomatrix
105	F4	Sandstone	1.1	0.44	0.33	Very coarse sand, medium sand, *medium sand*	m-w	72	5	3				1				12		3	4			Subfeldspathic Arenite	Pervasive alteration of plagioclase to fine-grained muscovite, forming pseudomatrix; Alteration of plagioclase to calcite cement that show rims of Fe-oxides in the crystals; Matrix is composed of fine-grained quartz and minor muscovite; Abundant monocrystalline quartz; Cubic pyrite with rims of Fe-oxides
119	F4	Sandstone	4.4	2.2	1.76	Granule, very coarse sand, *very coarse sand*	m	57		3		Tz					Tz	10	30					Subfeldspathic Arenite	Chlorite with anomalous blue interference colors; Micrite is replaced by fine- medium-crystalline dolomite; Dissolution of dolomite and later precipitation of calcite cement in the resultant pore space; Alteration of plagioclase; Abundant mono- and polycrystalline quartz; Recrystallized matrix is composed fine-grained quartz and minor muscovite

SAMPLE ID	FACIES	LITHOLOGY	CARBONATE GRAIN		CARBONATE MATRIX			CEMENT			TERRIGENOUSGRAINS						AUTHIGENIC COMPONENTS				ESTIMATED AVERAGE CRYSTAL-SIZE	CLASSIFICATION OF SEDIMENTARY PROTOLITH (Folk,1962; Dunham,1962)	COMMENTS
			Ooid	Peloid	Micrite	Microspar	Pseudospar	Spar	Dolomite	Quartz	K-feldspar	Plagioclase	Pyrite	Muscovite	Zircon	Tourmaline	Quartz	Chert	Feldspar	Muscovite			
102	F1	Carbonate-clast Conglomerate				5	9	40		15	1	10					20				Microspar: 22 μm Pseudospar: 44 -50 μm Spar: 50-220 μm Recrystallized matrix: <43 μm	Sparite, Crystalline carbonate	Neomorphism of micrite matrix to microspar, pseudospar and spar; Alteration of feldspar; Abundant authigenic quartz is filling elongated and apparently aligned pore space; Uncommon grain of microcline; Rare authigenic feldspar; Corrosion and dissolution of quartz grains; Fractures filled with calcite and most commonly with quartz
107	F1	Carbonate-clast Conglomerate	57			10	9	8	12	2							2				Microspar(inside ooids):11-12 μm Spar (inside ooids): 35-50 μm	Oomicrite, Ooid Packestone	Neomorphism of ooidal micrite to microspar and pseudospar; Abundant ooids and composite ooids; Replacement of ooids with quartz; Dolomitization of grains; Fractures filled with calcite and later replaced by quartz
108	F1	Carbonate-clast Conglomerate				92				4			2				2				Microspar: 18 μm	Microsparite, Mudstone	Fabric entirely obliterated by recrystallization of micrite to microspar; Presence of irregular, elongated pores filled with micrite, that was later on recrystallized by microspar or replaced partially by dolomite; Fractures filled with calcite and replaced afterward by quartz
111	F1	Carbonate-clast Conglomerate	70			20		5		5											Microspar matrix: 7-9 μm Microspar (inside ooids): 15 μm Spar: >75 μm	Oomicrite, Packestone	Examples of probable former ooids that have been micritized. Their micritic cortical fabric show only traces of preserved concentric structure; Recrystallization of ooidal micrite to microspar, specially in the nucleus; Neomorphism of micrite matrix to microspar; Unconnected pores that have been partially or completely filled with multiple generation of cements; Fractures filled with calcite and later replaced by quartz, specially along fracture walls.
125	F1	Carbonate-clast Conglomerate	1	2		12		40		40		5	Tz								Microspar: 16 μm Pseudospar: 80 μm	Sparite with quartz, Crystalline carbonate with quartz	Microfractures filled with calcite and quartz
127	F1	Carbonate-clast Conglomerate	57			10			28	5											Matrix: 8-11 μm Spar (inside ooids): 31-65 μm	Oomicrite, Ooid Packestone	Recrystallization of ooids to pseudospar. Commonly, micritic nucleus is still preserved; Neomorphism of micrite matrix to microspar; Fractures filled with calcite/dolomite and later replaced by quartz; Dolomitization of grains
158	F1	Carbonate-clast Conglomerate		15		35		20	8	3	Tz	2		Tz		Tz	16	Tz	Tz	1	Microspar: 17 μm Spar: 73 -110 μm Dolomite: 73 μm	Pelmicrite, Peloid Wackestone	Recrystallization (Neomorphism) of micrite matrix to microspar; Quartz grain are in average medium sand (0.55 mm); Replacement of medium crystalline dolomite in a micrite, forming a dolomitization front observed at the corner of the thin section; Corrosion and dissolution of quartz grains; Authigenic quartz is replacing microspar and/or filling pore space; Carbonate grains are in average 0.3 mm; Fractures filled with quartz
164	F1	Carbonate-clast Conglomerate				15		3	80	2											Microspar 12-22 μm Dolomite: 37-55 μm	Finely crystalline dolomite, Crystalline dolomite	Microspar formed by recrystallization of matrix; Partial dolomitization of matrix; Fractures filled with blocky calcite cement, that was replaced by quartz and muscovite; Patches of spar cements

Table II.3. Petrographic analysis of 8 carbonate-clasts samples from Channel 1 and 3 in the Castle Creek South study area.

SAMPLE ID	LITHOLOGY	CARBONATE GRAIN		CARBONATE MATRIX			CEMENT		TERRIGENOUSGRAINS							AUTHIGENIC COMPONENTS				ESTIMATED AVERAGE CRYSTAL-SIZE	CLASSIFICATION OF SEDIMENTARY PROTOLITH (Folk,1962; Dunham, 1962)	COMMENTS
		Ooid	Peloid	Micrite	Microspar	Pseudospar	Spar	Dolomite	Quartz	K-feldspar	Plagioclase	Pyrite	Muscovite	Zircon	Tourmaline	Quartz	Chert	Feldspar	Muscovite			
76	Carbonate-clast Debrite				5		5	88				Tz	Tz				2			Dolomite (matrix): 28-35 μm Dolomite (pores): 50-190 μm	Finely crystalline dolomite, Crystalline dolomite	Total dolomitization has masked the original texture; Two distinct types of dolomites: a finely crystalline dolomite that replaced the micritic matrix and a coarse to very coarse crystalline dolomite that replace micritic patches (apparently filling pores).; Microfractures filled with calcite, that locally has been replaced by quartz.; Coarse-grained dolomite shows zonation
77	Carbonate-clast Debrite				100															Microspar: 10-15 μm Pseudospar: 30-40 μm	Microbial Biolithite, Microbial Boundstone	Microbial-like fabric, showing layers of micrite (recrystallized to microspar or pseudospar) interbedded with layers of irregular, elongated cavities filled with micrite
78	Carbonate-clast Debrite			5				95	Tz											Dolomite (matrix): 32 μm Dolomite (pores): 62-110 μm	Finely crystalline dolomite, Crystalline dolomite	Total dolomitization has masked the original texture; Two distinct types of dolomites: a finely crystalline dolomite that replaced the micritic matrix and a coarse crystalline dolomite that replace micritic patches (apparently filling pores); Microfractures filled with calcite
79	Carbonate-clast Debrite						57	20									23			Spar: 157-275 μm	Sparite, Crystalline carbonate	Microfractures filled with calcite; Zoning in dolomite; Blocky calcite
80	Carbonate-clast Debrite				100							Tz					Tz			Microspar: 14-28 μm	Microsparite, Mudstone	Neomorphism of the micrite matrix to microspar to pseudospar; Microfractures filled with quartz
82	Carbonate-clast Debrite				98				2											Microspar: 4-10 μm	Microsparite, Mudstone	Recrystallization of the micrite to microspar; Presence of pressure-solution structures, such as stylolite; Common microfractures filled by calcite, that also were replaced by quartz or chert
83	Carbonate-clast Debrite				97							Tz					3			Microspar: 13-18 μm	Microsparite, Mudstone	Complete recrystallization of micrite to microspar; Common microfractures filled by calcite, that also were replaced by quartz
85	Carbonate-clast Debrite				15			55	30		Tz	Tz								Dolomite: 20-37 μm	Finely crystalline dolomite with quartz, Crystalline dolomite with quartz	Matrix mostly replaced by finely crystalline dolomite; Microspar formed by neomorphism of micritic matrix
109	Carbonate-clast Debrite				98				2											Microspar: 15-25 μm	Microbial Biolithite, Microbial Boundstone	Microbial-like structure consist of layers of micrite (recrystallized to microspar) interbedded with layers of irregular, elongated pores filled with micrite, that was later replaced by finely crystalline dolomite.
116	Carbonate-clast Debrite				76	23			1											Microspar: 8-25 μm Pseudospar: 40-60 μm	Microbial Biolithite, Microbial Boundstone	Microbial-like fabric showing layers of micrite (recrystallized to microspar or pseudospar) interbedded with layers of irregular, elongated cavities filled with micrite

Table II.4. Petrographic analysis of 10 carbonate-clast samples from debrite unit that underlies Channel 3 in the Castle Creek South study area.

PHOTOMICROGRAPHS

FACIES 1, SANDSTONE AND CONGLOMERATE

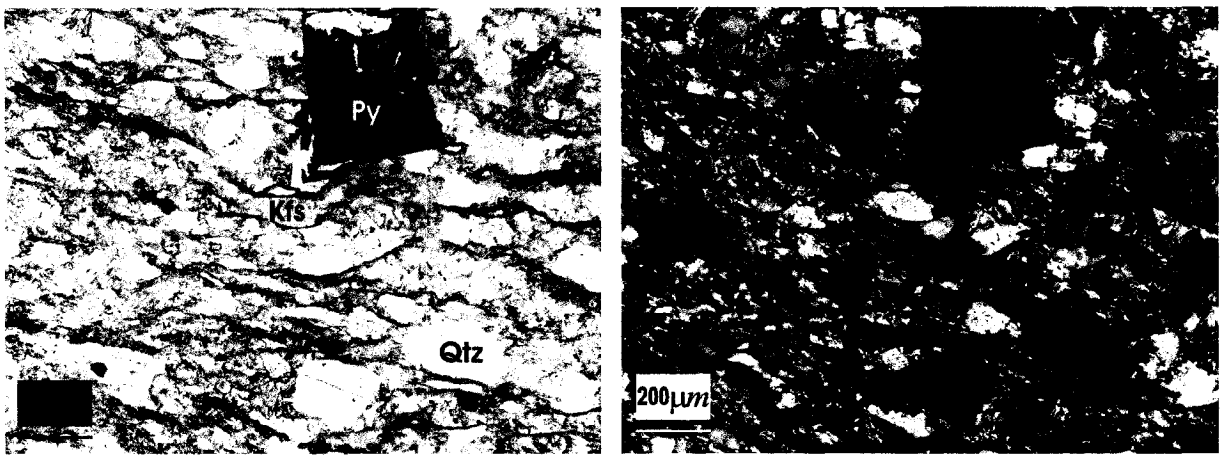

Figure II.1. Feldspathic arenite of facies F1, showing abundant recrystallized matrix of muscovite, chlorite, and fine-grained quartz. Monocrystalline quartz grains (Qtz) is the most common detrital constituent. Altered K-feldspar (Kfs) are also common. Fractured cubic pyrite (Py) with quartz between fragments and around the grain (arrow). Left photo, plane-polarized light. Right photo, same view under crossed polars.

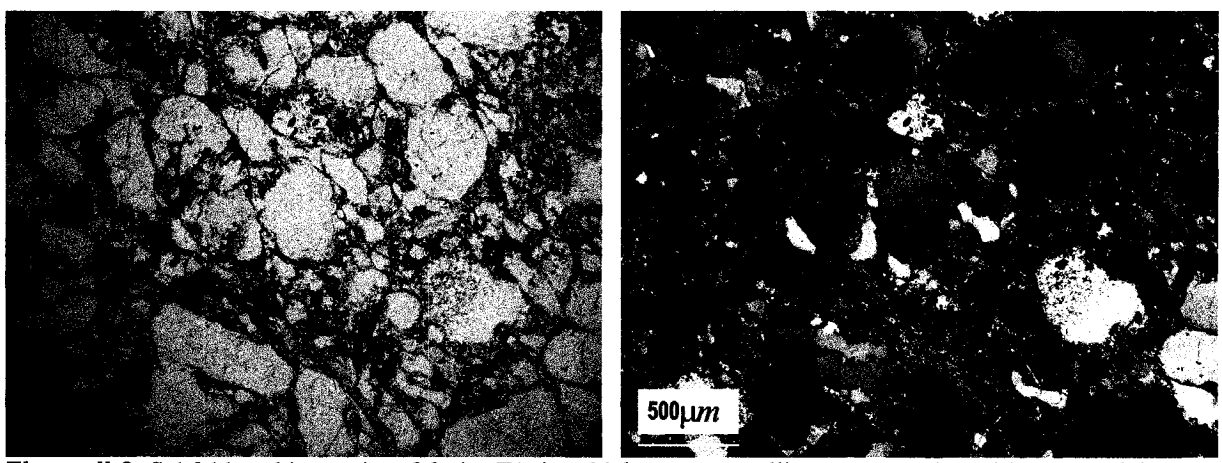

Figure II.2. Subfeldspathic arenite of facies F1, in which monocrystalline quartz grains with very undulatory extinction are more abundant. The recrystallized matrix is a mixture of fine-grained muscovite, chlorite. Authigenic muscovite are common. Dispersed pyrite framboids (black in left photo) are generally present. Left photo, plane-polarized light. Right photo, same view under crossed polars.

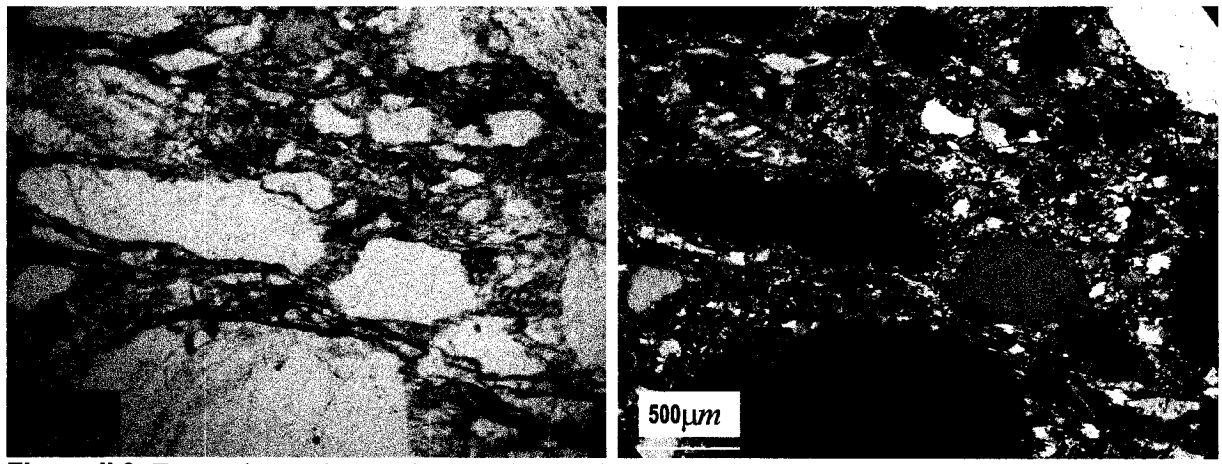

Figure II.3. Extremely poorly sorted, petromict conglomerate (Facies F1). Monocrystalline quartz clasts are pebble and granule size. Matrix is composed of coarse-sand grains of quartz and feldspar embedded in a recrystallized mixture of fine-grained quartz, muscovite and chlorite. Left photo, plane-polarized light. Right photo, same view under crossed polars.

Figure II.4. Perthitic feldspar in feldspathic arenite (facies F1). The light grey streaks in this photomicrograph are plagioclase exsolution lamellae in dark grey K-feldspar. Additionally, this grain shows evidence of deformation. Matrix is composed of fine-grained, dynamically recrystallized quartz neoblasts. Left photo, plane-polarized light. Right photo, same view under crossed polars.

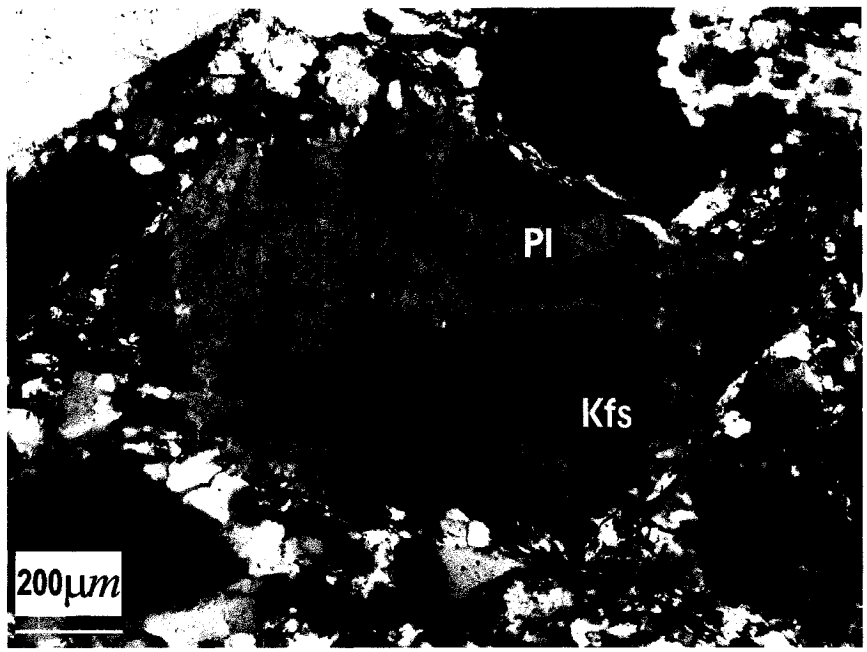

Figure II.5. Feldspar grain with perthite intergrowth in a subfeldspathic arenite (facies F1), exhibiting lamellae of plagioclase (Pl, light grey) in microcline (Kfs, dark grey). Microcline shows distinctive cross-hatched or tartan twinning. The plagioclase (probably albite) is "dirty" or "cloudy", owing to fine-grained alteration products (mainly clay minerals or white mica). The grain is surrounded by elongated aggregates of fine to medium recrystallized quartz, and muscovite. Crossed polars.

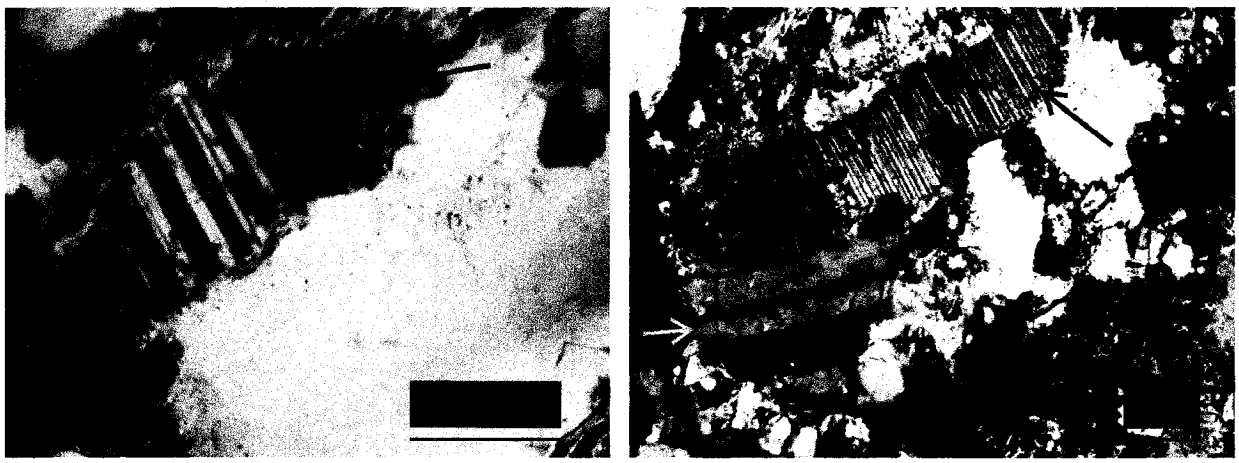

Figure II.6. Fragmented and altered plagioclase in a subfeldspathic arenite (facies F1). Left photo, plagioclase feldspar grain with multiple twinning that shows brittle deformation. The grain has been broken into fragments, which subsequently have been slightly deformed (arrow). Alteration halo of recrystallized, fine-grained muscovite envelopes the plagioclase grains. Right photo, a large grain of plagioclase with complex twinning that show albite twins (light grey, short arrow) that is combined at more or less regular intervals with pericline twins (dark to medium grey, long arrow). Plagioclase has been fractured and altered to calcite. Crossed polars.

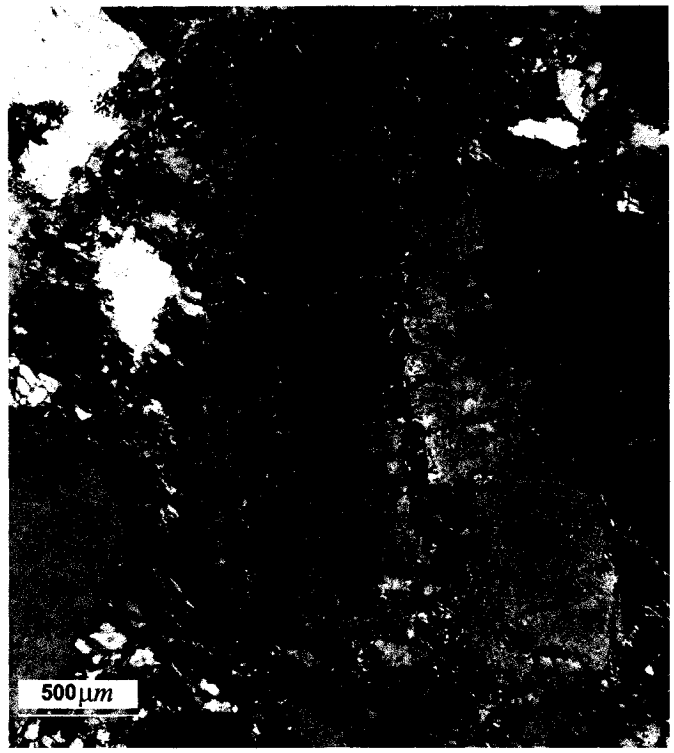

Figure II.7. Fragmented plagioclase in feldspathic arenite (facies F1). This large (pebble size) plagioclase grain shows microfractures and patchy alteration along exsolution lamellae. The highly birefringent, fine-grained alteration product is white mica, specifically muscovite. Crossed polars.

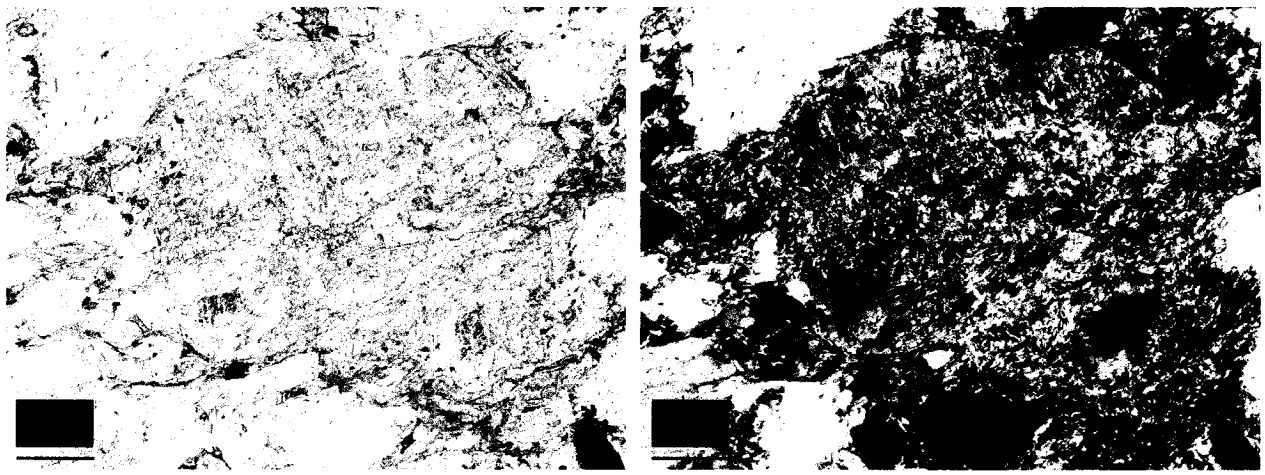

Figure II.8. A feldspar grain in the matrix of a petromict conglomerate (facies F1), which has been largely replaced by fine-grained white mica (muscovite). This grain is in a very advanced stage of alteration. The most common product of altered feldspars is the formation of pseudomatrix. Left photo, plane-polarized light. Right photo, same view under crossed polars.

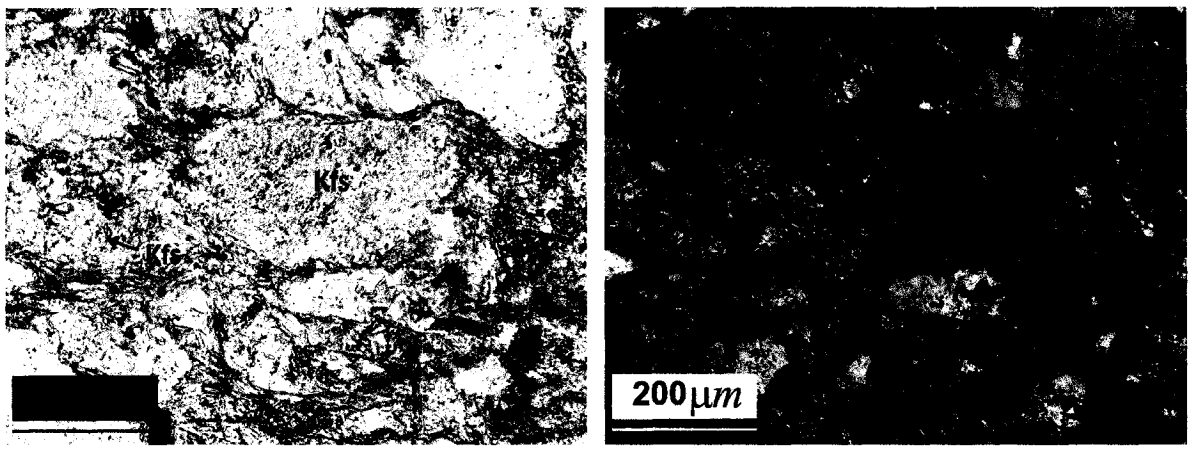

Figure II.9. Pseudomatrix in feldspathic arenite of facies F1. Psedudomatrix is the product of deformed, (partially or completely) altered and recrystallized feldspar grains. Commonly, relics of the feldspar grains (arrow) embedded with the matrix can be distinguished. Left photo, plane-polarized light. Right photo, same view under crossed polars.

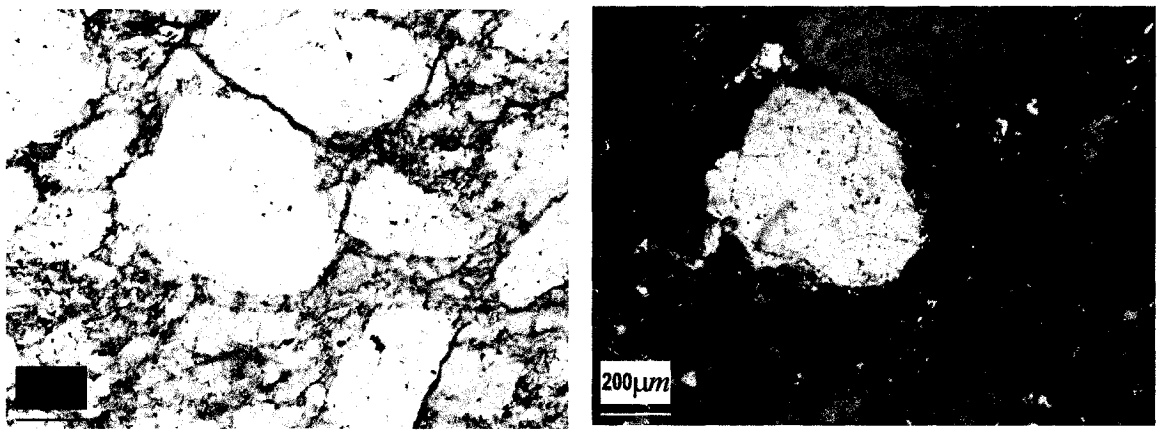

Figure II.10. Quartz overgrowth in petromict conglomerate (Facies F1). Some quartz grains show secondary overgrowth (forming a quartz cement, with dusty-looking inclusions) in optical continuity with the grain. Matrix is commonly a mixture of fine-grained quartz, muscovite and chlorite. Left photo, plane-polarized light. Right photo, same view under crossed polars.

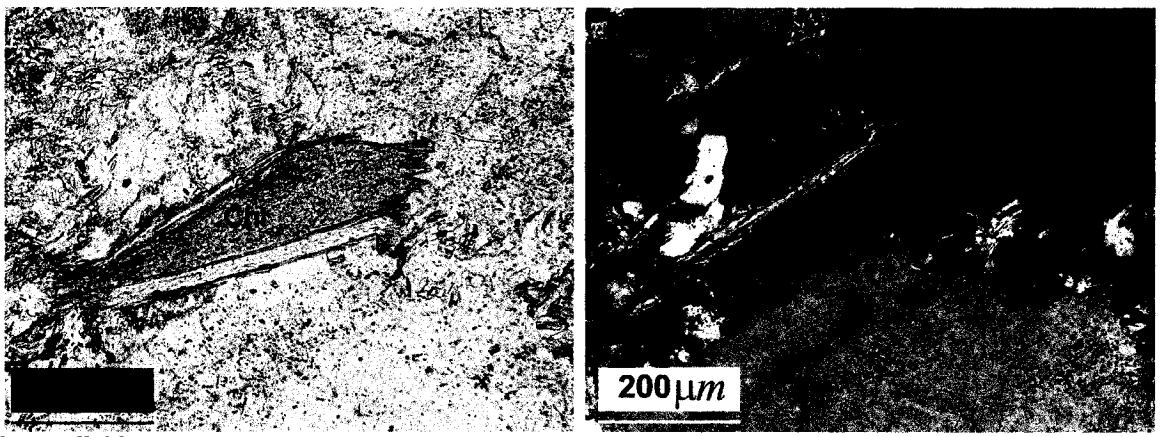

Figure II.11. Deformed chloritized grain (possibly shale) in a subfeldspathic arenite (facies F1), in which chlorite shows anomalous blue interference colors. Left photo, plane-polarized light. Right photo, same view under crossed polars.

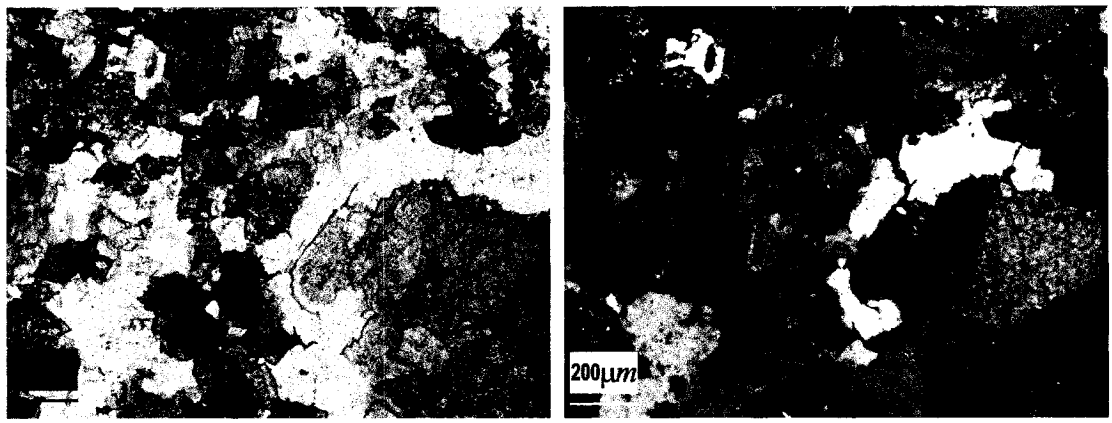

Figure II.12. Pore-filling carbonate cement in feldspathic arenite (facies F1). Plagioclase grains are locally replaced by calcite, showing scattered remnants of the original grain. Quartz corrosion is commonly observed. Left photo, plane-polarized light. Right photo, same view under crossed polars.

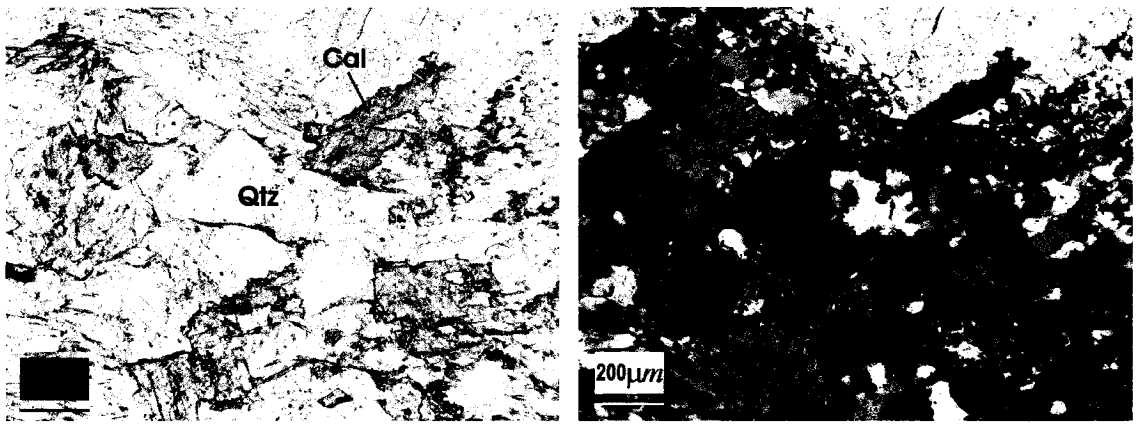

Figure II.13. Calcite cementation in a petromict conglomerate (facies F1). Polycrystalline quartz (Qtz) clasts with very undulose extinction are abundant in these strata. The blocky calcite (Cal) cement generally corroded and replaced quartz and feldspar clasts. Left photo, plane-polarized light. Right photo, same view under crossed polars.

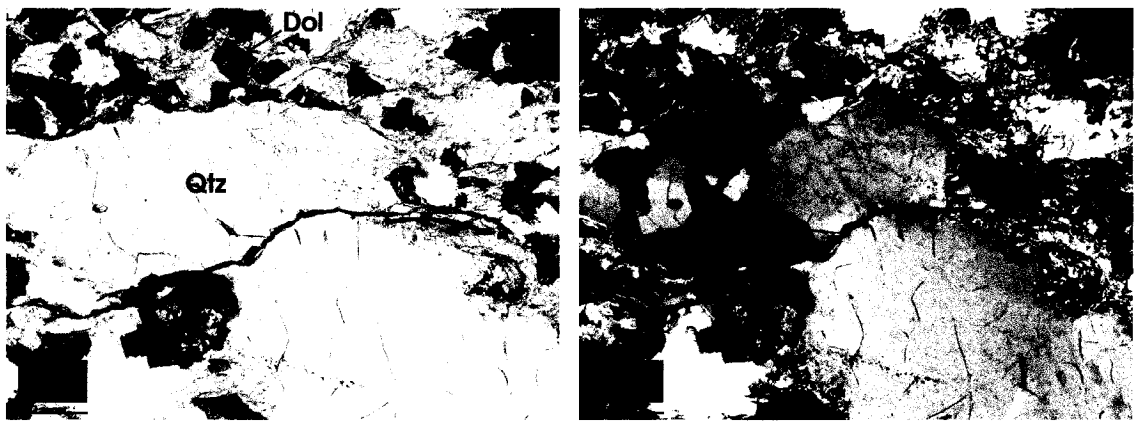

Figure II.14. Dolomitization of interstitial matrix and/or cement in a subfeldspathic arenite (facies F1). Polycrystalline quartz (Qtz) are relatively common in these sandstone. The dark brown color of euhedral dolomite crystals might indicate that they are iron-rich. Left photo, plane-polarized light. Right photo, same view under crossed polars.

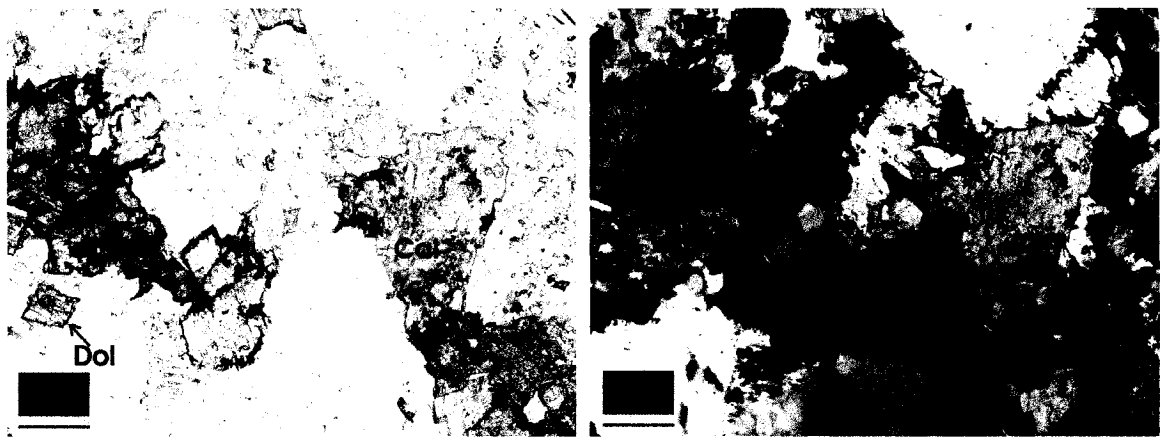

Figure II.15. Dedolomitisation in a subfeldspathic arenite (facies F1). Some euhedral authigenic dolomite crystals were dissolved and the resultant pore space filled by calcite. Left photo, plane-polarized light. Right photo, same view under crossed polars.

CARBONATE CLASTS, FACIES 1

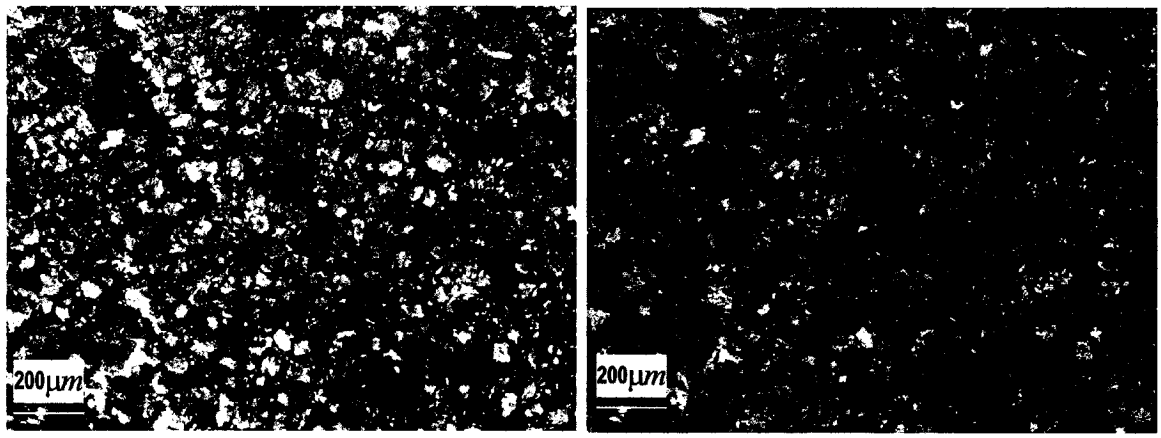

Figure II.16. Dolomitization in carbonate-clast conglomerate (facies F1). Micritic matrix has been completely dolomitized forming medium crystalline dolomite crystals. Left photo, plane-polarized light. Right photo, same view under crossed polars.

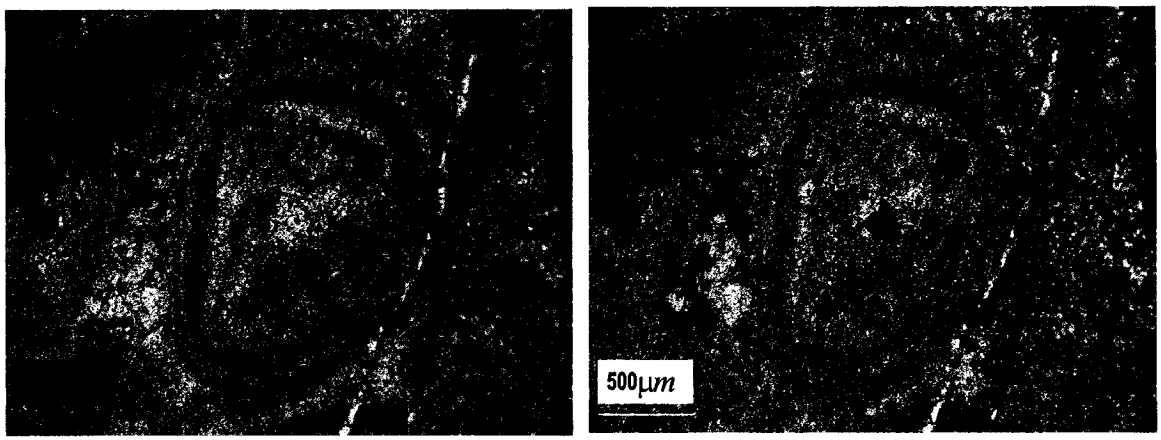

Figure II.17. Ooid grain in a carbonate-clast conglomerate (facies F1). The ooid shows multiple concentric layers corresponding to the original aragonitic coating that has been micritised (to microspar). The original interlayers formed by algal activity have been removed. This resulted in a gravitational collapse of the remaining cores within this grain, forming this rare internal fabric. The collapse was followed by infill with calcite cement of the moldic pores (pseudospar to spar size). Furthermore, interparticle pores were produced by the partial dissolution of the micritic matrix. These pores were later fully cemented by blocky calcite spar. Left photo, plane-polarized light. Right photo, same view under crossed polars.

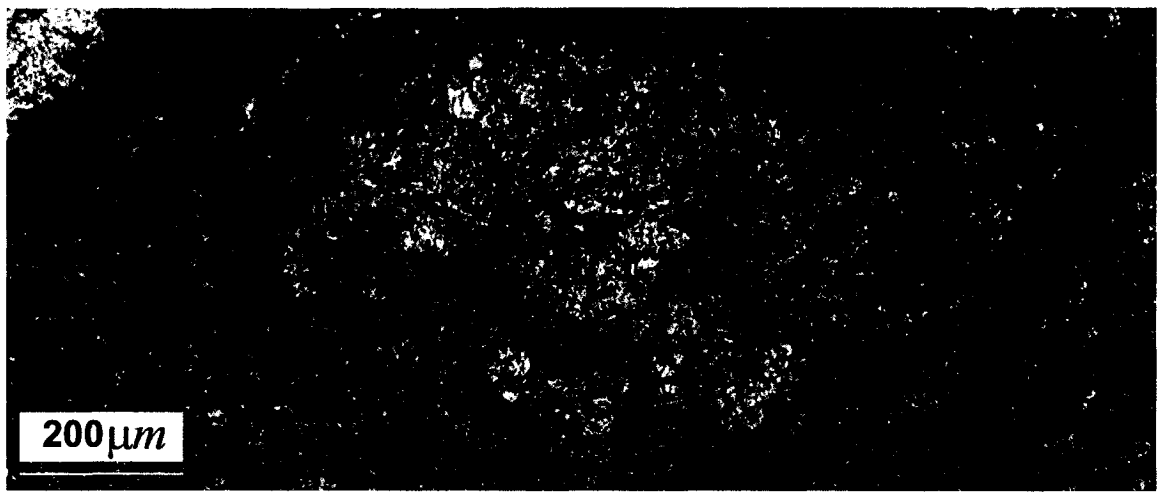

Figure II.18. Ooid from carbonate-clast conglomerate (facies F1). Ooids have micritic cortical fabrics with only traces of preserved concentric structure. Internally, ooid nuclei have been replaced by ferroan dolomite (i.e. the crystals are stained pale blue in this section). The surrounding micritic matrix has been neomorphosed to microspar, and later dolomitized. Plane-polarized light.

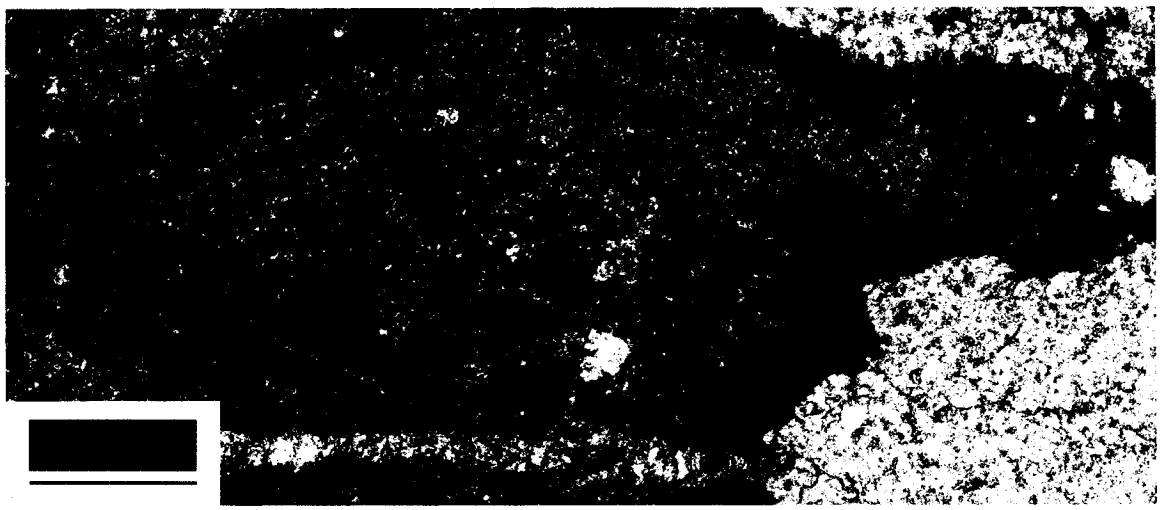

Figure II.19. Ooid in carbonate-clast conglomerate (facies F1). This ooid still preserves partially its original concentric lamination structure, even though the layers that correspond to the original aragonitic coating has been neomorphosed to microspar and selectively replaced by fine dolomite crystals (light blue stained). The dark interlayer lines and areas represent organic matter associated with microbial activity, that later were filled with micrite. The ooid was also partially fractured (bottom), in which the microfracture was filled by quartz. A secondary pore space (right side) was created and later filled by blocky ferroan calcite. Plane-polarized light.

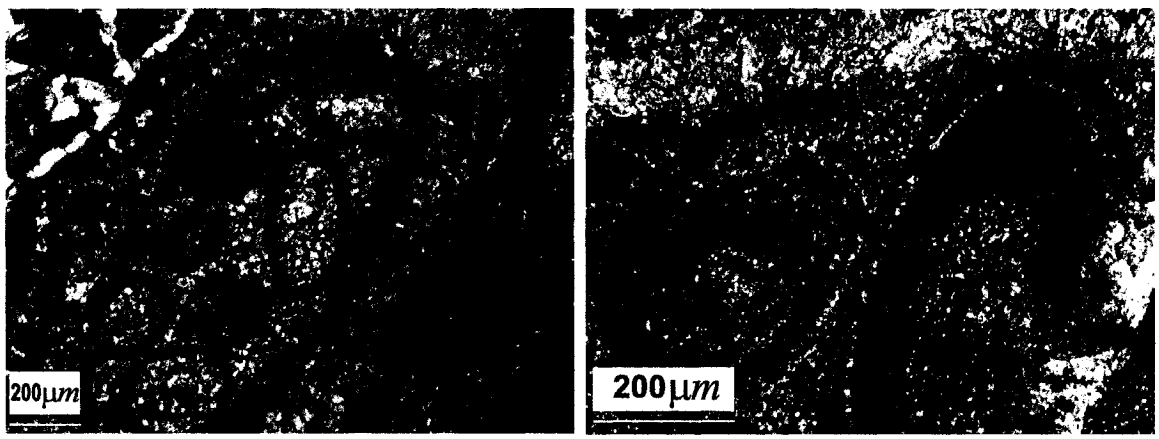

Figure II.20. Composite ooids in carbonate-clast conglomerate (facies F1). Composite ooids are formed when a small number of small ooids become enveloped by further oolitic coating (e.g. concentric lamellae). Internally, ooids have been replaced by finely to medium crystalline ferroan dolomite crystals (blue stained). Right photo, composite ooid is dissected by microfractures that are filled with quartz and calcite. Plane-polarized light.

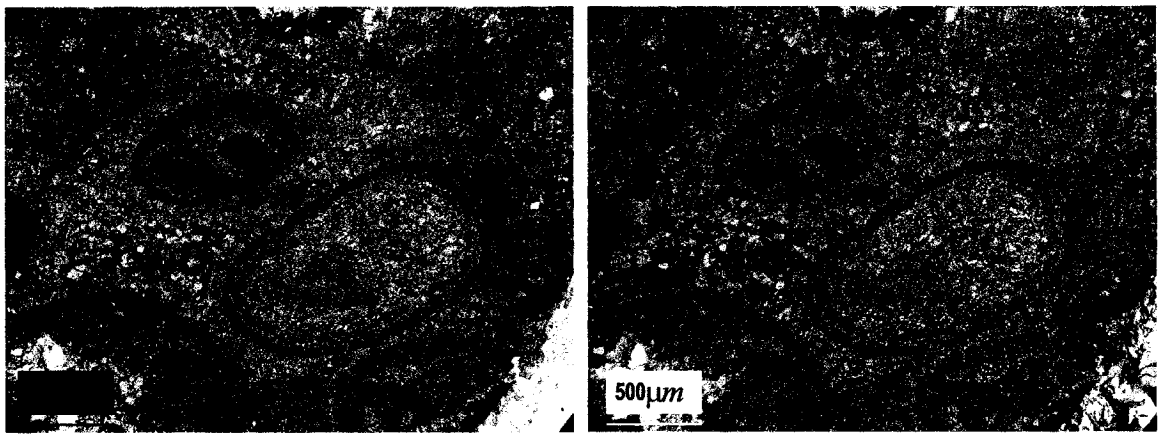

Figure II.21. Composite ooids in carbonate-clast conglomerate (facies F1). Composite ooids and ooidal components have preserved their concentric fabric, but some have been internally neomorphosed to microspar and also have been replaced by finely to medium crystalline ferroan dolomite. Two generations of cements are observed: the first generation is a more or less isopachous crust of bladed calcite around the ooids, and probably is associated with early diagenesis; the second generation is a void-filling blocky calcite cement. Indicators of later dolomitization are also observed.

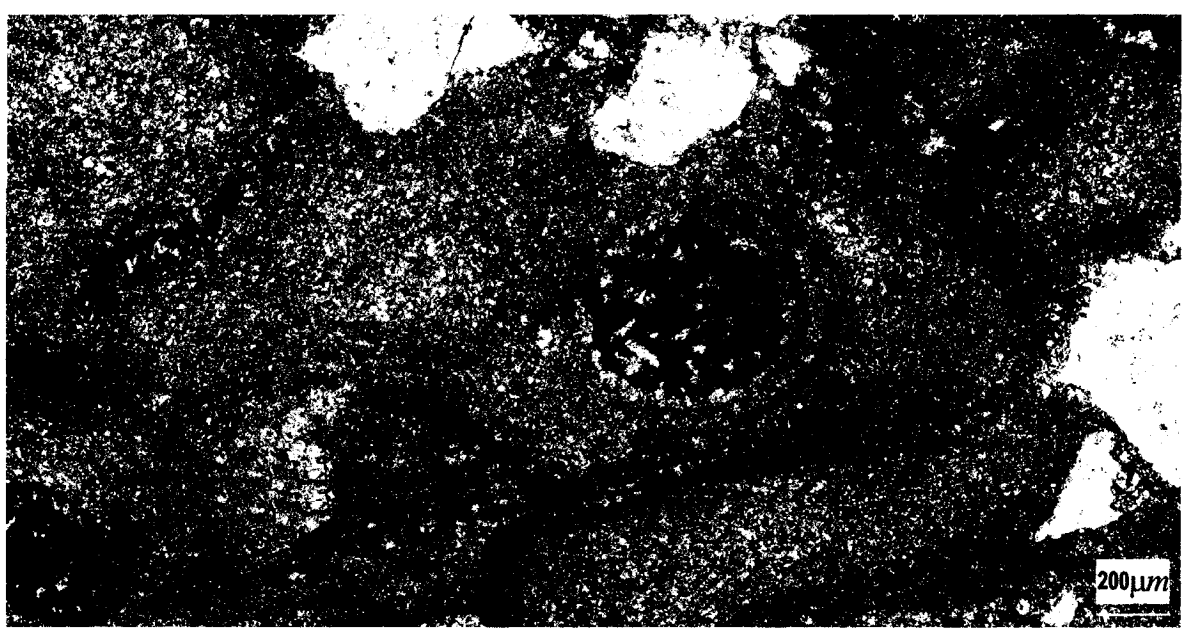

Figure II.22. Composite ooids in carbonate-clast conglomerate (facies F1) showing almost complete replacement by finely crystalline ferroan dolomite (blue stained) has partly obliterated the primary fabric. Some ooid nuclei are filled with micrite that is also partly replaced by medium dolomite crystals. Plane-polarized light.

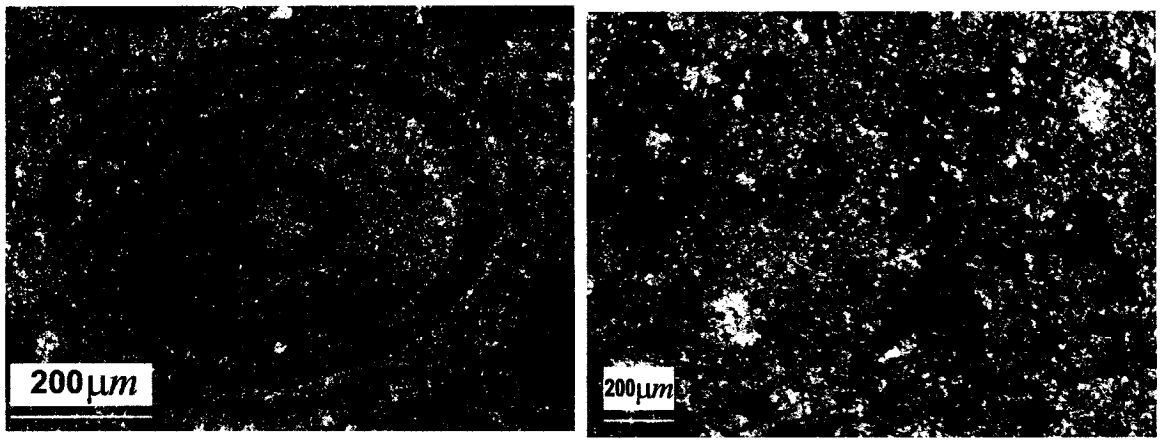

Figure II.23. Alteration of grain and matrix of carbonate-clast conglomerate. Left photo, selective alteration of ooid. Note the retention of the original textural character of the ooid. The original layers of aragonite were recrystallized to micrite, while the ooid nucleus and interlayers (with organic matter) were partially leached and the voids were subsequently filled with micrite that was later replaced by finely crystalline dolomite (blue stained). Right photo, a fenestral fabric that generally consists of a series of irregular cavities or pores that are larger than the grains. These pores were filled with micrite that subsequently has been neormorphosed to microspar. The grain/matrix framework that encased these pores has been completely obliterated by both recrystallization and dolomitization, and as a result it is extremely difficult to recognized the actual original fabric. Plane-polarized light.

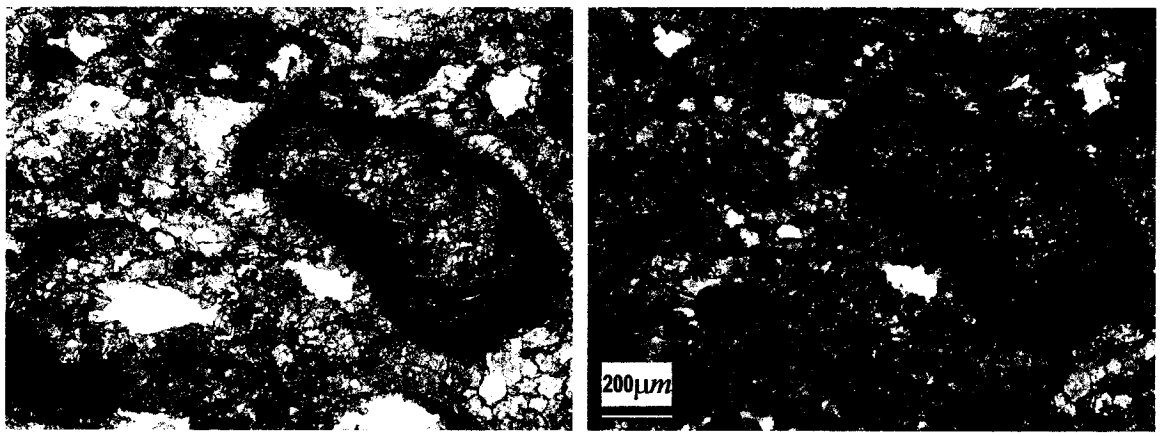

Figure II.24. Pelsparite-clast in conglomerate (facies F1). Peloid grains have been mostly recrystallized to microspar. The surrounded matrix has been totally neomorphosed to pseudospar and spar. Dispersed elongated quartz "grains" with irregular borders, but they were probably filling pores. A second-generation pore-filling blocky calcite cement was later precipitated (lower right corner). Left photo, plane-polarized light. Right photo, same view under crossed polars.

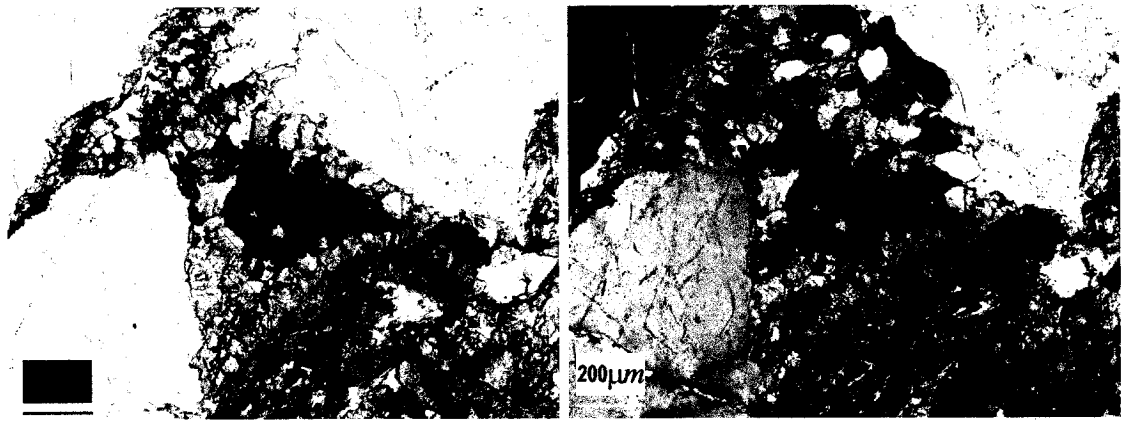

Figure II.25. Early calcite cement in carbonate-clast conglomerate. Partial dissolution of micritic matrix (dark brown) and rapid cementation of blocky or equant calcite cement that filled the residual pore space. This cement most probably formed during early in diagenesis. Left photo, plane-polarized light. Right photo, same view under crossed polars.

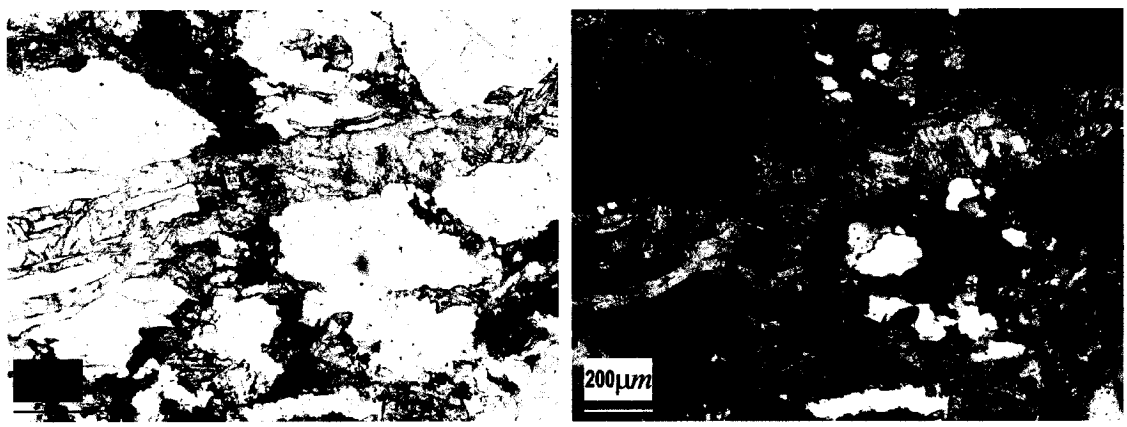

Figure II.26. Microfractures in carbonate-clast conglomerate facies F1. Fractures were filled with calcite cement from fluids that entered the open-space microfracture. Left photo, plane-polarized light. Right photo, same view under crossed polars.

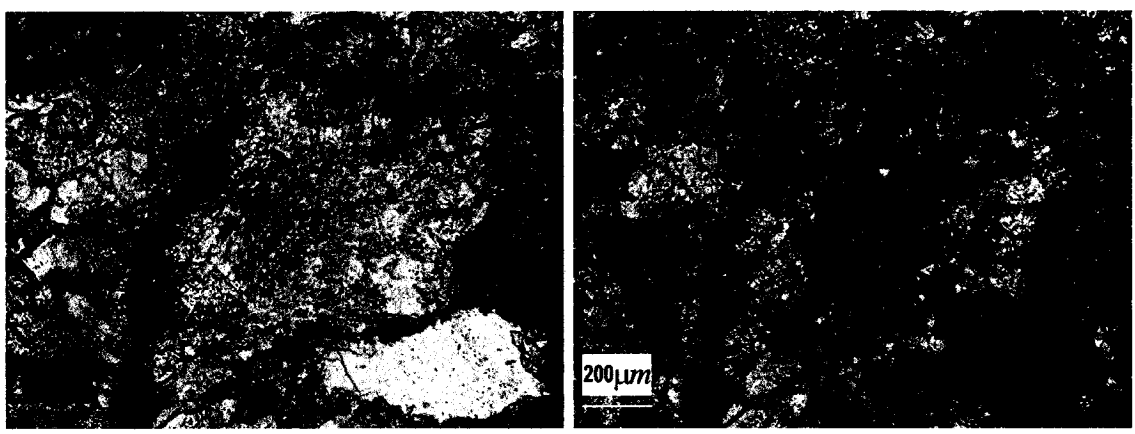

Figure II.27. Partial silicification of calcite in carbonate-clast conglomerate (facies F1). The apparent grain (center) that shows a clear brown border was initially replaced by sparry calcite cement, and then cemented by microcrystalline quartz or chert. Left photo, plane-polarized light. Right photo, same view under crossed polars.

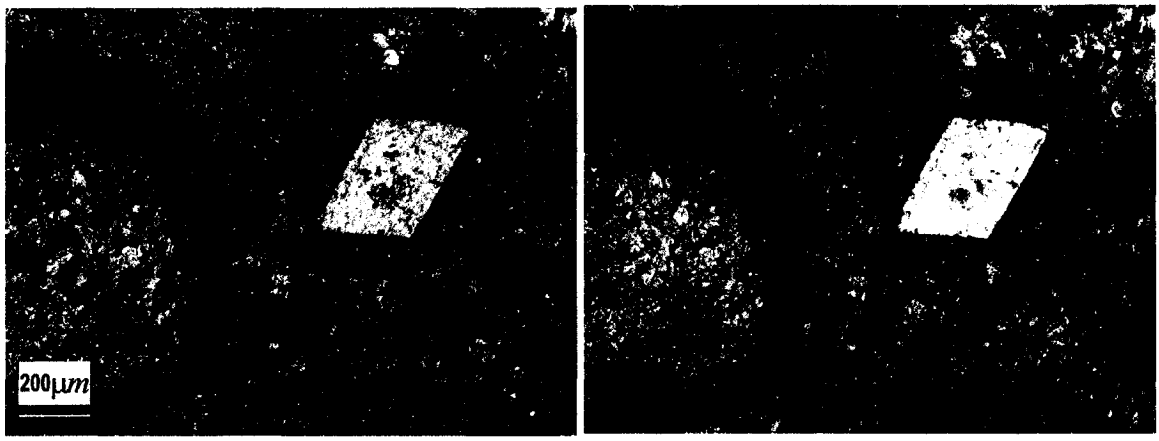

Figure II.28. Authigenic quartz in carbonate-clast conglomerate (facies F1). Euhedral authigenic quartz grain (right), with calcite inclusions indicating incomplete replacement of calcite by quartz. The ooid nucleus (left) has been dolomitized. Left photo, plane-polarized light. Right photo, same view under crossed polars.

CARBONATE CLASTS IN DEBRITE UNIT BENEATH CHANNEL 3

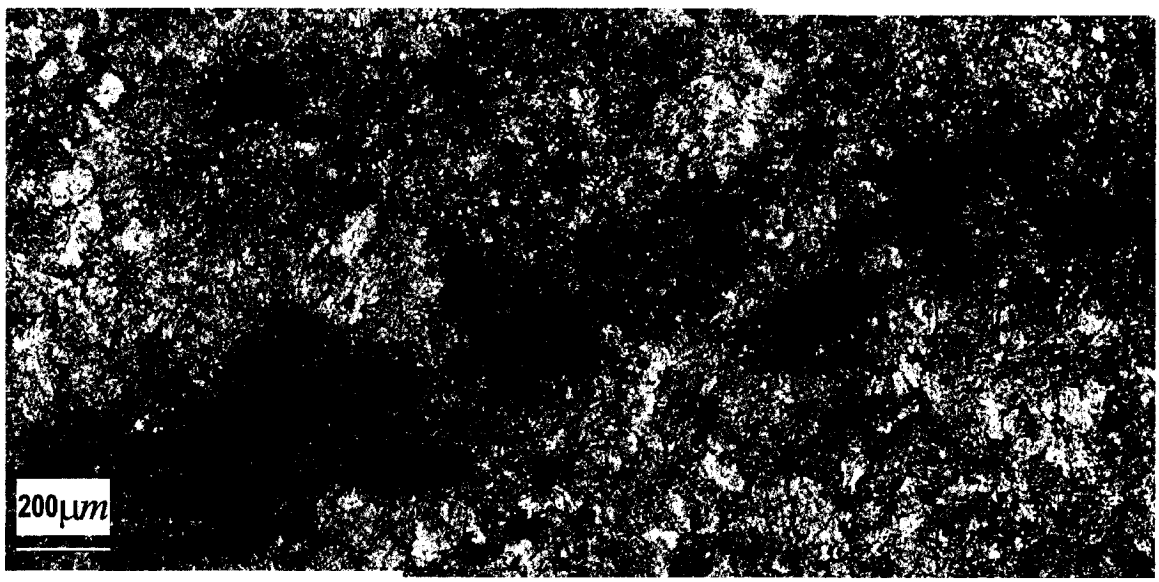

Figure II.29. Microbial structure in a carbonate-clast conglomerate (facies F1). The microbial laminated fabric in this sample consists of layers of neomorphosed micritic matrix (i.e. microspar or pseudospar) interbedded with layers of elongated fenestral pore-space now filled with micrite (dark brown), which corresponds to the structure of the original microbial mat. Plane-polarized light.

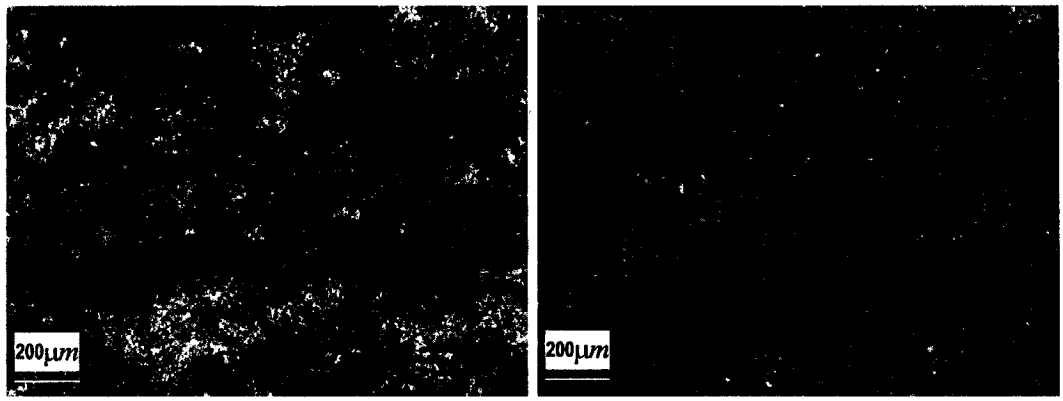

Figure II.30 Microbial fabric in fragment of carbonate embedded in debris-flow deposit. A goodt example of microbial facies, in which finely crystalline dolomitized matrix (blue stained) forms interlayers between elongated fenestral pore spaces filled with micrite (dark brown) that correspond with the original microbial mat structures. Plane-polarized light.

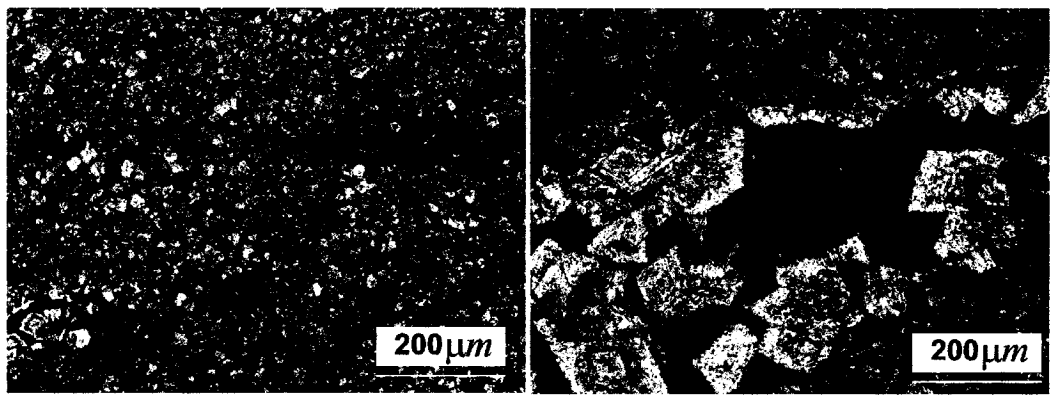

Figure II.31. Dolomitized microbial boundstone from carbonate-clast debrite. Layers of dolomitized crypto-algal lamination intercalated with laminoid fenestral pore-spaces filled with micrite (possible original microbial mat). The dolomite that replaced the matrix is medium to coarsely crystalline and has completely obliterated the primary fabric. Right photo, the dolomite in the fenestral fabric typically contains coarsely to very coarsely crystalline subhedral dolomite rhoms, which commonly are zoned with a more ferroan core (blue stained) and clear (non-ferroan) rim. Plane-polarized light.

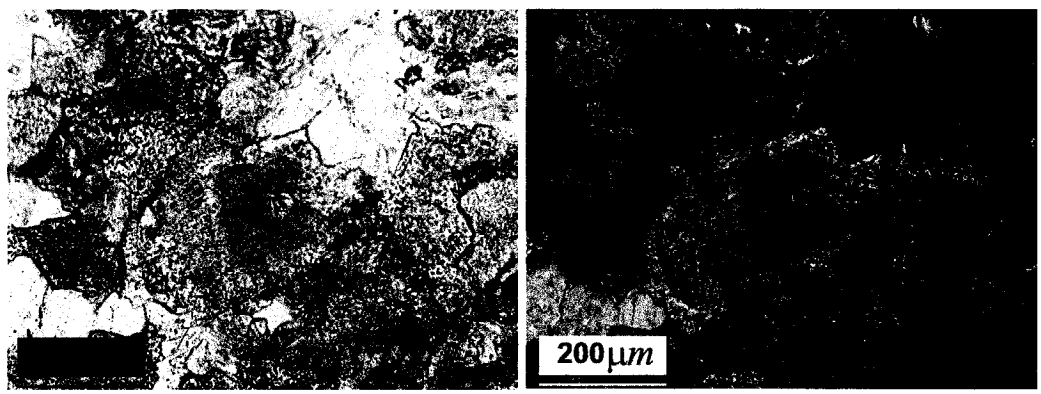

Figure II.32. Replacement dolomite in carbonate-clast debrite. Coarse dolomite rhombs replace the sparry calcite cement. The dolomite crystals show clear rims but "cloudy" cores due to the presence of small inclusions. Left photo, plane-polarized light. Right photo, same view under crossed polars.

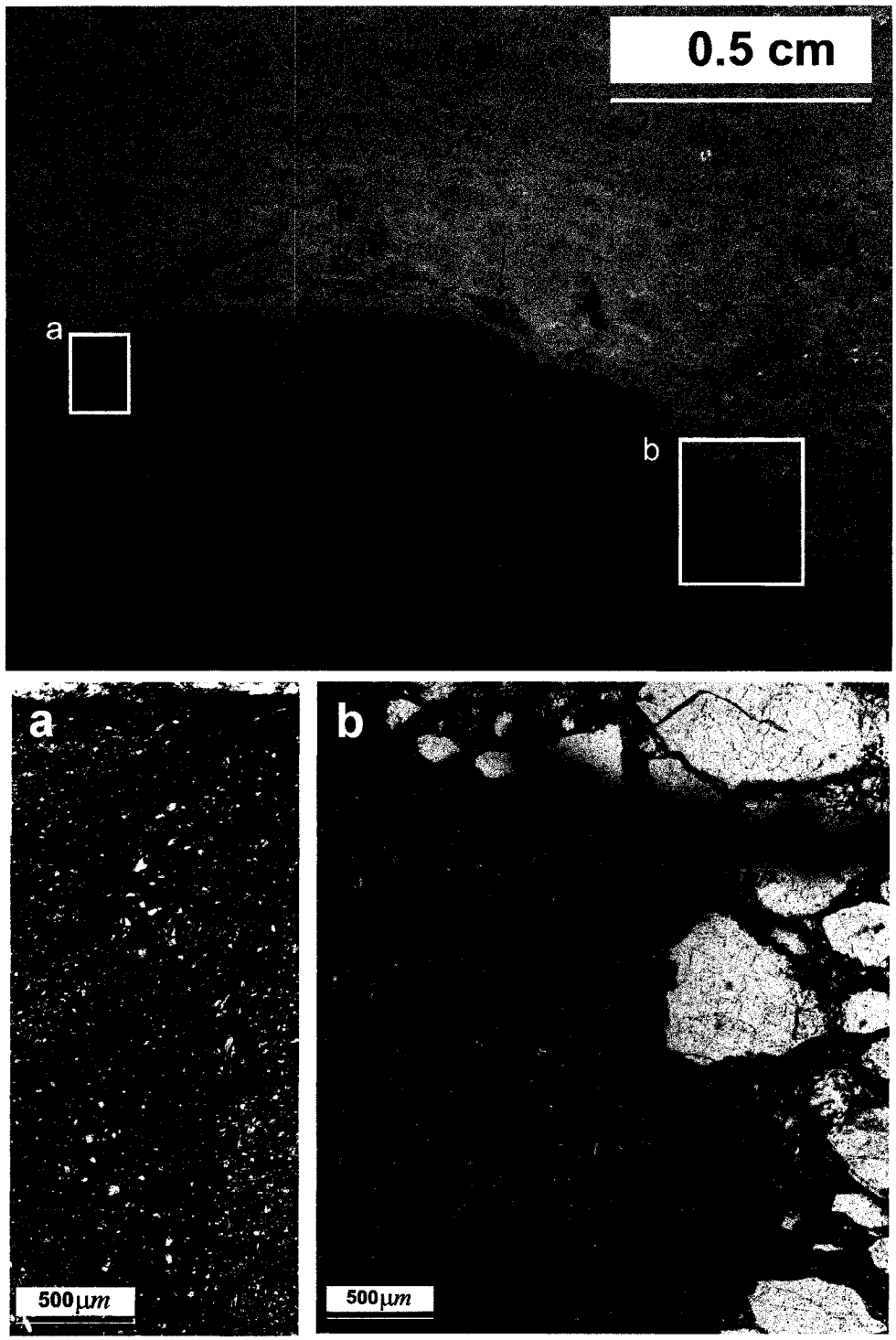

Figure II.33. A mudstone clast from the brecciated facies (facies F2.2) showing discrete fracture pore along longest margin that separate into further fragments (indicated by arrows). (a) Clast is also internally fractured where iron oxides were precipitated and spread laterally from percolating fluids (darker brown) and insoluble residues of quartz, opaque and clay minerals were concentrated. (b) Coarse quartz grains around the mudstone clast penetrate in the short margin, along diffuse lamination. Photo on the top, under incident light, and photos on the bottom (a and b) under plane polarized light.

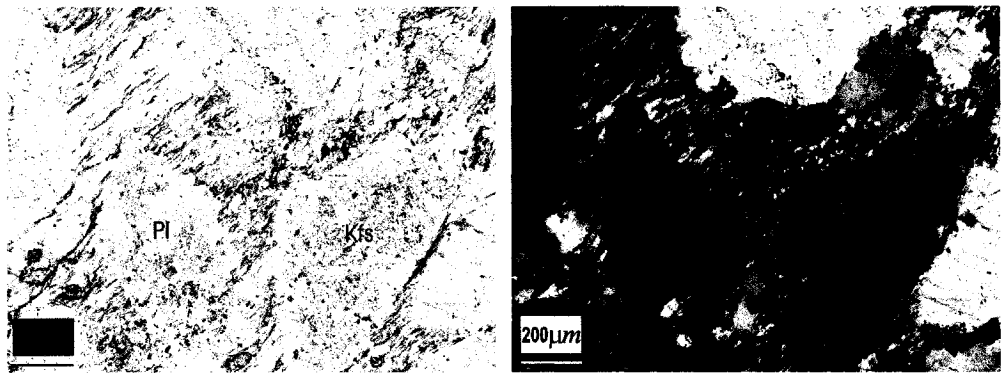

Figure II.34. Matrix from the breccia facies (facies F2.1) consist of coarse-sand grains of quartz and feldspar, and recrystallized matrix of fine-grained quartz, muscovite and chlorite. Left photo, feldspars are commonly altered (brownish areas). Right photo, the plagioclase grain (Pl) exhibits typical polysynthetic twins. Moreover, patchy exsolution lamellae of plagioclase (light grey streaks) can be seen in the K-feldspar (Kfs) grain and indicates perthite intergrowth. Left photo, plane-polarized light. Right photo, same view under crossed polars.

FACIES F3

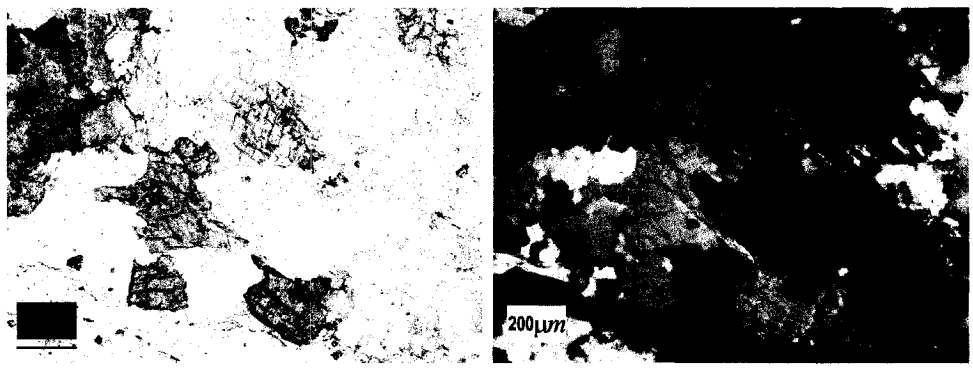

Figure II.35. Sub feldspathic sandstone of cross-stratified facies (facies F3), composed mostly of very coarse-sand, quartz grains cemented by very large crystals of calcite (high birrefrigent colors). Quartz grains are extensively corroded by the calcite cement. Left photo, plane-polarized light. Right photo, same view under crossed polars.

FACIES F4

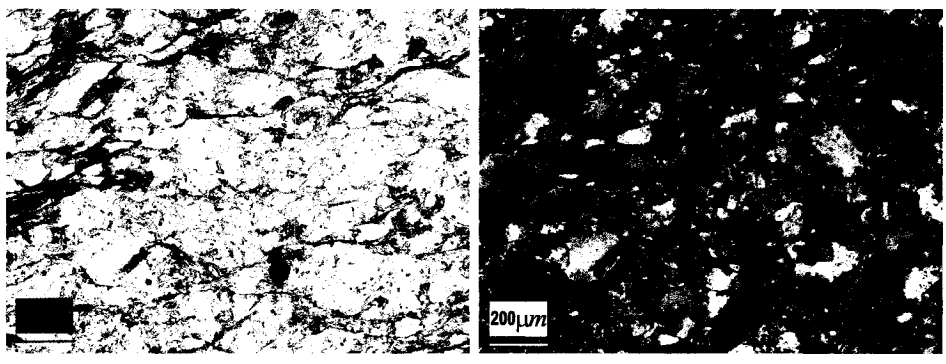

Figure II.36. Structureless sandstone (facies F4), consisting mainly of subangular to subrounded quartz and some altered feldspar grains. Grains are dispersed in a recrystallized matrix composed of fine-grained quartz, muscovite and chlorite. Left photo, plane-polarized light. Right photo, same view under crossed polars.

APPENDIX III. X-Ray Powder Diffraction Data

This appendix includes x-ray diffraction analyses and representative diffraction spectra of 34 bulk-rock samples of mudstone, mudstone-clast and carbonate-clast from channels 1 and 3 at the Castle Creek South study area (for more details about the preparation of these samples see Chapter 1, section 1.4.2). For sample location see Appendix 1.

The X-ray Powder Diffractometer is a theta-2theta (2θ) goniometer instrument, outfitted with a Cu rotating anode. It was set to scan between 0 to 70^{o} (2θ). The data were evaluated and minerals identified using the actualized mineral database published by International Center for Diffraction Data (ICDD).

	Sample ID	Facies	Lithology	Mineralogical composition								
				Quartz	Chlorite	Muscovite	Plagioclase	K-feldspar	Calcite	Dolomite	Ankerite?	Goethite
CHANNEL 1	112	F2	Mudstone-clast	X	X	X	X	X	X			
	115 (*)		Mudstone-clast	X	X	X	X		X			
	2 (*)	F4	Mudstone (Thin bedded turbidite)	X	X	X		X				
	99 (*)		Mudstone (Thin bedded turbidite)	X	X	X	X		X			
	135		Mudstone (Thin bedded turbidite)	X	X	X	X	X				
CHANNEL 3	102	F1	Carbonate clast	X		X	X		X	X	X	
	108		Carbonate clast	X		X				X	X	
	111 (*)		Carbonate clast	X		X	X			X	X	
	122 (*)		Carbonate clast	X						X	X	
	123		Carbonate clast	X		X	X			X	X	
	124		Carbonate clast	X		X			X	X	X	
	125		Carbonate clast	X						X	X	
	126		Carbonate clast	X						X	X	
	127		Carbonate clast	X			X			X	X	
	9	F2	Mudstone-clast	X	X	X	X	X				
	68 (*)		Mudstone-clast	X	X	X	X	X	X			
	69		Mudstone-clast	X	X	X	X	X	X			
	70		Mudstone-clast	X	X	X		X	X			
	47	F4	Mudstone (Thin bedded turbidite)	X	X	X	X		X			
	59		Mudstone (Thin bedded turbidite)	X	X	X	X		X			
	66 (*)		Mudstone (Thin bedded turbidite)	X	X	X	X		X			
	67		Mudstone (Thin bedded turbidite)	X	X	X						
	75		Mudstone (Thin bedded turbidite)	X	X	X	X		X			
	94 (*)		Mudstone (Thin bedded turbidite)	X	X	X	X	X				
UNDERLYING CHANNEL 3	105	Extra-channel deposits	Mudstone (Thin bedded turbidite)	X	X	X					X	
	113		Mudstone (Thin bedded turbidite)	X	X	X			X			
	120 (*)		Mudstone (Thin bedded turbidite)	X	X	X	X	X	X			
	18		Quartz- clast Debrite (Matrix)	X	X	X				X		
	84		Carbonate clast Debrite (Matrix)	X	X	X	X		X			
	88		Carbonate clast Debrite (Matrix)	X	X	X	X		X			
	76 (*)		Carbonate clast Debrite (Clast)	X		X				X	X	
	80		Carbonate clast Debrite (Clast)			X	X			X	X	
	81 (*)		Carbonate clast Debrite (Clast)	X						X	X	X
	82		Carbonate clast Debrite (Clast)	X		X				X	X	

(*) Diffractograms of these samples are shown below.

Table III.1. Mineralogical analysis of samples from Channel 1 and 3 using XRD

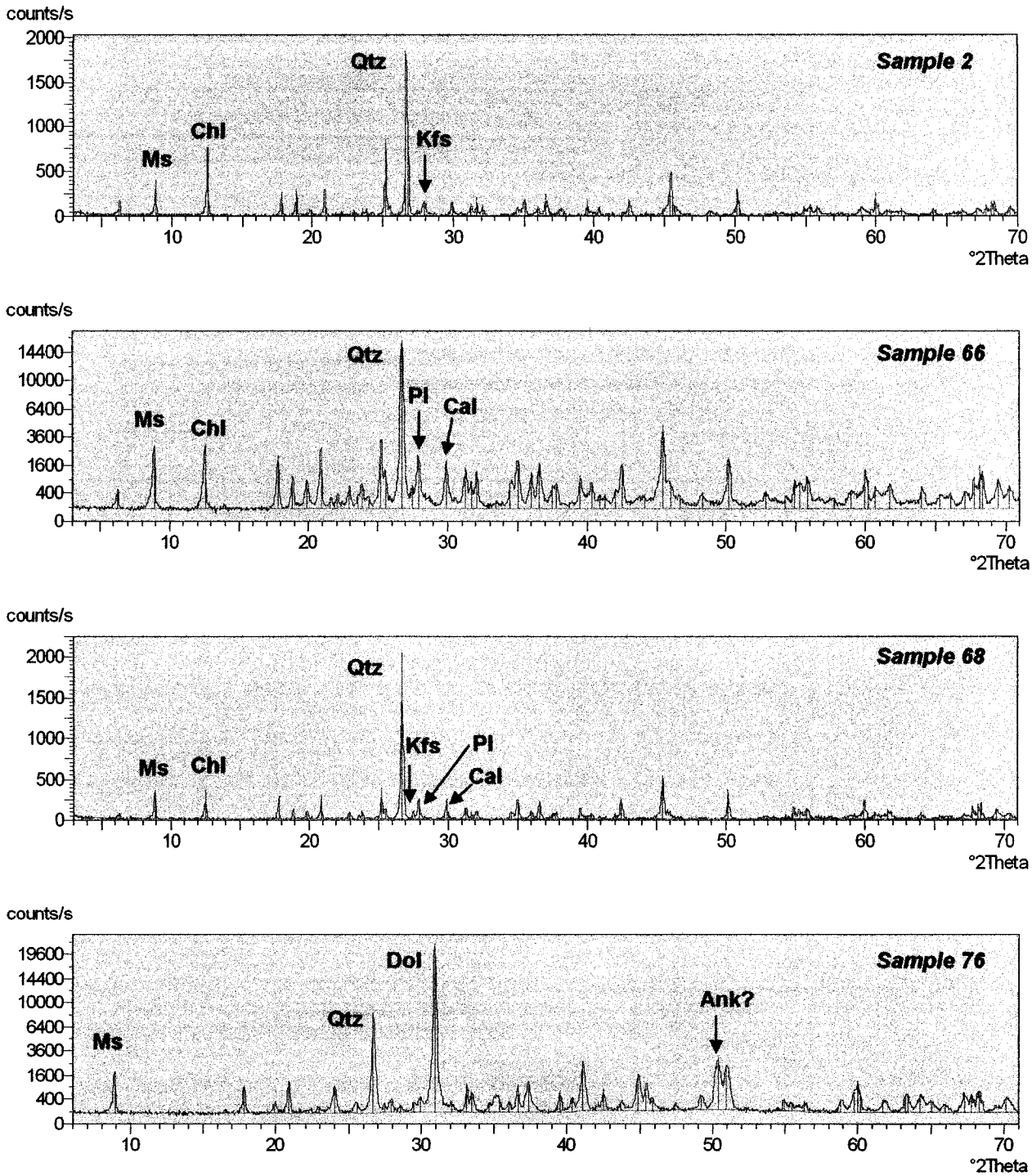

(Continued on next page)...

Figure III.1. X-ray diffractograms for samples from Channel 1 and 3 analyzed as random bulk powders. Important peaks are labeled as follows: Ank= Ankerite (descendent value), Cal = Calcite, Chl= Chlorite, Dol= Dolomite, Gt= Goethite, Kfs= K-feldspar, Ms= Muscovite, Pl = Plagioclase, Qtz= Quartz.

...Figure III. 1 (Continued)

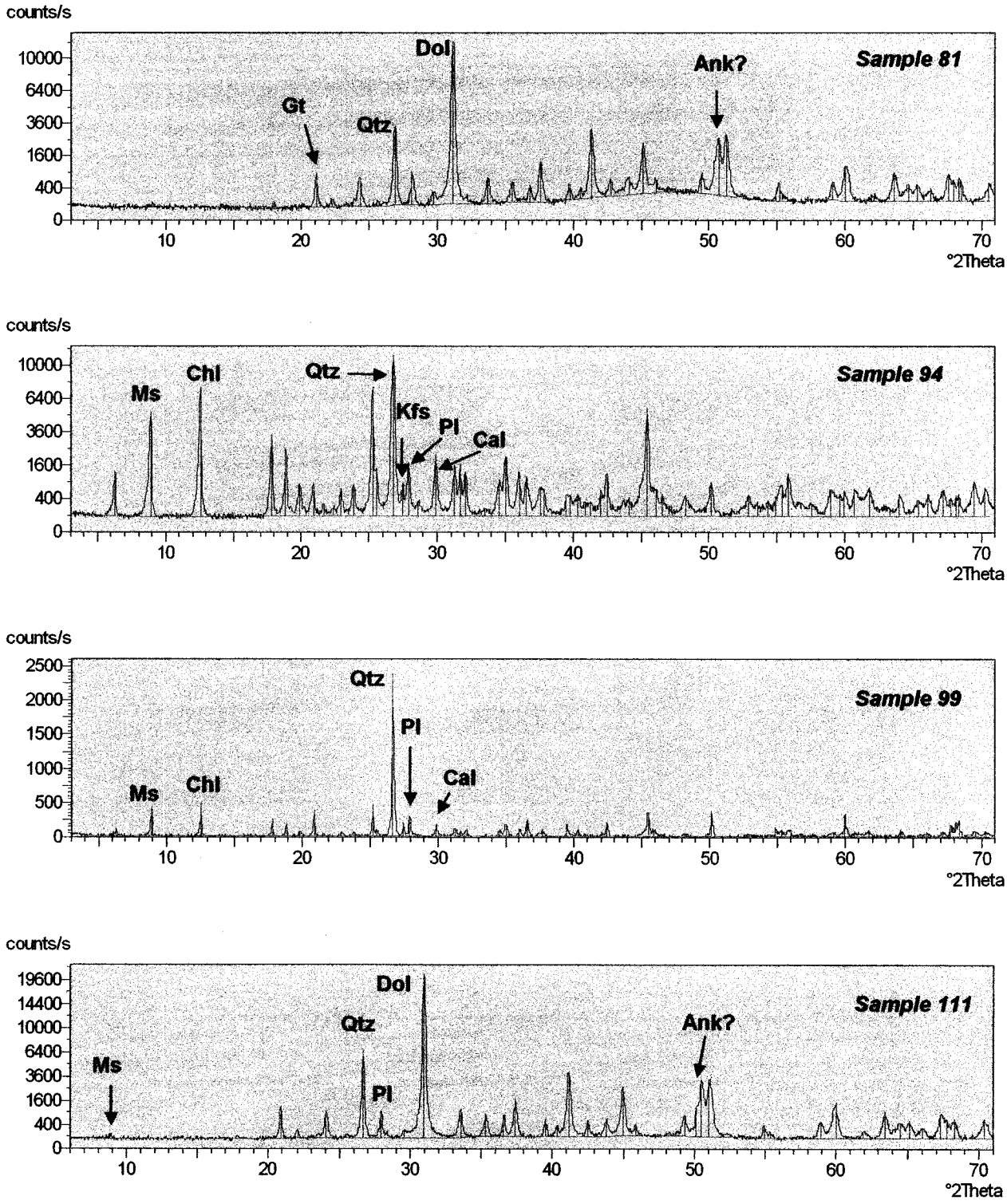

(Continued on next page)...

...Figure III. 1 (Continued)

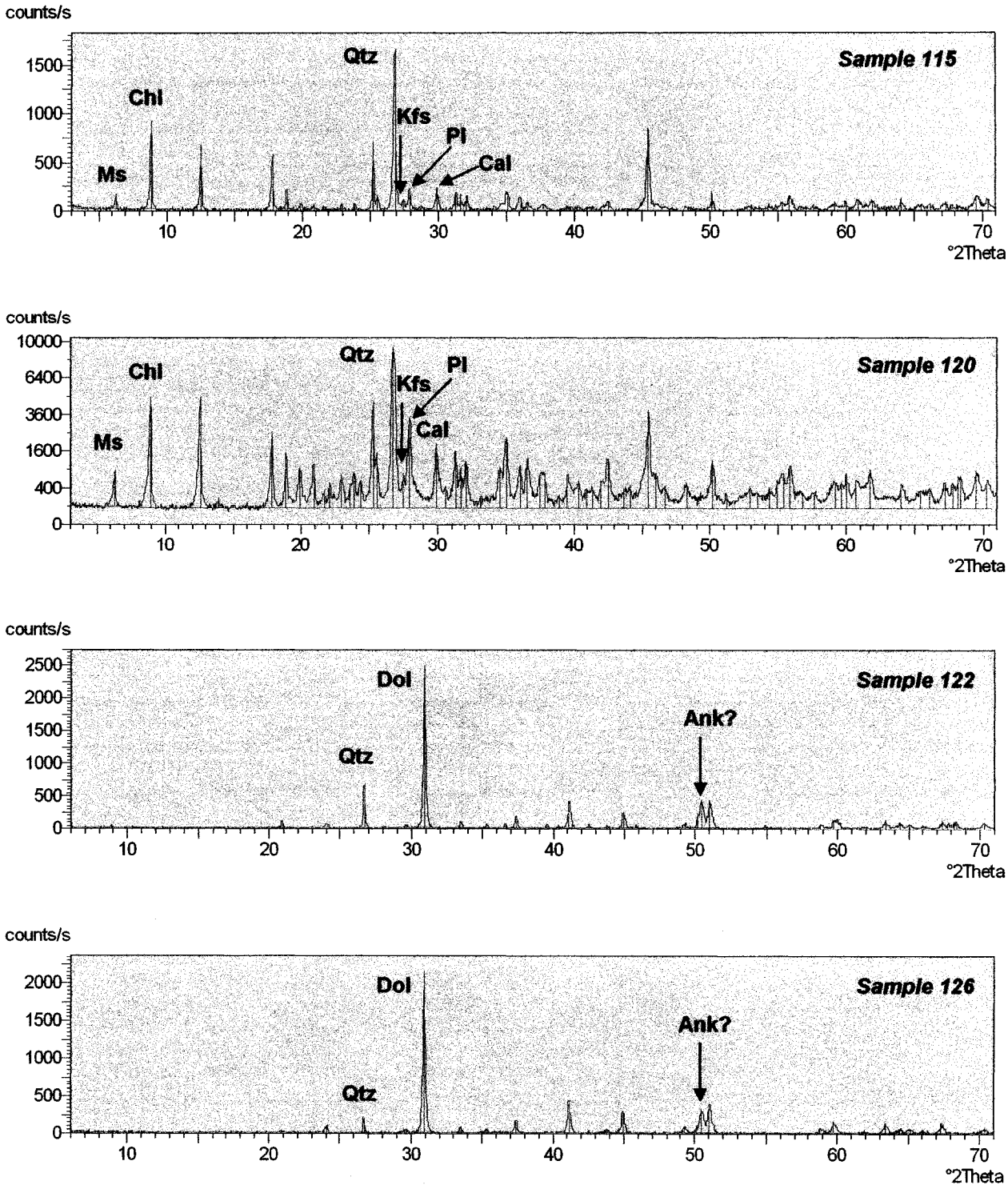

(Continued on next page)...

...Figure III. 1 (Continued)

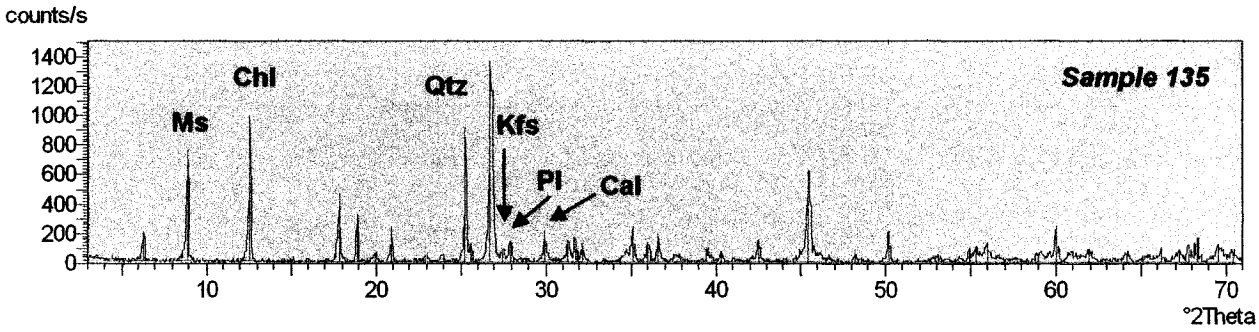

APPENDIX IV. Gamma Ray Profiles

This appendix contains the high-resolution spectral gamma-ray profiles of the outcrops using a portable gamma-ray scintillometer. Measurements were made ascending perpendicular to bedding and made every 75 cm. For detailed numerical data see EXCEL folder (.XLS files) included in the CD-ROM version of this work. The x-axis represents the gamma-ray counts and y-axis is the distance measured upward in meters.

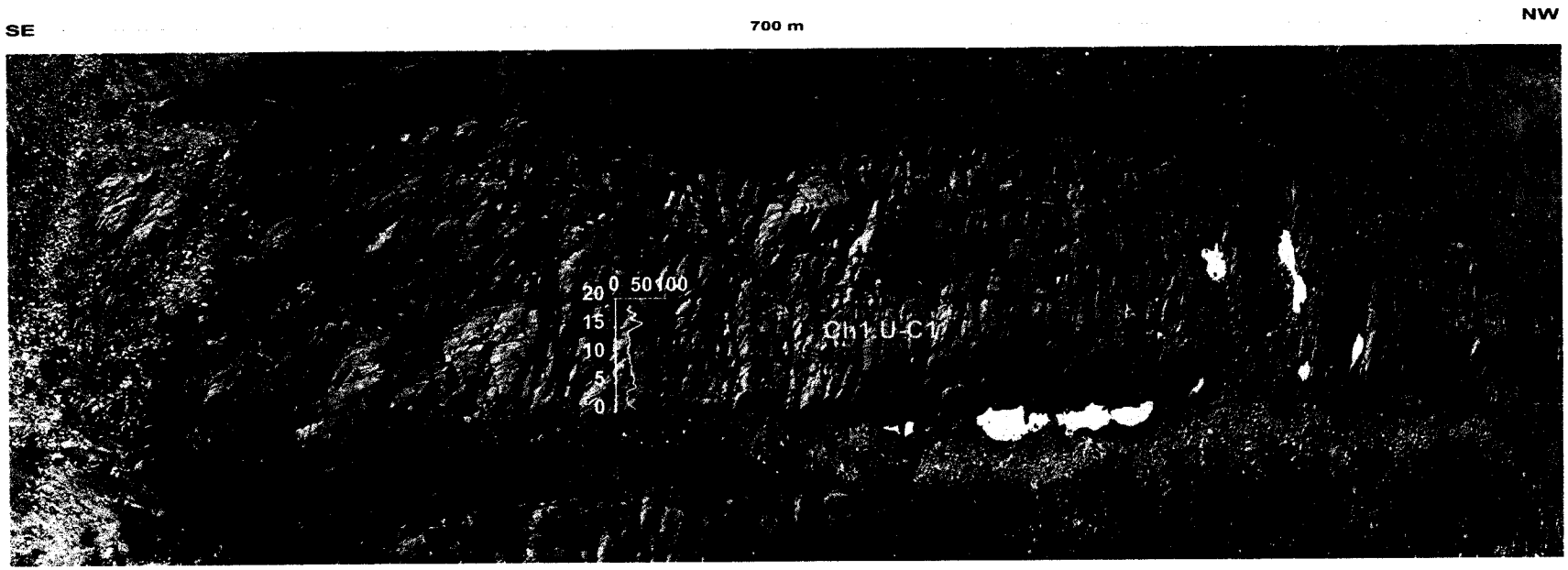

Figure IV.1. Gamma-ray curve for measured section in the axis of Channel 1. Note the low number of counts (<35), which is consistent with the sandstone/conglomerate composition of the beds in the channel fills.

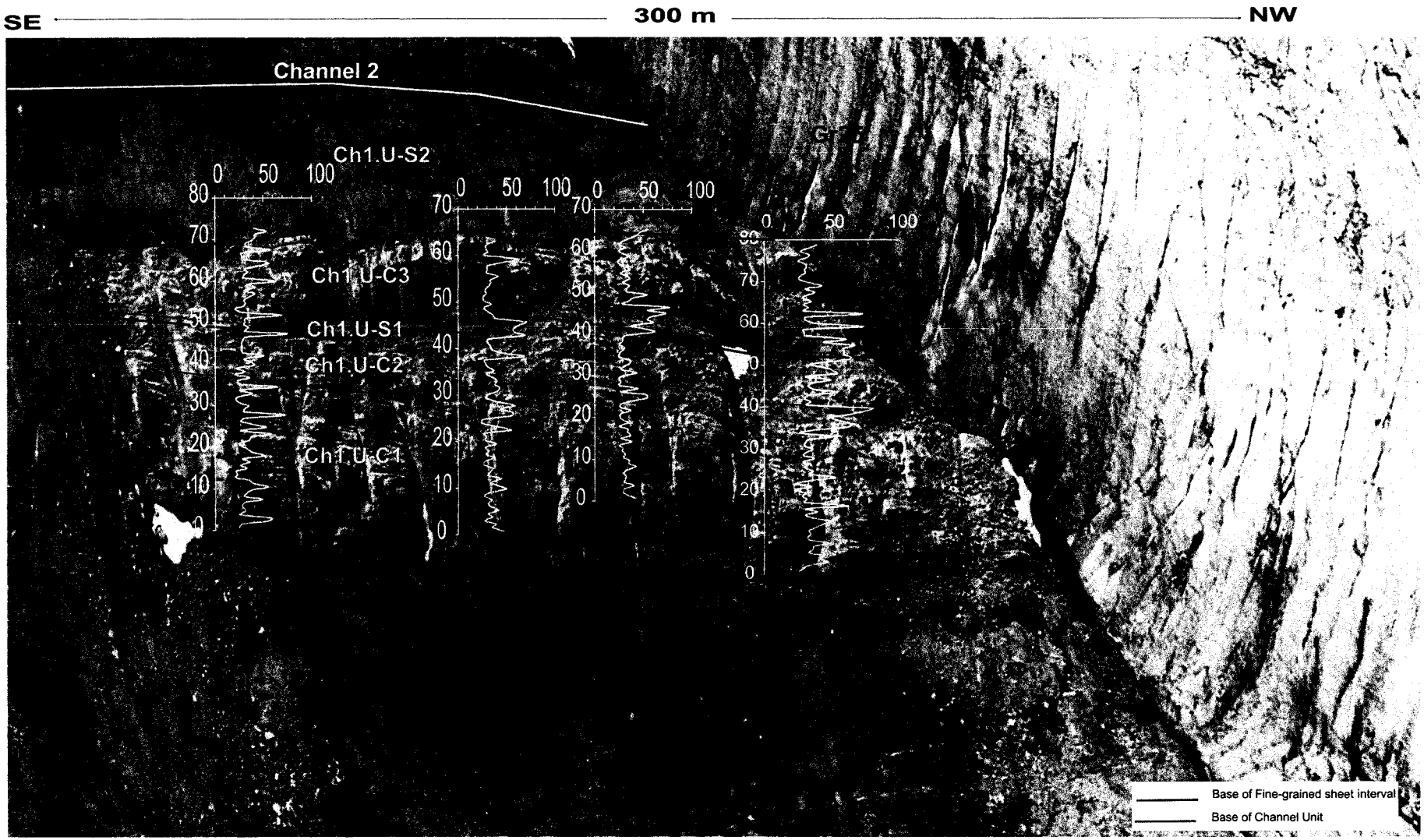

Figure IV.2. Geophysical gamma-ray logs for the marginal succession of Channel 1. Note the "blocky" character of the three major sandstone/conglomerate channel units that are abruptly separated by two fine-grained turbidite intervals with characteristic high gamma-ray counts.

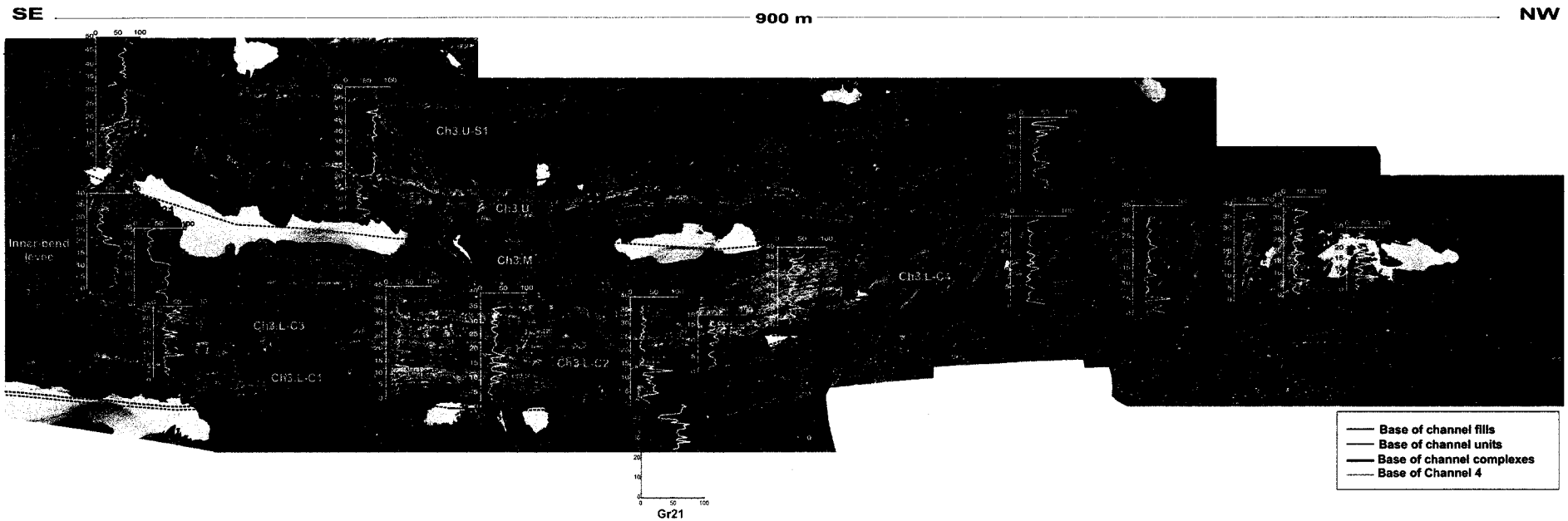

Figure IV.3. Gamma-ray logs for the intrachannel deposits of Channel 3. Note the sharp change from high to low gamma-ray counts, which coincides with changes from mostly fine-grained turbidites to coarse-grained, more thickly-bedded sandstone/conglomerate strata.

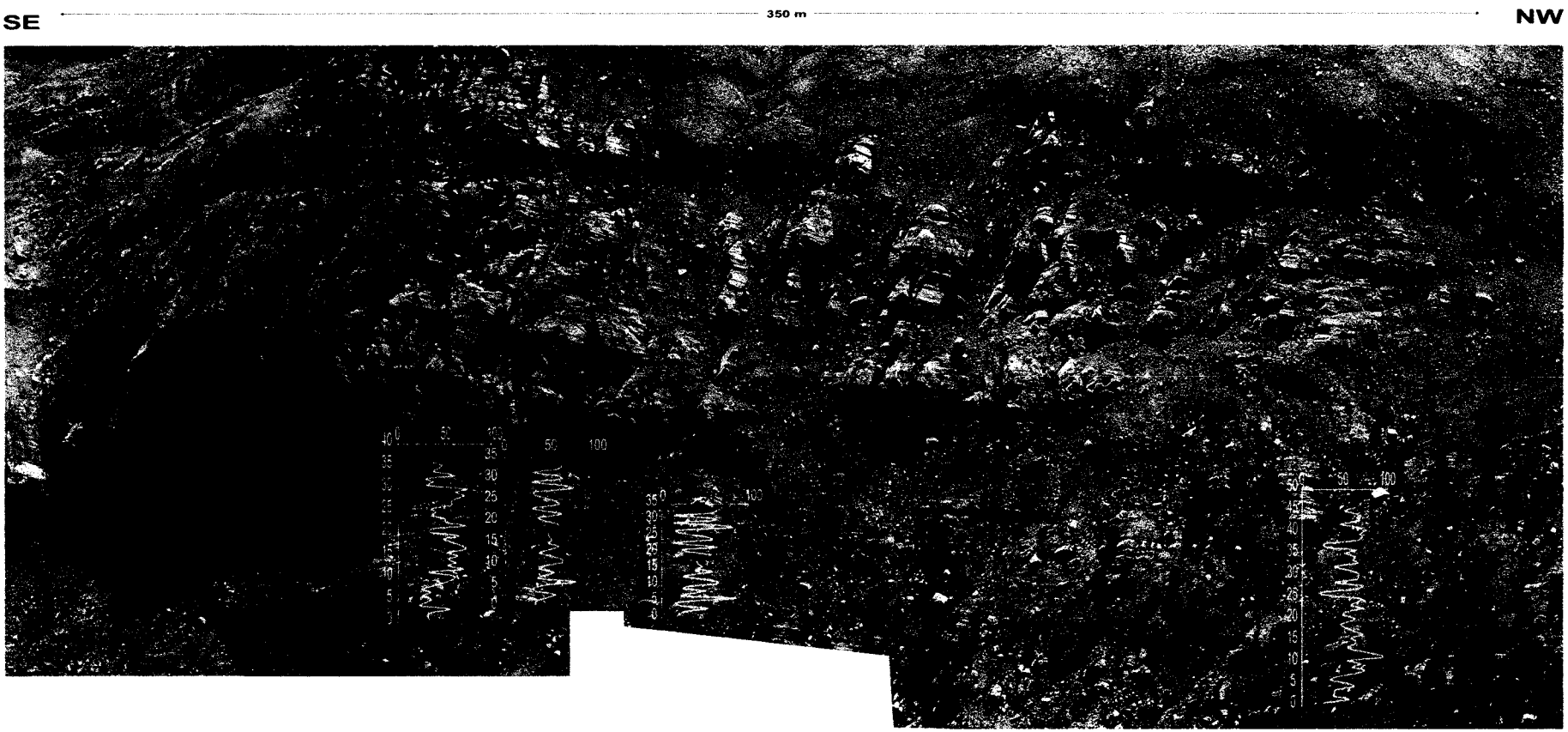

Figure IV.4. Gamma-ray logs for proximal levee deposits immediately beneath and adjacent to the strata in the Lower part of Channel 3. Note the correspondence between gamma-ray values and the characteristic heterolithic lithology (sandstone:low versus mud-rich: high).

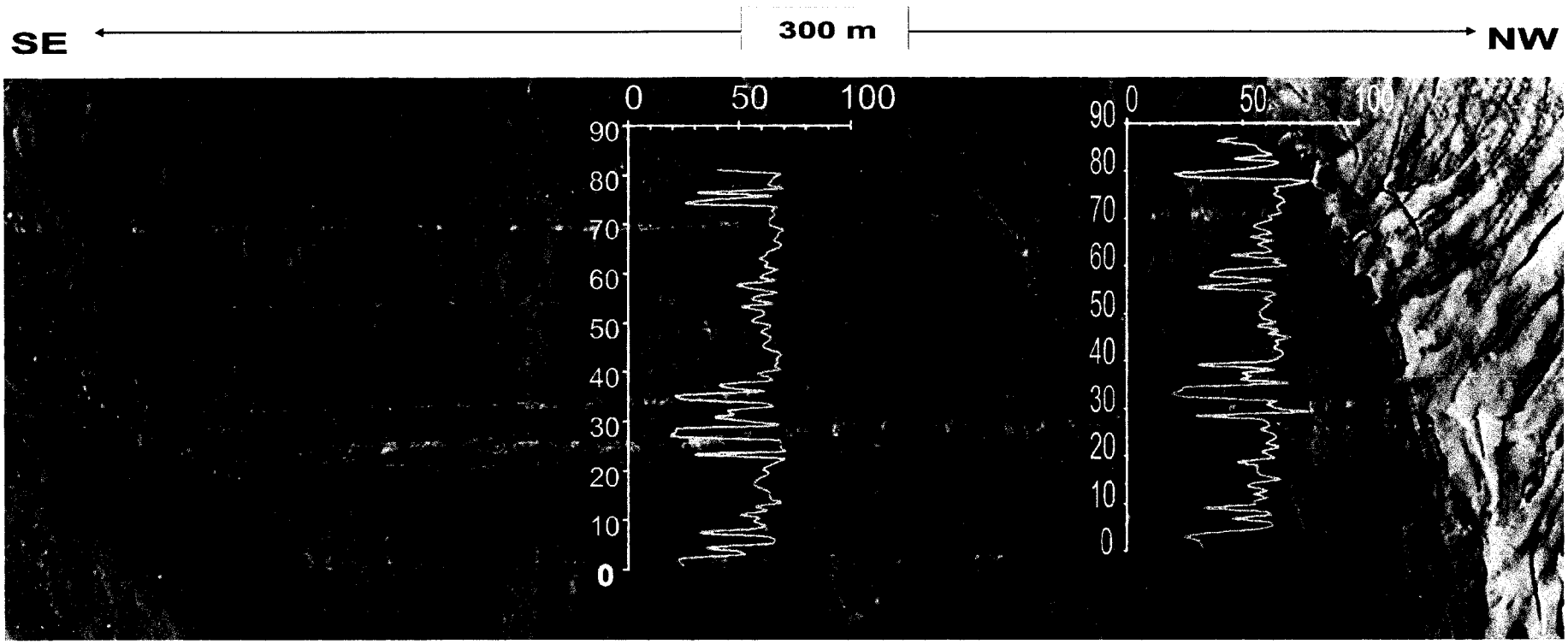

Figure IV.5. Gamma-ray logs for the distal levee deposits adjacent to the lower part of Channel 3. Note the characteristic spikey character of the gamma ray trace indicative of predominant mudstone-rich strata (high (>50) counts) intercalated with sandstone/conglomerate (low counts).

APPENDIX V. Facies distribution

This appendix tabulates data describing the nature of horizontal and vertical facies heterogeneity within channel units of Channel 1 and Channel 3. This quantitative analysis is based on data obtained from measured sections or logs. Percentages, which includes conglomerate and sandstone together formulate the net:gross values, and mudstone (including thin bedded heterolithic packages) which were calculated in order to compare the relatively distribution of facies proportions in the channel axis versus those near the margin. For more detailed numerical data see folder included in the CD-ROM version of this work.

Nomenclature of Facies and Subfacies

F1.Normally Graded to Massive Sandstone and Conglomerate
- F1.1. Normally Graded Sandstone and Conglomerate
  - F1.1a. Normally Graded Conglomerate to Sandstone
  - F1.1b. Normally Graded Sandstone
- F1.2. Massive Sandstone and Conglomerate
  - F1.2a. Massive Conglomerate
  - F1.2b. Massive Sandstone

F2. Mudstone-clast Breccia
- F2.1. Mudstone-clast Breccia
- F2.2. Mudstone-clast Brecciated facies

F3. Cross-stratified and Parallel stratified Sandstone
- F3.1. Cross-stratified Sandstone
- F3.2. Parallel-bedding Sandstone

F4. Sandstone interbedded with Mudstone and Unlaminated Mudstone
- F4.1 Sandstone interbedded with Mudstone
  - F4.1a. Structureless Sandstone and Mudstone
  - F4.1b. Laminated Sandstone and Mudstone
  - F4.1c. Rippled Sandstone and Mudstone
- F4.2. Mudstone

CHANNEL 1, *LOWER CHANNEL COMPLEX (Ch1.L)*

LOG	CHANNEL UNIT	LOG THICKNESS (m)	FACIES F1.1a			FACIES F1.1b			FACIES F1.2a			FACIES F1.2b			FACIES F2.1			FACIES F2.2			FACIES F3.1			FACIES F3.2			FACIES F4.1a			FACIES F4.1b			FACIES F4.1c			FACIES F4.2			COVER		% SANDSTONE	% MUDSTONE
			Total Thickness (m)	Avg. Bed Thickness (m)	%	Total Thickness (m)	Avg. Bed Thickness (m)	%	Total Thickness (m)	Avg. Bed Thickness (m)	%	Total Thickness (m)	Avg. Bed Thickness (m)	%	Total Thickness (m)	Avg. Bed Thickness (m)	%	Total Thickness (m)	Avg. Bed Thickness (m)	%	Total Thickness (m)	Avg. Bed Thickness (m)	%	Total Thickness (m)	Avg. Bed Thickness (m)	%	Total Thickness (m)	Avg. Bed Thickness (m)	%	Total Thickness (m)	Avg. Bed Thickness (m)	%	Total Thickness (m)	Avg. Bed Thickness (m)	%	Total Thickness (m)	Avg. Bed Thickness (m)	%	Total Thickness (m)	%		
21	Ch1L-C1 (axis)	12.70	4.89	1.55	38.5	3.14	1.07	19.8	0.56	0.56	4.4	5.37	1.64	42.1																											99.8	0.2
21.1	Ch1L-C1 (margin)	15.3	2.33	1.17	15.23	2.33	2.33	15.23	1.37	0.69	8.95	8.76	0.75	44.31							0.15	0.15	0.98	0.4	0.4	2.61							1.14	0.57	7.45	0.8	0.09	5.24			97.31	12.69
	Ch1L-C2 (margin)	4.97	0.88	0.44	17.71				0.84	0.84	16.9	1.77	0.89	35.61																						1.48	0.37	29.4			70.22	29.78
49	Ch1L-C2 (axis)	16.27	0.93	1.11	48.8	5.86	0.43	34.16	1.87	1.87	8.69	0.9	0.9	5.6										0.24	0.08	1.47				0.1	0.1	0.6	0.7	0.14	4.29	0.84	0.11	5.41			91.21	8.79

Table V.1. Chart of lithofacies distribution and percentage of sandstone in Lower Channel Complex of Channel 1 (Ch1.L). For Nomenclature see p. 246.

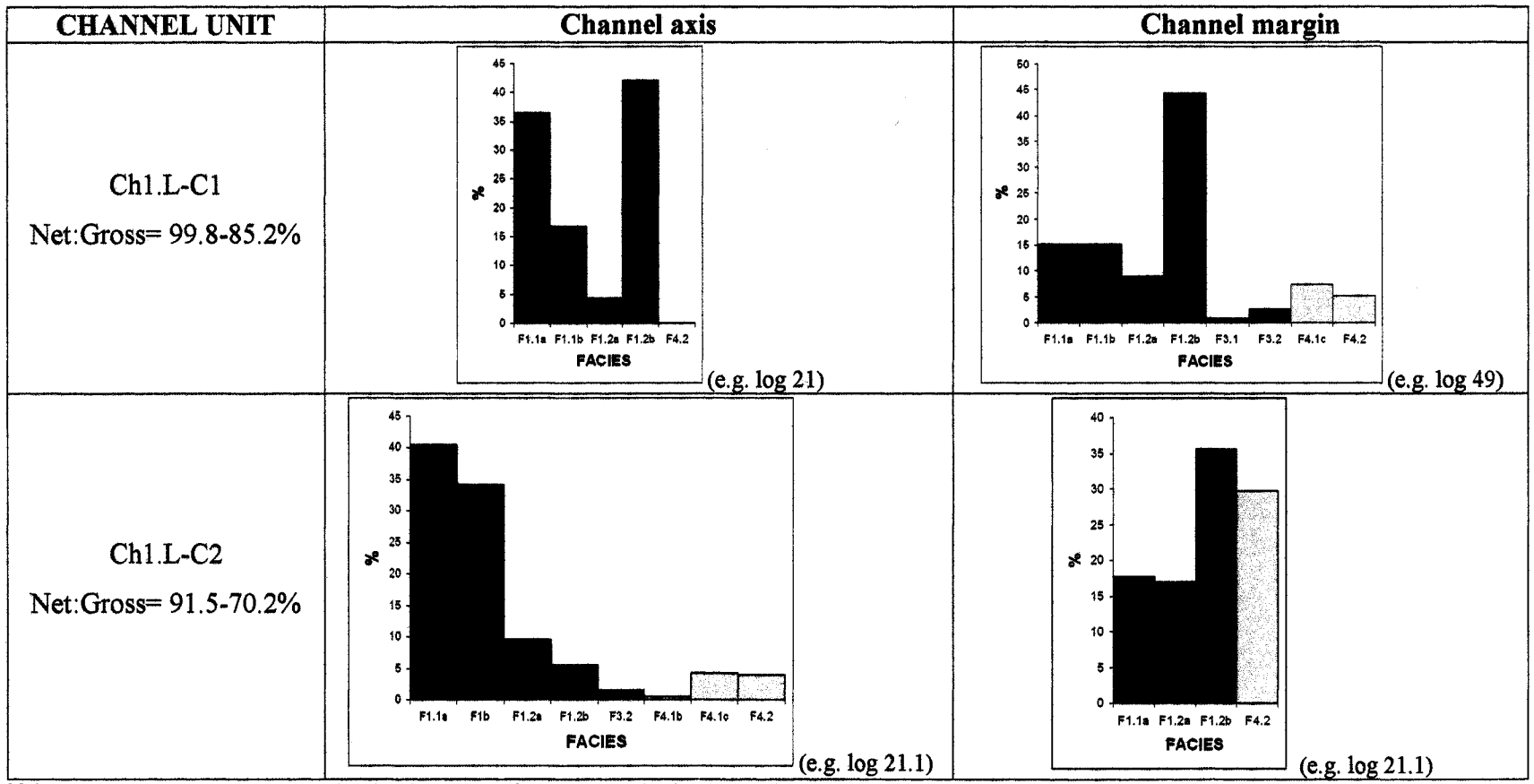

Figure V.1. Representative Facies types, distribution and N:G percentage in the Lower Channel Unit of Channel 1.

CHANNEL 1, *UPPER CHANNEL COMPLEX (Ch1.U)*

LOG	CHANNEL UNIT	LOG THICKNESS (m)	FACIES F1.1a			FACIES F1.1b			FACIES F1.2a			FACIES F1.2b			FACIES F2.1			FACIES F2.2			FACIES F3.1			FACIES F3.2			FACIES F4.1a			FACIES F4.1b			FACIES F4.1c			FACIES F4.2			COVER		% SANDSTONE	% MUDSTONE
			Total Thickness (m)	Ave. Bed Thickness (m)	%	Total Thickness (m)	Ave. Bed Thickness (m)	%	Total Thickness (m)	Ave. Bed Thickness (m)	%	Total Thickness (m)	Ave. Bed Thickness (m)	%	Total Thickness (m)	Ave. Bed Thickness (m)	%	Total Thickness (m)	Ave. Bed Thickness (m)	%	Total Thickness (m)	Ave. Bed Thickness (m)	%	Total Thickness (m)	Ave. Bed Thickness (m)	%	Total Thickness (m)	Ave. Bed Thickness (m)	%	Total Thickness (m)	Ave. Bed Thickness (m)	%	Total Thickness (m)	Ave. Bed Thickness (m)	%	Total Thickness (m)	Ave. Bed Thickness (m)	%	Total Thickness (m)	%		
12	Ch1.U-C1 (axial)	26.4	7.28	1.04	28.6	2.34	0.47	8.8	0.88	0.29	4	10.91	0.91	44.7	0.87	0.48	4							1.8	0.75	6.1										0.41	0.03	1.7			88.3	1.7
13	Ch1.U-C1 (axial)	30.85	8.18	0.87	15.9	4.04	0.37	13.1	10.69	0.81	34.5	8.18	0.82	26.5	0.26	0.13	0.8							1.83	0.64	5.9				0.62	0.27	2.7	0.1	0.1	0.3	0.07	0.01	0.2			90.7	9.3
14	Ch1.U-C1 (axial)	23.98	4.09	1.02	17.1	3.89	0.81	16.4	6.4	1.1	18.3	4.22	0.9	17.6	5.6	5.6	23.3							0.2	0.2	0.9				0.84	0.84	3.5	0.97	0.32	4.1	0.13	0.04	0.6			91.5	8.2
18	Ch1.U-C1	34.27	18.08	1.05	49.1	4.36	0.73	19.7	1.08	0.54	3.2	7.62	0.81	29.2										0.19	0.19	0.6	2.12	1.06	6.2	0.3	0.15	0.9	0.26	0.13	0.7	1.6	0.09	4.4			97.5	12.2
22	Ch1.U-C1	17.54	5.84	0.83	31.5	2.6	1.3	14.8	1.41	0.36	8	8.31	0.83	36	0.09	0.09	0.8																			0.87	0.1	5.4			94.5	5.5
61	Ch1.U-C1	23.14	5.14	0.86	23.5	13.23	0.74	57.2				0.2	0.2	0.8	0.6	0.3	2.6							0.19	0.1	0.8							3.04	0.76	13.1	0.74	0.06	3.2			83.7	16.3
31	Ch1.U-C1 (margin)	34.8	14.78	1.06	42.48	9.42	1.06	16.82	2.24	0.47	8.73	3.43	0.35	9.86	1.02	0.84	5.83	2.7	2.7	7.76	1.38	0.17	3.8				0.35	0.05-0.03	0.13	0.39	0.39	1.12	1.46	0.01-0.04	4.26	0.73	0.06	2.48			92.4	7.6
30	Ch1.U-C1 (margin)	28.16	13.09	1.01	34.3	10.87	0.99	28.49	3.17	0.79	9.31	4.13	2.07	16.89	2.69	0.87	7.66				1.31	0.22	3.49				0.42	0.053-0.03	1.4	0.08	0.08	0.21	1.88	0.02-0.04	4.49	0.71	0.06	1.98			91.43	8.57
29	Ch1.U-C1 (margin)	29.08	16.36	1.28	53.78	6.75	0.72	19.77	4.07	1.02	13.99	0.96	0.99	1.62	0.2	0.2	0.58				0.68	0.17	3.27							0.36	0.18	1.24	1.86	0.02-0.04	6.71	0.47	0.07	1.62			91.43	8.57
28	Ch1.U-C1 (margin)	27.02	18.8	1.11	58.47	1.09	0.96	3.46	1.34	1.34	4.96	1.39	0.33	5.43	0.06	0.06	0.53				1.36	0.17	4.62	0.09	0.09	0.39	0.63	0.3	3.66	0.16	0.16	0.64	2.02	0.03	7.31	0.36	0.09	1.39			87.22	12.79
26-26	Ch1.U-C1 (margin)	25.52	17.99	1.19	49.53	3.53	0.94	14.99	3.27	0.82	9.13	9.9	0.99	18.48	0.6	0.4	2.23				0.69	0.2	3.74	0.04	0.02	0.13				0.2	0.07	0.69	2.94	0.03-0.06	7.66	0.36	0.03	1.06			91.31	8.69
13	Ch1.U-C2 (axial)	16.17	0.89	0.89	4.85	6.11	0.98	37.88	1.27	1.27	8.37	9.8	0.91	45.8	1.03	1.03	12.73				0.07	0.07	0.45										0.37	0.14	1.28	0.17	0.03	1.02			97.1	2.9
48	Ch1.U-C2 (margin)	16.76	3.02	0.5	18.47	5.84	0.83	36.72				3.36	0.48	26.49	0.22	0.11	1.36	1.31	0.66	8.41	0.81	0.31	5.73	0.13	0.06	0.79	0.6	0.6	6.01				0.98	0.01-0.02	5.87	0.03	0.01	0.12			89.6	11
37	Ch1.U-C2 (margin)	15.84	4.18	1.05	26.39	5.69	0.95	37.18				3.23	0.65	24.39	0.56	0.19	3.47				0.27	0.18	5.04				0.1	0.1	0.63				0.8	0.4	5.04	0.68	0.1	4.39			87.44	12.56
39	Ch1.U-C2 (margin)	12.74	0.86	0.33	6.48	6.69	0.73	51.96				3.1	0.44	24.33	0.55	0.18	4.32				0.26	0.13	4.86							0.14	0.14	1.1	1.19	0.01-0.04	9.28	0.28	0.09	2.2			91.21	8.86
34	Ch1.U-C2 (margin)	19.99	17.66	1.19	46.48	3.53	0.94	13.99	3.27	0.82	8.13	9.9	0.99	16.49	0.6	0.4	2.23				0.69	0.2	3.74	0.04	0.02	0.13				0.2	0.07	0.69	2.94	0.03-0.06	7.66	0.36	0.03	1.06			91.31	8.69
27	Ch1.U-C2 (margin)	10.59	8.95	1.39	83.84	2.15	0.72	19.66				0.39	0.19	3.46							0.26	0.13	2.37										1.07	0.09-0.07	9.74	0.19	0.06	1.73			88.53	11.47
13	Ch1.U-C3 (axial)	7.69	0.83	0.83	10.79	1.26	0.42	16.36	0.38	0.38	4.89	4.26	0.94	55.36										0.24	0.24	4.48				0.25	0.25	3.25	0.33	0.33	4.29	0.05	0.05	0.66			91.8	8.2
47	Ch1.U-C3 (margin)	11.02	4.14	1.04	37.6	3.13	0.78	28.4	1.68	1.68	14.3	0.83	0.21	6.7				1.42	1.42	12.8										0.1	0.1	0.9				0.03	0.01	0.3			98.8	1.2
40	Ch1.U-C3 (margin)	13.84	11.75	1.18	81.4	3.92	0.98	28.8	0.33	0.11	1.3	0.83	0.21	4.4	0.06	0.06	0.3							0.24	0.24	4.48							1.28	0.02	9.8	0.21	0.11	1.1			92.52	9.9
27	Ch1.U-C3 (margin)	26.82	7.07	1.77	26.8	8.37	1.2	34.1	1.09	0.36	4.4	9.99	0.95	15.8										0.37	0.37	1.4				0.32	0.32	1.3	2.16	0.01-0.06	8.8	1.23	0.15	6.1			84.7	16.3

Table V.2. Chart of lithofacies distribution and percentage of sandstone in Upper Channel Complex of Channel 1 (Ch1.U). For Nomenclature see p. 246.

CHANNEL UNIT	Channel axis	Channel margin
Ch1.U-C1 Net:Gross= 98.3-83.7%	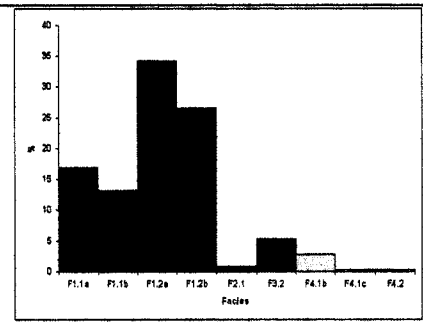 (e.g. log 13)	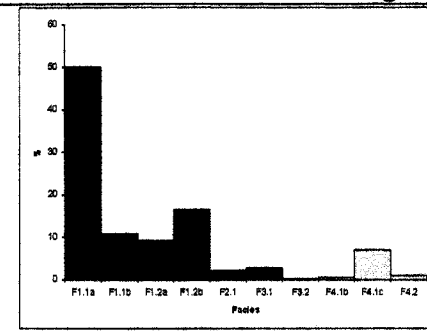 (e.g. log 25-26)
Ch1.U-C2 Net:Gross= 97.1-87.44%	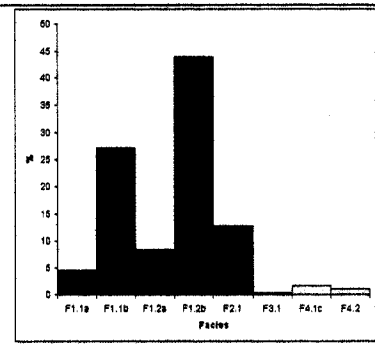 (e.g. log 13)	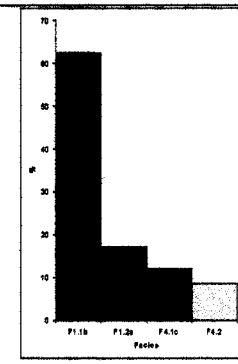 (e.g. log 27)
Ch1.U-C3 Net:Gross= 92.52-84.4 %	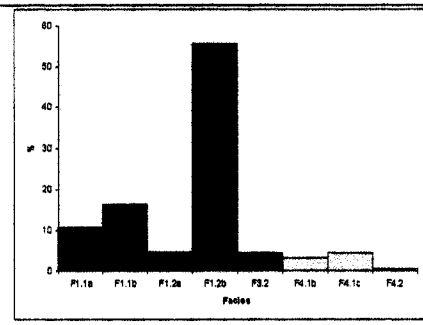 (e.g. log 13)	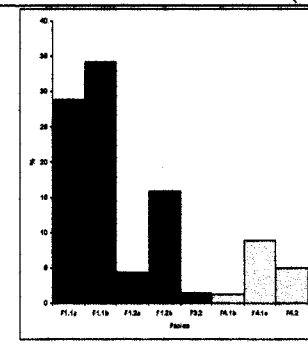 (e.g. log 27)

Figure V.2. Facies types, distribution and N:G percentage in the representative sections of Upper Channel Unit of Channel 1.

CHANNEL 3, *LOWER CHANNEL COMPLEX (Ch3.L)*

			FACIES F1.1a			FACIES F1.1b			FACIES F1.2a			FACIES F1.2b			FACIES F2.1			FACIES F2.2			FACIES F3.1			FACIES F3.2			FACIES F4.1a			FACIES F4.1b			FACIES F4.1c			FACIES F4.2			COVER			
LOG	CHANNEL	LOG	Total	Avg. Bed	%	Total	Avg. Bed	%	Total	Avg. Bed	%	Total	Avg. Bed	%	Total	Avg. Bed	%	Total	Avg. Bed	%	Total	Avg. Bed	%	Total	Avg. Bed	%	Total	Avg. Bed	%	Total	Avg. Bed	%	Total	Avg. Bed	%	Total	Avg. Bed	%	Total	%	% SANDSTONE	% MUDSTONE
	UNIT	THICKNESS (m)	Thickness (m)	Thickness (m)		Thickness (m)	Thickness (m)		Thickness (m)	Thickness (m)		Thickness (m)	Thickness (m)		Thickness (m)	Thickness (m)		Thickness (m)	Thickness (m)		Thickness (m)	Thickness (m)		Thickness (m)	Thickness (m)		Thickness (m)	Thickness (m)		Thickness (m)	Thickness (m)		Thickness (m)	Thickness (m)		Thickness (m)	Thickness (m)		Thickness (m)			
2	Ch3.L-C1	12.96	3.7	0.74	28.6	2.6	0.4	21.6	2.1	0.4	16.1	3.65	0.33	28.2																0.64	0.005-0.04	4.9				0.08	0.03	0.6			94.5	5.5
4	Ch3.L-C1 (margin)	18.76	4.45	1.11	23.7	3.9	1.3	20.8	9.37	0.85	49.9				0.1	0.1	0.6							0.15	0.15	0.8	0.04	0.04	0.2				0.62	0.01-0.03	3.3	0.13	0.07	0.7			95.7	4.2
6	Ch3.L-C1	7.68	2.35	2.35	31	2.72	1.36	35.9	1.2	1.2	15.9	0.7	0.7	9.2	0.6	0.15	7.9																					0.01	0.01	0.2			99.8	0.2
2	Ch3.L-C2	2.5				0.5	0.5	20				0.6	0.6	24	1.4	0.5	56																								100	0
5	Ch3.L-C2 (axis)	13.38	2.36	2.36	17.6							2.67	1.44	21.4	8	8	59.8																0.1	0.02-0.03	0.8	0.07	0.02	0.6			98.8	1.2
2	Ch3.L-C3 (margin)	11.46				0.95	0.48	8.3	1.5	0.8	13.1	7.4	0.4	65	0.28	0.28	2.4				0.4	0.4	3.5	0.06	0.06	0.7	0.55	0.28	4.7				0.05	0.02-0.04	0.1	0.3	0.04	2.2			93	7
5	Ch3.L-C3	9.26	0.98	0.98	10.4	0.38	0.38	4.1	4.72	1.9	51	1.54	1.54	16.9				1.17	0.59	12.6													0.12	0.02-0.04	1.2	0.07	0.02	0.8			98	2
7	Ch3.L-C3 (axis)	10.82										7.5	1.25	69.3	3.3	1.1	30.5																			0.02	0.01	0.2			99.8	0.2
5	Ch3.L-C4	10.4	2.31	0.77	22.2	1.89	0.95	18.2	2.81	7.24	27	2.85	0.41	27.4	0.2	0.2	1.9																0.15	0.02-0.03	1.4	0.19	0.02	1.9			96.7	3.3
7	Ch3.L-C4 (axis)	26.3	1.25	1.25	4.8	1.2	1.2	4.6				20.51	1.14	78	2.43	0.35	9.2																			0.91	0.1-0.05	3.4			96.6	3.4
10	Ch3.L-C4 (margin)	32.36				27.89	1.14	84.7				1.71	0.86	5.3	0.53	0.13	1.6							0.53	0.27	1.6							0.7	0.7	2.2	0.9		2.8	0.59	0.089	1.8			93.2	6.8
66	Ch3.L-C4 (margin)	23.94				15.13	0.72	63.2				3.95	0.49	16.5													0.95	0.48	3.97	1.57	0.05	6.56	1.22	0.05-0.3	5.1	1.12	0.1	4.67			79.7	20.3

Table V.3. Chart of lithofacies distribution and percentage of sandstone in Lower Channel Complex of Channel 3 (Ch3.L). For Nomenclature see p. 246.

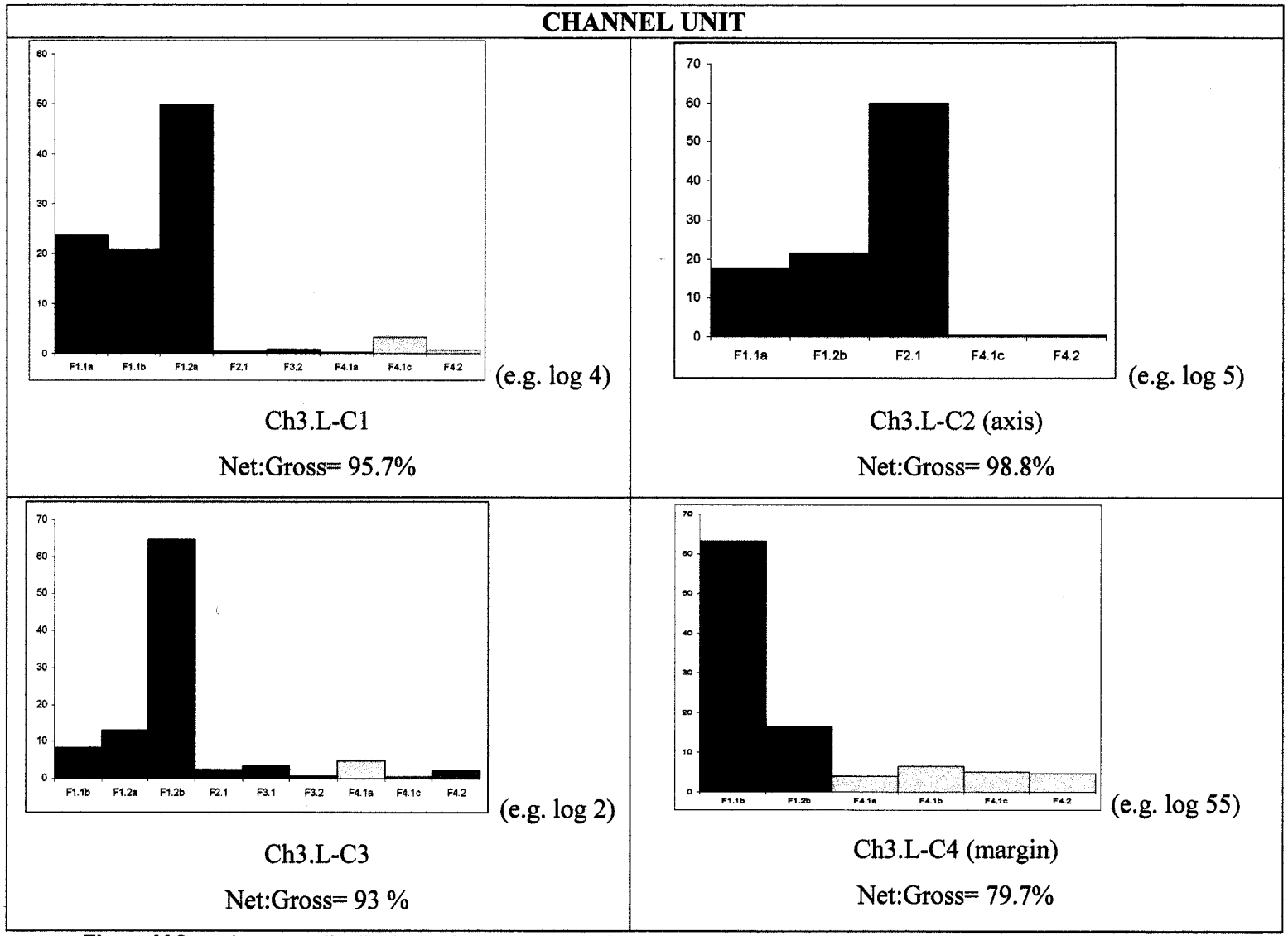

Figure V.3. Facies types, distribution and N:G percentage in representative sections of Lower Channel Complex of Channel 3.

CHANNEL 3, *MIDDLE AND UPPER CHANNEL COMPLEXES (Ch3.M and Ch3.U)*

LOG	CHANNEL UNIT	LOG THICKNESS (m)	FACIES F1.1a			FACIES F1.1b			FACIES F1.2a			FACIES F1.2b			FACIES F2.1			FACIES F2.2			FACIES F3.1			FACIES F3.2			FACIES F4.1a			FACIES F4.1b			FACIES F4.1c			FACIES F4.2			COVER		% SANDSTONE	% MUDSTONE
			Total Thickness (m)	Avg. Bed Thickness (m)	%	Total Thickness (m)	Avg. Bed Thickness (m)	%	Total Thickness (m)	Avg. Bed Thickness (m)	%	Total Thickness (m)	Avg. Bed Thickness (m)	%	Total Thickness (m)	Avg. Bed Thickness (m)	%	Total Thickness (m)	Avg. Bed Thickness (m)	%	Total Thickness (m)	Avg. Bed Thickness (m)	%	Total Thickness (m)	Avg. Bed Thickness (m)	%	Total Thickness (m)	Avg. Bed Thickness (m)	%	Total Thickness (m)	Avg. Bed Thickness (m)	%	Total Thickness (m)	Avg. Bed Thickness (m)	%	Total Thickness (m)	Avg. Bed Thickness (m)	%	Total Thickness (m)	%		
63	Ch3.M-C2	**12.18**	2.45	1.23	20.1	1.64	0.23	13.5	1.79	0.26	14.7										0.08	0.08	0.7							0.12	0.12	1	5.97	0.01-0.05	49	0.13	0.04	1			**49**	**51**
24	Ch3.M-C1	**15.99**	0.27	0.27	1.7	2.66	1.33	16.6	0.22	0.22	1.4	9.54	0.87	59.7	2.05	0.88	12.8							1.06	0.26	6.5										0.2	0.03	1.3			**98.7**	**1.3**
66	Ch3.U	**19**	1.66	0.95	8.8	15.2	0.76	79.8				0.56	0.56	2.9	1.35	0.45	7.3																			0.04	0.04	0.2			**99.8**	**0.2**

Table V.4. Chart of lithofacies distribution and percentage of sandstone in Middle and Upper Channel Complexes of Channel 3 (Ch3.M, Ch3.U).

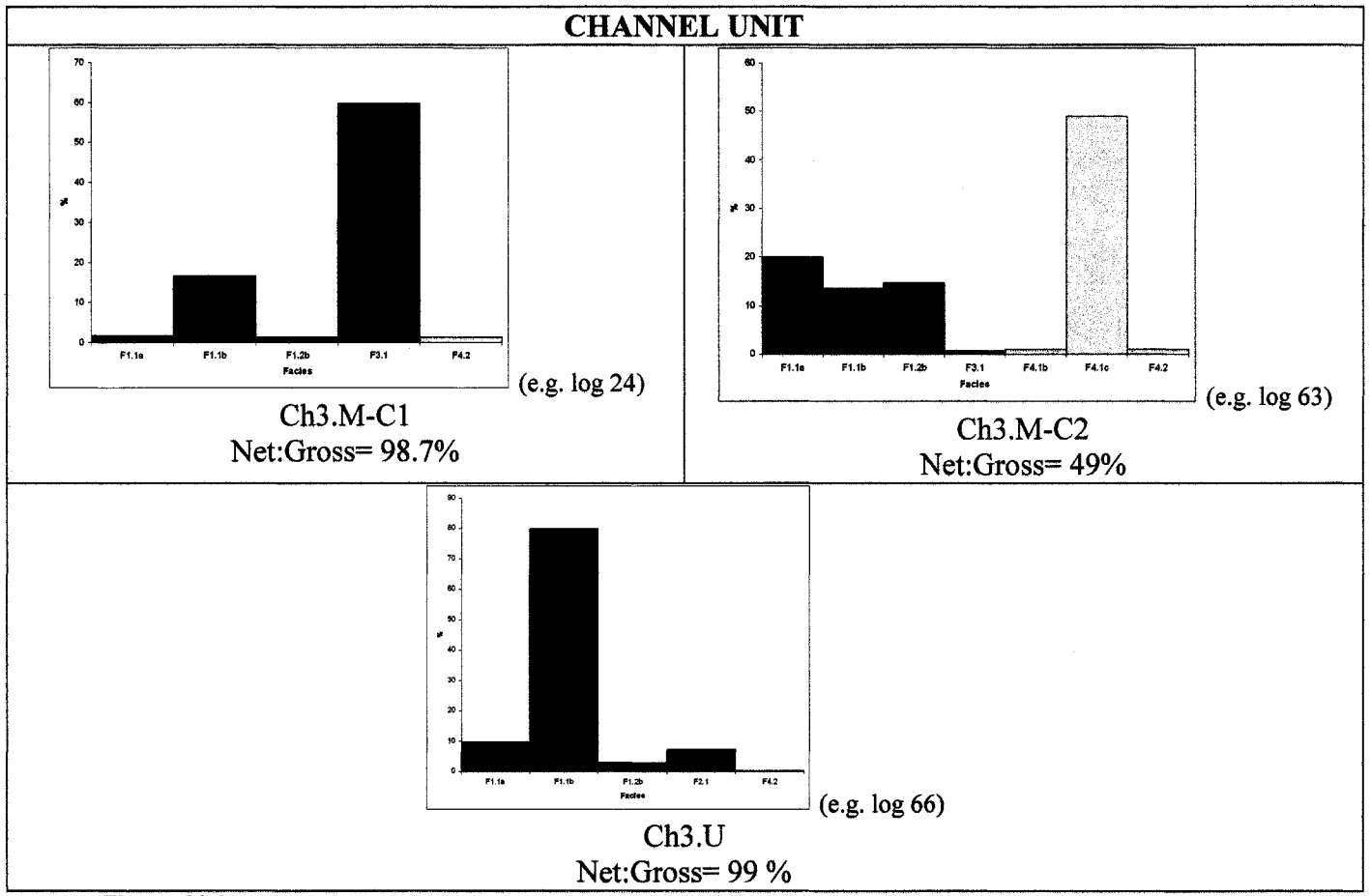

Figure V.4. Facies types, distribution and N:G percentage in the Middle and Upper Channel Units of Channel 3.

APPENDIX VI. Paper publication.

This appendix is a partial reproduction of the hardcopy- and CD-version papers 'Depositional Architecture and Evolution of a Deep-Marine Channel-Levee Complex: Isaac Formation (Windermere Supergroup), Southern Canadian Cordillera (Castle Creek South - Channel 3)' by Navarro U., L.; Z. Khan A. and R.W.C. Arnott, submitted and accepted for publication in a 'AAPG Atlas of Deepwater Outcrops', edited by T. Nilsen, Shew, G. Steffens, and J. Studlick, AAPG Special Publication, 2006.

Sections that are entirely part of the research project of graduate student Zishann A. Khan have been highlighted in this paper.

Depositional Architecture and Evolution of a Deep-Marine Channel-Levee Complex: Isaac Formation (Windermere Supergroup), Southern Canadian Cordillera (Castle Creek South - Channel 3)

Lilian Navarro U., Zishann A. Khan and R. William C. Arnott. Department of Earth Sciences, University of Ottawa, 140 Louis Pasteur St., K1N 6N5, Ottawa, ON, Canada.

Executive Summary

Channel 3 in the Castle Creek South study area (Figure 1; for geological overview look at Ross and Arnott, this volume) exposes a leveed channel system that is up to 90 m (300 ft) thick and extends at least 1.6 km (1 mi) laterally (Figure 2). The channel-levee system overlies an areally extensive, up to 80 m (260 ft)-thick carbonate-clast-rich debrite (D1). Locally, the debrite is overlain by a thick (up to 3 m; 10 ft), sheet-like, coarse-grained, sand-rich, heterolithic assemblage (L_o) interpreted to have been emplaced by relatively unconfined, high-density flows. These strata, in addition to topography along the top of the debrite, helped focus subsequent flows that ultimately formed Channel 3.

Channel 3 consists of four channel-fill units (C1 to C4) that stack in a lateral-offset pattern toward the northwest. These fills vary from 7 to 30 m (23 - 99 ft) thick, and have high N:G ratios (70 - 100 %). In their axis, channel-fill strata consist typically of thick-bedded (up to 3 m; 10 ft), massive to graded, pebble conglomerate and very coarse to medium sandstone, and mudstone-clast breccia that were deposited by high concentration, gravel- and sand-rich turbidity currents. In the upper part of Channel 3 (C3 and C4), strata near the margin of the channel consist of thick-bedded (up to 1.5 m; 5 ft) amalgamated sandstone that laterally become progressively more interbedded with siltstone and very fine to fine sandstone. These strata were deposited by low- to moderate-concentration flows.

Channel-fill strata are bounded on both sides by levee deposits. Adjacent to the northwest (outer-bend) margin, proximal levee (T1) units (L1 - L4) are laterally offset in the same direction as related channel units and consist predominantly of fine to medium sandstone, medium- to thick-bedded T_{cs} turbidites with a N:G up to 0.7. Laterally these strata commonly thin over lengths less than 300 m (984 ft) and thereafter persist as thin (< 15 cm, 6 in), very fine to fine sandstone and siltstone, commonly upper division turbidites (T_{cs}). It is these strata that make up the distal part of the outer bend levee (T2). Intercalated with distal strata are overbank splay deposits consisting of laterally extensive but discontinuous, up to 1 m (3.28 ft) thick, medium to coarse sandstone turbidites. On the opposite side of the channel fill, deposits forming the inner-bend levee (T3) fine and thin upward and consist predominantly of very fine sandstone and siltstone T_{cs} turbidites interbedded with uncommon medium sandstone beds more than 0.20 m (0.66 ft) thick. Outer and inner bend levee strata are interpreted to have been deposited by low- to moderate-concentration flows spilling out of the channel.

Aggradation and unidirectional migration of the entire system toward the northwest produced a composite terraced, erosive "flat and step" geometry along the outer-bend channel margin that sharply separates levee from channel-fill strata (Figure 7). These relationships support the notion that each channel-levee unit was formed by a common sequence of depositional events and that levee growth predated filling of the related channel unit.

Outcrop Summary	
Channel 3 (Castle Creek South)	
Location	
Specifics	Castle Creek area: Lat 53 - 53°25' N; Long 120°02' - 120°03 W
Region/ province/ state	British Columbia
Country	Canada
Formation Name	Isaac Formation
Age	Neoproterozoic (~569 - 607 Ma)
Basin Setting	Passive margin linked with the development of the proto-Pacific Ocean along the western margin of North America. Slope depositional system that shows a shoaling-upward upward trend from basin floor to shelf deposits.
Basin Size	~35,000 km^2 (11 700 mi^2; palinspastically unrestored)
General Outcrop Description and Stacking Pattern	Predominantly sand-rich system. An areally extensive mass transport complex (D1) occurs at the base of the study area. This element is overlain by Channel 3, which comprises four channel units (C1 - C4) that form a multilateral offset stacking pattern toward the northwest. Channel units are fringed by levee deposits (T1 - T3).
Depositional Setting Interpretation	Channel 3 was associated with multiple episodes of channel and levee growth that were in turn connected with the long term migration of the entire system progressively towards the northwest. In addition, the width of the channel belt decreased upwards, suggesting a change in flow conditions over time.
Overall Outcrop Dimensions in Panel	
Length	1.4 km (~ 870 mi)
Thickness	100 m (328 ft)
Average Net/Gross	70 - 100% (channel-fill strata) < 40 - 70% (levee strata)
Grain size range	Very fine sandstone to cobble conglomerate
Other	Periglacial outcrops occur along the periphery of fast-retreating Pleistocene glaciers. Outcrops are well-exposed on the steeply-dipping limb of a west-verging, SW-NE trending, overturned anticline. Minor normal faulting (offset < 0.5 - 2 m, 1.64 - 6.56 ft) and low grade metamorphism (primary sedimentary textures and structures have been preserved).

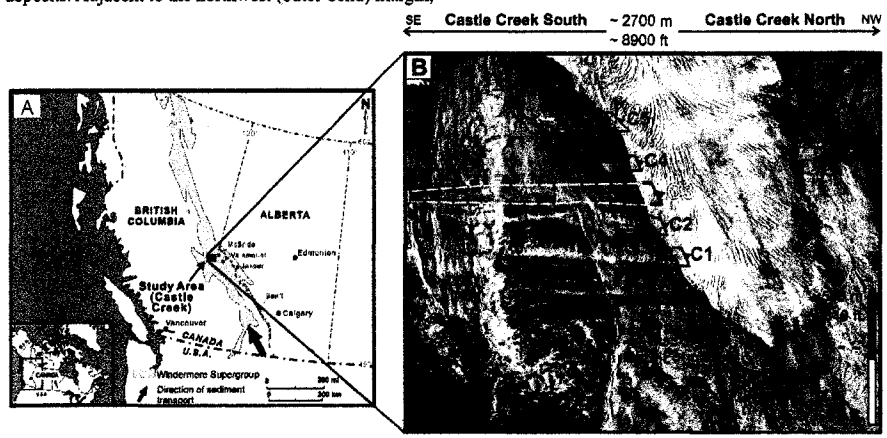

Figure 1. Location of the study area shown in relation to: (A) map of western Canada showing the distribution of Windermere strata. Outcrop distribution and inferred paleocurrent trend are from Ross and Murphy (1989) and Ross (1991). (B) Airphoto mosaic of the Castle Creek area in the Cariboo Mountains, British Columbia that illustrates the location of the main sandstone-rich channel fill units recognized in the Isaac Formation (C1-C6). Channel 3 is indicated by dashed rectangle (including adjacent levee deposits).

Architectural Element Number on Outcrop Photo or Interpretation

Channel-form Architectural Elements	C1	C2	C3	C4
Channel-form	Partial: erosive base and top	Partial: erosive base and top	Partial: erosive base and top	Partial: erosive base and top
Width	> 500 m (> 1640 ft)	> 550 m (1804 ft)	~600 m (1968 ft)	~600 m (1968 ft)
Thickness	20 - 30 m (66 - 98 ft)	15 m (49 ft)	7 - 15 m (23 - 49 ft)	10 - 30 m (33 - 98 ft)
Aspect ratio:Width/thickness	~1500/20= ~75 (one margin exposed)	~1000/15= ~66.6 (one margin exposed)	< 39	< 14
Net/Gross	80 - 95%	90 - 95%	88 - 100%	70 - 93%
Outcrop orientation for this element	Near vertical beds: strike 325-330°	Near vertical beds: strike 325-330°	Near vertical beds: strike 325-330°	Near vertical beds: strike 325-330°
Average paleocurrent	130-230°	NA	40°	NA
Typical facies Succession	Pebble to granule conglomerate and coarse to very coarse sandtone (Ta, rare Tb), partial Bouma sequences (Tacde, Tcde and Tade) are common at the top	Mudstone-clast breccia especially at the base, granule to pebble conglomerate and very to coarse sandstone (Ta)	Granule conglomerate, coarse to very coarse sandstone (Ta), and less commonly partial Bouma sequences (Tcde and Tde). Mudstone-clast breccia at the base.	Axis: coarse to very coarse sandstone (Ta), and granule conglomerate Margins: coarse to very coarse sandstone (Ta), and top of Bouma sequence (Tbc, Tcde, and Tde)
Channel infill bedding architecture	Complete to partial amalgamated, locally layered especially in upper part of fills	Amalgamated	Layered, SE margin convergence via onlap	Layered/ stratified toward the NW margin
Sand/Conglomerate Bed Architecture				
Bed length range	1 - > 500m (3 - > 1640 ft)	2 - > 500 m (7 - > 1640 ft)	100 - 400 m (328 - 1312 ft)	250 - 500 m (820 - 1640 ft)
Bed length average	30 - 50 m (98 - 164 ft)	100 m (328 ft)	175 m (574 ft)	300 m (984 ft)
Bed thickness range	0.02 - 3 m (0.7 - 10 ft)	0.5 - 8 m (2 - 26 ft)	0.06 - 2.3 m (0.2 - 7.5 ft)	0.01 - 2 m (0.03 - 7 ft)
Bed thickness average	0.5 - 0.9 m (1 - 3 ft)	1.2 m (3.93 ft)	0.6 m (2 ft)	0.3-1.4m (1-4.6 ft)
Texture - grain size range, average, and sorting	Fine sandstone to cobble conglomerate, very coarse sandstone to pebble conglomerate, poorly sorted	Fine sand to cobble, coarse sandstone to granule, poorly sorted	Very fine sandstone to cobble, coarse to granule, poorly sorted	Very fine to cobble, coarse sandstone, moderately to well sorted at margins
Channel-base shale drape coverage	2%	NA	NA	1%
Channel-base shale drape thickness	up to 2.5 m (8.2 ft)			1 m (3 ft)
Shale Bed Architecture				
Bed length range	0.5 - > 500 m (1.6 - >1640 ft; one margin is missing)	0.5 m - 2m (1.6 - 6.8 ft; one margin is missing)	75 - 200 m (246 - 656 ft)	250 - 500 m (820 - 1640 ft)
Bed length average	1 - 57 m (3 - 190 ft)	1 m (3 ft)	100 m (328 ft)	250 m (820 ft)
Bed thickness range	1 - 30 cm (0.4 - 12 in)	1 - 20 cm (0.4 - 8 in)	1 - 8 cm (0.4 - 3 in)	1 - 32 cm (0.4 - 12 in)
Bed thickness average	2 - 4 cm (0.8 - 2 in)	19 cm (7.4 in)	1 cm (0.4 in)	5 - 10 cm (2 - 4 in)

Thinbed Architectural Elements	T1 (NW proximal, including L_0)	T2 (NW distal, including L_0)	T3 (SE)
Length	> 420 m (> 1370 ft)	> 300 m (> 984 ft)	> 250 m (> 820 ft)
Thickness	Up to 52 m (741 ft)	80 m (262 ft)	up to 40 m (131 ft)
Net\Gross	56 - 70%	50% (increased by the ocurrence of overbank splay deposits)	40 - 55%
Texture - grain size range, average, and sorting	siltstone to very coarse sandstone, fine to medium sandstone average, moderately to well sorted	siltstone to medium sandstone predominant, well sorted	Siltstone to fines sandstone predominant, well sorted
Outcrop orientation for this element	Near vertical beds: strike 330°	Near vertical beds: strike 330°	Near vertical beds: strike 330°
Average paleocurrent	27°	Variable	---
Typical facies succesion	Typically partial Bouma sequences Ta-e, c[illegible]rsest beds occur[illegible] base of s[illegible]ction	Tc-e's interstratified with rare Tbc turbidites and overbank splay deposits Overbank splay deposits: massive to faintly laminated coarse to medium sandstone turbidites	Tc-e turbidites interbedded with rare Tab turbidites
Sand Bed Architecture			
Bed length range	50 - > [illegible] m (165 - > [illegible] ft)	50 - > 300 m (160 - > 984 ft)	30 - > 300 m (164 - > 328 ft)
Bed length average	> 420 [illegible] (> [illegible] ft)	> 300 m (> 900 ft)	> 300 m (> 984 ft)
Bed thickness range	3 - 100 [illegible] (1 - 39 in)	3 - 150 cm (1 - 59 in)	1 - 68 cm (0.4 - 32 in)
Bed thickness average	40 c[illegible] (16 in)	10 cm (4 in)	1 - 25 cm (0.4 - 10 in)
Shale Bed Architecture			
Bed length range	> 420 [illegible] (> 1380 ft)	> 300 m (> 984 ft)	> 300 m (> 328 ft)
Bed length average	NA	NA	NA
Bed thickness range	0.3 - 35 [illegible] (0.1 - 14	0.3 - 45 cm (0.1 - 18	1 - 10 cm (0.4 - 4 in)
Bed thickness average	10 [illegible] (4 in)	10 cm (4 in)	2 - 5 cm (1 - 2 in)

Debrite Architectural Elements	D1 Regional	D2 (local)
Length	> [illegible]00 m (> 45[illegible]2 ft)	50 m (164 ft)
Thickness	up to 90 m (29[illegible]2 ft)	up to 7 m (23 ft)
Net\Gross	NA	NA
Outcrop orientation for this element	Strike 330	Strike 330°
Average paleocurrent	NA	NA
Typical facies succesion	Mud-silty matrix, carbonate clasts and large interbedded sandstone rafts	mud-rich matrix, quartz pebbles

Analog Reservoirs or Fields	e.g. West Coast Africa, Gulf of Mexico and East Coast Canada

KHANSAW[illegible]K

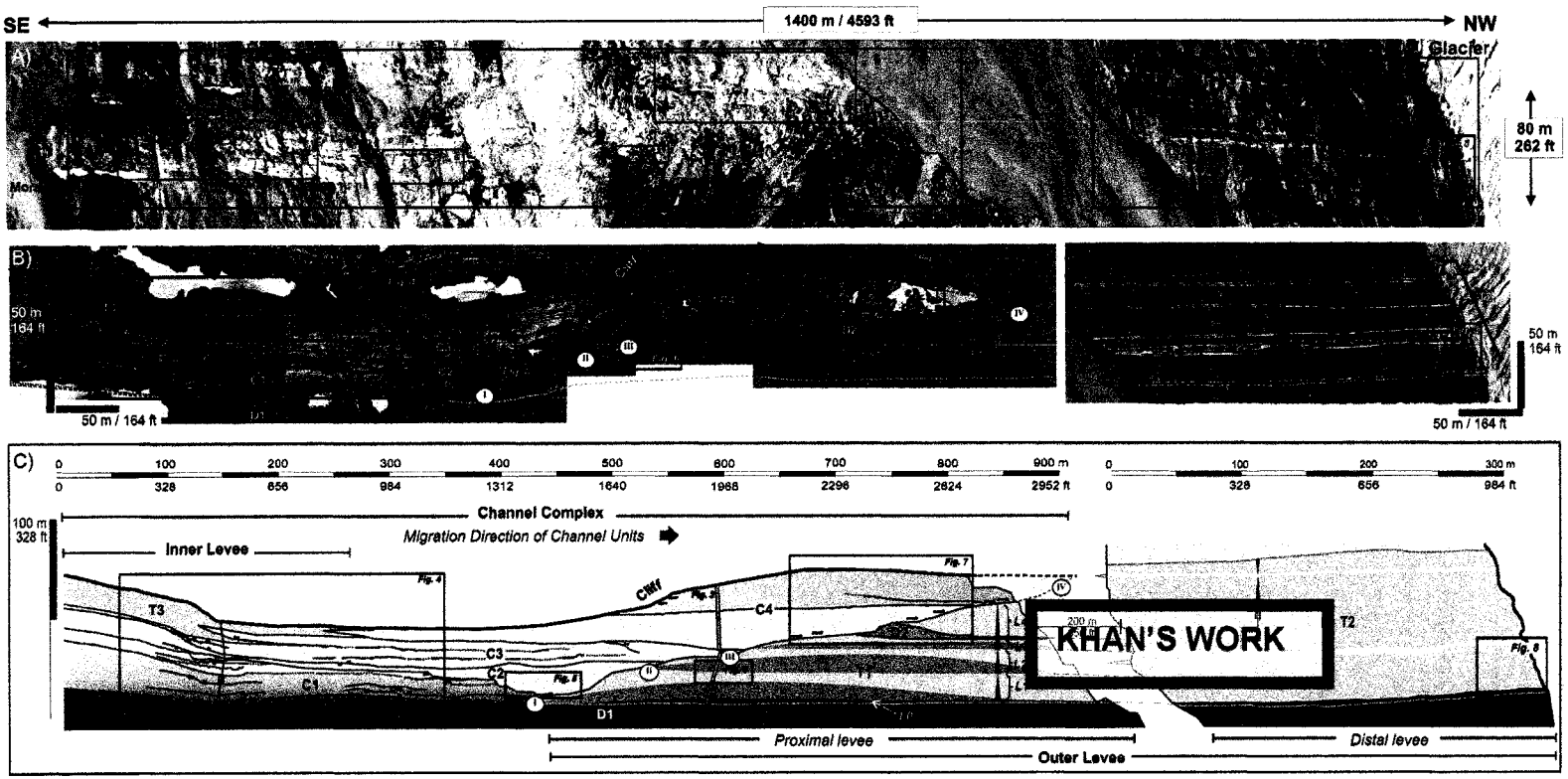

Figure 2. Vertical and lateral stacked channel-levee units of Channel 3, Castle Creek South. (A) Aerial photo showing the 1.4 km (0.9 mi) outcrop belt. (B) Photomosaic showing confined channel complex, highlighting the major channel fills and proximal and distal levee deposits. (C) Restored architectural panel that illustrates the channel network and levee deposits.

Channel units: Channel 3 consists of four channel units (C1-C4), each up to 30 m thick and individually comprising two or more genetically-related channel fills. Channel units exhibit upward changes in their configuration from wider, conglomerate- and sandstone-filled to narrower, mixed (sandstone-siltstone) filled channels (Fig. 3-5,7). Typically, channel fills show high bed amalgamation in the lower part of their axes, that laterally (especially evident in the upper channel units) and vertically is reduced due to the common ocurrence of siltstone interbeds.

Levee un ee deposits (T1) compris four distinct packages (T1-1 to 4) which ar divided into a sand-rich l ve a ne-ri upper part (light green; e Fig. 6 for more detail). These depos , especially strata makin packages, fine and thin laterally into the distal levee areas (T2, Fig. 8) where they are interstratified with numerous overbank-splay deposits. Along the southeast margin, fine-grained levee deposits (T3) interfinger with strata of the uppermost channel fills (Fig. 4).

KHAN'S WORK

Stacking Pattern: Channel 3 shows a complex vertical and lateral (offset) stacking pattern of both channel and levee units, reflecting the continuous migration of the channel system toward the northwest.

Composite Terraced basal surface: Migration of the channel axis of each unit eroded the cutbank, creating a composite terraced basal surface along the northwest margin, separating the channel fills and levee deposits (Fig. 7). Terraces suggest that channel and levee growths occurred episodically, after a period of erosion.

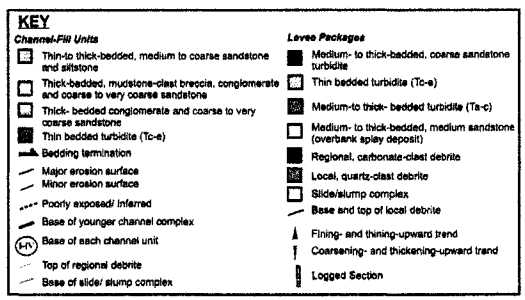

Figure 3. General Stratigraphic section of channel-levee deposits of Channel 3 illustrating contrasting lithological make up of proximal levee and channel-fill deposits.

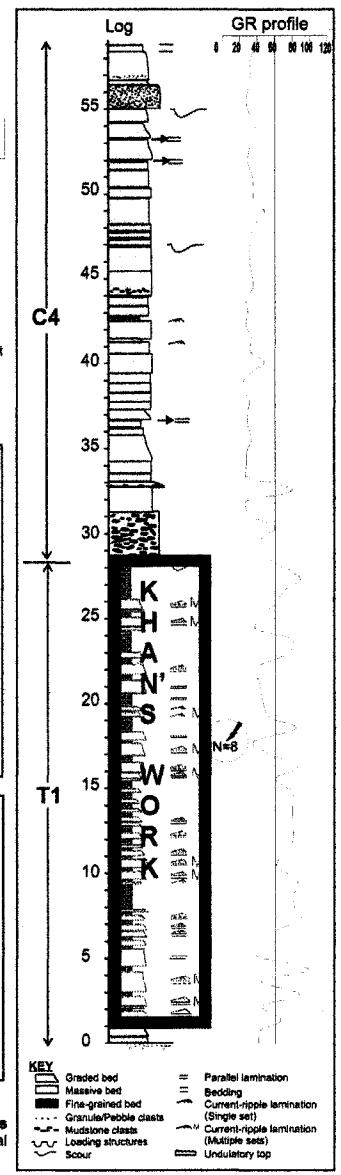

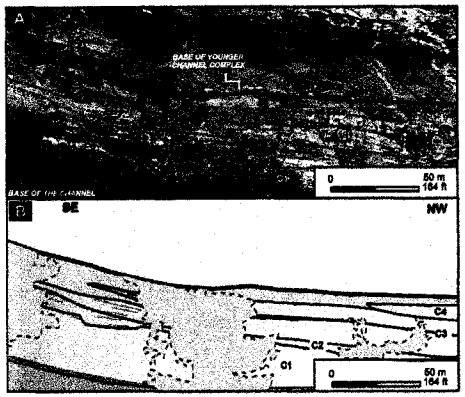

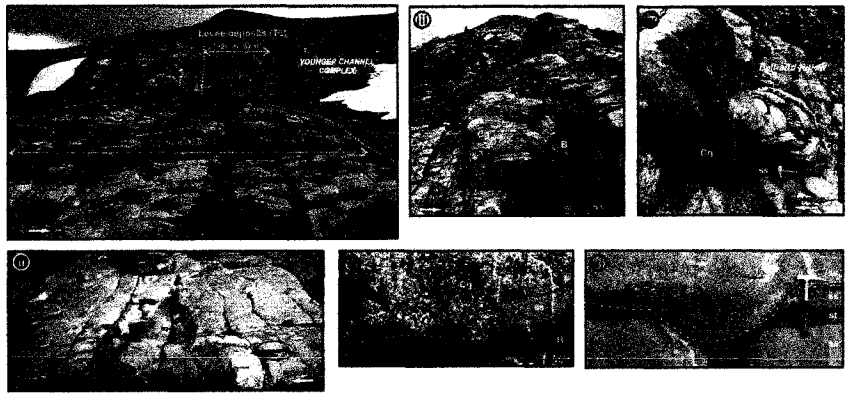

Figure 4. Channel and levee units along the SE margin of Channel 3. A) Uninterpreted, B) interpreted (see Key in Fig. 7). Channel fills of channel units C3 and C4 interfinger with thin bedded levee deposits, which are consider to be deposited by lower energy overbanking flows on the inner channel-bend (eg. Fig i); i-vi) strata in the axis of channels: Thick-bedded (up to 3 m, 10 ft), massive to graded conglomerate (Cg) and very coarse to coarse sandstone (ss), corresponding to Ta Bouma or R3/S3 Lowe sequences. Local mudstone-clast breccias are also observed. Siltstone interbeds (st, as shown in Fig. vi) are common toward the top of channel fills; vi-iv) in the channel axis, beds have common erosional (yellow dotted lines) and load bases, including ball-and-pillow and local combined (scour and load) structures. Toward the channel margin, coarse-grained strata tend to thin rapidly over a few hundred meters, and grade from (complete or partial) amalgamated sandstone to being interbedded with thin- to medium-bedded (up to 30 cm, 12 in) upper-division turbidites. Individual channel fills commonly fine and thin upward and laterally.

Figure 5. Example of a major erosion surface in Channel 3. The basal erosion surface of Channel-unit 3 (C2) is generally shallow (less than 1 m, 3.3 ft deep) but locally deeply scoured (up to 8 m, 26 ft deep), truncating the underlying channel-fill unit C1, which consists mostly granule to pebble conglomerate, including i) local carbonate clasts, and coarse to very coarse sandstone. Laterally extensive, mudstone (rip-up) clast breccia zones overlie the base of many channel fills and units. Although breccia layer are highly amalgamated, local lenses or remnants of conglomerate (Cg) and sandstone are observed.

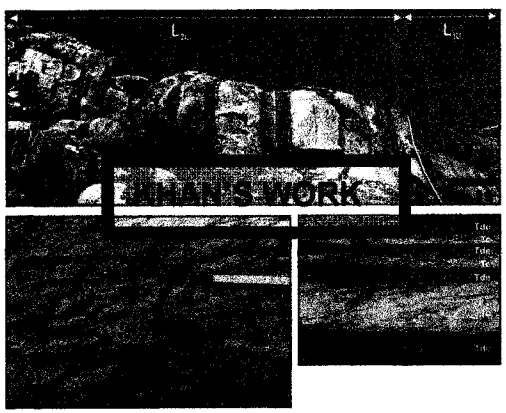

Figure 6. Proximal levee deposits adjacent to the NW margin of Channel 3 (view from SE). Proximal levee deposits comprise four units (L1-L4) which are commonly divided into lower and upper parts. The lower portion (in photo L_x corresponds to the lowermost portion of the second levee unit) consists of medium- to thick-bedded (up to 1 m, 3 ft), fine to medium sandstone turbidites (Ta-e Bouma sequences), including i) beds up to 40 cm (16 in) consisting of multiple, non-climbing, small scale (ripple) cross-laminated sets. The upper portion (in photo L_u corresponds to the uppermost portion of the first levee unit) consists predominantly of ii) thin bedded (< 15 cm, < 6 in), very-fine to fine sandstone and siltstone (Tcde turbidites).

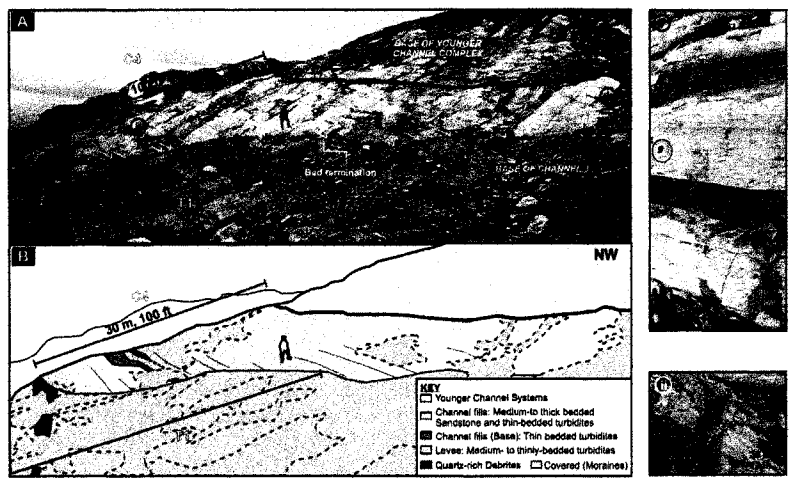

Figure 7. NW Channel margin of Channel 3. A)Uninterpreted, B) Interpreted. Intrachannel strata of the upper channel unit (C4) onlap fine-grained levee deposits and quartz-clast debrite. The irregularity of the margin is related to erosion along the outer channel bend or cutbank of the channel; i) strata near the margin of channel C4 are less amalgamated compared to the strata in the channel axis and is composed of medium- to thick bedded (up to 2 m, 7ft), coarse sandstone (Ta Bouma and S3 Lowe sequences) interbedded with thin-to medium- bedded (less than 40cm, 16in) siltstone and/or very fine to fine sandstone (Tcde turbidites). Beds thin toward the erosion surface; ii) up to 2 m/ 6.6 ft thick intervals of thin bedded, non-amalgamated, fine-grained turbidites (dark green in diagram) at the base of some channels are interpreted to be bypass facies deposited from the dilute tails of high-concentration flows.

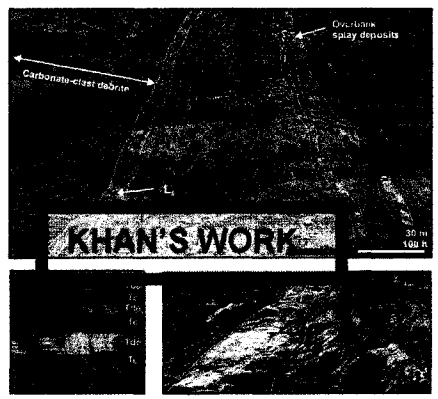

Figure 8. Distal levee deposits (view from NW). Debrite (D1) is abruptly overlain by an interval of medium to coarse sandstone (L_x). These strata, in turn, are overlain by distal levee deposits that comprise thinly-bedded turbidites interstratified with common overbank splay deposits. i) detailed view of thinly bedded (< 15 cm, < 6 in), very-fine to fine sandstone and siltstone turbidites (Tc-e); ii) intercalated overbank splay deposits which commonly comprise up to 5 m (13 ft) thick intervals of amalgamated, medium sandstone turbidites.

References

Ross, G.M. 1991. Geology, v.19, p.1125-1128

Ross, G.M. and Murphy, D.C. 1988. Geology, v. 16, p. 139-143

Depositional Architecture and Evolution of a Deep-Marine Channel-Levee Complex: Isaac Formation (Windermere Supergroup), southern Canadian Cordillera

(First Draft paper for Atlas of Deepwater Outcrops
AAPG Special Publication)

Navarro U., L., Khan, Z. and Arnott, R.W.C.

Department of Earth Sciences, University of Ottawa, Marion Hall, 140 Louis Pasteur, Ottawa, ON, Canada K1N 6N5

ABSTRACT

Channel 3 in the Castle Creek South study area exposes a leveed channel system that is up to 90 m (295 ft) thick and extends laterally for at least 1.6 km (1 mi). It overlies an areally extensive, thick, carbonate-clast-rich debrite, which in turn, is overlain locally overlain by a thick, coarse-grained, sand-rich, sheet-like deposit. In addition to the irregular topography along the top of the debrite, the overlying sand-rich deposit helped focus subsequent flows that ultimately localized and promoted the development of Channel 3.

Channel 3 comprises four channel-fill units bounded on both sides by genetically-related levee deposits. Channel-fill units are made up of two or more channel fills, which, in their axes, consist typically of thick-bedded, massive to graded, pebble conglomerate and very coarse to medium sandstone (T_a Bouma or R_3/S_3 Lowe sequences) and mudstone-clast breccia. The uppermost channel-fill units of Channel 3 show a distinct lateral trend in which strata become progressively more interbedded with siltstone and very fine to fine sandstone (T_{cde} turbidites). This trend is particularly well developed toward the channel margins. Proximal levee deposits occurring adjacent to the (northwest) outer-bend channel margin typically consist of fine-to medium-grained, medium- to thick-bedded T_{a-c} turbidites with a sandstone percentage of up to 70%. Laterally these strata commonly thin over lengths less than 300 m and then into the distal levee persist as thin bedded, very fine to fine sandstone and siltstone T_{cde} turbidites. In addition, overbank splays, which consist of laterally extensive but discontinuous, thick, coarse sandstone turbidites, are common in distal levee deposits. Inner-bend levees, on the other hand, consist of fine-grained, thin-bedded turbidites that also thin and fine laterally but are significantly thinner and finer grained compared to strata on the outer bend channel margin.

As a genetically-related pair, channel-fill and levee deposits are markedly different depending on which side of the channel they were formed. Along the outer-bend these strata are separated by a sharp erosive, terraced surface that suggests episodic channel-levee growth and long-term migration of the entire channel system toward the northwest. In contrast, along the inner-channel margin there is a distinct upward change in the spatial association of channel-fill and levee units. The lowermost part of the inner levee is truncated by the channel margin, probably associated with the earlier, more erosive nature of the channel. The uppermost part of the inner levee, on the other hand, interfingers with channel-fill deposits, suggesting deposition on the upper, lower-energy, inner-bend levee of a narrower channel.

INTRODUCTION

As land-based and shallow-water hydrocarbon reservoirs become progressively more depleted, exploration is being pushed increasingly into deeper water settings. Submarine levee-channel complexes are one of the most important elements of deep-water systems, and recently have proved to be economic hydrocarbon reservoirs. As a consequence, the analysis and establishment of accurate stratigraphic models for these systems is presently an area of much research (Normark, 1970, 1978; Pickering, 1982; DeVries and Lindholm, 1994; Manley *et al.*, 1997, Campion et al., 2000, Cronin et al., 2000; Pirmez et al., 2000; Kolla et al., 2001; Babonneau et al., 2002; Posamentier and Kolla, 2003; Beaubouef, 2004; among others). Unfortunately, current reservoir models commonly lack sufficient understanding of the small-scale distribution and geometry of the constituent architectural elements that relate channel-fill strata with their associated levee deposits. Such details are typically provided by outcrop analogues. However, in most places shale-rich levee deposits are typically poorly exposed because of surface weathering and vegetation cover. Channel 3 in Castle Creek South, on the other hand, is well exposed in vertically-dipping, periglacial strata, and as a consequence provides a rare opportunity to document the small- and large-scale associations between channel and genetically related levee-overbank deposits. The main objectives of this paper therefore will be to describe and discuss the spatial and temporal relationships between a deep-water channel and correlative strata in the adjacent levee/overbank setting. These details, in turn, will help

establish a channel-levee model that illustrates the evolution of these genetically related architectural elements. Ultimately, this will help to better understand and predict hydrocarbon potential and distribution in ancient channel-levee complexes.

CHANNEL 3 OF CASTLE CREEK AREA

Channel 3 in the Castle Creek South study area is located in east-central British Columbia, Canada, within the Neoproterozoic Isaac Formation (Fig. 1, for detailed geological setting and stratigraphy see Ross and Arnott, this volume). This channel-levee complex exposes an almost perpendicular-to-flow section through a leveed channel complex and occurs 600 m (1969 ft) above the contact between the Isaac Formation and Kaza Group (Fig. 2). It is well exposed in a laterally continuous outcrop (1.5-1.6 km-wide, 0.9-1 mi) that locally is obscured by glacial moraine and rubble. Periglacial conditions, especially along the margins of a fast-retreating Pleistocene glacier, yield lichen-free, commonly polished outcrop surfaces, even in fine-grained deposits. In general, the accessibility of the outcrops is very good, but local steep cliffs require major surfaces to be traced using visual observation.

Channel 3 is underlain by a significant, up to 90 m thick (296 ft), carbonate-clast, mud-rich, matrix-supported, areally extensive mass transport complex (Figure 3) which in turn is locally overlain by a thick (up to 3 m, 10 ft), coarse-grained, sand-rich, sheet-like deposit (Figure 3). The intrachannel part of Channel 3 is 80 m (262 ft) thick and is bounded on both sides by genetically-related levee deposits (Figure 3). Due to limited exposure of the southeast margin, the best estimate of the maximum lateral extent of the channel deposits is 1.5 km (0.9 mi). Because of the two-dimensionality of the outcrop face, accurate paleocurrent data of Channel 3 was difficult to obtain in the channel fills, but a small number of axes of three-dimensional current ripples and dunes indicate paleoflow toward the northeast (40°).

Levee strata flanking the northwest channel margin are well exposed and extend well beyond the limits of the study area (>1 km, 0.62 mi). These strata are truncated sharply along the channel margin. Based primarily on facies and stratigraphic relationships these strata are divided into proximal and distal levee deposits (Figure 3). Proximal levee deposits occur less than 500 m (1641 ft) away from the channel margin and are up to 56 m (184 ft) thick. Distal levee deposits occur greater than 500 m (1641 ft) away from the northwest channel margin and are up to 80 m (262 ft) thick.

Levee deposits occurring southeast of the channel margin are locally exposed laterally over 300 m (984 ft). The lower part of the southeast levee truncates against the channel margin, whereas the upper part interfingers with channel-fill strata. Ripple cross-laminated sandstone in the northwest and southeast levee indicate paleoflow toward 27°(NE) and 98°(E), respectively. Divergence of these two paleocurrents against the channel trend, suggests that levee deposition results from turbidity currents spilling out of the channel at both the outer-bend (northwest) and inner-bend (southeast) channel margin.

CHANNEL-FILL DEPOSITS

Channel 3 is 80 m (256 ft) thick and has been subdivided into four distinct main channel units (C1 to C4) that stack to form a channel complex and exhibit a lateral offset arrangement toward the northwest (Figure 3). Each channel unit comprises two or more channel fills, which are interpreted to be genetically related. The top of Channel 3 is abrupt and marked by the superposition of a new channel complex (Figure 4a).

Channel fills, in the lower part of Channel 3, are broad (at least 1.5 km and up to 15 m thick) and have high width/depth ratios (over 50). Conversely, channel fills in the upper part of Channel 3 are narrow (500 m/1641 ft wide and up to 30 m/98 ft thick) and have lower width/depth ratios (e.g. between 39 to 14). The lateral continuity of the channel fills, therefore, is high to intermediate (Clark and Pickering, 1996), and decreases toward the upper part of the channel complex.

Channel units are separated by major erosion surfaces that can be traced across the study area (~1 km, 0.62 mi). The basal surface of the channel complex is a smooth and shallow-dipping surface (<1°) that becomes steeper and more irregular along the channel margins, especially the northwest margin (Figure 3). In fact, this surface is a composite surface that indicates multiple episodes of channel growth. The lower part of the compound surface coincides with the base of channel unit C1 incises the top of a regionally extensive carbonate-clast rich debrite (D1). Erosion surfaces at the base of succeeding channel units (C2 to C4) are also shallow, parallel to the surface at the base of the Channel Complex and erode channel units. Locally, some surfaces deeply scour underlying channel units (up to 12 m, 40 ft deep), like C2 and C3. Laterally surfaces become steeper in the northwest margin, with gradients up to 25°, where in turn incises the adjacent levee deposits (T1) and quartz-clast debrite (D2).

Channel units are of the order of 7-30 m (23- 98 ft) thick and consist of a variety of sedimentary facies (Table 1, Figures 4a-g). At their base, different facies associations are recognized, including thinly-bedded sandstone interbedded with mudstone (facies CF1a), mudstone-clast breccia and inclined beds of massive sandstone interstratified with mudstone-clast breccia lenses. A fine-grained succession (CF1a) occurs at the base of C1 (Figure 5), is approximately 2 m (7 ft) thick and consists mostly of thin- to medium-bedded siltstone interbedded with normal graded, massive or parallel laminated, fine- to medium- grained sandstone (T_{b-e} turbidites according to Bouma, 1962) and are interpreted to have been deposited from the low-concentration tails of energetic turbidity currents. In contrast, matrix-supported breccia (facies CF2, Figure 4c, 6) overlies the base of C2 and locally C3. Breccias are up to 8 m (26 ft) thick, and consist of abundant, generally angular mudstone clasts dispersed in a poorly-sorted matrix of medium sandstone to pebble conglomerate (up to 3.5 cm, 1.4 in). Mudstone clasts are typically oriented parallel to the basal bedding contact, although disorganized fabrics and sand injections, similar to those described previously by Mutti and Nilsen (1981), occur locally. Breccia zones are highly amalgamated, including local lenses of conglomerate and sandstone. These breccia zones show variable lateral continuity that ranges from discontinuous lenses to hundred-meter continuous units (up to 500 m, 1640 ft long). This facies corresponds to the F3 division of Mutti (1992). Mudstone clasts were derived from a number of possible sources, including erosion of fine-grained strata associated with older channel fills or laterally adjacent levee deposits, or upstream erosion and downslope transport by sandy- and gravelly high-concentration turbidity currents (comparable to groups A and B respectively of Johansson and Stow, 1995). On the other hand, the inclined succession at the base of C4 is up to 3 m (10 ft) thick and composed of partially amalgamated, massive sandstone interstratified with mudstone-clasts breccia lenses (facies CF3 and CF2, Figure 7). It is similar to the semi-amalgamated lateral accretion package described by Abreu et al. (2003).

Basal facies associations represent bypass deposits that are overlain by channel fill. In general, lower channel units (C1 and C2) are composed mostly of pebble conglomerate, and upper channel units (C3 and C4) are distinguished by a predominance of sandstone and fine conglomerate. In their axis, channel fills are individually characterized by thick bedded (up to 2.5 m, 8.25 ft thick), normally-graded and massive, granule to pebbly conglomerate and coarse to very coarse sandstone (facies CF3; figure 4c-f). Beds are typically amalgamated and their lateral continuity is highly variable, ranging from tens to hundreds of meters. Coarse-grained deposits correspond to the T_a turbidite division (Bouma 1962), R_3 and S_3 divisions of Lowe (1982) or F5 division of Mutti (1992), and are interpreted to have been deposited by gravel- and sand-rich high concentration turbulent flows. Normal coarse-tail graded beds suggests differential grain settling during deposition from these concentrated flows (Mulder and Alexander, 2001), or a decrease in coarse sediment supply associated with an accumulative or rapid waning flow (Kneller and Branney, 1995; Kneller, 1995). Massive deposits, in contrast, suggest higher instantaneous rates of sediment deposition beneath a rapidly collapsing turbulent suspension (Middleton and Hampton, 1973; Arnott and Hand, 1989; Allen, 1991; Vrolijk and Southard, 1997; Russell and Arnott, 2003). Individual channel fills commonly show a fining- and thinning-upward trend, as does Channel 3 overall.

Toward the margin of channel fills, specifically channel units C3 and C4, coarse-grained strata tend to thin rapidly over 100 m (330 ft), and grade from (complete or partial) amalgamated sandstone (CF3) to less amalgamated, more interbedded thin- to thick-bedded coarse sandstone and thin- to medium-bedded upper-division turbidites (facies CF3 and CF1b respectively). Sandstones beds consist of T_a (Bouma, 1962) or S_3 (Lowe, 1982) and T_b turbidites, and respectively represent suspension deposition from concentrated flows and traction transport/deposition under upper-stage plane bed. Thinly bedded successions of T_{cd}, T_{cde} Bouma turbidites are related to deposition from lower-energy, low-concentration turbidity currents. The onlap and progressive thinning of beds near the margins of the uppermost channel fills (Navarro and Arnott, 2004; figure 8), is interpreted to indicate lower energy conditions along (McCaffrey and Kneller, 2001) along the periphery of larger flows that preferentially exploited the axis of the channel.

LEVEE DEPOSITS

Northwest Levee

Facies characteristics of Channel 3 levee strata are summarized in Table 1, and the detailed architecture of strata cropping out immediately northwest of the channel is illustrated in Figure 9. The basal 2-3 m (L_0) of the northwest levee complex consists mostly of medium to very-coarse sandstone ranging from 0.5-1.5 m thick (facies LF1, Figure 3 and 10a). This depositional element extends laterally toward the northeast and is truncated to the southeast by channel unit C1. This basal unit (L_0) is interpreted to represent deposition from relatively unconfined, moderate-density flows that formed a distributive depositional lobe.

L_0 is abruptly overlain by levee deposits, which immediately adjacent to the channel comprise four distinct levee packages (L_1-L_4, Figures 9 and 10b). Units L_1-L_3 range from 10-15 m thick and share common upward and lateral trends. The lower portion of these packages (denoted by $_L$) is composed predominantly of medium- to thick-bedded, fine to medium sandstone turbidites commonly T_{bc} and T_c turbidites, including beds up to 40 cm thick consisting of multiple, non-climbing, small-scale (ripple) cross-laminated sets (facies LF2a, Figures 10c,d). These medium to thick sandstone beds commonly thicken then thin laterally resulting in an overall "semi-elliptical" cross-sectional levee package geometry. Moreover, lower packages L_{1L} to L_{3L} are progressively laterally offset toward the northwest, a trend that is especially evident when comparing strata in L_{3L} with those in the underlying L_{2L} package (Figure 9). The upper portion of levee units L_1-L_3 (denoted by $_U$) consists predominantly of thin bedded, very-fine to fine sandstone and siltstone T_{cde} turbidites (facies LF2b) with less common medium beds (up to 35 cm) occurring in L_{1U}. The uppermost levee unit L_4 is 15 m thick and is composed entirely of facies LF2b. Accordingly, it is differentiated from underlying units by the absence of a medium- to thick-bedded, sandy basal portion.

Most beds occurring in the proximal levee are laterally continuous with the exception of some rare, thick (>1 m) T_{ab} and T_a beds that pinch-out in less than 40 m. Although pinching-out of beds is rare, medium to thick T_{bc} and T_c turbidites (facies LF2a) commonly thin laterally over lengths less than 200 m, whereafter they persist as thin bedded (< 15 cm), very-fine to fine sandstone turbidites (facies LF2b). As a consequence of this lateral trend, LF2b is the most common facies observed in the distal levee (Fig. 10e). Importantly, facies LF2b sandstone in both proximal and distal levee areas show negligible changes in thickness or grain size along their entire exposure (up to 600 m). Sand percentage in the most proximal levee regions are as high as 70%, which over a distance of 500 m decreases to less than 40% in the distal levee. Consequently, N:G ratio mainly varies as a function of lateral distance away from the channel margin.

Facies LF2a is interpreted to have been deposited by overbanking, high- to intermediate-concentrated turbidity flows. Lateral waning and thinning of these flows resulted in the loss of competence and deposited facies LF2b in more distal levee settings. Deposition of LF2b in northwest proximal levee settings, on the other hand, is associated with overspilling of lower concentrated

channel flows. The general lack of climbing ripple cross-lamination in the levee areas suggests that bedload transport continually exceeded the rate of suspension fallout (Allen, 1982).

A distinctive, up to 7 m thick layer sharply underlies the uppermost levee unit (L_4) and consists of silty mudstone with dispersed quartz pebble clasts (facies LF3, Figures 3 and 9) that is abruptly overlain by a thick (~1.5 m, 11.5 ft), coarse sandstone that fines laterally to medium sandstone and thins over 200 m to 40 cm. This silty mudstone unit, which is interpreted to be a debris-flow deposit (D2 in Figure 3), is truncated on one side by the channel wall of channel unit C4 and less than 50 m in the opposite direction pinches out. The occurrence of dispersed pebble quartz clasts indicates that this debrite was not the result of local levee failure, but instead came from upslope and traveled through the channel, and like other kinds of flows, overspilled at the channel bend. The overlying coarse bed is interpreted to have been deposited from the turbulent suspension that was maintained above the debris flow (Hampton, 1976; Fisher, 1983). Importantly, this debris-flow deposit would have abruptly added levee relief and as a consequence prevented completely the lower, denser parts of later flows from overspilling. This is the main reason for the absence of a sandy basal portion at the base of L_4.

A common facies association observed in the distal levee is thick, amalgamated, medium sandstone (facies LF4, Figure 10f). Beds range from 0.5-1.5 m thick and form amalgamated bed sets up to 4 m thick. These beds and bed sets are interpreted to be areally-restricted overbank splays that were deposited from turbulent flows that overtopped the channel margin (Posamentier and Kolla, 2003). These splay features are believed to have been deposited as a consequence of high levee relief, which effectively created greater backside slope relative to channel gradient. It is interpreted that high velocity, sand-rich turbidity currents were able to overcompensate the high frictional conditions associated with the rapid thinning of the flows as they quickly became unconfined. As a result, flows accelerated down the backsides of the proximal levee, essentially making the proximal levee area a zone of by-pass. A decrease in slope in more distal levee settings decreased flow velocity and competence, resulting in the deposition of splays.

Southeast levee

Deposits in the southeast levee consist predominantly of very fine sandstone and siltstone T_{cde} turbidites, which locally are with in the most proximal areas with interbedded thicker sandstone beds. These sandstone are typically medium- to thick-bedded (0.14- 0.5 m), fine to medium sandstone T_c turbidites composed of multiple (3 or 4) sets of non-climbing ripples (facies LF2a) occur (Figure 7), alike those commonly observed in the northwest proximal levee. Medium- to thick-bedded (>0.20 m thick) massive sandstone beds (facies LF2b, Figures 6 and 7) are also commonly found observed. Moreover, these levee deposits interfingers with channel-fill strata along the channel margin. These levee strata rapidly fine and thin laterally over a distance less than 50 m toward the southeast. These strata are interpreted to have been deposited by overbanking, lower-concentration turbidity flows.

EVOLUTION OF A CHANNEL-LEVEE COMPLEX

In the Castle Creek area, Channel 3 shows an evolution that can be subdivided into a period of slope instability followed by three recurring stages of levee growth followed by channel fill (Figure 11). Each stage is defined by particular channel geometry, channel and levee stacking pattern and the nature of levee deposits.

Incipient conditions

Prior to the inception of Channel 3 an up to 90 m (295 ft) thick, carbonate clast, mud-rich, matrix-supported, areally-extensive mass-transport complex blanketed the study area. Significant debris-flow deposits like this are commonly overlain by channel-levee systems (e.g. Weimer, 1991; Piper et al, 1997; Pirmez et al., 1997; Manley and Flood, 1998; Maslin et al, 1998; Beaubouef and Friedman, 2000; Brami et al, 2000; Winker and Booth, 2000; Samuels et al., 2003) that are

interpreted to coincide with episodes of sea level fall (Posamentier and Kolla, 2003). These debrites most probably formed a rugged, irregular sea-floor topography that helped focus subsequent relatively unconfined, turbidity currents downslope. At Castle Creek, these early flows probably emplaced thick, coarse-grained, potentially lobe-shaped deposits (LF1 and L_0 in Figure 11a). These strata, therefore, initiated the confinement of subsequent flows and as a result promoted the localization and development of Channel 3.

Stage 1

The first stage was characterized by levee aggradation and channel by-pass (Figure 11b). During this stage the channel was weakly confined, and as a consequence superelevation of turbidity currents as they rounded the bend aided in the overspill of the lower, higher-density part of highly stratified flows along the outer channel-bend, resulting in the deposition of the sandier, lowermost part of proximal levee packages on the northwest channel margin (facies LF2a). Lateral waning and thinning of these flows resulted in a loss of competence and reduction in sediment concentration, which in turn deposited facies LF2b in more distal levee settings. Superelevation of flows rounding the outer bend, resulted in comparatively diminished flow on the opposite, or inner-bend side of the channel. These lower energy flows resulted in the deposition of facies LF2b on the southeast inner-bend levee. During levee aggradation, highly efficient, largely bypassing flows were sculpting and widening the channel (Clark and Pickering, 1996; Mutti, 1992) due to disequilibrium between flow and slope conditions (Kneller, 2003; Samuels et al., 2003), forming laterally extensive erosion surfaces. These flows transported much of their sand and coarser sediments further basinward, leaving behind a residuum of thinly-bedded turbidites (facies CF1a), mudstone-clast breccia (facies CF2) and inclined package of sandstone and breccias (facies CF3 interbedded with CF2), typically in channel axes.

Stage 2

The second stage was distinguished by continued levee growth and the initiation of channel filling (Figure 11c). Increased channel confinement during the early part of stage 2 enabled only the upper, more dilute fraction of flows to overspill, resulting in the deposition of facies LF2b on both the northwest and southeast levees. Additionally, throughout stage 2, overbank splay deposits (facies LF4) were preferentially emplaced on the northwest distal levee.

The onset of channel filling was most probably related to an increase in sediment caliber and sediment flux. Initially channels were wide and began to fill with thick-bedded, normally graded and massive conglomerate and conglomeratic sandstone (facies CF3). Stratigraphically-upward thick, sandstone-dominated strata (facies CF3) become increasingly common, suggesting waning flow conditions or a decrease in sediment caliber and/or supply to the system.

Stage 3

In comparison to stages 1 and 2, channel aggradation increased significantly during stage 3 (Figure 11d), whereas overbanking processes were significantly diminished and as a consequence reduced channel-levee relief. Moreover, during this stage partially amalgamated sandstone (facies CF3) were deposited in the channel axis, and less amalgamated, more interbedded thick-bedded coarse sandstone and thin-bedded turbidites (facies CF3 and CF1b respectively) were emplaced toward the channel margins. Fining- and thinning-upward of channel-margin strata suggest that flows became gradually smaller, muddier and less dense, possibly as a result of rising relative sea level (Kneller, 2003). The end of Stage 3 is marked by channel abandonment and deposition of thin, fine sandstone turbidites (facies CF1b). The transition from Stage 3 to Stage 1 of the succeeding channel-levee unit is abrupt and marked by partial or complete erosion of the fine-grained channel abandonment succession at the top of the underlying unit.

Multiple episodes of channel- levee growth and migration

The four channel-levee units of Channel 3 exhibit a multilateral offset stacking pattern toward the northwest (Figure 3), which is interpreted to be associated with the long-term northwest migration of the entire system (Figure 11e). Importantly, migration of the channel axes of each channel unit eroded into outer channel bend, or cut bank, producing a composite terraced or erosive "flat and step" surface (sensu Eschard et al., 2004) that sharply separates levee from channel-fill deposits (Figure 8). This geometry strongly supports the interpretation that Channel 3 was formed by multiple (four) episodes of channel-levee growth, which individually comprise strata deposited from stages 1 to 3. Each episode was periodically interrupted by major events of channel re-incision that may be associated with fourth-order sea-level fall (Samuels et al., 2003), and as consequence caused the steeppening of the slope profile, loss of slope accommodation and resultant erosion, thereby promoting channelization (Imran et al., 1999; Pirmez et al., 2000). Re-incision events at the base of channel units C2 and C3 represent abrupt or punctuated migration of the channel system (in the sense of Deptuck et al., 2003; Kolla et al., 2001), leading to severe erosion of the preceding channel units. Erosion at the base of channel unit C4 (Figure 7), by contrast, is more subdued and was most likely related to a more gradual migration of the system (Deptuck et al., 2003).

Each reincision event was followed by periods of channel infilling that demonstrates that the channel was aggrading rapidly as it was migrating laterally. Channel aggradation is associated with an obvious diminution of flows conditions (e.g. flow competence, capacity and speed), and higher rates of channel aggradation certainly enhanced the preservation of sandy proximal levee deposits. More specifically, without sufficient rates of aggradation the unidirectional lateral shift of the channel would have eroded most of the proximal outer-bank levee deposits (Deptuck et al., 2003), and this may very well be the reason why thick bedded proximal levees are not commonly reported from the rock record.

Furthermore, the upward transition from wider, more erosive channels to narrower channels is recognized in Channel 3. This change in channel configuration is supported by the upward change of strata on southeast levee, were the lowermost part is truncated by the channel margin, probably associated with the earlier, more erosive nature of the channel, whereas in the uppermost part channel fill deposits interfingers with fine-grained levee deposits (Figure 8), suggesting deposition on the lower-energy inner-bend levee of a perhaps more sinuous channel. In addition, the width of the channel belt decreased, most probably as a consequence of changes in flow or slope conditions of the system, and is similar to earlier observations of some channels on the modern Indus Fan (McHargue, 1991; Deptuck et al., 2003).

RESERVOIR IMPLICATIONS

Based on sedimentologic and stratigraphic attributes, Channel 3 is comparable to modern offshore reservoirs in the Arabian Sea (McHargue, 1991) and West Africa (Kolla et al., 2001; Fonnesu, 2003; Abreu et al., 2003; Deptuck et al., 2003; Adeogba et al., 2005), and therefore, represents an important analog for predicting and estimating of stratal architecture of channel-levee hydrocarbon reservoirs.

Important reservoir analogies can be extrapolated from field observations relating the characteristics of the fills of Channel 3 with underlying deposits. First, the sheet-like deposits (L_0) that underlies Channel 3 is comparable to the transient fan of Adeogba et al. (2005), which could be a good local hydrocarbon reservoir because of its high N:G percentage and internal amalgamation, however due to its limited thickness it might difficult to be resolve on deep industry. Second, channel fills in the axial parts of Channel 3 have high reservoir quality with high vertical connectivity between them and high N:G ratios ranging from 80 to 100%. These fills consist almost exclusively of stacked, amalgamated clast-supported conglomerate and coarse-grained sandstone with a general lack of fine-grained strata. Nevertheless, fine-grained, laterally continuous turbidites do occur rarely at the

top of channel fills and would be expected to form local barriers to fluid flow. Likewise, mudstone rip-up clast breccias that commonly occur at the base of some channel fills could represent local permeability baffles, but more importantly reduce reservoir volume flow (Elliot, 2000). In most places, however, the overall fluid flow in these rocks is most probably affected very little due to good interconnectivity within the sand matrix surrounding the loosely packed mud-clasts. Third, reservoir quality decays as grain-size and bed thickness decrease vertically and laterally toward the channel margins. In the upper channel fills of Channel 3, N:G ratios decrease (from 93% to 70%) as strata become progressively less amalgamated. Typical thinning of beds toward the levee (similar in broad terms to the type A, pinch-out geometry of McCaffrey and Kneller, 2001) and common siltstone interbeds will most probably negatively affect the vertical connectivity between individual sandstone beds.

Levee deposits have recently proven to be important hydrocarbon reservoirs, for example from deep water Gulf of Mexico fields, including, Tahoe (Kendrick, 2000) and Ram/Powell (Clemenceau, 2000). However, seismic resolution is typically too coarse to identify and differentiate small-scale internal stratal attributes (DeVries and Linholm, 1994; Clemenceau et al., 2000). Thus, outcrop studies, like this one, can provide important insight into stratal architectures of reservoir-type facies in levee-overbank deposits. Levee deposits in Channel 3 are subdivided into two end-members: proximal and distal levee deposits. N:G ratios are up to 70% in the proximal levee and there is excellent lateral continuity of sandstone beds. Vertical communication, however, would be significantly reduced by laterally-continuous, interbedded siltstone layers. Laterally, N:G ratio decreases rapidly (<200 m, 656 ft) to less than 40% in distal levee settings. In the distal levee sandstone beds are consistently much thinner (<10 cm, 3.9 in) and are interbedded with siltstone more commonly. Moreover, these strata have good lateral continuity and based on the volumetric significance of these strata potentially present a good secondary hydrocarbon reservoir. Also, overbank splay sandstones, which occur in the distal levee, most likely represent good local reservoirs as they consist of tabular sandstones that extend over large areas providing excellent pathways for fluid flow and pressure communication (Posamentier and Kolla, 2003). Finally, sand-on-sand contacts between channel sandstone and levee deposits along the channel margin would certainly improve lateral continuity, but also vertical connectivity in distal levee strata, in addition to increasing N:G ratios locally.

CONCLUSIONS

Channel 3 of the Isaac Formation within the southern Canadian Cordillera is an excellent outcrop example of an ancient submarine channel-levee system, and thereby equivalent to those of the Cerro Toro Formation in southern Chile, Pab Formation in south-west Pakistan and Kirkgeçit Formation in Turkey. The fact that Channel 3 strata are so well preserved and are interpreted to have been deposited on a passive margin setting makes it an ideal analog for evaluating many modern deep-water channel-levee hydrocarbon reservoirs.

Channel 3 comprises four channel units that are flanked on both sides by genetically-related levee deposits: outer-bend (northwest) and inner-bend (southeast). These elements show complicated but distinctive facies and internal architectures that allow for the resolution of the temporal and spatial relationships between channel fill and levee architectural elements.

Channel units are individually separated by complex erosion surfaces. These units are laterally and vertically amalgamated, and each shows variations in lithofacies, geometry and internal bed amalgamation according to position (axial or marginal) within the channel fill. The upward variation from wide to narrow channel units is interpreted to be associated with adjustment in flow or slope conditions during the development of channel system.

Outer-bend levee deposits occurring along the northwest margin of Channel 3 are subdivided into proximal and distal areas depending on their proximity to the channel margin. Proximal levee deposits are made up of distinct levee packages that typically thin and fine upward and laterally.

Inner-bend levee beds are much thinner and finer than their outer-bend counterparts. In the distal areas, isolated, thicker and coarser overbank splay deposits are commonly interstratified with predominantly fine-grained, thinly-bedded turbidites.

Vertical and lateral staking patterns of channel and levee units are associated with a long-term migration of the system toward the northwest. This movement created a composite terrace surface along the northwest margin that was related to multiples episodes of channel-levee growth. These complex erosion surfaces are similar to those reported previously from outcrops in Pakistan and hydrocarbon systems in the Indus Fan. The rapid migration of each channel unit, in conjunction with significant channel aggradation, resulted in the preservation of outer levee deposits on the outer-channel bend (cut-bank side) and the development of inner levee in the opposite side to maintain the stability of the conduit margins during the infilling. We believed that channel-levee growth and migration were genetically associated, and the reason such relationships are not often documented with detail in the field is due to the poor exposure of fine-grained levee facies worldwide or the lack of sufficient detailed analyses of the internal architectural distribution of these deposits.

The model proposed here explains how repetitive chonostratigraphic relationships between levee and channel complexes occur. Detailed recognition of lithofacies, in addition to net-to-gross, stratal continuity and configuration of the composite architectural elements will hopefully provide useful comparative information to be considered in reservoir analyses in other deepwater systems.

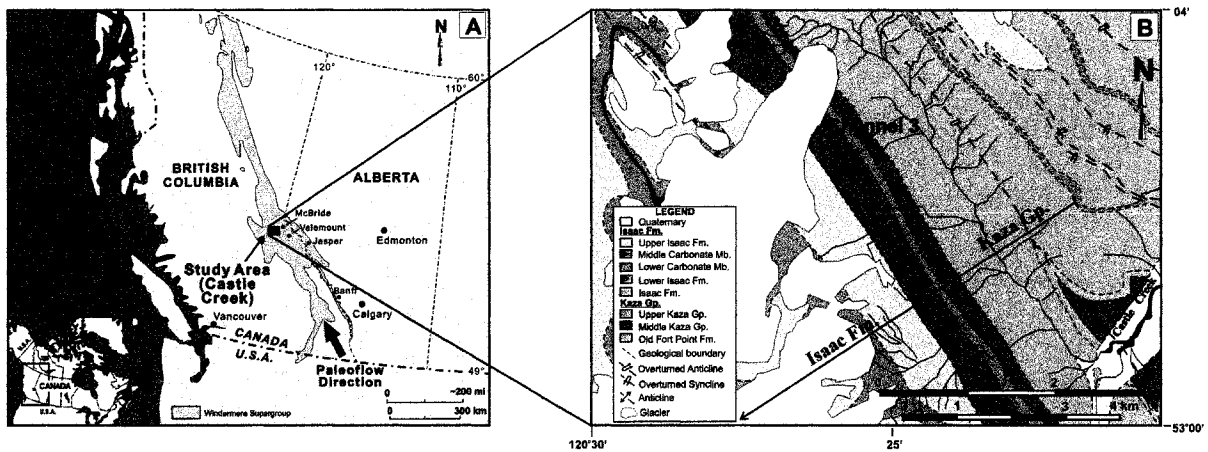

Figure 1. Location of the study area, indicated in relation to (A) map of western Canada showing the distribution of Windermere strata (outcrop distribution and inferred palaeocurrent trend are taken from Ross, 1991, and Ross and Murphy, 1989), and (B) map of the Cariboo Mountains, the most northerly range of the Columbia Mountains (modified from Ross and Ferguson 2003). Neoproterozoic (Hadrynian)rocks in this area are well-exposed on the steeply limb of a west-verging overturned anticline.

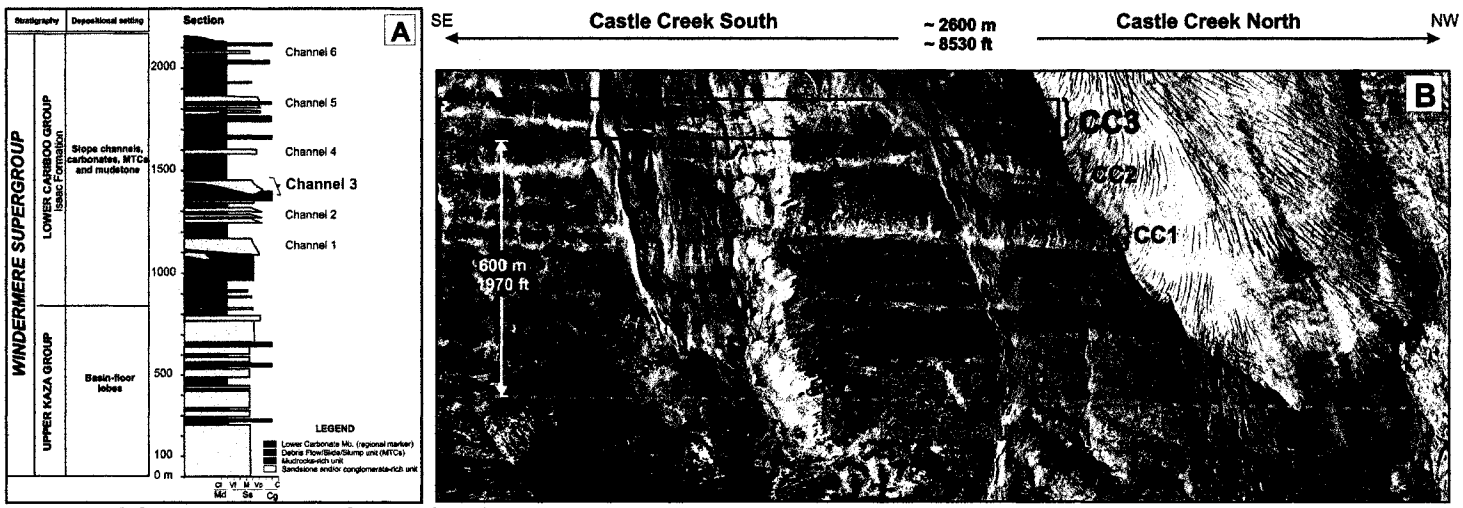

Figure 2. Location of Channel 3 in the Castle Creek area according to (A) Windermere Supergroup stratigraphy, and (B) Airphoto mosaic of the Castle Creek South area illustrating the location of the lowermost, sandstone-rich channel fill units recognized in the Isaac Formation (C1-C3). Channel 3 is indicated by red rectangle (including adjacent levee deposits)

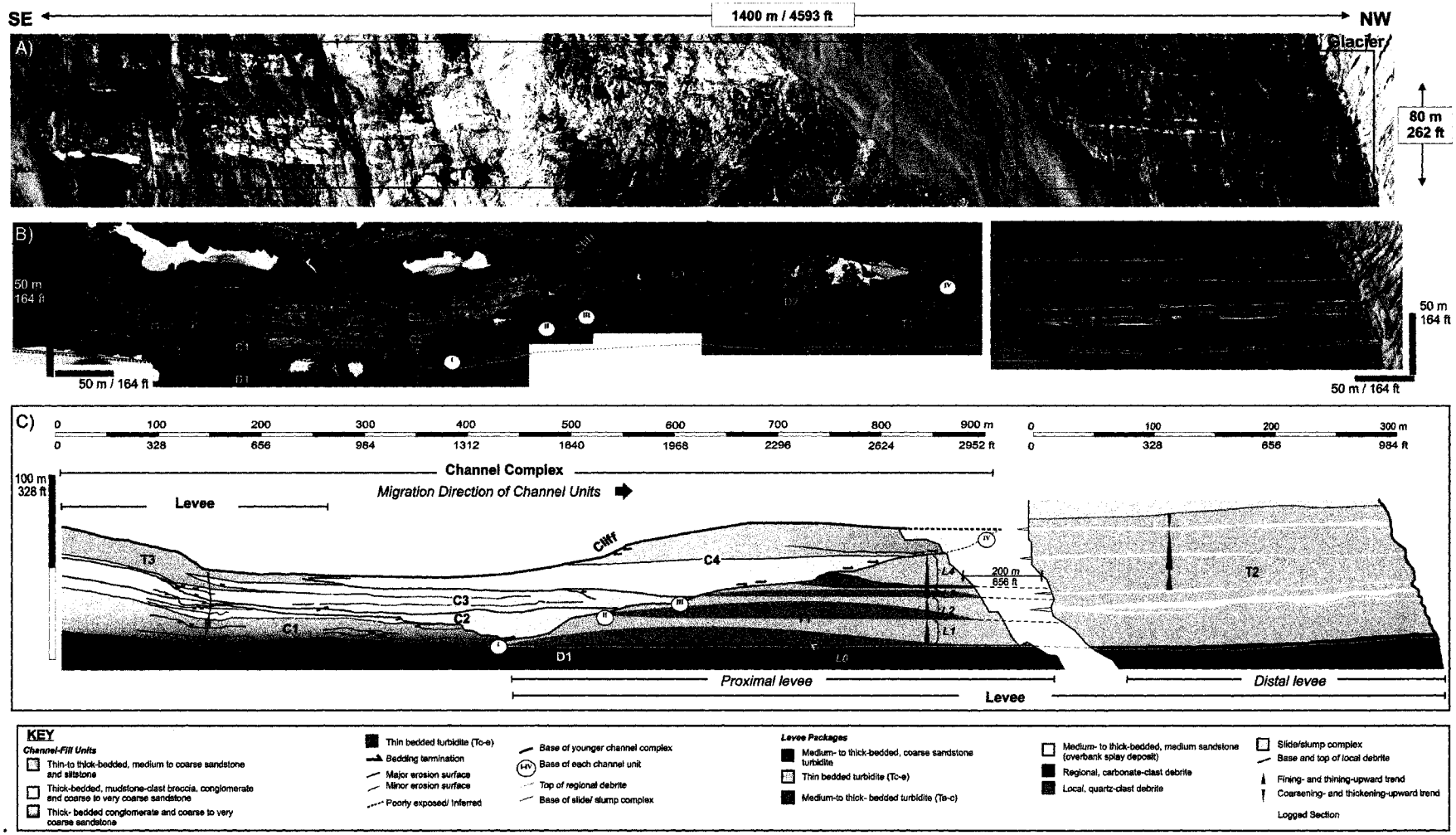

Figure 3. Vertical and lateral stacked channel-levee units of Channel 3, Castle Creek South. (A) Aerial photo showing the 1.4 km (0.9 mi) outcrop belt. (B) Photomosaic showing confined channel complex, highlighting the major channel fills and proximal and distal levee deposits. (C) Schematic architectural panel illustrating the channel network and coeval levee deposits.

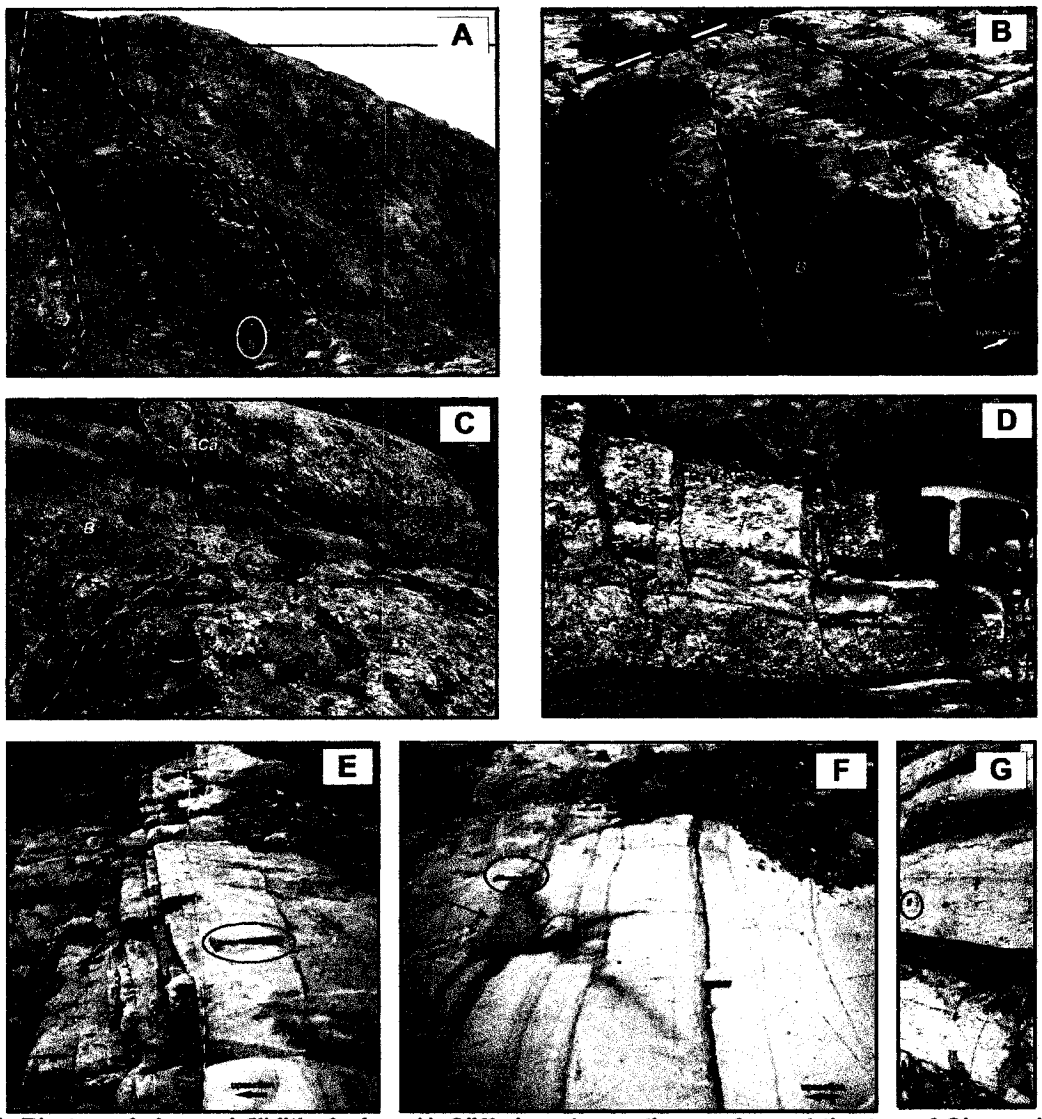

Figure 4. Photos of channel-fill lithofacies. A) Cliff-view: truncation surface at the top of Channel 3 where the younger channel complex is filled by laterally pinching thin-bedded turbidites (arrow); B) Step and shallow erosional surfaces at the base of amalgamated, thick mudstone-clast breccias. These deposits commonly occur at the base of channel units and eroded the underlying units; C) Poorly sorted, pebble clast-supported conglomerate with dispersed large carbonate clasts (brown-orange weathered, Ca) embedded into a quartz-rich matrix of grains from fine-sand to pebble size. This deposits occur in the channel unit 1, and are locally overlain by mudstone-clast breccia (B); D) Amalgamated, normally graded conglomerate beds in channel unit C1; E) massive and normally graded sandstone beds, with onlap bed termination toward the (southeast) channel margin; F) massive and normally graded sandstone beds in the channel axis, with local U-shaped scours (arrow); G) typical normally graded sandstone interbedded with siltstone/fine sandstone beds occur at the (northwest) channel margin of channel unit C4.

Figure 5. see Figure 3.17a

Figure 6. see Figure 3.17b

Figure 7. see Figure 3.17c.

Figure 8 and 9. Khan's work

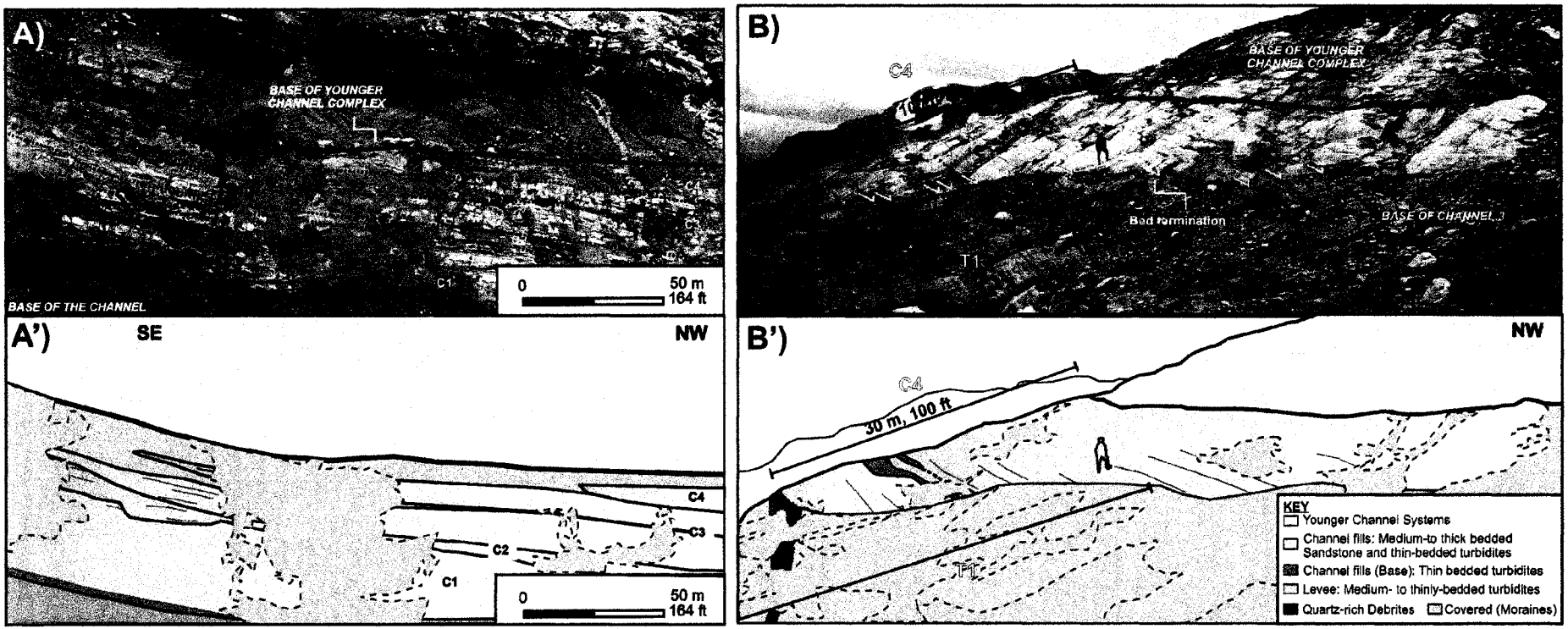

Figure 8. A-B) Uninterpreted, A'-B') interpreted. Channel and levee units along the SE and NW margins (A-A' and B-B' respectively) of upper channel fills of Channel 3. Channel fills of channel units C3 and C4 interfinger with thin bedded levee deposits that were deposited by lower energy overbanking flows on the inner channel-bend. In contrast, channel fills of channel unit C4 onlap quartz-clast debrite and fine-grained levee deposits. These latter strata are considered to have been deposited by more energetic overbanking flows on the outer channel bend, or cutbank side, of the channel.

Figure 11. See Fig. 4.4a-e

Table1. Facies association and general reservoir characteristics of channel-fill and levee deposits of Channel 3.

Architectural Element	Net: Gross and Bed continuity	Facies Association Name	Lithofacies Description	Lateral lithological changes	Depositional processes
Channel fills					
Width: > 375 m, 1230 ft Thickness: 7-30 m, 23-98.4 ft	Typical high N:G. Values decrease from the channel axis toward the margins: 0.8-1 to 0.7-0.93, respectively Variable continuity of individual beds, from less than 30 to 300 m. Beds, especially CF2 and CF3, in the channel axis are partially or completely amalgamated. In contrast, beds at the or near the channel margin are better stratified and show clear onlap and thin laterally, due to the occurrence of CF1.	CF1	***Thin to medium bedded sandstone interbedded with thinly bedded sandstone/siltstone (CF1a and CF1b)*** **CF1a**: Fine to medium sandstone and silty mudstone. Common massive, parallel and ripple cross-lamination. 0.01 to 0.30 m thick beds. Silty mudstone or siltstone beds are 0.02-0.35 m thick, occasional muddier bed (up to 0.11 cm). Interbeds of 0.01 – 0.31 cm thick, medium to coarse sandstone, commonly massive and parallel laminated, and 0.1-0.27 thick breccia that contain mudstone clasts embedded in a coarse sandstone matrix. **CF1b**: Medium to coarse sandstone, moderate to well sorted. Common massive, but also normal graded or parallel laminated. Beds are 0.05 -0.26 m thick with diffuse or sharp, non-erosive bases. Interbeds of fine to medium sand and silty mud. Common massive, parallel lamination and ripple cross-lamination. 0.01 to 0.3 cm thick beds. Silty mudstone or siltstone beds are 0.1-0.8 cm thick. Non- erosive bases. Flame structures are common.	CF1a succession typically overlies erosion surfaces and has conformable contacts with overlying beds at the channel margins, but tend to have erosive top contact in the channel axis. Successions thicken away from the channel axis. CF1b: Heterolithic intervals are more common toward the margins of the upper parts of the Channel 3, where finer sand (very fine sandstone) and thinners (<3 cm thick) beds predominate. Distinct siltstone drapes are also common and thicker (up to 0.32 m).	Deposition from low to medium-concentration steady depletive turbidity flows. Deposition from low to high-concentration turbidity currents with high sediment fallout rates, high energy upper- and lower-stage tractive conditions; followed by suspension deposition of silt and mud.
		CF2	***Medium to thick bedded, mudstone-clast rich breccia*** Dispersed pebble to boulder clasts in a medium sand to pebble matrix, extremely poorly sorted. Beds have common erosive bases and range from 0.2 - 8 m thick. Local injections are found.	Breccia are more common in the channel axis, and characteristically overlie areally extensive erosion surfaces	Sandy to gravelly high-concentration turbidity currents with abundant partially consolidated mud clasts.
		CF3	***Thick bedded, normal graded and massive conglomerate and sandstone*** Granule to pebble conglomerate in a coarse to very coarse matrix typical clast-supported conglomerate, 0.1 - 2.4 thick beds; well or poorly sorted. Local boulder carbonate clasts in the lower 0.2-0.25 m of the Channel 3. Coarse to very coarse sandstone. Distinctive erosive and sharp bases and also common undulatory bases associated with load and ball-and-pillow structures.	This lithofacies becomes predominantly more sandy near the channel margins, specifically in the northwest. Coarse and very coarse sand grain sizes, uncommon granules at the base. Beds are thin, and range from 0.4 - 1.5 m thick.	Differential settling or rapid suspension deposition from single or multiple gravelly or sandy high-concentration turbidity currents
Levee deposits					
Width: > 1000 m, 3280ft Thickness:5-80 m,3.28-262 ft	LF1 varies from 0.70 -0.90 N:G. LF2 N:G decreases away from channel margin from 0.70 – 0.40 LF1 beds are laterally discontinuous and amalgamated forming laterally extensive tabular units up to 5 m thick.	LF1	*Medium-to thick sandstone **(LF1a and LF1b)*** **LF1a**: Medium to coarse sandstone. Massive to normally graded, local development of dune cross-bedding, mud-clast horizons. Individual beds range in thickness from 0.2- 1.5 m. Unit thickness ranges from 2-5 m (6.56-16.4 ft). Bed bases are sharp to slightly erosive. **LF1b**: Similar to LF-1a but consists of medium-grained sandstone and also includes faint planar bedding. Individual beds range from 0.30-1.0 m, amalgamated units range from 2- 4 m. Diffuse or sharp, non-erosive to slightly erosive bases	LF1a is laterally continuous and occurs at the base of the levee succession. LF1b occurs in the distal levee (>500 m from channel margin) and is laterally continuous to the limit of the outcrop (>300 m) Both LF1a and LF1b are more common beyond the southeast margin in the upper part of Channel 3.	Relatively unconfined, depletive steady moderate-concentration turbidity currents.
	LF2 beds are commonly laterally continuous across the length of observed outcrop. Thicker beds (> 20 cm) fine and thin laterally but then persist as continuous thin turbidites (< 5 cm) to the limit of the outcrop.	LF2	*Medium bedded sandstone (LF-2a) interbedded with thin bedded sandstone-siltstone (LF-2b)* **LF2a**: fine to medium sandstone. Commonly normally graded, parallel laminated, multiple-set ripple cross-lamination. Common Bouma sequences include: T_{ab}, T_{bc}, and T_c. Beds are 0.20-1.5 m thick beds. Sharp, flat non-erosive bases. **LF2b**: grades from fine siltstone to fine sandstone. Ripple cross-laminated T_{cde} Bouma sequences. Beds are 0.03-10 cm thick with sharp conformable bases.	Up to 400 m lateral to the channel margin, beds are predominantly medium bedded T_{a-c} and interbedded with thin bedded T_{cde}'s. Thereafter, medium beds thin and persist as thin (<10 cm) turbidites. The distal levee, therefore, consists predominantly of T_{cde}'s interbedded with uncommon medium bedded turbidites.	Commonly low to moderate-concentration steady depletive turbidity flows.
		LF3	*Mud-Supported Conglomerate* An up to 7 m thick succession of mud rich matrix-supported conglomerate with dispersed quartz pebbles. Shallow, erosive base.	Unit is discontinuous (50 m long) and truncates against the channel fill to the southeast. It is overlain by a very coarse sandstone bed that pinch out to the northwest.	Debris flow generates from levee wall failure